

34  
N-70-1  
p.3



TECHNICAL REPORT N-70-1

# STRENGTH AND BEHAVIOR OF REINFORCED CONCRETE SLAB-COLUMN CONNECTIONS SUBJECTED TO STATIC AND DYNAMIC LOADINGS

Final Report  
by  
M. E. Criswell



US-CEC Property of the United States Government



RESEARCH CENTER LIBRARY  
U.S. ARMY ENGINEER WATERWAYS EXPERIMENT STATION  
VICKSBURG, MISSISSIPPI

December 1970

Conducted for Office of Civil Defense, Office of the Secretary of the Army  
Washington, D. C. 20310

Under Work Order No. OCD-PS-66-67, Work Unit 1127B

By U. S. Army Engineer Waterways Experiment Station, Vicksburg, Mississippi



TECHNICAL REPORT N-70-1

# STRENGTH AND BEHAVIOR OF REINFORCED CONCRETE SLAB-COLUMN CONNECTIONS SUBJECTED TO STATIC AND DYNAMIC LOADINGS

Final Report

by

M. E. Criswell



December 1970

## OCD REVIEW NOTICE

*This report has been reviewed in the Office of Civil Defense and approved for publication. Approval does not signify that the contents necessarily reflect the views and policies of the Office of Civil Defense.*

Conducted for Office of Civil Defense, Office of the Secretary of the Army  
Washington, D. C. 20310

Under Work Order No. OCD-PS-66-67, Work Unit 1127B

By U. S. Army Engineer Waterways Experiment Station, Vicksburg, Mississippi



TECHNICAL REPORT N-70-1

SUMMARY OF

**STRENGTH AND BEHAVIOR OF REINFORCED  
CONCRETE SLAB-COLUMN CONNECTIONS  
SUBJECTED TO STATIC AND DYNAMIC  
LOADINGS**

Final Report

by

**M. E. Criswell**



December 1970

**OCD REVIEW NOTICE**

*This report has been reviewed in the Office of Civil Defense and approved for publication. Approval does not signify that the contents necessarily reflect the views and policies of the Office of Civil Defense.*

Conducted for **Office of Civil Defense, Office of the Secretary of the Army**  
**Washington, D. C. 20310**

Under **Work Order No. OCD-PS-66-67, Work Unit 1127B**

By **U. S. Army Engineer Waterways Experiment Station, Vicksburg, Mississippi**

TA7  
W34  
No. N-70-1  
Top. 3

## SUMMARY

The primary objectives of this investigation were to study the strength and behavior of slowly (statically) loaded reinforced concrete slab-column connections and to determine the effect of rapid (dynamic) loading on the strength and behavior by comparison with the static test results.

Tests of 19 full-scale models of a connection and adjoining slab area are presented. The specimens consisted of a simply supported slab either 84 or 94 inches square and 6-1/2 inches thick loaded concentrically on a 10- or 20-inch-square stub column at the center of the slab. The main variables were the amounts of reinforcement in the slab ( $p = 0.75$  and 1.50 percent), the column size, and the loading speed. Eight specimens were loaded to failure statically, two were subjected to a very rapidly applied load of short duration, and nine were loaded to failure by a rapidly applied load with a rise time of 9 to 32 msec, a rate chosen to represent the conditions at the connections in a blast-loaded structure.

The behavior of the statically and dynamically loaded specimens was very similar. Failure deflections increased 25 to 50 percent at the rapid loading rate chosen. The strength of specimens failing in shear after flexural yielding was reached ( $p = 0.0075$ ) increased 18 percent with rapid loading. The strength of the more heavily reinforced specimens ( $p = 0.0150$ ) increased 26 percent. These increases could be adequately explained by the effects of the high strain rates on material strengths.

The static test results are compared with 12 shear strength prediction methods. All methods, including those of ACI Code 318-63, became less



conservative with the larger column size. The strengths of the specimens with  $p = 0.0075$  were best predicted by a yield-line formula for flexural strength.

The failure of connections with square columns was shown to start at the column corners and progress toward the column centerlines.

Differences between the mechanism of shear failure in slabs and beams are examined. The shear-compression failure mechanism is shown to be not strictly applicable for slabs failing in shear. The consistent drop in radial concrete strains measured on the compression side of the test specimen is explained by a reversal in radial moments as the flexural strength is approached and by the effects of the orthogonal reinforcement pattern. The effects of several variables on the shear strength and the moment distribution in the slab throughout the loading history are discussed.

## Foreword

This report is based on a thesis prepared by Mr. M. E. Criswell of the Nuclear Weapons Effects Division (NWED) of the U. S. Army Engineer Waterways Experiment Station (WES) in partial fulfillment of the requirements for the degree of Doctor of Philosophy in the Department of Civil Engineering, University of Illinois, Urbana, Illinois.

The investigation was conducted at WES during the period April 1966 to December 1969 under the general direction of Dr. M. A. Sozen, Professor of Civil Engineering, University of Illinois, Mr. G. L. Arbuthnot, Chief, NWED, and Mr. W. J. Flathau, Chief, Protective Structures Branch, NWED. The work was sponsored by the Office of Civil Defense and conducted under Work Order No. OCD-PS-66-67, Work Unit 1127B.

Directors of WES during the investigation and the preparation of this report were COL John R. Oswalt, Jr., CE, COL Levi A. Brown, CE, and COL Ernest D. Peixotto, CE. Technical Directors were Mr. J. B. Tiffany and Mr. F. R. Brown.

TABLE OF CONTENTS

	Page
FOREWORD . . . . .	iii
LIST OF TABLES . . . . .	viii
LIST OF FIGURES . . . . .	ix
NOTATION . . . . .	xviii
CONVERSION FACTORS, BRITISH TO METRIC UNITS OF MEASUREMENT . . . . .	xxiv
SUMMARY . . . . .	xxv
CHAPTER	
1 INTRODUCTION. . . . .	1
1.1 THE PROBLEM . . . . .	1
1.2 OBJECTIVE OF THE STUDY . . . . .	2
1.3 SCOPE. . . . .	3
1.4 DEFINITIONS. . . . .	4
2 REVIEW OF PREVIOUS RESEARCH . . . . .	6
2.1 STATIC TESTS . . . . .	6
2.1.1 Investigations of the Basic Strength and Behavior of Slab-Column Connections Failing in Shear . . . . .	6
2.1.2 Other Investigations of Slab-Column Connections. . . . .	19
2.1.3 Performance of Connections in Slab Systems . . . . .	24
2.1.4 Design Specifications for Static Loadings. . . . .	27
2.1.5 Test Results . . . . .	29
2.1.6 Parameters Affecting Connection Strength . . . . .	30
2.2 DYNAMIC TESTS. . . . .	34
3 DESIGN OF THE EXPERIMENTAL INVESTIGATION. . . . .	36
3.1 RATIONALE OF THE TEST PROGRAM. . . . .	36
3.2 TEST VARIABLES . . . . .	37
3.3 PROTOTYPE AND MODEL SCALE. . . . .	39
3.4 TEST PROGRAM . . . . .	40
3.5 TEST SPECIMENS . . . . .	41
3.6 LOADING OF THE TEST SPECIMENS. . . . .	43
3.6.1 Support and Load Locations . . . . .	43
3.6.2 Dynamic Loading Rate . . . . .	44
4 EXPERIMENTAL PROCEDURE. . . . .	50
4.1 SPECIMEN MATERIALS AND FABRICATION . . . . .	50
4.1.1 Concrete . . . . .	50

## CHAPTER

4.1.2	Reinforcement . . . . .	50
4.1.3	Forming, Casting, and Curing of Specimens . . . . .	51
4.1.4	Material Tests . . . . .	52
4.2	TEST EQUIPMENT AND PROCEDURES . . . . .	54
4.2.1	Loading Device . . . . .	54
4.2.2	Test Setup . . . . .	54
4.2.3	Static Tests . . . . .	56
4.2.4	Dynamic Tests . . . . .	56
4.3	TEST MEASUREMENTS AND INSTRUMENTATION . . . . .	57
4.3.1	Load Measurement . . . . .	57
4.3.2	Deflection and Acceleration Measurements . . . . .	58
4.3.3	Strain Measurements . . . . .	59
4.3.4	Data Recording and Reduction . . . . .	60
5	EXPERIMENTAL RESULTS . . . . .	62
5.1	STATIC TESTS . . . . .	62
5.2	DYNAMIC TESTS . . . . .	63
6	STRENGTH AND BEHAVIOR OF STATICALLY LOADED SLAB-COLUMN CONNECTIONS . . . . .	66
6.1	RESULTS OF DUPLICATE TESTS . . . . .	67
6.2	LOAD-DEFLECTION RELATIONSHIPS . . . . .	67
6.3	CRACK PATTERNS . . . . .	69
6.4	THE FAILURE SURFACE . . . . .	71
6.5	INTERNAL CRACK FORMATION . . . . .	74
6.6	CONCRETE STRAINS . . . . .	76
6.6.1	S2000 Series . . . . .	77
6.6.2	S4000 Series . . . . .	78
6.7	STEEL STRAINS . . . . .	80
6.7.1	S2000 Series . . . . .	80
6.7.2	S4000 Series . . . . .	81
6.8	FAILURE OF THE CONNECTION SPECIMENS . . . . .	82
6.8.1	S4075 Specimens . . . . .	82
6.8.2	S4150 Specimens . . . . .	84
6.9	COMPARISON OF MEASURED AND PREDICTED QUANTITIES . . . . .	85
6.9.1	Flexural Strength . . . . .	85
6.9.2	Shear Strength . . . . .	87
6.9.3	Deflections and Stiffnesses . . . . .	92
6.10	AN EXAMINATION OF SLAB-COLUMN CONNECTION BEHAVIOR . . . . .	95
6.10.1	Current Concepts of Connection Behavior . . . . .	95
6.10.2	Comparison of Beam and Column Connections . . . . .	97
6.10.3	Moments in an Idealized Connection . . . . .	100
6.10.4	Calculated Stress Distribution Near the Column Face . . . . .	106
6.10.5	Effects of an Orthogonal Reinforcement Pattern . . . . .	107
6.10.6	Effect of Column Size . . . . .	112

## CHAPTER

6.10.7	Effect of Column Shape . . . . .	114
6.10.8	Effects of the Reinforcement Ratio . . . . .	115
7	STRENGTH AND BEHAVIOR OF DYNAMICALLY LOADED SLAB-COLUMN CONNECTIONS . . . . .	117
7.1	DYNAMIC STRENGTH OF MATERIALS . . . . .	117
7.1.1	Steel Tensile Strength . . . . .	117
7.1.2	Concrete Compressive Strength . . . . .	117
7.1.3	Concrete Tensile Strength . . . . .	118
7.2	VERY RAPID LOADING . . . . .	118
7.2.1	Loads Applied . . . . .	118
7.2.2	Behavior . . . . .	122
7.2.3	Analysis . . . . .	124
7.3	RAPID LOADING . . . . .	124
7.3.1	Loads and Accelerations . . . . .	127
7.3.2	Deflections and Velocities . . . . .	129
7.3.3	Crack Patterns and the Failure Surfaces . . . . .	131
7.3.4	Internal Crack Formation . . . . .	132
7.3.5	Concrete Strains . . . . .	135
7.3.6	Steel Strains . . . . .	136
7.3.7	The Effect of Loading Speed on Connection Performance . . . . .	139
7.3.8	Analysis of Strength Increase . . . . .	141
7.4	PERFORMANCE OF SLAB-COLUMN CONNECTIONS IN A BLAST-LOADED STRUCTURE . . . . .	141
7.4.1	Types of Loading . . . . .	142
7.4.2	Useful Dynamic Connection Strengths and Deflections . . . . .	144
7.4.3	Approximate Blast Resistance of Slabs as Limited by the Connections . . . . .	144
8	SUMMARY, CONCLUSIONS, AND RECOMMENDATIONS . . . . .	146
8.1	OBJECTIVES AND SCOPE . . . . .	147
8.2	DESCRIPTION OF THE EXPERIMENTAL PROGRAM . . . . .	147
8.2.1	Test Specimens . . . . .	147
8.2.2	Experimental Procedure . . . . .	148
8.3	BEHAVIOR OF SLAB-COLUMN CONNECTIONS FAILING IN SHEAR . . . . .	148
8.3.1	Idealized Connection Model . . . . .	150
8.3.2	Connections with Rectangular Columns . . . . .	151
8.3.3	Effect of Reinforcement Ratio . . . . .	151
8.3.4	Effect of Column Size . . . . .	151
8.4	STRENGTH OF THE TEST SPECIMENS . . . . .	151
8.4.1	Statically Loaded Specimens . . . . .	153
8.4.2	Dynamically Loaded Specimens . . . . .	154
8.5	CONCLUSIONS . . . . .	154
8.5.1	Statically Loaded Specimens . . . . .	154
8.5.2	Mechanism of Shear Failure . . . . .	155



## CHAPTER

8.5.3	Very Rapidly Loaded Specimens. . . . .	156
8.5.4	Rapidly Loaded Specimens . . . . .	156
8.6	RECOMMENDATIONS FOR FUTURE RESEARCH. . . . .	157

LIST OF REFERENCES . . . . .	159
------------------------------	-----

TABLES . . . . .	166
------------------	-----

FIGURES. . . . .	185
------------------	-----

## APPENDIX

A	THE 200-KIP LOADER. . . . .	291
B	DATA FROM THE STATIC TESTS. . . . .	299
C	DATA FROM THE DYNAMIC TESTS . . . . .	331
D	SHEAR STRENGTH ANALYSIS OF SLABS WITH TWO-WAY REINFORCEMENT BY THE METHODS OF KINNUNEN-NYLANDER AND KINNUNEN. . . . .	377

LIST OF TABLES

TABLE	Page
3.1	EXPERIMENTAL PROGRAM. . . . . 166
4.1	PROPORTIONS OF CONCRETE MIXTURES. . . . . 167
4.2	MILL-DETERMINED PROPERTIES OF NO. 5 REINFORCEMENT . . . . . 168
4.3	WES-DETERMINED PROPERTIES OF NO. 5 REINFORCEMENT. . . . . 169
4.4	CONCRETE CYLINDER TEST RESULTS. . . . . 170
5.1	SUMMARY OF TEST RESULTS . . . . . 171
6.1	OBSERVED RELATIVE DUCTILITIES OF STATICALLY TESTED SPECIMENS. . 172
6.2	COMPARISON OF CALCULATED FLEXURAL CAPACITIES AND TEST RESULTS . 173
6.3	COMPARISON OF CALCULATED SHEAR STRENGTHS AND TEST RESULTS . . . 174
6.4	STRENGTHS AND SLAB ROTATIONS PREDICTED BY METHODS OF KINNUNEN-NYLANDER AND KINNUNEN. . . . . 175
6.5	ULTIMATE UNIT SHEAR STRESS OF STATICALLY LOADED SPECIMENS . . . 176
7.1	STRAIN-RATE EFFECT ON LOWER YIELD STRESS OF STEEL IN TENSION. . 177
7.2	STRAIN-RATE EFFECT ON CONCRETE STRENGTH . . . . . 178
7.3	SHEAR FORCE TRANSFERRED BY THE VERY RAPIDLY LOADED SPECIMENS. . 179
7.4	LOADS AND DEFLECTIONS OF THE RAPIDLY LOADED SPECIMENS . . . . . 180
7.5	COMPARISON OF STATIC AND DYNAMIC CONNECTION STRENGTHS . . . . . 181
7.6	CALCULATED CONNECTION-STRENGTH INCREASE DUE TO RAPID LOADING. . 182
7.7	EFFECT OF RAPID LOADING ON FAILURE DEFLECTION . . . . . 183
7.8	EQUIVALENT UNIFORM PRESSURE CAPACITIES OF PROTOTYPE SLAB SYSTEM. . . . . 184

LIST OF FIGURES

Figure		Page
1.1	Concrete floor systems without beams . . . . .	185
2.1	Stages of flexural behavior from Hognestad (1953). . . . .	186
2.2	Idealized connection model from Kinnunen and Nylander (1960) .	187
2.3	Shear reinforcement for slab-column connections. . . . .	188
2.4	Observed strengths of column footings failing in shear . . . .	189
2.5	Observed strengths of connections of normal weight concrete failing in shear . . . . .	190
2.6	Observed strengths of lightweight concrete and/or prestressed connections failing in shear . . . . .	191
2.7	Comparison of strengths predicted by various methods . . . . .	192
3.1	Slab-column connection specimen. . . . .	193
3.2	Slab reinforcement for 2075 Series specimens . . . . .	194
3.3	Slab reinforcement for 2150 Series specimens . . . . .	194
3.4	Slab reinforcement for 4075 Series specimens . . . . .	195
3.5	Slab reinforcement for 4150 Series specimens. . . . .	195
3.6	Plan view of slab system showing location of contraflexure lines. . . . .	196
3.7	Loading of the connection model. . . . .	197
3.8	Column load and moment from a quasi-static traveling wave. . .	198
3.9	Early response of an elastoplastic system loaded with a linearly decaying load . . . . .	199
4.1	Specimen form with reinforcement in place. . . . .	200
4.2	Typical static stress-strain curve for flexural reinforcement.	201
4.3	Typical static stress-strain curves for concrete control cylinders. . . . .	201

Figure		Page
4.4	Reaction structure and loading device. . . . .	202
4.5	Section through reaction structure . . . . .	203
4.6	Detail of slab support . . . . .	203
4.7	Slab supports. . . . .	204
4.8	Detail of column area. . . . .	204
4.9	Testing arrangement . . . . .	205
4.10	Completed testing arrangement prior to test. . . . .	205
4.11	Location of deflection and acceleration transducers. . . . .	206
4.12	Deflection and acceleration transducers and mounts . . . . .	207
4.13	Crack detection assembly . . . . .	207
4.14	Strain gage layout for S2000 Series. . . . .	208
4.15	Strain gage layout for Specimens D2075-1, D2075-2, and D2150-1. . . . .	209
4.16	Strain gage layout for Specimens D2075-3, D2150-2, and D2150-3. . . . .	210
4.17	Strain gage layout for S4000 and D4000 Series. . . . .	211
4.18	Diagram of instrumentation system. . . . .	212
5.1	Deflections before and after failure . . . . .	213
5.2	Load-deflection curves for the statically tested connections .	214
5.3	Posttest photographs of Specimen S2075-1 . . . . .	215
5.4	Posttest photographs of Specimen S2075-2 . . . . .	216
5.5	Posttest photographs of Specimen S2150-1 . . . . .	217
5.6	Posttest photographs of Specimen S2150-2 . . . . .	218
5.7	Posttest photographs of Specimen S4075-1 . . . . .	219
5.8	Posttest photographs of Specimen S4075-2 . . . . .	220

Figure	Page
5.9	Posttest photographs of Specimen S4150-1 . . . . . 221
5.10	Posttest photographs of Specimen S4150-2 . . . . . 222
5.11	Load-time curves for very rapidly loaded specimens . . . . . 223
5.12	Load-time curves for rapidly loaded specimens with 10-inch columns. . . . . 224
5.13	Load-time curves for rapidly loaded specimens with 20-inch columns. . . . . 225
5.14	Crack patterns of very rapidly loaded specimens. . . . . 226
5.15	Column side of Specimen D2075-2. . . . . 227
5.16	Posttest photographs of Specimen D2075-3 . . . . . 228
5.17	Posttest photographs of Specimen D2150-1 . . . . . 229
5.18	Posttest photographs of Specimen D2150-2 . . . . . 230
5.19	Posttest photographs of Specimen D2150-3 . . . . . 231
5.20	Posttest photographs of Specimen D4075-1 . . . . . 232
5.21	Posttest photographs of Specimen D4075-2 . . . . . 234
5.22	Posttest photographs of Specimen D4075-3 . . . . . 236
5.23	Posttest photographs of Specimen D4150-1 . . . . . 238
5.24	Posttest photographs of Specimen D4150-2 . . . . . 239
6.1	Events and stages of the load-deflection curve . . . . . 241
6.2	Idealized load-deflection curves . . . . . 242
6.3	Comparison of quarterspan and corner deflections with column deflections . . . . . 243
6.4	Sequence of cracking as determined by crack pattern. . . . . 244
6.5	Section through failure cone . . . . . 244
6.6	Slab thickness change versus column deflection, S4000 Series . 245
6.7	Deflection and load traces immediately before failure. . . . . 246



Figure		Page
6.8	Maximum concrete strains, S2000 Series . . . . .	247
6.9	Variation of concrete strains with column deflection, S2000 Series . . . . .	248
6.10	Distribution of concrete strains along slab centerline, S4000 Series . . . . .	249
6.11	Variation of concrete strains with column deflection, S4000 Series . . . . .	250
6.12	Concrete strains at column face, S4075 Specimens . . . . .	251
6.13	Distribution of steel strains along slab centerline, S4000 Series . . . . .	252
6.14	Variation of steel strain with column deflection, S4000 Series . . . . .	253
6.15	Concrete strains versus steel strains, Specimen S4075-1. . . . .	254
6.16	Concrete strain versus steel strain, Specimen S4150-2. . . . .	255
6.17	Predicted yield-line pattern . . . . .	256
6.18	Comparison of actual and predicted yield-line patterns . . . . .	257
6.19	Comparison of ACI Code equation with static test results . . . . .	258
6.20	Comparison of calculated connection stiffnesses with the test results . . . . .	259
6.21	Yield-line pattern for a circular slab loaded on a circular column . . . . .	260
6.22	Free-body diagrams . . . . .	261
6.23	Elastic moments in a circular slab with a fixed center column . . . . .	262
6.24	Elastic moments for a circular slab loaded along a centrally located hole . . . . .	263
6.25	Elastic moments in a circular slab loaded along a circular ring . . . . .	264
6.26	Determination of load and radial moments for a circular slab at yield-line completion . . . . .	265

Figure	Page
6.27	Moments in a circular slab at yield-line completion. . . . . 266
6.28	Moments and shears at yield-line completion for two column sizes. . . . . 266
6.29	Decrease in radial moments with yield-line formation . . . . . 267
6.30	Column deflection and moments 5 inches from the column face. . 268
6.31	Finite-element representation of axially symmetric connection. 269
6.32	Stresses in an uncracked slab-column connection. . . . . 270
6.33	Stresses in a slab-column connection with an inclined crack. . 271
6.34	Uniaxially loaded slab with reinforcement 45 degrees from applied moment . . . . . 272
6.35	Effect of moment ratio on stresses in the direction of smaller principal moment, reinforcement 45 degrees from principal moment . . . . . 273
7.1	Load and deflection traces, Specimens D2075-1 and D2075-2. . . 274
7.2	Determination of dynamic load characteristics. . . . . 275
7.3	Comparison of quarterspan and corner deflections with column deflections. . . . . 276
7.4	Acceleration-, velocity-, and displacement-time curves, Specimen D2075-3 . . . . . 277
7.5	Acceleration-, velocity-, and displacement-time curves, Specimen D2150-1 . . . . . 278
7.6	Acceleration-, velocity-, and displacement-time curves, Specimen D2150-2 . . . . . 279
7.7	Acceleration-, velocity-, and displacement-time curves, Specimen D2150-3 . . . . . 280
7.8	Concrete strain distribution and strain rates. . . . . 281
7.9	Steel strain distribution and strain rates . . . . . 282
7.10	Comparison of static and dynamic connection strengths. . . . . 283
7.11	Typical applied load-deflection curves, D2000 Series . . . . . 284

Figure		Page
7.12	Typical applied load-deflection curves, D4000 Series . . . . .	285
7.13	Connections in a building. . . . .	286
7.14	Usefulness of postfailure resistance . . . . .	287
7.15	Reinforcement in flat plates and flat slabs near columns . . .	288
8.1	Idealized connection model . . . . .	289
8.2	Comparison of observed and calculated strengths, static tests. . . . .	290
A.1	Cutaway view of the 200-Kip Loader . . . . .	297
A.2	Potential and actual applied load-stroke curves. . . . .	298
B.1	Deflections and concrete strains, Specimen S2075-1 . . . . .	300
B.2	Steel strains, Specimen S2075-1. . . . .	301
B.3	Deflections and concrete strains, Specimen S2075-2 . . . . .	302
B.4	Steel strains, Specimen S2075-2. . . . .	303
B.5	Deflections and concrete strains, Specimen S2150-1 . . . . .	304
B.6	Steel strains, Specimen S2150-1. . . . .	305
B.7	Deflections and concrete strains, Specimen S2150-2 . . . . .	306
B.8	Steel strains, Specimen S2150-2. . . . .	307
B.9	Deflections and concrete strains, Specimen S4075-1 . . . . .	308
B.10	Concrete and steel strains, Specimen S4075-1 . . . . .	309
B.11	Deflections and concrete strains, Specimen S4075-2 . . . . .	310
B.12	Concrete and steel strains, Specimen S4075-2 . . . . .	311
B.13	Deflections, Specimen S4150-1. . . . .	312
B.14	Concrete strains, Specimen S4150-1 . . . . .	313
B.15	Deflections and concrete strains, Specimen S5140-2 . . . . .	314
B.16	Concrete and steel strains, Specimen S4150-2 . . . . .	315

Figure	Page
B.17 Tracing from Recorder 1, Specimen S4075-1. . . . .	316
B.18 Tracing from Recorder 2, Specimen S4075-1. . . . .	317
B.19 Tracing from Recorder 3, Specimen S4075-1. . . . .	318
B.20 Tracing from Recorder 1, Specimen S4075-2. . . . .	319
B.21 Tracing from Recorder 2, Specimen S4075-2. . . . .	320
B.22 Tracing from Recorder 3, Specimen S4075-2. . . . .	321
B.23 Tracing from Recorder 2, Specimen S4150-1. . . . .	322
B.24 Tracing from Recorder 3, Specimen S4150-1. . . . .	323
B.25 Tracing from Recorder 1, Specimen S4150-2. . . . .	324
B.26 Tracing from Recorder 2, Specimen S4150-2. . . . .	325
B.27 Tracing from Recorder 3, Specimen S4150-2. . . . .	326
B.28 Profiles of slab failure surface, Specimen S4075-1 . . . . .	327
B.29 Profiles of slab failure surface, Specimen S4075-2 . . . . .	328
B.30 Profiles of slab failure surface, Specimen S4150-1 . . . . .	329
B.31 Profiles of slab failure surface, Specimen S4150-2 . . . . .	330
C.1 Tracing from Recorder 1, Specimen D2075-1. . . . .	332
C.2 Tracing from Recorder 1, condensed records, Specimen D2075-1 .	333
C.3 Tracing from Recorder 2, Specimen D2075-1. . . . .	334
C.4 Tracing from Oscillograph 1, Specimen D2075-1. . . . .	335
C.5 Tracing from Recorder 1, Specimen D2075-2. . . . .	336
C.6 Tracing from Recorder 1, condensed records, Specimen D2075-2 .	337
C.7 Tracing from Recorder 2, Specimen D2075-2. . . . .	338
C.8 Tracing from Oscillograph 1, Specimen D2075-2. . . . .	339
C.9 Tracing from Recorder 1, Specimen D2075-3. . . . .	340

Figure		Page <sup>1</sup>
C.10	Tracing from Recorder 3, Specimen D2075-3. . . . .	341
C.11	Tracing of load, acceleration, and deflection records, Specimen D2150-1 . . . . .	342
C.12	Tracing of concrete and steel strain records, Specimen D2150-1 . . . . .	343
C.13	Tracing of steel strain records, Specimen D2150-1 . . . . .	344
C.14	Tracing of load and steel strain records, Specimen D2150-2 . . . . .	345
C.15	Tracing of acceleration records, Specimen D2150-2 . . . . .	346
C.16	Tracing of deflection, concrete strain, and steel strain records, Specimen D2150-2 . . . . .	347
C.17	Tracing of concrete strain records, Specimen D2150-2 . . . . .	348
C.18	Tracing of load, acceleration, and steel strain records, Specimen D2150-3 . . . . .	349
C.19	Tracing of acceleration and steel strain records, Specimen D2150-3 . . . . .	350
C.20	Tracing of concrete strain records, Specimen D2150-3 . . . . .	351
C.21	Tracing of load, acceleration, and steel strain records, Specimen D4075-1 . . . . .	352
C.22	Tracing of concrete and steel strain records, Specimen D4075-1 . . . . .	353
C.23	Tracing of concrete strain records, Specimen D4075-1 . . . . .	354
C.24	Tracing of deflection records, Specimen D4075-1 . . . . .	355
C.25	Tracing of load, acceleration, and steel strain records, Specimen D4075-2 . . . . .	356
C.26	Tracing of deflection records, Specimen D4075-2 . . . . .	357
C.27	Tracing of concrete strain records, Specimen D4075-2 . . . . .	358
C.28	Tracing of load, acceleration, and steel strain records, Specimen D4075-3 . . . . .	359
C.29	Tracing of deflection records, Specimen D4075-3 . . . . .	360



Figure	Page
C.30	Tracing of concrete strain records, Specimen D4075-3 . . . . . 361
C.31	Tracing of load, acceleration, and steel strain records, Specimen D4150-1 . . . . . 362
C.32	Tracing of deflection, load, and concrete strain records, Specimen D4150-1 . . . . . 363
C.33	Tracing of concrete strain records, Specimen D4150-1 . . . . . 364
C.34	Tracing of load, acceleration, and deflection records, Specimen D4150-2 . . . . . 365
C.35	Tracing of deflection, steel strain, and concrete strain records, Specimen D4150-2 . . . . . 366
C.36	Tracing of concrete strain and steel strain records, Specimen D4150-2 . . . . . 367
C.37	Profiles of slab failure surface, Specimen D2075-3 . . . . . 368
C.38	Profiles of slab failure surface, Specimen D2150-1 . . . . . 369
C.39	Profiles of slab failure surface, Specimen D2150-2 . . . . . 370
C.40	Profiles of slab failure surface, Specimen D2150-3 . . . . . 371
C.41	Profiles of slab failure surface, Specimen D4075-1 . . . . . 372
C.42	Profiles of slab failure surface, Specimen D4075-2 . . . . . 373
C.43	Profiles of slab failure surface, Specimen D4075-3 . . . . . 374
C.44	Profiles of slab failure surface, Specimen D4150-1 . . . . . 375
C.45	Profiles of slab failure surface, Specimen D4150-2 . . . . . 376
D.1	Solution of $f(\alpha)$ , from Kinnunen-Nylander (1960) . . . . . 385
D.2	Solution of $f(\alpha)$ , $\gamma = 0.35$ , from Kinnunen (1963) . . . . . 386
D.3	Solution of $\eta$ , from Kinnunen (1963) . . . . . 387
D.4	Solution of $\lambda$ , $\gamma = 0.35$ , from Kinnunen (1963) . . . . . 388

## NOTATION

- $a$  = radius of a circular slab simply supported at the perimeter;  
span length of a slab in the  $x$  direction; side dimension of a square slab
- $A_s$  = area of tensile reinforcement
- $b$  = perimeter of the loaded area (column); column radius of an axisymmetric slab; span length of a slab in the  $y$  direction; width of a beam
- $b_o$  = perimeter of the section located  $d/2$  from the loaded area (column)
- $b_1$  = perimeter of the section located  $d$  from the loaded area (column)
- $B$  = diameter of a round column
- $c$  = diameter of a circular slab simply supported at the perimeter
- $c_o$  = radius to the shear crack at the level of the reinforcement
- $C$  = compressive force of concrete
- $C, C_1, C_2$  = resultant concrete compressive forces
- $d$  = effective depth of a reinforced concrete section, the distance from the compressive face to the centroid of the reinforcement
- $d'$  = effective depth less collar recess, if any
- $d\phi$  = central angle of a slab sector
- $D$  = flexural rigidity of a slab
- $D_g$  = flexural rigidity of an uncracked section
- $e$  = eccentricity of load resultant
- $E$  = modulus of elasticity

- $E_c$  = modulus of elasticity of concrete  
 $E_s$  = modulus of elasticity of steel  
 $f'_c$  = compressive cylinder strength of concrete  
 $f_{ce}$  = average effective concrete prestress  
 $f_s$  = stress in the tensile reinforcement  
 $f_{sp}$  = concrete tensile splitting strength  
 $f_{up}$  = ultimate concrete prestress  
 $f_y$  = yield strength of the reinforcement  
 $f(\alpha)$  = function of the angle from the horizontal to the force  $T$   
 acting on the conical shell, Appendix D  
 $F$  = total dynamic load acting on one slab panel  
 $F_e$  = effective prestressing force per cable  
 $g$  = acceleration of gravity, 32.2 ft/sec<sup>2</sup>  
 $I$  = moment of inertia  
 $I_a$  = average of cracked and uncracked section moment of inertia  
 $I_{cr}$  = moment of inertia of a fully cracked section  
 $I_{gross}$  = moment of inertia of an uncracked section  
 $jd$  = internal moment arm, the distance from the resultant force of  
 the reinforcement to the resultant concrete compressive force  
 $k = KE_c I_a / L^4$  = effective stiffness of a slab  
 $K$  = stiffness, a constant dependent upon the slab support size  
 $K_y$  = constant defined by Equation D.16  
 $l_s$  = distance from the face of the column to the load position  
 $L$  = span length of a slab panel measured from center to center of  
 supports  
 $m$  = unit moment capacity; number of half sine waves in the  $x$  di-  
 rection of a vibrating plate

- $M$  = bending moment in beam
- $M_r$  = radial moment, the moment acting on a section of constant radius
- $M_t$  = tangential moment, the moment acting along a radial line
- $M_u$  = average ultimate resisting moment of the slab per unit width within the "pyramid of rupture," an area  $(r+2d)$  square under a square column
- $M_x$  = moment acting on the x face
- $M_y$  = moment acting on the y face
- $M_l$  = radial moment at the column face
- $n$  = number of half sine waves in the y direction of a vibrating plate; number of sectors in the yield-line pattern for a circular slab
- $p$  = flexural reinforcement ratio
- $P$  = applied load on the column; maximum dynamic force
- $P_m$  = maximum applied column load
- $P_{yl}$  = flexural strength by yield-line theory
- $P_1, P_2$  = calculated column load capacities in Appendix D
- $q = pf_y/f'_c$  = reinforcement index
- $Q_e$  = resistance at yielding of an elasto-plastic system
- $r$  = side dimension of a square column, one-fourth of the column perimeter; radius; column diameter
- $r_y$  = radius to which yielding in the slab extends
- $R$  = resistance mobilized in one slab panel
- $R_1, R_2, R_3, R_4$  = force resultants
- $s$  = spacing of reinforcement bars

- $S$  = spacing of prestressing cables
- $t$  = time; total slab thickness
- $t_d$  = duration time of a positive pressure loading
- $t_{50}$  = duration of a linearly decaying pressure curve passing through an overpressure-time curve at 50 and 100 percent of the peak pressure
- $T$  = natural period of vibration; tensile force of the reinforcement; inclined compressive force acting on the conical shell of a connection model
- $T_1, T_2$  = resultant reinforcement tensile forces
- $v$  = unit shear stress
- $v_b$  = unit shear stress at the column face
- $v_r$  = unit shear stress at a radius  $r$
- $v_u$  = ultimate unit shear stress
- $V$  = total shear transferred from the slab to the column; total shear on a beam section
- $V_c$  = column load
- $V_{calc}$  = calculated shear strength
- $V_e$  = shear capacity of an eccentrically loaded connection
- $V_{flex}$  = shear load equal to the flexural strength as given by the yield-line analysis
- $V_o$  = shear capacity of a concentrically loaded connection
- $V_{test}$  = observed shear strength
- $V_u$  = ultimate shear strength
- $w$  = uniform load; weight of a unit slab area
- $w(x,y)$  = deflection out of the plane of a slab at point  $(x,y)$
- $W$  = maximum slab deflection



$x$  = coordinate; displacement  
 $\dot{x}$  = velocity  
 $\ddot{x}$  = acceleration  
 $X_e$  = yield deflection of an elasto-plastic system  
 $y$  = coordinate; deflection of the column face before punching shear failure relative to the supports; depth of the compressive zone remaining above the inclined crack of a slab  
 $y_c$  = deflection of the column to the slab supports after punching shear failure  
 $y_s$  = deflection of the slab adjacent to the column to the slab supports after punching shear failure  
 $z$  = internal lever arm of a reinforced concrete section  
 $\alpha$  = ratio of smaller to larger principal moment; angle from the horizontal to the force  $T$  acting on the conical shell of a connection model  
 $\beta$  = angle between the reinforcement and the principal moment direction  
 $\gamma$  = proportion of total load supported by reinforcement doweling and the vertical component of the steel force  
 $\Delta$  = increment of load or moment  
 $\epsilon$  = strain  
 $\dot{\epsilon}$  = strain rate  
 $\eta$  = coefficient of reduction of the reinforcement force because of a two-way reinforcement pattern  
 $\eta'$  = value of  $\eta$  used for design  
 $\theta$  = slope of the inclined crack; angle; change in reinforcement orientation

$\lambda$  = distance from the slab compressive surface to the resultant concrete compressive force divided by the depth of the compressive zone above the inclined cracks of a slab

$\mu$  = mass per unit area of a slab

$\nu$  = Poisson's ratio

$\sigma_t$  = stress in the conical shell at failure

$\phi$  = capacity reduction factor

$\phi_o$  = ratio of ultimate shear capacity to the flexural capacity of a slab given by yield-line analysis

$\psi$  = rotation of the slab sectors at failure

$\psi_{\text{calc}}$  = calculated rotation of slab sectors at failure

$\psi_{\text{test}}$  = observed rotation of slab sectors at failure

$\omega$  = natural circular frequency

CONVERSION FACTORS, BRITISH TO METRIC UNITS OF MEASUREMENT

British units of measurement used herein may be converted to metric units as follows.

Multiply	By	To Obtain
feet	0.3048	meters
inches	25.4	millimeters
square inches	645.16	square millimeters
cubic feet	0.02831685	cubic meters
megatons	0.9071847	gigagrams
pounds	0.4535924	kilograms
kip	4.448222	kilonewtons
kip per inch	0.1751268	meganewtons per meter
pounds per inch	0.1751268	kilonewtons per meter
pounds per square foot	47.88026	newtons per square meter
pounds per square inch	6.894757	kilonewtons per square meter
kip per square inch	6.894757	meganewtons per square meter
inch-pounds	0.1129848	meter-newtons
inch-pounds per inch	0.4535924	meter-newtons per meter

## SUMMARY

The primary objectives of this investigation were to study the strength and behavior of slowly (statically) loaded reinforced concrete slab-column connections and to determine the effect of rapid (dynamic) loading on the strength and behavior by comparison with the static test results.

Tests of 19 full-scale models of a connection and adjoining slab area are presented. The specimens consisted of a simply supported slab either 84 or 94 inches square and 6-1/2 inches thick loaded concentrically on a 10- or 20-inch-square stub column at the center of the slab. The main variables were the amounts of reinforcement in the slab ( $p = 0.75$  and 1.50 percent), the column size, and the loading speed. Eight specimens were loaded to failure statically, two were subjected to a very rapidly applied load of short duration, and nine were loaded to failure by a rapidly applied load with a rise time of 9 to 32 msec, a rate chosen to represent the conditions at the connections in a blast-loaded structure.

The behavior of the statically and dynamically loaded specimens was very similar. Failure deflections increased 25 to 50 percent at the rapid loading rate chosen. The strength of specimens failing in shear after flexural yielding was reached ( $p = 0.0075$ ) increased 18 percent with rapid loading. The strength of the more heavily reinforced specimens ( $p = 0.0150$ ) increased 26 percent. These increases could be adequately explained by the effects of the high strain rates on material strengths.

The static test results are compared with 12 shear strength prediction methods. All methods, including those of ACI Code 318-63, became less

conservative with the larger column size. The strengths of the specimens with  $p = 0.0075$  were best predicted by a yield-line formula for flexural strength.

The failure of connections with square columns was shown to start at the column corners and progress toward the column centerlines.

Differences between the mechanism of shear failure in slabs and beams are examined. The shear-compression failure mechanism is shown to be not strictly applicable for slabs failing in shear. The consistent drop in radial concrete strains measured on the compression side of the test specimen is explained by a reversal in radial moments as the flexural strength is approached and by the effects of the orthogonal reinforcement pattern. The effects of several variables on the shear strength and the moment distribution in the slab throughout the loading history are discussed.

## CHAPTER 1

### INTRODUCTION

#### 1.1 THE PROBLEM

The behavior of reinforced concrete slab-column connections is not yet well defined or understood, even when these connections are loaded slowly. The strength and behavior of these connections resulting with dynamic loading rates is needed to adequately define the blast resistance of structures containing them. This investigation has sought to provide some insight into the complex response of these connections when subjected to either static or dynamic loads.

The response of these connections to loading is important because the strength and ductility of many reinforced concrete flat-plate and flat-slab floor systems will be governed not by their flexural behavior but by the strength and rotational capacity of the slab-column connections. These floor systems are currently widely used and apparently will remain so.

The flat-slab system originated in the early 1900's (Sozen and Siess, 1963).<sup>\*</sup> This system includes a thickened slab area in the column vicinity and extending below the rest of the slab, the drop panel, and an enlargement at the top of the column, the column capital. Builders and architects have found that a cheaper and more visually appealing slab often can be constructed by making the entire column the size of the needed capital and by using the necessary drop panel depth throughout the entire slab. Indeed, for many buildings with small floor loads, the column size is already

---

<sup>\*</sup> References are arranged in alphabetical order in the List of References. The number in parentheses refers to the year of publication.

sufficient and the minimum slab thickness provisions control the slab depth. Thus, the flat-plate system evolved from its parent, the flat slab. Both systems are shown in Figure 1.1. The clean architectural lines, the minimum floor system depth, the minimum obstruction to utility and duct placement, and the simplicity of forming the flat plate have all contributed to its wide usage in newer buildings.

The flat plate and, to a lesser extent, the flat slab have one serious structural weakness. The entire floor load must be transferred to the column over a small area and at the location of maximum flexural bending moments. The connections also commonly transfer bending and twisting moments into the columns, especially at exterior columns or if lateral loads act on the structure.

The structural collapse due to a slab-column connection failure may be catastrophic and involve a large slab area. The lack of strength and rotational capacity in the connection can not only force an undesirable failure mode to occur, but can also preclude the development of otherwise useful slab strength resulting from moment redistribution, membrane action, and strain-hardening of the reinforcement. These effects are mobilized with large slab deflections. The energy absorption capacity of the entire system can be appreciably reduced because of the inclusion of relatively brittle connections.

## 1.2 OBJECTIVE OF THE STUDY

The general objective of this investigation was to study experimentally the strength and behavior of reinforced concrete slab-column connections representative of those used in conventional flat-plate and flat-slab

buildings at both static and dynamic loading rates. Specifically, the objectives were as follows:

1. To study the response of the connections when loaded at either static or dynamic rates.
2. To determine the relationship between static and dynamic strength and behavior.
3. To extend the range of parameters studied experimentally to include specimens typical of a larger proportion of actual structures.
4. To examine the adequacy and limitations of existing strength prediction equations.
5. To study the mechanism of failure in slab-column connections.

### 1.3 SCOPE

Nineteen full-scale models of the area around and including the slab-column connection of a reinforced concrete flat-plate floor system were tested. Eight static and 11 dynamic tests were conducted.

The models consisted of a 6-1/2-inch-thick\* slab either 84 or 94 inches square with a concentric load applied on a 10- or 20-inch-square stub column located at the center of the slabs. The effective slab depth was nominally 5 inches. The edges of the connection slab were simply supported on rollers with the corners free to rise.

Two flexural reinforcement ratios, two column sizes, and static and dynamic loading rates were included. No compression or shear reinforcement was used. The average concrete compressive strength was 4600 psi and the

---

\* A table of factors for converting British units of measurement to metric units is included on page xxiv.



nominal yield stress of the reinforcing steel was 48,000 psi. The rise times for all but two of the dynamic tests ranged from 9 to 32 msec.

#### 1.4 DEFINITIONS

The following definitions will apply throughout this report:

Static denotes occurring over a period of time measured in minutes or hours.

Dynamic indicates taking place in less than many times the natural frequency of the system considered, a period of time usually measured in fractions of a second. Dynamic loading will be used to describe both impact and very rapid loading, where inertial forces are very important, and rapid loading, a loading applied in a time near to or several times the natural period and resulting in much smaller inertial considerations.

Punching shear failure is a failure of the connection caused by excessive shear forces transverse to the slab. The column and a truncated pyramid or conical portion of the slab above the column, the failure cone, is punched through the slab.

Failure of the slab-column connection occurs when the continuity between the slab and the column is destroyed, the time at which the column moves relative to the compression surface of the slab. Some resistance to load remains after failure because of the tensile membrane action of the reinforcing bars crossing the failure zone until collapse, the point at which all reinforcing bars crossing the column area have fractured or have been torn from the slab.

A shear failure is a punching shear failure occurring before general flexural yielding is developed in the connection specimen.

A flexural-shear failure is a punching shear failure taking place after general flexural yielding.

## CHAPTER 2

### REVIEW OF PREVIOUS RESEARCH

#### 2.1 STATIC TESTS

Numerous studies of the shear strength of slabs have been reported over the last 60 years. Three closely related problems have been studied: (1) the shear strength of column footings, (2) the shear strength of slab-column connections, and (3) the shear strength of bridge decks with arbitrarily placed loads.

In the discussion to follow, past investigations principally concerned with the basic strength and behavior of slabs failing in shear will be reviewed first. Next, studies concerned primarily with special cases, including the strength of prestressed and/or lightweight aggregate concrete slabs, the effects of eccentric loadings, and the effects of shear reinforcement, will be briefly outlined. Tests of slab system models failing in shear will then be discussed and code provisions presented. Finally, findings of these past experiments and the primary factors indicated to affect connection strength will be summarized.

2.1.1 Investigations of the Basic Strength and Behavior of Slab-Column Connections Failing in Shear. An important early investigation is the extensive study of column and wall footings by Talbot (1913). Approximately twenty of the eighty-three 5-foot-square column footings loaded on a bed of springs were judged to have failed as a result of excessive diagonal tension. Many of the other slabs failed first in bond or flexure with a punching shear failure following.

Unit shear stress was computed by:

$$v = \frac{V}{4(r + 2d)jd} \quad (2.1)$$

Where:  $v$  = unit shear stress

$V$  = total shear transferred from the slab to the column

$r$  = side dimension of a square column

$d$  = effective depth of the slab

$jd$  = internal moment arm, the distance from the tensile reinforcement to the resultant concrete compressive force

The total shear transferred  $V$  was calculated as the load acting on the slab outside of an area  $r + 2d$  on a side under the column.

Diagonal tension, not pure shear, was observed to govern the punching shear failure. Equation 2.1 was advanced only to provide an index value to the likelihood of a diagonal tension failure.

Diagonal cracking was thought to occur first at or near the level of the flexural reinforcement. Higher shear strengths were noted with increasing amounts of flexural reinforcement.

Results of eight thick slabs simply supported at the edges and loaded at the center were reported by Graf (1938). Six contained shear reinforcement. Shear strength was found to increase with concrete strength, but at a lower rate than direct proportionality. Some influence of the flexural cracking on the shear strength was suggested.

Another extensive study of reinforced concrete footings was reported by Richart (1948). No design recommendations were made. The 140 column footings were designed to fail by either flexure, bond, or diagonal tension according to the contemporary design practice. Many footings designed to

fail in bond failed initially as a result of excessive diagonal tension. Nominal unit shear stresses at failure varied from 0.05 to 0.09  $f'_c$ , where  $f'_c$  is the concrete compressive strength. Most of the footings showing appreciable distress initially in flexure or bond were destroyed by a punching shear failure.

Richart explicitly noted that the punching shear failure is primarily a diagonal tension failure and warned that the use of nominal shear as a direct measure of diagonal tension resistance may not always be consistent.

The use of a critical section closer than  $d$  from the column face was suggested.

The increase in shear strength with increasing amounts of flexural reinforcement observed in these tests was credited to doweling action of the reinforcement. It was also observed that the shear (diagonal tension) capacity did not increase directly in proportion to the concrete compressive strength as was assumed at that time (1948).

Richart's test results were reevaluated by Hognestad (1953). The influence of the flexural strength on the ultimate shear strength was explicitly included in the following empirical equation:

$$v_u = \frac{V_u}{7bd/8} = \left( 0.035 + \frac{0.07}{\phi_o} \right) f'_c + 130 \text{ psi} \quad (2.2)$$

Where:  $v_u$  = ultimate unit shear strength

$V_u$  = ultimate shear strength

$b$  = perimeter of the loaded area (column)

$\phi_o$  = ratio of the ultimate shearing capacity of the slab to the ultimate flexural capacity calculated by the yield-line theory

The shearing stresses were calculated at the column face since this yielded the most consistent results and was thought to be indicative of the final failure, which was believed to be a shearing off of the compression zone above the diagonal tension crack and around the loaded area.

Four stages of flexural action were recognized as shown in Figure 2.1. The effect of flexure in determining the shear strength was expected to be different in these various stages. Failures occurring in the plastic-flexural stage, Stage IV, were considered to be primarily flexural failures and were not included in obtaining Equation 2.2.

Tests of thirty-nine 6-foot-square slabs, of which thirty-four failed in shear, were reported by Elstner and Hognestad (1956). Most slabs were simply supported along all four edges and loaded on stub columns located at the center. In order to model the connections in flat-slab and flat-plate systems instead of a column footing, an edge loading condition and a slender slab geometry than those used by Richart (1948) and by Talbot (1913) were chosen.

Major variables included concrete strength, amounts of tensile and compressive reinforcement, column size, support and loading conditions, distribution of tensile steel, and shear reinforcement.

The following equation was obtained from the test results:

$$v_u = \frac{V_u}{7(4rd)/8} = \frac{V_u}{7bd/8} = 333 \text{ psi} + \frac{0.046f'_c}{\phi_o} \quad (2.3)$$

Again, slabs reaching the plastic-flexural stage were considered to have failed in flexure, not in shear.

Concentration of the reinforcement over the column increased the slab stiffness slightly, but did not increase the shear strength. Compressive

reinforcement also did not appreciably change the shear strength. The shear reinforcement used was not fully effective, mainly because of the difficulty of providing adequate anchorage for the bars used as shear reinforcement.

Whitney (1957) reevaluated the test results of Richart (1948) and of Elstner-Hognestad (1956) and proposed the following ultimate shearing strength formula which differed radically from those previously proposed:

$$v_u = \frac{V_u}{4d(r + d)} = 100 \text{ psi} + \frac{0.75M_u}{d^2} \sqrt{d/l_s} \quad (2.4)$$

Where:  $M_u$  = average ultimate resisting moment per unit width of the slab within the base of the pyramid of rupture, an area  $(r + 2d)$  square

$l_s$  = distance from the face of the column to the load position

A number of slabs with large reinforcing ratios were judged to have failed in bond and were not considered in obtaining Equation 2.4.

This equation introduces the shear span  $l_s$  and an intermediate critical section  $d/2$  away from the column face. The  $j$  term is dropped. Unlike previous equations, Equation 2.4 states that the shear strength is primarily a function of the moment capacity near the column; the only influence of concrete strength is its effect on  $M_u$ . The moment capacity of the rest of the slab does not enter in Whitney's expression.

An extensive test series using forty-three 6-foot-square slab-column connections was reported by Moe (1961). Principal variables included the effects of holes near the column, concentration of flexural reinforcement

over the column, column size and shape, eccentricity of the load, and selected types of shear reinforcement.

The strengths of the slabs tested by Richart (1948) and by Elstner-Hognestad (1956) as well as several included in Moe's tests were statistically studied with the following expression resulting:

$$v_u = \frac{V_u}{4rd} = \left[ 15 \left( 1 - \frac{0.075r}{d} \right) - 5.25\phi_o \right] \sqrt{f'_c} \quad (2.5)$$

This may be rewritten in a more convenient form by eliminating  $\phi_o$ :

$$v_u = \frac{V_u}{4rd} = \frac{15 \left( 1 - \frac{0.075r}{d} \right) \sqrt{f'_c}}{1 + \frac{5.25bd \sqrt{f'_c}}{V_{flex}}} \quad (2.5a)$$

Where:  $V_{flex}$  = shear load causing flexural failure as predicted by the yield-line theory

$$b = 4r$$

Among the conclusions of this study were: (1) the influence of the concrete compressive strength can be expressed by  $\sqrt{f'_c}$ , (2) the critical section governing shear strength is at the column face, (3) concentration of flexural reinforcement over the column does not increase shear strength, (4) adequate anchorage of shear reinforcement is problematical in thin slabs, (5) the effect of holes near the column may be accounted for by using a net critical section perimeter, and (6) approximately one-third of any unbalanced moment transferred by an interior column connection is transferred by nonuniformly distributed shear forces with unbalanced slab moments and torsional moments transferring the remainder.



Diagonal cracks were visually observed to form at about 60 percent of the ultimate load in some of the connections with large holes in the slab near the column.

Moe notes that Equation 2.5 was derived from tests using an  $r/d$  ratio of 3.1 and less, and should not and cannot be used with larger  $r/d$  ratios. A shear capacity of zero is predicted by this equation if  $r/d = 8.67$  and  $\phi_o = 1.0$ .

The following equations were suggested by Moe for design use:

$$v = \frac{V}{bd} = \left( 9.23 - \frac{1.12r}{d} \right) \sqrt{f'_c} \quad \text{if } r/d \leq 3 \quad (2.6a)$$

$$v = \frac{V}{bd} = \left( 2.5 + \frac{10d}{r} \right) \sqrt{f'_c} \quad \text{if } r/d > 3 \quad (2.6b)$$

Where  $b = 4r$ .

Kinnunen and Nylander (1960) reported a theoretical and experimental program including the testing of 61 circular slab-column connections loaded on the perimeter and supported on a centrally located column. Eighteen of the connections contained a preformed conical-shaped diagonal crack placed at 45 degrees and extending about three-fourths through the slab. Ring, radial, and two-way orthogonal reinforcement patterns were used.

The first inclined cracking was reported to have occurred at 45 to 75 percent of the ultimate load.

The specimens containing the preformed crack behaved somewhat similarly to the corresponding initially uncracked slabs. The strength and deflections at failure were decreased, however, to an average of 68 and 51 percent, respectively, of comparable initially uncracked connections. More

decreases in both strength and deflection resulted with ring reinforcement than with two-way reinforcement.

An idealized mechanical model of the slab with the inclined crack was developed (Figure 2.2). It was used in deriving equations predicting shear strength and deflection at failure.

The slab sector outside the shear crack and bounded by radial cracks was assumed to rotate as a rigid body about the root of the shear crack and to be supported on a conical shell. Forces acting on the slab sector were then derived and are, except for the applied load and reaction, proportional to the slab rotation. The shear capacity is evaluated from the equilibrium conditions at failure. Failure is considered to have occurred when the concrete on the compression side of the slab reaches a strain at which it can no longer offer increasing confinement for the very highly stressed conical shell. The failure criterion consists of reaching a limiting value for the tangential strain on the concrete surface and under the crack root (point A in Figure 2.2b). The limiting values used are empirical and were selected to give reasonable agreement with the test results of the slabs reinforced with ring reinforcement only.

Several lengthy equations result from the idealized model. These equations, contained in Appendix D, are time consuming to solve even when available graphical aids (Rao, et al., 1968) are used. Iteration is required to evaluate a given design. A correction factor derived from the test results is included to account for the higher strengths and larger deflections observed with two-way reinforced specimens.

The model is acknowledged to be only an idealization. Kinnunen-Nylander state that the actual mechanism of failure in the concrete above

the crack is quite complex and is not necessarily a compressive failure. The compressive stress in the conical shell was considered to constitute only a measure of the risk of failure in the actual case.

Kinnunen (1963) modified the formulas of Kinnunen-Nylander (1960) to account for the doweling forces and the vertical component of the bar forces (membrane forces) that exist with the two-way reinforcement pattern. These two effects are credited with supporting 35 percent of the applied load. The effect of lack of polar symmetry resulting from the use of an orthogonal reinforcement pattern was also examined analytically. The formulas needed to evaluate the shear strength of a connection design by this method are contained in Appendix D.

A report by a joint American Concrete Institute (ACI) and American Society of Civil Engineers (ASCE) committee, ACI-ASCE Committee 326 (now Committee 426), "Shear and Diagonal Tension," was published in 1962 (ACI-ASCE, 1962). Available pertinent research, including several investigations not included in this review, was summarized and a design procedure for shear in slabs developed. This report had great influence on the provisions adopted for the 1963 ACI Standard Building Code (ACI, 1963). Earlier ACI Code requirements for shear in slabs are also reviewed in the Committee 326 report.

The recommendations for slab shear analysis contained in the Committee 326 report drew heavily from the work of Moe (1961). The three principal variables recognized as affecting the shear strength are the concrete strength, the relationship of the size of the loaded area (column size) to the slab thickness, and the relationship between the shear and moment near the loaded area.

Equation 2.5 (Moe) is the starting point for the Committee 326

equation. A value of 1.0 was inserted for  $\phi_o$  because of the desirability of shear strength being equal to or above the flexural capacity in actual construction. The following equation results:

$$v_u = \frac{V_u}{bd} = \left( 9.75 - \frac{1.125r}{d} \right) \sqrt{f'_c} \quad (2.7)$$

This expression yields a shear capacity  $V_u$  of zero for a point load ( $b = 4d$  is zero) and a  $v_u$  of zero or less at large  $r/d$  values, both unacceptable. Equation 2.7 was then replaced by a hyperbolic equation:

$$v_u = \frac{V_u}{bd} = 4 \left( \frac{d}{r} + 1 \right) \sqrt{f'_c} \quad (2.8)$$

This equation gives a finite shear capacity  $V_u$  at all  $r/d$  values, is below nearly all test data available then, and approaches  $v_u = 4\sqrt{f'_c}$  as the  $r/d$  value increases.

This value rather than the much lower nominal shear stress of  $1.9\sqrt{f'_c}$  recommended for beams was chosen on the basis of wide-beam tests reported by Diaz de Cossio (1962). These tests indicated that the unit shear strength of beams increases significantly with an increasing width to depth ratio. A multiplication factor of  $\frac{1.65 b/d}{0.375 + (b/d)}$ , where  $b$  = beam width, was suggested to account for this effect. It is interesting to note that Committee 326 recommends that the shear stress be checked across the width of slabs containing connections with large  $r/d$  ratios assuming the slab to be a wide beam, and that the expression for beam shear includes no influence of beam width.

The final Committee 326 equation was obtained by defining the critical section at a location  $d/2$  away from the column instead of at the face. Equation 2.8 then becomes:

$$v_u = \frac{V_u}{4(r+d)d} = \frac{V_u}{4b_o d} = 4.0 \sqrt{f'_c} \quad (2.9)$$

Where  $b_o$  = perimeter of the critical section .

The Committee 326 report also discusses slabs with openings near the column, moment transfer at the slab-column connections, and shear reinforcement.

Yitzhaki (1966) proposed the following strength prediction equation for relatively thin slabs failing in shear:

$$V_u = 8 \left(1 - \frac{q}{2}\right) d^2 \left(149.3 + 0.164pf_y\right) \left(1 + \frac{0.5r}{d}\right) \quad (2.10)$$

Where:  $q$  = reinforcement index =  $pf_y/f'_c$

$p$  = flexural reinforcement ratio

$f_y$  = yield strength of the reinforcement

Yitzhaki formulated this empirical equation after examining the results of various connection tests including at least 28 carried out under his supervision. Several of the 11 tests reported by Rosenthal (1959) were included.

Equation 2.10 yields a very simple expression for the nominal shear stress at a distance  $d$  from the column face:

$$v_u = \frac{V_u}{\left(1 - \frac{q}{2}\right) d (4r + d)} = 149.3 + 0.164pf_y \quad (2.11)$$

Concrete strength properties do not enter in determining the value of  $v_u$  as defined by Equation 2.11.

The equations of Yitzhaki lend themselves well to graphical presentation and comparison with flexural strength.

An expression for a balanced reinforcement ratio, one producing equal flexural and shear strengths, was derived. Yitzhaki suggested as a design procedure that a sufficient proportion of the flexural reinforcement over the column be bent down and adequately anchored to act as shear reinforcement if shear is critical. His test results appear to support this procedure.

Another method for calculating the shear strength of slabs was presented by Reimann (1963). The method is fundamentally a flexural analysis and draws heavily from the work of Kinnunen-Nylander (1960).

The connection capacity is calculated using an anisotropic and axially symmetric plate analysis. The degree of the anisotropy, which results from the predominantly radial crack pattern, is a function of the ratio of the flexural reinforcement percentage to the balanced reinforcement percentage. The failure load is related to the tangential moment at the column face. No iteration is necessary. The solution for several intermediate steps is presented in charts.

Test results from 16 octagonal-shaped models of the connections in lift slabs were reported by Tasker and Wyatt (1963) along with design recommendations for shear in all flat plates. The lift slab configuration was chosen for testing because it was judged the most critical form of the flat plate for shear.

A variation of Moe's equation (Equation 2.5a) was given as the best fit to their test results:

$$\frac{V_u}{bd\sqrt{f'_c}} = \frac{8.27 \left( 1 + \frac{1.21d}{r} \right)}{1 + \frac{5.25bd\sqrt{f'_c}}{V_{flex}}} \quad (2.12)$$

Where  $b$  = perimeter of the column collar or the base of the outermost cage of adequate shear reinforcement.

A second equation was presented as a reasonable lower bound suitable for design:

$$\frac{V_u}{bd\sqrt{f'_c}} = 2.5 + \frac{10}{(r/d) + 1} \quad (2.13)$$

Where  $b$  = perimeter of effective support.

Concentration of reinforcement over the column area was reported to be beneficial by both increasing strength and reducing deflections at design load levels.

Andersson (1964) reported tests of 12 lift-slab connections, four being posttensioned. The strength and the stiffness of the steel collar were found to influence the strength and behavior of the connection in shear.

Taylor and Hayes (1965) published test results from 22 small (35-inch-square) slabs loaded by small, square, centrally located plates. The effect of edge restraint (fixity) was studied. Restraining the edges of slabs containing reinforcement increased the shear strength by 0 to 60 percent. More increase occurred with lower flexural steel ratios. The restrained slabs containing no reinforcement were stronger than the simply-supported slabs with 1.57 percent flexural reinforcement.

Long and Bond (1967) reported a theoretical analysis of the punching shear problem for round slabs containing two-way flexural reinforcement and no shear reinforcement. Elastic and isotropic plate theory with several approximations was used to compute the stresses in the concrete compression zone at the column face even at failure. The failure load is found using

an octahedral shear stress failure criterion for concrete. Several correction factors are also employed. The results of four small test specimens are included in the report.

2.1.2 Other Investigations of Slab-Column Connections. Many other studies investigating special loadings, shear reinforcement, prestressing, and lightweight materials have added significantly to the knowledge on shear failures in slabs and have explored many configurations used in actual buildings.

Prestressed and/or Lightweight Concrete Connections. The shear strength of lift slabs was investigated by Scordelis, et al. (1958), using 15 specimens of which 12 were prestressed. Variables included concrete strength, size of the steel collar cast with the slab and surrounding the column, slab thickness, amount of prestressing, and amount of collar recess above the bottom of the slab.

The equations of Elstner-Hognestad (Equation 2.3) and Whitney (Equation 2.4) predicted the observed results much better than the then-current 1956 ACI Code (ACI, 1956) which gave a scattering factor of safety. As would be expected, prestressing increased shear strength and decreased the angle of the failure surface.

The following expression was presented as a fit to the experimental results:

$$\frac{V_u}{bdf'_c} = 0.175 - 0.0000242f'_c + 0.000020 \frac{F_e}{S} \quad (2.14)$$

Where:  $b = 4r$

$F_e$  = effective prestress force per cable

$S$  = cable spacing



Results from a series of eleven 3-foot-square prestressed connection models using lightweight aggregate concrete were reported by Grow and Vanderbilt (1966). Only the effective prestress force was varied.

Two equations fitting the data were reported:

$$V_u = (0.360 + 0.30f_{ce})bd' \quad (2.15)$$

$$V_u = (0.190 + 0.53f_{up})bd' \quad (2.16)$$

Where:  $V_u$  = shear capacity, kips

$f_{ce}$  = average effective concrete prestress, ksi

$f_{up}$  = ultimate concrete prestress, ksi

$b$  = perimeter of loaded area

$d'$  = effective slab depth less collar recess, if any

The strength and behavior of nonprestressed connections containing lightweight aggregate concrete have been reported by Hognestad, et al. (1964), by Mowrer and Vanderbilt (1967), and by Ivy, et al. (1969).

Hognestad, et al., reproduced three slab geometries tested by Moe (1961) using two lightweight aggregates for each slab geometry. The project was conducted to facilitate including provisions for lightweight aggregate concrete in the 1963 ACI Code (ACI, 1963).

A modified form of Moe's equations (Equations 2.5 and 2.5a) using the concrete splitting strength  $f_{sp}$  rather than the square root of the compressive strength was suggested:

$$v_u = \frac{V_u}{bd} = \left[ 2.24 \left( 1 - \frac{0.075r}{d} \right) - 0.784\phi_o \right] f_{sp} \quad (2.17)$$

or, eliminating  $\phi_o$  :

$$v_u = \frac{2.24 \left(1 - \frac{0.075r}{d}\right) f_{sp}}{1 + \frac{0.784 b d f_{sp}}{V_{flex}}} \quad (2.17a)$$

These are merely Moe's equations (Equation 2.5 and 2.5a) with  $f_{sp}$  substituted for  $6.7\sqrt{f'_c}$ .

Results from two test series including 51 slabs, 43 using lightweight aggregate concrete, were presented by Mowrer-Vanderbilt. Amount of reinforcement, concrete strength, and hole patterns around the columns were varied in the first series. The main variable in the second series was the ratio of the column side to the slab effective depth, the  $r/d$  ratio. Connection specimens with  $r/d$  ratios of 2 through 8 were tested. The amount of reinforcement and edge fixity were also varied.

An equation similar to Moe's (Equation 2.5a) was found to fit the results of these tests:

$$\frac{v_u}{bd\sqrt{f'_c}} = \frac{9.7 \left(1 + \frac{d}{r}\right)}{1 + \frac{5.25bd\sqrt{f'_c}}{V_{flex}}} \quad (2.18)$$

Where  $b$  = perimeter of the column less holes.

The effect of slab edge fixity could be accounted for by its effect on  $V_{flex}$ , the flexural capacity as calculated by the yield-line method.

Ivy, et al., reported tests of fourteen connection specimens constructed of lightweight aggregate concrete, ten with a size and geometry similar to the slabs tested by Elstner-Hognestad (1956) and four full-size (24-inch-square columns,  $r/d = 4.27$ ) models of the connection area of the

prototype flat-plate structure tested by Hatcher, et al. (1961) (one-quarter scale), and by Guralnick and La Fraugh (1963) (three-quarter scale). Three types of lightweight aggregates were used. Equation 2.17a (Hognestad, et al.) reasonably predicted the experimental strengths.

Eccentrically Loaded Connections. Connections transferring moments as well as shear frequently occur in structures and have received limited attention in the reported research. The addition of moment has been found to reduce the capacity in shear.

A method for analyzing connections transferring moments was presented by Di Stasio and Van Buren (1960). The moment transferred in excess of that which the reinforcement crossing a section  $d$  from the column face could support was assumed to be transferred by nonuniformly distributed vertical shearing stresses at that section. No tests were conducted nor were any test results used to derive or check the equations.

Moe's study (Moe, 1961) included 12 connections tested with eccentric loads. He assumed a constant proportion of one-third of the unbalanced moment of the slab was transferred by vertical shear and gave the following interaction formula:

$$\frac{V_e}{V_o} = \frac{1}{1 - \frac{e}{r}} \quad (2.19)$$

Where:  $V_e$  = shear strength of eccentrically loaded connection

$V_o$  = shear strength of concentrically loaded connection

$e$  = eccentricity of load resultant

Committee 326 (ACI-ASCE, 1962) adopted a method similar to that suggested by Moe; a proportion of the unbalanced moment was assumed to be

resisted by unevenly distributed shear forces.

The Commentary to the 1963 ACI Code (ACI, 1965) includes a slightly modified form of the Di Stasio-Van Buren formula and retains the concept that only the moment which cannot be transferred by the flexural steel need be considered when examining the shear stresses.

Hanson and Hanson (1968) reported the results of a series of 17 slab-column connection tests. Shear only, moment only, and one intermediate loading case were included. One exterior column model was included. Rectangular and square columns, some with holes along two parallel faces, were used. Both Moe's equation (Equation 2.19) and a modified form of the Committee 326 equation were found to give good results.

Tests of three exterior column-slab connections were reported by Andersson (1966). Eccentricity of the column load was shown to have a considerable influence both on the ultimate load and on the primary mode of failure (shear or flexure).

Six full-scale exterior connections were tested by Beresford (1967). The observed failure loads were from 2.00 to 2.21 times the permissible working load calculated with the method of Di Stasio-Van Buren (1960).

Connections with Shear Reinforcement. Because of the inherent weakness of slab-column connections in shear, methods of providing shear reinforcement have received considerable attention. Figure 2.3 shows some of the configurations considered. Elstner-Hognestad (1956) and Yitzhaki (1966) used bent bars. Moe (1961) considered the use of both steel plates and shearheads fabricated from bars (Figures 2.3c and 2.3g).

Test results from 28 slabs containing several types of bar shear reinforcement were published by Andersson (1963). Both two-way and radial

flexural reinforcement patterns were included. The failure cracks in the more heavily shear-reinforced slabs occurred outside of the shear reinforcement; the shear reinforcement acted to enlarge the effective column area. Bent-up radial bars and vertical continuous stirrups (Figure 2.3b and 2.3e) placed around the column were judged the best methods for placing shear reinforcement. Adequate shear reinforcement appreciably increased the deflections at punching shear failure. Shear reinforcement was most beneficial when the concrete strength was low, the flexural reinforcement ratio high, and/or the column size was small.

Another method of increasing the shear strength is to embed structural shapes in the slab and over the column area. This method is also sometimes used with lift slabs.

W. H. Wheeler (1935) patented a shear reinforcing procedure which used two pairs of crossing structural steel shapes in a pattern similar to that shown in Figure 2.3h.

Tests of 21 slabs, most reinforced with structural sections placed as shown in Figure 2.3h or 2.3i, were reported by Corley and Hawkins (1968) with design recommendations. The structural shapes increased the shear strength considerably by increasing the apparent column size. The proposed design procedure presented would allow an increase in shear of up to 75 percent for connections containing structural shapes of sufficient stiffness and length.

2.1.3 Performance of Connections in Slab Systems. The most realistic tests of the slab-column connections have been the relatively few tests of the slab systems containing them.

A series of multiple-panel reinforced concrete floor slab tests was

conducted at the University of Illinois in the late 1950's and early 1960's. One flat-plate and two flat-slab structures were included in the five nine-panel one-quarter-scale slabs of this program. Three one-sixteenth-scale slabs were also constructed and tested.

The test of the flat-plate model was reported by Hatcher, et al., (1961). This slab contained three 5-foot bays in each direction and was a model of a prototype designed in accordance with the 1956 ACI Code (ACI, 1956) for a working live load of 70 psf (total load of 155 psf).

The capacity of the slab was controlled by a punching shear failure at an interior column at a total load of 360 psf applied over the entire slab surface. The measured shear was slightly above that predicted by Moe (Equation 2.5 with  $\phi_o = 1.0$ ) or by Committee 326 (Equation 2.9). A small moment was also being transferred by the connection.

However, the report notes that a higher-than-normal shear strength should be expected because the small-aggregate concrete used in the model had a much higher tensile strength than would typical construction concrete with the same compressive strength. The report also warns that had the structure been loaded with weights a violent failure would have occurred rather than the quite gentle failure observed with the relatively stiff loading system used.

The test of a three-quarter-scale (45-foot-square) model of the flat-plate prototype used by Hatcher, et al. (1961), was reported by Guralnick-La Fraugh (1963). The concrete compressive strength was significantly higher (4715 psi versus 2510 psi) than in the one-quarter-scale model.

The larger model also failed by punching shear at an interior column and at a total load of 369 psf. The unit shear observed is 15 percent

below that given by the equation of Committee 326 (Equation 2.9) and 17 percent below that given by Equation 2.5 (Moe) with  $\phi_o = 1.0$ . Guralnick-La Fraugh classified the failure as a secondary shear failure because extensive yielding had occurred near the column. Median panel deflection at the time of failure was approximately 1.80 inches, 1/100 of the span.

Three 1/28-scale models of this same prototype were tested to failure by Lee (1964). Concrete strengths ranged from 2510 to 2670 psi. All three models failed by punching shear at an interior column and at 102, 103, and 117 percent of the load carried by the quarter-scale model.

Experimental results from three flat-slab systems were reported by Self (1964). The slabs were 10 feet square with four interior supports either 10 or 13 inches in diameter forming a 66-inch-square interior bay. Self calculated shear capacity with the intermediate formula of Committee 326 (Equation 2.8) with a critical perimeter of  $\pi \times (\text{column diameter} + d)$  used for  $b$  rather than  $4r$  to account for the support shape. He reasoned that "inclined cracking" governed the shear strength of round columns rather than "shear compression," the mechanism he expected to govern with square columns. Two of the three slabs failed by punching shear and after extensive steel yielding.

Several multiple-panel flat-plate models have been tested in Australia (Blakey, 1963 and 1967). One reinforced concrete flat-plate model failed by shear at an exterior column after local yielding. The final collapse occurred when all slab-column connections were destroyed and the slab literally dropped to the column footings. The two most critical design problems with flat plates according to Blakey are preventing shear failures at the columns and avoiding troublesome slab deflections.

A large-scale prestressed, lightweight concrete flat plate tested by Gamble (1964) failed in shear at an interior column and at a larger load than predicted by the formulas generally used at that time. The columns were quite small. The failure was described as brittle and occurred at a small slab deflection (0.66-inch maximum deflection, 9- by 12-foot bay size).

As reported by Feld (1964), a building containing flat-plate construction partially collapsed during construction in 1956. Although official reports did not include the cause of failure, the probable cause was excessive shear at the columns. During the casting of the fourth floor slab, a section about 72 by 144 feet collapsed suddenly. All four floors dropped into the basement with most of the columns remaining standing. The third floor was 20 days old and reshored. Some shear reinforcement was provided. Rather large utility ducts were placed along parallel sides of some interior columns and reinforcement continuity was interrupted.

2.1.4 Design Specifications for Static Loadings. The American Concrete Institute Standard 318, "ACI Standard Building Code Requirements for Reinforced Concrete," has served as the design specification for nearly all recently constructed buildings in the United States.

The provisions for shear in slabs and in footings contained in the currently used 1963 ACI Code, ACI 318-63 (ACI, 1963), follow closely the recommendations of the Committee 326 report (ACI-ASCE, 1962).

The allowable unit shear stress  $v_u$  for the ultimate strength design method is given by

$$v_u = \frac{V_u}{b_o d} = 4\phi\sqrt{f'_c} \quad (2.20)$$



Where:  $b_o$  = perimeter of the critical section located  $d/2$  from the concentrated load or reaction area (column)

$\phi$  = capacity reduction factor to account for possible material understrength and equal to 0.85 for diagonal tension (shear)

The shear stress  $v_u$  is limited to  $0.6\phi$  times the splitting strength for lightweight aggregate concrete but not to exceed that given by Equation 2.20.

The allowable unit shear stress may be increased up to 50 percent with shear reinforcement, but only if the slab is at least 10 inches thick. The shear reinforcement is assumed to be one-half as effective as in beams.

The member must also be checked for beam shear across its entire width.

The value of  $b_o$  is reduced if holes in the slab are located within ten slab thicknesses from the column.

The additional shears created by transfer of bending moment at the connection must be considered, although no method for analysis is given in ACI 318-63 itself. A method similar to that proposed by Di Stasio-Van Buren (1960) is suggested in the Commentary for the 1963 ACI Code (ACI, 1965).

Provisions for the working stress design method are identical except the  $\phi$  factor is dropped and the allowable stresses are reduced by one-half.

The 1956 ACI Code (ACI, 1956) provisions for shear are quite typical of those in earlier ACI Codes also. Only the working stress design method is included, and the allowable shear is given as a portion of the compressive strength of the concrete.

Unit shear was calculated at a distance  $d$  from the loaded area:

$$v = \frac{V}{jdb_1} \quad (2.21)$$

Where:  $b_1$  = perimeter of the critical section  $d$  from the loaded area

The following shear stresses were allowed:

$v = 0.025f'_c \leq 85$  psi when 25 percent of the column flexural reinforcement passes through the critical section

$v = 0.030f'_c \leq 100$  psi when more than 50 percent of the column strip flexural reinforcement passes through the critical section

$v = 0.030f'_c \leq 75$  psi for footings

2.1.5 Test Results. The reported test results from concentrically loaded slabs without shear reinforcement and represented to have failed primarily in shear are shown in Figures 2.4 through 2.6. The unit shear at failure acting on the section located at the column face and divided by  $\sqrt{f'_c}$  is plotted against the ratio of the column size (column perimeter divided by 4) to the effective slab depth, the  $r/d$  ratio.

The 1963 ACI Code expression with  $\phi = 1.0$  and modified for a critical section at the column face (Equation 2.8) is also plotted for comparison. It must be remembered, however, that most of the test results should lie above the ACI Code provisions because (1) the ACI Code equation is intended to be a reasonable lower bound, and (2) most specimens tested were designed to fail in shear, a condition discouraged by the ACI Code. Therefore, many test specimens had a flexural strength considerably above the capacity in shear and benefited from the resulting moment-shear interaction. Moe's equation (Equation 2.5) with two values of  $\phi_o$ , the ratio of shear strength to flexural strength, is plotted in Figure 2.5 to illustrate the

possible magnitude of shear strength increase with increased flexural strength.

Many of the equations presented in this chapter are compared in Figure 2.7. A flexural strength equal to the shear strength ( $\phi_o = 1$ ) was assumed in plotting these curves. Several equations have obvious limitations. For example, Equations 2.3 and 2.5 are not applicable for very small or large  $r/d$  ratios. Equations 2.6, 2.13, 2.20, and 2.21 are design equations and are intended to be below a majority of the data.

Other equations for concentrically loaded slabs involve other variables and could not be plotted on the axes chosen. Several of these equations differ considerably from those included in Figure 2.7.

2.1.6 Parameters Affecting Connection Strength. It is instructive to examine the influence assigned to the various parameters by past investigators. This discussion will be limited to concentrically loaded slabs using normal weight concrete.

Concrete Strength. Early reports assumed that the unit shear capacity increased in direct proportion to the concrete compressive strength, although it was recognized that excessive diagonal tension in the concrete precipitated the failure. Richart (1948) noted that shear capacity rose less rapidly than the compressive strength. This was later explicitly stated by Hognestad (1953). Moe (1961) expressed the shear strength as a function of the concrete tensile strength, a quantity assumed to be proportional to the square root of the compressive strength. The current ACI Code (ACI, 1963) follows this reasoning. Concrete strength was ascribed even less influence by Whitney (1957) and Yitzhaki (1966). Both limited the influence of concrete strength to its effect on the flexural capacity,

a minor effect for underreinforced sections.

Connection Size Effect. No size effect per se has been identified, although the increased tensile strength of the small-aggregate concrete often necessary in small-scale specimens may appreciably increase the shear strength for concrete of a given compressive strength.

Flexural Strength of the Slab. Talbot (1913) noted in his early tests that shear capacity increased with increased flexural reinforcement and that low flexural capacities did not necessarily prevent a final failure by shear. Hognestad (1953) introduced the ratio  $\phi_0$  of shear to flexural strength as a parameter influencing shear strength. Flexural strength is the most influential variable in the methods of Yitzhaki (1966) and Whitney (1957).

All investigators have considered specimens reaching general flexural yielding as having performed satisfactorily in shear regardless of the final mode of failure. The strength and ductility of connections failing after general yielding in the column area have received little attention.

Definition of the Critical Section. The location of the critical section is doubly important with slabs because the area available to resist shear as well as the total shear load changes with the assumed critical section location.

The nominal shear stress was calculated at  $d$  away from the loaded area by early investigators and codes. Just as in beams, the shear at this location was assumed to govern diagonal cracking.

Hognestad (1953) calculated unit shear stress at the perimeter of the loaded area because the destruction of the concrete compression zone at that location appeared to control the shear failure. Moe (1961) and most

recently proposed methods also assume that the column outline defines the critical location. A location  $d/2$  from the column face has also been suggested. Moe states that the question of correct critical location has two answers: inclined cracking occurs away from the column face and the final failure takes place near the column periphery.

The calculated nominal shear value has long been recognized as only a convenient and relative measure of the critical stresses. It is indicative of neither the actual distribution nor the absolute magnitude of the stresses. Because the unit shear is only a nominal measure, the depth of the critical section has lately been defined as being simply  $d$  rather than  $jd$ .

When comparing unit shear stresses, care must be taken that the critical sections assumed are the same.

Relative Size of the Column and Slab Depth. The maximum shear stress was not explicitly expressed as a function of the relative size of the column and slab until Moe (1961) did so in Equation 2.5. Moe reasoned that smaller columns resulted in a higher nominal shear stress capacity because of the more beneficial triaxial stress conditions at the critical section, the column outline.

Defining the effect of relative column size and selecting the critical section are interrelated problems. An effect of column size on the shear capacity of connections is inherently included in many equations, probably unknowingly so in at least the early cases, by using a critical section placed at some distance away from the column face. The perimeter of such a location increases at a slower rate with increasing column sizes than does the column perimeter.

Committee 326 (ACI-ASCE, 1962) and the 1963 ACI Code (ACI, 1963) intentionally chose the method of recognizing the effect of relative column size by using a critical section away from the column face since this simplified the shear capacity formulas.

Few test results are available for connections with large column size to slab depth ratios, especially for nonprestressed slabs constructed with normal weight concrete.

Slab Slenderness. The effect of this parameter, corresponding to the shear span, or  $M/Vd$  ratio, in beams, has not been experimentally investigated and is included only in the equation proposed by Whitney (Equation 2.4).

Concentration of Reinforcement Over the Column. Several ACI Building Codes, including the 1956 edition (ACI, 1956), allowed greater shear stresses if the flexural reinforcement was concentrated within the critical section for shear. Whitney's formula (Equation 2.4) agrees with this by considering only the flexural capacity in the column area. Tasker-Wyatt (1963) reported experimental evidence of such a strength increase.

In contrast, Elstner-Hognestad (1956) reported no such strength increase with concentration of reinforcement over the column. Moe (1961) observed a slight decrease in shear strength when the flexural reinforcement was concentrated over the column.

It is agreed that concentration of the bars over the column more closely follows the elastic moments in the slab and increases the slab system stiffness.

Compressive Reinforcement. Elstner-Hognestad (1956) reported no strength increases resulted from the use of compression steel. Gamble

(1964) notes that compression steel may help hold the structure together once punching failure has occurred.

Shear Reinforcement. Both Moe (1961) and Elstner-Hognestad (1956) reported shear reinforcement as not being fully effective, especially in thin slabs, because of problems in adequately anchoring the shear reinforcement. The 1963 ACI Code (ACI, 1963) follows this approach.

An opposite viewpoint is expressed by Yitzhaki (1966) and Andersson (1963). They state that properly designed shear reinforcement is quite effective even in thin slabs.

In contrast to the early viewpoint that shear reinforcement in slabs functions similarly to stirrups in beams, several recent experimenters have stated that effective shear reinforcement should function by increasing the apparent column size, thus forcing the shear crack and failure to occur further from the column.

## 2.2 DYNAMIC TESTS

No dynamic tests of slab-column connections or column footings have been reported. Dynamic tests of columns, slabs, and several other structural members have been conducted, however, and are of interest as these test results suggest the type of behavior to be expected with dynamic loading. A review of tests conducted to determine the dynamic properties of materials is included in Chapter 7.

A large series of static and dynamic tests to failure of reinforced concrete columns was reported by Reinschmidt, et al. (1964). One hundred and fifty-four dynamic tests and 51 static tests of 5-inch-square columns of various lengths and with various amounts and differing patterns

of reinforcement were included. An average strength increase of 29 percent over the static strength was found for columns loaded concentrically with an average rise time of 30 msec, several times the longitudinal natural period of the columns.

The strength of dynamically loaded shear keys has been investigated by Hansen, et al. (1961). Loads with rise times of 25 to 40 msec were used. Dynamic loading increased the strength 15 to 70 percent depending on the amount of transverse stress acting on the key.

One of the several studies of dynamically loaded beams is that reported by Keenan (1965). Nine large beams with a span-to-depth ratio of about 9 and containing shear reinforcement were tested. Three were loaded statically and six were loaded dynamically with a uniformly distributed step load. The observed shear at cracking and at first yielding of a stirrup increased an average of 88 and 59 percent, respectively, with dynamic loads.

Denton (1967) reported a 27 to 43 percent increase in the load-carrying capacity of fairly slender simply supported two-way reinforced concrete slabs. A blast load with a long decay time was used.



## CHAPTER 3

### DESIGN OF THE EXPERIMENTAL INVESTIGATION

#### 3.1 RATIONALE OF THE TEST PROGRAM

A test series seeking to define the effect of rapid loading must be designed in full view of the available knowledge of the behavior of slab-column connections loaded statically.

The static strength and behavior of slab-column connections are not well understood, even after a number of extensive studies. This is evident from the differing influences assigned to some variables, as noted in Chapter 2, and from the lack of an accurate, complete, and commonly accepted solution for this problem.

All available methods for calculating the shear strength of these connections involve either approximate theoretical solutions, often including experimental constants, or are fits to experimental results. The emergence of a general analytical solution has thus far been precluded by the difficult theoretical problems resulting from the complexity of the stress distributions near the column, the lack of a proven theory of failure for triaxially stressed concrete, and the nonlinearity and nonhomogeneity of the highly stressed and cracked reinforced concrete at the critical sections.

The understanding of this problem has also been slowed and the solution made more difficult by the large number of parameters which do or may possibly influence the connection strength and behavior. The effects of many variables are interdependent; thus, isolating the influence of only one variable can be very difficult.

Because of the incomplete state of knowledge regarding the static

connection strength, an unsophisticated test program was thought desirable to define the effect of loading speed. A maximum of useful information should result from experimentally determining a quantitative relationship between the strength of slowly and dynamically loaded connections over a reasonable range of the most important variables.

It is assumed that with the help of a well-defined relationship giving the effect of loading speed, plausible projections of the effect of other variables may be made into the dynamic range from existing information available from static tests.

Both static and dynamic tests are necessary to allow a direct comparison of the strengths and behaviors at the two loading rates.

An accurate evaluation of the effects of loading speed requires the comparison of well-defined data points. The scatter observed in previous tests dictates that, as a minimum, duplicate tests be conducted to establish that the quantities being compared are themselves meaningful. The size and complexity of the connection specimen will necessarily limit the amount of repetition to below what is desired for statistical analysis.

To serve the intended goal of evaluating conventional construction, the connection specimens tested must be representative of those commonly included in buildings. This includes connections supposedly designed to prevent a shear failure from governing the connection behavior.

Thus, the test program will include duplicate testing at both static and dynamic loading rates of typical connections including a limited range of the most important parameters.

### 3.2 TEST VARIABLES

The results of past experimental programs indicate that three variables

are most influential in determining the static capacity of concentrically loaded slab-column connections. These three are: (1) the concrete strength, expressed either by the compressive or tensile strength; (2) the flexural moment capacity of the slab in the vicinity of the column, usually related to the flexural reinforcement ratio  $p$ ; and (3) the relative size of the column and the slab, commonly expressed as the ratio of the side dimension of an equivalent square column  $r$  to the effective depth of the slab  $d$ .

The flexural reinforcement ratio and the column size as well as the loading rate are the variables selected for inclusion in this test program.

Flexural reinforcement ratios of 0.75 and 1.50 percent were selected. The lower value of  $p = 0.75$  percent is near the minimum commonly used and found to produce economical structures, while the higher value of 1.50 percent is near the upper bound of common usage; the requirements for shear in recent ACI Codes (ACI, 1956 and 1963) have acted to discourage the use of higher reinforcement ratios in the column strip.

The two values of  $r/d$ , the ratio of column side to effective slab depth, of 2 and 4 were also selected to bracket a majority of common practice conditions. The  $r/d$  ratio of the connections in many flat plates, especially those in shorter structures with small column loads, can be near 2. Much of the reported research also clusters about this lower value. The higher  $r/d$  value of 4 can occur in lower floors of multistory flat-plate buildings. Flat slabs commonly have a  $r/d$  ratio of 4 or more. This larger  $r/d$  value is also of interest because of the scarcity of information on the static strength of connections with  $r/d$  ratios of 4 or

larger and constructed of normal weight concrete without prestressing, as noted in Chapter 2.

The chosen nominal compressive strength of 4000 psi is typical of the actual concrete strength in a majority of construction. A design strength of 3000 to 4000 psi has been fairly common in recent years, and actual strength normally exceeds the specified design strength.

The dynamic loading speeds selected are discussed in Section 3.6.2.

The nominal reinforcement yield strength of 48,000 psi selected represents a value between the average actual strength of intermediate- and hard-grade reinforcement.

The scope of this investigation was limited to concentrically loaded interior connections.

### 3.3 PROTOTYPE AND MODEL SCALE

The prototype selected is a flat-plate structure with a column spacing of 17 feet 6 inches. The overall slab depth is 6-1/2 inches with an average effective depth of 5 inches. The slab is supported on either 10- or 20-inch-square columns.

The allowable design live load for the prototype, as controlled by the flexural capacity, may be found from the flexural capacity of the connection area, the provisions and moment distributions contained in Chapter 21 of the 1963 ACI Code (ACI, 1963), and the assumed geometry and dimensions. Using the ultimate strength design method and the specified load factors, the prototype design live load capacity varies from approximately 85 psf for  $p = 0.75$  percent and the smaller column to 250 psf for  $p = 1.50$  percent and the larger column.

The connection specimens tested in this investigation are full-scale models of the prototype connection and adjacent slab areas. Any possible size effects are thus avoided. Also avoided is the possible distortion of the relative shear and flexural strengths resulting from the usually higher-than-normal ratio of tensile to compressive strength common with the small-aggregate concrete often necessary with small-scale models.

### 3.4 TEST PROGRAM

The experimental test program for this investigation is shown in Table 3.1. Two specimens containing each of the four combinations of geometric variables are included for static testing and three for dynamic testing because of the larger scatter expected with dynamic testing. The third dynamic test of a specimen type may be omitted if not deemed necessary.

The specimens and the corresponding test will be designated as follows:

S or D indicating static or dynamic test

2 or 4 indicating a 10- or 20-inch-square column ( $r/d = 2$  or  $4$ )

075 or 150 indicating a flexural reinforcement ratio of either 0.0075 or 0.0150

-1, -2, or -3 indicating the number of the test with this combination of variables

For example, the designation S4075-2 indicates the second statically tested specimen with an  $r/d$  ratio of 4 (20-inch-square column) and a flexural reinforcement ratio of 0.0075.

### 3.5 TEST SPECIMENS

The specimens designed for use in this investigation consisted of an 84- or 94-inch-square reinforced concrete slab 6-1/2 inches in total thickness and with a 10- or 20-inch-square stub column 15 inches high cast monolithically at the center of the slab (Figure 3.1). The slab portion of these full-size models was reinforced with deformed No. 5 reinforcing bars uniformly distributed across the section. The flexural reinforcement was proportioned to give an ultimate moment capacity in each direction equal to that obtained with the stated nominal reinforcing ratio and an effective depth of 5 inches. Figures 3.2 through 3.5 show the reinforcement layout for all slabs. The steel percentages and spacings for the two layers differ because of the 5/8-inch difference in effective depths.

The specimens were designed to be simply supported along all four edges with the corners free to rise.

The chosen specimen configuration includes the immediate connection area and an adjacent portion of the slab. The slab area included is approximately that located within the negative moment region around the column and inside the line of contraflexure, the line of zero principal moment.

The conditions at the boundary of any model of a continuous structure should ideally be identical to those at the location in the structure being modeled. These boundary conditions often cannot be satisfied exactly, especially with plates and slabs, without testing the entire structure. Therefore, the configuration of the model was chosen to best represent the actual conditions using a practical model.

The slab in the model is extended out to the line of contraflexure because this moment-free boundary is easily provided by a simple support.

Round (Kinnunen-Nylander, 1960), octagonal (Tasker-Wyatt, 1963), and, more often, square slabs (Elstner-Hognestad, 1956, and Moe, 1961) have been used to represent the shape of the contraflexure location. The computed shape of the contraflexure line for a square, uniformly loaded interior panel supported on square columns and assuming isotropy and homogeneity is shown in Figure 3.6 (Mowrer-Vanderbilt, 1967). The location of the contraflexure line has also sometimes been assumed to be at one-fifth the span from the column centerline.

The 35-inch shear span (distance from the support to the column) used in this investigation is one-sixth the assumed prototype bay size of 17 feet 6 inches.

Reproducing exactly the other boundary conditions at the slab periphery is also not feasible in a usable model of the connection area. The distribution of the shear forces and the deflections at the edge of the slab are quite complex for even an elastic plate. Reproducing these conditions would, at best, be very difficult unless multipanel slab models were used.

With the isolated connection model used in this program, the corners of the slab lift off the support; consequently, all the shear enters the slab along approximately the middle half of each side. This is consistent with the trend of the behavior of the slab system. More deflection occurs in the prototype at the location of the corner of the model (the model is inverted) and the shear forces are larger near the column line than along the diagonals in the slab system at the model perimeter location.

The location and shape of the contraflexure line and the distributions of the other conditions at the boundary of the model are not constant in a reinforced concrete slab system. Cracking of the slab produces changes in

the relative stiffnesses of various sections and directions. Redistribution of moments can and does take place in the slab system, causing the location of the contraflexure line to shift. The model used does not include these effects of continuity, nor are possible inplane forces included.

Despite the above approximations of the model used, the strengths observed with the use of these isolated connection models are thought to closely approximate the strength of the connections in an actual slab system. The few large-scale flat-plate structures tested to ultimate (Guralnick and La Fraugh, 1963, and Magura and Corley, 1969) failed in the connection regions at a shear stress near that expected from tests of isolated connections.

Failure of the model to provide the indeterminacy which allows the magnitude of shear being transferred to increase even after general yielding occurs in the column area is probably the greatest defect of the models used in this and most other studies of connection shear strength.

### 3.6 LOADING OF THE TEST SPECIMENS

3.6.1 Support and Load Locations. The connection specimens were loaded on the column only and supported only at the slab periphery. This may appear contradictory to the prototype loading condition, a uniform load acting over the entire slab, but is not for the following reason (also see Figure 3.7): for an interior column, the load from a tributary area approximately  $L$  on a side, where  $L$  is the column spacing, is supported on a column. Using the assumptions contained in Section 3.5, the span of the model used is  $0.38L$  and  $0.43L$  for the two column sizes chosen. For the connection model with the larger columns, the proportion of the load placed



outside the model area and entering this area as shear on the perimeter is:

$$L^2 - (0.43L)^2 = 0.815L^2$$

This increases to  $0.855L^2$  for the smaller column size. Load placed directly over the column is not transferred through the connection, but is supported directly by the column. Thus, only a small portion of the load transferred by the connection is from the uniform load acting over the specimen area.

A uniform load applied only over the slab area with the slab edges free would model the conditions at a column footing, not those of a slab-column connection. These two problems are closely related, the models used are very similar, and the shear strengths are nearly the same despite the differences in loading.

3.6.2 Dynamic Loading Rate. The rise time for the dynamic loading case was chosen to be typical of the loading rates that a connection in the prototype slab system would experience with blast loadings.

The column load is the reaction of a dynamically loaded structural system. For this reason, the behavior of the slab system must be examined. As noted by Biggs (1964), the dynamic reactions of a real structure have no relationship to the spring force in the equivalent single-degree-of-freedom system so often used to analyze dynamically loaded structural elements.

The chosen rise time of 20 to 40 msec was arrived at by considering two effects: (1) the crossing time of the pressure wave front from a nuclear blast, and (2) the time needed for the slab to deflect and thus transfer the load to the connection.

Temporarily neglecting the dynamic effects, the rise time of the

column load resulting from a slowly traveling pressure wave is approximately equal to the time needed for the pressure wave to travel 1.2 span lengths, as is shown in Figure 3.8. For an overpressure level of 10 psi, the pressure wave travels at 1400 ft/sec (Brode, 1964). The crossing time for this wave velocity over 1.2 times the prototype span (17 feet 6 inches) is 15 msec.

The dynamically applied load acting on the slab is not instantaneously transferred to the connections; inertial forces support a portion of the load and slow the flow of load to the supports.

The rise time of the reactions of an elastoplastic slab loaded uniformly across its length by a decaying pressure loading is approximately equal to the time for the slab to reach yielding. Biggs (1964) approximates the dynamic column load of a slab system so loaded as:

$$V_c = 0.16F + 0.84R \quad (3.1)$$

Where:  $V_c$  = column load

$F$  = dynamic load acting on one panel

$R$  = resistance mobilized in one panel

$V_c$  will have a maximum value very near the time of general slab yielding.

The natural period of vibration for the slab system is needed to examine the dynamic effects. This quantity is given approximately by the following expression (Anderson, et al., 1961, page 98):

$$T = 5\sqrt{\frac{w}{kg}} \quad (3.2)$$

Where:  $w$  = weight per unit slab area

$k$  = effective stiffness =  $KE_c I_a / L^4$

$g$  = acceleration of gravity,  $32.2 \text{ ft/sec}^2$

$K$  = constant dependent on relative support size

$E_c$  = modulus of elasticity of concrete

$I_a$  = average of cracked and uncracked section moment of inertia

$L$  = average column spacing

Assuming an average column size of 15 inches, a reinforcement ratio near the column of 0.011, and an average reinforcement ratio in the slab of one-half of that over the column, the calculated natural period of the slab is 80 msec.

Using a numerical procedure (Newmark, 1962), the time to yield for an elastoplastic system having this natural period can be found to be 0.25 times the natural period (Figure 3.9), or 20 msec, when the system is loaded by a linearly decaying load pulse with a peak equal to the yield resistance and a duration of 800 msec, which is the  $t_{50}$  value for the 15-psi overpressure level from a 1-megaton device (Newmark and Haultiwanger, 1962, Figure 3.7). This load is near the maximum capacity of a slab system of normal ductility since it would drive the equivalent single-degree-of-freedom elastoplastic system to a maximum deflection of seven times the yield deflection in a time of  $1.85T$  (Melin and Sutcliffe, 1959, Chart 1). Smaller overpressures would result in slightly longer times to yield.

The rise times from the two effects discussed above will interact in a complex manner to determine the actual rise time of the column load.

Nearly all blast-loaded connections will be loaded with some moment either because of their placement in a lateral-load resisting frame or because of the unsymmetrical conditions resulting from the traveling wave. The inertial forces would act to decrease the moments from the traveling

wave; the moments shown in Figure 3.8 would not be reached. As previously mentioned, this program was limited to the case of eccentrically loaded connections.

The only practical loading method available in the laboratory to test the connection specimens of dynamic rates was to apply the dynamic load on the column, although loading and moving the periphery of the slab would be more representative of the prototype loading conditions.

Only small deviations from the actual prototype conditions were expected to result from the chosen loading methods because the rise time chosen exceeds the natural period of the connection model. Inertial forces in the slab at the time of failure were expected to be small.

The calculated fundamental natural periods of the connection models are listed below for both a fully cracked and a fully uncracked slab.

Slab Size	Calculated Natural Period T		
	Uncracked Slab	Cracked Slab p = 0.0075	Cracked Slab p = 0.0150
	msec	msec	msec
84 inches square (10-inch column)	9.5	21.0	16.2
94 inches square (20-inch column)	12.8	28.4	21.9

The slab was assumed to deflect into the shape given by:

$$w(x,y) = W \sin \frac{m\pi x}{a} \sin \frac{n\pi y}{b} \quad (3.3)$$

Where:  $w(x,y)$  = deflection at point  $(x,y)$

$W$  = maximum deflection of the slab

m = number of half sine wave shapes in the x direction

n = number of half sine wave shapes in the y direction

a = span length of slab in the x direction

b = span length of slab in the y direction

This is the deflection shape for a slab simply supported along all four sides with the corners tied down. The natural circular frequency for such a slab (Timoshenko and Woinosky-Krieger, 1959, page 334) is:

$$\omega = \frac{2\pi}{T} = \pi^2 \sqrt{\frac{D}{\mu} \left( \frac{m^2}{a^2} + \frac{n^2}{b^2} \right)} \quad (3.4)$$

Where:  $\omega$  = natural circular frequency

T = natural period of vibration

D = plate stiffness

$\mu$  = mass per unit area of slab

For the fundamental mode, m = n = 1 .

The mass of the column was considered by multiplying the natural periods calculated from Equation 3.4 by the square root of the ratio of the effective slab mass with the stub column to that without the column. The effective mass was assumed proportional to the integral of the mass multiplied by deflection over the slab area. This increased the value of T by 4 percent for the smaller column size and by 12 percent for the larger column size.

Both the mass of the loading system and the freedom of the slab corners to rise would increase the natural period.

The calculated natural period of the full-scale connection model is significantly less than that of the slab system. This should be expected because the connection area is only a part of the slab system. The period

of an assemblage of elements in series is greater than the period of any individual element.

## EXPERIMENTAL PROCEDURE

## 4.1 SPECIMEN MATERIALS AND FABRICATION

4.1.1 Concrete. A Type II cement also meeting the requirements of Type I was used for all specimens. The fine and coarse (3/4-inch maximum size) aggregates were both crushed limestone of Tennessee origin.

The concrete mixture was determined using trial batches and was designed to produce a 28-day strength of 4000 psi for cylinders cured similarly to the connection specimens. The proportions used for each specimen are listed in Table 4.1. All batches had a measured slump of 1-1/2 to 2-1/2 inches.

The change in mixture proportions starting with Specimen S4150-1 resulted from having to change cement on rather short notice when the bulk cement supply being used for several programs became exhausted. Physical tests of the second shipment of cement indicated that a lower water-cement ratio would be needed to maintain the desired strength. Three slabs were cast before cylinder tests indicated that this was not so. The two D4150 Specimens were cast with the lower water-cement ratio in order to match the concrete used in the companion statically tested specimens.

4.1.2 Reinforcement. All flexural reinforcement placed in the slabs was commercially obtained intermediate-grade No. 5 steel bars meeting the requirements of ASTM Specification A15 (ASTM, 1964) and with deformations conforming to ASTM Specification A305 (ASTM, 1964). Bars from two heats having the mill-determined properties listed in Table 4.2 were received in untagged bundles.

The No. 6 bar used for the column reinforcement and the No. 3 bar used as column ties were intermediate-grade deformed steel bars.

4.1.3 Forming, Casting, and Curing of Specimens. The specimens were cast with the column down and in wooden forms. A platform constructed with a 3/4-inch plastic-coated plywood deck formed the slab surface and 6-1/2-inch-high dimension-lumber walers bolted to the platform formed the specimen sides. A separate column form fit into the center of the platform and was used to facilitate changing the column size and stripping the forms.

After the form was oiled lightly and the column steel placed, the slab reinforcement was inserted into holes in the walers and tied to form a sturdy mat. This procedure was used to insure the proper bar spacing and height even after the forms had been trucked to the casting facility.

The bars in the slab were also tied to lifting lugs located about 15 inches from each corner and supported near the column either by tying one or more slab bars in each direction to the column steel or by placing four individual high chairs 10 to 12 inches from the column face. These chairs were fabricated from 1/4-inch-diameter smooth wire. The second method was adopted for later specimens because the ties between the slab reinforcement and the column steel of some of the earlier specimens slipped during transportation and had to be retied.

Strain gages were mounted on selected bars prior to placing the bars in the form.

The distance of the reinforcement above the form in the vicinity of the column was measured immediately prior to casting.

A 2-1/2-inch-outside-diameter aluminum conduit was placed at the center of the column to form the hole needed for the loading pull bar to pass through. This conduit, the column steel, and the lifting lugs terminated 1/8 inch below the level of the finished surface.



A form with all reinforcement in place is shown in Figure 4.1.

The concrete was mixed in three batches of 11 or 15 ft<sup>3</sup> for the Series 2000 and 4000 specimens, respectively, using a 16-ft<sup>3</sup> Maxon tilting drum mixer. A butter mix of approximately 1 ft<sup>3</sup> preceded the mixing of the three batches used to cast the slab.

Ten control cylinders were cast from the first batch and three from each of the other two batches. The cylinders were cast in standard 6- by 12-inch steel molds and vibrated for 15 seconds using an internal vibrator with a 1-1/4-inch-diameter round head.

After the control cylinders were cast, the concrete in each batch was carefully placed in the forms in the following sequence.

1. The first batch was placed in and immediately around the column.
2. The second batch was next placed in a donut-shaped area around the first.
3. The third was placed in the corner areas of the slab.

The concrete was then vibrated using internal vibrators and the surface was screeded with a wooden screed supported on the walers forming the edge of the slab. During initial set, 2 to 2-1/2 hours after casting, the surface was finished using a steel trowel.

The specimens were cured under wet burlap for 7 days and then air-cured until testing.

The control cylinder molds were removed approximately 24 hours after casting. Curing was the same as for the companion connection specimen.

4.1.4 Material Tests. The properties of the No. 5 deformed bars used to reinforce the slabs were determined from tensile tests using 18-inch lengths of bar selected at random.

Each of six bar specimens was instrumented with two 1/4-inch foil-type electrical strain gages placed diametrically opposite to obtain stress-strain curves. Only enough deformations were removed to allow the placement of the gages. No deformations were removed from the other bar lengths tested. Two small punch marks were placed 8 inches apart prior to testing the bar as a reference for measuring elongation. The bars were loaded at a rate of 55,000 to 70,000 psi/min in the elastic region. The determined properties of the reinforcement are listed in Table 4.3 and were calculated using the nominal cross sectional area of the bar.

All bars exhibited a ductile failure, with necking and fracture occurring between the elongation punch marks. All bars had a well-defined yield point and yield plateau. Limited results from the gaged bars, indicated strain hardening started at a strain of  $18,000 \times 10^{-6}$ . A typical stress-strain curve for the reinforcement is shown in Figure 4.2.

The results from the concrete control cylinder tests are listed in Table 4.4. Typical load-deflection curves obtained from specimens instrumented with 6-inch-long strain gages are shown in Figure 4.3.

The cylinders tested in compression were capped with Cylcap, a sulphur-based compound, and tested in accordance with ASTM Specification C39 (ASTM, 1964).

The split cylinder strengths were determined by loading 6- by 12-inch cylinders on their side in accordance with the U. S. Army Corps of Engineer Specification CRD-C 77-61 (WES, 1949). Strips of 1/8- by 1-inch pressed wood 12 inches long were placed between the cylinder and the testing machine head and table to provide a uniform distribution of load along the cylinder length. The load was applied at a rate of 17,000 lb/min.

For most specimens, two cylinders were tested at 4 weeks to determine the 28-day compressive strength. The remaining cylinders were broken the day of the corresponding slab-column connection test. The compressive strengths listed in Table 4.4 are the average of five cylinders for Batch 1 and the average of three cylinders for Batches 2 and 3. The split-cylinder tensile strengths were determined for Batch 1 only and are the average of three cylinder breaks.

Most, if not all, of the concrete at the location of the shear failure was from Batch 1. Therefore, the strengths of Batch 1 will be used in the shear strength calculations. The average strengths of the three batches will be used in the flexural strength calculations.

## 4.2 TEST EQUIPMENT AND PROCEDURES

4.2.1 Loading Device. The 200-Kip Loader, an open-loop hydraulic testing device capable of producing both static and dynamic loads, was used for all tests. The operation and capabilities of this device are discussed in Appendix A.

4.2.2 Test Setup. The slab-column connection models were simply supported along all four edges by rollers placed on a massive-reinforced concrete reaction structure surrounding the loading device and bolted to the two 30-inch-deep plate girders supporting the loader (see Figures 4.4 and 4.5).

Details of the supporting arrangement are shown in Figures 4.6 and 4.7. The supports consisted of a 3- by 5/8-inch cold-drawn steel plate placed atop a 1-inch-diameter cold-finished steel roller. This roller was placed atop a 3- by 3/8-inch steel flat which in turn rested on an 8- by 5/8-inch cold-drawn steel plate attached to the reaction structure with thirty-six 1/2-inch-diameter bolts and embedded Deco anchors. An epoxy filler was

placed in the void between the plate and the reaction structure after the plate had been leveled at the 36 bolt locations to within  $\pm 0.003$  inch of flatness.

After the walers had been struck from the connection specimen, the tension slab surface of all but the first specimen was whitewashed to aid in photography. The specimens were then carefully flipped over, the column form removed, and, after two or more days elapsed to allow the concrete surface to dry thoroughly, strain gages were applied on the concrete surface.

The connection specimen was then placed in the reaction structure. The specimen was set onto a plastic layer of mortar spread atop the upper steel plate. This insured proper seating of the slab and support.

A 1-inch-thick steel plate the size of the column was then seated atop the stub column with mortar. For the 20-inch-square column, a 10-inch-square plate was placed upon the 20-inch-square plate. The plates were included to help spread the applied load over the column cross section.

A WES-manufactured load cell was next placed on this plate, and a 2-inch-diameter pull bar was inserted through the load cell and the hole formed through the stub column and connected to the loader. Details of the area around the column are shown in Figure 4.8.

To complete the test arrangement, deflection gages were mounted on an aluminum frame spanning the reaction structure. The completed testing arrangement is shown in Figures 4.9 and 4.10.

After testing, the specimens were closely examined and posttest photographs were taken. The cover over the reinforcing bars immediately outside the area of shear failure was removed and the bars flame-cut, allowing the column and failure cone of the slab to be removed from the rest of the slab.

The failure surface was then examined. Profiles of the failure surface were plotted for the last 13 specimens.

4.2.3 Static Tests. The static loadings were obtained by using the 200-Kip Loader as a hydraulic cylinder (Appendix A). After all instrumentation leads and equipment were installed and checked, the loader ram was slowly moved down, loading the specimen.

The load in the first four static tests was applied in 15 to 20 increments. No advantage was seen in step loading nor was this necessary because of the continuous recording system used. The last four statically loaded specimens were loaded at a nearly constant deflection rate. All static tests were completed in 10 to 20 minutes.

4.2.4 Dynamic Tests. The 200-Kip Loader was operated in the dynamic loading mode as described in detail in Appendix A. After the instrumentation was completed and checked, the low-bulk modulus oil in the loading system was pressurized. A 500- to 700-pound preload was maintained on the specimen prior to the dynamic test. The dynamic load was produced when the fluid pressure below the loader piston was relieved by the controlled breaking of a double-rupture disk valve. The resulting pressure imbalance loaded the piston, and, via the pull bar, the connection specimen. Recorders were started four or more seconds before the test and shut off two or more seconds after failure.

The column was pulled down several inches immediately after failure because of the expansion needed to reduce the pressure above the piston and thus restore equilibrium after the resistance drop associated with the connection failure.

For the first two dynamic tests, the loader was equipped with the

maximum size orifice disk in order to produce a very fast loading rate by offering the least resistance for the fluid escaping through the orifice plate and rupture disk assembly. The behavior of the loader with the connection specimens was uncertain because the loader had previously been used only to test much stiffer resisting elements. Loading rates faster than the designed were preferable to extremely long rise times.

This arrangement resulted in a nearly impulsive load. A short load duration resulted from the large deflection of the connection specimen and the small stroke needed to release the pressure in the pressure tanks connected to the chamber above the piston.

Larger pressure tanks and smaller orifice plate openings were used for the remainder of the dynamic tests to obtain sufficient stroke and the desired rise times.

#### 4.3 TEST MEASUREMENTS AND INSTRUMENTATION

4.3.1 Load Measurement. The load cell constructed for this investigation was located immediately above the stub column of the specimen (Figures 4.8 and 4.9). It consisted of an instrumented 5-3/4-inch length of 4-1/4-inch-outside-diameter by 3/4-inch-wall-thickness heat-treated mechanical tubing turned to a 3.600-inch outside diameter in the center region. Two sets of four 1/4-inch-gage-length epoxy-backed foil strain gages (Budd C6-141-B) were placed in two full-bridge configurations on the reduced center section. Vertically and horizontally oriented gages were placed at 90 degrees around the load cell. Gages located diametrically opposite were used for each channel.

Two load channels were included in the load cell as a check of the accuracy, especially for the dynamic tests, and to have a backup record in

case of gage failure or loss of record during a dynamic test.

The response of both bridges was linear within the loading range of 0 to 250,000 pounds. Strains of  $26.74 \times 10^{-6}$  and  $26.55 \times 10^{-6}$  corresponded to 1000 pounds of load.

4.3.2 Deflection and Acceleration Measurements. Deflections were measured on either side of the column on the slab surface, on the side of one column, at one slab corner over the supports, and at one quarterspan point of the slab for all specimens. The gage layout is illustrated in Figure 4.11.

The three deflection measurements near and on the column were obtained with 7-inch-capacity linear potentiometers manufactured by Topp Industries. The corner and quarterpoint deflections were measured with  $\pm 5/8$ -inch-capacity Collins linear variable differential transformers (LVDT). A  $\pm 5/8$ -inch-capacity Collins LVDT identified as D2a was added in some tests.

Both types of deflection gages were clamped to the aluminum deflection bridge with mounting brackets (Figures 4.8 and 4.12). The gage probes were attached to 1-inch-square metal pads using a short length of Shrinktubing as shown in Figure 4.12. The pull pads were attached to the slab or column surface with Epocast, a two-phase epoxy glue.

Four additional deflection gages were added for the last nine slabs. Their function was to detect the formation of internal diagonal cracking in the column vicinity indirectly by measuring the thickness change between the top and bottom slab surfaces to which the gage assembly was attached. These assemblies, shown in Figure 4.13, utilized  $\pm 1/10$ -inch-capacity Collins LVDT's and were located as shown in Figure 4.11. A  $1/4$ -inch-diameter hole was drilled through the slab to permit the  $5/32$ -inch-diameter shaft to

extend freely through the slab.

Three 500-g-capacity Consolidated Electronics Corporation (CEC) accelerometers were placed in the positions shown in Figure 4.11 for the dynamic tests only. The transducer above the column was attached to the 10-inch-square plate below the load cell with four small screws. The two accelerometers located on the slab, one near the column and the other at a quarter-span point, were attached to the slab with 1/4-inch lead anchors and a base plate as shown in Figure 4.12.

4.3.3 Strain Measurements. Concrete strains on the compression (column) side of the slab and strains of the flexural reinforcement were measured at the locations shown in Figures 4.14 through 4.17. The gage layout was modified during the test program when examination of earlier test data indicated changes would be desirable.

The steel strains were measured using Budd C6-141-B epoxy-backed foil gages. These gages have a nominal grid size of 1/4-inch length by 1/8-inch width and a resistance of  $120 \pm 0.2$  ohms.

After two or three deformations were removed from the reinforcement and the surface was smoothed with emery cloth and cleaned, the gages were bonded to the bar using a heat-curing epoxy. The lead wires were then soldered to the gage tabs and the gages waterproofed with successive layers of three synthetic rubber compounds, Gagekote 1, 2, and 5.

Two strain gages located diametrically opposite were used at each gage location for the first seven tests. The two gages formed the active arms of a four-arm bridge circuit designed to eliminate output from bending.

One gage at each location was used for the remainder of the test program because the effects of bending of the reinforcement were thought to be



small and the two-gage configuration often complicated determining when one of the gages failed or was damaged, thus ending the valid range of strain information.

Concrete strains were measured using Budd C6-1161-B epoxy-backed foil gages with a 1-inch-long by 3/32-inch-wide grid. The gage resistance was  $120 \pm 0.2$  ohms.

The concrete voids at the gage location were filled to insure proper gage adhesion by spreading a thin layer of Epocast onto the concrete surface and later sanding this material off until the concrete was again exposed. The gages were bonded to the concrete with Eastman 910, the leads attached, and the gages waterproofed with Gagekote 1, 2, and 5.

The 1-inch gage length selected for the concrete was a compromise between the short length needed to measure strains in regions of high strain gradients and the length of two or more times the maximum aggregate size necessary to most accurately measure concrete strains (Cooke and Seddon, 1956).

4.3.4 Data Recording and Reduction. Figure 4.18 is a block diagram of the instrumentation system used.

B and F Instruments, Inc., balance units and a WES-constructed balance unit provided excitation to the gages and contained the calibration and balancing circuitry.

The signal from all transducers except the Collins LVDT gages was amplified by Dana Model 2000 dc operational amplifiers before entering the recorders.

Three 14-channel magnetic tape recorders, a Sangamo 3500, an Ampex CP-100, and an Ampex ES-100 unit, served as the primary data recording

system. For the tests of Specimens D2075-1 and D2075-2, it was necessary to record most steel strain data with a CEC 5-124 direct writing oscillograph recorder instead of the Ampex ES-100 recorder. One channel of each magnetic tape was used for timing and another internally used by the recorder, leaving 12 available data channels per tape. A recording speed of 7-1/2 in/sec was used in the static tests. For the dynamic tests, 60 in/sec was used. The oscillograph recorder was operated at 160 in/sec.

Calibration for the data was provided by electrically inserting a known equivalent gage output into the circuitry of each data channel and recording the resulting output for a brief period prior to each test. For most transducers, this calibration procedure was accomplished by switching in a known resistance in parallel with one active gage arm of the balancing bridge circuit. Plus or minus one-percent resistors were used for the calibration. When the data were reduced, the calibration values were corrected to account for the effect of the cable resistance between the transducer and the calibration circuitry.

The data recorded on magnetic tape were later reproduced on photographic paper using the tape output as the input to a CEC oscillograph recorder. The resulting data traces were manually scaled to reduce the data. Several acceleration records were digitized and doubly integrated with the aid of a digital computer.

## CHAPTER 5

### EXPERIMENTAL RESULTS

All test results are contained in this chapter and in Appendixes B and C. Discussions of these results are contained in the two subsequent chapters on connection behavior.

The records contained in Appendixes B and C which are not shown throughout the entire test were terminated either when the transducer failed (most common with strain gages on the reinforcement) or when the traces were obviously no longer valid. In several instances, a recording channel either became electrically saturated or overdrove the recording equipment when the gage output significantly exceeded that predicted. Some traces returned to a valid range after being overranged. The nonlinear portions of these traces are identified in the traced records.

#### 5.1 STATIC TESTS

All eight slab-column connections tested under static loading conditions failed suddenly when the stub column and a portion of the slab were pulled through the deflected slab in the manner shown in Figure 5.1. The drop in resistance and the loss of continuity associated with the punching failure allowed the slab outside the column area to spring back towards its undeflected position. The operation of the loader pulled the column portion down farther after failure. Some resistance remained after failure because of the tensile membrane action of the reinforcing steel.

The maximum loads and the deflections at failure for these eight connection specimens along with the observed specimen properties are tabulated in Table 5.1. The measured effective depth often varied from the 5.00-inch nominal dimension and resulted in small changes in the  $r/d$  and  $p$  values from the nominal values listed in Chapter 3. The average effective depth

at the column is listed for Specimen S4075-2. The depth at the south column face of this slab was 0.17 inch less than at the opposite face as a result of the column form being tilted approximately 1/2 degree during casting.

The load-deflection curves for the static tests are shown in Figure 5.2. The center deflections plotted in the load-deflection curves are the averages of deflections measured at three locations: two on the slab at the north and south faces of the column (D1 and D2 in Figure 4.11) and one on the column (D3 in Figure 4.11). The descending portion at the ends of the curves occurred in the final few seconds prior to failure.

Complete deflection, concrete strain, and steel strain data plotted as a function of the applied load are presented in Appendix B (Figures B.1 through B.16). Tracings of the oscillograph records for the last four static tests are shown in Figures B.17 through B.27.

Photographs of the connection specimens after testing are presented in Figures 5.3 through 5.10. The cracks have been marked in several photographs. Photographs of the column and failure surface were taken after the loose concrete cover was removed, the reinforcing bars cut, and the column portion lifted from the slab.

Profiles of the failure surface of four Series S4000 specimens are presented in Figures B.28 through B.31.

The gage locations were not consistently numbered for all tests. All data are for the gage numbers presented in Chapter 4, which are not always the same as the location numbers visible in some of the photographs contained in this chapter.

## 5.2 DYNAMIC TESTS

A punching shear failure occurred in nine of the eleven specimens

tested under dynamic conditions. The two specimens loaded with a very rapidly applied force of short duration, Specimens D2075-1 and D2150-2, were driven to large flexural deflections unaccompanied by complete punching shear failures.

The results of the dynamic tests are summarized in Table 5.1. The rise times, failure times, and maximum connection resistances listed in Table 5.1 were not always uniquely defined or readily apparent from the records. The determination of these quantities and the reason for not using the absolute maximum applied load as the connection resistance are discussed in Section 7.3.1.

The load-time curves for the dynamically loaded connections are presented in Figures 5.11, 5.12, and 5.13. Tracings of all dynamic records obtained are contained in Appendix C (Figures C.1 through C.36).

Deflection records for Specimens D2075-3 and D2150-2 were lost due to instrumentation difficulties. Acceleration records of these two tests and the preceding two tests were doubly integrated in order to recover the deflection information and to determine how the deflections so obtained compared with those measured directly. The accelerations were digitized by an analog-to-digital data reduction unit and numerically integrated using a digital computer. The results are shown in Figures 7.4 through 7.7. The large accelerations resulting from the slab rebounding after failure overranged several acceleration channels and complicated the integration procedure.

Neither deflection information nor the magnitude of the accelerations was obtained for Specimen D4150-1.

Photographs of the slabs after testing are included in Figures 5.14 through 5.24. The profiles of the failure surface of the dynamically loaded specimens failing by punching shear are presented in Figures C.37 through C.45.

## CHAPTER 6

### STRENGTH AND BEHAVIOR OF STATICALLY LOADED SLAB-COLUMN CONNECTIONS

The behavior of the specimens with the two reinforcing ratios differed considerably. The specimens with the higher reinforcement ratio ( $p = 0.0150$ ) exhibited a rather brittle behavior and failed before general flexural yielding was reached in the slab. Their failures were caused primarily by shear distress and will be designated as shear failures. The specimens with the lower reinforcement ratio ( $p = 0.0075$ ) failed in shear only after appreciable general flexural yielding. Their failures will be designated as flexural-shear failures.

Approximately one-fourth of the maximum resistance remained after failure, with the load being supported by the tensile membrane action of the flexural reinforcing bars. The connections were not tested to collapse so that the concrete cover would remain intact and the crack patterns could be examined.

The loads measured by the two load cell channels agreed closely, varying by a maximum of 3 percent at failure. The average value has been used when both channels operated.

The cracking load of Specimen S4150-1 was relatively low. Appreciable load was accidentally placed on this connection while positioning the loader ram for the test and may have been sufficient to cause some damage before the test.

Specimen S4075-2 failed at a significantly smaller deflection and a slightly smaller load than did its companion specimen. The column of this connection was tilted slightly during casting, causing the slab depth to be

smaller at one column face. This suggests that ductilities of lightly reinforced connections may be quite sensitive to material and load eccentricities.

## 6.1 RESULTS OF DUPLICATE TESTS

The duplicate tests indicated that the capacities of the slab-column connections were quite reproducible. The ratios of the strengths of the stronger connections to the strength of the weaker of the pair were as follows:

S2075 - 1.062

S2150 - 1.054

S4075 - 1.039

S4150 - 1.003

Some difference in the strengths of the companion slabs resulted from their slightly differing concrete strengths and effective slab depths.

The ratios of the observed to predicted strength (see Section 6.9) for the two specimens of each pair differed slightly less than the ratio of the connection strengths listed above. The use of the average observed and predicted strengths of the duplicate tests as the static connection properties appears reasonable. These average values will be utilized in Chapter 7 when comparing the static and dynamic strengths of the connection specimens.

## 6.2 LOAD-DEFLECTION RELATIONSHIPS

A short descending branch of the load-deflection curve was observed in all the static tests (see Figure 5.2) during the last 2 to 10 seconds



before failure. Failure occurred at from 94 to 98 percent of the maximum load. This ratio depended on the characteristics of the test setup as well as those of the specimens. The descending portion of the curve was detectable only through the use of continuous instrumentation and a relatively stiff loading device.

Although the descending portion of the load-deflection curve is of definite importance in studying the behavior of the connections, it cannot serve as a useful and visible indication of impending failure, especially for connections loaded with dead weight.

Critical events in the load-deflection response of the specimens are summarized in Figure 6.1. Initially, the slab was uncracked and quite stiff. A significant decrease in the stiffness accompanied cracking of the slab, and a second decrease began with the start of significant yielding of the reinforcement. The load-deflection curve became nearly horizontal as yielding of the reinforcement extended throughout the slab. The transitions between these three stages were gradual because of the gradual spread of both cracking and yielding throughout the slab. The general yielding stage was not reached in the more heavily reinforced specimens.

The ductilities of the connection specimens may be approximated by idealizing the load-deflection curves as an elastoplastic curve as shown in Figure 6.2. The curves were chosen to fit the observed data by minimizing the area between the actual and the fitted curves and by maintaining the observed energy, the area under the load-deflection curve. The approximate deflections at general flexural yielding are also shown in Figure 6.2.

The ductilities, stiffnesses, and energy absorption capacities indicated by the elastoplastic curves are listed in Table 6.1. Both the

ductility and stiffness values are quite sensitive to the fit of the curve.

Ductilities of the more heavily reinforced slabs ranged from 1.5 to 1.9 and those of the more lightly reinforced slabs ranged from 2.7 to 4.9 using the elastoplastic curves. The more lightly reinforced slabs possessed significantly more energy-absorbing capacity because of their larger ultimate deflections.

The failure deflections are also compared in Table 6.1 with the general yielding deflection and with the span of the connection specimen slab. The more heavily reinforced slabs failed at a deflection of 0.7 to 0.9 percent of the span length. The more lightly reinforced slabs failed at a deflection of 1.5 to 2.0 percent, roughly twice the deflection of the specimens with  $p = 0.0150$ . The failure deflection increased by approximately one-third with the larger column size.

The measured quarterspan and corner deflections are compared with the center deflections for three tests in Figure 6.3. The quarterspan deflections were slightly over one-half the center deflection, as they should be because of the elastic curvature of the slab being concave toward the column side. After yielding began, the increase in the quarterspan deflection was very close to one-half the center deflection.

The slab corners lifted off the supports at a rate of approximately one-fourth the downward deflection of the column throughout the test. Because of the upward deflection of the corners, the slabs were effectively supported only along the middle half of each side.

### 6.3 CRACK PATTERNS

The cracks observed on the tensile surface of the slabs after failure

are shown in Figures 5.3 through 5.10. The crack patterns consisted primarily of radial cracks throughout the slab surface and two main circumferential cracks, one roughly following the column outline and the other outlining the larger dimension of the failure cone. Considerable amounts of concrete cover were often torn off along and outside the outer circumferential crack. The shape of the outer circumferential crack was much more irregular in the lighter reinforced slabs, especially in S2075-2 (Figure 5.4a).

No circumferential cracking was found outside the failure cone and only limited circumferential cracking was observed between the two main circumferential cracks, especially in the specimens with the smaller reinforcement ratio.

Although the tension surface of the slab could not be viewed during the test, the available experimental evidence suggests that the intermediate circumferential cracks in the slabs with the smaller column size had not formed before failure. Such evidence includes:

1. Although yielding of the reinforcement was quite general in the lightly reinforced slabs and flexural cracking was well developed, little intermediate cracking was seen even after failure in flexural-shear. The crack pattern of Specimen S2075-2 (Figure 5.4a) is a good example.

2. In several specimens, the outer circumferential crack was not complete. One such specimen was S2150-1 (Figure 5.5). The segment without the outer circumferential crack had a circumferential crack only at the column outline.

3. The intermediate circumferential cracks, when present, were not generally continuous. Nor were these cracks usually locally continuous

across the radial cracks. This indicates that the radial cracks formed first (Figure 6.4).

It is concluded that the intermediate circumferential cracks of the connections with the 10-inch column formed after failure and as a result of the tensile reinforcement draping over the column and failure cone, as shown in Figure 6.5.

The cause of the intermediate circumferential cracking of the connections with the larger column is not as clear. Several cracks in the vicinity of the column faces, especially those parallel to the reinforcement nearer the tension surface (to the left and right of the column in Figures 5.7a, 5.8a, 5.9a, and 5.10a), have the appearance of flexural cracks.

Radial cracking extended toward but did not always reach the edge of the slab in the more heavily reinforced specimens. The radial cracking in the specimens with  $p = 0.0075$  extended to the edges, and distinct yield lines had formed before failure.

Torsional cracking developed on the slab edges at the ends of the radial cracks reaching the edge. These torsional cracks were quite wide at the yield line cracks.

Some bond cracking or splitting was observed on the edges of Specimen S4150-1 (Figure 5.9b). This cracking developed after failure and only where much concrete cover was torn loose by the tensile reinforcement mat and an insufficient length of cover remained to anchor these bars adequately.

#### 6.4 THE FAILURE SURFACE

The slabs failed along a surface formed by inclined cracks in the

immediate vicinity of the column. The failure surface had a shape approximating the surface of a truncated cone spreading out from the column. This is illustrated in Figures 5.4 through 5.10 which show the failure cones and Figures B.28 through B.31 which show the profiles of the failure surface.

Some loose concrete fragments were found in the slab when the column was removed, indicating either that two or more inclined cracks developed close together in the failure zone or that the postfailure cracking of the failure cone suggested in Figure 6.5 did occur.

The failure surfaces were quite irregular. The angle of the line from the column face to the intersection of the shear crack with the closer steel layer varied considerably within a given slab but was usually 20 to 30 degrees from the horizontal for all slabs. The angle of the failure surface did not appear to be dependent on the reinforcing ratio. However, the failure surface was usually dished into the failure cone for the higher reinforcing ratio and away from the failure cone for the smaller ratio, particularly for the smaller size (compare Figure 5.4b with Figures 5.5c and 5.6b).

In the S2000 Series, the failure angle tended to decrease at the corners in the lightly reinforced connections and increase at the corners in the more heavily reinforced specimens. No discernible pattern was apparent with the larger column size (S4000 Series).

The column outline on the compression slab surface was followed quite closely by the failure cone in all of the more heavily reinforced connections. The slope of the crack near the column was nearly 45 degrees, noticeably steeper than the average slope of the failure crack.

The failure crack did not always follow the column face with the

smaller reinforcing ratio, but sometimes deviated from the column outline near the center of the column face. A very large deviation can be seen in Figure 5.7b, a photograph of the column side of Specimen S4075-1. The cracking at the end of the peninsula shape shown extending from the column in this figure was nearly vertical (see Figure 5.7d) and had the appearance of a flexural crack extending from the column side of the slab. This specimen may have failed from excessive shear at the column corners and along three column faces, leaving the column area cantilevering out from the fourth side, which then failed in flexure from a moment of opposite sign of that for which the slab was reinforced.

The failure crack of the more lightly reinforced specimens normally intercepted the slab compressive surface at a very small angle, especially Specimen S2075-2 (Figure 5.4), leaving very thin sections of the slab above the failure crack.

The failure cone was markedly flared near the slab tensile face, particularly with the larger reinforcing ratio, and intercepted the surface at a flat angle quite unlike that to be expected for a flexural crack. The surface cracks at the failure location were not flexural cracks, but resulted from a splitting action of the tensile reinforcement after the shear crack had formed and the reinforcement attempted to carry the applied load by dowel action. The irregular crack outline, the incompleteness of the cracking circle in several specimens, and the crack location far from the column face all support this observation.

The absence of circumferential flexural cracks (except at the column face) in the slabs of the specimens with the 10-inch columns indicates that the inclined cracks forming the failure surface originated inside the slab and spread to both faces.

The inclined cracks along the column faces in the connections with the larger columns may have originated from flexural cracks.

## 6.5 INTERNAL CRACK FORMATION

The development of inclined cracking in the vicinity of the column was detected indirectly by measuring change in the slab thickness at four locations (Figure 4.11) as described in Section 4.3.2. The measured changes in slab thickness are the sum of the small vertical material strains and vertical width of any cracks crossing the gage location. This indirect method of measuring crack width, while not highly sensitive, yielded considerable information on the internal cracking of the specimens. The gages measuring slab thickness changes appeared to drift appreciably, especially Gage D9 and all gages in the test of Specimen S4150-2.

The changes in slab thickness are plotted against the column deflection in Figure 6.6. Initiation of inclined cracking could not be precisely and incontrovertibly detected. As can be seen in Figure 6.6 but is better illustrated by the traced records (Figures B.18, B.21, B.23, and B.26), the observed slab thicknesses generally increased gradually throughout most of the test. The inclined cracks did not open rapidly at the time of their formation and generally opened appreciably only after 90 percent or more of the ultimate load was reached.

Two distinct slope changes are visible in most of the curves in Figure 6.6, the first at a very small slab thickness change and at a column deflection of about 0.2 inch and a second near the ultimate load. The first change in slope is thought to correspond to the initiation of inclined cracking and occurred at a load of 45 to 55 kips for both reinforcing ratios. Cracking appears to have developed first near the corners (Gages D6 and D7).

The crack widths increased significantly first near the corner, at Gages D6 and D7. A very distinct jump in the slab thickness was recorded simultaneously at these two locations in the more lightly reinforced slabs (Figures B.18 and B.21). These sudden increases in slab thickness occurred at a deflection of 0.94 and 0.95 inch for Specimens S4075-1 and S4075-2, respectively, after general yielding had developed and at 98 to 100 percent of the maximum load. These internal cracks opened quickly and were quite large at the time of failure, exceeding the approximately 1/16-inch capacity of instrumentation as set up.

No distinct jumps in the slab thicknesses were detected at the column corners in the more heavily reinforced connections, but significant increases were measured at roughly 90 percent of the maximum load. These values increased to 0.009 to 0.020 inch at the time of failure, significantly less than with the smaller reinforcing ratio.

The cracks opened at the column face (Gages D8 and D9) only immediately before or simultaneously with failure and at or after the maximum load was recorded. A pronounced opening of these cracks prior to failure was detected only for Specimens S4075-1 and S4150-2. In these two specimens, crack opening was simultaneous at locations D8 and D9. Expanded records immediately before failure are shown in Figure 6.7 for these two specimens. A noticeable decrease in the load and an increase in the column deflection began concurrently with the cracking at the column face of these two specimens.

The inclined cracks near the center of the column face did not open before failure for Specimens S4075-2 and S4150-1. The probable explanation is that the inclined cracks opened first at one or more of the other column



faces and failure quickly progressed around the column at the time of failure. The slab area adjacent to all four column faces should not be expected to independently form large cracks simultaneously; even small random properties should preclude this.

Local disturbances of the slab near the gages, while unavoidable, should have been small because of the small size of the hole (1/4-inch diameter) drilled through the slab to accommodate the gage probe.

The results of the slab-thickness measurements indicate that the connection specimens experienced major shear distress first at the area of the column corners and only immediately before failure at the column faces. Although inclined cracks generally formed at all gaged locations at a load appreciably below the ultimate, the opening of the cracks in the corner areas did not indicate imminent failure of the connection as did the opening of cracks near the column face.

## 6.6 CONCRETE STRAINS

Concrete strains were measured at various locations on the compressive side of the slab and in the column area (Figures 4.14 through 4.17) as described in Section 4.3.3. All the concrete strain data obtained for the static tests are contained in Appendix B (Figures B.1 through B.16).

The observed phenomena discussed below will include (1) the distribution of the concrete strains along the column face and along the slab centerline, (2) a reversal of the concrete strains observed at all gaged locations on the slab except at some locations adjacent to the column face on the specimen centerline, and (3) the distribution of the vertical load near the base of the stub column.

6.6.1 S2000 Series. Concrete strains were measured only near the column face on the column (compression) side of the slab for the specimens with the 10-inch column size.

Maximum concrete strains (Figure 6.8) at the centerline were substantially larger than at the column corners and were above  $2000 \times 10^{-6}$  at one or more faces of each specimen. The maximum concrete strain measured was  $2650 \times 10^{-6}$ , which is below the limiting compressive strain for unconfined concrete. The magnitude and distribution of the maximum concrete strains were not clearly different for the specimens with different flexural reinforcement ratios.

Figure 6.9 shows the strain history as a function of column deflection. The strains along the centerlines were normally slightly larger than the corner strains at low load levels and did not reverse strain direction until very near the maximum load, if at all.

For the S2150 specimens, the strains at the column centerline increased nearly linearly with the deflection. Several gages in the specimens with the higher reinforcing ratio showed increasing compression until failure, while several in the specimens with the smaller reinforcement ratio quickly moved from a compressive strain of over  $2000 \times 10^{-6}$  to or near a tensile strain in the final seconds before failure. Concrete strains at failure near the corners were from 0 to 60 percent of the maximum strain recorded by the gage in the more lightly reinforced slabs. Lesser amounts of reversal were seen with the more heavily reinforced slabs, especially in Specimen S2150-2.

The strains near the column corner reached a maximum at a column deflection of 0.5 to 0.6 inch for all S2000 Series specimens.

6.6.2 S4000 Series. The concrete-strain distribution measured along the centerline of the S4000 Series specimens are shown in Figure 6.10 at various loads up to the load at which the strains began to reverse. As should be expected, the strains increased as the column face was approached.

Large reversal of the concrete strains were measured at locations away from the column face. (See Figure 6.11 which compares the strains measured on the west side of the column with the center deflection.)

The strains away from the column face, C1 through C4 and C7 through C10, consistently reached their maximum values at the same time and at a center slab deflection of approximately 0.6 inch for the S4150 Specimens and 0.7 inch for the S4075 Specimens (Figure 6.11). The strains decreased quite steadily with increasing deflection until near failure. A significant strain decrease was seen even at 20 inches from the column face.

The extent of this strain reversal and its consistent occurrence at a deflection at which yielding appeared to be spreading throughout the slab strongly suggests that this phenomenon is not related to the shear response of the connection, but rather to the flexural behavior of the slab.

Comparison of the three strains measured along the east face (C5, C11, and C12) shows that the strains consistently reversed first nearer the column corners for both reinforcement ratios.

As shown by Figure 6.12 for the more lightly reinforced specimens and in Figures B.14 and B.15 for the S4150 Specimens, the strain 9 inches from the centerline (C12) reversed first and at about 90 percent of the maximum load, then decreased before failure to near one-third of its maximum value. This gage recorded only small changes during the final seconds before failure. The strain at C11, located 4-1/2 inches from the centerline, decreased

at near the maximum load and usually slightly before the gage at the centerline.

Comparison of the concrete strains measured by Gages C12, C11, and C5 indicates that the failures were progressive and originated at the column corners, a hypothesis consistent with the observed pattern of the crack openings discussed in the previous section and with the strains measured on the column.

The vertical strains on the column face and at the centerline (C13) were small, under  $60 \times 10^{-6}$ , throughout most of the loading history and tensile for all specimens except Specimen S4150-1 (Figures B.10, B.12, B.14, and B.16). Near or at the maximum load, the strain measured at this location moved in the compressive direction. The compressive strain measured 1 inch from the column corner (C14) decreased significantly prior to failure. Thus, near failure, the load coming down the center of the column face increased while that at the corner decreased.

The strains measured on the column also show the highly uneven distribution of the load transferred by the connection. The column load was very highly concentrated at the column corners. The maximum vertical strains measured near the corner of the column (C14) of the S4075 connection correspond to stresses of 1900 to 2100 psi. This stress over the entire column area would produce a column load of 760 to 840 kips, over ten times the actual applied load. This concentration of load at the column corners and the tension at the column face both are reasonable when the bowl-like deflected shape of the slab as tested is considered. The slab attempts to deflect least relative to the supports at the column corners; a column unattached to the slab would be in contact with the slab only at the column

corners. The slab, in attempting to retain a doubly-curved shape throughout, tries to separate from the column at the column centerline, and tensile stresses result.

The experimental results show that the column load, and therefore the shear transfer, is initially concentrated at the corner of the column. Before the connection failure, the resistance of the connection in this region decreases. The column load, following the remaining resistance, shifts away from the corner and towards the center of the column face.

The assumed nominal shear distribution ( $v = V/bd$ ) is very much an idealization not only of the distribution throughout the slab depth, but also of the distribution around the critical section, at least for rectangular columns.

## 6.7 STEEL STRAINS

The locations of the strain gages on the reinforcement are shown in Figures 4.14 through 4.17. The strains measured are plotted as a function of applied load in Figures B.2 through B.16.

6.7.1 S2000 Series. The 16 strain gages of the S2000 Series specimens, all placed on the reinforcement either at or 5 inches from the column face, showed little strain until the slab began to crack, then indicated a steady increase until yielding was reached near the column face. The steel strains then increased rapidly or stabilized at or slightly below the yield strain of  $1700 \times 10^{-6}$  depending on the proximity of the gage to the circumferential flexural crack following the column outline. Yielding was reached before the flattening of the load-deflection curve identified as the start of significant yielding in Figure 6.1. No unusual behavior was detected near failure.

Several of the steel strain traces, while appearing valid, showed unexplainable and unrealistic variations, especially during the test of Specimen S2150-1. These variations may have resulted when one of the two strain gages at each location became damaged.

6.7.2 S4000 Series. The gage configuration was changed for the S4000 Series to ten gages placed on one reinforcement bar located under the line of concrete gages.

The distribution of the steel strains along the instrumented bar is shown in Figure 6.13 for two tests. At the higher load levels, the strains at 10 inches from the column were consistently higher than at 5 inches out for the S4075 Specimens, suggesting that more cracking activity existed at the former location. Strains along the gaged bar of Specimen S4150-2 did not increase as rapidly as the column face was approached as was expected from the calculated elastic moments.

As shown in Figure 6.14, the rate of straining decreased with increasing slab deflection after a deflection of about 0.3 inch was reached. The magnitude of the strains then often stabilized or decreased slightly, especially in the more lightly reinforced slabs. These events are attributed to the moment distribution associated with the formation of the flexural yield-line pattern, a topic discussed later in this chapter. Even with large deflections, yielding strains were measured only near the column face. Gages S4 and S7, located 5 inches from the column face, often recorded strains of  $1500 \times 10^{-6}$  but seldom indicated significant yielding.

The observed steel strains are plotted against the corresponding concrete strains at the same location in Figures 6.15 and 6.16. The results are much more irregular than was expected. The slope increase in the

curves at Locations 3, 4, and 7 of Specimen S4075-1 may indicate the presence of diagonal cracking. The downturned tail of the concrete strain versus steel strain curves results from the decrease in the concrete strain near the ultimate load and the decreased rate of the reinforcement straining. The steepness of Curves 5 and 6 of Specimen S4150-2 may result from stress concentrations in the compression zone near the column.

A sudden increase of Strains S8, S9, and S10 of Specimen S4075-1 (Figure B.10) was recorded in the final seconds before failure, a time of great interest in studying the connection behavior.

## 6.8 FAILURE OF THE CONNECTION SPECIMENS

The use of continuous recording equipment for the static tests provided the opportunity of examining the gage readings throughout the final few seconds before failure and the interaction of the various measured quantities throughout the entire test. Much can be determined about the failure mechanism of these specimens by examining these records, especially for the S4000 Series specimens.

6.8.1 S4075 Specimens. For Specimen S4075-1, the influence of the opening of the inclined cracks near the corner (D6 and D7) can be observed in the traced records (Figures B.17, B.18, and B.19). The concrete strains away from the column face on the same side of the column (C8, C9, and C10) began a more rapid decrease and the strain near the column face (C6) increased simultaneously with the opening of the corner crack. The opening of the corner cracks appeared to hasten the concrete strain decrease throughout the slab and increased the compressive strain at the center of the column face.

When the inclined crack opened at the west column face (D8 and D9) 3 seconds prior to failure, the deflections increased and the resistance dropped as noted in Section 6.4. Also at this time, there was a rapid increase in the compressive concrete strain on the slab west of the column (C7 through C10). The corresponding steel strains registered sudden increases in tension. The concrete strain at the west column face (C6) dropped rapidly to near zero while the concrete strains along the centerline east of the column moved rapidly in the tensile direction.

This evidence points to the following failure mechanism for Specimen S4075-1. The slab failed first at the corners, and the shear capacity of these regions was lost. Failure of the entire connection followed later and started when the inclined crack at one face, the west face in this case, opened and propagated to the compressive surface, rendering the slab area adjacent to this column face ineffective in transferring the load. The column then tilted slightly toward the west, increasing the moment carried in the slab to the west of the column and reducing it to the east. Some slight tilting of the column was possible with the test setup used and was observed, although not measured. The crack pattern for this specimen (Figure 5.7a) also suggests that the column tilted toward the west (the right side of the photograph). Punching followed as the areas remaining to transfer the shear were unable to do so and the formation of the crack forming the failure cone was quickly completed.

In the records of Specimen S4075-2 (Figures B.20, B.21, and B.22), a very definite decrease in the concrete strain away from the column (C8, C9, and C10) began simultaneously with the opening of the cracks in the adjacent corner (D6 and D7).



No opening of the inclined crack near the west column face (D8 and D9) was recorded before failure. This indicates that the failure of this specimen began at another column face, very probably by an inclined crack opening near the east column face 4 seconds before failure. At this time, the concrete strains along the centerline of the east side of the slab began to move in the compressive direction and the strains at the east column face were very low. Simultaneously, the concrete strains on the west half of the slab moved rapidly in a tensile direction. This pattern is nearly identical with that accompanying the opening of the cracks along the west column face of Specimen S4075-1.

6.8.2 S4150 Specimens. The failure mechanisms for the S4150 Specimens are less clear. For Specimen S4150-1, initiation of failure appeared to be neither at the east nor at the west face (Figures B.23 and B.24). No crack opening was detected at the west column face prior to failure, and the concrete strains along the centerline were all moving in a tensile direction. Gage C13 showed increasing load coming down the center of the east face immediately before failure, and C11 measured a sudden drop in compressive strain 4-1/2 inches from the centerline, a drop probably indicating that the inclined crack had propagated to the surface at that location.

For Specimen S4150-2, the concrete gages away from the column (Figures B.25, B.26, and B.27) also all moved rapidly toward tension immediately before failure at both sides of the column. A sizable increase in the inclined cracking width was detected near the west column face at about 1/4 second prior to failure (Figure 6.7b), but it is unclear whether the final failure initiated at that face.

Changes were noted in a number of traces at the time of the sudden decrease in strain registered by Gage C12, located on the slab surface near the southeast corner of the column, an event associated with at least a partial failure of that corner of Specimen S4150-2. The load coming down the corner (measured by C14) dropped and the strain at the column face 5-1/2 inches from the corner (C11) began a more rapid increase. A distinct increase in the strain rates of Gages C2 and C3 also took place.

Four seconds prior to failure, the strain at C11 reversed at a rate which became very rapid immediately before failure, at which time C13 and C14 showed another pronounced increase in the portion of load coming down the center of the column face, further indicating that failure of the column face section takes place last at the centerline.

## 6.9 COMPARISON OF MEASURED AND PREDICTED QUANTITIES

6.9.1 Flexural Strength. The flexural strength of the test slabs can be calculated from the yield-line theory. The appropriate yield-line pattern for the slabs tested, the pattern compatible with the physical restraints on the slab and predicting the smallest capacity, is that shown in Figure 6.17 (Elstner-Hognestad, 1956). The location of the corner levers is chosen to minimize the predicted strength obtainable with the yield lines originating from the corners of the column.

The flexural strength predicted by the yield-line theory is:

$$V_{\text{flex}} = 8m \left( \frac{1}{1 - \frac{r}{a}} - 3 + 2\sqrt{2} \right) = 8m \left( \frac{1}{1 - \frac{r}{a}} - 0.1716 \right) \quad (6.1)$$

Where:  $m$  = unit moment capacity of the slab

$r$  = column side dimension

$a$  = slab span

$$m = \rho f_y d^2 \left( 1 - 0.5 \frac{\rho f_y}{f'_c} \right) \quad (6.2)$$

Where:  $\rho$  = reinforcement ratio

$f_y$  = yield strength of the reinforcement

$d$  = effective slab depth

$f'_c$  = concrete compressive strength

The location of the yield lines forming the corner levers is at  $\left( 1 - \frac{\sqrt{2}}{2} \right) (a - r) = 0.293 (a - r)$  from the corners. These corner levers rotate about the  $x - x$  axes shown in Figure 6.17 causing the corners of slab to lift from the supports.

The predicted and actual yield-line patterns for two specimens reaching general yielding are compared in Figure 6.18. The predicted pattern formed in all the more lightly reinforced specimens.

Yield-line theory assumes that the slab segments bounded by the yield lines remain plane. Thus, the quarterpoint deflection is one-half the column deflection. The corners of the idealized yield-line structure rise 0.293 times the column deflection.

As shown in Figure 6.3, the measured quarterpoint deflection for Specimen S2075-2, a lightly reinforced slab, approached one-half the column deflection. The observed corner rise was slightly less than that predicted by the yield-line model for all three slabs included in Figure 6.3.

The predicted flexural capacities are compared with the observed capacities of the statically tested connections in Table 6.2. The dead load of the test specimens has been neglected in the calculations. Calculations not reproduced here showed that the inclusion of the slab and the stub column dead load would reduce the predicted applied column load capacity by

approximately 1050 and 1600 pounds for the smaller and larger column size, respectively, and would move the calculated yield-line locations by 0.06 to 0.13 inch.

The yield-line analysis predicted the strength of the four lightly reinforced ( $p = 0.0075$ ) specimens very closely, the average ratio of the observed to predicted value being 0.991.

Slab strength is commonly above the values calculated by the yield-line analysis because of the effects of (1) compressive membrane action at low slab deflections resulting from edge restraint or support friction, (2) strain hardening of the reinforcement, (3) tensile membrane action accompanying large slab deflections, and (4) extension of the slab past the supports. These effects were small in the connection tests. The largest deflection before failure was 28 percent of the slab thickness, insufficient to develop appreciable tensile membrane action. The long, flat-topped yield region of the reinforcement stress-strain curve indicates that the strain hardening region should not have been reached, and the roller supports minimized the support friction which is necessary for substantial compressive membrane action. The coefficient of rolling friction for steel on steel is very small, approximately 0.006 (Meriam, 1966, p. 311).

The more heavily reinforced specimens reached 82 and 88 percent of the yield-line capacities for the smaller and larger column size, respectively.

6.9.2 Shear Strength. The observed strength of the eight statically tested specimens included in this project are compared with the capacities given by many of the existing expressions for predicting the shear strength of slab-column connections in Tables 6.3 and 6.4.

The equations of Kinnunen-Nylander (1960) and Kinnunen (1963) are

directly applicable only to circular columns and slabs. The values necessary for their equations were determined, as detailed in Appendix D, by assuming a circular column and slab with perimeters equal to those of the specimens tested. The capacities given by the equations of Kinnunen-Nylander were increased 10 percent as recommended for connections containing two-way reinforcement.

Before discussing these results, it must be noted that the applied load, and consequently the shear capacity, of the more lightly reinforced specimens was limited by the flexural capacity of the slab. Because the rotation of the slab edges was not restrained, there was little increase in load after general yielding was reached in the slab. These four tests may be considered ductility or performance tests of slab-column connections with the strength of the connection controlled primarily by flexure.

These connections were generally predicted to fail in flexure, and did in the sense that general flexural yielding was reached in the connection area. For purposes of limit design and protective shelter use, where the criterion of failure is the strength of the structure and large deflections may be allowed, these connections did not display adequate ductility or rotational capacity to allow full moment redistribution and possible development of membrane stresses. For these purposes, the connections failed prematurely in shear. Simply attaining general flexural yielding in the areas of the connection is of secondary importance when large deflections of the structure containing the connection are acceptable.

Specimens with  $p = 0.0075$ . The test results of the lightly reinforced specimens demonstrate very clearly that the mere prediction of a shear capacity above the flexural capacity of the specimen guarantees

neither that a punching shear failure will be prevented nor that the connection will have an adequate rotational capacity.

The calculated shear capacities of the specimens with the smaller reinforcement ratio (Series S2075 and S4075) exceeded the observed strength with the exception of the values predicted by the methods given by Kinnunen-Nylander and Kinnunen (Table 6.4). Whitney's method (Table 6.3) also indicated a lower strength than that observed for the S2075 Specimens. The overprediction of connection strength by most methods should be expected because the flexural capacity limited the loads carried by these specimens. Nor is it unexpected that the methods of Kinnunen-Nylander, Kinnunen, and Whitney are closest to the test results since these methods give considerable weight to the flexural strength of the slab.

Several of the expressions for shear strength, notably those of Moe and Elstner-Hognestad, are expressly stated to be applicable only if the value of  $\phi_o$ , the ratio of the shear strength to the flexural strength, is one or less.

The important point for the specimens with  $p = 0.0075$  in Table 6.3 is that slab-column connections may ultimately fail as a result of punching shear at less than 60 percent of the shear strength predicted by several of the methods (Equations 2.3, 2.6, and 2.20 for the S4075 Series) if extensive flexural yielding and subsequent rotation develops in the connection area.

No shear-strength theory predicted the flexural-shear capacity more closely than did the yield-line formula for flexural capacity.

Specimens with  $p = 0.0150$ . All the shear-strength equations are applicable for the more heavily reinforced ( $p = 0.0150$ ) connections.

Equations 2.6, 2.13, and 2.20 should underestimate the connection strength as these three are intended to be lower-bound equations suitable for design and do not include the beneficial effects resulting when the flexural strength exceeds the shear strength. Equations 2.17 and 2.18 are primarily intended for use with lightweight aggregate concrete, but should also be valid for normal weight concrete. Equations 2.3 and 2.5 were derived from test data with  $r/d$  values smaller than 4 and would be expected to be more successful for the specimens with the smaller columns.

The strengths of the connections with a 10-inch column were within 5 percent of that predicted by Equations 2.3 and 2.5.

The capacities of the S4150 Series were overestimated at least 7 percent by all equations except by Equation 2.13 and by the methods of Kinnunen-Nylander and Kinnunen (Table 6.4). These three methods underestimated the connection strength by a maximum of 8 percent.

All of the equations became less conservative with the larger column size, especially Equations 2.3, 2.4, 2.13, and 2.20. These four were 25 to 30 percent less conservative at the larger column size. Moe's equation, using either the concrete compressive strength (Equation 2.5) or the splitting strength  $f_{sp}$  (Equation 2.17) best followed the change in strength with the column size change and also best predicted the connection capacities. The average ratio of test to calculated values were closer with Equations 2.6 and 2.10, but there was considerable more variance with column size. Equations 2.12 and 2.18 consistently overestimated the connection strength.

Comparison of the Test Results with the Methods of ACI 318-63. The observed unit shears at the column face for all the statically tested

specimens are compared with the unit shears predicted by the 1963 ACI Code (Equation 2.20 of this report) in Figure 6.19. Table 6.5 lists the nominal unit shear strengths for critical sections located at the column face and at  $d/2$  from the column face. The latter is the critical section used by Equation 2.20. This equation, using a critical section at the column face and  $\phi = 1.00$  becomes:

$$v_u = \frac{V_u}{bd} = 4 \left( 1 + \frac{d}{r} \right) \sqrt{f'_c} \quad (2.8)$$

From Figure 6.19, the decrease in unit shear strength with increasing  $r/d$  values is seen to be much higher than that predicted by the ACI Code. The S4150 connections failed at 92 percent of the value predicted by this design equation, while the two S2150 connections failed considerably (34 percent) above the ACI Code provisions (Table 6.3).

The test results add to the evidence shown in Figure 2.5 that the decrease in unit shear strength is greater with increasing  $r/d$  ratios than that given by the ACI Code provisions and that a majority of the limited number of normal weight concrete connections tested to date with  $r/d$  values of 4 or more have tended to fail below the ACI Code provisions.

As mentioned in Chapter 2, the ACI Code accounts for the influence of the  $r/d$  ratio by using a critical section away from the column face, thereby increasing the critical section less rapidly than the column perimeter. To account for the  $r/d$  effect shown by the connections with  $p = 0.0150$ , such a section would have to be located at  $3.05d$  from the column face instead of at  $d/2$ . A 100 percent increase in the column perimeter (from 40 to 80 inches) increased the connection capacity only by an average of 28 percent, even with 20 percent stronger concrete in the



connections with the larger columns. The strength added by the additional 10 inches at each column face with the 20-inch columns is equivalent to a unit shear of  $1.97\sqrt{f'_c}$  acting on this added perimeter.

The S4150 connections were more highly stressed in flexure ( $\phi_o = 0.88$  versus  $\phi_o = 0.82$  for the S2150 connections) than the S2150 connections. If Moe's equation (Equation 2.5) is used to project the test results to a common  $\phi_o$  value, a critical section 2.10d from the column face is found necessary to account for the r/d effect, still an extreme location.

The fallacy of assuming that connections weak in flexure will not fail in shear unless the capacity given by the ACI Code equation is somehow approached is clearly shown in Figure 6.19 by the points representing the flexural-shear failures of the connection specimens with  $p = 0.0075$ .

The 1963 ACI Code equation was derived to be applicable at a  $\phi_o$  value of one (ACI-ASCE, 1963). Because of the favorable interaction of shear and flexural strength, the ACI Code equation should be less conservative for connections with a  $\phi_o$  greater than one (connections with a calculated flexural strength below the shear strength), the condition encouraged by the ACI Code.

6.9.3 Deflections and Stiffnesses. The deflection, or rotation, capacity of slab-column connections has not received great attention in the literature.

As noted in Chapter 2, several researchers have observed that even most "flexurally controlled" connections will eventually be destroyed by the column punching through the slab. The lack of information about the ductility of these connections failing in flexural-shear might be interpreted as implying that adequate rotational capacity in the connection

exists and the final punching shear failure is not of practical interest. This is not so.

Predictions of the rotation of the slab outside of the column are obtained as an intermediate step in the lengthy shear capacity analysis of Kinnunen-Nylander (1960) and Kinnunen (1963). The expressions of Kinnunen were obtained specifically for two-way reinforced connections and those of Kinnunen-Nylander for the stiffer ring reinforcement pattern.

The rotations predicted by both of the above methods as well as the observed values are included in Table 6.4. The rotations computed by Kinnunen's method are of the proper magnitude for both reinforcing ratios. The increase in ultimate deflection with increasing column size was not as large as that predicted.

The stiffnesses of the connection area can be calculated approximately using medium-thick plate theory.

As an alternative to analyzing the case of a square slab with its corners free to rise and loaded by a square column, a difficult problem to solve, the slab-column connection geometry may be approximated by an axially symmetric circular shape.

The slab-column connections described in this report were idealized as simply supported circular slabs of radius  $a$  and loaded by a centrally located rigid cylinder with radius  $b$  and fixed to the slab. The deflection of such a slab, for a Poisson's ratio of zero (Roark, 1965), is:

$$y = \frac{P}{16\pi D} \left[ \frac{3a^4 - b^4 - 2a^2b^2 - 8a^2b^2 \ln \frac{a}{b} - 4a^2b^2 \left( \ln \frac{a}{b} \right)^2}{a^2 + b^2} \right] \quad (6.3)$$

Where:  $y$  = deflection of the stiff cylinder relative to the supports

$P$  = applied load

$D$  = flexural rigidity =  $EI$  per unit width

$E$  = modulus of elasticity

$I$  = moment of inertia

The column and slab diameters have been chosen to retain the actual slab and column perimeters.

The calculated stiffnesses  $K = P/y$  are shown superimposed on the observed load-deflection curves in Figure 6.20. The stiffnesses resulting with an uncracked section ( $I = I_{\text{gross}}$ ), a fully cracked section ( $I = I_{\text{cr}}$ ), and a partially cracked section [ $I = I_a = 1/2(I_{\text{gross}} + I_{\text{cr}})$ ] are shown.

The stiffness of the connection specimens before cracking was usually very close to that predicted using the gross slab section, as it should be.

The average stiffness of the specimens up to the start of the yielding of the reinforcement was satisfactorily given by assuming a fully cracked section. The stiffnesses calculated with the cracked section averaged 85 percent (ranging from 74 to 107 percent) of the stiffnesses of the fitted elastoplastic load-deflection curves (see Figure 6.2 and Table 6.1).

Thus, a bilinear resistance function reasonably representing the connection specimen behavior can be obtained by using an elastic portion with the stiffness computed from Equation 6.3 (assuming a fully cracked section) extending up to the connection capacity followed by a plastic segment (stiffness equal to zero).

The observed ductilities of the statically tested specimens using the elastoplastic curve described above are tabulated as follows. The yield deflections are calculated as the test capacity divided by the stiffness from Equation 6.3.

Specimen	Yield Deflection	Ductility	Specimen	Yield Deflection	Ductility
	inches			inches	
S2075-1	0.462	2.66	S4075-1	0.510	3.53
S2075-2	0.434	3.04	S4075-2	0.491	2.69
S2150-1	0.440	1.39	S4150-1	0.513	1.58
S2150-2	0.417	1.29	S4150-2	0.514	1.40

The ductilities determined in this manner are lower and more consistent within duplicate tests than those obtained from the curves of Figure 6.2.

#### 6.10 AN EXAMINATION OF SLAB-COLUMN CONNECTION BEHAVIOR

The behavior of slab-column connections has not yet been adequately explained. The test results of this investigation have added to the evidence that this behavior is indeed complicated. In this section, the behavior of the connections is examined from a more theoretical viewpoint. Both explanations for some of the behavior and difficulties precluding an exact analysis of the problem at this time are discussed. Differences between beam and column connections are presented, and the flexural behavior at all stages of loading is examined. An explanation is offered for the reversal of concrete strains measured near failure on the slab portion of the connection specimens. The effects of column size, column shape, and other variables on the shear strength are discussed.

##### 6.10.1 Current Concepts of Connection Behavior. The behavior of

slab-column connections in shear has often been compared to shear in beams with certain beneficial conditions added or assured which explain the higher unit shear strength at the face of the column.

The three main beneficial effects added or assured in slab-column connections are:

1. The inclined, or shear, crack must occur near the column face; sections farther from the column have a larger perimeter and are thus less critical. In a beam, the width of all sections is the same and the shear crack is thereby freer to move away from the point of loading.

The crack location near the column precludes a diagonal tension, or instability, failure. A stable inclined crack forms near the column, creating a three-dimensional tied arch. Failure takes place at a higher load and when the concrete in the compression zone over the truncated conical crack becomes overstressed.

Because the inclined crack does not lead to immediate instability, the failure load and not the cracking load may be safely used in the design of connections, while the inclined cracking load must ordinarily be considered the ultimate useful capacity of beams of normal proportions.

2. The bending of the slab in both directions results in the compression zone of the concrete above the shear crack being compressed in the circumferential direction also. This lateral support, also called slab action or the biaxial effect, has been credited with substantially increasing the strength of the compression zone and thus the connection capacity. Kupfer, et al. (1969), report, however, that the strength increase of concrete loaded with equal biaxial stresses over that of uniaxially stressed concrete is of the order of 15 percent, certainly not a large increase.

3. The location of the compression zone immediately adjacent to the column face insures that the vertical compression resulting from the dispersion of the column load into the slab, comparable to the vertical stresses in the soil near a column footing, acts over much or all of the critical compression zone, further confining the concrete above the inclined crack and increasing its strength.

6.10.2 Comparison of Beam and Column Connections. The additional dimension added to the beam shear problem by the slab-column connections introduces a number of important differences in addition to those mentioned in Section 6.10.1. These differences play a significant role in explaining the behavior of the connections. They also warn against merely cutting out a strip of the connection and analyzing it as a modified beam.

Three differences and the resulting implications follow.

1. Lack of Symmetry. Only for the case of round columns on round slabs containing ring reinforcement is the slab-column connection axially symmetric. With either two-way reinforcement or square columns, cases including almost all connections of interest, axial symmetry does not exist and there is no one typical section.

Different locations around the column should be expected to crack at different times, carry different loads, and fail at different times and at different capacities.

The capacity of the slab-column connection is not necessarily the sum of the strengths of all the sections around the perimeter: the failure can be progressive. Some sections may fail before others reach their ultimate capacity.

2. Different Moment Distribution. The moment distribution in slabs

is more complex and unlike that of beams. The introduction of tangential moments, corresponding to moments which would act along the sides of a beam, greatly alters the moment distribution and crack pattern of slabs from that of a beam strip.

In the slab of a connection with a small column, the main cracking in the slab is along radial lines, not in the circumferential direction except at the column face. This can be seen from the yield-line pattern of a circular slab with a circular column (Figure 6.21). Square slabs with small columns develop roughly the same radial crack pattern (Figure 6.17). Obviously, no such radial cracks can form in a beam. It will be shown later that the tangential moments exceed the radial moments throughout nearly all of the slab even for the elastic range, and thus cracking should be mainly in the radial direction.

A most important consequence of the flexural behavior is that the inclined, or shear, cracks in a slab form at right angles to the main flexural crack pattern. Therefore, inclined cracking is less likely to develop from a flexural crack in a slab than in a beam.

The mechanism of inclined crack opening in slabs also differs from that in beams. The inclined cracks do not necessarily open rapidly, and the stress in the reinforcement crossed by the crack need not increase rapidly after cracking as it does when a tied-arch geometry forms in a beam.

The slab can and does carry moment in the tangential direction. The deflection of the slab which must follow from the rotation resulting from any shear crack opening is possible only if the tangential strains and therefore the tangential moments increase. Such an increase can occur only with increasing load.

Thus, unlike a beam, in which the inclined cracks usually develop from flexural cracks and can open widely soon after their formation, the inclined cracks in a slab often form at uncracked sections and are restrained from opening by the stiffness of a slab in a tangential direction. Increasing amounts of flexural reinforcement in a slab can increase the shear strength by the same mechanisms as those operating in a beam and by increasing the tangential stiffness of the slab, thereby offering further control of the crack width and propagation.

3. Inadequacy of Statics. The equations of statics alone are not sufficient to determine the forces at and above the shear crack of a slab.

For a beam, the total compression in the concrete zone above the crack must necessarily equal the force in the steel at the location where the inclined crack crosses the steel, i.e.  $C = T$  in Figure 6.22a, if support friction and any horizontal component of the interlocking forces along the crack are neglected. This follows not from the equilibrium of the section inside the shear cracks, but from the requirement of horizontal equilibrium on the portion shown to the right in Figure 6.22a.

For the slab-column connection, it does not follow that  $C_1$  and  $T_1$  shown in Figure 6.22b (the concrete compressive force and steel tensile force, respectively, acting on the column area) are equal. The horizontal equilibrium for the failure cone gives  $T_1 - C_1 = T_1 - C_1$ , a trivial equation placing no restriction on  $C_1$ . Equilibrium of half the slab outside of the column area requires only that  $C_1 + C_2 = T_1 + T_2$ , i.e. the total horizontal steel force across the entire slab equals the entire horizontal concrete force across the slab (again disregarding any horizontal forces acting at the supports or slab edges and any net horizontal forces from



interlocking along the inclined crack). No unique restriction of the value of  $C_1$  is given by statics; statics can be satisfied even if  $C_1$  or  $C_2$  is zero. Compatibility must also be employed to determine the value of  $C_1$ .

As the inclined crack of the slab enters the compression zone and/or when the concrete above the inclined crack is stressed above its linear range, the total stiffness of the concrete above the crack is reduced and proportionately more of the compression forces will be carried by the areas away from the column face. The force  $C_1$  is controlled and the resulting concrete compressive stress limited by the stiffness of the area remaining above the inclined cracks. This "compression release mechanism" has major ramifications in determining the crack geometry and the final failure of the concrete above the inclined crack.

Horizontal compression is needed to turn the inclined crack orientation toward the horizontal. A progressive decline in compressive force (not stress) above the crack with crack propagation upward would make the unchecked propagation of the crack entirely through the section much more likely than in a beam.

If the inclined crack does turn and a distinct and stable compression zone forms above the crack, the limitation of the compression stresses without a mechanism to limit the shear stresses may result in the concrete above the crack truly failing in shear, not primarily in compression.

6.10.3 Moments in an Idealized Connection. The development of the inclined cracking leading to a shear failure is critically influenced by flexure. For this reason, the flexural moments acting in the slab will be explored.

The moment distribution in the slab at various levels of flexural action will be examined using the idealized case of a round slab with a round column at its center. Medium-thick plate theory (with homogeneous and isotropic materials) will be used except where otherwise noted. A Poisson's ratio of zero will be assumed. A connection with a 5-inch-radius column and a 40-inch-radius slab will be examined unless otherwise stated.

First Cracking. Initially, the connection will behave elastically and as a slab with a fixed column located at the center.

The moments for this case (Timoshenko and Woinosky-Krieger, 1959, pages 58-61) are:

$$M_r = -\frac{a^2 b^2}{a^2 - b^2} M_1 \left( \frac{1}{a^2} - \frac{1}{r^2} \right) - \frac{P}{4\pi} \left[ \ln \frac{r}{a} + \frac{\ln \frac{a}{b}}{a^2 + b^2} \left( b^2 - \frac{a^2 b^2}{r^2} \right) \right] \quad (6.4)$$

$$M_t = -\frac{a^2 b^2}{a^2 - b^2} M_1 \left( \frac{1}{r^2} + \frac{1}{a^2} \right) - \frac{P}{4\pi} \left\{ \ln \frac{r}{a} - 1 + \ln \frac{b}{a} \left[ \frac{b^2}{a^2 - b^2} + \frac{a^2 b^2}{r^2 (a^2 - b^2)} \right] \right\} \quad (6.5)$$

Where:  $M_r$  = radial moment, moment acting on a section of constant radius

$a$  = radius of the slab

$b$  = radius of the column

$M_1$  = radial moment at the column face

$r$  = radius at which  $M_r$  and  $M_t$  are computed

$P$  = load applied on the column

$M_t$  = tangential moment, moment acting on a radial line

$$M_1 = \frac{P}{4\pi \left( \frac{a^2}{b^2} + 1 \right)} \left[ \left( \frac{a^2}{b^2} - 1 \right) + \frac{2a^2}{b^2} \ln \frac{b}{a} \right] \quad (6.6)$$

These moments are plotted in Figure 6.23.

By far the largest elastic moment is the radial moment at the column face. First cracking occurs at that location. The radial moments decrease rapidly away from the column face and are smaller than the tangential moments further than 7-1/2 inches from the column face.

With the first cracking, the slab is no longer homogeneous and plate theory becomes approximate.

First Yielding. To examine this level of flexural behavior, the inexact assumptions will be made that all sections have cracked and that a uniform slab stiffness exists throughout the slab in all directions. With these assumptions, Equations 6.4, 6.5, and 6.6 are again applicable.

First yielding is predicted to be at the column face and occurs when  $M_r$ , the radial moment, reaches  $m$ , the unit flexural capacity of the slab. The load at first yielding is  $m/0.4030 = 2.48m = P$ .

At yielding around the column face, the radial stiffness at this location is destroyed. Increments of load above that causing first yielding effectively act on a slab with a hole in the middle, the load being applied to the perimeter of the interior hole.

For this condition, the following formulas apply (Timoshenko and Woinowsky-Krieger, 1959, pages 52 and 59):

$$\Delta M_r = -\frac{\Delta P}{4\pi} \left[ \ln \frac{r}{a} + \frac{b^2}{a^2 - b^2} \left( 1 - \frac{a^2}{r^2} \right) \ln \frac{b}{a} \right] \quad (6.7)$$

$$\Delta M_t = -\frac{\Delta P}{4\pi} \left[ \ln \frac{r}{a} - 1 + \frac{b^2}{a^2 - b^2} \left( 1 + \frac{a^2}{r^2} \right) \ln \frac{b}{a} \right] \quad (6.8)$$

Where:  $\Delta M_r$  = increment of radial moment

$\Delta P$  = load increment

$\Delta M_t$  = increment of tangential moment

The distribution of these moments is shown in Figure 6.24.

The additional load applied after yielding is reached around the column is primarily supported by additional tangential moments. The radial moments, especially in the inner half of the slab, increase much less rapidly than before first yielding.

Start of Radial Yielding. The tangential moments will increase until the yield moment is reached next to the column face.

At this time, the connection may be analyzed as a solid slab with a ring load at the column face. This satisfies the condition that, at the column face,  $M_r = M_t = m$  at this load level. Equal stiffness throughout the slab again must be assumed.

The radial and tangential moment distributions at the time the tangential moment first reaches yielding are shown in Figure 6.25 and are given by the following equations (Timoshenko and Woinowsky-Krieger, 1959, pages 63 and 64):

$$M_r = -\frac{P}{8\pi} \left( 1 - \frac{a^2 - b^2}{a^2} - \frac{b^2}{r^2} + 2 \ln \frac{r}{a} \right) \quad (6.9)$$

$$M_t = -\frac{P}{8\pi} \left( -1 - \frac{a^2 - b^2}{a^2} + \frac{b^2}{r^2} + 2 \ln \frac{r}{a} \right) \quad (6.10)$$

The tangential moments are considerably larger than the radial moments, more so at larger radii.

The load at this level is  $m/2.046 = 4.89m = P$ .

Completion of the Yield-Line Pattern. The yield-line pattern is completed when the radial yield lines extent to the edge of the slab forming the pattern shown in Figure 6.21.

At this load level, all the forces acting on a slab sector are known. The load capacity and the radial moment distribution may be obtained from statics only.

A free-body diagram of one of  $n$  identical pie-shaped sectors assumed to form around the slab is shown in Figure 6.26a. No shears or twisting moments act along the radial lines because of symmetry. The number of segments is assumed to be large enough that small angle approximations can be used.

Moment equilibrium about the support gives:

$$\frac{P}{n} (a - b) = \frac{2\pi r b}{n} + \frac{2\pi m}{n} (a - b) \quad (6.11)$$

or, simplified

$$P_{yl} = 2\pi m \left( \frac{a}{a - b} \right) = \text{yield-line flexural strength} \quad (6.11a)$$

For a slab with  $a = 40$  inches and  $b = 5$  inches,  $P_{yl} = 7.18m$ .

The radial moment distribution is determined simply by the moment equilibrium equation about point A shown in Figure 6.26b. This equation is:

$$\frac{2\pi}{n} \left[ M_r r + m \left( \frac{a}{a - b} \right) (r - b) - mr \right] = 0 \quad (6.12)$$

which reduces to

$$M_r = \frac{m}{r} \left[ \frac{b(a - r)}{a - b} \right] = \text{unit radial moment} \quad (6.12a)$$

The resulting distributions of  $M_r$  and  $M_t$  at completion of the yield lines are shown in Figure 6.27. The tangential moment  $M_t$  equals the ultimate unit moment  $m$  at all radii, as required for the yield lines

to form. The radial moment  $M_r$  drops very quickly away from the column face, being 0.25m and 0.50m at only 9.7 and 3.9 inches, respectively, away from the column face.

The unit shear distribution plotted in Figure 6.27 is the same at all loading levels and is found simply from geometry:

$$v_r = \frac{b}{r} v_b = \frac{P}{2\pi r} \quad (6.13)$$

Where:  $v_r$  = unit shear at radius  $r$

$v_b$  = unit shear at the column face

Both the radial moment and the unit shear decrease much less rapidly as the column size increases. This is illustrated in Figure 6.28, which shows the shears and moments with two column sizes,  $b = 5$  and 10 inches, for slabs with the same distance from the support to the column face and at the yield-line load level.

The radial moments at other loading stages can also be shown to decrease more rapidly with decreasing column size. Connections with smaller  $r/d$  ratios should thus be expected to be stronger in shear because of the smaller moments at the cracking location and the more favorable moment-shear interaction.

For the same unit shear at the column face, the unit shear at the location of the inclined cracking is considerably less for the smaller column. At 2-1/2 inches from the column face ( $d/2$  if the slab effective depth is 5 inches), the shear is 80 percent of that at the column face for the larger column ( $b = 10$  inches), but only 67 percent for the smaller column ( $b = 5$  inches). An increase in shear capacity as measured by unit shear at the column face should result from this more rapid decrease in shear with smaller column sizes.

A most interesting phenomenon is seen by comparing the radial moments at the time of first tangential yielding and at a full yield-line development. The radial moments decrease significantly as the radial yield lines form, as is shown in Figure 6.29. This "moment release" with increasing load after the radial yield lines begin to form is greatest in the outer portions of the slab.

With the aid of Figures 6.23 through 6.27, the approximate load-moment relations can be obtained for the idealized slab. Figure 6.30 shows the moments at a location 5 inches from the column face as well as the calculated load-column deflection curve. This figure indicates that yielding at the column face does not appreciably change the stiffness of the idealized connection but that a significant decrease of stiffness accompanies the start of radial yielding.

The behavior of a square slab should be similar to that of this model in areas away from the immediate column area. The smaller radial moment increase after yielding at the column face and its decrease with the radial yield-line formation is consistent with the observed stabilization and/or decrease of the strains observed in the tests described in this report.

6.10.4 Calculated Stress Distribution Near the Column Face. A finite-element analysis of an axially symmetric connection was made using an available computer program (Desai, 1968) to obtain information of the stress distribution near the column face of both an uncracked slab and one containing an arbitrary inclined crack.

A constant strain element and the grids shown in Figure 6.31 were used. The elements were assumed to deform linearly with applied force. The connection analyzed had a 64-inch-diameter slab, an 8-inch-diameter

column, an effective depth of 4.03 inches, and a flexural reinforcement ratio of 0.0150. The crack angle (45 degrees) and depth (0.70d) correspond to the geometry of the preformed cracks in the slab tested by Kinnunen-Nylander (1960).

The analysis is approximate for several reasons, including:

(1) cracking does not take place in the analysis to relieve the unrealistically large concrete tensile stresses, (2) the analysis does not consider that concrete strength and stiffness at high stresses are nonlinear and dependent on confinement, (3) bond slippage of the reinforcement was not modeled except by extending the crack over an appreciable width, and (4) the reinforcement was modeled as a steel plate rather than as a network of bars.

The stresses in the column-slab junction area for the uncracked slab are shown in Figure 6.32. The maximum tension in the reinforcement is slightly inside the column face. At the level of the top slab surface, the column load is highly concentrated at the outside of the column with sizable vertical tension at the column center. The concrete compressive stress increases quite rapidly as the column is approached.

Figure 6.33 shows the computed stresses near the top of the preformed inclined crack in the connection. Large tensile stresses around the crack root indicate that this crack would propagate further. The concrete above the crack and near the column face is very highly stressed with all three principal stresses being compressive.

6.10.5 Effects of an Orthogonal Reinforcement Pattern. Behavior of a slab containing two-way reinforcement is different from that predicted by plate theory in at least two important ways not previously noted in this chapter: (1) all cracked sections do not have the same stiffness, and



(2) inplane forces will be created in a slab having orthogonal reinforcement.

Section Stiffness. The stiffness of the cracked sections in a slab with isotropic (equal moment capacity in all directions) two-way reinforcement is not equal at all locations and in all directions. Rather, the section stiffness decreases as the angle between the reinforcement and the crack crossing it approaches 45 degrees and as the ratio between the smaller and larger principal moment decreases. It follows that the magnitude of the maximum concrete compressive strains and the depth to the neutral axis are also dependent on these two values. These section properties have been discussed in detail by Lenschow and Sozen (1966).

A circular slab with two-way reinforcement will be stiffer along radii parallel to the reinforcement. Consequently, more moment will be carried in these directions after cracking and before the yield lines are totally developed. Shear and twisting moments will also exist along most radial lines during this stage.

In the test specimens, both smaller stiffness along the diagonals and the rise of the slab corners increased the proportion of the moment carried by the areas parallel to the reinforcement and crossing the column.

Because of the complex and changing distribution of stiffnesses throughout the slab, conventional plate theory, however refined, should be expected to only approximate both the strain distributions and magnitudes. The stiffness of the slab obtained with plate theory will also necessarily be approximate.

Inplane Forces. A more important consequence of the two-way reinforcement pattern is the creation of inplane forces within the slab.

When the component of the reinforcement forces in any direction multiplied by the lever arm of an equally reinforced beam strip without axial load is larger than the applied moment in that direction, the excess tensile force acts as an internally created prestressing force. This condition will generally exist with orthogonal reinforced slabs, even those with equal moment capacity in orthogonal directions ("isotropic"), except when the principal moments are perpendicular to the reinforcement or when the principal moments are of equal value.

The existence of this self-induced prestressing action can easily be demonstrated by examining a slab with the reinforcement placed at 45 degrees to the applied moment and with the smaller principal moment equal to zero, the case shown in Figure 6.34a.

Although a component of the steel force exists in the  $y$  direction, no external moment has been applied in this direction. To satisfy equilibrium, the resultant concrete force must act collinearly with this steel force in the  $y$  direction as is shown in Figure 6.34c. The resulting concrete stress distribution is identical to that resulting from an externally applied inplane force at the level of the reinforcement. Compressive stresses will act parallel to the cracks on the tension side of the slab.

If  $d$ , the effective depth, is more than two-thirds the slab thickness, the concrete stress on the "compression side" of the slab will be tensile in the  $y$  direction. Lenschow-Sozen (1966) observed tensile strains exceeding those attributable to a Poisson's ratio effect on this side of a slab with the moment and reinforcement pattern of Figure 6.34a.

At first glance, the presence of concrete in compression at the same level and direction as a tensile component from the reinforcement appears

incompatible. The stress condition is possible because of a slight rotation of the reinforcement direction shown exaggerated in Figure 6.34d. The action is analogous to four tensile links arranged in a square with two opposite corners pulled apart (points b in Figure 6.34d) and with a compression strut between the other two corners (points a).

Figure 6.35 illustrates the effect of the moment ratio on the concrete stresses and neutral axis location for a slab with orthogonal reinforcement placed at 45 degrees to the principal moments. The concrete has been assumed to be within its elastic range and unable to support tension below the neutral axis. A small difference in the principal moments will greatly decrease the concrete stress and drop the neutral axis of the section. The decrease in the maximum concrete compressive stress is much more rapid than the decrease in the moment being carried.

The expressions describing the self-induced prestressing are quite involved if (1) the flexural cracks form at an angle of other than 0 or 45 degrees to the reinforcement, (2) all or part of the reinforcement is in the elastic range and the reinforcement is not at 0 or 45 degrees to the principal moments, and/or (3) the reinforcement is not isotropic. The magnitude of the self-induced prestress generally decreases as the crack more closely follows the direction of the reinforcement.

At completion of the yield-line pattern of a circular slab, all bars except those parallel to a segment centerline will cross radial yield lines, although the bar crossing the yield line at a small angle will reach yield only with large yield-line rotations. Generally, the inplane forces created will be largest at complete yield-line formation.

In the idealized slab-column connection examined in Section 6.10.3,

the tangential moments exceeded the radial moments except very near the column. The area where the radial moment was the larger moment decreased after yielding at the column face. At the yield-line formation, the tangential moments were several times the radial moment throughout most of the slab. Sizable inplane forces will result along the radial lines. A similar behavior would be expected of a square slab loaded on a small square column.

The behavior of a connection in shear should be expected to approach that of a partially prestressed radial element with bonded reinforcement. The shear strength of the connection will be increased by these inplane forces. The size of the compressive block is increased, a condition less favorable for crack formation and propagation, and the concrete stresses are lessened, making destruction of the compression zone by crushing more unlikely. The rotation needed to open any inclined cracks is hindered.

The creation of the inplane forces also helps explain some other phenomena observed in the tests and further warns against expecting elastic plate theory and beam moment concepts to accurately describe the moments and stresses in a slab.

The large decrease in concrete stresses observed in the test discussed earlier in this chapter resulted from both the radial moment decrease with yield-line formation and the creation of inplane stresses made possible by the difference between the radial and tangential moments, a difference which increased as the yield-line formation was completed.

This phenomenon also provides a mechanism by which appreciable moment can be carried in the direction of the smaller principal moment without sufficient concrete tension developing to crack the section on the "tension

side." This explains how a slab can be cracked only from the larger principal moment even though the smaller principal moment also exceeds the cracking moment of a beam strip of comparable strength.

6.10.6 Effect of Column Size. The experimental evidence presented in Chapter 5 and the previous discussion of the stress conditions near the column suggest three primary effects of the column size on the ultimate unit shear stress measured at the column face. These are the effects resulting from (1) the shear distribution in the slab, (2) variations in the moment distribution, and (3) relative effect of the corners of connections with rectangular columns.

Shear Distribution. The unit shear stress drops more rapidly away from the face of a smaller column (Figure 6.28 and Equation 6.13). Thus, for a given unit shear at the column face, the unit shear at the location of inclined cracking is less and the inclined cracking less likely with decreasing column size. The steeper shear gradient with smaller column size also tends to attract the inclined crack to a location nearer the column. The later inclined cracking and better crack location control with smaller columns will result in an increase of the unit shear capacity.

Moment Distribution. The ratio of the radial moment to the tangential moment increases with an increasing column size and the moments decrease less rapidly away from the column location (see Section 6.10.3). With very large columns, the decay of radial moments between the load and the supports approaches the linear decay of a beam. The tangential moments become smaller and less important with increasing column size.

These differences in moment distribution with large columns reduce the unit shear capacity of the connection in several ways. Larger radial

moments result in a less favorable shear-moment interaction and increase the likelihood that circumferential flexural cracks will form in the slab. This increases the probability that the inclined crack can develop from a flexural crack rather than at a location free from circumferential cracking. Control of the crack propagation and width also decreases with increasing column size. This results from the tangential moments having less effect on the slab stiffness and rotation about the root of the inclined cracking being less restrained.

A less beneficial biaxial stress condition near the column face will result with the larger column size because of the smaller tangential moments.

The magnitude of the self-induced prestressing resulting from the orthogonal reinforcement pattern will also decrease as the ratio of the radial moment to tangential moment increases.

Effect of the Corners. The areas of the slab near the corners of a rectangular column and those adjacent to the column sides became more distinct as the column size ( $r/d$  ratio) increases. The behavior of these two areas differ, resulting in a change in the efficiency of the connections with changing column size. The corner areas of most connections with square columns will fail first. The shear stress must then be carried by the areas adjacent to the column face. The strength of the connection is necessarily less than the sum of the strengths of the corner and column face regions; the connection is not fully effective.

The decrease in efficiency accompanying the progressive failure and resulting from the difference in behavior of the corner and column face regions is largest with the intermediate column sizes ( $r/d$  values from about 3 to 7).

With very small columns (small  $r/d$  ratios), all of the column perimeter is effectively in the corner areas and the efficiency of the connection is high. With very large columns, the strength contribution of the column face areas dominates and the efficiency will again be high.

As the  $r/d$  ratio becomes very large, the strength and behavior of the connection approaches that of a wide beam. The strength of wide beams has not been extensively investigated, although the results of tests reported by Diaz de Cossio (1962) indicate a sizable increase in strength for wide beams over the strength of beams of normal widths.

It appears prudent, however, to expect the unit shear strength of connections with very large  $r/d$  ratios to approach the strength of a typical beam strip rather than the value of  $4\sqrt{f'_c}$  assumed in obtaining the 1963 ACI Code (ACI, 1963) expression for slab-column connection strength, unless future test results substantiate a beneficial effect from beam width.

6.10.7 Effect of Column Shape. The effect of the column shape is interrelated with the  $r/d$  ratio. In connections having very small  $r/d$  ratios, the shape of the column will not greatly affect the connection performance; the slab is effectively point loaded for all column shapes. For connections having the usual values of  $r/d$ , the column shape should affect both the strength and behavior of the connection. With very large  $r/d$  ratios, the behavior of all connections approaches that of a wide beam and column shape again becomes less important.

Rectangular Column. As already noted, the shear transfer is initially concentrated at the corners of a rectangular column. The strength of these corner regions should also be higher than that of regions adjacent to the column faces for several reasons:

1. Any beneficial effects from a biaxial stress condition will be largest in the corner areas. Little stress can be developed in the slab parallel and immediately adjacent to the column face because of the much higher stiffness of the column.

2. Larger radial (beam strip) moments and more circumferential flexural cracking will exist along the face of large columns than at the corner regions. Inclined cracking can more often form from flexural cracks in areas adjacent to the column faces than at the corners.

3. The inclined crack can form farther from the column along the column face than at the corners without increasing the crack perimeter. The shear gradient is less along the column face and also results in less confinement of the crack location.

4. The corner regions will be the areas of maximum self-induced prestressing with the usual reinforcement pattern.

As discussed in Section 6.10.6, the differences in the loading and behavior of the corner and column face areas lead to a progressive failure and reduce the effectiveness of connections with rectangular columns.

Round Columns. Both the load and the connection strength will be more evenly distributed around the perimeter of a round column than around a rectangular column. Distinct corner regions do not exist and the failure should be less progressive. The efficiency of the connection will be higher than for a rectangular column. On this basis, connections with the intermediate (and usual)  $r/d$  ratios and round columns should be slightly stronger than connections with rectangular columns of an equal perimeter.

#### 6.10.8 Effects of the Reinforcement Ratio.

Shear Failures. Increasing amounts of flexural reinforcement increase



the connection shear strength in several ways: (1) the depth of the concrete compression block is increased, (2) the slab becomes stiffer and the inclined crack is better restrained, and (3) the addition of more reinforcement also increases the load which can be supported by dowel forces.

Flexural-Shear Failures. If the reinforcement ratio is small and extensive flexural yielding is reached, the flexural strength of the slab can control the shear capacity of the connection more directly. The radial yield lines near the column corners will help destroy the ability of the corner regions to support shear and may limit the shear capacity of the connection to only slightly more than the resistance along the four column faces. The large rotations accompanying general flexural yielding will hasten the destruction of the concrete above any inclined cracks.

STRENGTH AND BEHAVIOR OF DYNAMICALLY LOADED  
SLAB-COLUMN CONNECTIONS

## 7.1 DYNAMIC STRENGTH OF MATERIALS

The strengths of both concrete and steel increase with increasing strain rates. Before discussing the results from the tests of the dynamically loaded specimens, strain-rate effects on the strength of concrete and steel will be reviewed. No dynamic material property determinations were conducted as a part of this project, but a limited amount of information is available in the literature.

7.1.1 Steel Tensile Strength. Table 7.1 lists the increase in the lower yield stress of structural- and intermediate-grade steels for various strain rates as reported in several references.

An upper yield is often observed in dynamic tests of machined steel specimens and is more strain-rate sensitive than is the lower yield stress. The upper yield is of secondary interest, however, because as-rolled reinforcement usually does not have a distinct upper yield and because the strength of a reinforcing bar after yielding and before strain hardening begins is determined by the lower yield stress. Higher strength steels and the postyield strength of all steels are less strain-rate sensitive than is the lower yield strength of a mild steel.

The modulus of elasticity of steel appears to be relatively insensitive to the strain rate.

7.1.2 Concrete Compressive Strength. Observed increases in the compressive strength of concrete resulting from rapid straining are listed in Table 7.2.

The percentage strength increase has been observed to decrease with

higher strength concrete and with the dryness of the concrete (Cowell, 1966).

Watstein (1953) reported an increase of 10 and 24 percent in the secant modulus (up to a strain of  $1000 \times 10^{-6}$ ) of concrete in compression with 2500 and 6500 psi concrete strained at 0.1 per second. Cowell (1966) observed increases of intermediate value.

7.1.3 Concrete Tensile Strength. In the few tests reported to date, concrete has been found to be more strain sensitive in tension than in compression. The results of the reported tests, all using split cylinder specimens, are also listed in Table 7.2.

The effect of rapid loading on the concrete modulus of elasticity in tension has not been clearly established.

## 7.2 VERY RAPID LOADING

7.2.1 Loads Applied. The loads acting on the first two dynamically tested connection, Specimens D2075-1 and D2075-2, were applied very rapidly. The time to maximum load was 2.2 and 2.4 msec for the first and second tests, respectively. The loads decayed rapidly because of the sizable slab deflection and the large loader stiffness resulting from the use of the small-volume pressure tanks then available.

The peak loads were 2.43 (for D2075-1) and 3.00 (for D2075-2) times the static connection strength. The loads decayed to below the static capacity in approximately 10 msec (Figure 7.1). The oscillations in the loads are due mainly to the dynamic response of the loader itself.

### 7.2.2 Behavior.

Loads. A punching shear failure did not occur in either test. Two of

the column corners of Specimen D2075-2 were pushed approximately 1/4 inch into the slab (see Figure 5.15b) indicating that the connection strength in shear was approached, although not reached.

The flexural response of the connections was as would be expected for a slab loaded dynamically over a small central area. During the first few milliseconds, the slab responded primarily in modes other than the fundamental mode. The mass of the slab first acted to fix the outer portions of the slab, causing moments near the quarterspan to be of opposite sign to those of a slowly loaded slab. The momentum imparted to the slab while the load was large drove the slab to a large deflection and to flexural distress after the applied load dropped. Shear was most critical before the applied load dropped below the static connection capacity. The danger of shear and flexural failure thus occurred at distinctly different times for these two tests.

Cracking. The photographs of the tension side of the slabs (Figure 5.14) show a very distinct radial yield-line pattern with circumferential cracks near the column face. No circumferential cracks could be found away from the column face, indicating that neither flexural cracks nor inclined (shear) cracks reaching the surface had formed between the radial cracks away from the column face.

Some crushing of the concrete above the flexural yield lines and several circular cracks can be seen on the column side of the slab in Figures 5.15a and 5.15c. The circular cracks near the slab corners probably formed in the first few milliseconds when the corner mass acted to hold the corner down. The circular cracks nearer the column probably resulted from the initial moments causing tension on the column side and not from tensile membrane cracking.

Accelerations. Maximum accelerations of near 130 g's and 190 g's were measured near the column and slightly before the load peak for D2075-1 and D2075-2, respectively. These and other records are contained in Figures C.1 through C.8.

Deflections. The maximum column deflections measured were 1.85 and 2.95 inches, respectively, for D2075-1 and D2075-2. Maximum column deflection was reached at about 21 msec for both specimens (see Figure 7.1). The corner and quarterspan deflections initially lagged the center deflection by about 2 msec.

The condensed deflection records (Figures C.2 and C.6) indicate that an appreciable content of higher modes of the connection specimen were excited, especially at the corners of the slab. The observed period of the fundamental mode for the highly cracked Specimen D2075-2 was 31 msec, higher than the 21-msec period calculated for the cracked slab (see Section 3.6.2).

Steel Strains. Limited steel strain data for Specimen D2075-1 indicated a steel strain rate of approximately 0.6 per second at the gaged locations (Figure 4.15) during the elastic straining of the reinforcement. These instrumentation channels were very noisy.

A majority of the steel strains measured in Specimen D2075-2 indicated yielding prior to 5 msec. Elastic strain rates varied from 0.48 to 1.2 per second with an average of 0.73 per second (Gages S9, S10, and S16 not considered).

Concrete Strains. The locations of the concrete strains measured are shown in Figure 4.15.

The three concrete strains measured along the column centerline and 10 or more inches from the column face (C1, C2, and C3) were all initially

tensile, reflecting the early moment distribution discussed earlier. Peak tensile strains of near  $125 \times 10^{-6}$  and  $150 \times 10^{-6}$  were reached in 2 to 3 msec, approximately the time of the peak load. No tensile strain was recorded by Gage C4, located 5 inches from the column face, during the first few milliseconds.

Maximum compressive strains were recorded by Gages C1, C2, and C3 at 11 (for D2075-1) and 7 (for D2075-2) msec, corresponding to center deflections of 1.1 and 0.8 inches. These maxima were quite small, varying from  $70 \times 10^{-6}$  to  $260 \times 10^{-6}$ .

As the test progressed, these strains again became tensile. This last reversal resulted from the same factors causing reversal in the static tests, i.e. radial moment decrease with yield-line formation and self-induced forces, and not from tensile membrane action only. The deflections at strain reversal were roughly 50 percent greater than in the static tests.

The concrete strains measured near and perpendicular to the column face reached a peak of near  $1300 \times 10^{-6}$  for Specimen D2075-1 and  $2300 \times 10^{-6}$  for D2075-2. Both peaks occurred at about 10 msec.

Gage C7, located 2 inches from the column corner of Specimen D2075-1, and Gages C5, C6, and C7 located along the column face of D2075-2 recorded large tensile strains following sizable compressive strains. These gages failed at near 13 msec, probably reflecting shear distress at that time and at those locations. After the test, a crack was found crossing the three gages of Specimen D2075-2 mentioned above.

The observed concrete strain rates up to the time of the compressive peak were as listed below:

Gage	Specimen D2075-1	Specimen D2075-2
C1	0.031 per second	0.051 per second
C2	0.044	0.074
C3	0.028	0.070
C4	0.100	0.064
Average C1 through C4	0.051	0.065
C5	0.130	0.32
C6	0.150	0.24
C7	0.135	0.30
C8	0.138	0.20
Average C5 through C8	0.138	0.26

### 7.2.3 Analysis.

Flexure. The response of the connection specimens in flexure will be approximated by idealizing the specimen as a single-degree-of-freedom system loaded with a force decreasing linearly with time. Its resistance is assumed to be elastoplastic.

The slab resistance will increase because of the strain-rate effect on materials. The flexural strength of underreinforced slabs, such as those tested, is governed almost exclusively by the steel strength. An average strain rate of 0.6 per second corresponding to a steel yield stress increase of about 30 percent (Table 7.1) will be assumed. The complex and varying strain distribution throughout the slab renders the selection of one typical reinforcement strain rate necessarily approximate.

An equivalent single-degree-of-freedom system with a stiffness of 141 kips/in (cracked-section stiffness from Figure 6.20), a natural period of 21 msec (tabulation, Section 3.6.2), a resistance of 85 kips (1.30 times 65 kips, the static flexural capacity), and a yield deflection of 0.60 inch will be examined.

The loading curves will be idealized by the triangular force pulses shown in Figure 7.1. These were chosen to preserve the impulse up to the time of maximum deflection.

The predicted deflections of such an elastoplastic system loaded with this forcing function (Melin-Sutcliffe, 1959) are 2.6 and 3.4 inches for Specimens D2075-1 and D2075-2, respectively, 132 and 116 percent of the observed deflections of 1.85 and 2.95 inches. This represents reasonable agreement considering the assumptions and approximations of the analysis and the sensitivity of the predicted deflections to small load changes.

Shear. Table 7.3 lists the shear forces transferred by the very rapidly loaded specimens. The inertial force of the column and the potential shear cone have been subtracted from the applied load to determine the load transferred by the connection.

Both the maximum shear force transferred (1.88 and 2.25 times the static strength) and the average shear force transferred during the time from 1 to 9 msec (1.60 and 1.72 times the static strength) are larger than those explainable by the strength increase indicated for the concrete in compression. The measured strain rate near the column face and the data in Table 7.2 would suggest an increase of about 35 percent in the concrete compressive strength.

Concrete tensile strain rates at the critical locations were not measured. The tensile strength of the concrete may have sufficiently increased with the very rapid loading to prevent the formation of inclined cracks.

Besides the strain-rate effect on the material properties, a second loading-rate effect also affected the strength in shear. The load duration was too short relative to the specimen's natural period to allow the slab to



deflect enough for any inclined cracks to open appreciably before the load had decreased to below the static capacity.

### 7.3 RAPID LOADING

All nine of the specimens loaded under dynamic conditions approximating those resulting from a blast loading failed when the column and a portion of the slab punched through. The specimens with the higher reinforcement ratio ( $p = 0.0150$ ) failed before sufficient deflection was mobilized to develop the full flexural strength. The lower reinforcement ratio specimens ( $p = 0.0075$ ) displayed considerable flexural yielding before punching failure occurred.

The instrumentation records from these nine tests are contained in Appendix C (Figures C.9 through C.36).

7.3.1 Loads and Accelerations. The characteristics of the loads acting on the specimens in this series of tests are listed in Table 7.4.

The rise times of the loads, although not uniquely defined by the records, were near the desired values of 20 to 40 msec (see Section 3.6.2). The applied load rose to about 50 kips during the first 4 to 5 msec, then increased more gradually and rounded off to a nearly level plateau. The rise times listed in Table 7.4 are necessarily approximate and were found as illustrated in Figure 7.2.

Throughout the tests, a variation in loading due to the dynamic response of the loading device itself was clearly observable. Figures 5.12 and 5.13, the load-time traces for these nine tests, show that the pattern of variation in the loading traces was remarkably similar for all tests. A fundamental period of near 5.8 msec is indicated for the loading device used in these tests.

The largest expansion tanks available (see Appendix A) were used with the loader for all tests in this series in order to provide an adequate deflection capability without excessive load decay. A slightly smaller orifice disk was used for the test of Specimen D4075-3 than for the other eight tests in order to produce a longer rise time than those obtained in the other two tests of D4075 Specimens.

From soon after the rise time was reached to immediately before failure, the measured accelerations were small, usually 10 g's or less. The movement of the acceleration traces corresponded closely to the variations of the applied load (see Figure 7.2). The average acceleration over this time was nearly zero; thus, the column was being pulled down at a nearly constant velocity and the average inertial loading was small. This was expected with the loader under the conditions of these tests, as is explained in Appendix A.

The difference between the applied load curve and an average load curve during the time between the rise time and failure (Figure 7.2) was partially supported by inertial forces of the column area and not entirely transferred as shear by the critical sections. For this reason, the maximum resistance was taken as the peak of the average load curve and not the maximum applied load. The locations in time of the maximum resistances are noted on the load traces in Appendix C.

The maximum applied loads of the D4075 Specimens occurred soon after the rise time and in fairly sharp peaks. For the other specimens, the maximum applied load was reached near the determined maximum resistance.

The failure times of the specimens are listed in Table 7.4 and were determined from changes observed in the accelerations and strains recorded

near the column and from the load traces as shown in Figure 7.2. Because of the finite mass of the specimen and loading system and the large expansion in time of the records, the punching failure did not appear to form instantaneously but instead over a small (usually 1 to 3 msec) period of time.

In some tests, the failure appeared to have developed in stages. For example, trace changes indicative of failure can be seen near both 54 and 60 msec elapsed time in the test of Specimen D2075-3 (Figures C.9 and C.10). Many instrumentation channels in the test of D4075-3 indicated failure at around 112 msec, others at 140 msec (Figures C.28, C.29, and C.30). The failure of this last mentioned connection specimen was significantly more gradual than those of the other tests and a distinct failure time could not be definitely established.

The acceleration records obtained during the rapid tests are contained in Appendix C. Accelerometers were included in these tests primarily to measure the accelerations near the time of failure and for possibly determining velocities and deflections by integration of the acceleration records.

The maximum accelerations measured during the first few milliseconds of the tests generally ranged between 20 and 50 g's. The accelerations decreased after the specimen began to deflect appreciably and were lowest near the time of the punching failure.

The largest accelerations were measured after failure when the slab rebounded and the column was pulled down. The acceleration of the column (Gage AC1) and the quarterspan point (Gage AC3) after failure were larger for specimens with the larger reinforcement ratio. This resulted from the larger load available at failure to accelerate the column portion and the larger slab stiffness acting to spring the slab upward.

The accelerations of the quarterspan point of the three D4075 Specimens after failure were considerably smaller than those of the other specimens, suggesting that the failures of these three specimens were more gradual than the failures of the other connections tested.

The accelerometer mounted on the slab near the base of the column (Gage AC2) did not always remain on the slab portion after failure but was sometimes pulled down with the column. This gage often remained attached to only a thin portion of the slab and measured very high accelerations.

7.3.2 Deflections and Velocities. The average deflections measured in the column region at the time of failure for each dynamic test are listed in Table 7.4. The individual gage readings at failure are marked in the figures of Appendix C.

The downward motion of the slab at failure resulted in the maximum deflections being reached slightly after the connection was judged to have failed. The failure deflections are approximate because of the impreciseness of the failure times.

The failure deflections were quite consistent for specimens with similar properties. They increased with the larger column size (larger  $r/d$  ratio) and with the smaller slab reinforcement ratio.

The quarterspan and corner deflections were nearly one-half and one-fourth of the column deflections, as is shown in Figure 7.3 for two specimens. The nonlinear shape of the curves of Figure 7.3, especially 7.3a, reflects primarily the first mode deflection shape of the slab being superimposed on the deflection shape of a slab centrally loaded. A natural period of about 15 msec is thus indicated for Specimen D2150-1.

The acceleration records for the tests of Specimen D2075-3 and the

D2150 Specimens were doubly integrated to obtain velocity information and to recover deflection information for Specimens D2075-3 and D2150-3. The results are presented in Figures 7.4 through 7.7.

The accelerations of Specimens D2150-1 and D2150-2 were doubly integrated primarily to compare the deflections derived for accelerations with those measured directly during the tests. The deflections obtained in these two ways are noted in Figures 7.5 and 7.6. Except for the deflection obtained from Accelerometer AC1 of Specimen D2150-1, the two deflections differ by less than 15 percent.

The deflections derived from the two accelerations measured on or near the column of Specimens D2075-3 and D2150-3 are similar in magnitude and the quarterpoint deflections are roughly one-half of the column deflections. This is another confirmation of the reliability of the data obtained. The deflections at failure listed in Table 7.4 for these two specimens are the average of the two deflections at the column calculated from acceleration measurements.

No deflection information was obtained for Specimen D4150-1 because the deflection instrumentation and the calibration circuitry for the accelerometer channels both failed to function.

The velocity-time curves of the column and slab quarterspan are also displayed in Figures 7.4 through 7.7. The largest velocities occurred after failure.

The time of the maximum velocity before failure was from 11 to 12 msec from the start of loading for all twelve acceleration records integrated. Maximum velocities of the column prior to failure were near 4 ft/sec for Specimen D2075-3 and from 2 to 3-1/2 ft/sec for the D2150 Specimens.

Velocities at failure were roughly one-half the maximum velocities reached prior to failure.

7.3.3 Crack Patterns and the Failure Surfaces. The crack patterns of the slab tensile surfaces of the dynamically loaded connections were similar to those of the corresponding static tests except that more concrete cover was usually torn off around the punching shear crack location and the circumferential cracks around the column were wider. These differences resulted from the columns being pulled down farther in the dynamic tests. Photographs of the slab tensile surface are included with other photographs of the dynamically tested connections in Figures 5.16 through 5.24.

A radial crack pattern with distinct flexural yield lines formed in the slabs with the lower reinforcement ratio. A close examination of the specimens with the higher reinforcement ratio revealed a radial pattern of narrow cracks in the slab outside of the failure area.

The surfaces of the failure cone were also generally similar for the statically and dynamically tested connections. Profiles of the slab failure surfaces of the dynamically tested connections are included in Figures C.37 through C.45. The slope of the failure crack did not appreciably change with the reinforcement ratio.

The intersection of the failure surface and the column side of the slab was noticeably flatter with the lower reinforcement ratio, especially for Specimen D2075-3. The slope near the column face with the larger reinforcement ratio was often near 45 degrees.

The crack angle near some corners of the D2150 Specimens, particularly Corner 2 of Specimen D2150-2 (Figure C.39), was much steeper than the rest.

The average crack angle of the failure surface of the slab was 25 to

35 degrees from the horizontal, about 5 degrees larger than in the statically tested connections.

The cracks forming the failure cone often surfaced on the compression side of the slab at a considerable distance away from one or more column faces in the D4075 Specimens (see Figures 5.20, 5.21, and 5.22), more so than in the static tests. These cracks usually surfaced at a very small angle to the horizontal.

The failure crack along the side marked 1-4 of Specimen D4075-2 (side below column in Figure 5.21c) is notable because of its location far from the column face (about 18 inches away) and its nearly vertical direction (Figure 5.21e). The probable sequence of failure for this specimen is that three sides failed first in shear leaving the column area cantilevering from the fourth side. This fourth side then failed in flexure.

Circumferential cracks formed near the corners on the column side of the slab of several specimens (see Figures 5.21c and 5.22a). These cracks formed from the flexural stresses resulting from inertial forces holding the corners down during the first few milliseconds of the test.

Most of the radial cracks on the column side seen in Figures 5.22 and 5.23 were either crushing over yield lines or yield-line cracks which extended to the compression surface during handling of the specimen after testing.

The radial cracks on the column side roughly following the centerline of slab of the two D4150 Specimens (Figures 5.23 and 5.24) were formed during the rebound of the slab after failure.

Bond splitting was seen in Specimen D4150-2 and is shown in Figure 5.24f. The reinforcement had been flame cut even with the slab edge

prior to the test. At other locations of the D4150-2 connections, the bars outside of the failure cone were completely unbonded (Figures 5.23a and 5.24c).

The strength of the specimens, however, was not controlled by bond. Bond distress was seen only when the concrete cover was ripped off to near the slab edge. This happened after the column and the slab had separated.

Torsion cracks developed on the sides of all the dynamically tested connections.

7.3.4 Internal Crack Formation. The five specimens with the larger column were instrumented with small-stroke deflection gages to detect internal cracking and crack opening indirectly by measuring changes in the slab thickness. These measurements were less successful in the dynamic tests than in the static tests. In the dynamic tests, this instrumentation was consistently noisy and did not produce the resolution needed to determine cracking. The records for Specimen D4150-2 varied considerably and unexplainably from those of the other four tests. The measured changes in slab thickness are contained in Appendix C along with the other records of each test.

The measured slab thickness increases before failure were consistently larger in the dynamic tests than in the corresponding static tests.

The pattern of slab thickness changes did not differ noticeably for the two reinforcement ratios.

In most cases, Gage D7, located 7 inches from the column centerline and 5 inches from the column face (Figure 4.11), recorded the first large crack width. Gage D6, located on the slab diagonal, next detected wide cracking. Except for Specimen D4150-2, Gages D8 and D9, located along the centerline,



recorded similar deflection magnitudes and patterns. Both usually indicated a rapidly increasing slab thickness close to the time of failure.

Gages D8 and D9 of Specimen D4075-3 both recorded a very rapid thickness increase beginning at 114 msec, appreciably before that of Gage D6 and the probable failure time. Perhaps significant is that the failure of this specimen was notably gradual and may have been very progressive in nature. These two records were also the lone indication in any of the tests of failure occurring first at the column face rather than near the column corners.

7.3.5 Concrete Strains. The concrete strains recorded during the dynamic tests displayed many of the characteristics of the strains of the corresponding static tests. The strain records for each test are contained in Appendix C.

Away from the column face, tensile concrete strains of very low magnitude were often recorded during the first few milliseconds. This phenomenon, not observed in the static tests, resulted from the initial higher mode response of the slab.

Just as in the static tests, the strains on the column side of the slab away from the column displayed a significant reversal. The strains at these locations increased in compression at a fairly constant rate with time after the first few milliseconds, reached a peak compressive value considerably before the specimen failed, and then decreased.

Very distinct peak concrete compressive strains were measured at a column deflection of 0.65 to 0.80 inch for the specimens with  $p = 0.0075$  and were followed by a nearly linear (both with time and deflection) decrease until the time of failure. These strains often reached tension before failure of the connection specimen.

The peaks in the concrete strain records were much more rounded for the specimens with the larger reinforcement ratio. A leveling off of the concrete strain magnitudes began with a column deflection of about  $1/3$  to  $1/2$  inch, with a gradual decrease following.

This strain reversal, like that of the static tests, resulted from the flexural response of the slab. As explained in Chapter 6, the reversal is primarily caused by the drop in the radial moments and the self-induced prestressing of the slab which begins when the slab deflects sufficiently to initiate the formation of radial yield lines.

The strain reversal in the slabs with the small reinforcement ratio appeared to be more sudden and to occur at a slightly larger deflection with dynamic loading than with static loading.

The concrete strains at a time slightly before the strain reversal are shown in Figure 7.8 for four specimens, one with each combination of column size and reinforcement. The average strain rate, which is the average slope of the strain-time trace up to the time the strains began to level off, is also shown for these tests.

The concrete strains measured on all specimens tended to decrease in magnitude as the distance from the column increased. Consequently, the strain rates at the various gage locations varied considerably.

The measured concrete compressive strain rates generally varied from approximately 0.012 per second at the gage location farthest away from the column to above 0.15 per second adjacent to the column face.

The concrete strains measured adjacent to the column reached higher values than in the companion static tests. Compressive strains in excess of  $4000 \times 10^{-6}$  were recorded for Specimens D4075-2 and D4150-2,

indicating that concrete crushing was at least approached at the column face of these connections. The maximum recorded compressive concrete strains adjacent to the center of the column face exceeded  $2500 \times 10^{-6}$  near at least one column face of all specimens except D2075-3 and differed considerably within similar specimens.

The behavior of the strains adjacent to the column and on the slab centerlines differed in pattern as well as magnitude in similar specimens, even when the failure geometries were nearly identical. Gage C5 of Specimen D2150-1 recorded increasing strain (maximum of  $3820 \times 10^{-6}$ ) until very near the time of failure. The strains at the column centerline of Specimen D4075-2 (Gages C5 and C6) exceeded  $4000 \times 10^{-6}$  at the time of failure. The more usual pattern was for these strains to reach a peak before failure and after the strains away from the column had reversed. These strains decreased at varying rates until failure. Gage C5 of Specimen D2150-3 recorded a tensile strain before the time of failure.

Just as in the static tests, the concrete strains along the column face tended to be smaller away from the centerline and often reversed first near the corner, especially with the larger column size. One notable exception was observed with Specimen D2150-3. The strain gage 1 inch outside the column corner (C8) registered increasing strain (Figure C.20) until the time of failure, and indicated the largest concrete strain recorded in the test of Specimen D2150-3.

The strains measured on the columns of the D4000 Series indicated a movement of the column load away from the column corners near failure very similar to that observed in the static tests.

Gage C13, mounted vertically at the center of a column face, initially

recorded tensile strains of up to  $70 \times 10^{-6}$  (for the D4150 connections) or small compressive strains, thus showing that most of the column load and shear transfer was initially concentrated near the corners of the column.

The strain indicated by Gage C14, placed vertically on the column near a corner, reached a maximum and then decreased before failure for all specimens. The strain at failure ranged from 55 percent (for D4075-3) to 74 percent (for D4075-1) of the maximum values for the D4075 Specimens and near 75 percent of the maximum for the two D4150 Specimens.

This decrease and the sizable compressive strain increment registered by Gage C13 at times near failure resulted from more vertical force traveling down the center of the column face and entering the adjoining slab as shear at later times. As in the static tests, the ability of the dynamically tested specimens to transfer shear was lost first in areas near the column corner.

7.3.6 Steel Strains. The same basic behavior was displayed by the steel strains in the dynamic tests as in the static tests. The complete steel strain records are contained in Appendix C.

Little movement of the steel strains was recorded during the first few milliseconds of the dynamic tests because of the initial higher mode response of the slab and because the slab had not yet cracked nor deflected appreciably.

The steel strains increased at a nearly linear rate with time and deflection after the first few milliseconds. Most of the strains away from the column face leveled off to a distinct plateau at a time closely corresponding to the maximum concrete strain peaks at these locations. This

leveling off of the strain magnitudes resulted from the stabilization and decrease of the radial moments accompanying the beginning of radial yield-line formation as explained in Section 6.10.3. The steel strains remained fairly constant from the start of radial yielding until the failure of the connection. Some increased slightly while others decreased with no apparent pattern.

The magnitude of the steel strains and the rates of straining decreased with the distance from the column. The strain magnitudes at a time before the start of yield-line formation and the average strain rates for the reinforcement in four specimens, one with each combination of column size and reinforcement ratio, are shown in Figure 7.9.

The strain rates of the reinforcement generally varied from about 0.10 per second at the gages farthest from the column to approximately 0.3 per second near the column. The strain rate was determined by the average slope of the strain-time curve before the strains began to level off.

#### 7.3.7 The Effect of Loading Speed on Connection Performance.

Strength. The strength of the specimens loaded at a rate comparable to the loading rates probable in blast-loaded structures was consistently larger than the strength of the specimens loaded slowly, as can be seen in Figure 7.10, a bar graph comparing the strength of the statically and dynamically loaded specimens.

The approximate magnitude of the strength increase at the loading rate selected can be obtained by comparing the average strength observed at the two loading speeds for the specimens of each basic geometry and strength. This comparison is shown in Table 7.5. The average ratio of dynamic strengths of the specimens to the static strengths is 1.26.

Because the various specimens within the four groups had slightly different properties, a direct comparison of the observed static and dynamic strengths to determine the effect of loading speed is somewhat approximate. The dynamically tested specimens usually contained stronger reinforcement and often had a slightly larger measured effective depth (Table 5.1).

Because an analytical expression stating the effect of the different variables is lacking in the case of a shear failure, it is not possible to normalize all the results shown above with respect to the material and geometrical properties of the specimens. However, part of these differences may be eliminated by normalizing the results of the specimens with  $p = 0.015$  on the basis of the parameter  $d\sqrt{f'_c}$  and the results of the specimens with  $p = 0.0075$  on the basis of the parameter  $pd^2f_y$ . The parameter  $d\sqrt{f'_c}$  was chosen because the unit shear  $V/bd$  is assumed to be related to  $\sqrt{f'_c}$  for shear failures. The parameter  $pd^2f_y$  relates to the flexural strength of the specimen.

The normalized ratios of dynamic strength to static strength are also given in Table 7.5. In Series 2075 and 4075, the maximum load was controlled primarily by flexure. In Series 2150 and 4150, the maximum load was controlled by shear. The normalized ratios given in Table 7.5 imply that the increase in strength due to rapid loading was slightly larger for shear failures. The strength increase was slightly larger for specimens with the larger  $r/d$  ratio.

A more elaborate approach to determining the effect of loading speed is to compare the ratio of experimental strength to the predicted static capacity for the connections tested at the two loading rates. This, however, requires that a particular theory for predicting the shear strength

be chosen. The results will vary with the theory adopted, but the differences will be small because the variations in the specimen properties were not large.

Moe's equation for analysis (Equation 2.5a) and the yield-line (flexure) equation (Equation 6.1) will be used in the comparisons. The strength increases due to the loading speed computed in this manner are listed in Table 7.6. The variation of the increases displayed by the duplicate tests is small.

Moe's shear capacity expression (Equation 2.5a) and the yield-line (flexure) equation (Equation 6.1) will be assumed applicable for the specimens with a reinforcement ratio of 0.0150 and 0.0075, respectively. The strength increases with dynamic loading for the four basic connections resulting from this method of comparison are included in the last column of Table 7.5.

The calculated ratios for the 2075 and 4075 Specimens are the same as the normalized ratios because the calculated yield-line capacity is nearly proportional to  $\rho f_y d^2$ . The use of Equation 2.5a to normalize the results for the specimens with  $\rho = 0.0150$  yielded ratios which differed little from the ratios normalized with respect to the parameter  $\sqrt{f'_c}$ .

Deflections. The ultimate deflections of the statically and dynamically loaded specimens are compared in Table 7.7. Ultimate deflections were 25 to 50 percent larger for the rapidly loaded specimens. A larger increase was observed with the larger column size ( $r/d = 4$ ).

The applied load versus column deflection curves for typical dynamic tests are plotted and compared with a companion static test in Figures 7.11 and 7.12. Because inertial forces are included in the applied load, these

applied load-deflection curves are not strictly resistance curves, especially at very small deflections when the accelerations were appreciable. At larger deflections and prior to failure, a smooth curve fitted through the plotted curve should reasonably represent the resistant curve for the reasons discussed in Section 7.3.1.

7.3.8 Analysis of Strength Increase. The increase in connection strength with the loading rate can be attributed primarily to the increase of the material strengths accompanying the large strain rates resulting from the faster loading.

The controlling strain rate for the connection can be obtained only approximately from the test data. The strain rates differ in time and location throughout the slab, and those measured are not necessarily representative of the strain rates at the locations of failure. However, the strength increase with rapid straining is claimed to be a function of the logarithm of the strain rate and increases rather slowly, usually 10 to 15 percent for a tenfold increase in the strain rate. Differences of several hundred percent in the strain rate values should produce less inaccuracy than the scatter of the test results included in Tables 7.1 and 7.2.

The strengths of the connection specimens failing in shear may be controlled by the compressive strength of the concrete above the inclined crack. The concrete near the column is likely to be confined. Choosing a failure strain of  $6000 \times 10^{-6}$ , an average time to failure of 60 msec (near the test average), and assuming a linear rate of straining, a strain rate of 0.10 per second for the controlling concrete area is obtained. A strength increase of about 25 percent corresponds to this strain rate (Table 7.2). This is very near the strength increases of 23 and 29 percent for the



2150 and 4150 Specimens, respectively, obtained by comparing the proportion of the calculated capacities for static loadings observed with the static and dynamic loading speeds (last column of Table 7.5).

It is possible that some of the shear failures resulted primarily from concrete tensile failures. Assuming the concrete reaches a failure stress of 550 psi in 60 msec results in a strain rate (using  $E = 3,000,000$  psi) of 0.003 per second and an indicated tensile strength increase for the concrete of near 20 percent (from Table 7.2). This percentage is also close to the observed strength increases for the specimens with the higher reinforcement ratio.

The flexural strength of the slab depends on the stress and, therefore, on the strain of the reinforcement throughout the slab. These strains vary from very high values at the circumferential crack near the column face to much smaller values near the edges of the slab and perpendicular to the column face. Assuming an average steel strain at failure ( $t = 0.060$  second) of three times the yield strain of  $1800 \times 10^{-6}$  (yield stress of 55 ksi) gives an average strain rate of 0.10 per second, which corresponds to an increase in the steel tensile stress of about 15 percent (Table 7.1). This increase corresponds closely to the strength increases of 16 and 21 percent displayed by the specimens with the smaller reinforcement ratio (Table 7.5), those primarily controlled by their flexural strength.

The slightly larger strength increase displayed by the specimens failing primarily in shear is consistent with the slightly larger strength increase for the concrete than for the reinforcement.

The strength increase of connections with properties near or within the range included in this test program and loaded at similar rates to those

used for the rapidly loaded specimens can be satisfactorily expressed by the increase in the predicted strengths obtained by using suitable dynamic material strengths rather than static material strengths. The term  $\sqrt{f'_c}$  should be replaced by the strain rate strength increase factor times  $\sqrt{f'_c}$  and not by the square root of the dynamic compressive concrete strength.

The punching shear strengths of connections loaded with an impulse or with a very rapidly decaying load (such as the load on Specimens D2075-1 and D2075-2) will increase more than that given by the procedure suggested above.

#### 7.4 PERFORMANCE OF SLAB-COLUMN CONNECTIONS IN A BLAST-LOADED STRUCTURE

7.4.1 Types of Loading. Few connections in a blast-loaded structure will be concentrically loaded as were the specimens in this test series. The actual loading conditions must be found experimentally or by a dynamic structural analysis. A few qualitative remarks on the loadings of the connections in a building follow.

Connections at four levels in a structure are shown in Figure 7.13. Connections at the roof, such as those marked A, may transfer substantial vertical loads. Higher overpressures will act above the roof slab than below it, a difference depending on the filling time and structural integrity of the walls of the top floor. Detonations at a high angle from the horizontal will produce large vertical forces on the roof. The connections may also transfer sizable moments to the column. Some moment at the column will result from the blast load crossing the slabs, an asymmetrical condition, although this would probably not act concurrently with the largest shear load. Additional moments will result from the participation of the

floor-column framework in the lateral load resisting system of the building. These moments could act concurrently with the maximum shear loading on the connection.

As a first approximation only, the increases in strength and rotation capacity of dynamically loaded slab-column connections transferring appreciable moment may be assumed equal to the increases observed in the concentrically loaded test specimens.

The blast loading will usually add little to the vertical load transferred by the connections at intermediate floors, such as those marked B. The pressures acting above and below these floors will usually be nearly equal. Large moments may act on the connection from the lateral loading of the structure, especially at lower floors of tall buildings without effective shear walls. The ability of the connections to transfer these moments resulting from lateral loading may be critical in determining if the structure will remain standing.

The connections located over the basement area, such as those identified as C, must transfer sizable vertical forces since the blast pressure ingresses quite slowly into most basement areas, with a large pressure difference resulting across the first floor slab. Just as at the roof, moments from the blast crossing the slab and from the lateral loading are possible.

The column footings, marked D, behave similarly to the slab-column connections. The column-footing connections will very often be the most concentrically loaded connections in a blast-loaded structure.

Connections at the exterior of the structure will be subjected to more moment loading because of the connection geometry.

#### 7.4.2 Useful Dynamic Connection Strengths and Deflections. The

loading in the lower overpressure regions is of comparatively long duration, especially with the higher-yield weapons. For this reason, the maximum useful dynamic load capacities of blast-loaded buildings and building elements will not greatly exceed the static strengths.

The portion of the connection load-deflection curve after the punching shear failure was not given great attention in the previous sections because it will generally not be a useful portion of the resistance curve.

After punching failure, the resistance of the connection is provided by the tensile membrane action of the reinforcing mat. The vertical component of the steel force increases with deflection and the postfailure connection resistance increases until the reinforcement ruptures or tears loose from the slab. Idealized load-deflection curves including the postfailure resistance and the resulting strain energy curves are shown in Figure 7.14a. The postfailure curves for the connections tested were similar to the lower curve.

Energy principles state that a system can be at rest (have no kinetic energy) only if the strain energy of the system is equal to the work done by the forces acting on it.

The work-deflection curve of the time dependent forcing function shown in Figure 7.14b is indeterminate until the deflection-time history of the system is known, but will have a shape similar to that of the family of curves labeled 1 through 4. The system will fail, i.e., will not reach zero velocity, unless the work and strain energy curves cross, as they do for Cases 1 and 2. Any gradually decaying dynamic load large enough to have a work curve passing over the strain energy curve at the point of punching shear failure (such as Case 3) will not intercept the strain energy curve

unless the postfailure strength is large. The postfailure portion of the curve could be useful in the case of impulse loading, Case 5. Even a relatively large postfailure strength may not increase the blast-resistance appreciably: compare the increase of Curve 3 or 4 over Curve 2.

Total collapse of the connection models was prevented only by a very rapid load drop after the punching failure.

The postfailure strengths of the connections tested should be slightly less than those of as-built slab systems. Typical reinforcement contained in flat plates and slabs is shown in Figure 7.15. In all cases, the bottom bars crossing the shear cone may be terminated near the column. Such bars are not adequately anchored to offer appreciable postfailure strength. The concrete cover over the top bars is not sufficient to prevent the bars from ripping the cover off, as was the case in the tests. The top bars in the specimens tested extended to  $L/5$  or  $L/4.47$  from the column centerline, slightly less than the length of the top bars in slabs reinforced as shown in Figure 7.15a. Thus, the reinforcement bars in the slab-column connection specimens had slightly less anchorage length than would exist in a slab system.

The bent bars of the slabs reinforced with bent and straight bars (Figure 7.15b) would be effective in providing some postfailure strength.

7.4.3 Approximate Blast Resistance of Slabs as Limited by the Connections. An upper bound of the pressure level which could act on the prototype slab systems without punching failure may be found by equating the test results to the force resulting from a uniform pressure acting over the prototype bay size (17 feet 6 inches square). The results are listed in Table 7.8.

The connection specimens tested dynamically failed at a finite velocity. A loading the specimens could have survived is necessarily lower than those of the tests. Any load eccentricity would further decrease the connection strength.

This method also omits the intricacies of a complete dynamic analysis and is therefore approximate. Although the maximum resistance and the maximum applied load capacity are not necessarily the same in the case of dynamic loading, the two are nearly equal for long-duration loads with a finite rise time acting on a system with some ductility.

The maximum blast overpressures of sizable duration which could be supported by the prototype slabs for the connection models without collapse would be no more than  $1\text{-}1/4$  to  $3\text{-}1/3$  psi.

## CHAPTER 8

### SUMMARY, CONCLUSIONS, AND RECOMMENDATIONS

#### 8.1 OBJECTIVES AND SCOPE

The primary objectives of this investigation were to study the strength and behavior of slowly (statically) loaded reinforced concrete slab-column connections and to determine the effect of rapid (dynamic) loading on the strength and behavior of these connections.

The number and range of test variables were deliberately limited to allow duplicate testing of specimens with each combination of variables at both static and dynamic loading rates.

Nineteen full-scale models of the connection and adjoining slab area of a flat-plate floor system were tested. Eight specimens were loaded to failure in 10 to 20 minutes. Nine of the eleven dynamically tested specimens were subjected to rapid loading having a rise time of 9 to 32 msec, the approximate rise time expected at the connections of a blast-loaded structure. The remaining two specimens were tested very rapidly with load rise times of 2.2 and 2.4 msec.

The slab reinforcement ratios were 0.0075 and 0.0150. No compressive reinforcement was used.

The specimens had  $r/d$  ratios ( $r$  = side dimension of a square column and  $d$  = effective slab depth) of either 2 or 4.

Concrete strength varied from 3860 to 5600 psi. All reinforcement had a nominal static yield stress near 48,000 psi.

All loads were applied concentrically onto the column.

Two specimens with each combination of  $r/d$  ratio and reinforcement percentage were tested at static loading rates. Three specimens with each

combination were tested dynamically except that only two were tested with the combination of  $p = 0.0150$  and  $r/d = 4$ . The strength and behavior of specimens tested at the two loading rates are compared.

## 8.2 DESCRIPTION OF THE EXPERIMENTAL PROGRAM

8.2.1 Test Specimens. The connection specimens used simulate the area of a flat plate including the column and extending approximately to the lines of contraflexure (lines of no principal moment). The prototype slab system was assumed to have a 17-1/2-foot column spacing.

The specimens consisted of a 6-1/2-inch-thick reinforced concrete slab either 84 or 94 inches square with a 10- or 20-inch-square stub column 15 inches high located at the center (Figure 3.1). The nominal effective slab depth was 5 inches. The slabs were simply supported on an 80- or 90-inch span with the corners free to rise.

The reinforcement was proportioned to give the same flexural resistance in either direction. All reinforcement was evenly spaced across the slab parallel to the edges.

8.2.2 Experimental Procedure. All specimens were loaded with the 200-Kip Loader, an open-loop hydraulic device capable of producing both static and dynamic loads (Figure 4.9).

The perimeter of the slabs was supported on rollers placed on a massive reinforced concrete reaction structure. The specimens were tested in an inverted position.

Measurements included the applied load and the deflections at the column, at one corner of the slab, and at one of the quarterpoints of the span (Figure 4.11). Strain gages were placed at various locations on the



reinforcement and on the concrete compressive surface (Figures 4.14 through 4.17). Accelerations were measured on top of the column, near the base of the column, and at one of the quarterpoints of the span for the dynamically loaded specimen (Figure 4.11). Instrumentation to determine the initiation and opening of inclined (shear) cracks was added for the specimens with the larger column size.

All data were continuously recorded. Except for the integration of some acceleration traces, the data were reduced by scaling paper records produced by playing the tapes back through an oscillograph recorder.

### 8.3 BEHAVIOR OF SLAB-COLUMN CONNECTIONS FAILING IN SHEAR

The inclined crack formation and the consequent shear failure of a slab subjected to a concentrated load differ considerably from these processes in a beam because of certain structural characteristics of the slab. These characteristics will be explained first with the aid of an idealized model. More realistic configurations will then be examined.

8.3.1 Idealized Connection Model. The model, shown in Figure 8.1a, consists of a round slab loaded by a round column. The flexural reinforcement is placed in an orthogonal pattern (Figure 8.1b) and is of sufficient quantity to insure that shear failure occurs before general flexural yielding is reached in the slab. The ratio of the column radius to the slab depth is less than two.

The unit shear stress decreases rapidly away from the column because the potential crack perimeter increases with the radius. Inclined cracking is thus forced to occur near the column outline.

The radial moments in the linearly elastic isotropic slab also decrease

rapidly away from the column face. After the first crack (a circumferential crack nearly directly under the column outline) forms, the tangential moments exceed the radial moments at all points away from the immediate vicinity of the column. Subsequent cracking will be in the radial direction.

A sector of the model bounded by two radial cracks is shown in Figure 8.1c.

Unlike the flexure-shear crack in a beam, the inclined crack is not initiated by a flexural crack but develops in an uncracked section. The inclined crack begins near the center of the slab and propagates toward both slab surfaces.

Before inclined cracking, the parabolic shear stress distribution should be approached. Consequently, the load at inclined cracking for symmetrical slabs with small columns should be near that resulting from a nominal unit shear stress of two-thirds the concrete tensile strength at  $d/2$  from the column face. On the basis of a tensile strength of  $6\sqrt{f'_c}$ , the unit shear stress at cracking would be  $4\sqrt{f'_c}$ .

In addition to the more rapid decrease in the elastic moments in the model than in a beam, there are two other effects which have an important influence on the response of the slab. Both act to lower the radial stresses in the slab.

1. As yielding develops in the reinforcement crossing the radial cracks, the radial moments in the slab decrease even though the load is increasing (Section 6.10.3).

2. Whenever the principal moments differ and are not parallel to the reinforcement, inplane forces will be internally created in the slab.

The tangential moments usually exceed the radial moments, resulting in an excess of tensile force in the radial direction at the level of the reinforcement. The excess must be balanced by a resultant compressive force on the concrete (Figure 8.1c) which acts to prevent or control any circumferential cracks, including inclined cracks. Because the reinforcement is usually in the lower third of the section, tensile concrete stresses are added to the concrete near the compressive surface. Strain reversals caused by these two phenomena were observed in the tests (Figure 6.11).

Once the inclined crack does form, the tangential moments also restrain the opening of the crack. The crack can open only by a rotation of the slab sector in a vertical plane. This rotation necessitates an increase in the tangential strains and, therefore, an increase in the tangential moments and in the applied load.

The stress conditions in the concrete above the inclined crack also differ from those in a beam. The magnitude of the radial compressive force is not dictated by statics as it is in a beam, but also depends on compatibility. Much of the compressive force flows to areas of the slab away from the column, more so as the stiffness of the area above the inclined crack decreases. Because of this mechanism controlling compressive stresses and the absence of any control of the shear stresses, the concrete above the inclined crack fails primarily from excessive shear stresses.

8.3.2 Connections with Rectangular Columns. For the more usual case of rectangular columns, the failure becomes more complex because the axial symmetry is lost.

Most of the load is initially concentrated near the corners of the column. Although the corner areas should be slightly stronger in shear than

areas adjacent to the column face, inclined cracking and shear distress occur first near the column corners. When the ability of the corner regions to carry shear is lost, the areas adjacent to the column faces must transfer the load.

The shear failure with a square column is progressive. The connection is not fully effective: the connection strength is less than the sum of the strengths of the corner and column face areas.

8.3.3 Effect of Reinforcement Ratio. Larger reinforcement ratios increase the slab stiffness, the depth of the concrete compressive zone, and the amount of shear which may be carried by dowel forces. All three increase the shear strength.

Most slabs reaching general flexural yielding will eventually fail in shear. Failures of such connections are designated as flexural-shear failures.

8.3.4 Effect of Column Size. As the column size increases, the stress conditions in the slab approach those in a wide beam. Inclined cracks can more often develop from flexural cracks parallel to the column outline, especially in areas adjacent to the faces of rectangular columns. The final failure will approach the shear-compression model as the column size increases.

The efficiency of square columns increases with very large column sizes because the relative amount of the perimeter near the corner decreases. With very small columns, column shape becomes unimportant as all columns effectively apply a point-load to the slab.

## 8.4 STRENGTH OF THE TEST SPECIMENS

8.4.1 Statically Loaded Specimens. The average unit shear strength

$v_u$  of the two slowly loaded connection specimens with each configuration were:

Series	r/d Ratio	Reinforce- ment	$v_u = \frac{V_u}{(r + d)d}$	$\frac{v_u}{\sqrt{f'_c}}$
			pct	psi
S2075	2	0.75	224	3.36
S2150	2	1.50	353	5.28
S4075	4	0.75	153	2.35
S4150	4	1.50	266	3.71

The strengths of duplicate specimens varied by a maximum of 6 percent.

The test results are compared with the calculated yield-line flexural strength and the strengths given by twelve shear capacity equations in Figure 8.2. Three of the four series displayed an ultimate unit shear strength below the 1963 ACI Code (ACI, 1963) prediction of  $4\sqrt{f'_c}$  (the material understrength factor  $\phi = 1$  because material strengths were known), which is intended to represent a reasonable lower bound to experimental data.

The strength of the four S2075 and S4075 Specimens was controlled primarily by the flexural strength of the slab in the connection area, even though a punching-shear failure did occur after general flexural yielding was reached. The yield-line flexural analysis closely predicted the strengths of the S2075 and S4075 Specimens.

The 1963 ACI Code provisions for shear strength are applicable for the S2150 and S4150 Specimens. The two S4150 Specimens failed below the unit

shear stress of  $4\sqrt{f'_c}$  given by the 1963 ACI Code, as have a very large proportion of other reported specimens with  $r/d$  ratios of 4 or more.

8.4.2 Dynamically Loaded Specimens. The ratio of the dynamic capacity of the rapidly tested specimens to the static strength of the companion static tests for the four specimen configurations were:

Series	Ratio
2075	1.15
2150	1.23
4075	1.20
4150	1.29

A punching-shear failure occurred in all nine of the rapidly loaded specimens. The D2075 and D4075 Specimens developed appreciable flexural yielding before failure and failed at approximately 2 to 2-1/2 times the deflection of the more heavily reinforced specimens.

The expected material strength increases at the strain rates developed in the rapid tests are 25 percent for concrete in compression and 15 percent for steel in tension. These increases correspond closely to the observed strength increases of the specimens with  $p = 0.0150$  and  $0.0075$ , respectively. The strength of the specimens failing in flexural-shear (D2075 and D4075) were controlled primarily by the steel strength. The strength of the other specimens depended more heavily upon the concrete strength.

Large flexural deflections without a punching shear failure occurred in the two specimens tested with very rapidly applied loads of short duration. The average shear forces during an 8-msec interval were 1.60 and 1.72 times the static shear strength. Deflections of the slab were small during this period of high shear, i.e., less than 40 percent of the maximum deflection.

## 8.5 CONCLUSIONS

8.5.1 Statically Loaded Specimens. Among the 12 analysis and design methods studied, the ones that resulted in the smallest deviations from the measured strengths were the method proposed by Moe (1961) and given in Equation 2.5, and Moe's method modified to include concrete tensile strength (Hognestad, et al., 1964) as given by Equation 2.17. These methods, which should not be used with slab-column connections having  $r/d$  ratios larger than 4, overestimated the observed strengths by an average of 7 percent. The decrease in the unit shear stress with the  $r/d$  ratio was larger than indicated by any of the 12 methods (see Figure 8.2a).

Connections weak in flexure and reaching general flexural yielding are likely to fail ultimately by punching shear. Such flexural-shear failures occurred in some tests at less than 60 percent of the shear capacity calculated according to the 1963 ACI Code (ACI, 1963). The strengths of the specimens which experienced flexural-shear failures were closely predicted by the yield-line theory (Equation 6.1).

For shear failures, calculations based on the 1963 ACI Code resulted in strength underestimates of 25 percent for the specimens with the smaller column size ( $r/d = 2$ ). The 1963 ACI Code was slightly unconservative for the larger columns ( $r/d = 4$ ). Use of a unit shear strength approaching  $3\sqrt{f'_c}$  at large  $r/d$  ratios appears advisable.

The failure surface of the connection specimens tested had a shape approximating the surface of a truncated cone spreading out from the column. The angle of the failure surface varied considerably, but was generally 20 to 30 degrees from the horizontal.

Punching shear failure occurred at a center deflection of from 0.7 to 2.0 percent of the span of the specimen. The failure deflections of the

specimens with  $p = 0.0075$  were slightly over twice those of the specimens with  $p = 0.0150$ . Failure deflections increased by about one-fourth as the  $r/d$  ratio was increased from 2 to 4.

The stiffness of the elastic portion of the elastoplastic idealization of the static resistance curve was near that given by elastic plate theory (Equation 6.3) using a fully cracked section modulus. The ductilities of the specimens in this program ranged from 1.3 to 3.5 using the elastic stiffness calculated by Equation 6.3.

8.5.2 Mechanism of Shear Failure. Flexural cracking is in the radial direction for connections with small  $r/d$  ratios except at the column outline. The possibility of circumferential flexural cracking away from the column outline increases as the  $r/d$  ratio increases.

The inclined crack in connections with small or moderate  $r/d$  ratios forms in an uncracked region and not from a flexure crack.

The shear-compression failure model used for many beams failing in shear does not describe the failure of the compression zone above the inclined cracks in slab connections failing in shear, especially with the lower  $r/d$  ratios. The compressive stresses at the column face can be redistributed to other parts of the slab. This redistribution results in the concrete above the inclined crack failing primarily from excessive shear, not compression.

The stiffness provided by the tangential moments of a slab helps control the propagation and opening of inclined cracks.

A sizable reversal of the concrete strains on the surface opposite the reinforcement can develop at large slab deflections. This phenomenon is related to the decrease in radial moments accompanying yield-line formation and by the creation of inplane forces resulting when the reinforcement



direction deviates from the principal moment direction.

With square columns, inclined cracking starts near the corners of the column. Shear resistance is also lost first at the corners. The strength of connections with square columns is necessarily less than the sum of the strengths of the areas near the column corners and those near the column face because of the progressive nature of the failure.

8.5.3 Very Rapidly Loaded Specimens. The two specimens loaded very rapidly transferred an average shear force of 1.6 and 1.7 times the static strength during an 8-msec period before yielding was general in the slab. Neither slab failed by punching shear. Strain-rate effects on the material strength accounted for about one-half of this strength increase.

Shear and flexure can be critical at different times for slabs subjected to very rapidly applied loads of short duration.

8.5.4 Rapidly Loaded Specimens. The failure mechanism and crack patterns were similar to those resulting with static loadings.

The shear strength of the slab-column connections increased slightly more than the flexural strength with rapid loading. The increase in strength with rapid loading averaged 18 percent for the specimens failing primarily in flexure (those with  $p = 0.0075$ ) and 26 percent for those failing in shear ( $p = 0.0150$ ). The strength increases of the specimens with  $p = 0.0075$  and  $0.0150$  corresponded closely to the material strength increases expected for the steel and concrete, respectively, at the strain rates reached in the tests.

Failure deflections increased 25 to 50 percent over the static test values with the rapid loading rate used.

The blast resistance of the prototype slab systems, which were chosen

to bound the properties of most flat-plate structures, will be limited to 1.3 to 3.5 psi by the strength of the slab-column connections.

Resistance provided after shear failure by tensile membrane action of the reinforcement will not normally be a usable portion of the resistance curve.

## 8.6 RECOMMENDATIONS FOR FUTURE RESEARCH

More information is needed on the response and behavior of eccentrically loaded connections at static loading rates. The effect of loading speed on eccentrically loaded connections should also be determined. Most connections in a blast-loaded building will transfer some moment as well as shear.

A large proportion of the connections in a slab system are located either at the corners or along the sides of the building. The behavior of these connections has not been adequately explored.

Additional experimental data points are needed on the performance of connections weaker in flexure than in shear, the condition encouraged in design. An empirical expression predicting the ductility or failure deflection of the connections failing in flexural-shear would be very useful both in design and analysis of dynamically loaded structures. The effect of edge restraint, which allows increasing load after the slab has reached general yielding in the column area, on the strength and failure deflection of specimens weak in flexure has not been adequately investigated.

Connection model tests using  $r/d$  ratios larger than 4 are desirable both to model the connections in flat slabs and to assess the magnitude of the decrease in the ultimate unit shear strength with increasing column

size. The strength of wide beams is a lower limit to the strength of connections with very large columns and has not been adequately investigated.

Dynamic testing of prototypes or models of slab systems containing slab-column connections will more directly determine the performance of the connections in a blast-loaded structure.

More and better information concerning the probable load-time history acting on a connection in a blast-loaded structure is needed.

## LIST OF REFERENCES

- American Concrete Institute, "Commentary on Building Code Requirements for Reinforced Concrete (ACI 318-63)," Special Publication SP-10, 1965, Detroit, Mich.
- American Concrete Institute Committee 318, "ACI Standard Building Code Requirements for Reinforced Concrete (ACI 318-56)," Proceedings, American Concrete Institute, Vol 52, May 1956, pp 913-986.
- \_\_\_\_\_, "ACI Standard Building Code Requirements for Reinforced Concrete (ACI 318-63)," Proceedings, American Concrete Institute, Vol 60, June 1963, pp 809-816.
- American Concrete Institute-American Society of Civil Engineers Committee 326, "Shear and Diagonal Tension," Proceedings, American Concrete Institute; "Part 1, General Principles," Vol 59, Jan 1962, pp 1-30; "Part 2, Beams and Frames," Vol 59, Feb 1962, pp 277-334; "Part 3, Slabs and Footings," Vol 59, Mar 1962, pp 353-396.
- American Society for Testing and Materials, "1964 Book of ASTM Standards"; 1964, Philadelphia, Pa.
- Anderson, F. E., Jr., et al., "Design of Structures to Resist Nuclear Weapons Effects," ASCE Manuals of Engineering Practice No. 42, 1961, American Society of Civil Engineers, New York, N. Y.
- Andersson, J. L., "Genomstansning av Lift Slabs (Punching of Lift Slabs)," Bulletins of the Division of Building Statics and Structural Engineering No. 49 (in Swedish), 1964, Royal Institute of Technology, Stockholm, Sweden; also Nordisk Betong No. 3, 1964.
- \_\_\_\_\_, "Genomstansning av plattor understödda av pelare vid fri kant (Punching of Slabs Supported on Columns at Free Edges)," Bulletins of the Division of Building Statics and Structural Engineering No. 61 (in Swedish), 1966, Royal Institute of Technology, Stockholm, Sweden.
- \_\_\_\_\_, "Punching of Concrete Slabs with Shear Reinforcement," Transactions No. 212, 1963, Royal Institute of Technology, Stockholm, Sweden.
- Atchley, B. L. and Furr, H. L., "Strength and Energy Absorption Capabilities of Plain Concrete Under Dynamic and Static Loadings," Proceedings, American Concrete Institute, Vol 64, Nov 1967, pp 745-756.
- Beresford, F. D., "Tests of Edge Column Connections of a Flat Plate Structure," The Institution of Engineers, Australia, Civil Engineering Transactions, Vol CE 9, No. 2, Oct 1967, pp 235-241.

- Biggs, J. M., Introduction to Structural Dynamics, McGraw-Hill, New York, 1964, pp 212-219.
- Blakey, F. A., "Australian Experiments with Flat Plates," Proceedings, American Concrete Institute, Vol 60, Apr 1963, pp 515-525.
- \_\_\_\_\_, "Design of Flat Slabs," Concrete, Vol 1, No. 10, Oct 1967, pp 361-362.
- Brode, H. L., "A Review of Nuclear Explosion Phenomena Pertinent to Protective Construction," Report No. R-425-PR, p 39, May 1964, The RAND Corporation, Santa Monica, Calif.
- Cooke, R. W. and Seddon, A. E., "The Laboratory Use of Bonded-Wire Electrical-Resistance Strain Gages on Concrete in the Building Research Station," Magazine of Concrete Research, Vol 8, No. 22, Mar 1956, pp 31-38.
- Corley, W. G. and Hawkins, N. M., "Shearhead Reinforcement for Slabs," Proceedings, American Concrete Institute, Vol 65, Oct 1968, pp 811-824.
- Cowell, W. L., "Dynamic Properties of Plain Portland Cement Concrete," Technical Report R447, June 1966, U. S. Naval Civil Engineering Laboratory, Port Hueneme, Calif.
- \_\_\_\_\_, "Dynamic Tests of Concrete Reinforcing Steels," Technical Report R394, Sept 1965, U. S. Naval Civil Engineering Laboratory, Port Hueneme, Calif.
- Denton, D. R., "A Dynamic Ultimate Strength Study of Simply Supported Two-Way Reinforced Concrete Slabs," Technical Report No. 1-789, July 1967, U. S. Army Engineer Waterways Experiment Station, CE, Vicksburg, Miss.
- Desai, C. S., Solution of Stress-Deformation Problems in Soil and Rock Mechanics Using Finite Element Methods, Ph. D. thesis, University of Texas, Austin, Tex., Aug. 1968.
- Diaz de Cossio, Roger, discussion of "Shear and Diagonal Tension" (ACI-ASCE, 1962), Proceedings, American Concrete Institute, Vol 59, Sept 1962, pp 1323-1333.
- Di Stasio, J. and Van Buren, M. P., "Transfer of Bending Moment Between Flat Plate Floor and Column," Proceedings, American Concrete Institute, Vol 57, Sept 1960, pp 299-314.
- Elstner, R. C. and Hognestad, E., "Shearing Strength of Reinforced Concrete Slabs," Proceedings, American Concrete Institute, Vol 53, July 1956, pp 29-58.

- Feld, J., "Lessons from Failures of Concrete Structures," American Concrete Institute Monograph Series, Monograph No. 1, 1964, pp 30-32.
- Gamble, W. L., "An Experimental Investigation of the Strength and Behaviour of a Prestressed Concrete Flat Plate," Report T8.0-9, 1964, Commonwealth Scientific and Industrial Research Organization, Division of Building Research, Melbourne, Australia; also "Experimental Lightweight Flat Plate Structure, Part 8 - Test to Failure of a Prestressed Slab," Constructional Review, Vol 37, No. 10, Oct 1964.
- Graf, O., "Strength Tests of Thick Reinforced Concrete Slabs Supported on All Sides Under Concentrated Loads (Versuche über die Widerstandsfähigkeit von allseitigen aufliegen dicken Eisenbetonplatten unter Einzellasten)" (in German), No. 88, 1938, Deutscher Ausschuss für Eisenbeton, Berlin.
- Grow, J. B. and Vanderbilt, M. D., "A Study of the Shear Strength of Lightweight Prestressed Concrete Flat Plates," Structural Research Report No. 2, Dec 1966, Civil Engineering Department, Colorado State University, Fort Collins, Colo.; also Journal of the Prestressed Concrete Institute, Vol 12, No. 4, Aug 1967, pp 18-28.
- Guralnick, S. A. and La Fraugh, R. W., "Laboratory Study of a 45-Foot-Square Flat Plate Structure," Proceedings, American Concrete Institute, Vol 60, Sept 1963, pp 1107-1185; also Portland Cement Association, Research and Development Laboratories, Bulletin D70, Skokie, Ill.
- Hansen, R. J., Nawy, E. G., and Shah, J. M., "Response of Concrete Shear Keys to Dynamic Loading," Proceedings, American Concrete Institute, Vol 57, May 1961, pp 1475-1490.
- Hanson, N. W. and Hanson, J. M., "Shear and Moment Transfer Between Concrete Slabs and Columns," Journal of the PCA Research and Development Laboratories, Portland Cement Association, Vol 10, No. 1, Jan 1968, pp 2-16.
- Hatcher, D. S., Sozen, M. A., and Siess, C. P., "A Study of Tests on a Flat Plate and Flat Slab," Structural Research Series 217, July 1961, Department of Civil Engineering, University of Illinois, Urbana, Ill.; also "Tests on a Reinforced Concrete Flat Plate," Journal of the Structural Division, Proceedings, American Society of Civil Engineers, Vol 91, Oct 1965, pp 205-231.
- Hognestad, E., "Shearing Strength of Reinforced Concrete Column Footings," Proceedings, American Concrete Institute, Vol 50, Nov 1953, pp 189-208.
- Hognestad, E., Elstner, R. C., and Hanson, J. A., "Shear Strength of Reinforced Structural Lightweight Aggregate Concrete Slabs," Proceedings, American Concrete Institute, Vol 61, June 1964, pp 643-655.

- Ivy, C. B., Ivey, D. L., and Buth, E., "Shear Capacity of Lightweight Concrete Flat Slabs," Journal of the American Concrete Institute, Vol 66, No. 6, June 1969, pp 490-494.
- Keenan, W. A., "Dynamic Shear Strength of Reinforced Concrete Beams - Part I," Technical Report R395, Dec 1965, U. S. Naval Civil Engineering Laboratory, Port Hueneme, Calif.
- Kinnunen, S., "Punching of Concrete Slabs with Two-Way Reinforcement with Special Reference to Dowel Effect and Deviation of Reinforcement from Polar Symmetry," Transactions No. 198, 1963, Royal Institute of Technology, Stockholm, Sweden.
- Kinnunen, S. and Nylander, H., "Punching of Concrete Slabs Without Shear Reinforcement," Transactions No. 158, 1960, Royal Institute of Technology, Stockholm, Sweden.
- Kupfer, H., Hilsdorf, H. K., and Rüsçh, H., "Behavior of Concrete Under Biaxial Stresses," Journal of the American Concrete Institute, Vol 66, No. 8, Aug 1969, pp 656-666.
- Lee, S. T., Behavior of Micro-Concrete Flat Plate Structure, M.S. thesis, Massachusetts Institute of Technology, Cambridge, Mass., Mar 1964.
- Lenschow, R. J. and Sozen, M. A., "A Yield Criterion for Reinforced Concrete Under Biaxial Moments and Forces," Structural Research Series No. 311, July 1966, Department of Civil Engineering, University of Illinois, Urbana, Ill.
- Long, A. E. and Bond, D., "Punching Failure of Reinforced Concrete Slabs," Proceedings, The Institution of Civil Engineers, London, Vol 37, May 1967, pp 109-162.
- Lundeen, R. L., "Dynamic and Static Tests of Plain Concrete Specimens," Miscellaneous Paper No. 6-609, Report 1, Nov 1963, U. S. Army Engineer Waterways Experiment Station, CE, Vicksburg, Miss.
- Magura, D. D. and Corley, W. G., "Tests to Destruction of a Multipanel Waffle Slab Structure," Full-Scale Testing of New York World's Fair Structures, Volume II, The Rathskeller Structure, Publication 1721, Building Research Advisory Board, National Academy of Sciences, Washington, D. C., 1969, pp 10-135.
- McHenry, D. and Shideler, J. J., "Review of Data on Effect of Speed in Mechanical Testing of Concrete," Symposium of Speed on Testing of Non-Metallic Materials, ASTM Special Technical Publication No. 185, 1956, pp 72-82; also reprinted as Portland Cement Association, Research and Development Laboratories, Development Department Bulletin D9, Skokie, Ill.

- Melin, J. W. and Sutcliffe, S., "Development of Procedures for Rapid Computation of Dynamic Structural Response," Structural Research Series 171, Jan 1959, Department of Civil Engineering, University of Illinois, Urbana, Ill.
- Meriam, J. L., Statics, Wiley, New York, 1966.
- Moe, J., "Shearing Strength of Reinforced Concrete Slabs and Footings Under Concentrated Loads," Development Department Bulletin D47, Apr 1961, Portland Cement Association, Research and Development Laboratories, Skokie, Ill.
- Mowrer, R. D. and Vanderbilt, M. D., "Shear Strength of Lightweight Aggregate Reinforced Concrete Flat Plates," Proceedings, American Concrete Institute, Vol 64, Nov 1967, pp 722-729.
- Newmark, N. M., "A Method of Computation for Structural Dynamics," Transactions, American Society of Civil Engineers, Vol 127, Part I, 1962, pp 1406-1435.
- Newmark, N. M. and Haltiwanger, J. D., "Air Force Design Manual, Principles and Practices for Design of Hardened Structures," Technical Documentary Report No. AFSWC-TDR-62-138, Dec 1962, Air Force Special Weapons Center, Kirtland Air Force Base, N. Mex.
- Norris, C. H., et al., Structural Design for Dynamic Loads, McGraw-Hill, New York, 1959, pp 21-27.
- Rao, K. S. S., Rengaraju, V. R., and Ranganatham, B. V., "Charts for the Punching Shear Analysis of Reinforced Concrete Slabs," Indian Concrete Journal, Vol 42, No. 6, June 1968, pp 242-248.
- Reimann, H., Zur Bemessung von Dünnen Plattendecken auf Stützen Ohne Kopf gegen Durchstanzen (The Proportioning of Thin Slabs Supported on Columns Without Capitals Against Punching), Dr.-Ing. thesis (in German), Technischen Hochschule, Stuttgart, Jan 1963.
- Reinschmidt, K. F., Hansen, R. J., and Yang, C. Y., "Dynamic Tests of Reinforced Concrete Columns," Proceedings, American Concrete Institute, Vol 61, Mar 1964, pp 317-333.
- Richart, F. E., "Reinforced Concrete Wall and Column Footings," Proceedings, American Concrete Institute, Vol 45, Oct and Nov 1948, pp 97-127 and 237-260.
- Roark, R. J., Formulas for Stress and Strain, 4th ed., McGraw-Hill, New York, 1965.
- Rosenthal, E., "Experimental Investigation of Flat Plate Floors," Proceedings, American Concrete Institute, Vol 56, Aug 1959, pp 153-166.



- Scordelis, A. C., Lin, T. Y., and May, H. R., "Shearing Strength of Prestressed Lift Slabs," Proceedings, American Concrete Institute, Vol 55, Oct 1958, pp 485-506.
- Seabold, R. H., "Dynamic Shear Strength of Reinforced Concrete Beams - Part II," Technical Report R502, pp 52-56, Jan 1967, U. S. Naval Civil Engineering Laboratory, Port Hueneme, Calif.
- Self, M. W., "Ultimate Strength of Reinforced Concrete Flat Slabs," Journal of the Structural Division, Proceedings, American Society of Civil Engineers, Vol 90, Aug 1964, pp 205-233.
- Siess, C. P., "Behavior of High-Strength Deformed Reinforcing Bars Under Rapid Loading," unnumbered report, Feb 1962, Department of Civil Engineering, University of Illinois, Urbana, Ill.
- Sozen, M. A. and Siess, C. P., "Investigation of Multiple-Panel Reinforced Concrete Floor Slabs; Design Methods--Their Evolution and Comparison," Proceedings, American Concrete Institute, Vol 60, Aug 1963, pp 999-1027.
- Talbot, A. N., "Reinforced Concrete Wall Footings and Column Footings," Bulletin No. 67, Mar 1913, Engineering Experiment Station, University of Illinois, Urbana, Ill.
- Tasker, H. E. and Wyatt, R. J., "Shear in Flat-Plate Construction Under Uniform Loading," Special Report No. 23, Oct 1963, Australian Commonwealth Experimental Building Station, Sydney, Australia.
- Taylor, R. and Hayes, B., "Some Tests on the Effect of Edge Restraint on Punching Shear in Reinforced Concrete Slabs," Magazine of Concrete Research, Vol 17, No. 50, Mar 1965, pp 39-44.
- Timoshenko, S. and Woinowsky-Krieger, S., Theory of Plates and Shells, 2d ed., McGraw-Hill, New York, 1959.
- U. S. Army Engineer Waterways Experiment Station, CE, "Handbook for Concrete and Cement," Aug 1949 (with quarterly supplements), Vicksburg, Miss.
- Watstein, D., "Effect of Straining Rate on the Compressive Strength and Elastic Properties of Concrete," Proceedings, American Concrete Institute, Vol 49, Apr 1953, pp 729-744.
- Wheeler, W. H., "Frame for Concrete Columns," U. S. Patent No. 2,000,543, May 7, 1935, U. S. Patent Office, Washington, D. C.
- Whitney, C. S., "Ultimate Shear Strength of Reinforced Concrete Flat Slabs, Footings, Beams, and Frame Members Without Shear Reinforcement," Proceedings, American Concrete Institute, Vol 54, Oct 1957, pp 265-298.

Wright, R. N. and Hall, W. J., "Loading Rate Effects in Structural Steel Design," Journal of the Structural Division, Proceedings, American Society of Civil Engineers, Vol 90, Oct 1964, pp 11-37.

Yitzhaki, D., "Punching Strength of Reinforced Concrete Slabs," Proceedings, American Concrete Institute, Vol 63, May 1966, pp 527-542.

TABLE 3.1 EXPERIMENTAL PROGRAM

Specimen	Reinforcement Ratio	Loading Speed
	pct	
10-Inch-Square Column:		
S2075-1	0.75	Static
S2075-2	0.75	Static
S2150-1	1.50	Static
S2150-2	1.50	Static
D2075-1	0.75	Dynamic
D2075-2	0.75	Dynamic
D2075-3	0.75	Dynamic
D2150-1	1.50	Dynamic
D2150-2	1.50	Dynamic
D2150-3	1.50	Dynamic
20-Inch-Square Column:		
S4075-1	0.75	Static
S4075-2	0.75	Static
S4150-1	1.50	Static
S4150-2	1.50	Static
D4075-1	0.75	Dynamic
D4075-2	0.75	Dynamic
D4075-3	0.75	Dynamic
D4150-1	1.50	Dynamic
D4150-2	1.50	Dynamic
D4150-3	1.50	Dynamic

TABLE 4.1 PROPORTIONS OF CONCRETE MIXTURES

Specimen	Cement-Sand-Gravel Ratio by Weight	Water-Cement Ratio by Weight
----------	------------------------------------	------------------------------

## Cement Shipment RC-579:

S2075-1	1:3.43:4.26	0.717
S2075-2	1:3.43:4.26	0.717
S2150-1	1:3.43:4.26	0.717
S2150-2	1:3.43:4.26	0.717
D2075-1	1:3.23:4.01	0.682
D2075-2	1:3.36:4.17	0.693
D2075-3	1:3.43:4.26	0.717
D2150-1	1:3.43:4.26	0.717
D2150-2	1:3.43:4.26	0.717
D2150-3	1:3.43:4.26	0.717
S4075-1	1:3.43:4.26	0.717
S4075-2	1:3.43:4.26	0.717

## Cement Shipment RC-608:

S4150-1	1:3.05:3.94	0.664
S4150-2	1:3.05:3.94	0.664
D4075-1	1:3.05:3.94	0.664
D4075-2	1:3.43:4.26	0.717
D4075-3	1:3.43:4.26	0.717
D4150-1	1:3.05:3.94	0.664
D4150-2	1:3.05:3.94	0.664

TABLE 4.2 MILL-DETERMINED PROPERTIES OF NO. 5 REINFORCEMENT

Heat Number	Yield Strength	Ultimate Strength	Flow in 8 Inches	Bend Test	Manganese Content	Phosphorous Content	Sulphur Content	Carbon Content
	psi	psi	pct		pct	pct	pct	pct
10858	50,396	70,740	22	Satisfactory	0.62	0.004	0.047	0.30
10540	50,919	74,675	25	Satisfactory	0.64	0.016	0.062	0.31

TABLE 4.3 WES-DETERMINED PROPERTIES OF NO. 5 REINFORCEMENT

Bundle of Steel	Specimens Using This Steel	Number of Specimen Tests	Range of Yield Strengths	Average Yield Strength	Average Ultimate Strength	Flow in 8 Inches
			psi	psi	psi	pct
1	S2075-1 S2075-2 S2150-1 S2150-2 S4075-1 S4075-2 S4150-1	9	47,100 to 49,190	47,940	72,500	26.0
2	D2075-1 D2075-2 D2150-1 S4150-2 D4075-1	8	48,060 to 49,190	48,710	74,300	25.9
3	D2075-3 D2150-2 D2150-2 D4075-2	8	48,710 to 51,450	50,160	77,260	23.7
4	D4075-3 D4150-1 D4150-2	7	46,610 to 47,900	47,200	73,300	21.0

TABLE 4.4 CONCRETE CYLINDER TEST RESULTS

Specimen	Age at Test	28-Day Compressive Strength, Batch 1 <sup>a</sup>	Compressive Strength at Time of Test				Split Cylinder Strength, Batch 1 <sup>c</sup>
			Batch 1 <sup>b</sup>	Batch 2 <sup>c</sup>	Batch 3 <sup>c</sup>	Average	
	days	psi	psi	psi	psi	psi	psi
S2075-1	55	--	4700	4680	5210	4860	430
S2075-2	45	--	4210	4320	4720	4470	475
S2150-1	42	4100	4290	4370	4720	4460	445
S2150-2	31	4160	4370	3910	4290	4190	445
D2075-1	42	4440	4870	5730	--	5300	525
D2075-2	42	4090	4180	4670	4860	4570	465
D2075-3	54	3880	4480	4920	4860	4750	475
D2150-1	43	--	4310	4290	4250	4280	465
D2150-2	40	3650	4140	4890	4740	4590	460
D2150-3	30	4460	4740	4750	4550	4680	440
S4075-1	43	3800	3860	3960	4270	4030	395
S4075-2	42	4200	4670	4940	4760	4790	485
S4150-1	41	5090	5140	5150	5140	5140	435
S4150-2	42	--	5180	4850	5350	5130	485
D4075-1	45	--	5310	5080	5140	5180	480
D4075-2	41	4340	4300	4010	4010	4110	370
D4075-3	28	4180	4180	4570	4620	4460	435
D4150-1	40	4650	5020	5170	5390	5190	545
D4150-2	38	5480	5600	5290	5420	5440	465

- <sup>a</sup> Average of two cylinder tests.  
<sup>b</sup> Average of five cylinder tests.  
<sup>c</sup> Average of three cylinder tests.

TABLE 5.1 SUMMARY OF TEST RESULTS

r/d = ratio of column size to effective slab depth; p = flexural reinforcement ratio; d = measured effective slab depth;  $f'_c$  = compressive strength of concrete in the column vicinity;  $f_y$  = yield stress of the reinforcement.

Specimen	Measured r/d	p	d	$f'_c$	$f_y$	Maximum Connection Resistance	Column Deflection at Failure <sup>a</sup>	Rise	Time to
								Time	Failure
			inches	psi	psi	pounds	inches	msec	msec
S2075-1	2.10	0.00789	4.75	4700	47,950	65,200	1.23		Static
S2075-2	2.08	0.00780	4.81	4210	47,950	61,300	1.32		Static
S2150-1	2.05	0.01537	4.88	4290	47,950	104,400	0.61		Static
S2150-2	2.08	0.01560	4.81	4370	47,950	99,000	0.54		Static
171	D2075-1	2.08	4.81	4870	48,710	157,500 <sup>b</sup>	1.85 <sup>b</sup>	2.2	b
	D2075-2	2.08	4.81	4180	48,710	193,900 <sup>b</sup>	2.95 <sup>b</sup>	2.4	b
	D2075-3	2.03	4.93	4480	50,160	79,100	1.75	26	54
	D2150-1	2.01	4.97	4310	48,710	129,800	0.80	24	50
	D2150-2	2.03	4.93	4140	50,160	125,800	0.64	22	31
	D2150-3	2.03	4.93	4740	50,160	134,300	0.71	22	45
	S4075-1	4.00	5.00	3860	47,950	77,000	1.80		Static
S4075-2	4.10	4.88 <sup>a</sup>	4670	47,950	74,100	1.32		Static	
S4150-1	4.05	4.94	5140	47,950	130,200	0.81		Static	
S4150-2	4.05	4.94	5180	48,710	130,500	0.72		Static	
D4075-1	4.00	5.00	5310	48,710	95,000	2.40	9	62	
D4075-2	4.00	5.00	4300	50,160	94,000	2.62	9	81	
D4075-3	4.00	5.00	4180	47,200	92,100	2.76	30	140	
D4150-1	4.07	4.91	5020	47,200	163,500	c	32	57	
D4150-2	4.07	4.91	5600	47,200	169,400	1.14	28	51	

<sup>a</sup> Average at column face.

<sup>b</sup> No failure.

<sup>c</sup> No record, instrumentation difficulties.



TABLE 6.1 OBSERVED RELATIVE DUCTILITIES OF STATICALLY TESTED SPECIMENS

Specimen	Stiffness of Fitted Elasto-Plastic Curve	Ductility, Ratio of Failure Deflection to Deflection at Start of Plastic Curve	Energy Absorption Capacity	Failure Deflection	Ratio of Failure Deflection to General Yielding Deflection	Ratio of Failure Deflection to Span Length
	lb/in		in-lb	inches		pct
S2075-1	142,000	2.7	65,000	1.23	1.6	1.54
S2075-2	168,000	3.8	67,500	1.32	1.7	1.65
S2150-1	294,000	1.8	44,000	0.61	a	0.76
S2150-2	291,000	1.6	36,000	0.54	a	0.68
S4075-1	205,000	4.9	122,800	1.80	2.5	2.00
S4075-2	190,000	3.4	83,300	1.32	1.8	1.47
S4150-1	236,000	1.5	69,200	0.81	a	0.90
S4150-2	337,000	1.9	67,800	0.72	a	0.80

<sup>a</sup> Did not reach general yielding stage.

TABLE 6.2 COMPARISON OF CALCULATED FLEXURAL CAPACITIES AND TEST RESULTS

Specimen	Calculated Unit Moment Capacity, m	Calculated Flexural Capacity $V_{flex}$	Observed Failure Load $V_{test}$	Ratio of Observed Load to Calculated Capacity, $\phi_o$
	in-lb/in	kips	kips	
S2075-1	8,210	63.8	65.2	1.022
S2075-2	8,290	64.4	61.3	0.952
S4075-1	8,590	76.5	77.0	1.006
S4075-2	8,440	75.2	74.1	0.985
S2150-1	16,100	125.1	104.4	0.835
S2150-2	15,750	122.4	99.0	0.809
S4150-1	16,500	147.1	130.2	0.885
S4150-2	16,750	149.3	130.5	0.874

TABLE 6.3 COMPARISON OF CALCULATED SHEAR STRENGTHS AND TEST RESULTS

Specimen	Test Results $V_{test}$	Equation 6.1 Yield Line Elstner- Hognestad (1956)		Equation 2.3 Elstner- Hognestad (1956)		Equation 2.4 Whitney (1957)		Equation 2.5 Moe (1961) Analysis		Equation 2.6 Moe (1961) Design		Equation 2.10 Yitzhaki (1966)	
		$V_{calc}$	$\frac{V_{test}}{V_{calc}}$	$V_{calc}$	$\frac{V_{test}}{V_{calc}}$	$V_{calc}$	$\frac{V_{test}}{V_{calc}}$	$V_{calc}$	$\frac{V_{test}}{V_{calc}}$	$V_{calc}$	$\frac{V_{test}}{V_{calc}}$	$V_{calc}$	$\frac{V_{test}}{V_{calc}}$
		kips	kips	kips	kips	kips	kips	kips	kips	kips	kips	kips	kips
S2075-1	65.2	63.8	1.022	88.4	0.786	55.9	1.165	79.4	0.821	89.5	0.728	75.2	0.867
S2075-2	61.3	64.4	0.952	81.7	0.750	56.6	1.083	78.3	0.783	86.2	0.711	76.0	0.807
Average	63.2		0.987		0.768		1.124		0.802		0.720		0.837
S4075-1	77.0	76.6	1.006	148.6	0.518	98.2	0.784	96.5	0.798	124.3	0.620	119.1	0.646
S4075-2	74.1	75.2	0.985	150.4	0.493	96.3	0.769	96.8	0.765	131.7	0.562	117.0	0.633
Average	75.6		0.996		0.506		0.778		0.782		0.591		0.640
Average for Specimens with $p = 0.0075$			0.991		0.638		0.950		0.792		0.655		0.738
S2150-1	104.4	125.1	0.835	99.3	1.051	82.9	1.259	105.6	0.988	88.7	1.177	95.3	1.096
S2150-2	99.0	122.4	0.809	98.2	1.008	81.8	1.211	104.2	0.950	87.8	1.128	93.9	1.055
Average	101.7		0.822		1.030		1.235		0.969		1.153		1.076
S4150-1	130.2	147.1	0.885	181.4	0.718	141.9	0.917	147.2	0.885	140.8	0.925	147.4	0.883
S4150-2	130.5	149.3	0.874	182.5	0.715	143.5	0.910	148.5	0.879	141.3	0.923	148.4	0.880
Average	130.4		0.880		0.717		0.914		0.882		0.924		0.882
Average for Specimens with $p = 0.0150$			0.851		0.873		1.074		0.926		1.038		0.979

Specimen	Test Results $V_{test}$	Equation 2.12 Tasker-Wyatt (1963) Analysis		Equation 2.13 Tasker-Wyatt (1963) Design		Equation 2.17 Hognestad et al. (1964)		Equation 2.18 Mower- Vanderbilt (1967)		Equation 2.20 1963 ACI Code (ACI, 1963) $\phi = 1.0$	
		$V_{calc}$	$\frac{V_{test}}{V_{calc}}$	$V_{calc}$	$\frac{V_{test}}{V_{calc}}$	$V_{calc}$	$\frac{V_{test}}{V_{calc}}$	$V_{calc}$	$\frac{V_{test}}{V_{calc}}$	$V_{calc}$	$\frac{V_{test}}{V_{calc}}$
		kips	kips	kips	kips	kips	kips	kips	kips	kips	kips
S2075-1	65.2	81.9	0.797	74.6	0.874	76.9	0.848	90.0	0.725	76.9	0.848
S2075-2	61.3	80.9	0.758	71.7	0.855	81.8	0.750	88.9	0.690	74.0	0.829
Average	63.2		0.777		0.865		0.799		0.708		0.839
S4075-1	77.0	99.6	0.773	111.8	0.650	94.6	0.814	111.4	0.691	124.3	0.620
S4075-2	74.1	99.7	0.744	119.0	0.623	98.8	0.750	112.5	0.659	132.8	0.558
Average	75.6		0.758		0.637		0.782		0.675		0.589
Average for Specimens with $p = 0.0075$			0.768		0.750		0.791		0.691		0.714
S2150-1	104.4	110.0	0.950	73.9	1.416	106.6	0.979	120.1	0.869	76.1	1.372
S2150-2	99.0	108.1	0.916	73.1	1.354	104.6	0.947	118.2	0.837	75.4	1.314
Average	101.7		0.933		1.385		0.963		0.852		1.343
S4150-1	130.2	151.0	0.862	126.9	1.029	139.9	0.930	170.4	0.764	141.3	0.921
S4150-2	130.5	152.5	0.856	127.4	1.024	149.0	0.876	172.0	0.759	141.9	0.920
Average	130.4		0.859		1.027		0.903		0.761		0.921
Average for Specimens with $p = 0.0150$			0.896		1.206		0.933		0.807		1.132

TABLE 6.4 STRENGTHS AND SLAB ROTATIONS PREDICTED BY METHODS OF KINNUNEN-NYLANDER AND KINNUNEN

For these calculations, an equivalent circular column and slab were assumed as described in Appendix D.

Specimen	Test Results $V_{test}$	Observed Rotation $\psi_{test}$	Kinnunen-Nylander (1960)(Bulletin 158)				Kinnunen (1963)(Bulletin 198)			
			$y/d^a$	$\psi_{calc}$	$V_{calc}^b$	$\frac{V_{test}}{V_{calc}}$	$y/d^a$	$\psi_{calc}$	$V_{calc}$	$\frac{V_{test}}{V_{calc}}$
	kips	radians		radians	kips			radians	kips	
S2075-1	65.2	0.0276	0.255	0.0119	52.2	1.249	0.226	0.0182	52.0	1.254
S2075-2	61.3	0.0296	0.252	0.0119	53.6	1.143	0.222	0.0184	53.2	1.151
					Average	1.196			Average	1.202
175 S4075-1	77.0	0.0404	0.219	0.0219	74.1	1.039	0.166	0.0430	62.5	1.232
S4075-2	74.1	0.0296	0.199	0.0268	72.8	1.018	0.151	0.0480	60.9	1.216
					Average	1.029			Average	1.244
Average of $p = 0.0075$ slabs						1.112				1.213
S2150-1	104.4	0.0137	0.381	0.0084	80.3	1.299	0.354	0.0123	83.2	1.255
S2150-2	99.0	0.0121	0.380	0.0085	79.1	1.251	0.354	0.0125	82.2	1.205
					Average	1.275			Average	1.230
S4150-1	130.2	0.0182	0.317	0.0173	129.0	1.009	0.264	0.0283	119.6	1.089
S4150-2	130.5	0.0162	0.318	0.0173	130.0	1.003	0.266	0.0281	121.1	1.078
					Average	1.006			Average	1.084
Average of $p = 0.0150$ slabs						1.141				1.157

<sup>a</sup>  $y$  = distance from top of shear crack to compressive surface;  $d$  = effective slab depth.

<sup>b</sup> Values have been increased 10 percent as recommended by Kinnunen-Nylander for slabs containing two-way reinforcement.

TABLE 6.5 ULTIMATE UNIT SHEAR STRESS OF STATICALLY LOADED SPECIMENS

r = side dimension of square column; d = effective slab depth; v = unit shear stress; b = column perimeter.

Specimen	Concrete Strength $f'_c$	Observed Shear Stress $V_{test}$	Measured r/d Ratio	Critical Section at Column Face		Critical Section at d/2 from Column	
				$v = \frac{V_{test}}{bd}$	$\frac{v}{\sqrt{f'_c}}$	v	$\frac{v}{\sqrt{f'_c}}$
	psi	lb		psi		psi	
S2075-1	4700	65,200	2.10	343	5.01	233	3.39
S2075-2	4210	61,300	2.08	319	4.91	215	3.32
S2150-1	4290	104,400	2.05	535	8.17	359	5.49
S2150-2	4370	99,000	2.08	514	7.78	347	5.26
S4075-1	3860	77,000	4.00	192	3.10	154	2.48
S4075-2	4670	74,100	4.10	187	2.76	152	2.22
S4150-1	5140	130,200	4.05	329	4.60	264	3.69
S4150-2	5180	130,500	4.05	334	4.62	267	3.72

TABLE 7.1 STRAIN-RATE EFFECT ON LOWER YIELD STRESS OF STEEL IN TENSION

Reference	Strength Increase at Given Strain Rate $\dot{\epsilon}$					Notes
	0.03/sec	0.10/sec	0.3/sec	1.0/sec	Other	
	pct	pct	pct	pct	pct	
Wright and Hall (1964)	11	15	21	27	--	Low (0.17 pct) carbon steel, lower yield point. Data given as 4.5-, 6-, 8.5-, and 11-ksi strength increase over the strength at $\dot{\epsilon} = 10^{-4}/\text{sec}$ . Yield stress of 40 ksi assumed
Cowell (1965)	10	13	17	19	--	Intermediate grade, lower yield point, $f_y = 50.6$ ksi at $\dot{\epsilon} = 10^{-3}/\text{sec}$ . Machined specimens of 0.505-inch diameter
Siess (1962)	--	--	--	--	33	As received No. 6 intermediate grade reinforcement. $\dot{\epsilon} \cong 0.6/\text{sec}$ . Static $f_y = 47$ ksi
Denton (1967)	--	--	--	--	18	Machine No. 2 reinforcement. Static $f_y = 51.6$ ksi. Elastic $\dot{\epsilon} = 0.19/\text{sec}$
Norris, et al. (1959)	10	14	18	23	--	Design curve for structural steel. Data given as time to yield
Newmark-Haltiwanger (1962)(Air Force Design Manual)	13	20	26	35	--	Design curve, intermediate grade reinforcement. Data given as time to yield
Seabold (1967)	--	--	35	47	--	0.146-inch-diameter smooth wire. Static $f_y = 36$ ksi. Ultimate and upper yield increased 12 and 59 percent, respectively, at $\dot{\epsilon} = 0.3/\text{sec}$

TABLE 7.2 STRAIN-RATE EFFECT ON CONCRETE STRENGTH

Reference	Strength Increase at Given Strain Rate $\dot{\epsilon}$						Notes
	0.003/sec	0.01/sec	0.03/sec	0.10/sec	0.3/sec	3.0/sec	
	pct	pct	pct	pct	pct	pct	
Compression:							
Watstein (1953)	--	--	28	38	48	--	$f'_c = 2500$ psi, nominal
	--	--	18	23	29	--	$f'_c = 6500$ psi, nominal 3- by 6-inch cylinders. Air dried 3 days prior to testing
Cowell (1966)	--	--	22	28	37	--	$f'_c = 3900$ psi, tested "wet"
	--	--	14	20	28	--	$f'_c = 4800$ psi, tested dry
	--	--	19	25	34	--	$f'_c = 7400$ psi, tested "wet"
	--	--	11	15	20	--	$f'_c = 8700$ psi, tested dry 3- by 9-inch cylinders. "Wet" and dry concrete exposed to 2 or 21 days, respectively, to 20 percent relative humidity prior to testing
Lundeen (1963)	--	--	--	--	--	35	1-1/2- by 3-inch cylinders. $f'_c = 2000$ to 4000 psi. Air dried 7 days prior to testing
Atchley and Furr (1967)	--	--	48	50	53	--	$f'_c = 2500$ psi, nominal
	--	--	39	41	45	--	$f'_c = 3700$ psi, nominal
	--	--	42	48	54	--	$f'_c = 5000$ psi, nominal 6- by 12-inch cylinders. Air dried 1 day prior to test
Newmark-Haltiwanger (1962) (Air Force Design Manual)	--	--	25	34	44	--	Design curve
McHenry and Shideler (1956)	--	--	23	29	36	--	Curve fitted to data then available
Norris, et al. (1959)	--	--	17	24	33	--	Design curve
Tension:							
Cowell (1966)	37	44	53	65	--	--	$f'_c = 3900$ psi, tested "wet"
	18	23	30	44	--	--	$f'_c = 4800$ psi, tested dry
	33	40	49	62	--	--	$f'_c = 7400$ psi, tested "wet"
	20	24	30	40	--	--	$f'_c = 8700$ psi, tested dry Split cylinder tests using 3- by 6-inch cylinders. "Wet" and dry concrete exposed 2 or 21 days, respectively, to 20 percent relative humidity prior to testing
Keenan (1965)	22	32	45	70	--	--	$f'_c = 2280$ psi, split cylinder tests using 4- by 8-inch cylinders. Data given as stress rate. $E_c = 3,300,000$ psi assumed
Lundeen (1963)	--	--	--	--	73	--	$f'_c = 2000$ to 4000 psi. Split cylinder tests using 6- by 12-inch cylinders

TABLE 7.3 SHEAR FORCE TRANSFERRED BY THE VERY RAPIDLY LOADED SPECIMENS

Maximum Shear						
Specimen	Accelerometer	Maximum Applied Load	Acceleration at Maximum Load	Inertial Load of Column Area <sup>a</sup>	Maximum Shear Transferred <sup>b</sup>	Maximum Shear Loading/Static Strength <sup>c</sup>
		kips	g's	kips	kips	
D2075-1	AC1	157.5	97	32.7	124.8	1.92
	AC2	157.5	112	37.8	119.7	1.84
				Average	122.2	1.88
D2075-2	AC1	193.9	122	41.1	152.8	2.35
	AC2	193.9	160	53.9	140.0	2.15
				Average	146.4	2.25

Average Values from 1 to 9 msec						
Specimen	Accelerometer	Average Applied Load	Average Acceleration	Average Inertial Load	Average Shear Transferred	Average Shear Loading/Static Strength
		kips	g's	kips	kips	
D2075-1	AC1	118.0	42	14.1	103.9	1.60
	AC2	118.0	40	13.5	104.5	1.61
				Average	104.2	1.60
D2075-2	AC1	134.0	69	23.2	110.8	1.70
	AC2	134.0	63	21.2	112.8	1.73
				Average	111.8	1.72

<sup>a</sup> Acceleration in g's times 337 pounds (weight of column, steel plate atop column, and truncated pyramid portion of the slab under the column with sides 30 degrees to the horizontal).

<sup>b</sup> Maximum load minus inertial loading.

<sup>c</sup> From Table 6.3, static strength = 0.99 times yield-line flexural strength = 65 kips for Specimens D2075-1 and D2075-2.



TABLE 7.4 LOADS AND DEFLECTIONS OF THE RAPIDLY LOADED SPECIMENS

Specimen	Rise Time	Time of Failure	Maximum Applied Load	Maximum Resistance	Center Deflection at Ultimate
	msec	msec	kips	kips	inches
D2075-3	26	54	79.8	79.1	1.75 <sup>a</sup>
D2150-1	24	50	130.3	129.8	0.80 <sup>b</sup>
D2150-2	22	31	129.6	125.8	0.64 <sup>b</sup>
D2150-3	22	45	136.5	134.3	0.71 <sup>a</sup>
D4075-1	9	62	105.6	95.0	2.40 <sup>b</sup>
D4075-2	9	81	102.7	94.0	2.62 <sup>b</sup>
D4075-3	30	140 <sup>c</sup>	104.0	92.1	2.76 <sup>b</sup>
D4150-1	32	57	170.4	163.5	d
D4150-2	28	51	176.3	169.4	1.14

<sup>a</sup> From doubly integrated acceleration record.

<sup>b</sup> From deflection gage records.

<sup>c</sup> Initial signs of failure observed at 112 msec.

<sup>d</sup> No record.

TABLE 7.5 COMPARISON OF STATIC AND DYNAMIC CONNECTION STRENGTHS

Series	Average Static Strength	Average Dynamic Strength	Strength Ratio (Dynamic/Static)	Normalized Strength Ratio <sup>a</sup>	Strength Ratio Based on Predicted Strength <sup>b</sup>
	kip	kip			
2075	63.3	79.1	1.25	1.15	1.15
2150	101.7	130.0	1.28	1.24	1.23
4075	75.6	93.7	1.24	1.20	1.20
4150	130.4	164.8	1.26	1.27	1.29
		Average	1.26	1.22	1.22

<sup>a</sup> Series 2075 and 4075 normalized by  $pd^2f_y$ . Series 2150 and 4150

<sup>b</sup> normalized by  $d\sqrt{f'_c}$ .

Ratio of average observed to calculated static strength ratios for dynamic and static tests. Series 2075 and 4075 calculated by Equation 6.1. Series 2150 and 4150 calculated by Equation 2.5a.

TABLE 7.6 CALCULATED CONNECTION-STRENGTH INCREASE DUE TO RAPID LOADING

Specimen	Observed Dynamic Strength	Predicted Static Strength	Ratio of Observed Dynamic to Predicted Static Strength	Average Ratio of Observed to Predicted Strength - Static Tests <sup>a</sup>	Ratio of Dynamic to Static Strength <sup>b</sup>
	kip	kip			
Equation 2.5a (Moe, 1961):					
D2075-3	79.1	83.9	0.94	0.80	1.18
D2150-1	129.8	108.6	1.20	0.97	1.24
D2150-2	125.8	107.3	1.17	0.97	1.21
D2150-3	134.3	112.2	1.20	0.97	1.24
				Average	1.23
D4075-1	95.0	103.8	0.92	0.78	1.17
D4075-2	94.0	101.2	0.93	0.78	1.19
D4075-3	92.1	97.3	0.95	0.78	1.21
				Average	1.19
D4150-1	163.5	144.0	1.14	0.88	1.29
D4150-2	169.4	148.2	1.15	0.88	1.30
				Average	1.29
Equation 6.1 (Yield-Line Analysis, Elstner-Hognestad, 1956):					
D2075-3	79.1	69.2	1.14	0.99	1.15
D2150-1	129.8	129.0	1.01	0.82	1.22
D2150-2	125.8	132.1	0.95	0.82	1.16
D2150-3	134.3	132.4	1.02	0.82	1.24
				Average	1.20
D4075-1	95.0	78.5	1.21	1.00	1.21
D4075-2	94.0	80.0	1.18	1.00	1.18
D4075-3	92.1	75.8	1.22	1.00	1.22
				Average	1.20
D4150-1	163.5	144.2	1.13	0.88	1.29
D4150-2	169.4	144.7	1.17	0.88	1.33
				Average	1.31

<sup>a</sup> Average ratio for the two similar statically tested specimens from Table 6.3.

<sup>b</sup> Ratio of Column 4 to Column 5.

TABLE 7.7 EFFECT OF RAPID LOADING ON FAILURE DEFLECTION

Specimen	Failure Deflection	Average Failure Deflection for Series	Average Failure Deflection for Companion Static Tests	Ratio of Dynamic to Static Failure Deflection
	inches	inches	inches	
D2075-3	1.75	1.75	1.28	1.37
D2150-1	0.80	0.72	0.58	1.25
D2150-2	0.64			
D2150-3	0.71			
D4075-1	2.40	2.59	1.80 <sup>a</sup>	1.44
D4075-2	2.62			
D4075-3	2.76			
D4150-1	No record	1.14	0.77	1.49
D4150-2	1.14			

<sup>a</sup> Failure deflection of S4075-1 only. Failure deflection of S4075-2 low and probably influenced by geometric asymmetry.

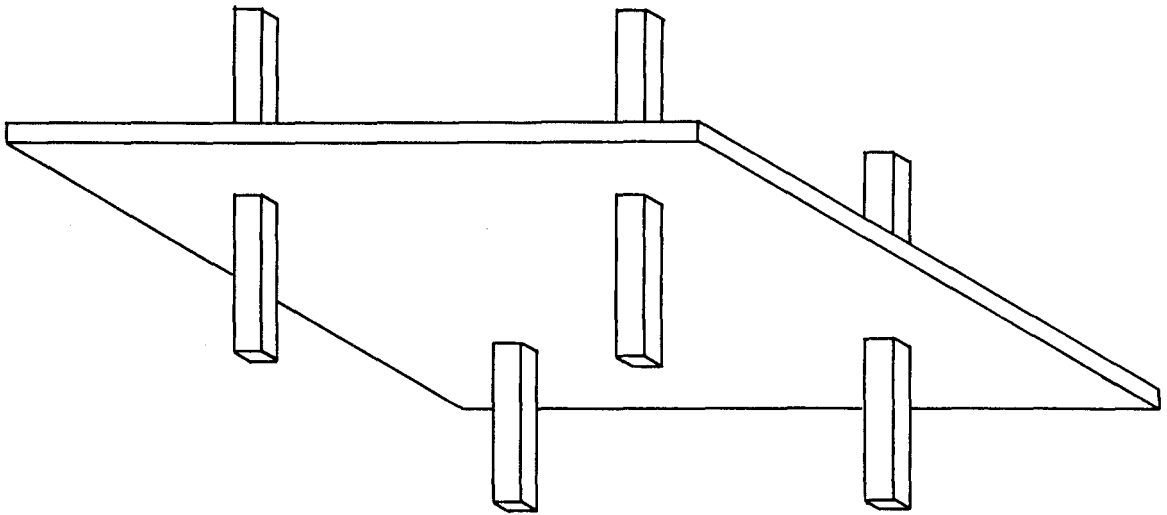
TABLE 7.8 EQUIVALENT UNIFORM PRESSURE CAPACITIES OF PROTOTYPE SLAB SYSTEM

Specimen	Maximum Resistance	Equivalent Total <sup>a</sup> Failure Pressure	Dead Load of the Slab	Equivalent Net Failure Pressure
	kips	psi	psi	psi
Static Tests:				
S2075-1	65.2	1.49	0.55	0.94
S2075-2	61.3	1.40	0.55	0.85
S2150-1	104.4	2.38	0.55	1.83
S2150-2	99.0	2.26	0.55	1.71
S4075-1	77.0	1.77	0.55	1.22
S4075-2	74.1	1.70	0.55	1.15
S4150-1	130.2	2.99	0.55	2.44
S4150-2	130.5	3.00	0.55	2.45
Dynamic Tests:				
D2075-3	79.1	1.80	0.55	1.25
D2150-1	129.8	2.96	0.55	2.41
D2150-2	125.8	2.87	0.55	2.32
D2150-3	134.3	3.06	0.55	2.51
D4075-1	95.0	2.19	0.55	1.64
D4075-2	94.0	2.16	0.55	1.61
D4075-3	92.1	2.12	0.55	1.57
D4150-1	163.5	3.76	0.55	3.21
D4150-2	169.4	3.90	0.55	3.35

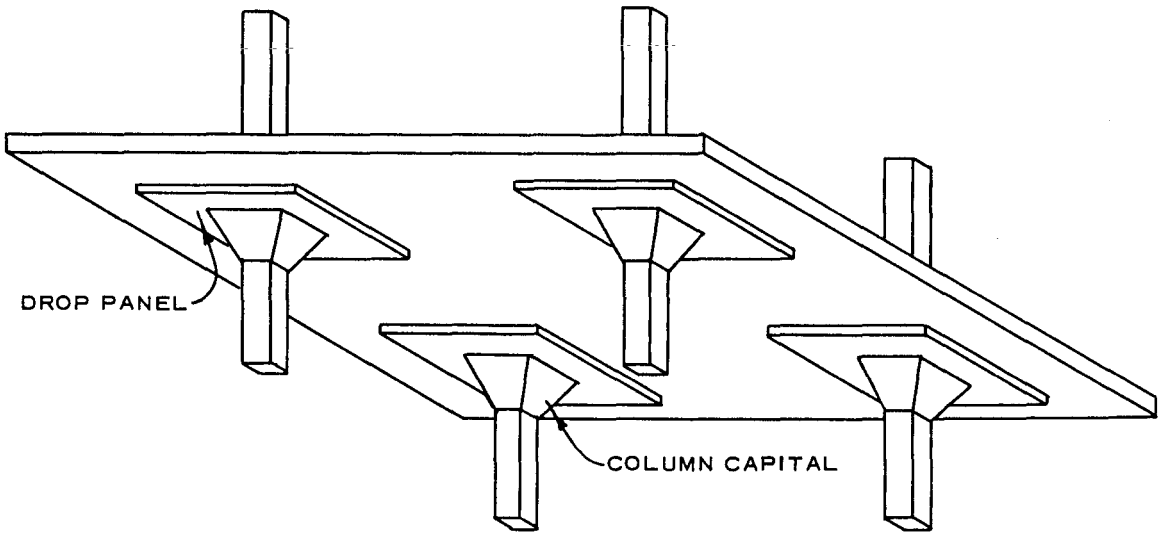
<sup>a</sup> Maximum resistance ÷ contributory area.

$$\begin{aligned}
 \text{Contributory area} &= (\text{bay size})^2 - (\text{column size} + \text{effective depth})^2 \\
 &= 43,875 \text{ in}^2 \text{ for 10-inch column} \\
 &= 43,475 \text{ in}^2 \text{ for 20-inch column}
 \end{aligned}$$

Prototype bay size = 17 feet 6 inches (210 inches)



a. FLAT-PLATE SYSTEM



b. FLAT-SLAB SYSTEM

Figure 1.1 Concrete floor systems without beams.

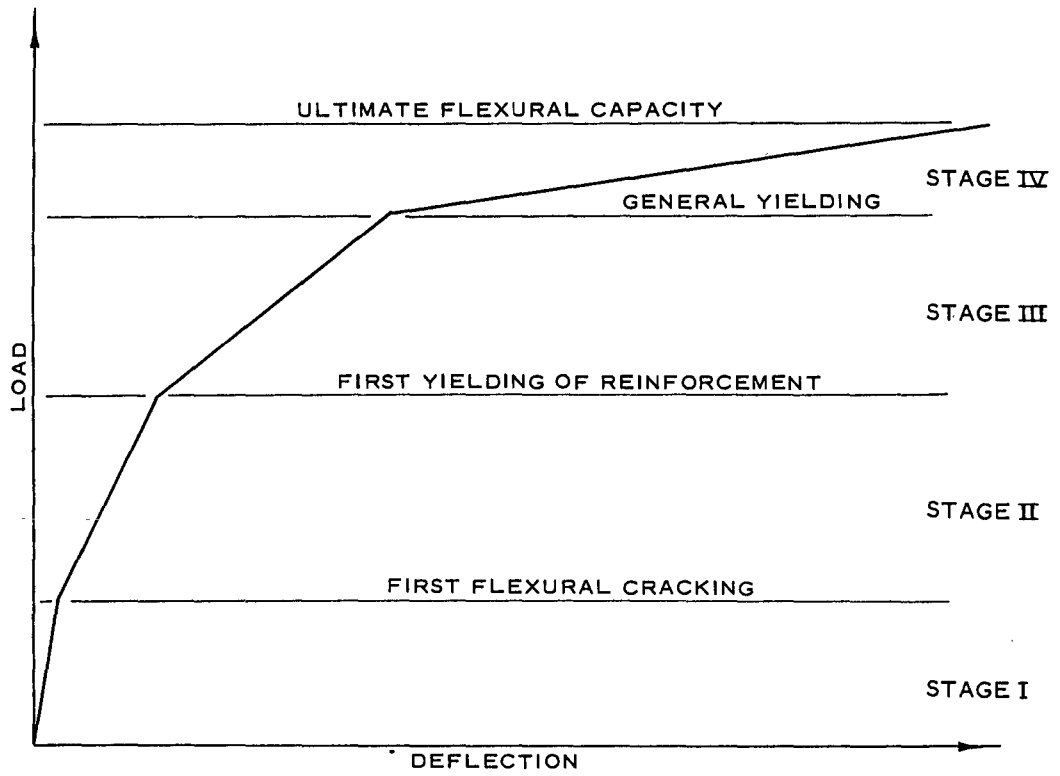
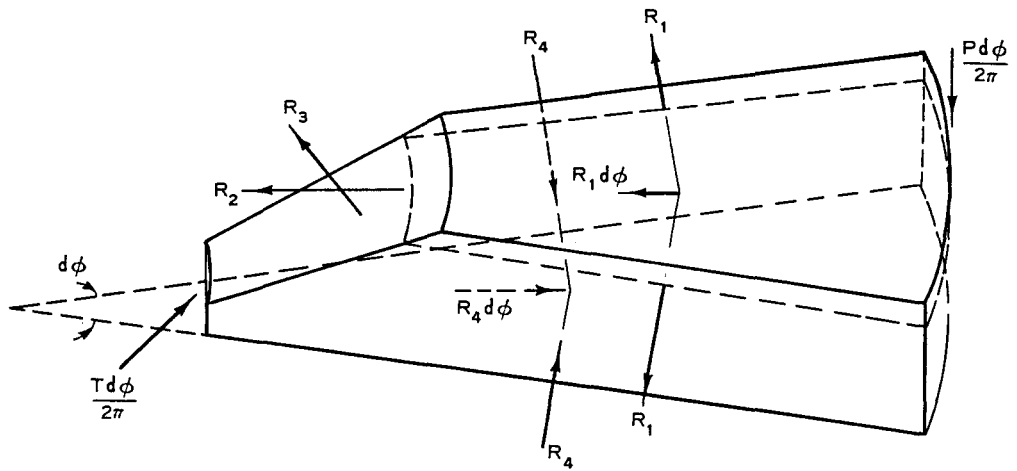
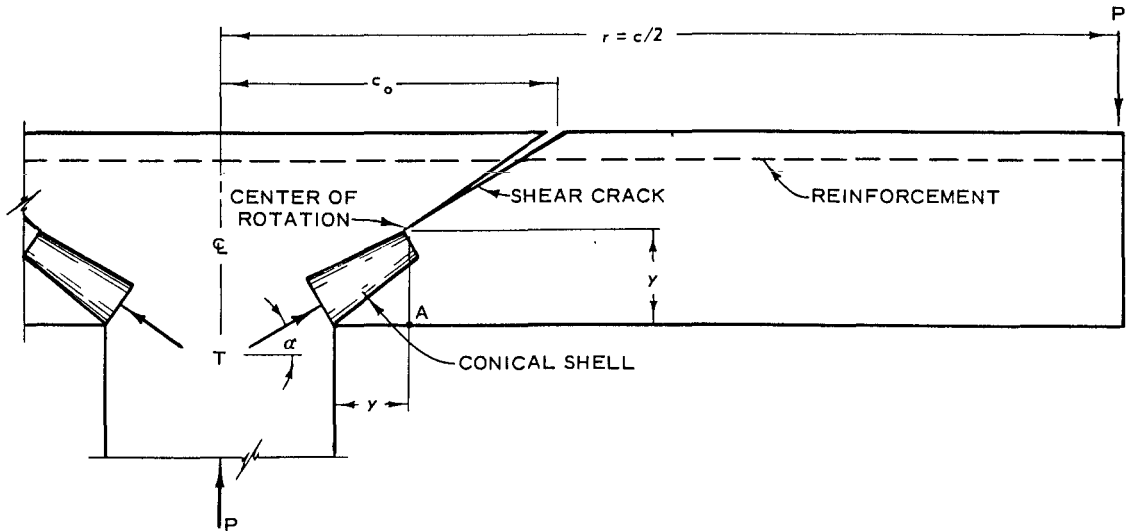


Figure 2.1 Stages of flexural behavior from Hognestad (1953).



a. FORCES ACTING ON A SLAB SEGMENT



b. ASSUMED GEOMETRY OF THE CONNECTION

LEGEND

- P = APPLIED LOAD AT THE SLAB PERIPHERY
- T = INCLINED COMPRESSIVE FORCE ACTING ON THE CONICAL SHELL
- $R_1$  = RESULTANT PERPENDICULAR TO RADIAL CRACK OF THE REINFORCEMENT
- $R_2$  = RESULTANT PERPENDICULAR TO SHEAR CRACK OF THE REINFORCEMENT
- $R_3$  = RESULTANT OF SHEAR REINFORCEMENT, IF ANY
- $R_4$  = TANGENTIAL RESULTANT OF THE CONCRETE COMPRESSIVE STRESSES

Figure 2.2 Idealized connection model from Kinnunen and Nylander (1960).



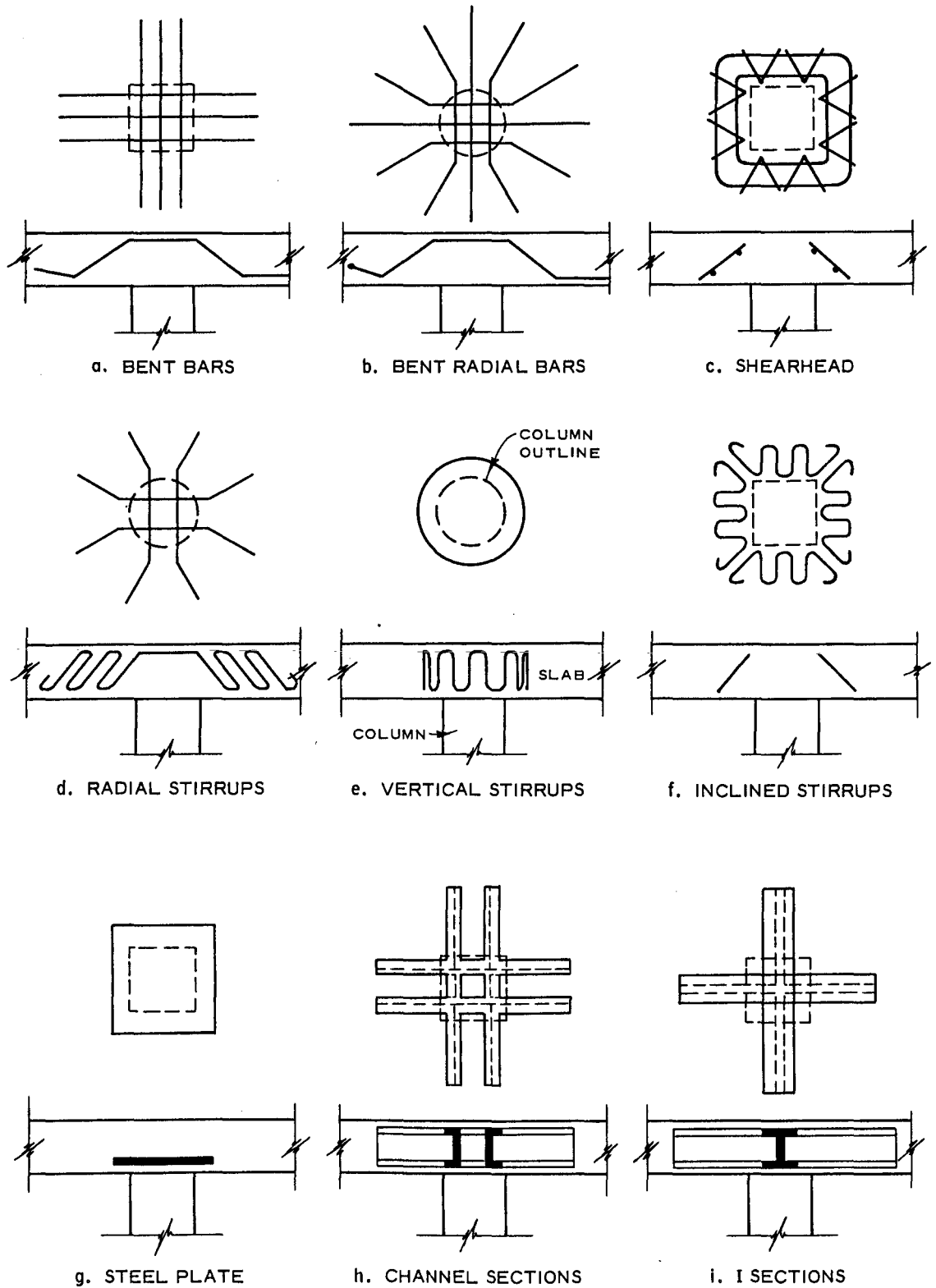


Figure 2.3 Shear reinforcement for slab-column connections.

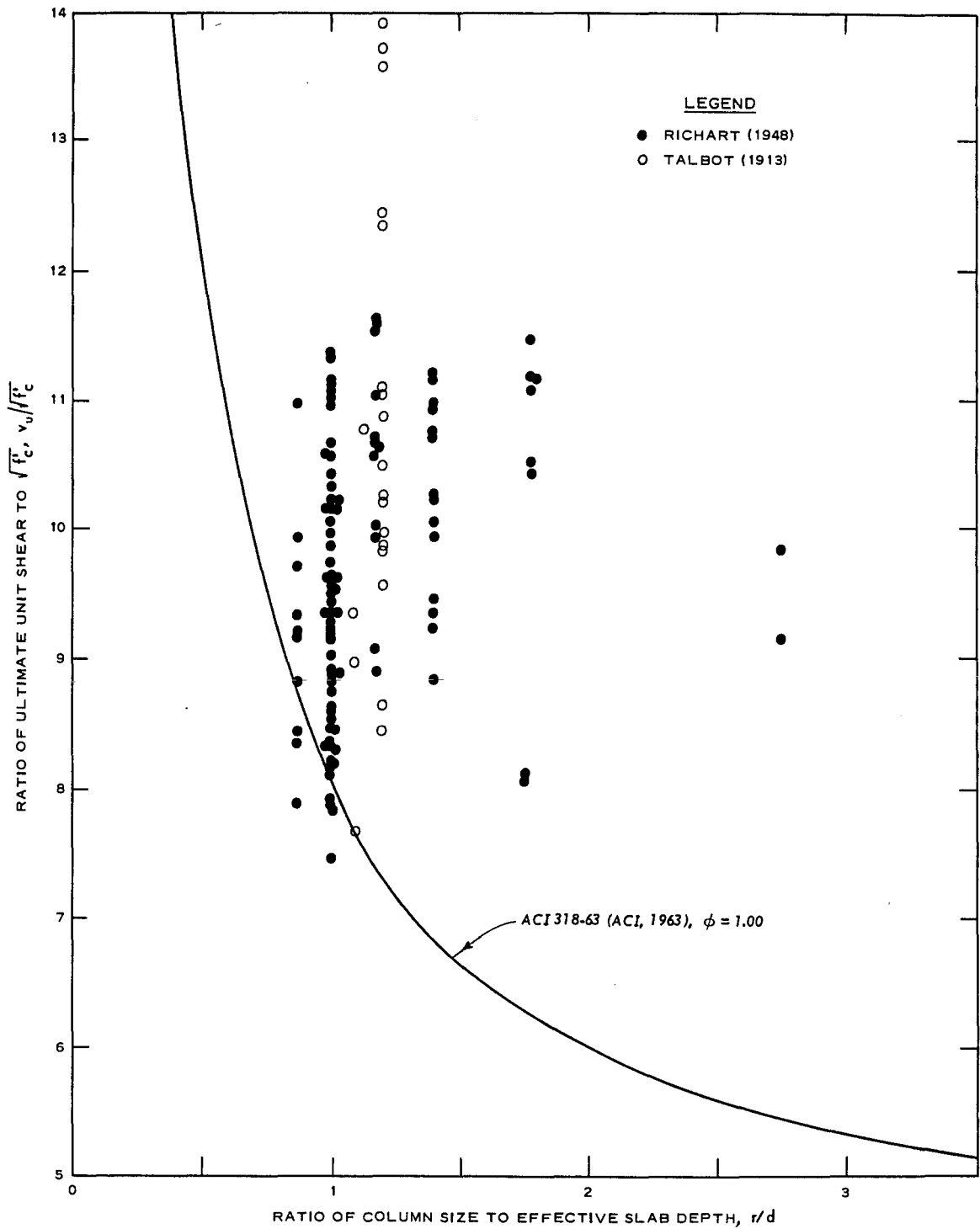


Figure 2.4 Observed strengths of column footings failing in shear.

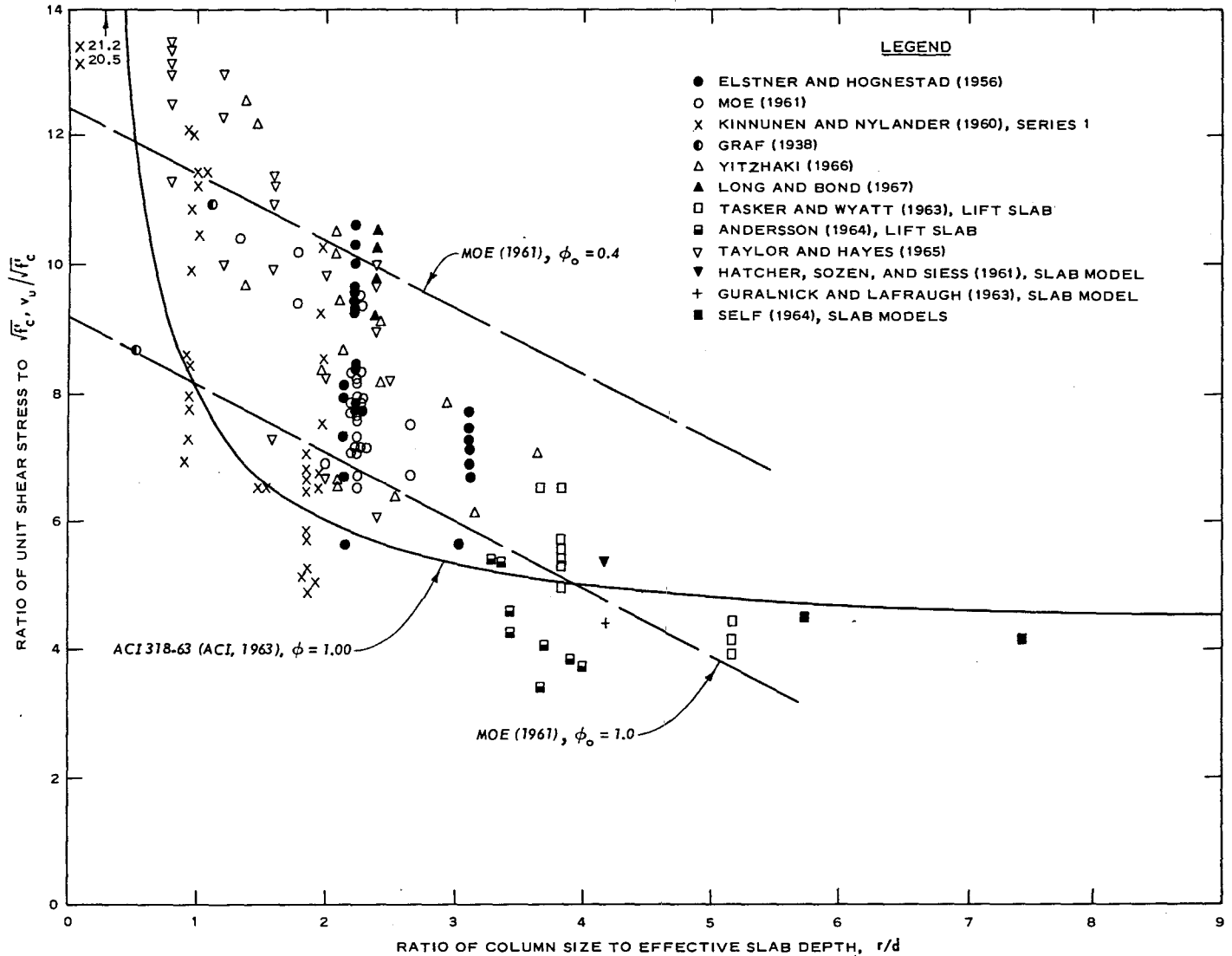


Figure 2.5 Observed strengths of connections of normal weight concrete failing in shear.

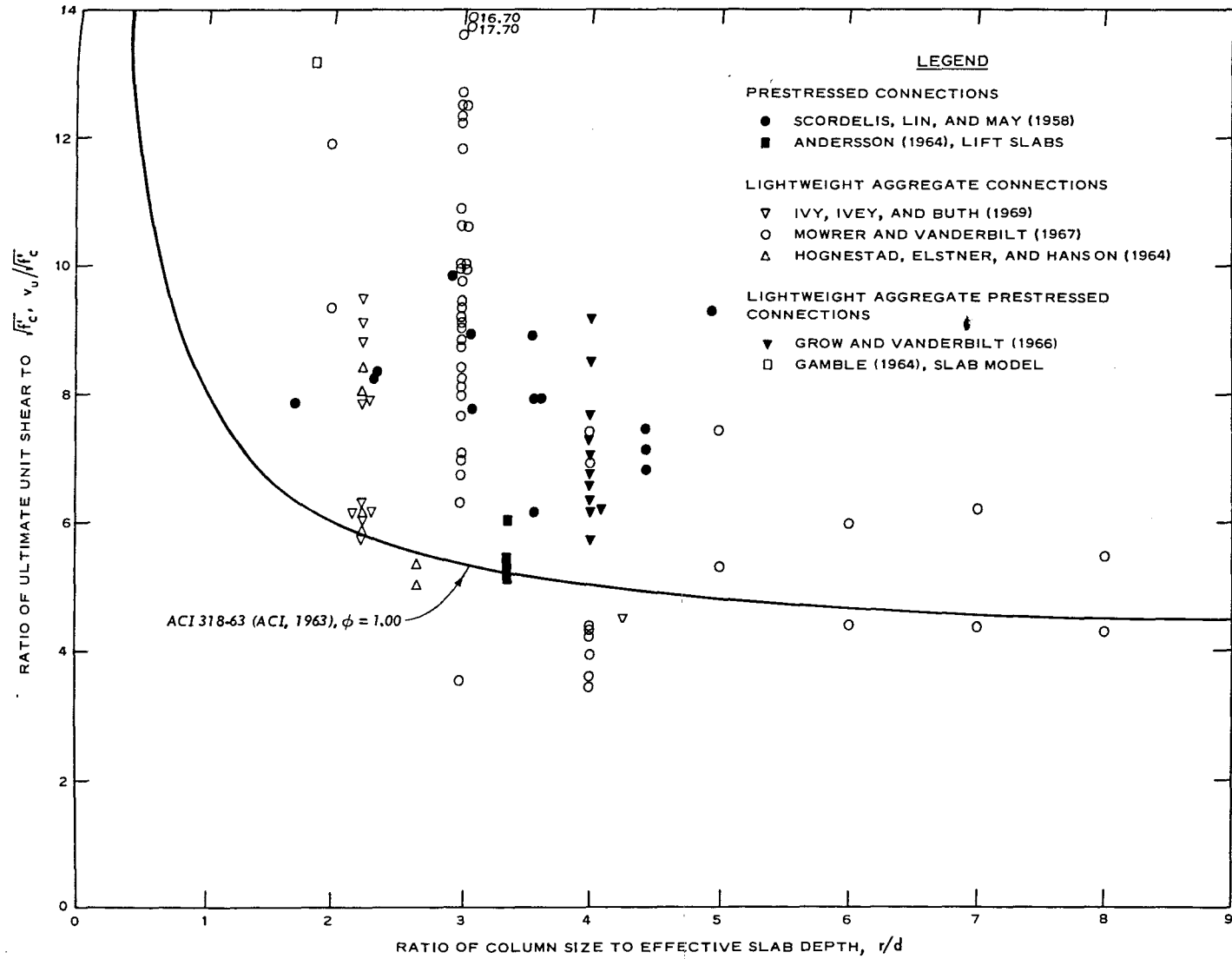


Figure 2.6 Observed strengths of lightweight concrete and/or prestressed connections failing in shear.

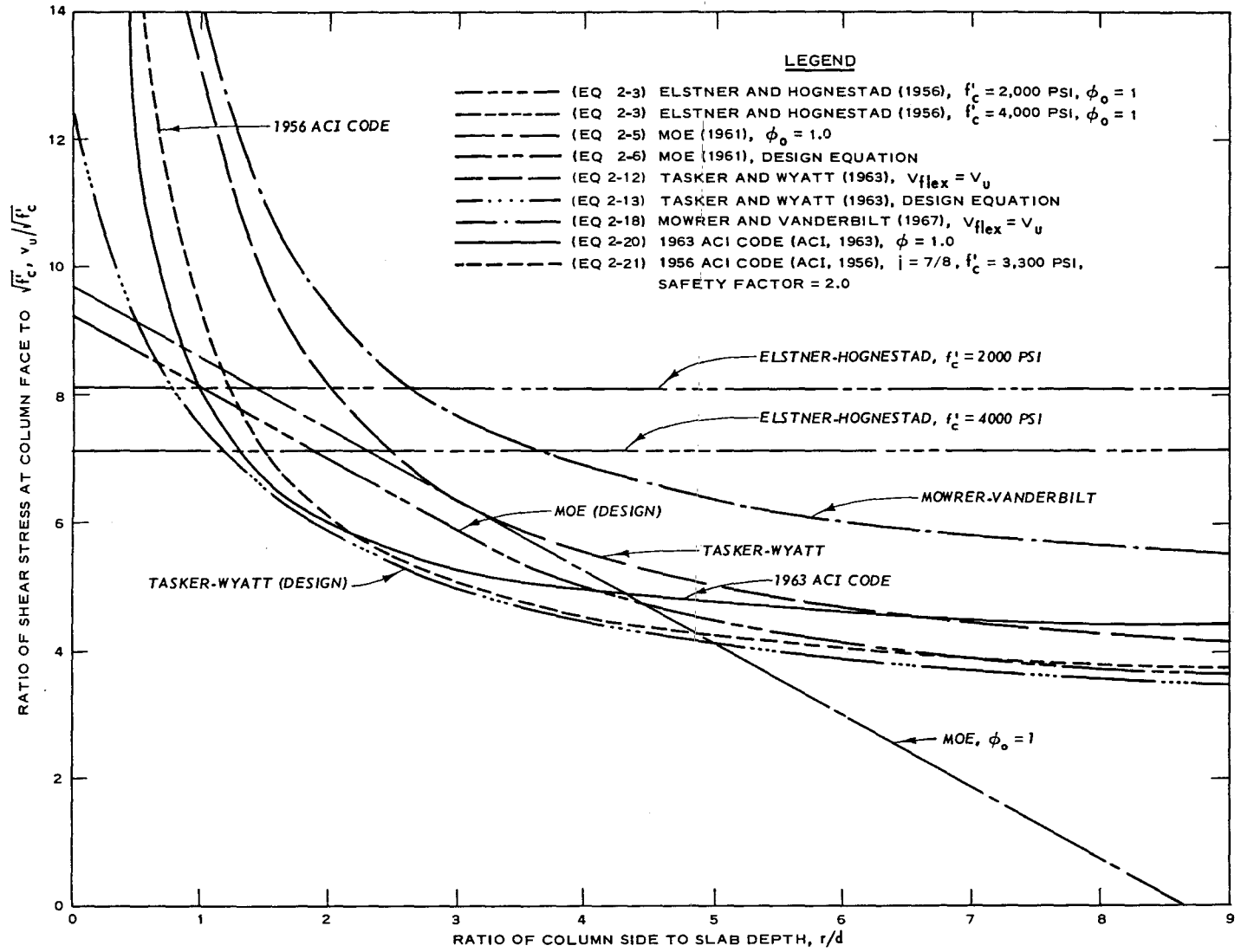


Figure 2.7 Comparison of strengths predicted by various methods.

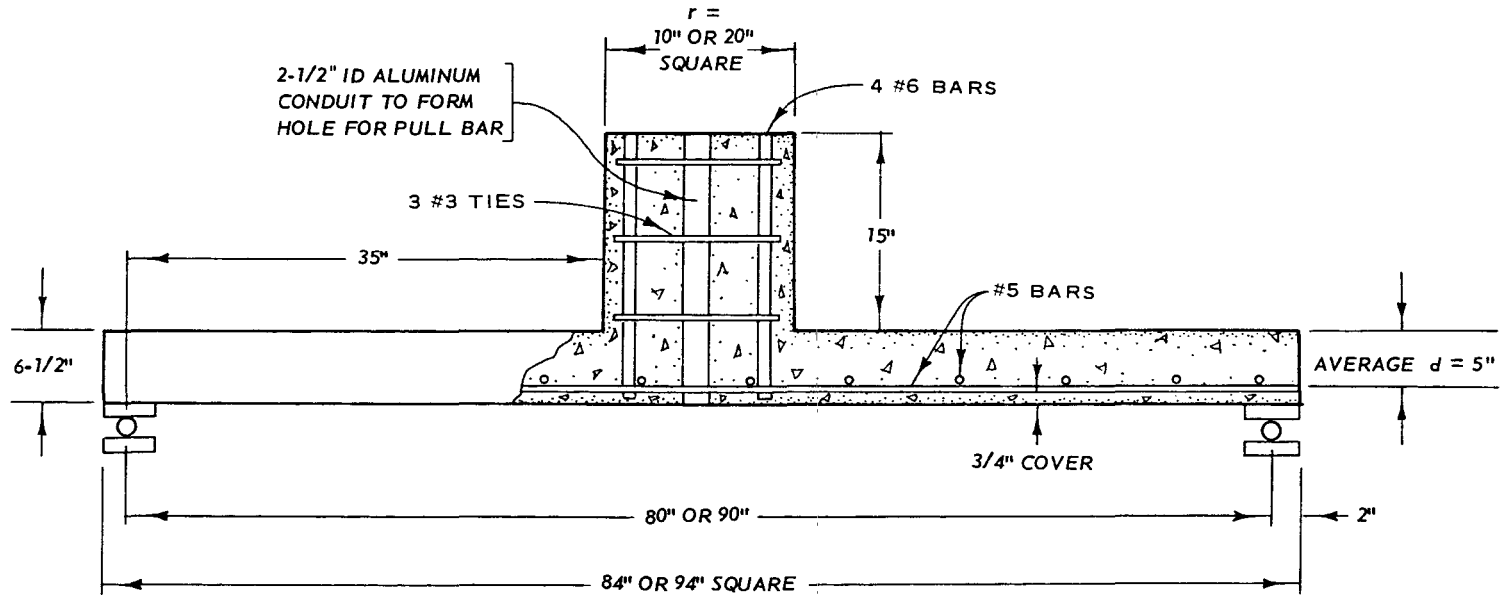


Figure 3.1 Slab-column connection specimen.

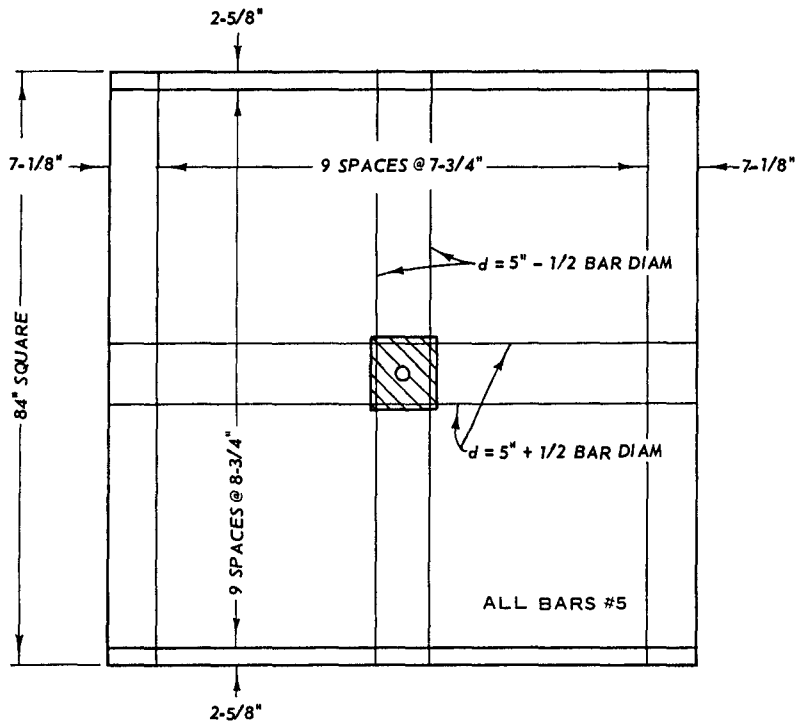


Figure 3.2 Slab reinforcement for 2075 Series specimens.

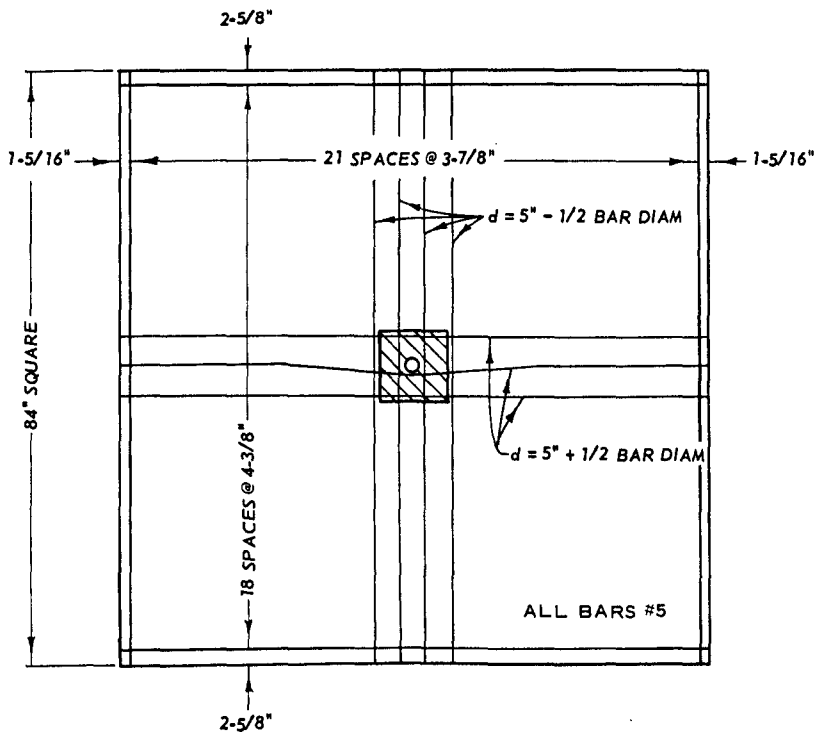


Figure 3.3 Slab reinforcement for 2150 Series specimens.

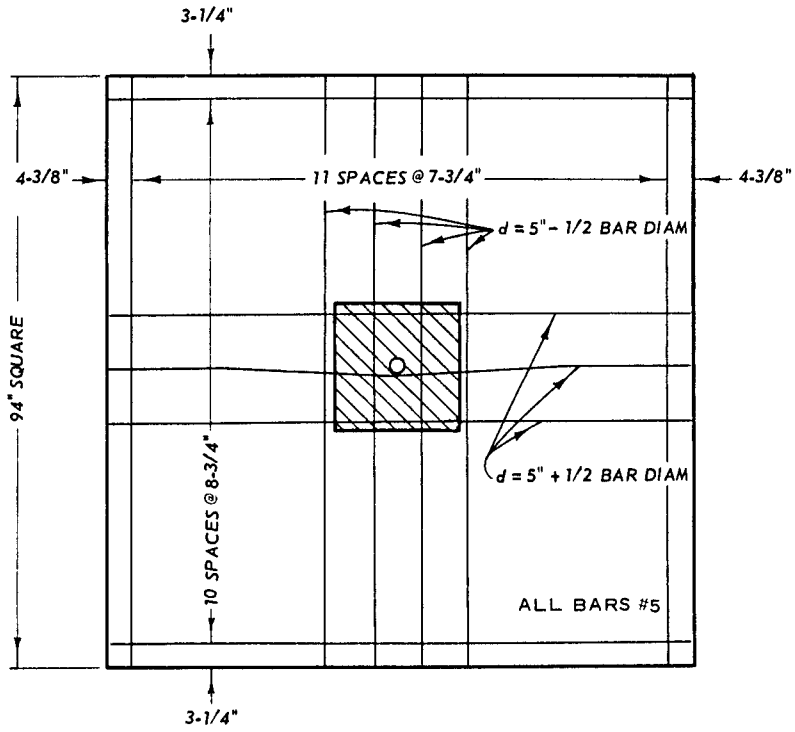


Figure 3.4 Slab reinforcement for 4075 Series specimens.

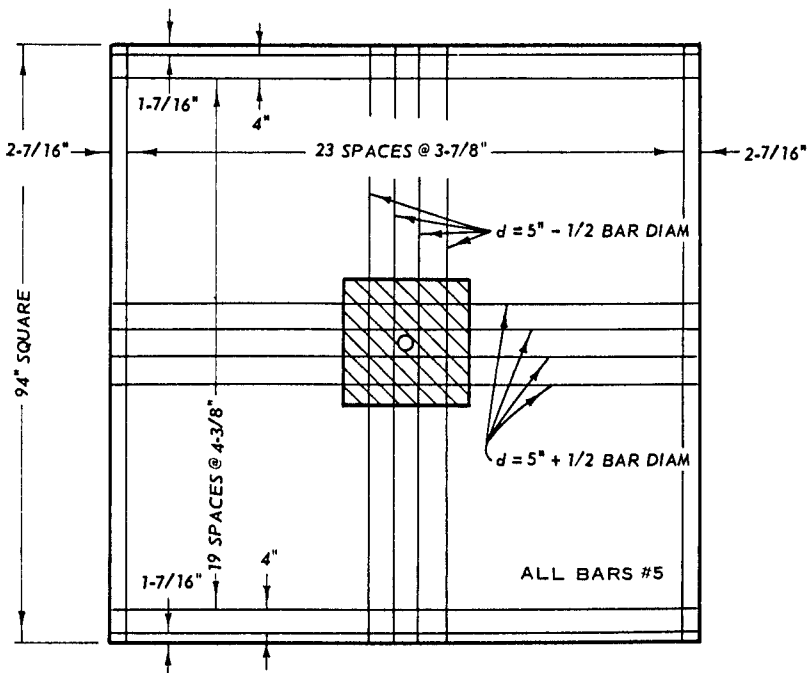


Figure 3.5 Slab reinforcement for 4150 Series specimens.



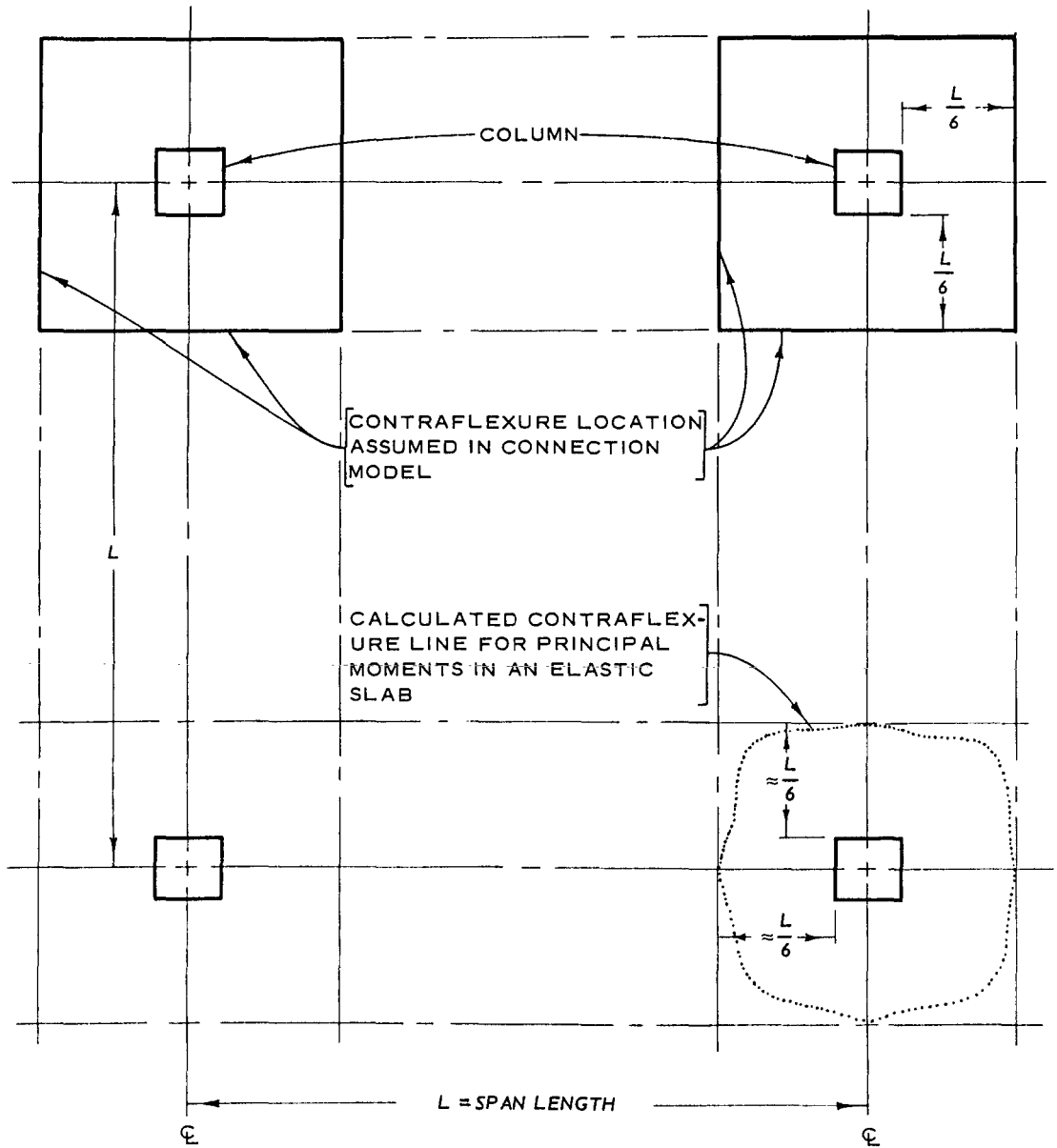
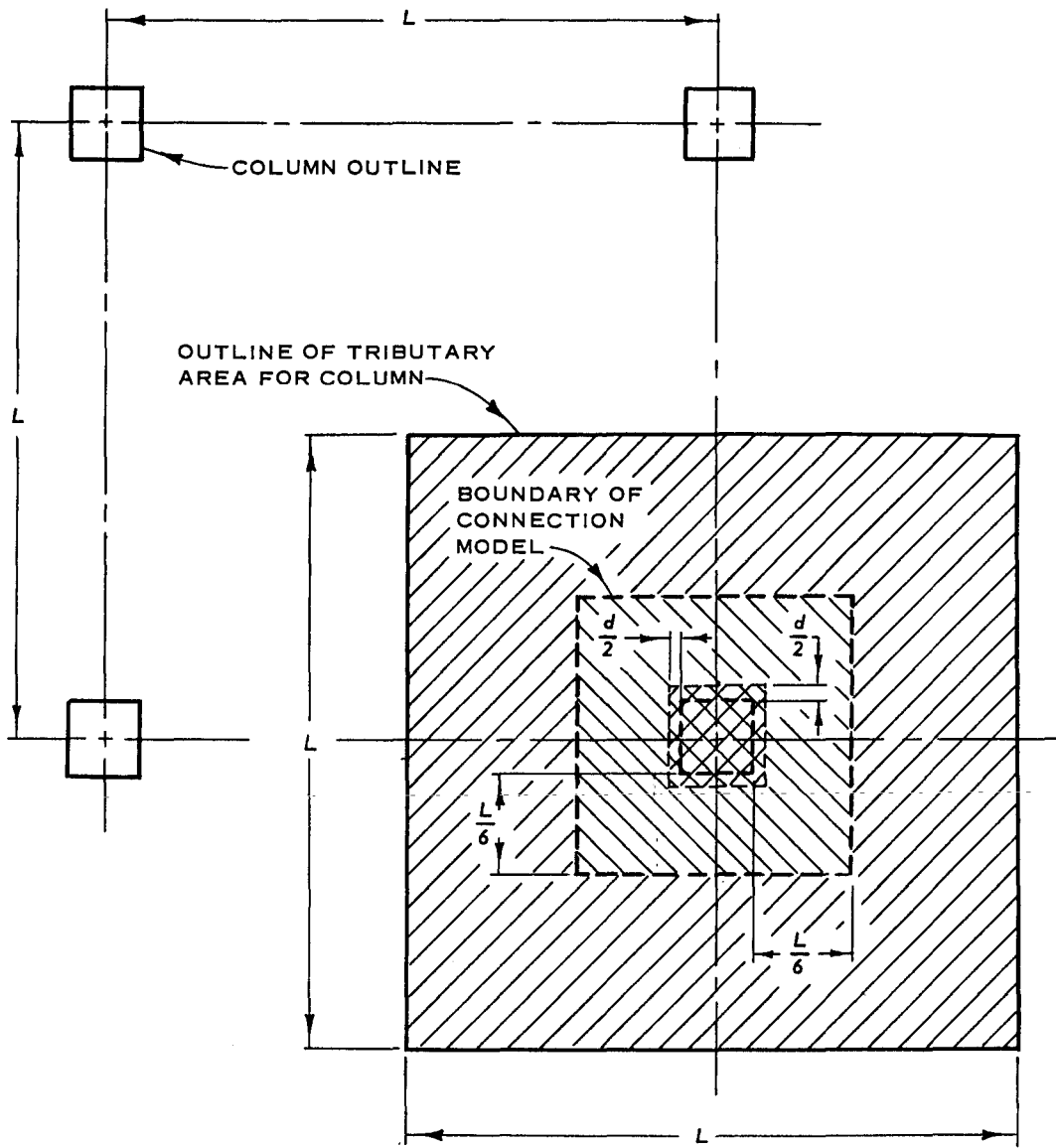


Figure 3.6 Plan view of slab system showing location of contraflexure lines.



LEGEND




-  LOAD ENTERING MODEL AREA AS SHEAR
-  UNIFORM LOAD ACTING ON MODEL SLAB AREA
-  UNIFORM LOAD ASSUMED TO BE CARRIED DIRECTLY BY THE COLUMN

Figure 3.7 Loading of the connection model.

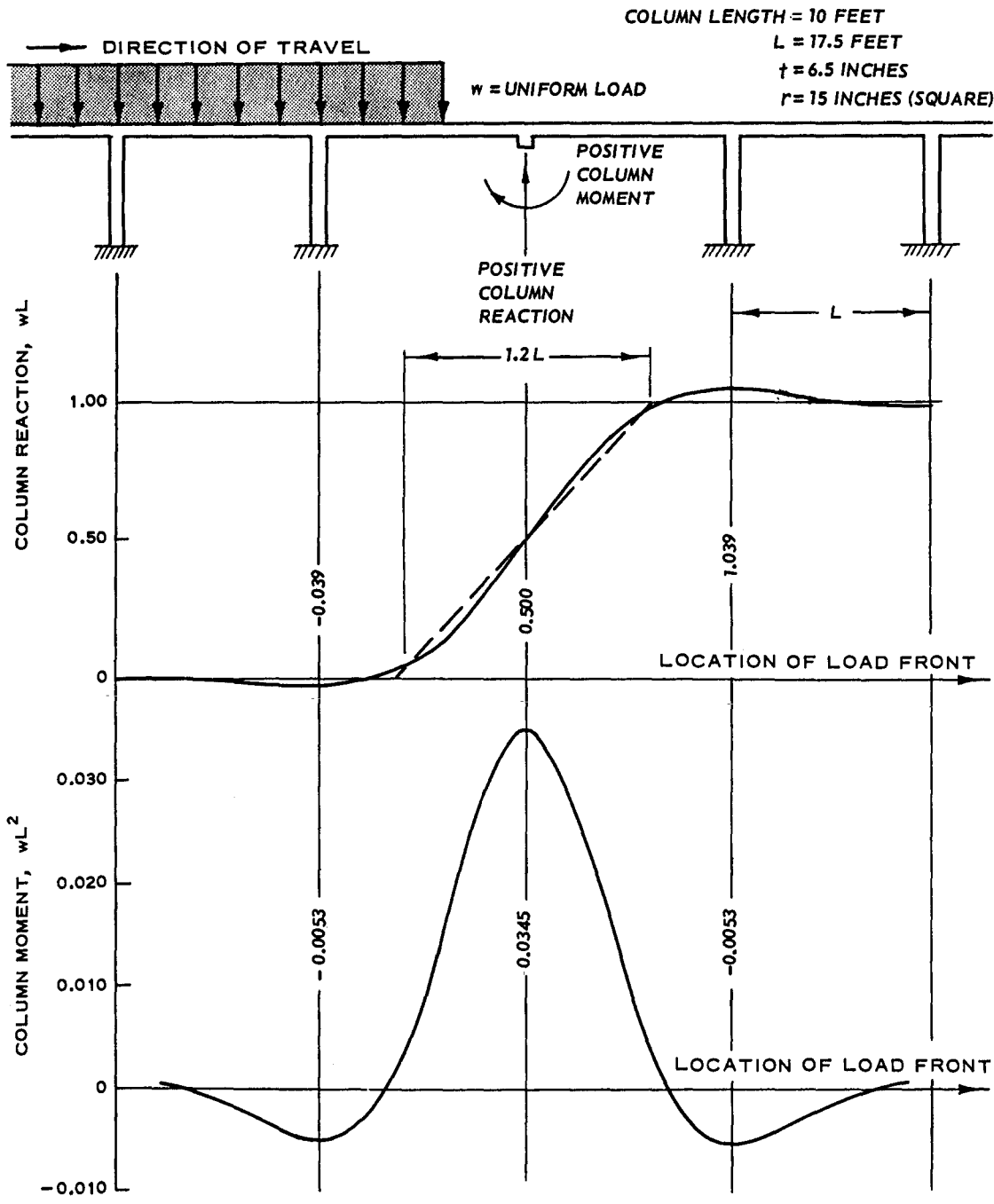


Figure 3.8 Column load and moment from a quasi-static traveling wave.

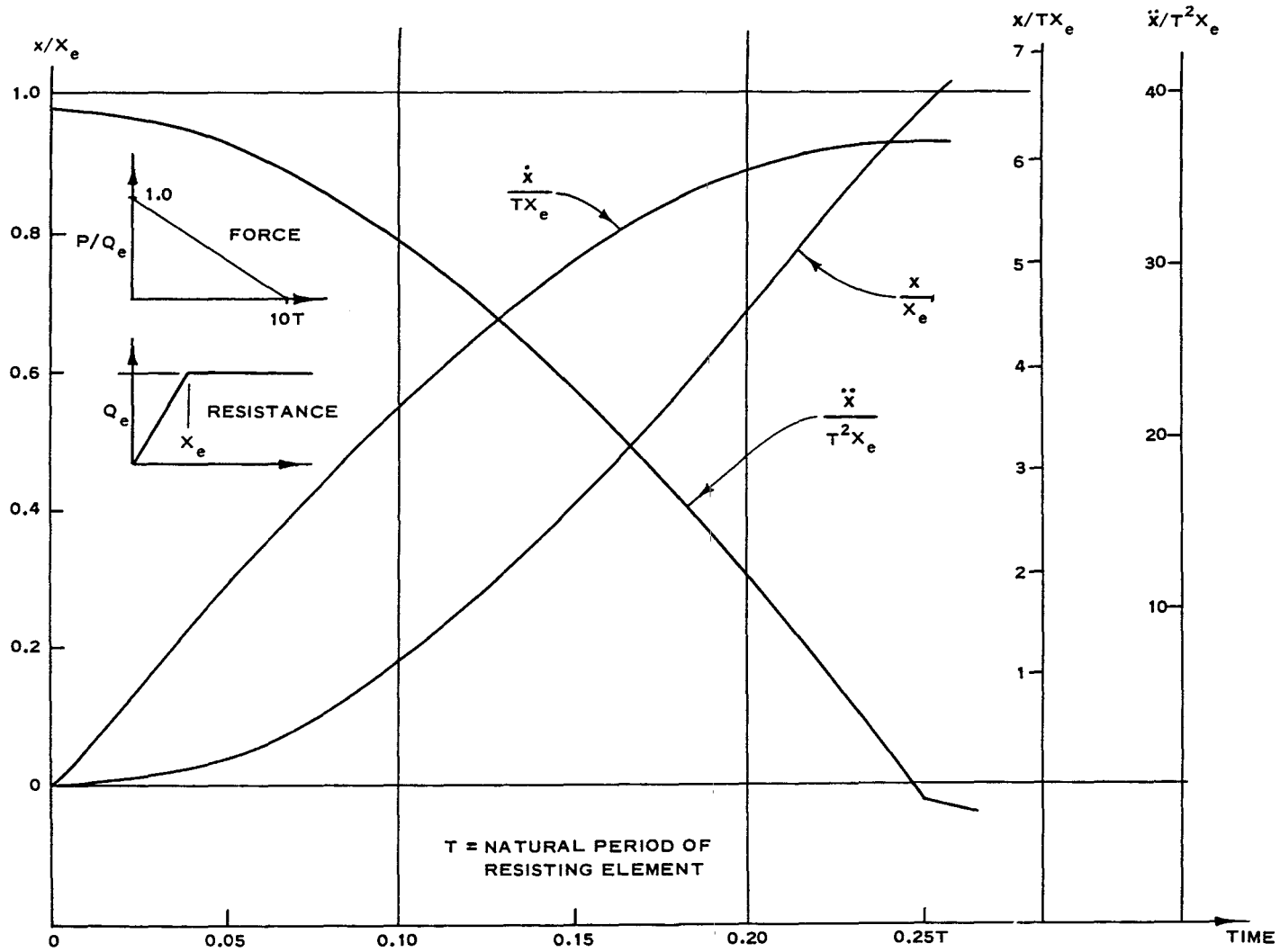


Figure 3.9 Early response of an elastoplastic system loaded with a linearly decaying load.

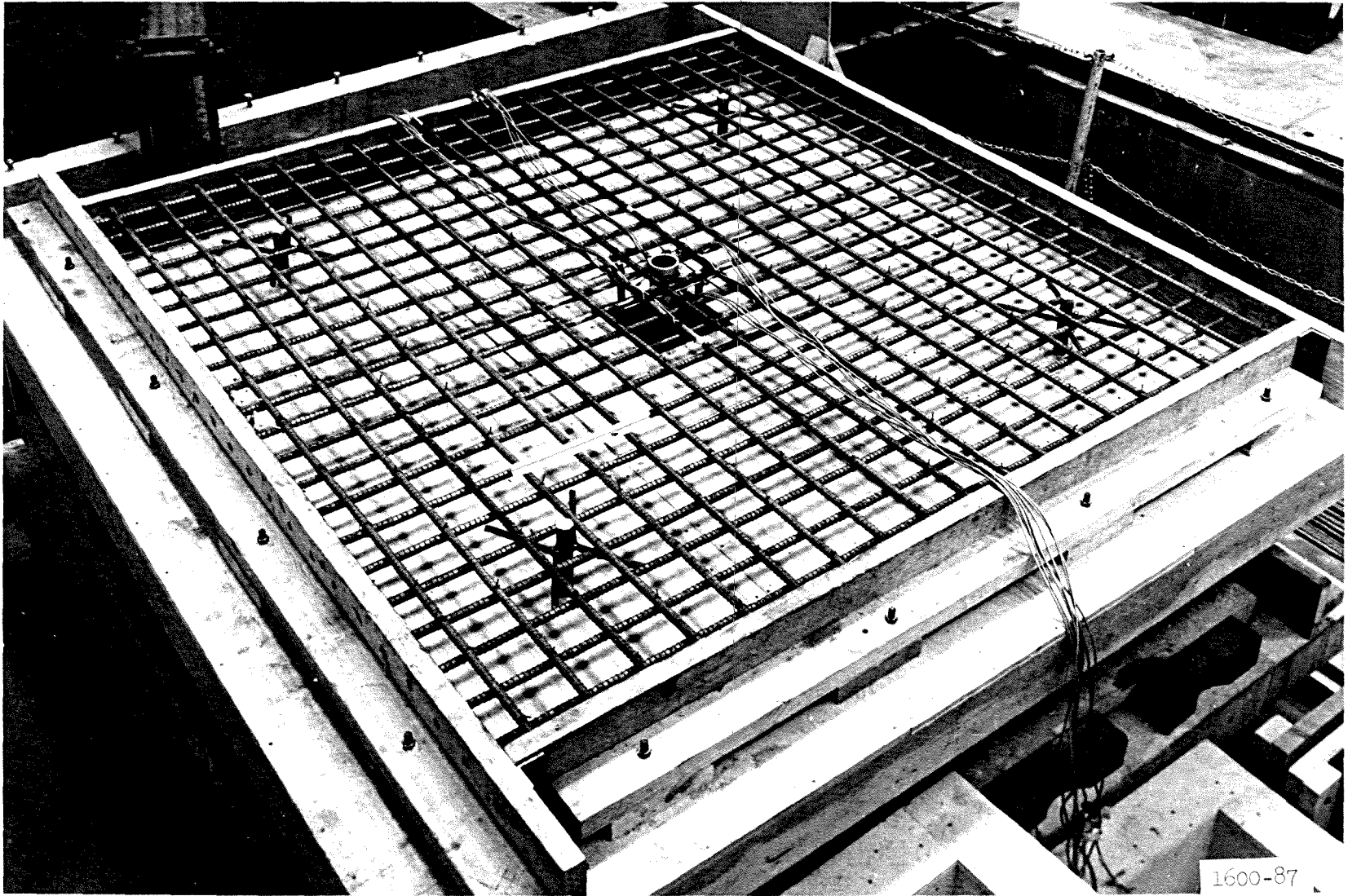


Figure 4.1 Specimen form with reinforcement in place,  $p = 0.0150$ .

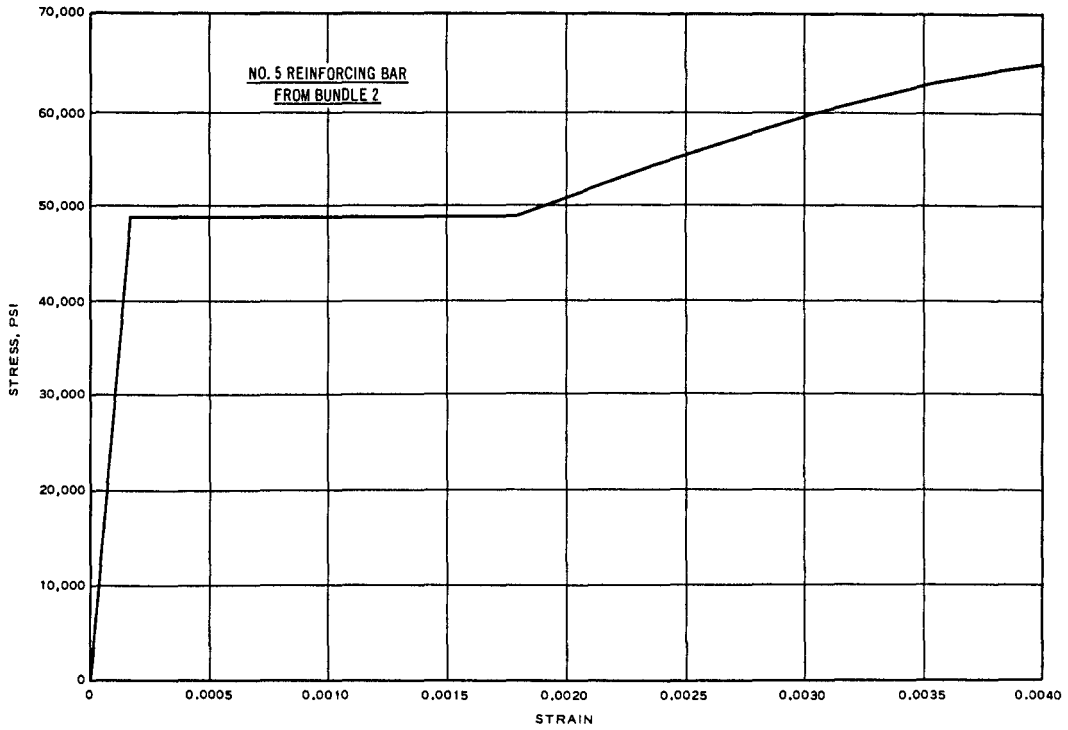


Figure 4.2 Typical static stress-strain curve for flexural reinforcement.

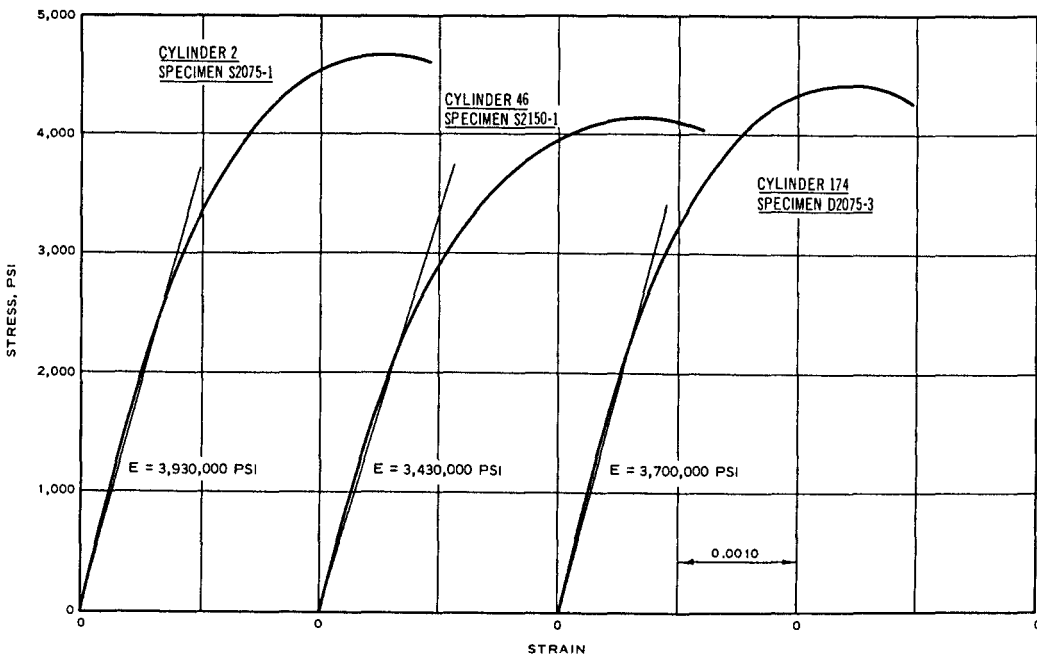


Figure 4.3 Typical static stress-strain curves for concrete control cylinders.

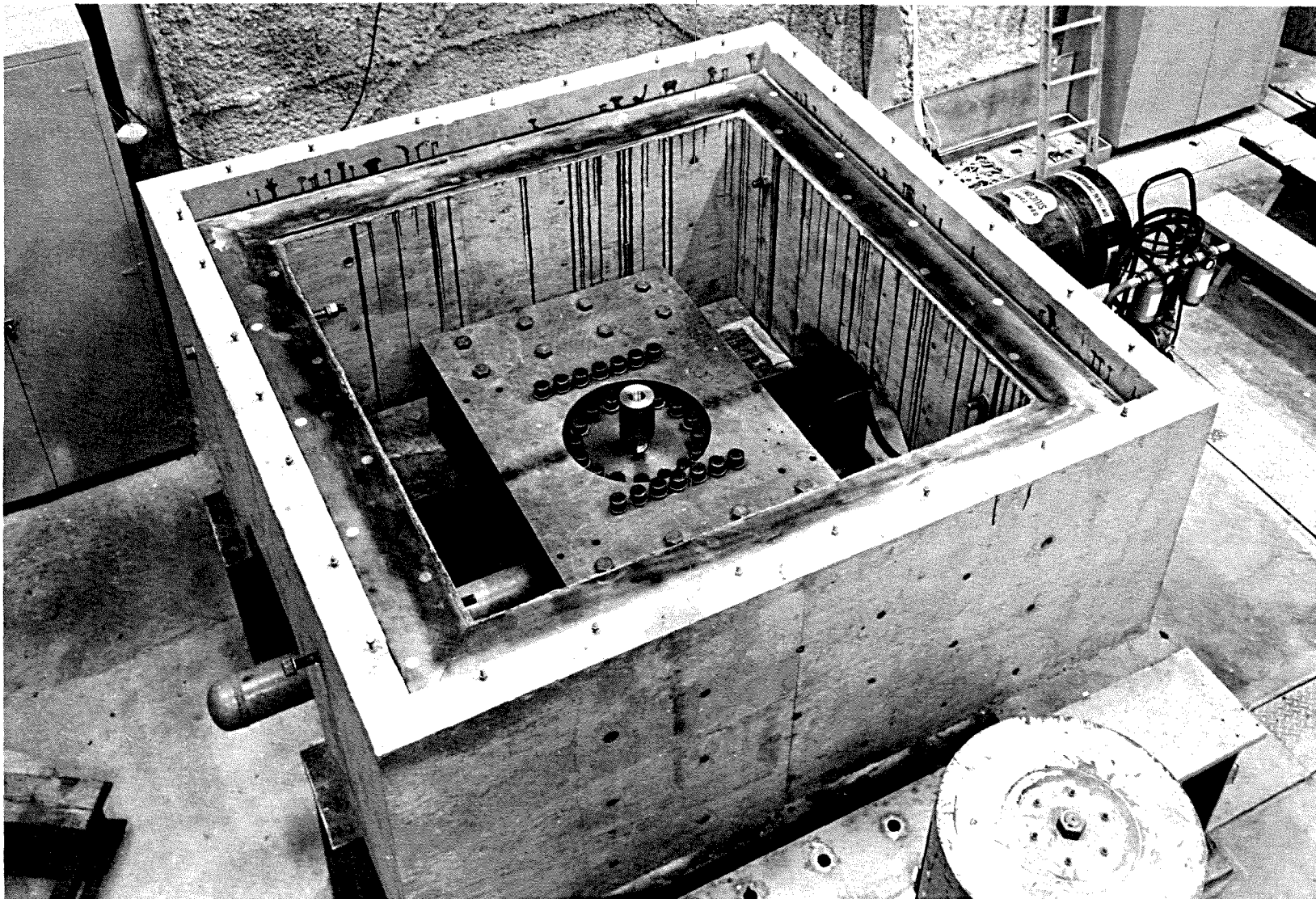


Figure 4.4 Reaction structure and loading device.

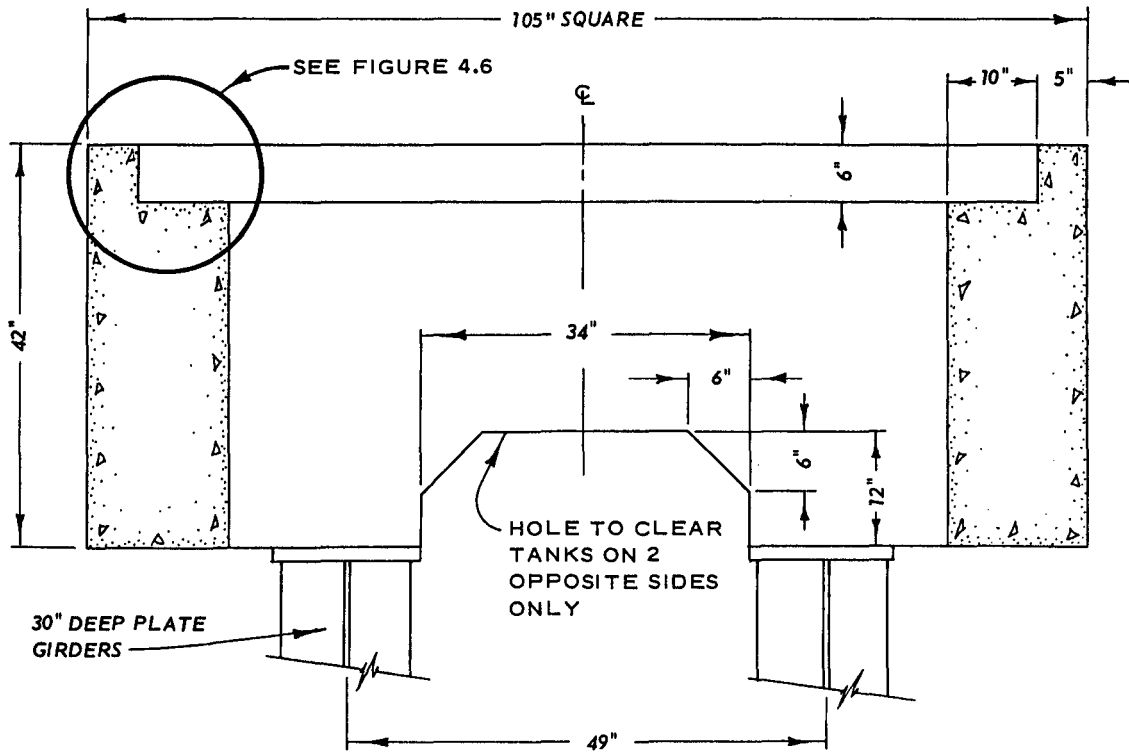


Figure 4.5 Section through reaction structure.

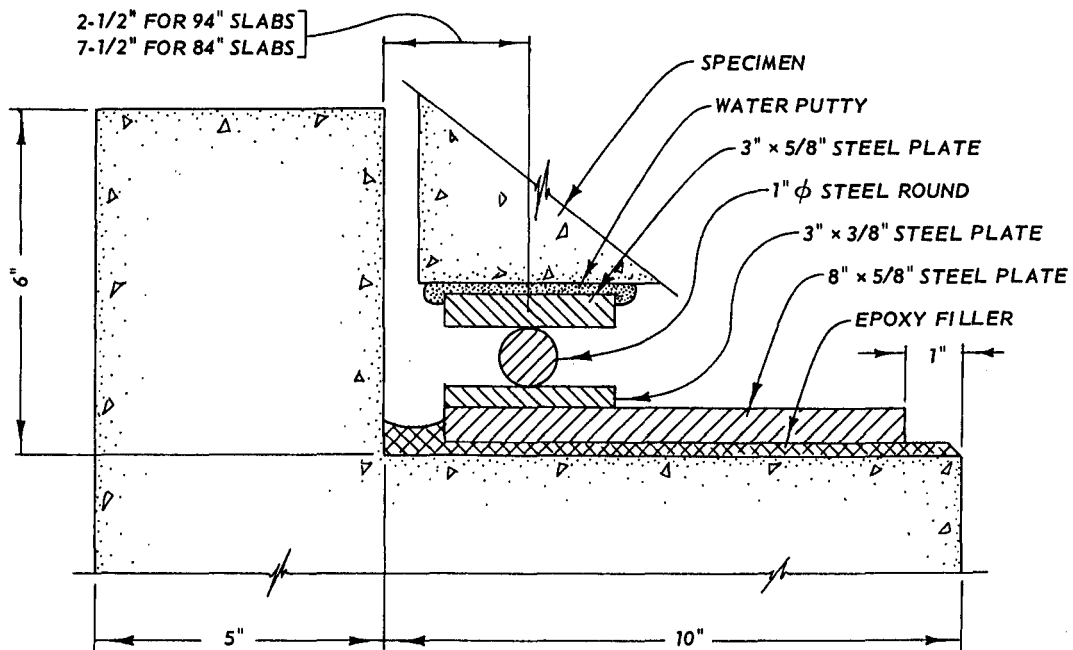


Figure 4.6 Detail of slab support.



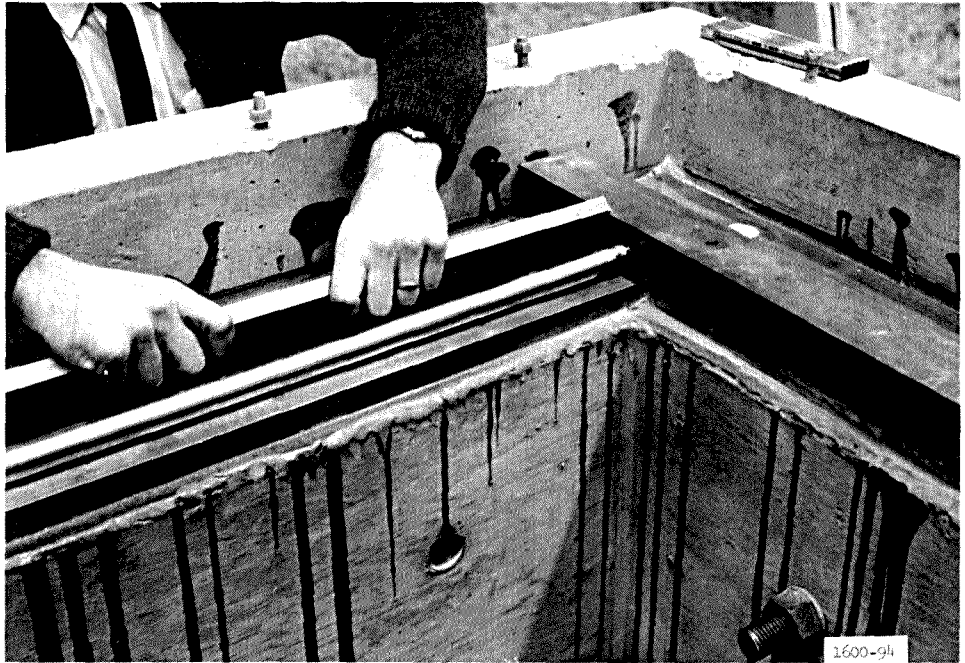


Figure 4.7 Slab supports.

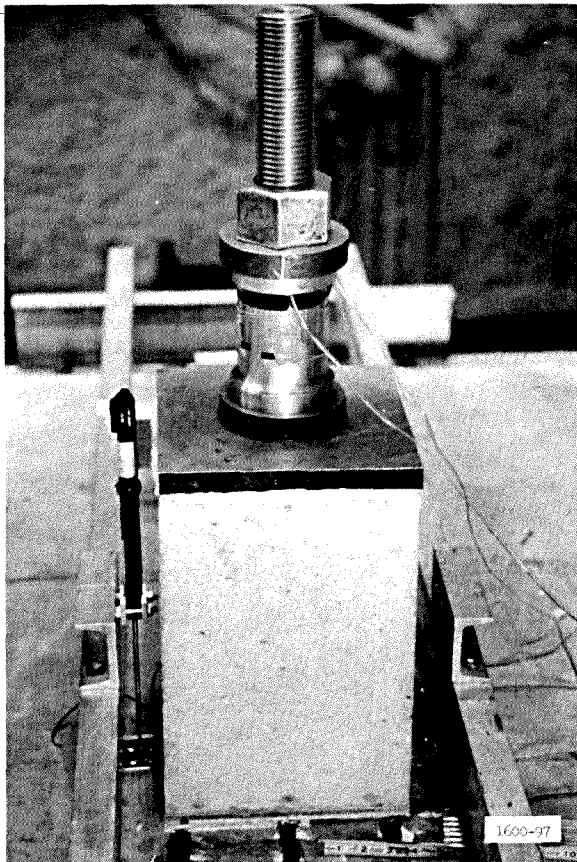


Figure 4.8 Detail of column area.

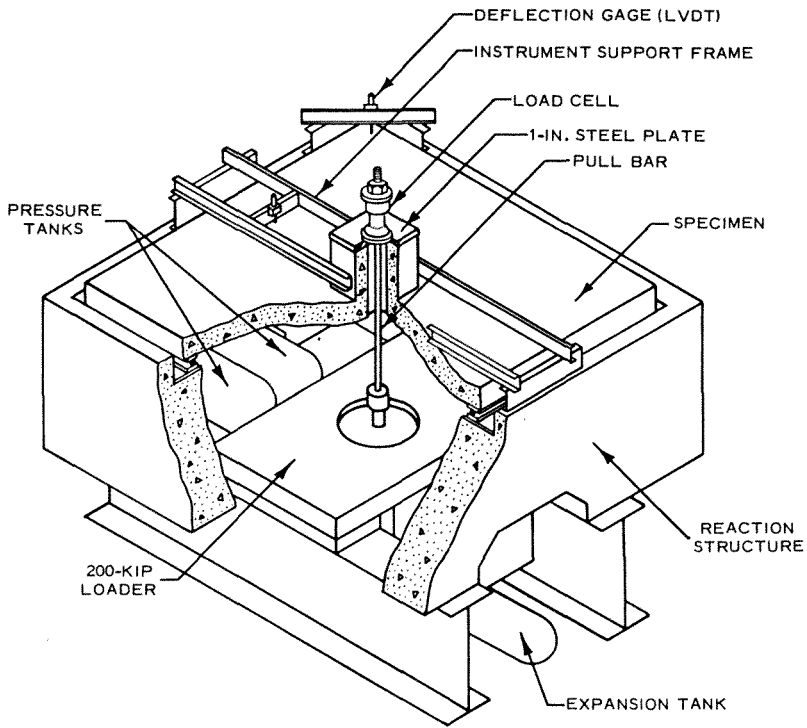


Figure 4.9 Testing arrangement.

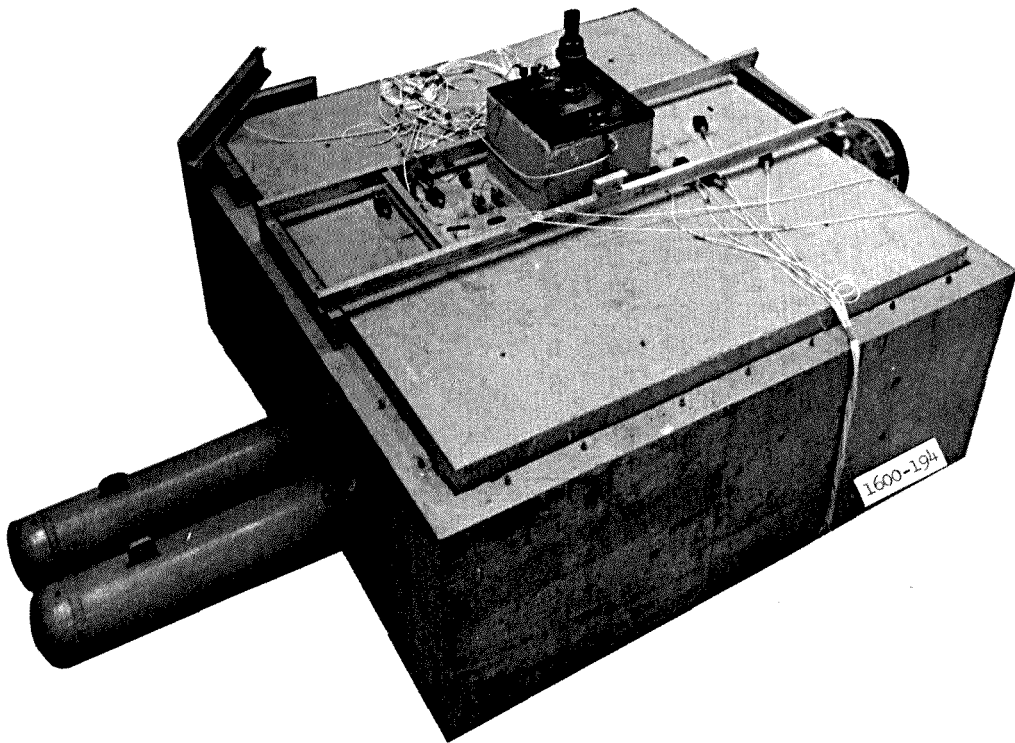
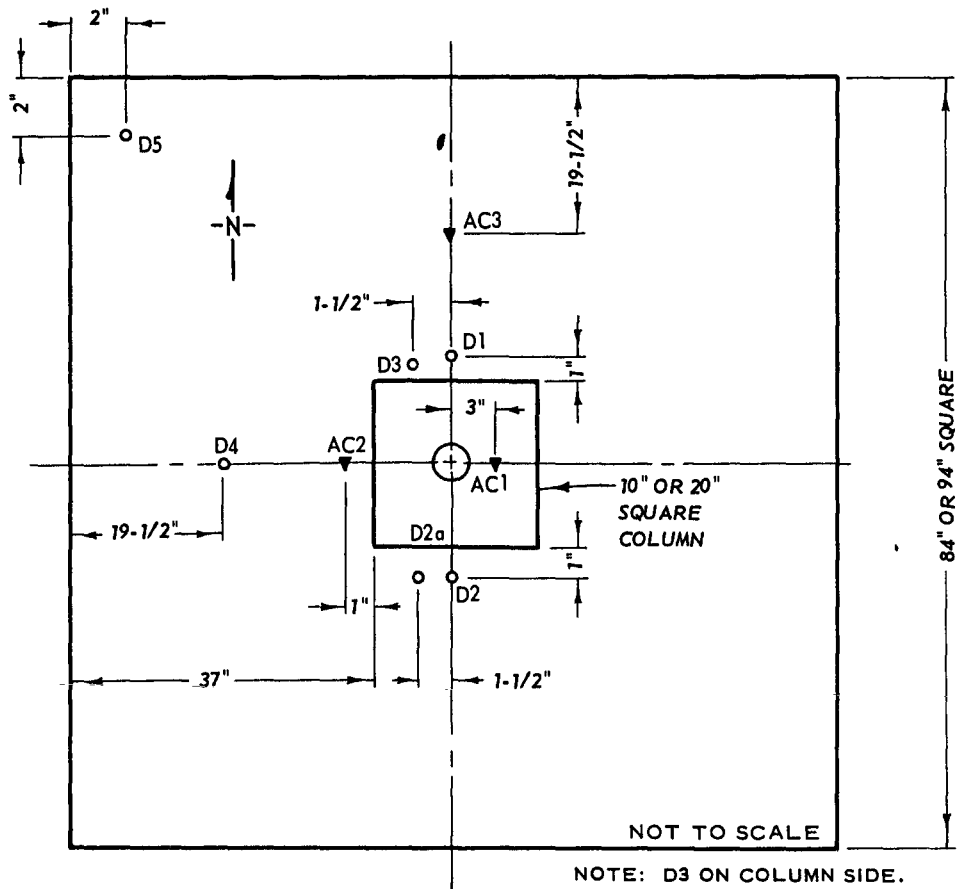
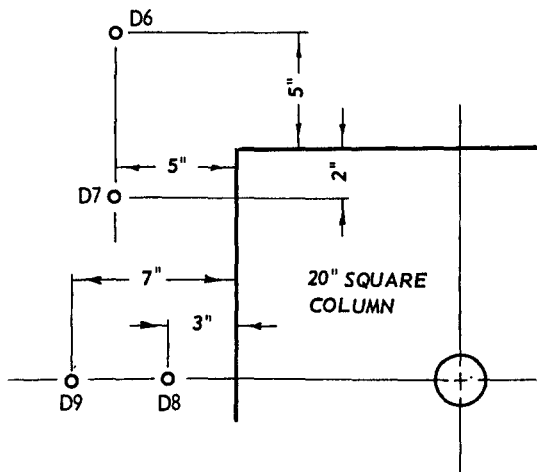


Figure 4.10 Completed testing arrangement prior to test.



NOTE: D3 ON COLUMN SIDE.  
AC1 AT TOP OF COLUMN.



D1-D5 - DEFLECTION GAGES  
ON ALL SPECIMENS

D6-D9 - CRACK FORMATION  
GAGES, USED WITH  
LARGER COLUMN ONLY

AC1-AC3 - ACCELEROMETERS,  
DYNAMIC TESTS ONLY

Figure 4.11 Location of deflection and acceleration transducers.

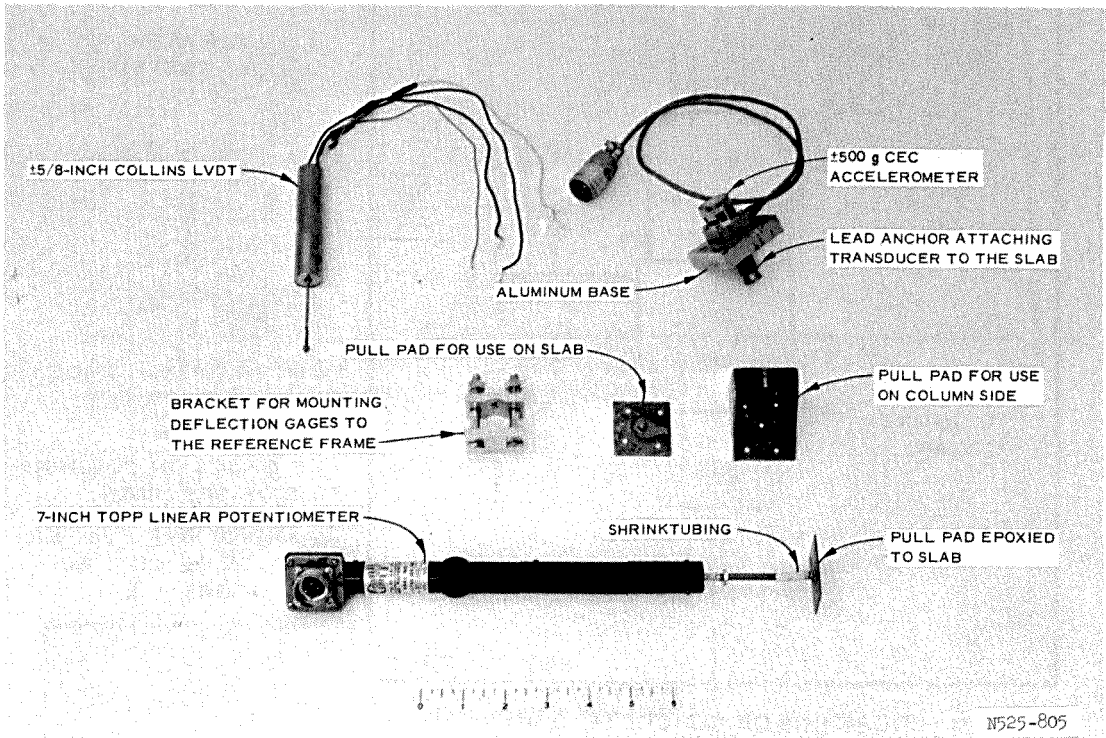


Figure 4.12 Deflection and acceleration transducers and mounts.

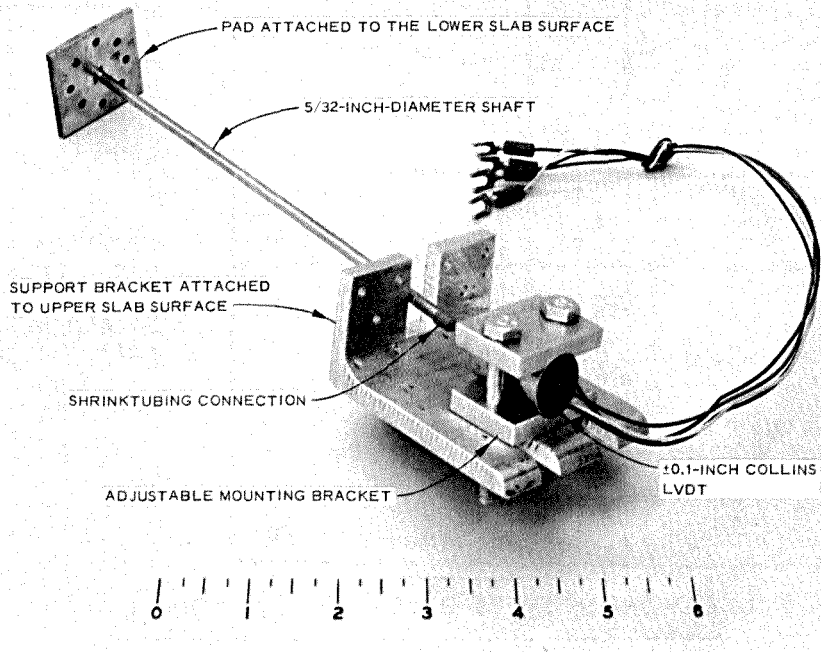


Figure 4.13 Crack detection assembly.

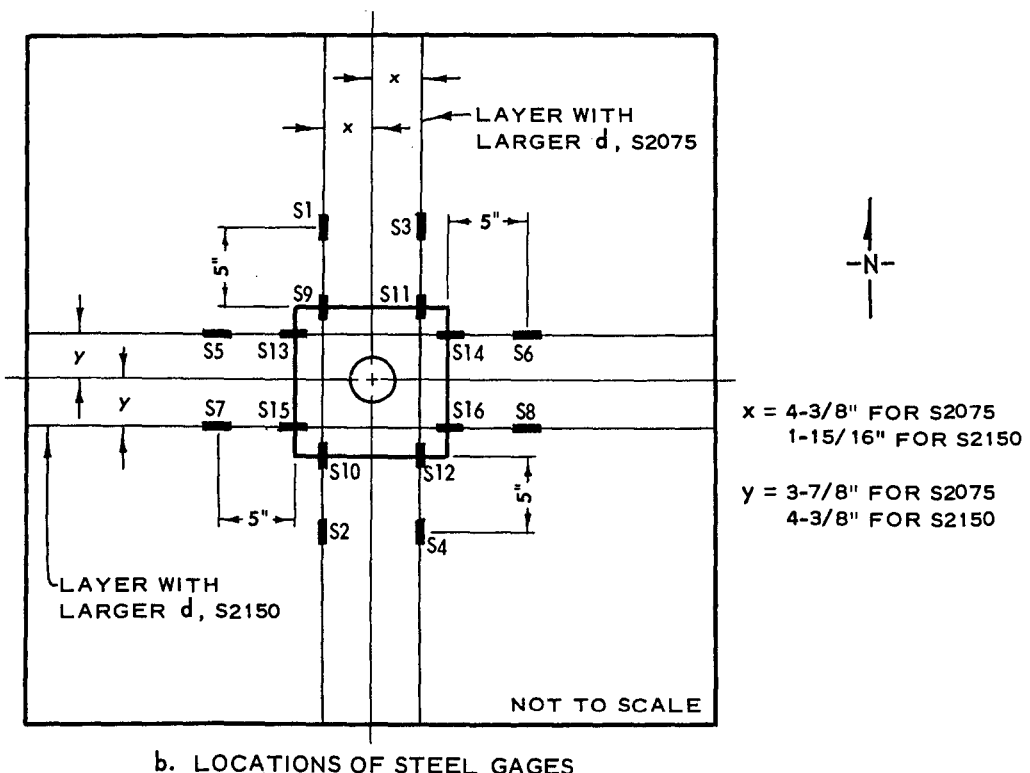
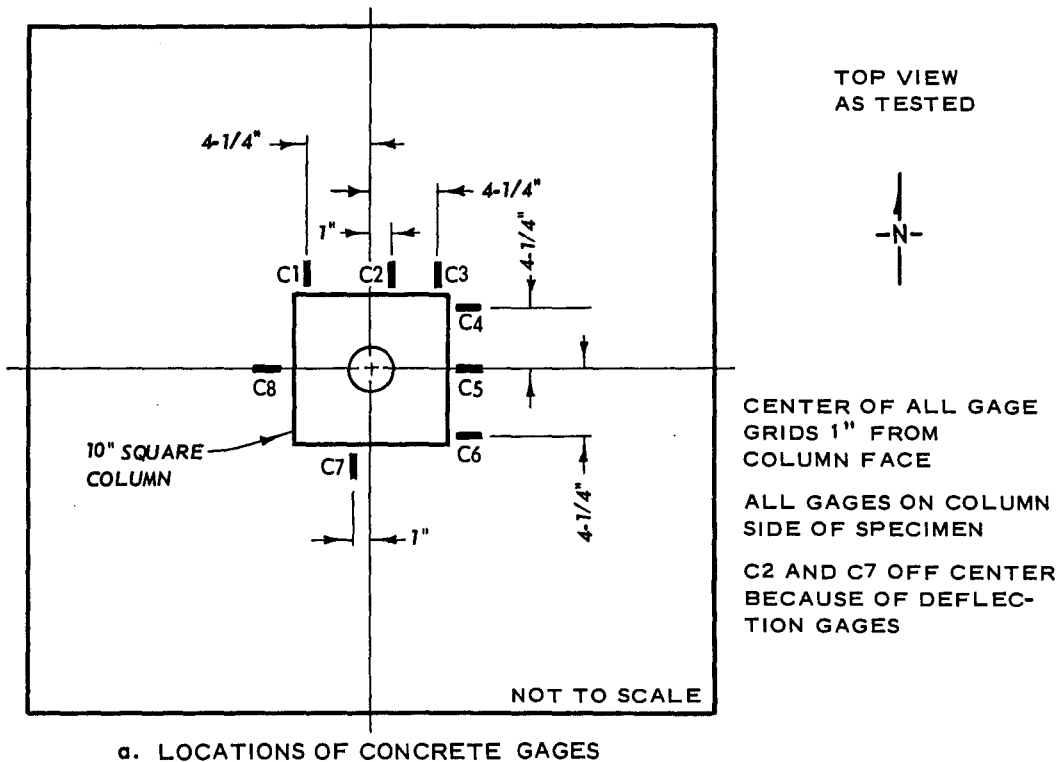


Figure 4.14 Strain gage layout for S2000 Series.

NOTE: LOCATIONS OF STEEL GAGES IDENTICAL  
TO THOSE SHOWN IN FIG. 4.14b

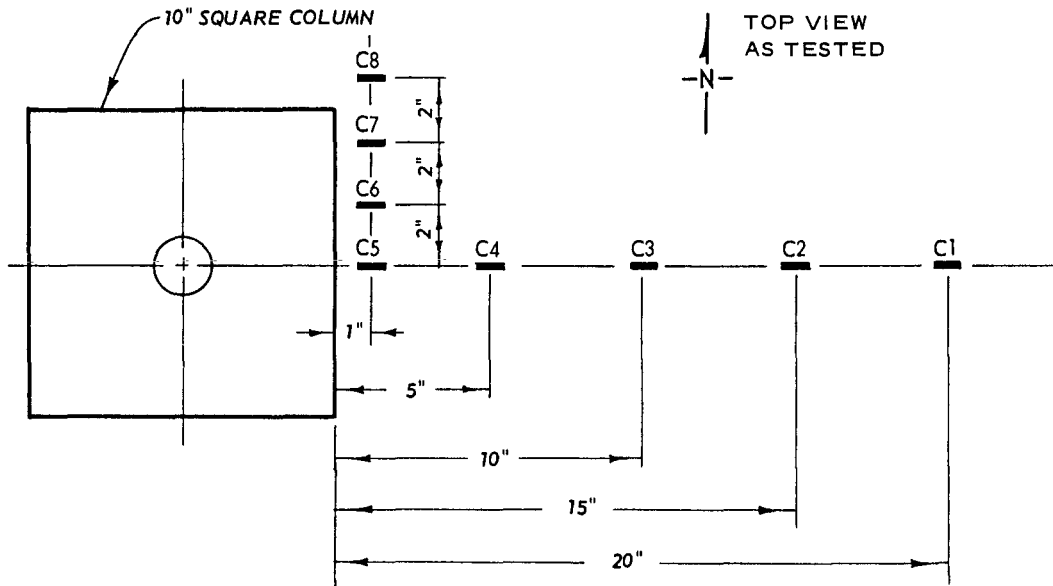
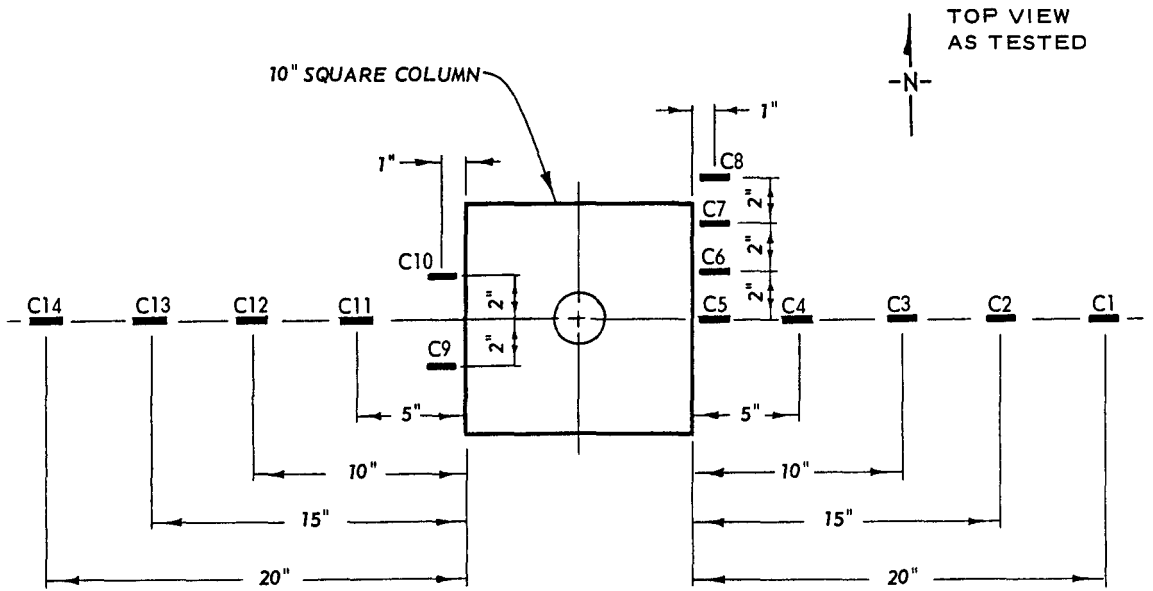
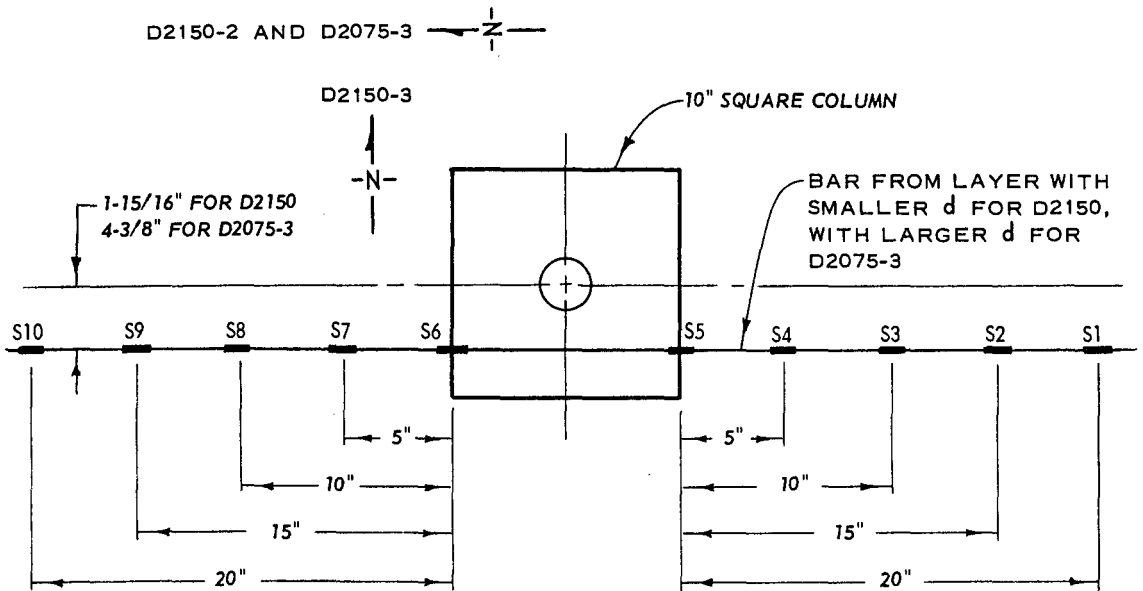


Figure 4.15 Strain gage layout for Specimens D2075-1, D2075-2, and D2150-1.

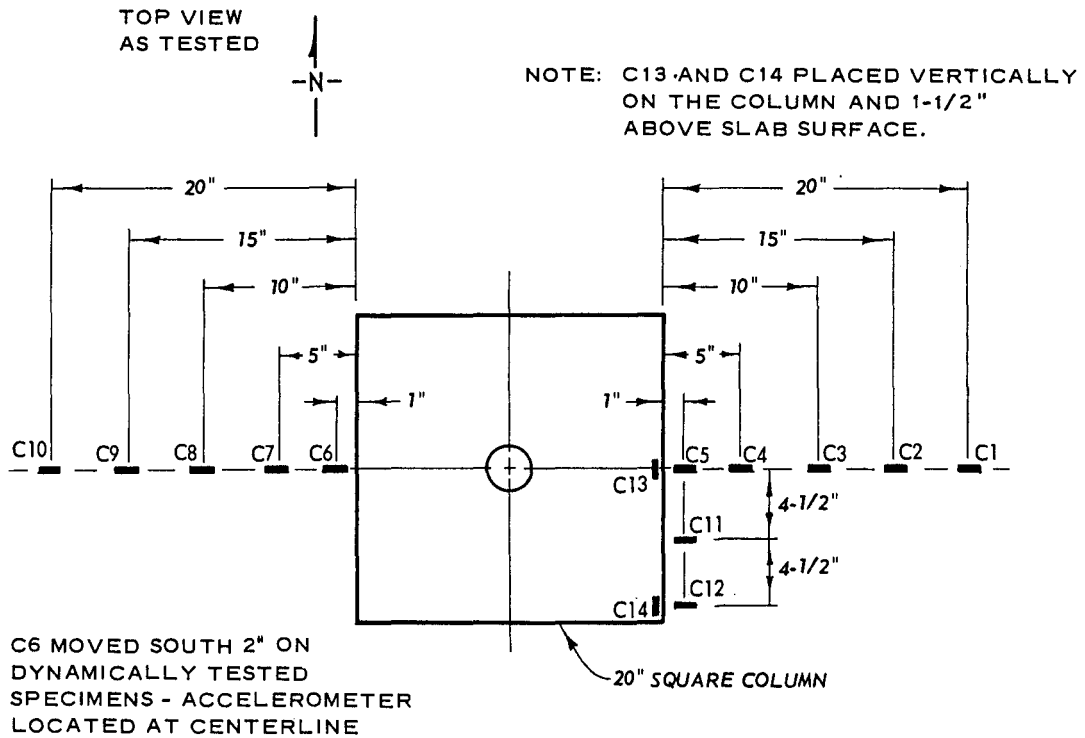


a. LOCATION OF CONCRETE GAGES

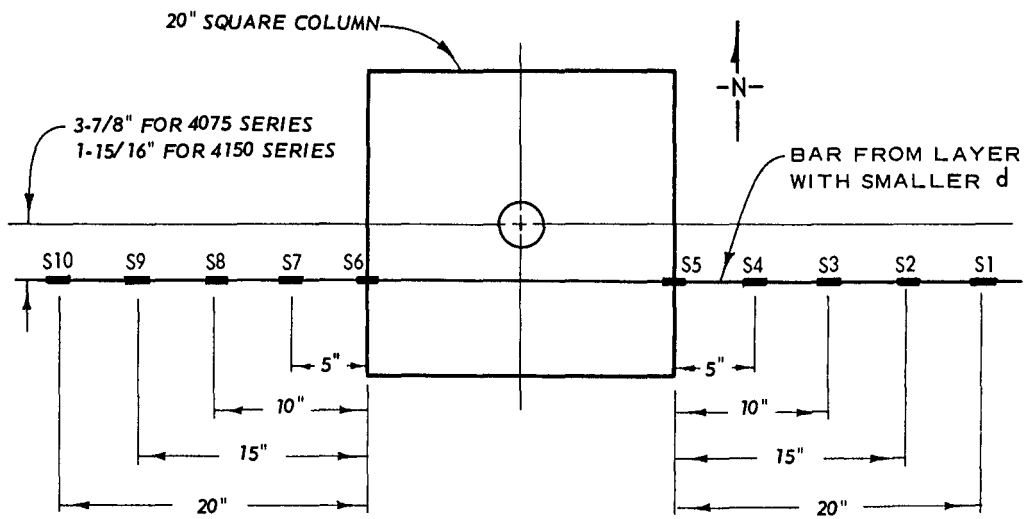


b. LOCATION OF STEEL GAGES

Figure 4.16 Strain gage layout for Specimens D2075-3, D2150-2, and D2150-3.



a. LOCATION OF CONCRETE GAGES



b. LOCATION OF STEEL GAGES

Figure 4.17 Strain gage layout for S4000 and D4000 Series.



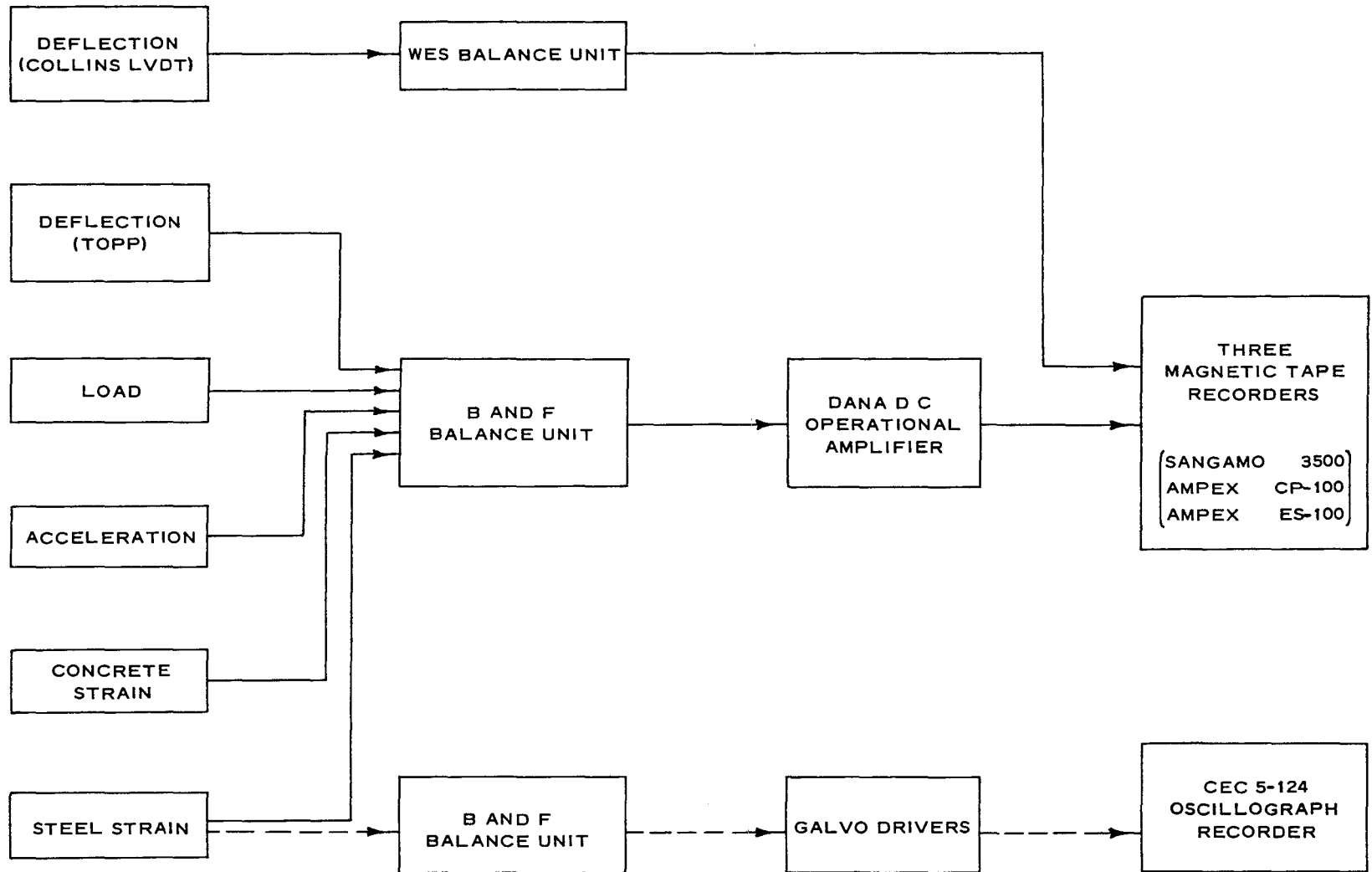


Figure 4.18 Diagram of instrumentation system.

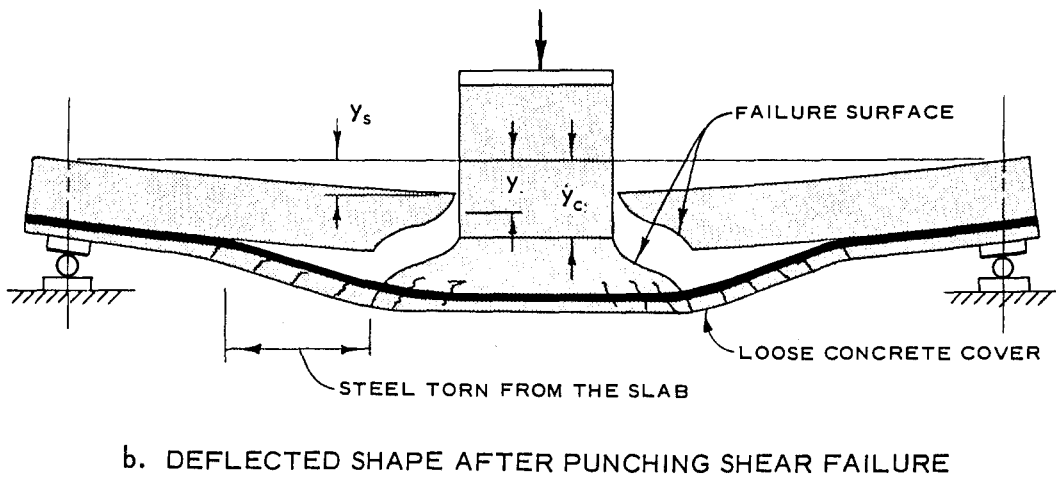
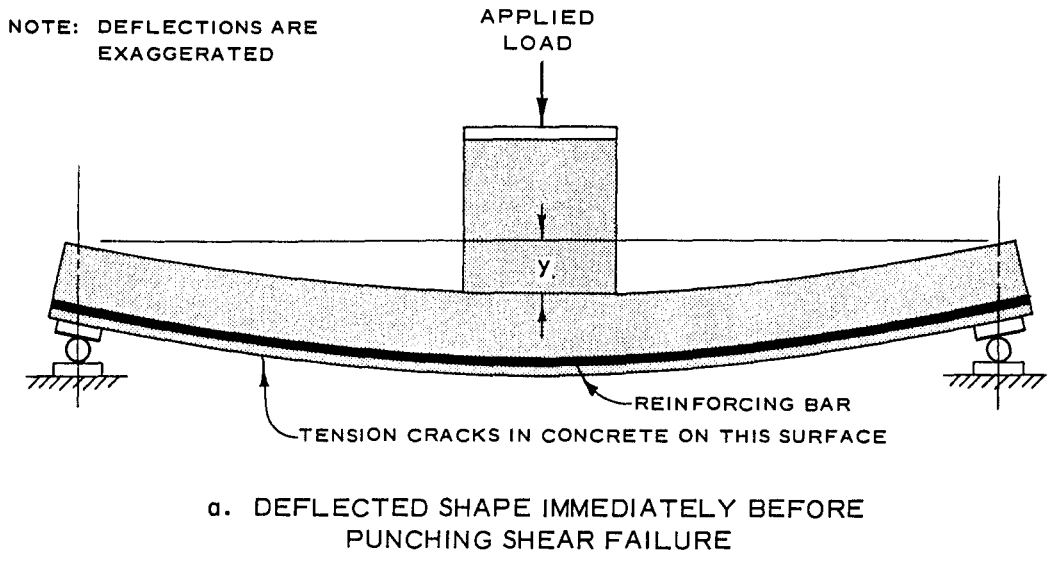
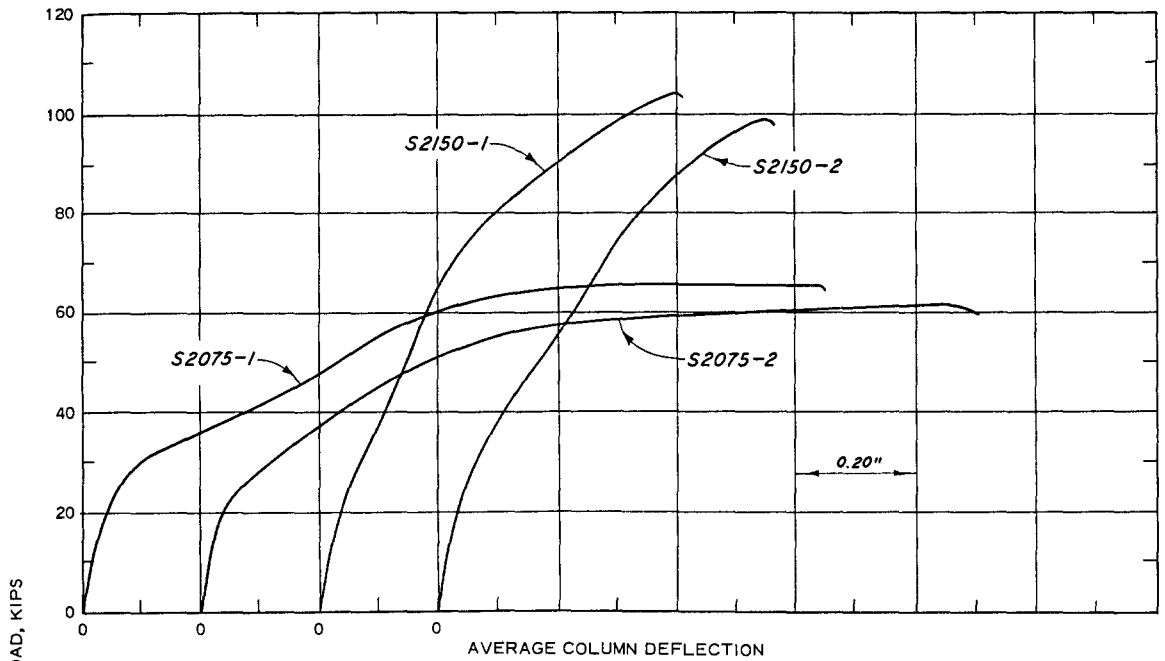
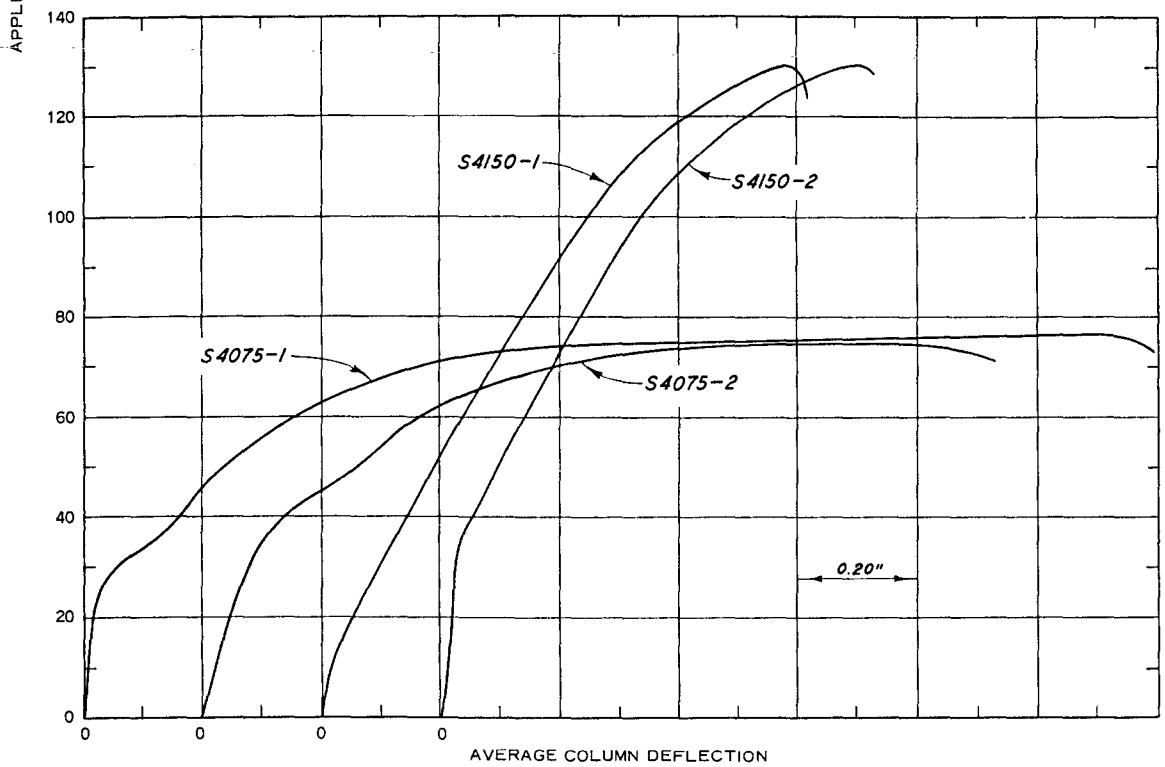


Figure 5.1 Deflections before and after failure.

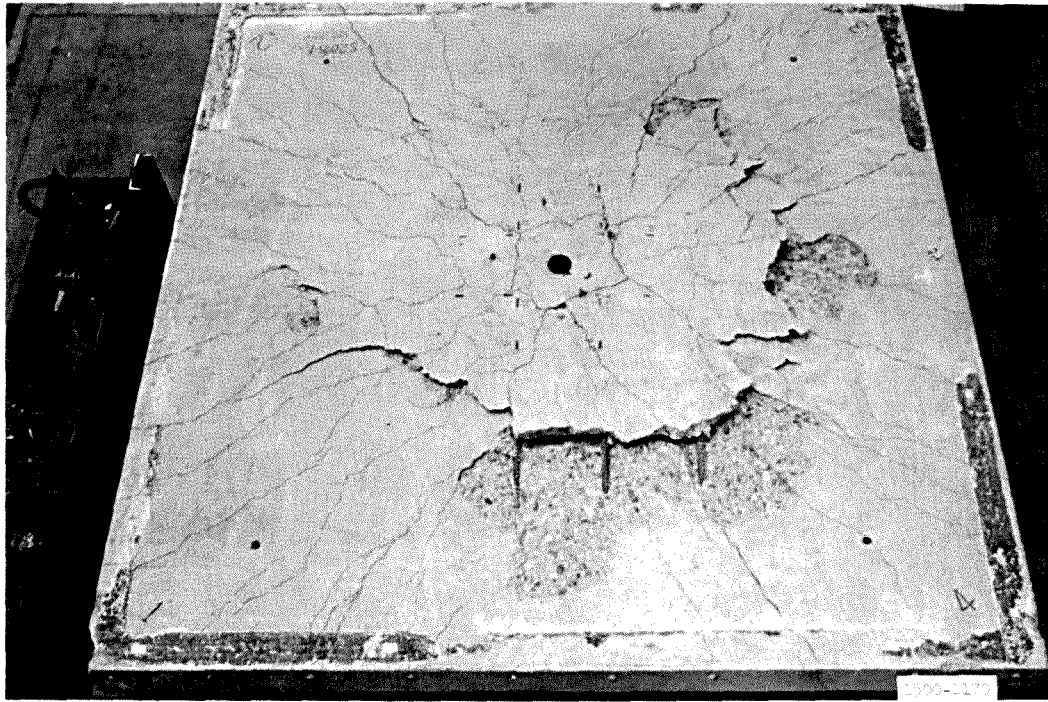


a. CONNECTIONS WITH A 10-INCH-SQUARE COLUMN

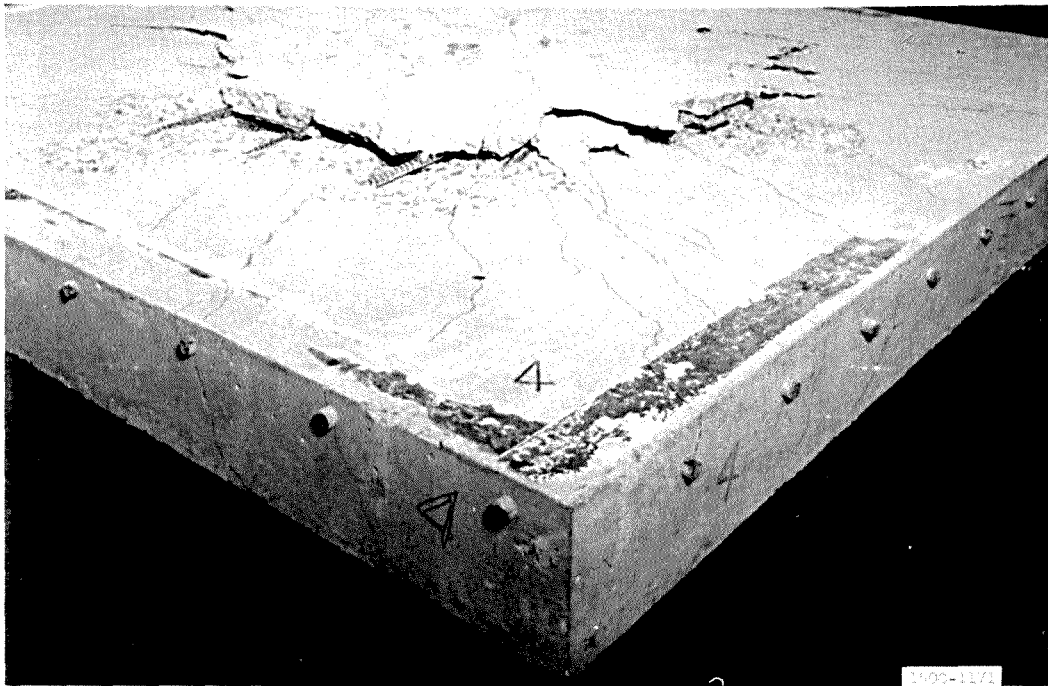


b. CONNECTIONS WITH A 20-INCH-SQUARE COLUMN

Figure 5.2 Load-deflection curves for the statically tested connections.



a. Crack pattern, cracks marked.

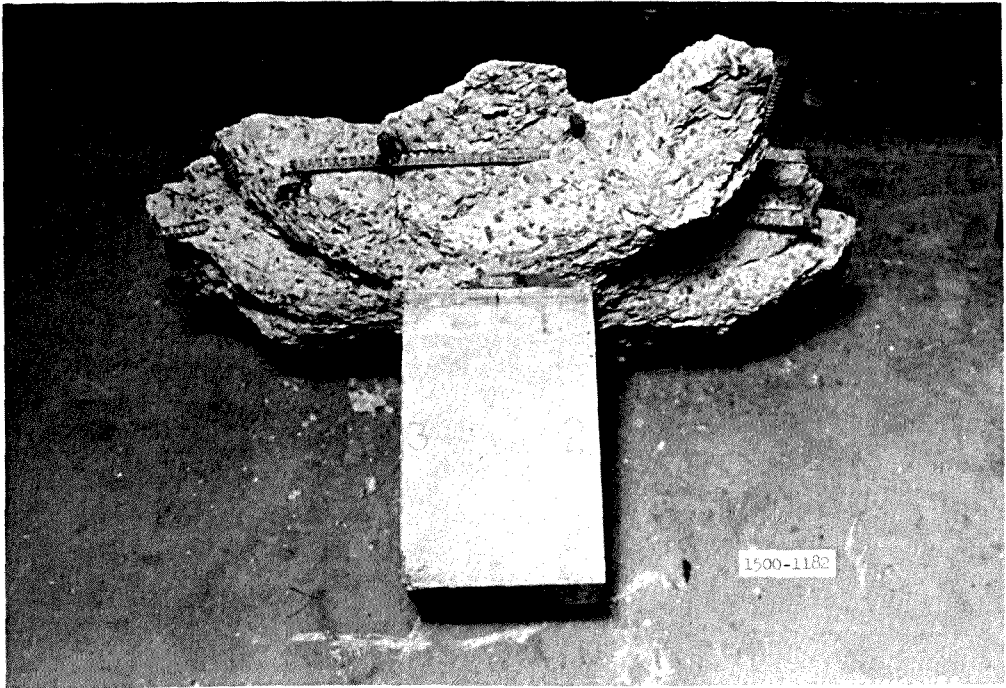


b. Detail of a corner, cracks marked.

Figure 5.3 Posttest photographs of Specimen S2075-1.



a. Crack pattern.

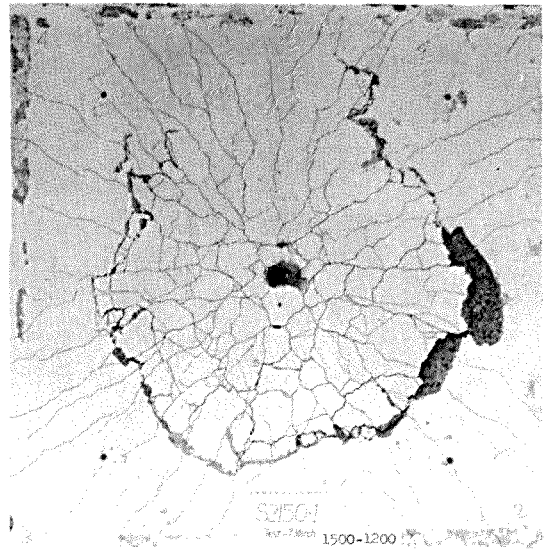


b. Column and failure cone.

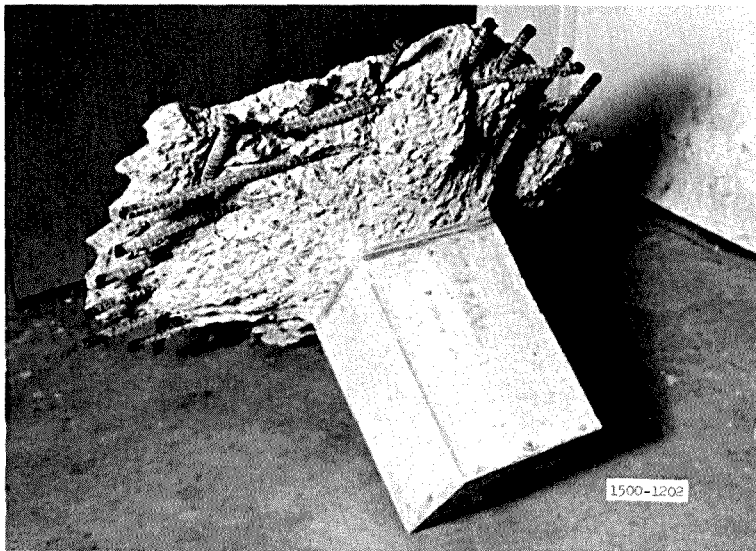
Figure 5.4 Posttest photographs of Specimen S2075-2.



a. Crack pattern.

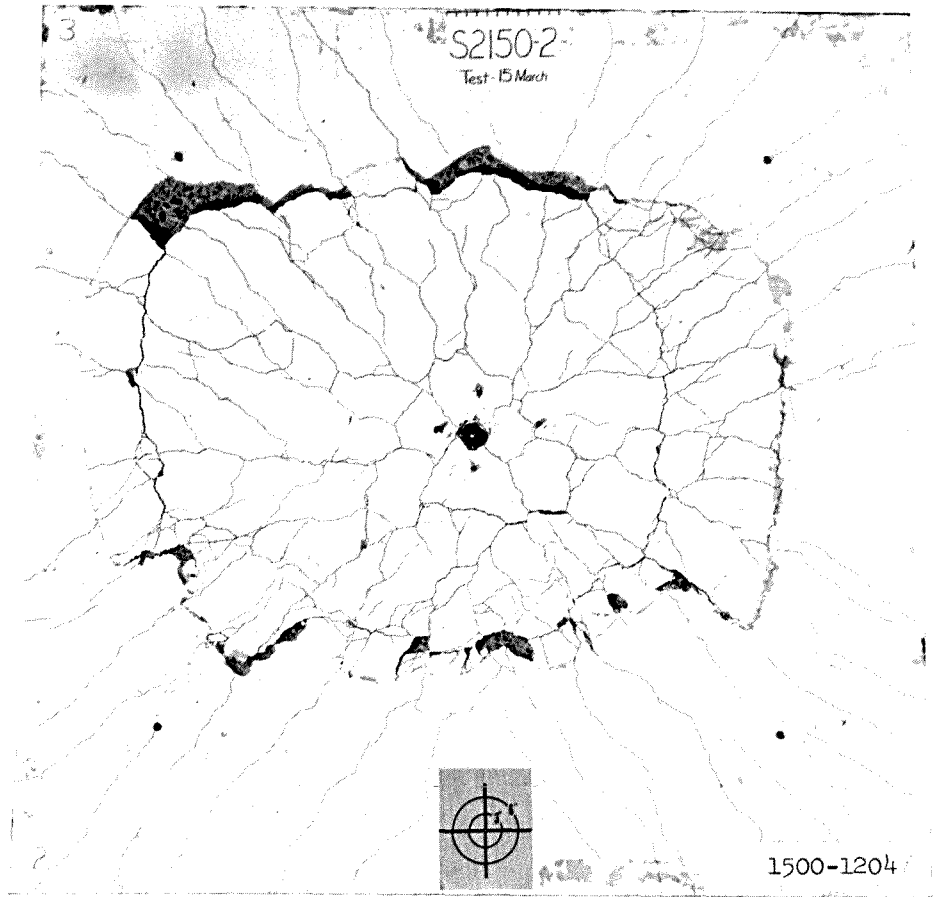


b. Crack pattern, cracks marked.

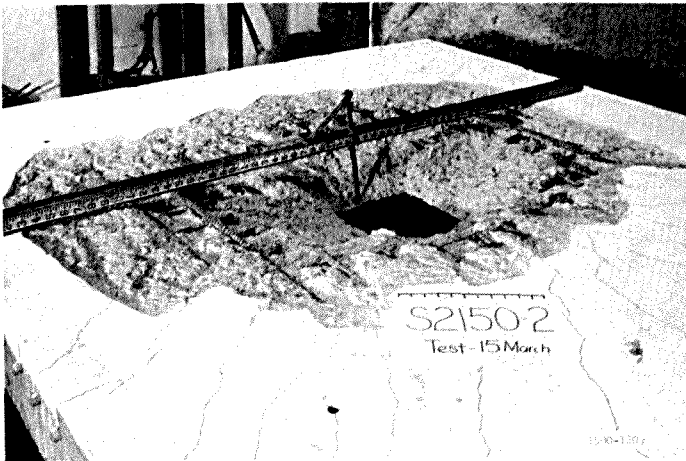


c. Column and failure cone.

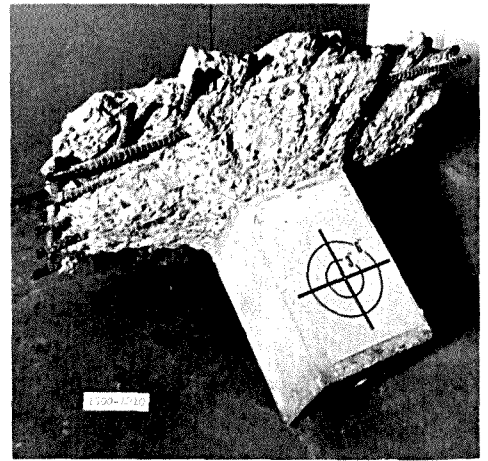
Figure 5.5 Posttest photographs of Specimen S2150-1.



a. Crack pattern, cracks marked.

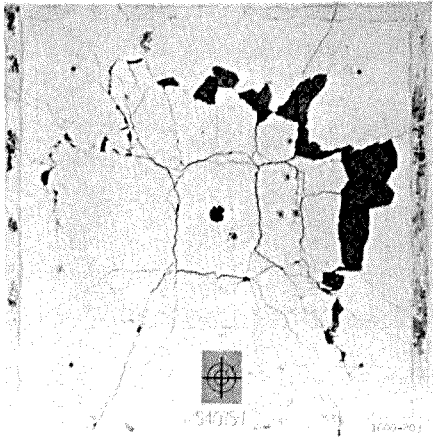


b. Column and failure cone.

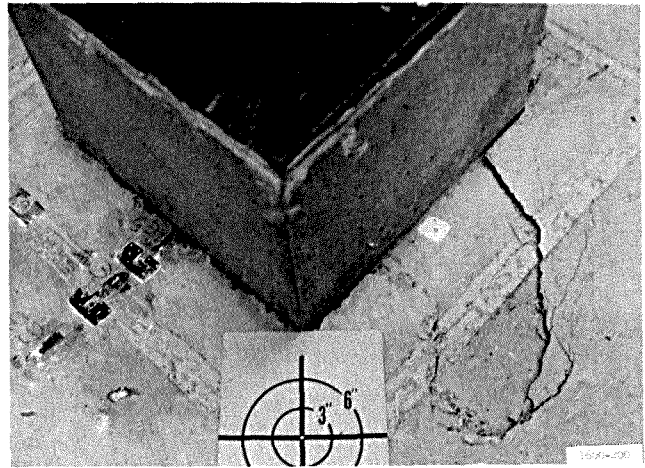


c. Slab with column removed.

Figure 5.6 Posttest photographs of Specimen S2150-2.



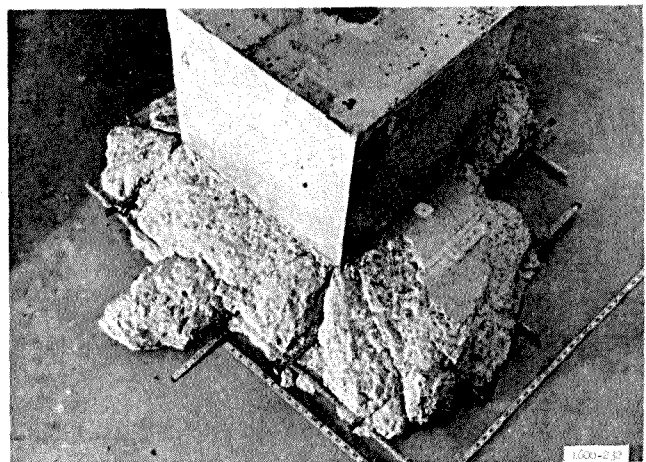
a. Crack pattern.



b. Detail of column side of slab.



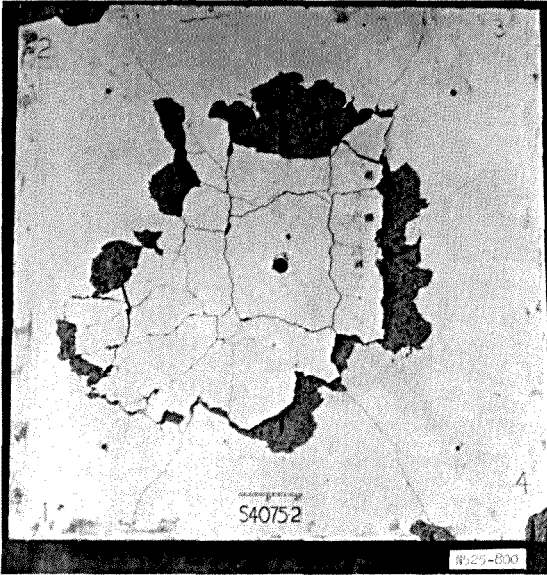
c. Column removed,  
cracks marked.



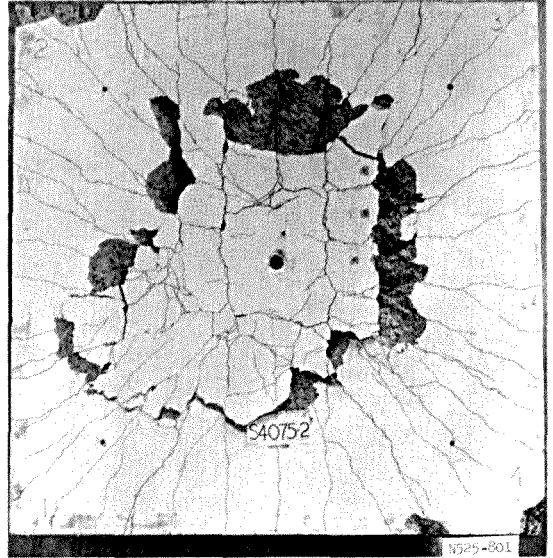
d. Column and failure cone.

Figure 5.7 Posttest photographs of Specimen S4075-1.

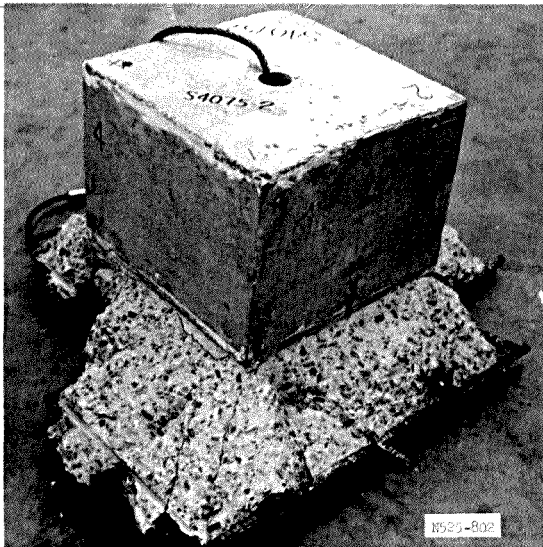




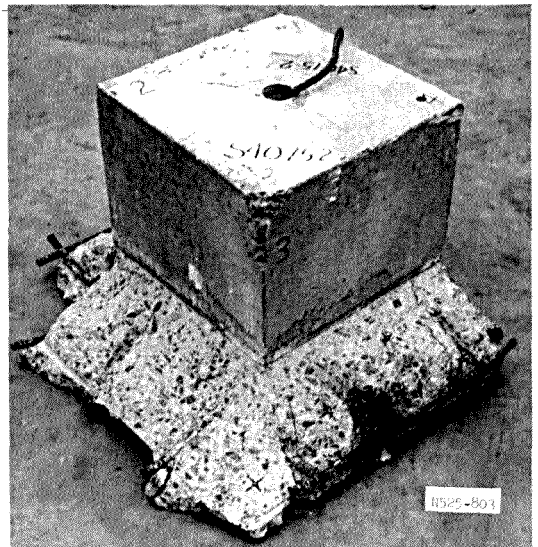
a. Crack pattern.



b. Crack pattern, cracks marked.



c. Column and failure cone.

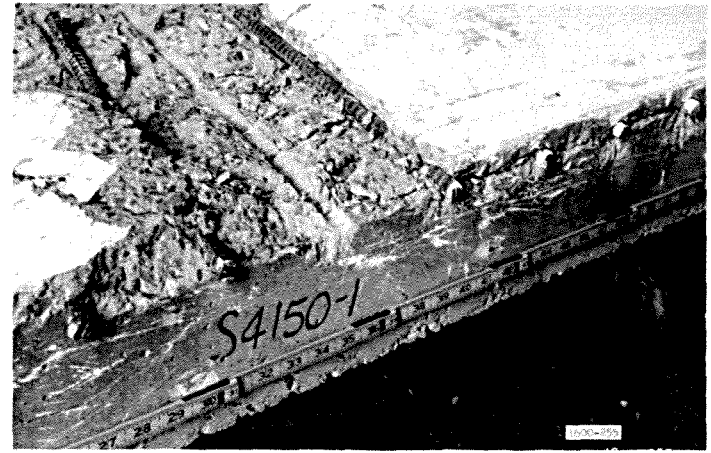


d. Column and failure cone.

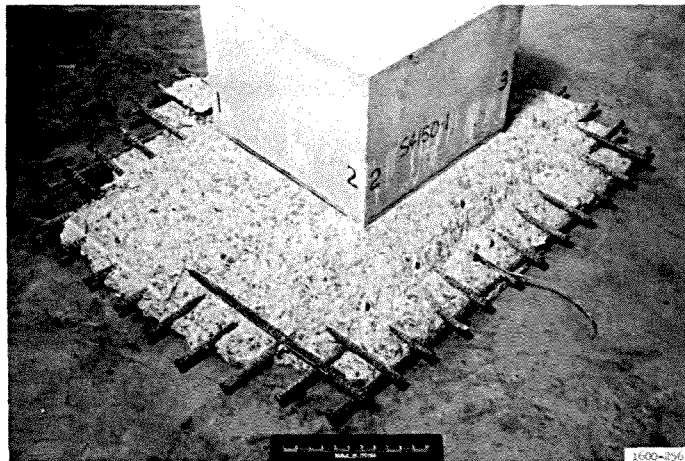
Figure 5.8 Posttest photographs of Specimen S4075-2.



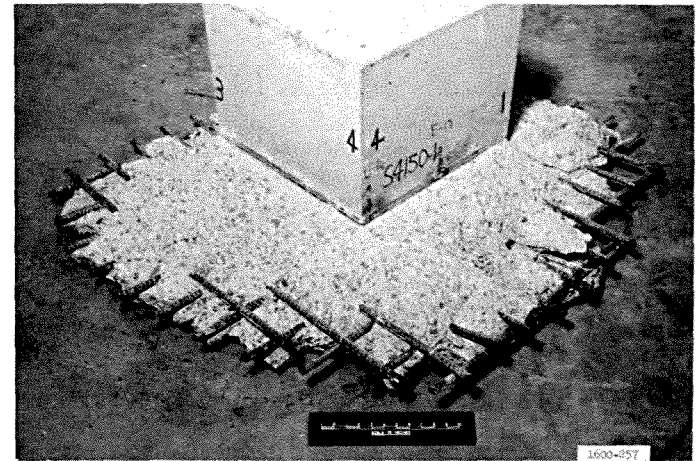
a. Crack pattern.



b. Detail of slab edge, column removed.

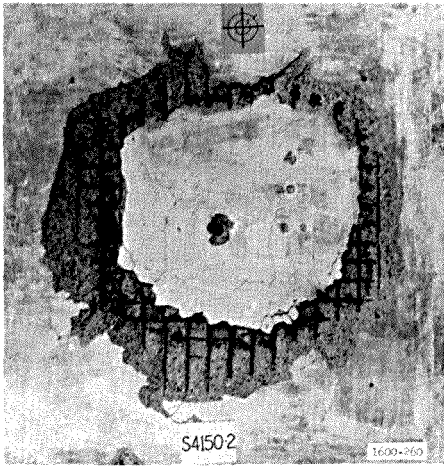


c. Column and failure cone.

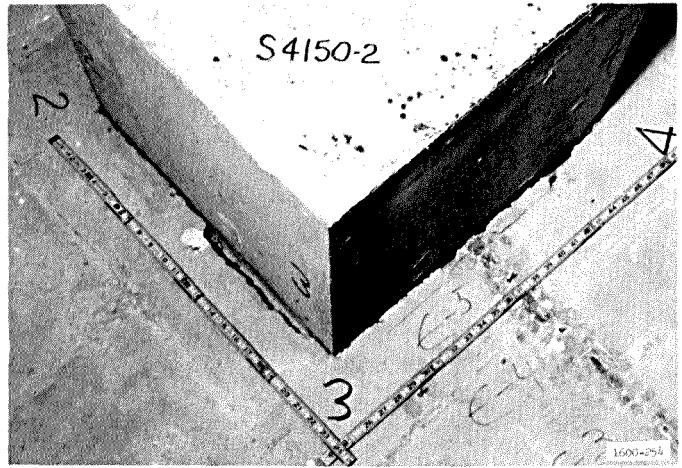


d. Column and failure cone.

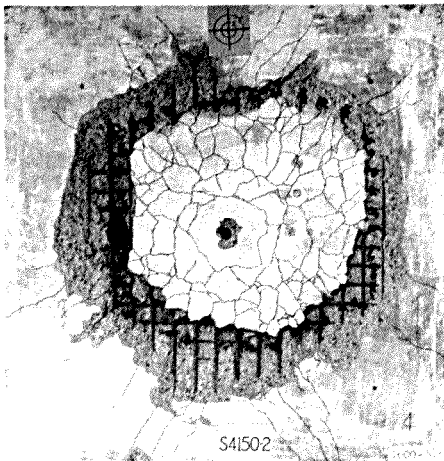
Figure 5.9 Posttest photographs of Specimen S4150-1.



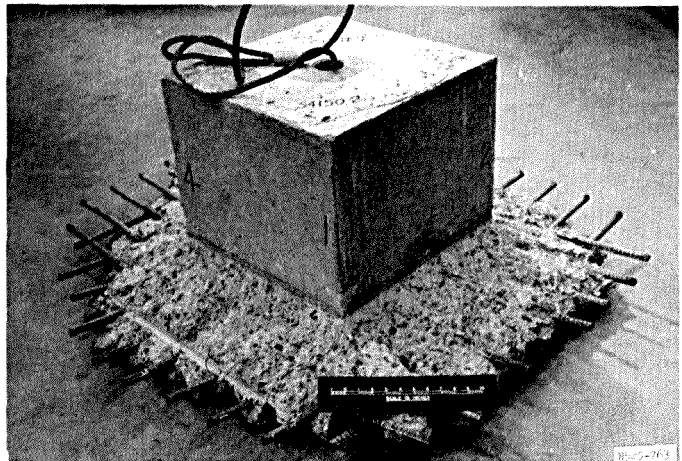
a. Crack pattern, bars cut.



b. Detail of column side of slab.



c. Crack pattern, cracks marked.



d. Column and failure cone.

Figure 5.10 Posttest photographs of Specimen S4150-2.

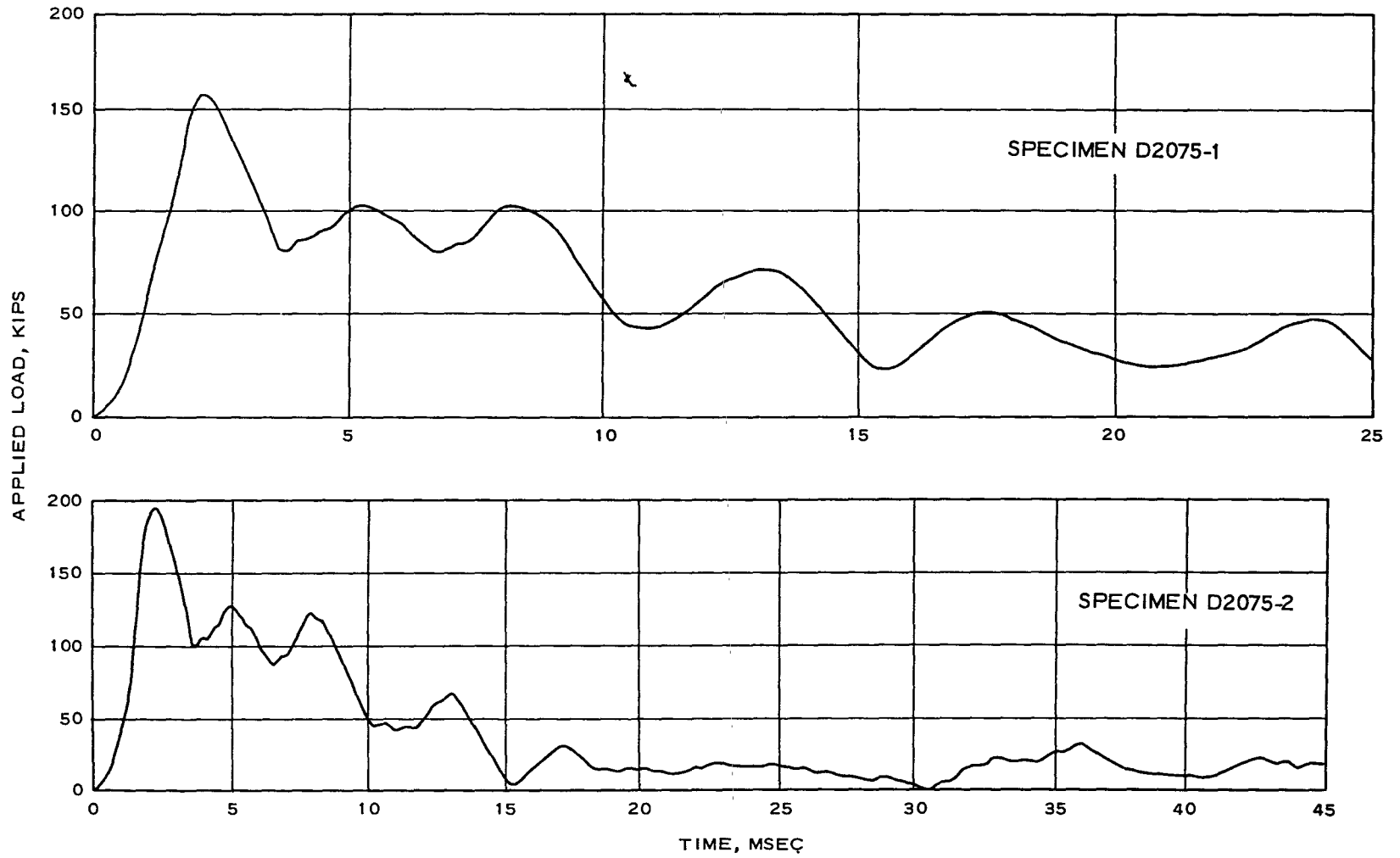
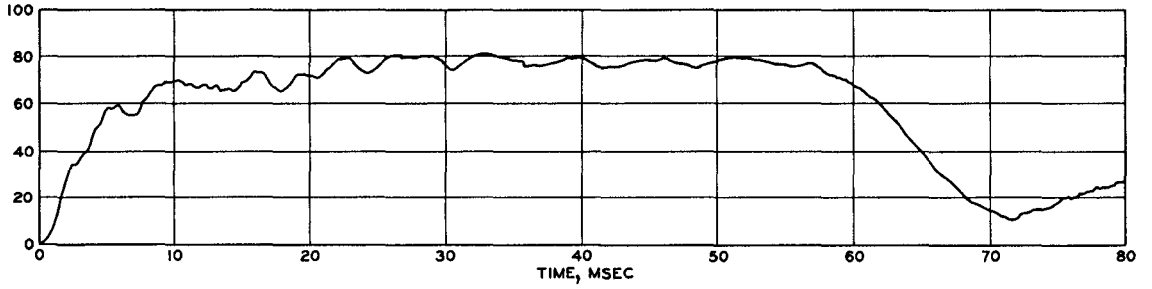
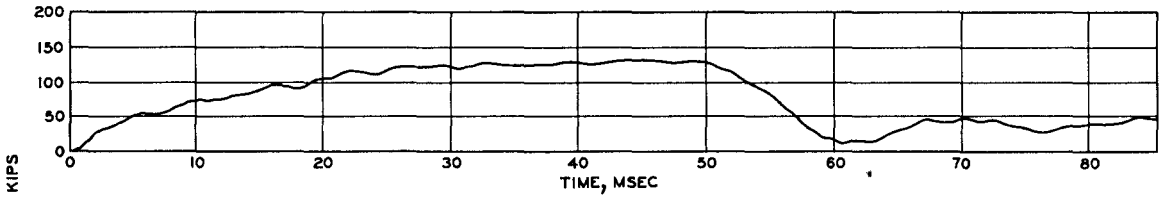


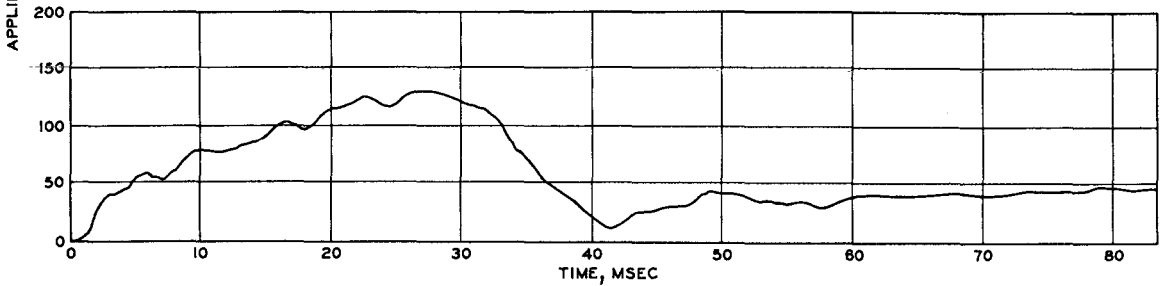
Figure 5.11 Load-time curves for very rapidly loaded specimens.



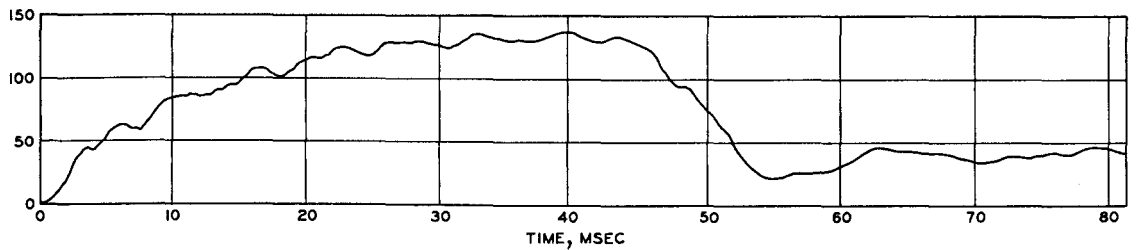
a. SPECIMEN D2075-3



b. SPECIMEN D2150-1

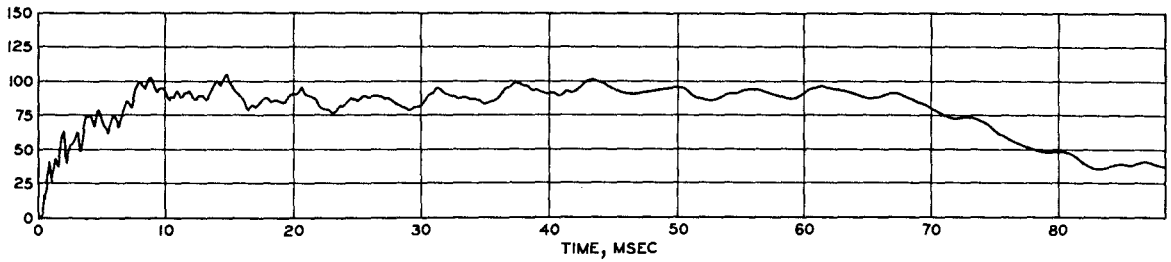


c. SPECIMEN D2150-2

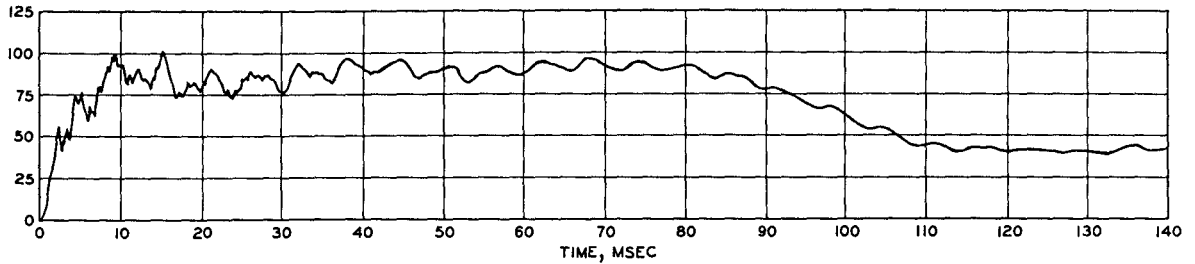


d. SPECIMEN D2150-3

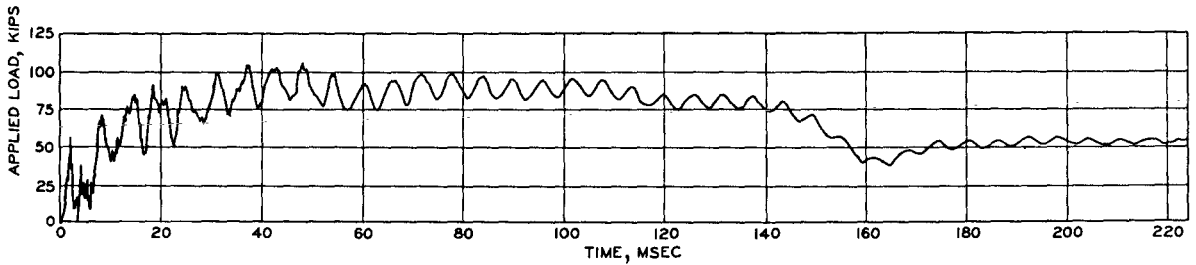
Figure 5.12 Load-time curves for rapidly loaded specimens with 10-inch columns.



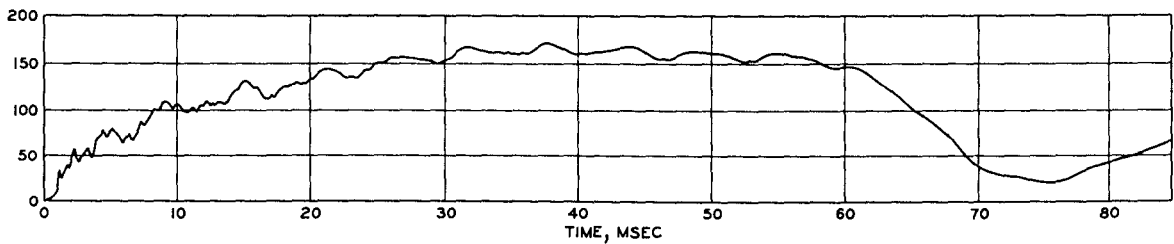
a. SPECIMEN D4075-1



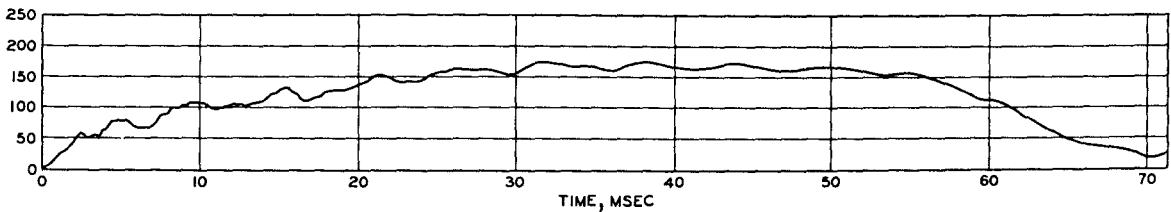
b. SPECIMEN D4075-2



c. SPECIMEN D4075-3

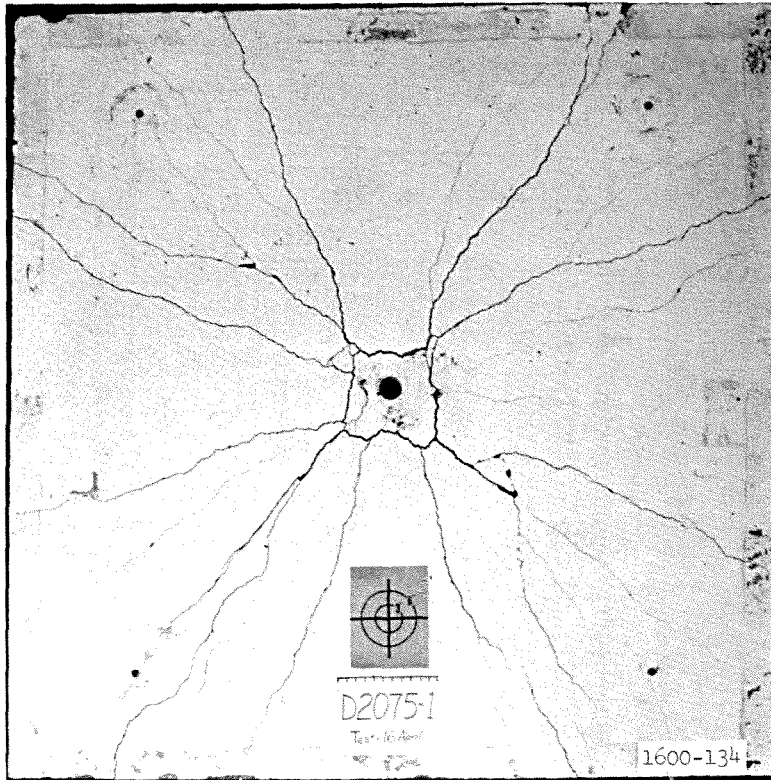


d. SPECIMEN D4150-1



e. SPECIMEN D4150-2

Figure 5.13 Load-time curves for rapidly loaded specimens with 20-inch columns.



a. Specimen D2075-1.

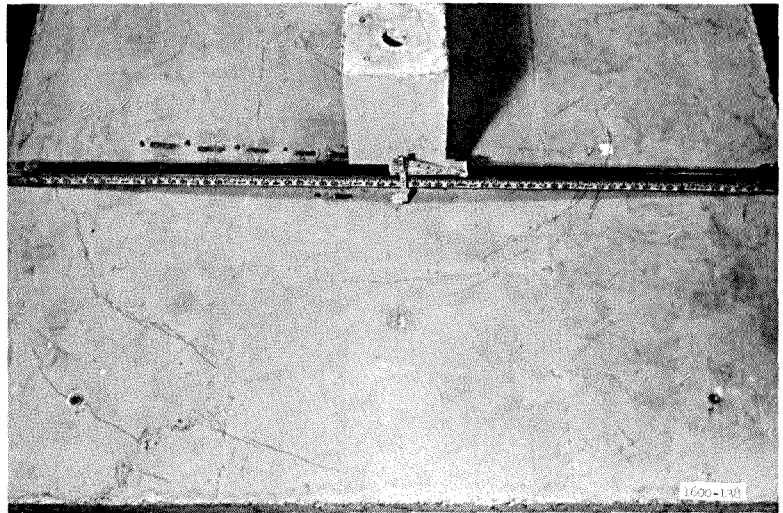


b. Specimen D2075-2.

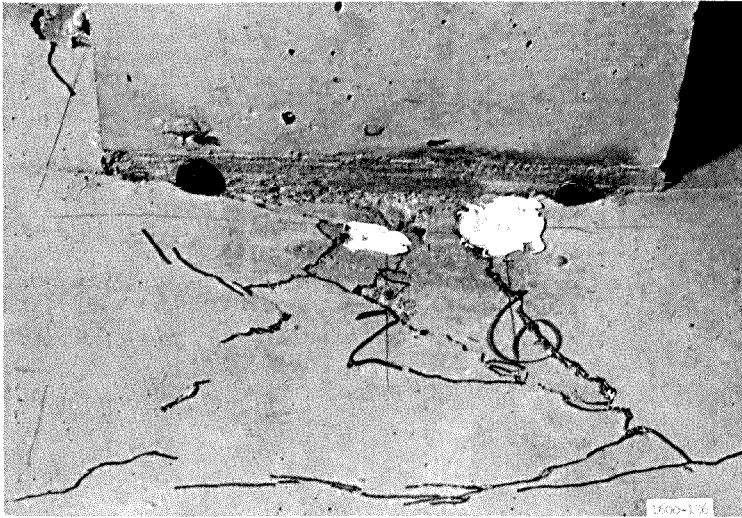
Figure 5.14 Crack patterns of very rapidly loaded specimens.



a. Column side crack pattern, cracks marked.



b. Detail near column.



c. Side view.

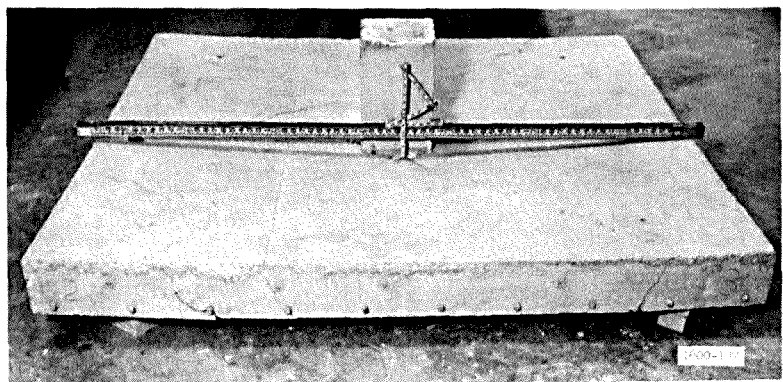
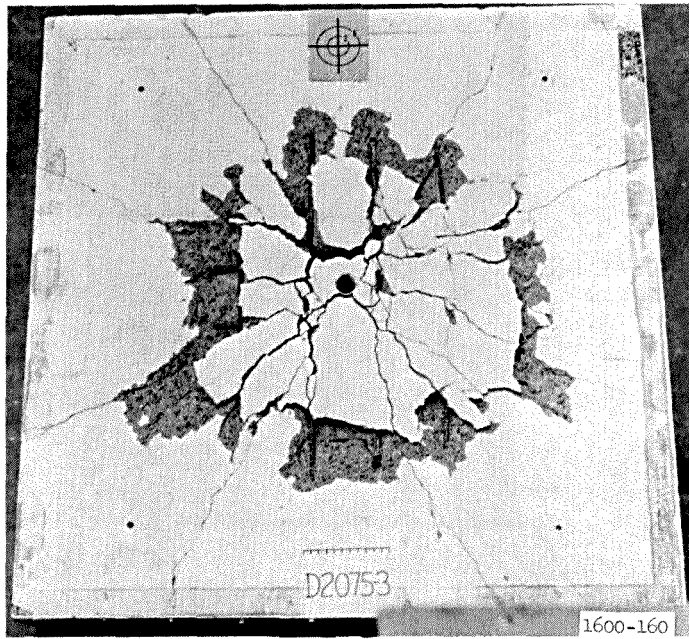
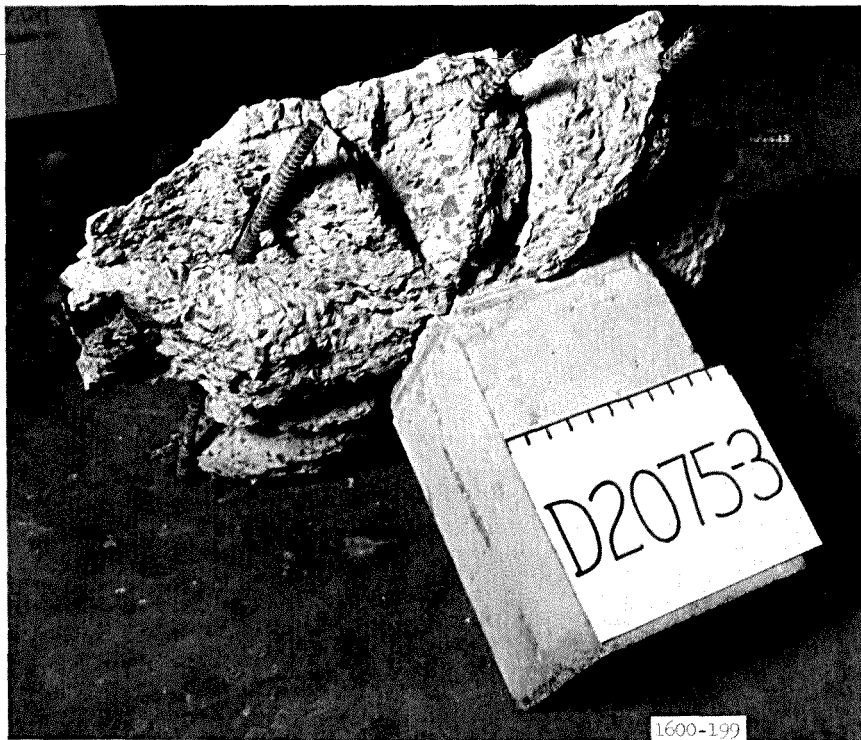


Figure 5.15 Column side of Specimen D2075-2.



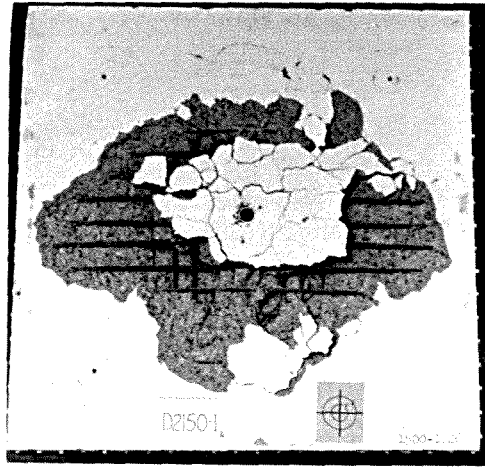


a. Crack pattern.

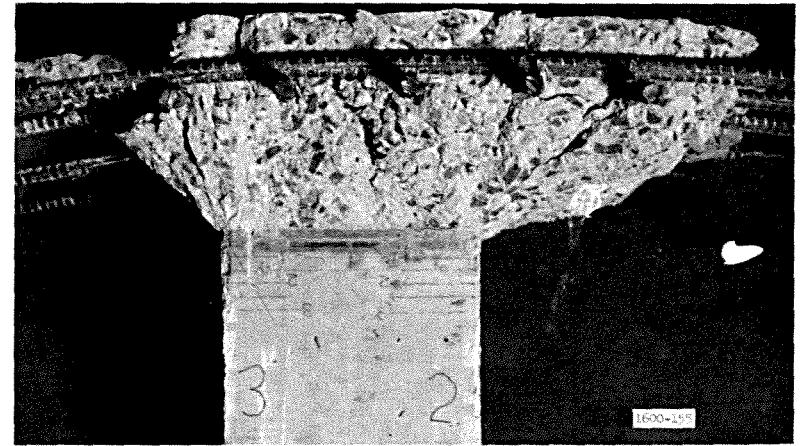


b. Column and failure cone.

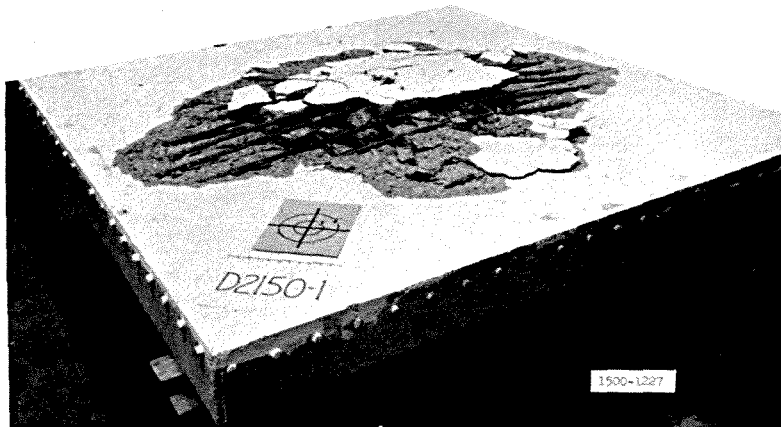
Figure 5.16 Posttest photographs of Specimen D2075-3.



a. Crack pattern.



b. Column and failure cone.



c. Oblique view of tensile surface.

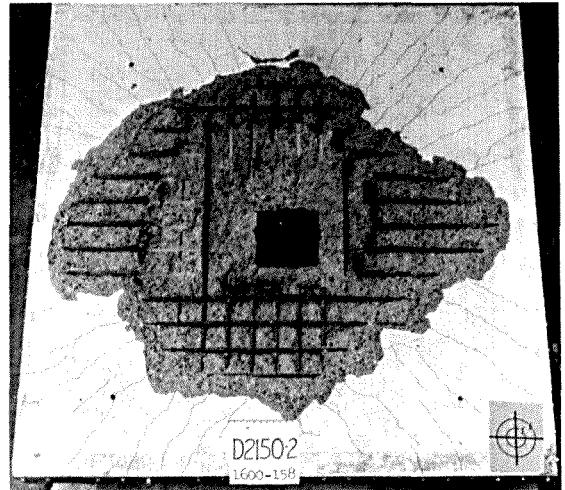


d. Slab with column removed.

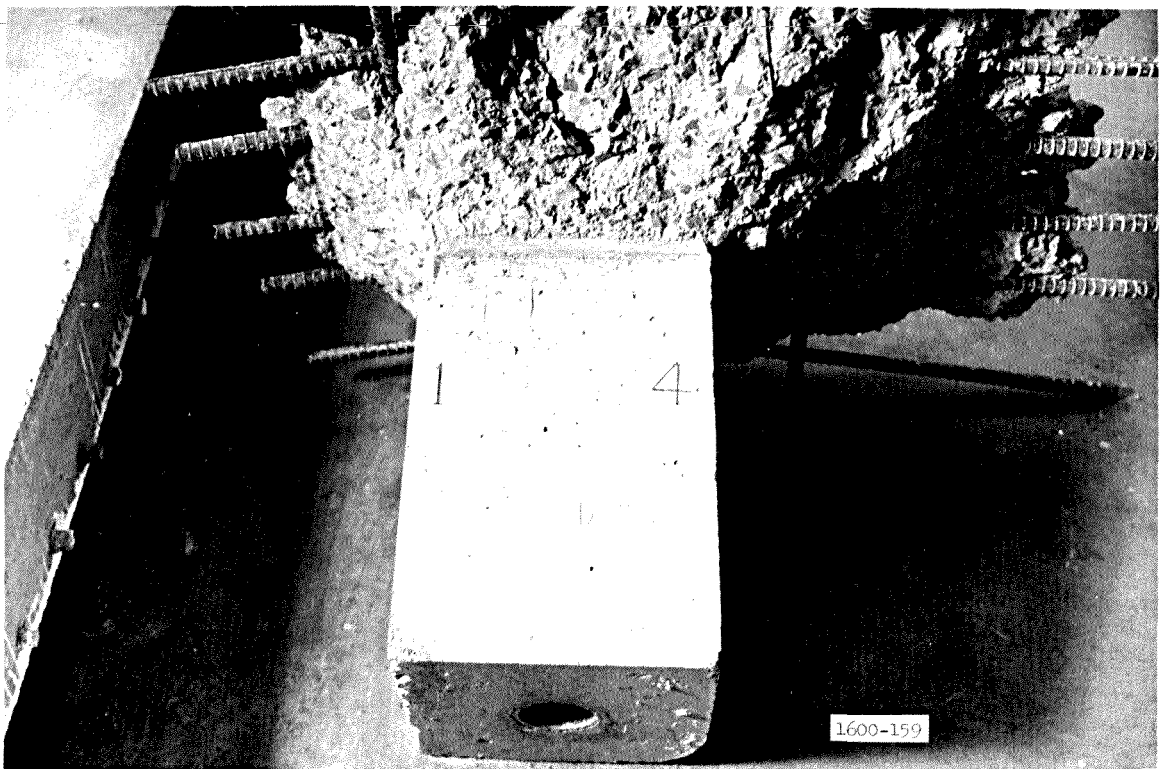
Figure 5.17 Posttest photographs of Specimen D2150-1.



a. Crack pattern.

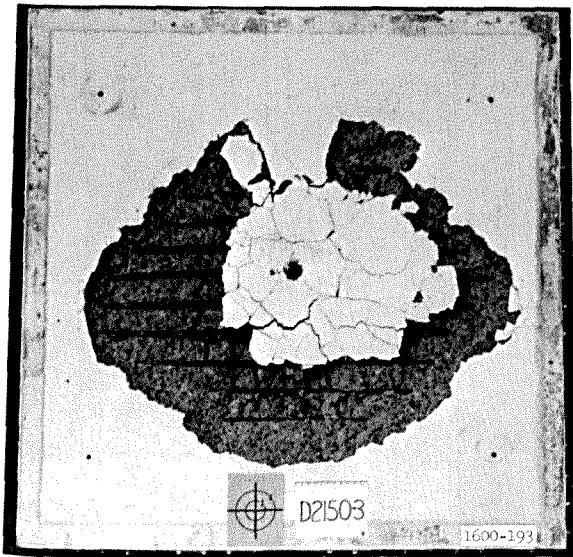


b. Crack pattern, column removed, cracks marked.

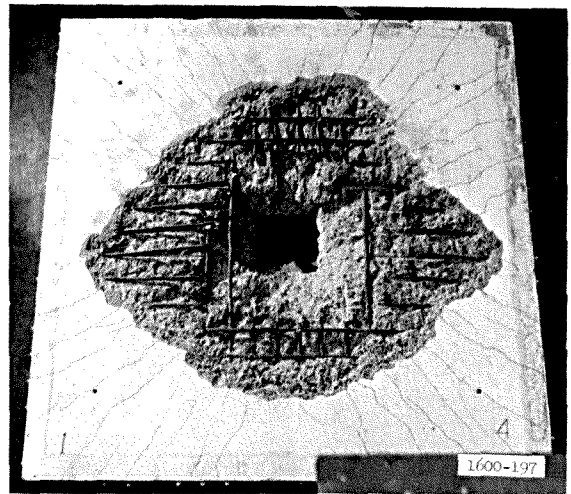


c. Column and failure cone.

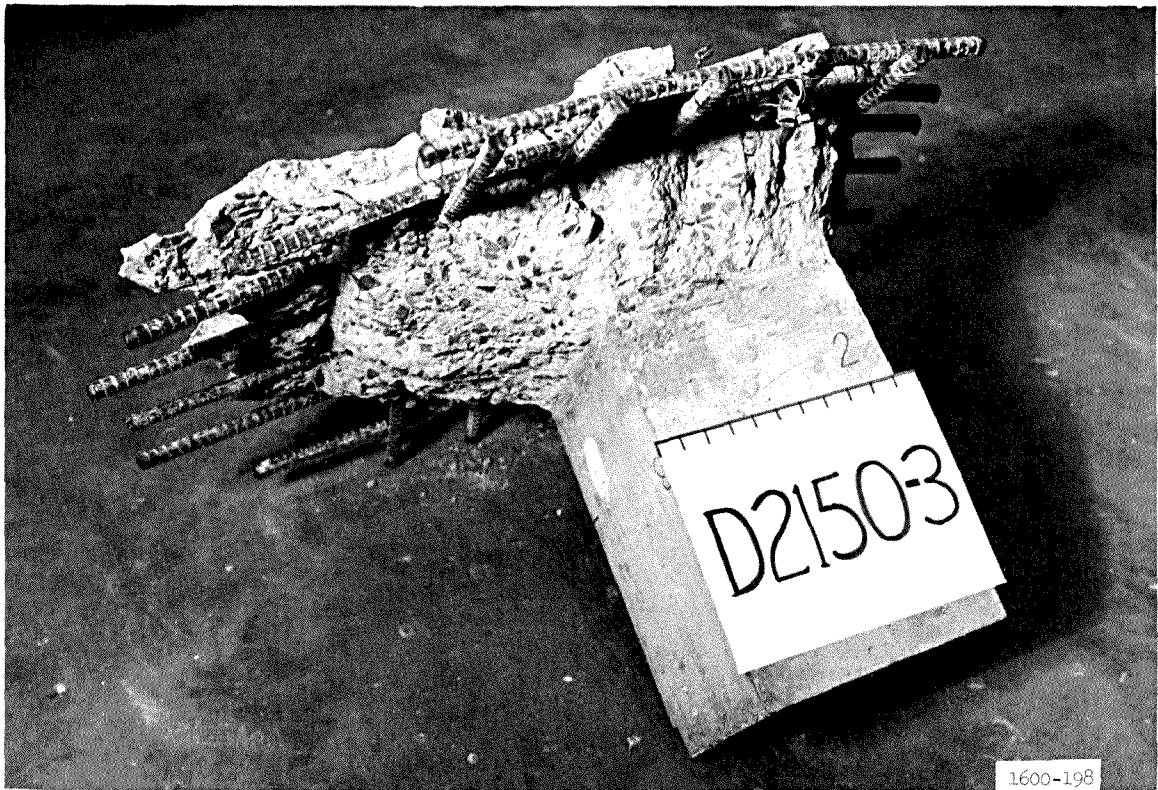
Figure 5.18 Posttest photographs of Specimen D2150-2.



a. Crack pattern.



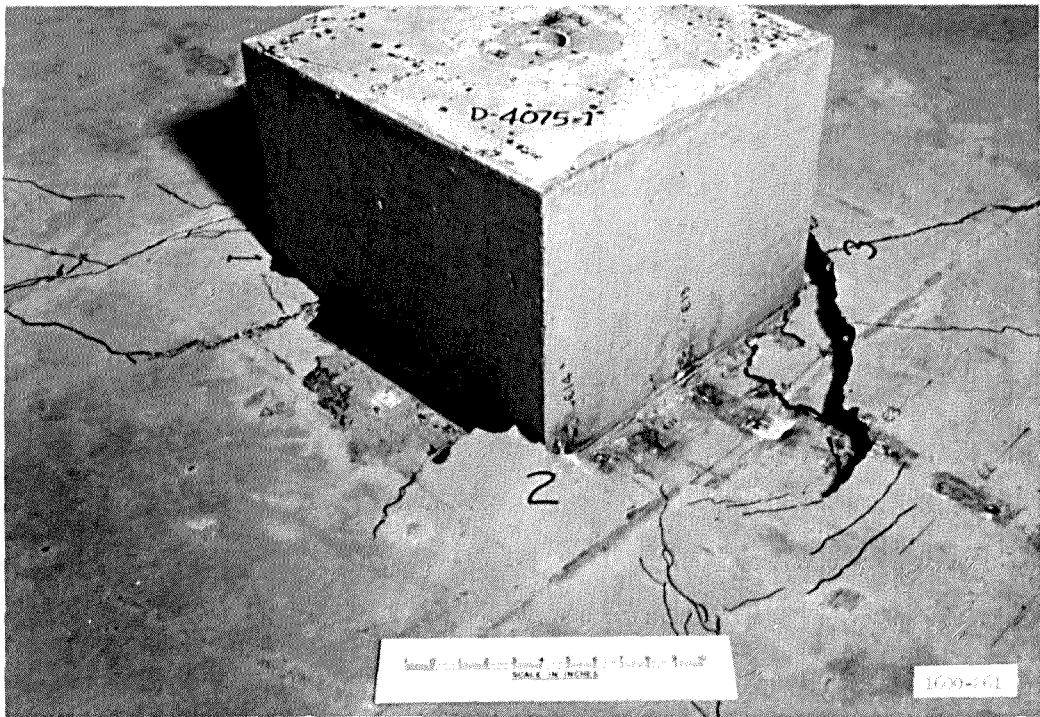
b. Crack pattern, column removed, cracks marked.



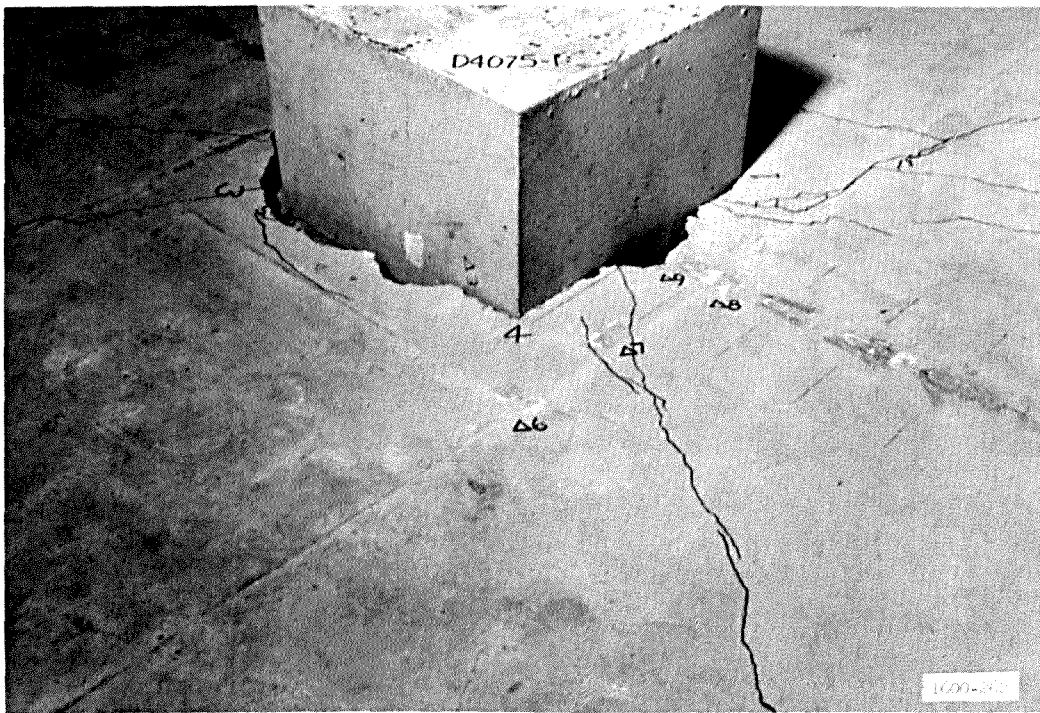
c. Column and failure cone.

Figure 5.19 Posttest photographs of Specimen D2150-3.



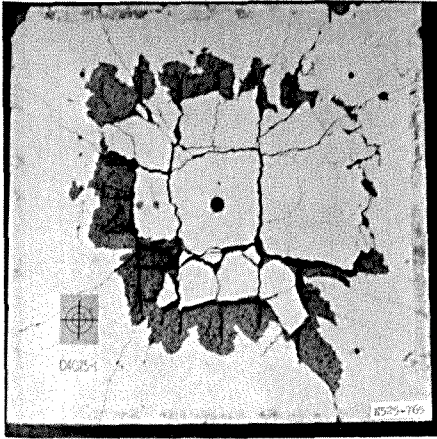


a. Column side of slab, cracks marked.

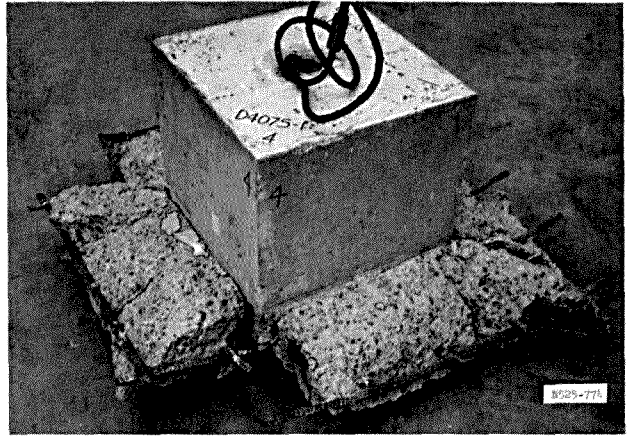


b. Column side of slab, cracks marked.

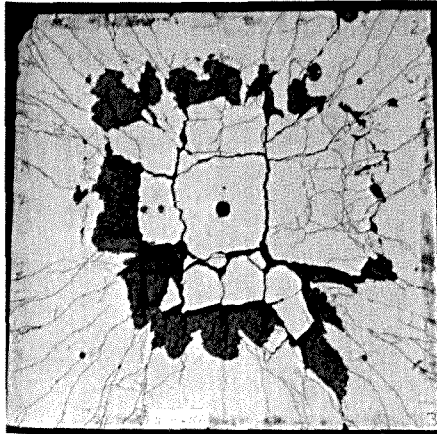
Figure 5.20 Posttest photographs of Specimen D4075-1 (Sheet 1 of 2).



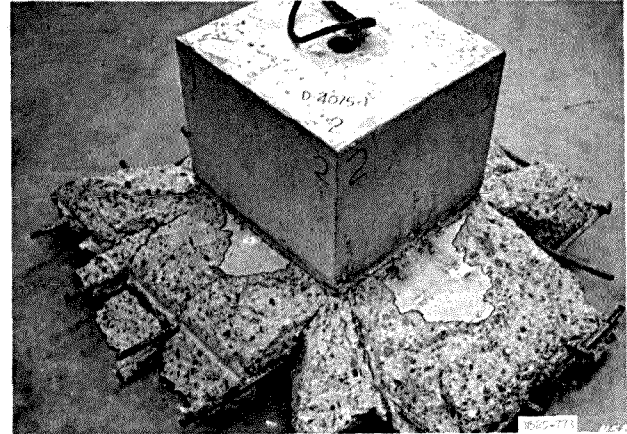
c. Crack pattern.



d. Column and failure cone.

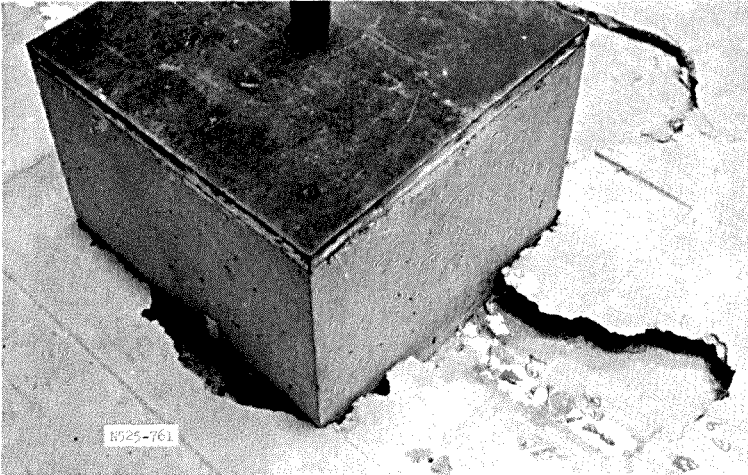


e. Crack pattern,  
cracks marked.

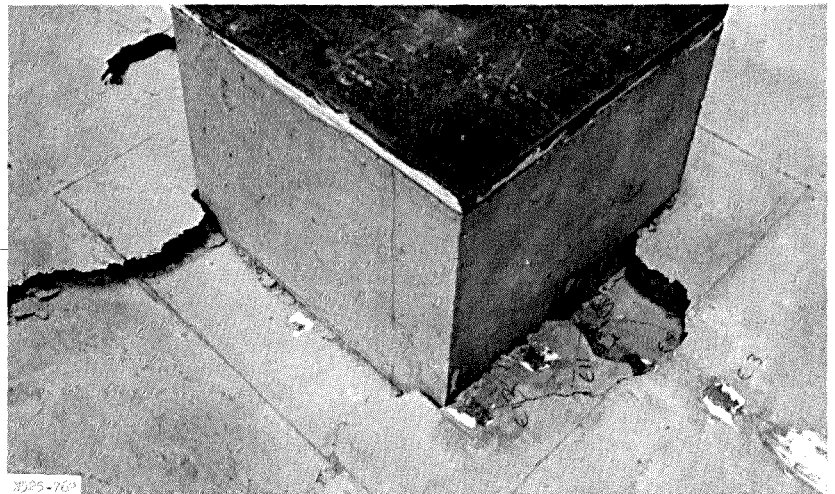


f. Column and failure cone.

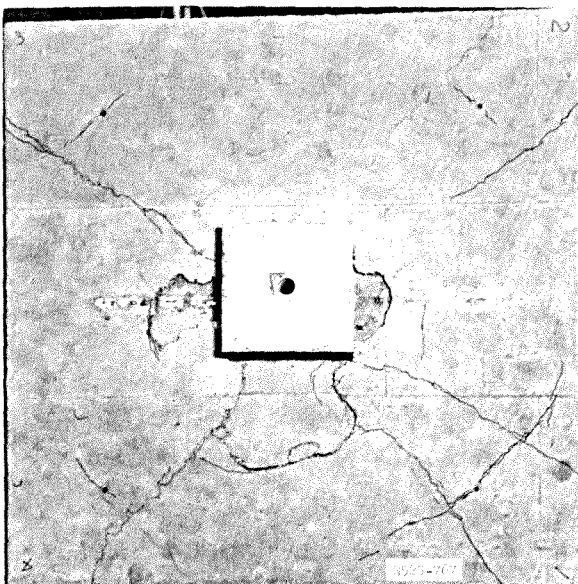
Figure 5.20 (Sheet 2 of 2).



a. Detail of failure, column side.

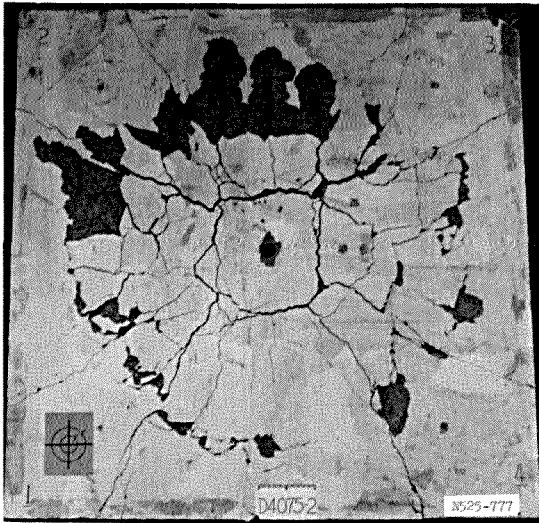


b. Detail of failure, column side.

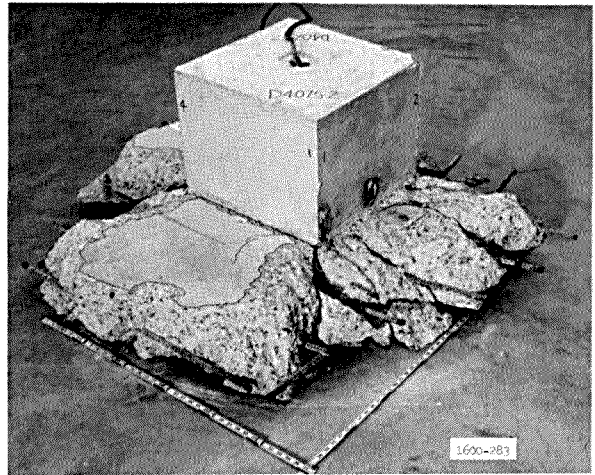


c. Column side crack pattern, cracks marked.

Figure 5.21 Posttest photographs of Specimen D4075-2 (Sheet 1 of 2).



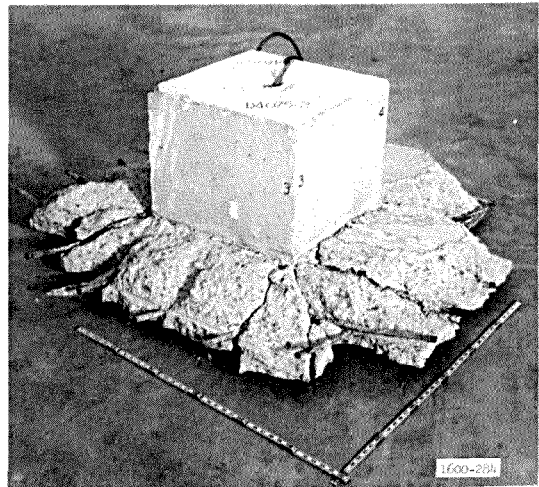
d. Crack pattern.



e. Column and failure cone.



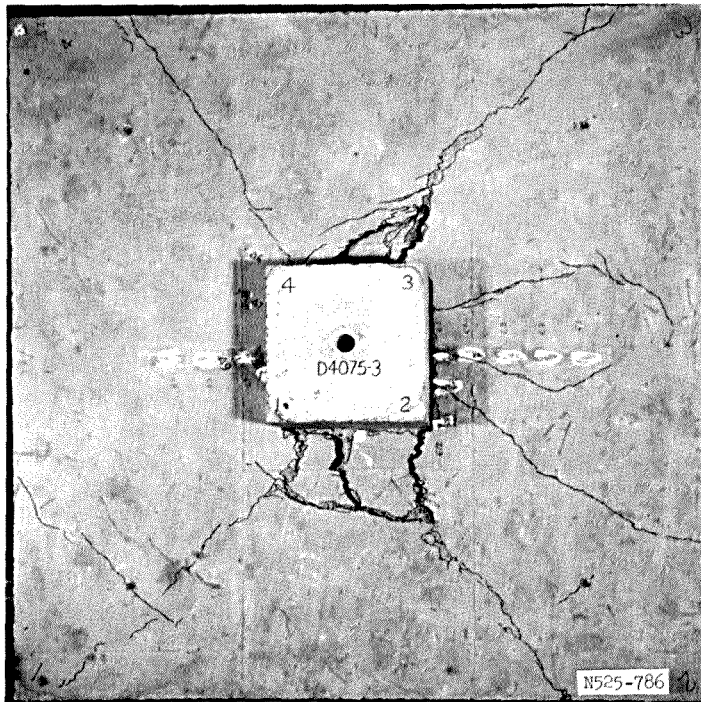
f. Slab with column removed,  
cracks marked.



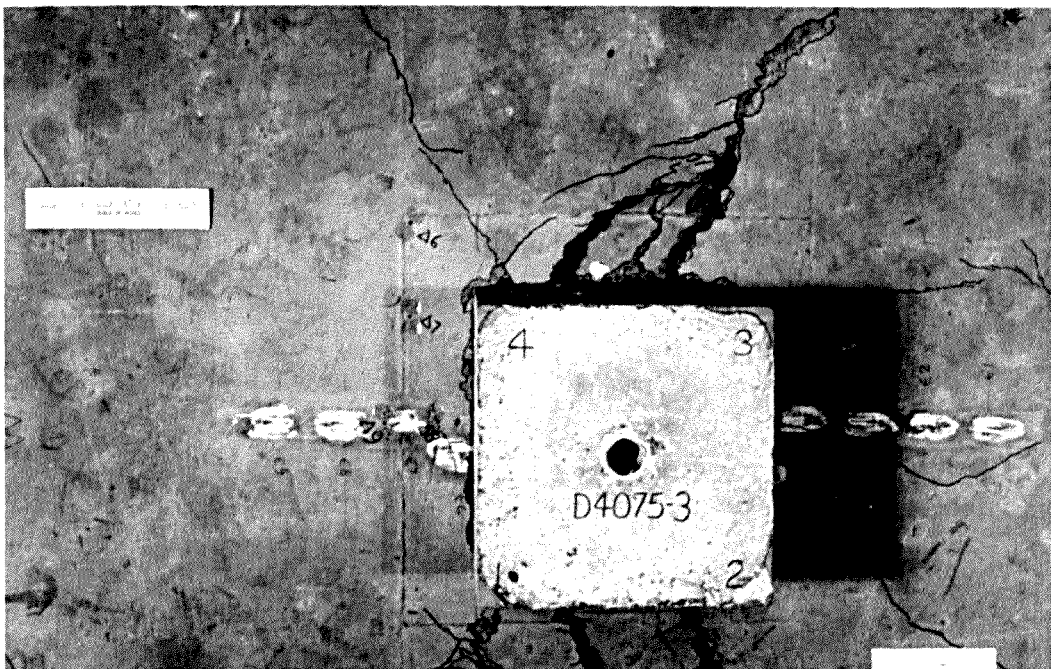
g. Column and failure cone.

Figure 5.21 (Sheet 2 of 2).



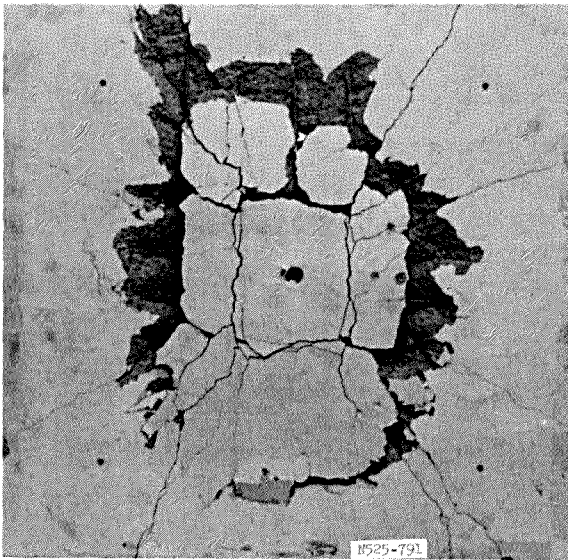


a. Crack pattern on column side, cracks marked.



b. Detail of column side.

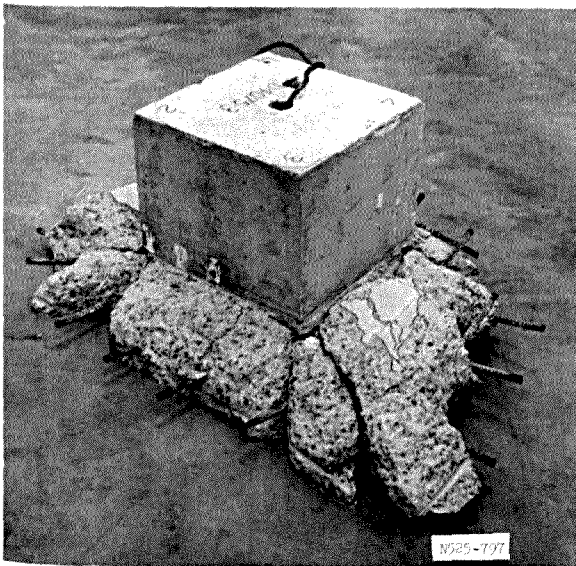
Figure 5.22 Posttest photographs of Specimen D4075-3 (Sheet 1 of 2).



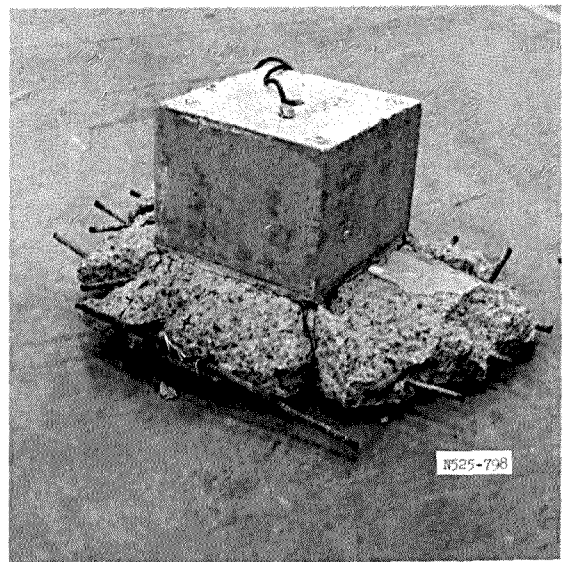
c. Crack pattern.



d. Slab with column removed.

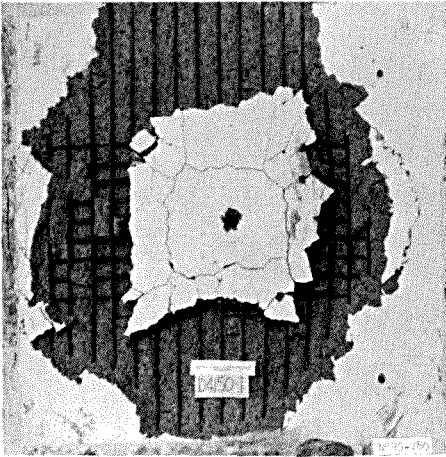


e. Column and failure cone.

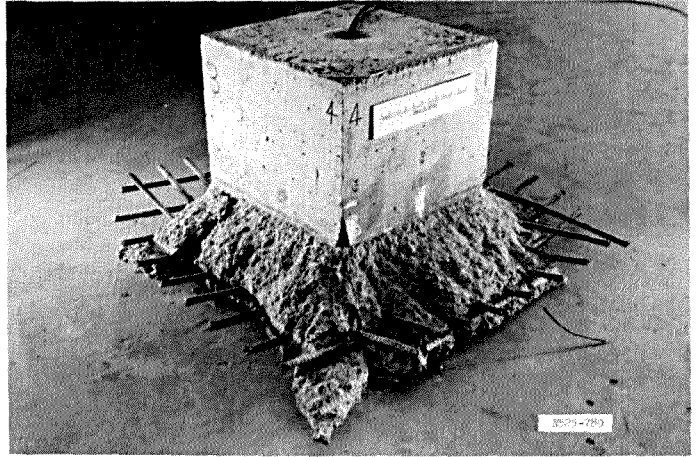


f. Column and failure cone.

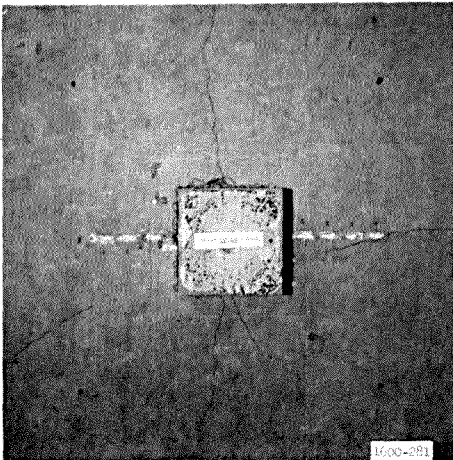
Figure 5.22 (Sheet 2 of 2).



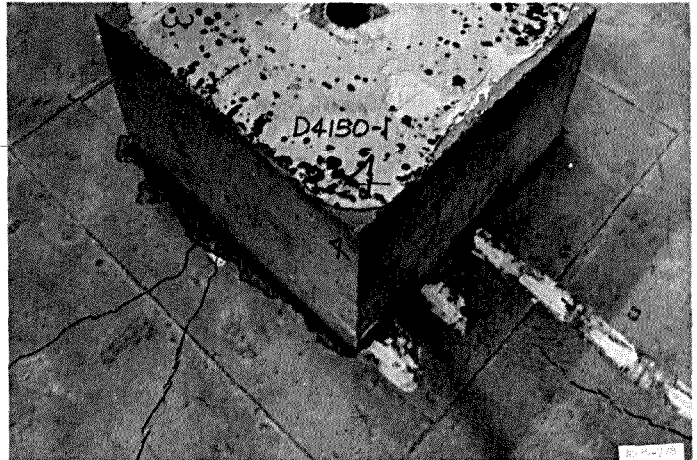
a. Crack pattern.



b. Column and failure cone.



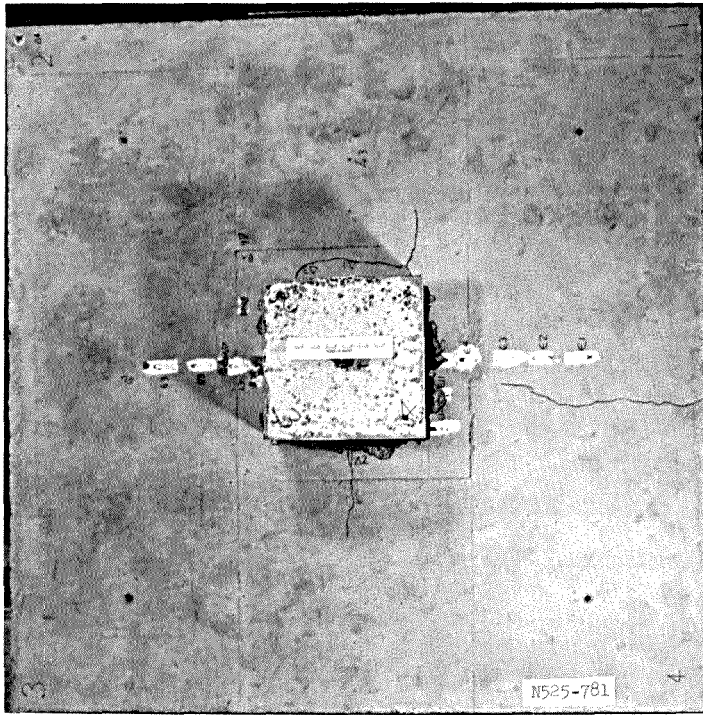
c. Column side,  
cracks marked.



d. Detail of column side.

Figure 5.23 Posttest photographs of Specimen D4150-1.





a. Column side, cracks marked.

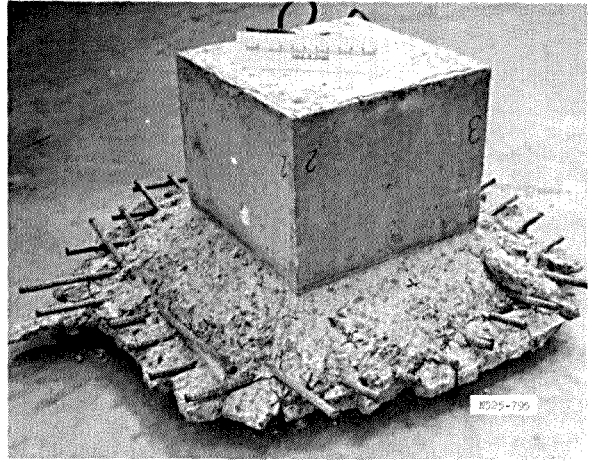


b. Detail of column side.

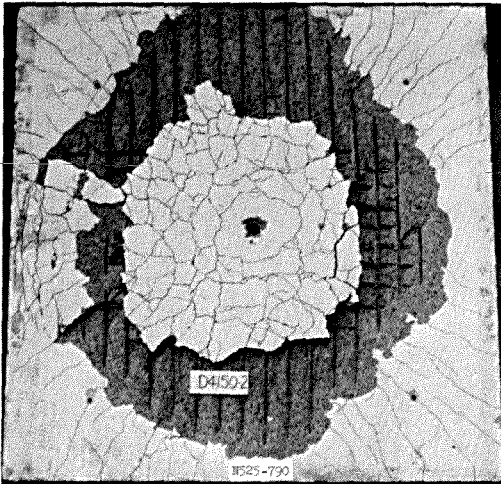
Figure 5.24 Posttest photographs of Specimen D4150-2 (Sheet 1 of 2).



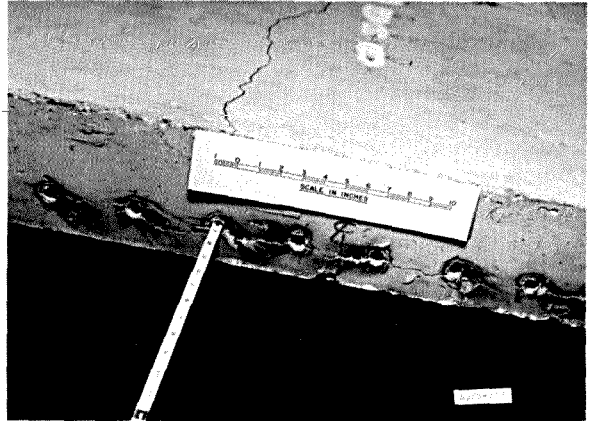
c. Crack pattern.



d. Column and failure cone.

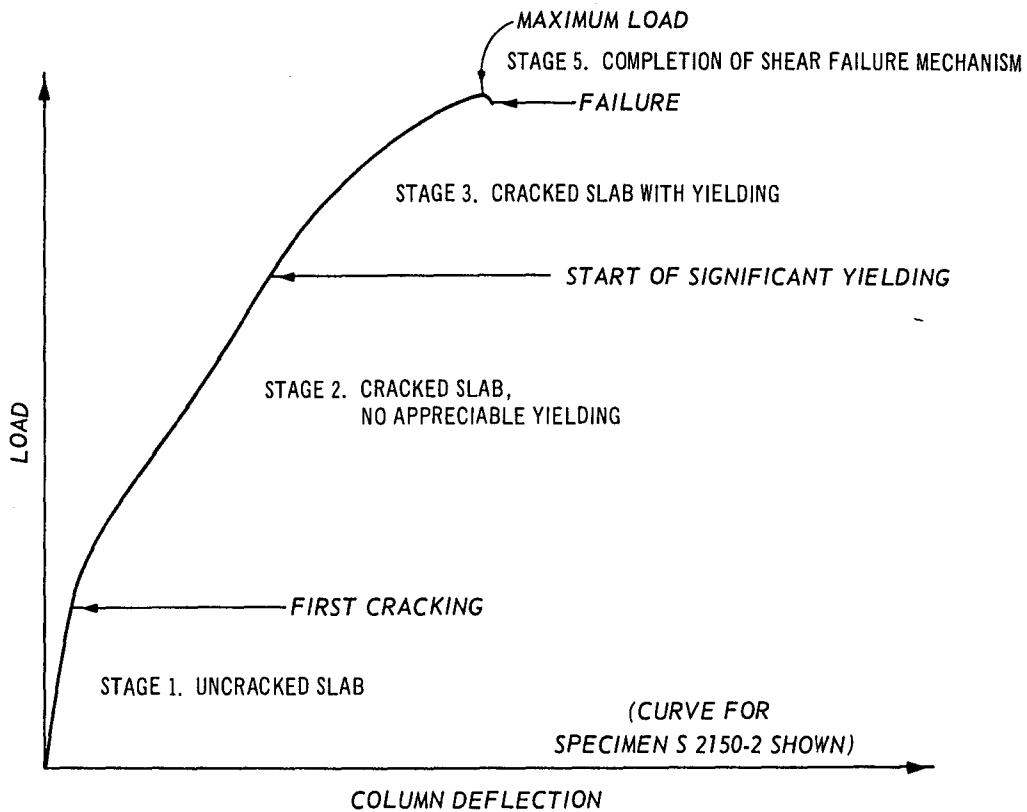


e. Crack pattern,  
cracks marked.

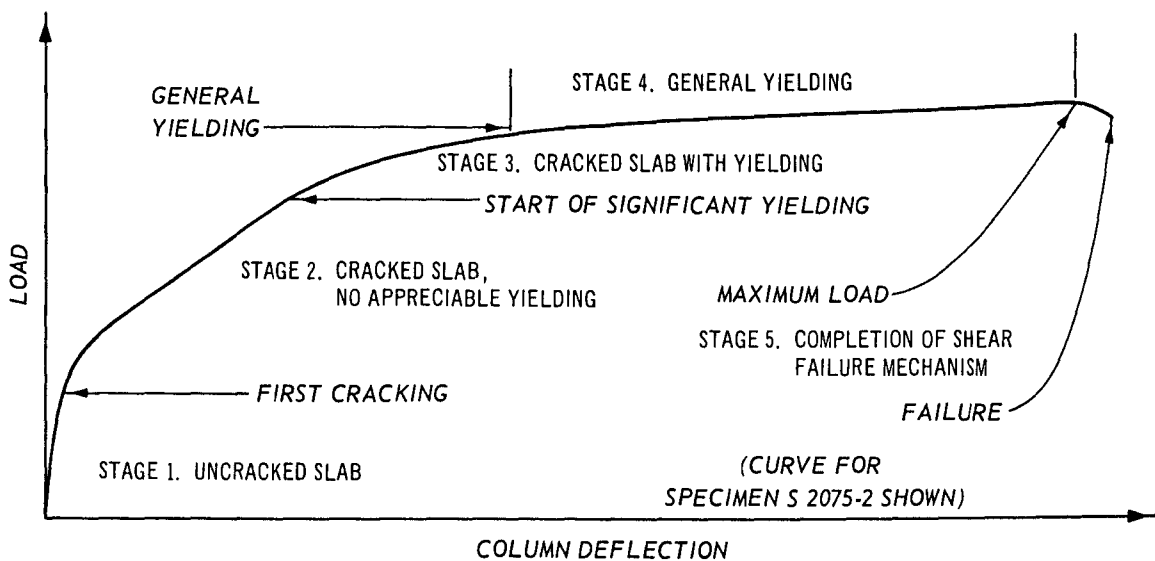


f. Cracking at level of  
reinforcement.

Figure 5.24 (Sheet 2 of 2).



a. SPECIMENS WITH  $p = 0.0150$



b. SPECIMENS WITH  $p = 0.0075$

Figure 6.1 Events and stages of the load-deflection curve.

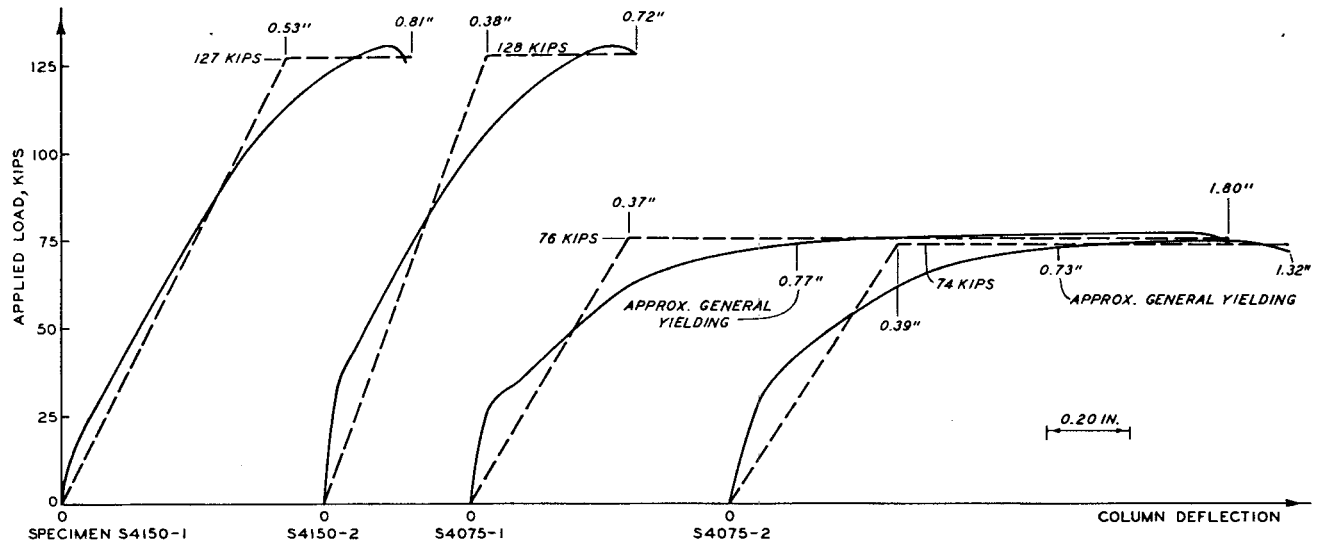
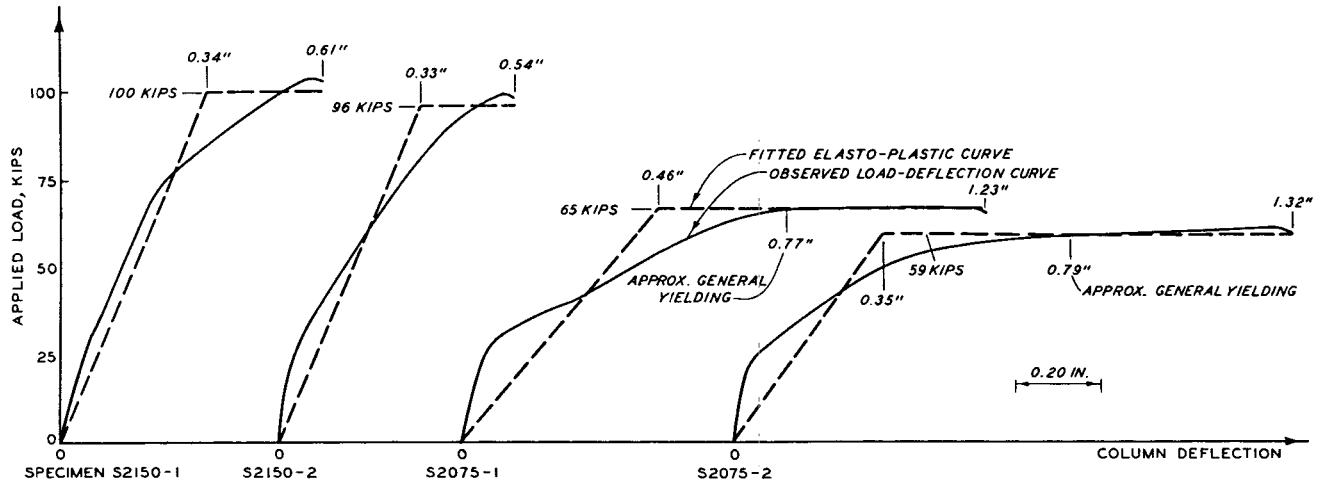
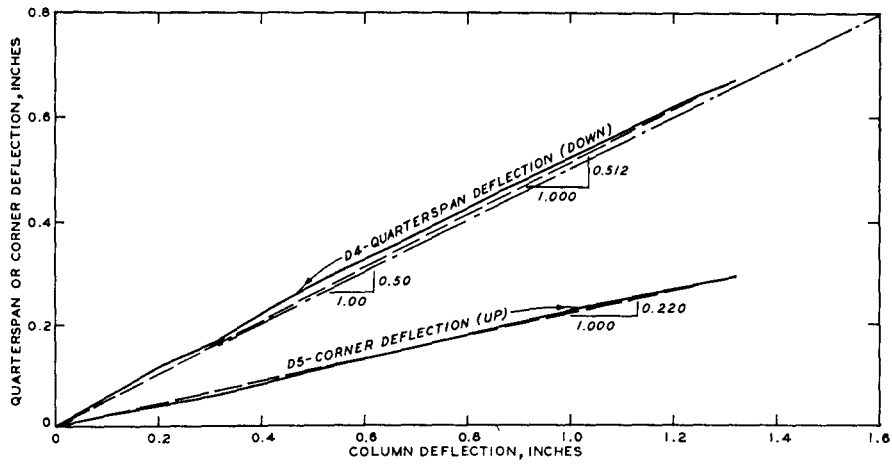
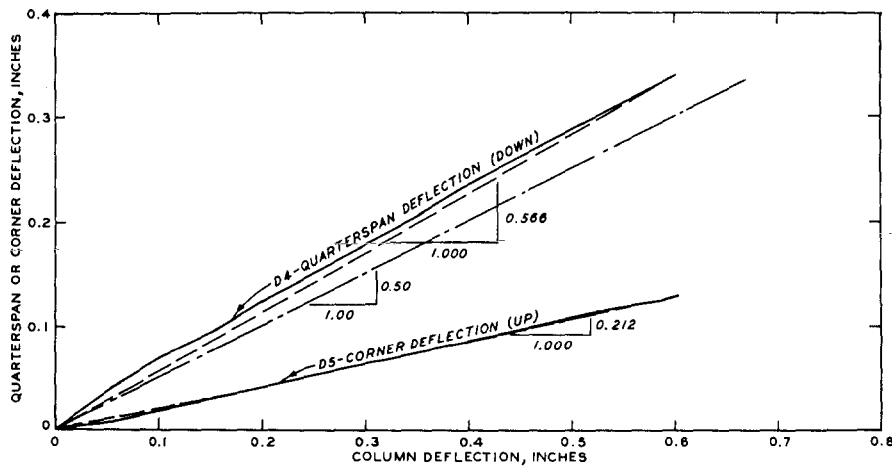


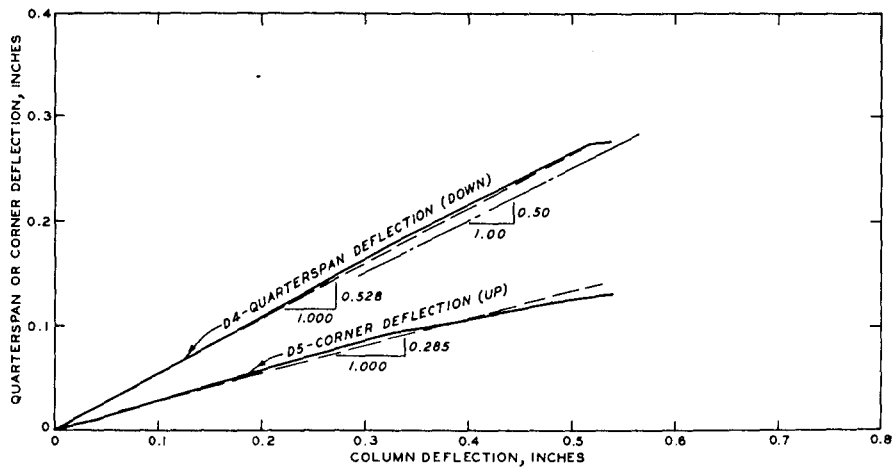
Figure 6.2 Idealized load-deflection curves.



a. SPECIMEN S2075-2



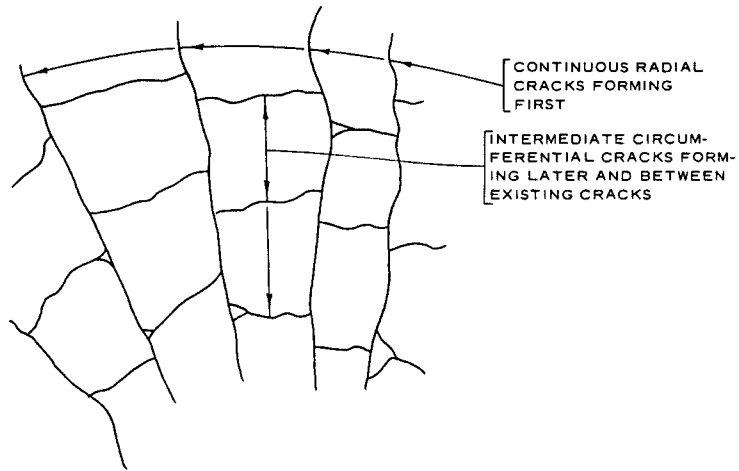
b. SPECIMEN S2150-1



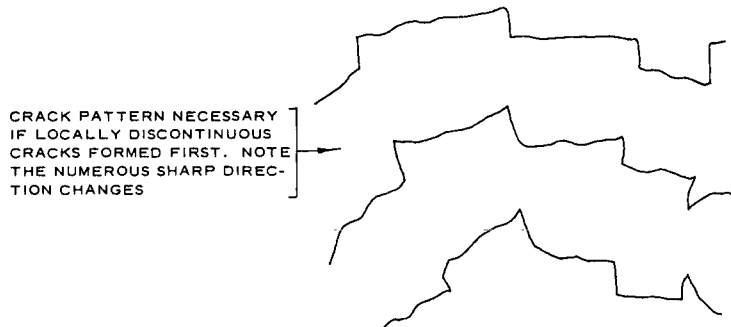
c. SPECIMEN S2150-2

Figure 6.3 Comparison of quarterspan and corner deflections with column deflections.





a. FINAL CRACK PATTERN



b. UNLIKELY INTERMEDIATE CRACK PATTERN

Figure 6.4 Sequence of cracking as determined by crack pattern.

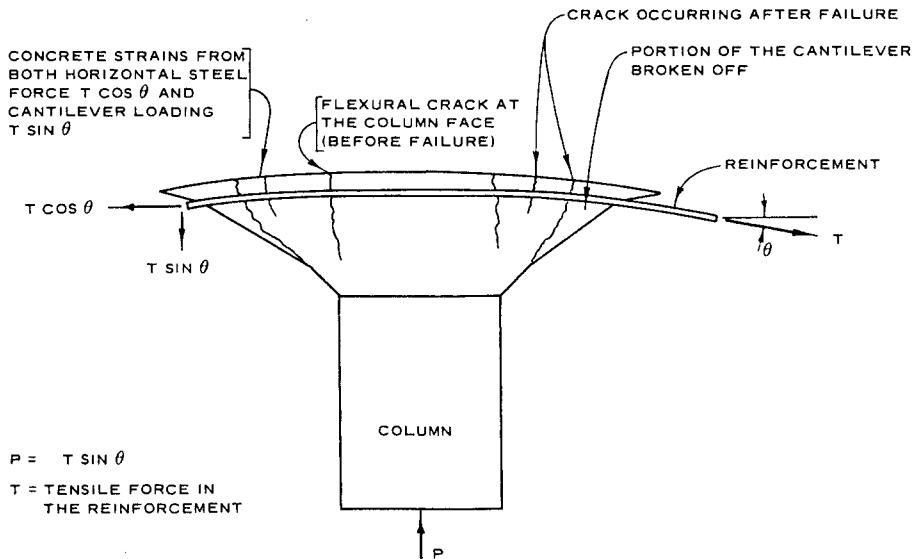


Figure 6.5 Section through failure cone.

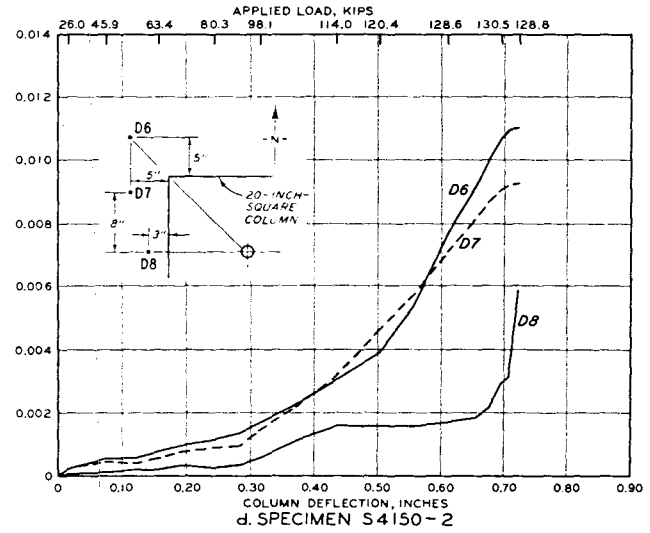
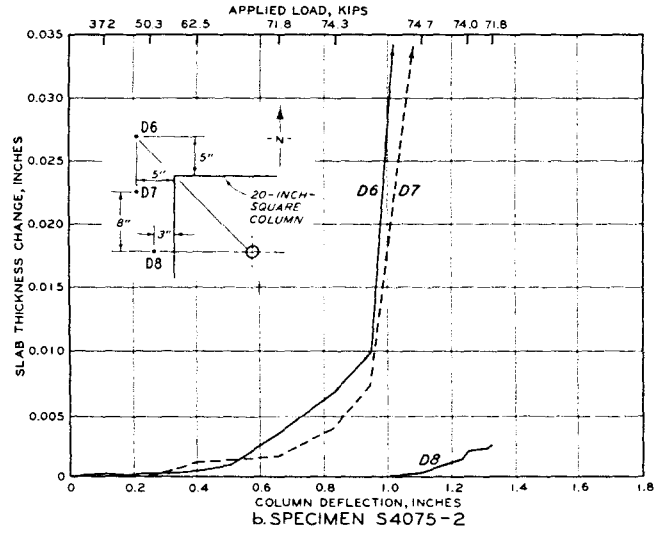
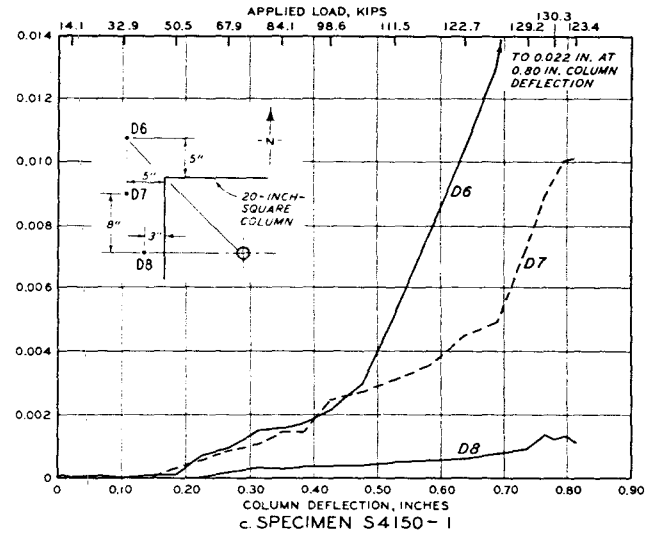
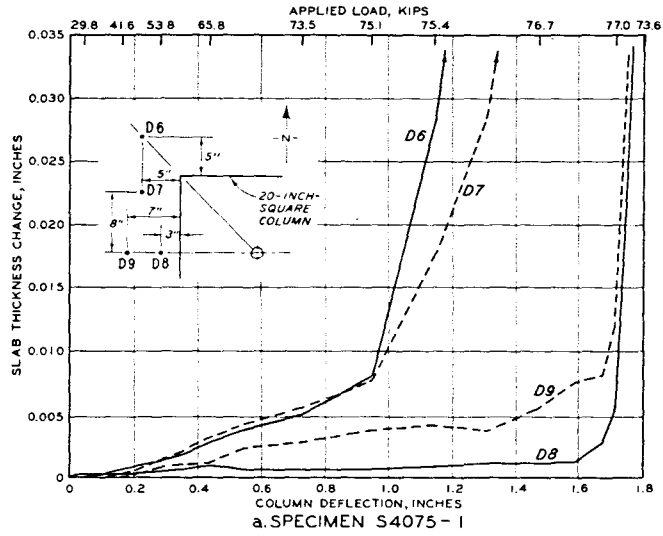
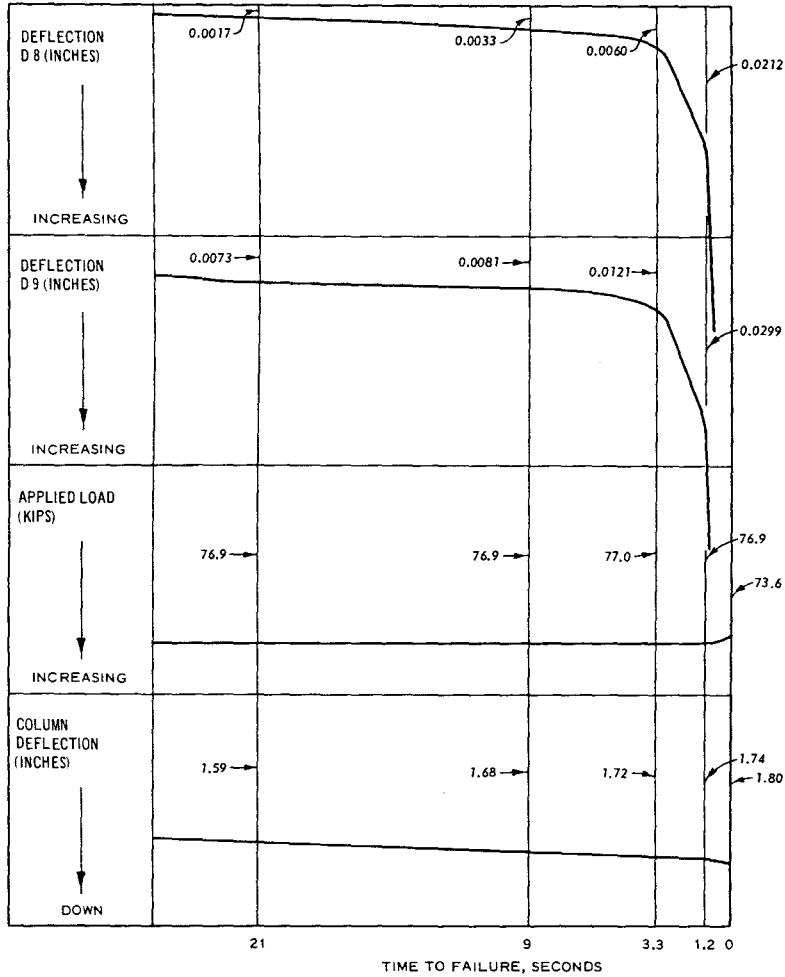
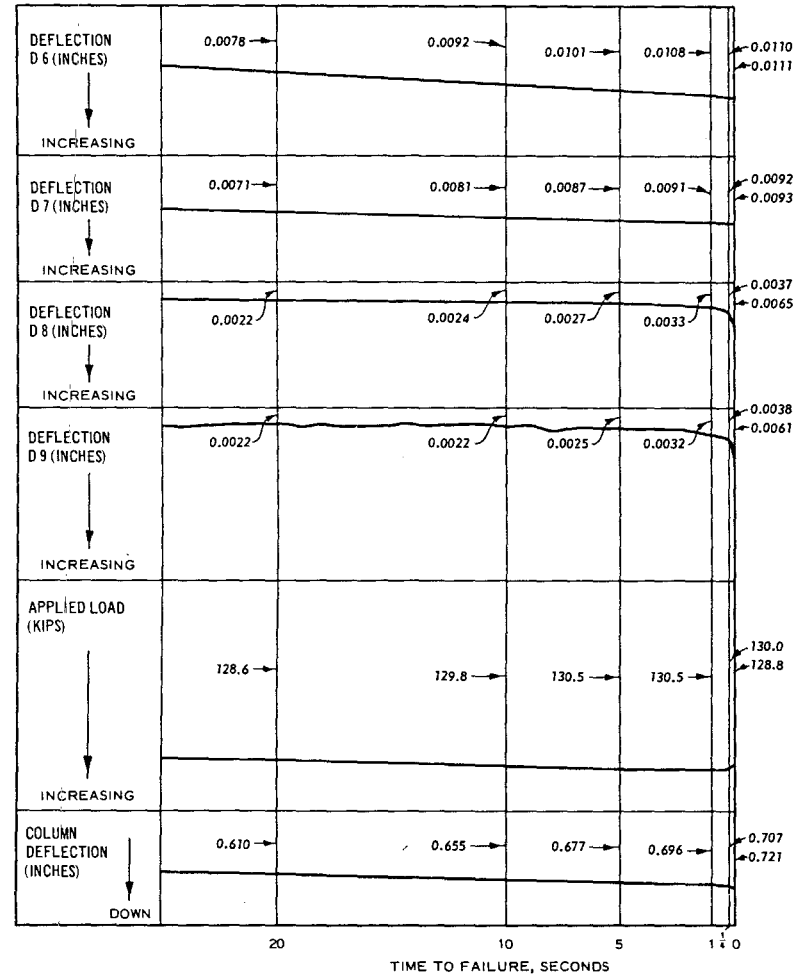


Figure 6.6 Slab thickness change versus column deflection, S4000 Series.

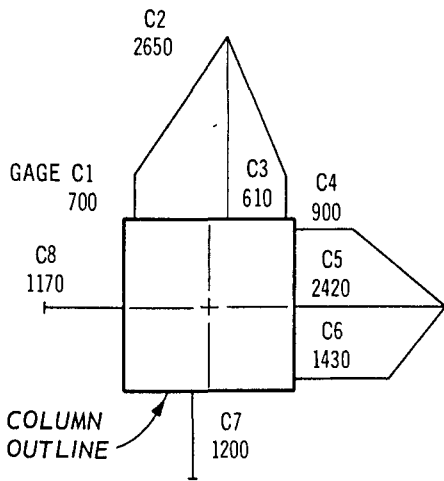


a. SPECIMEN S4075-1

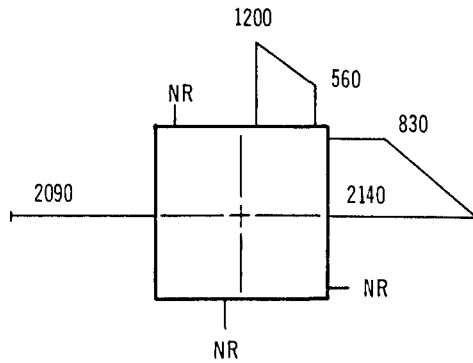


b. SPECIMEN S4150-2

Figure 6.7 Deflection and load traces immediately before failure.



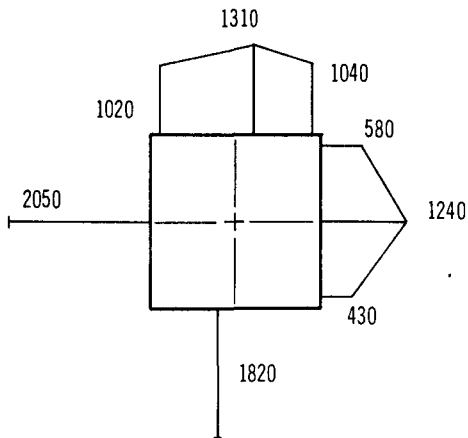
a. SPECIMEN S 2075-1



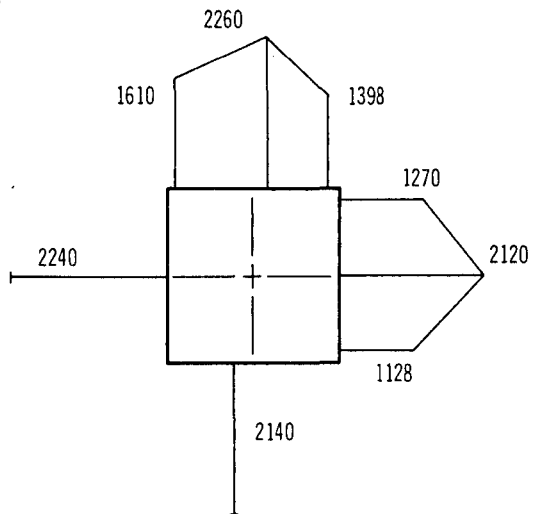
b. SPECIMEN S 2075-2

NOTE: NR = NO RECORD

ALL STRAINS COMPRESSIVE AND  
WITH UNITS  $10^{-6}$



c. SPECIMEN S 2150-1



d. SPECIMEN S 2150-2

Figure 6.8 Maximum concrete strains, S2000 Series.

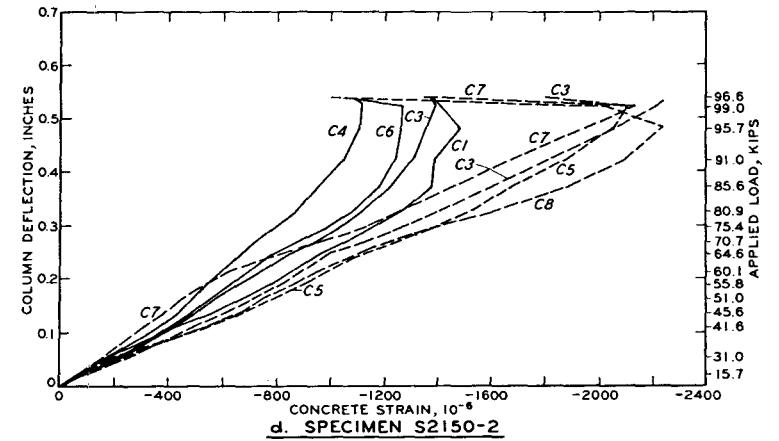
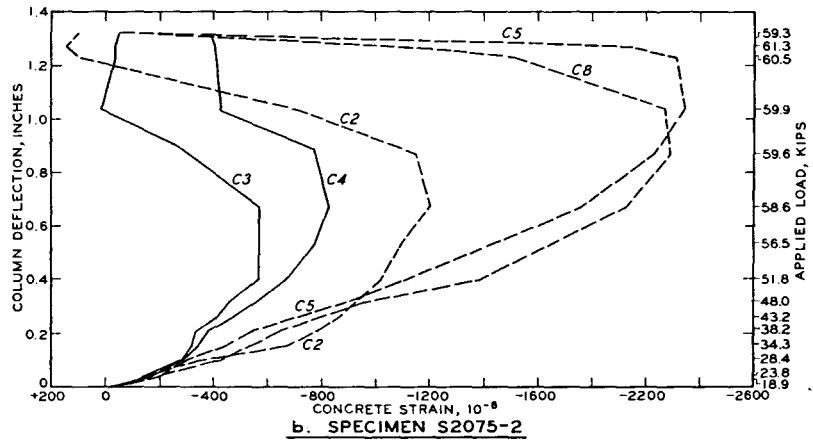
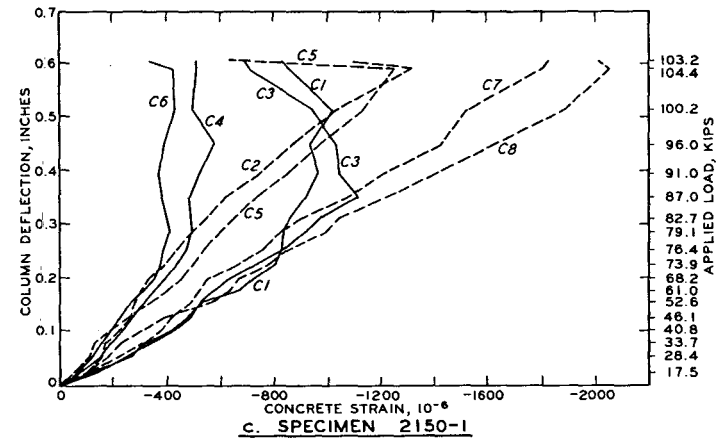
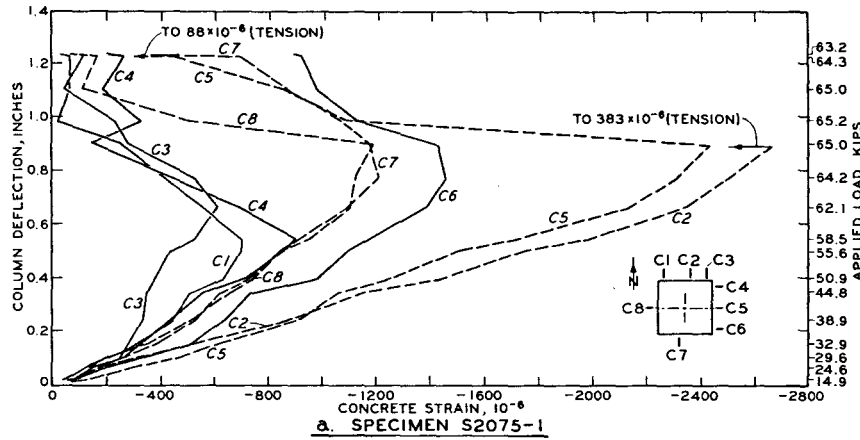
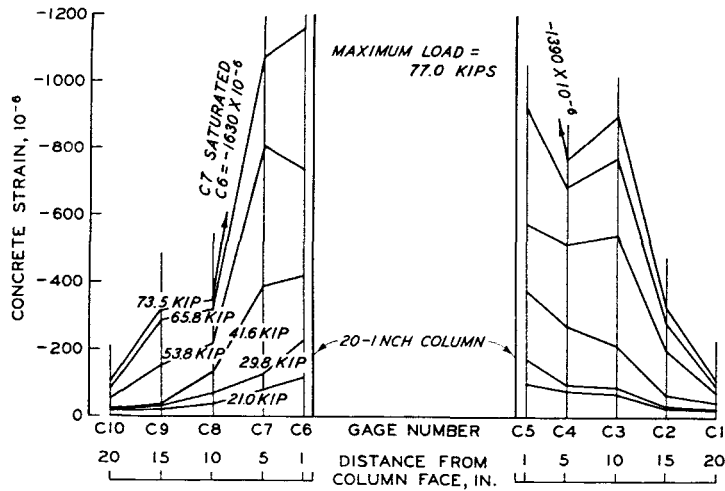
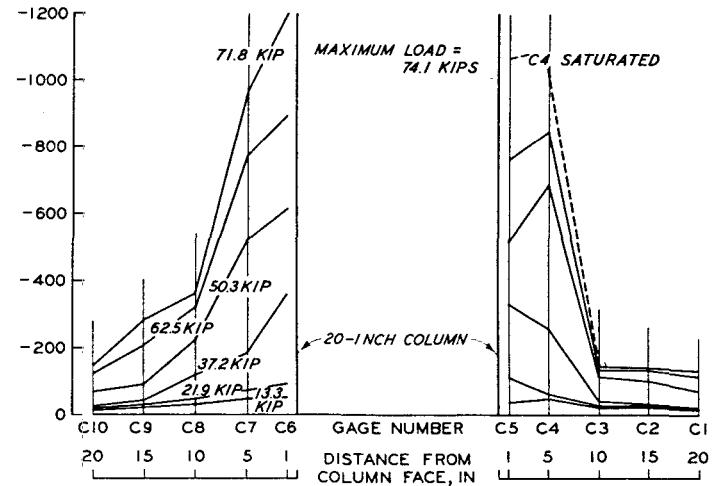


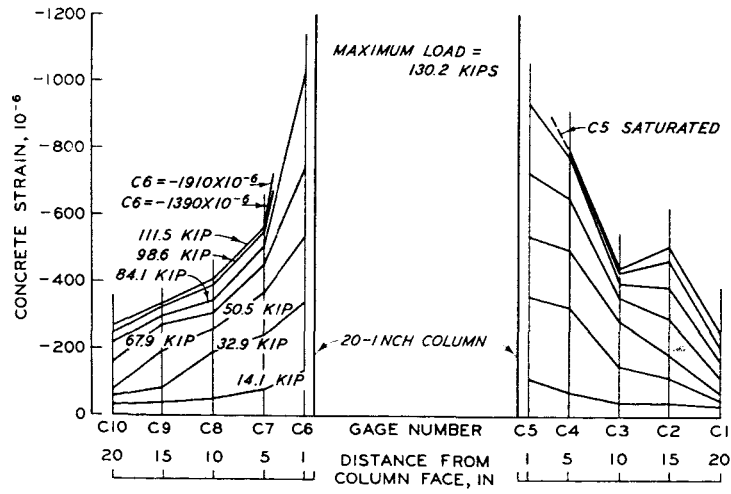
Figure 6.9 Variation of concrete strains with column deflection, S2000 Series.



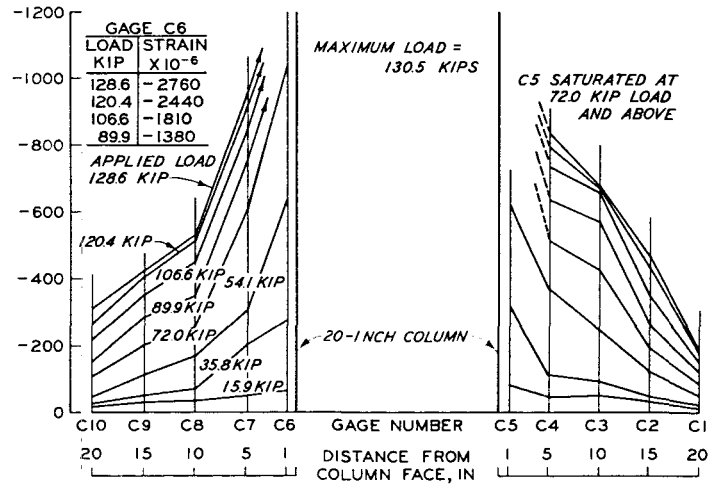
a. SPECIMEN S4075-1



b. SPECIMEN S4075-2



c. SPECIMEN S4150-1



d. SPECIMEN S4150-2

Figure 6.10 Distribution of concrete strains along slab centerline, S4000 Series.

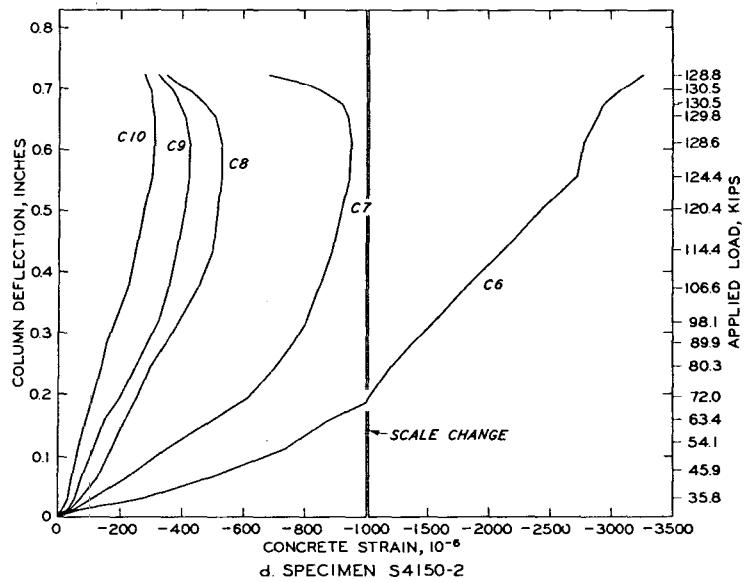
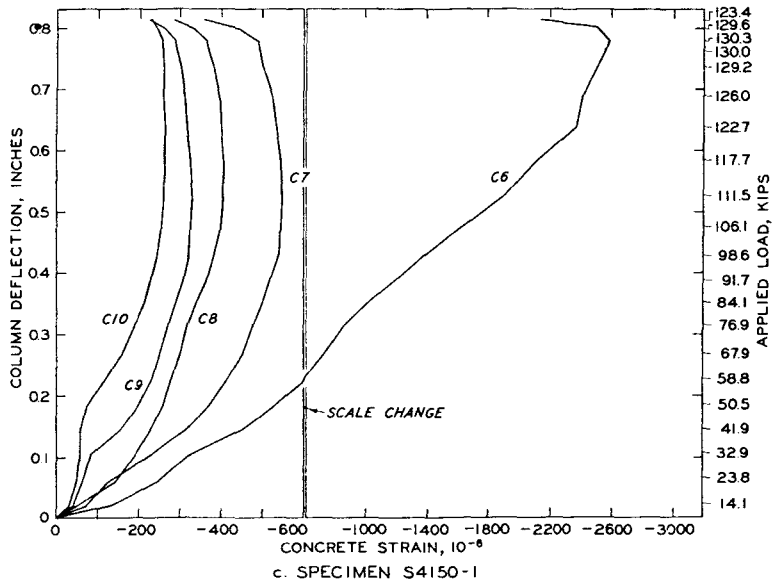
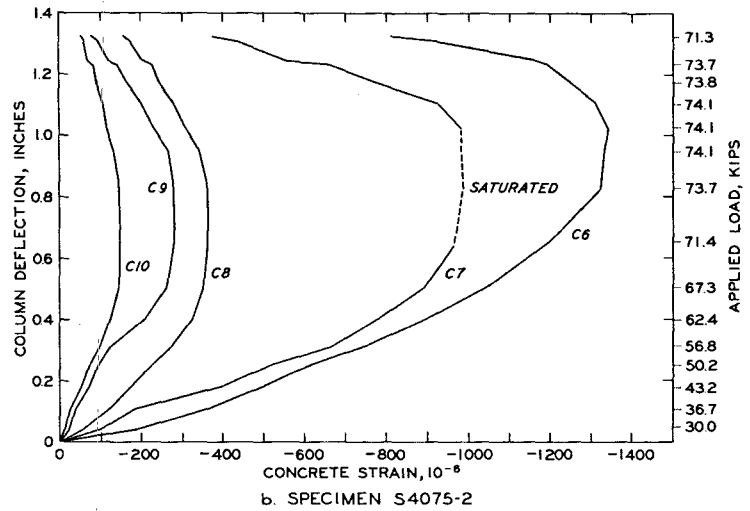
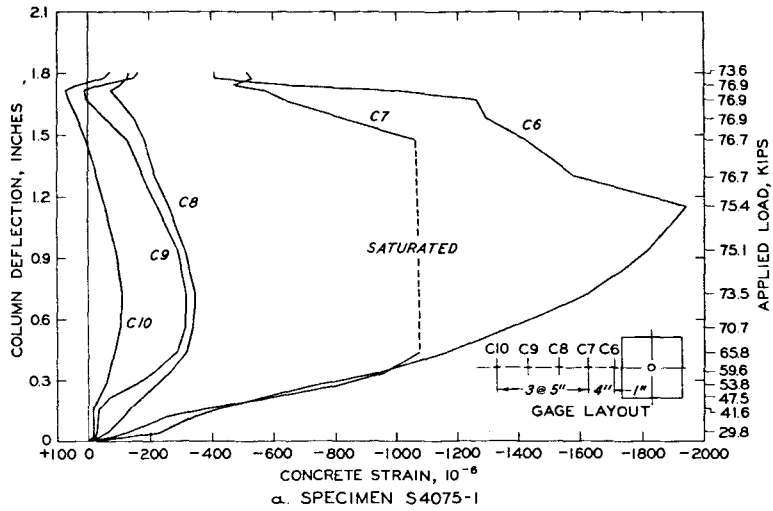


Figure 6.11 Variation of concrete strains with column deflection, S4000 Series.

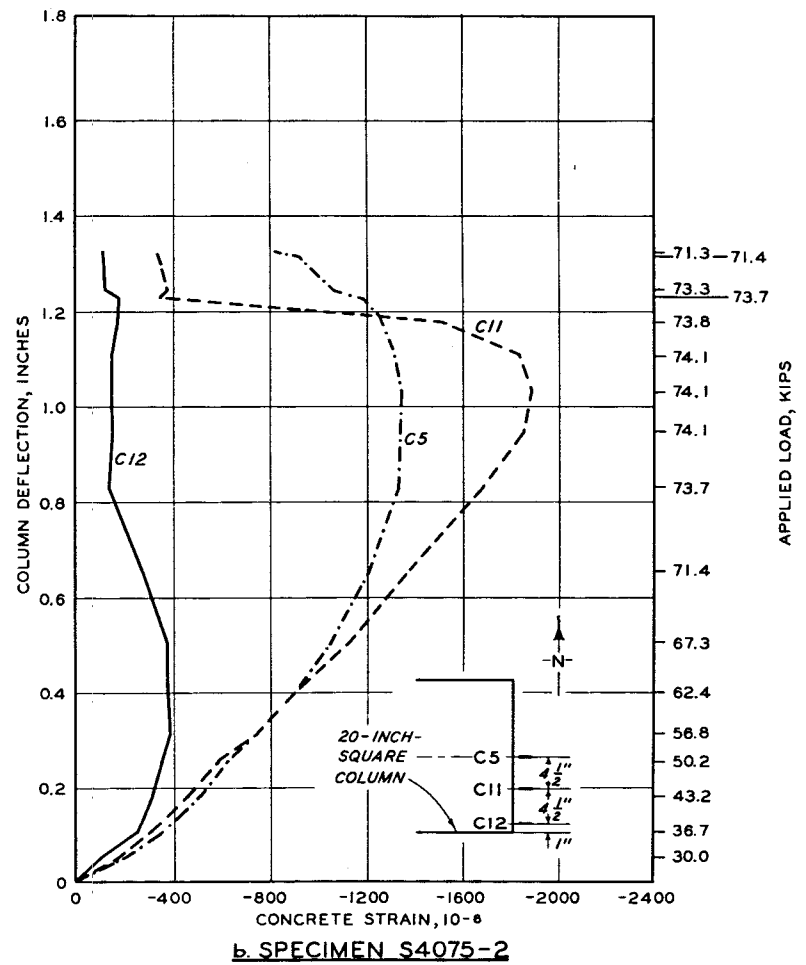
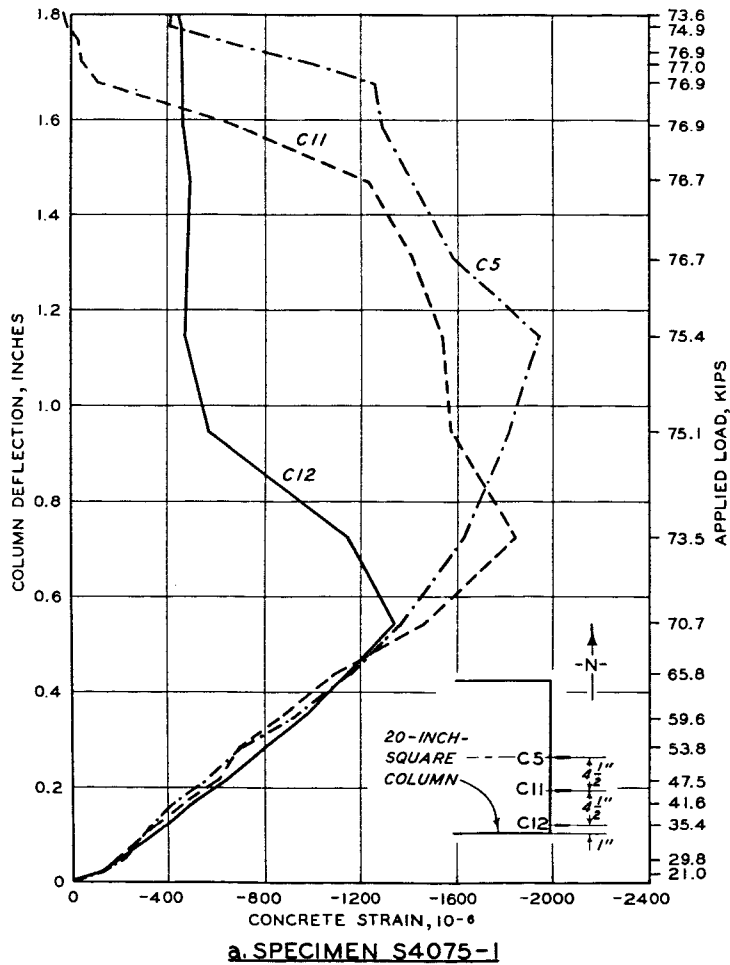
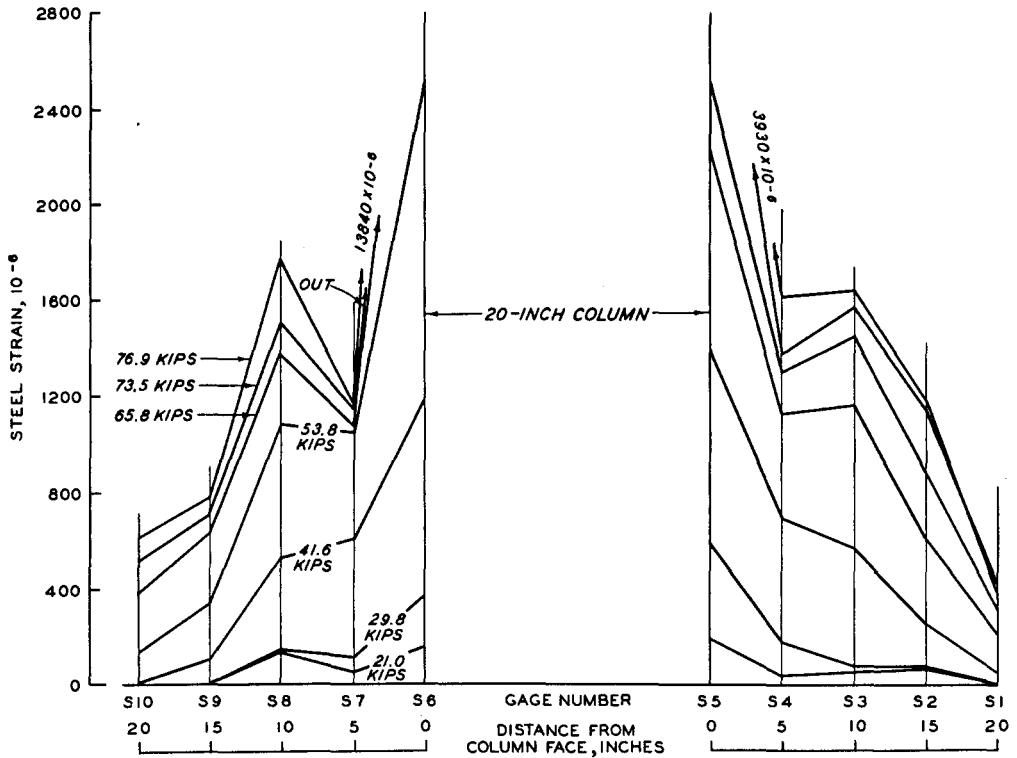
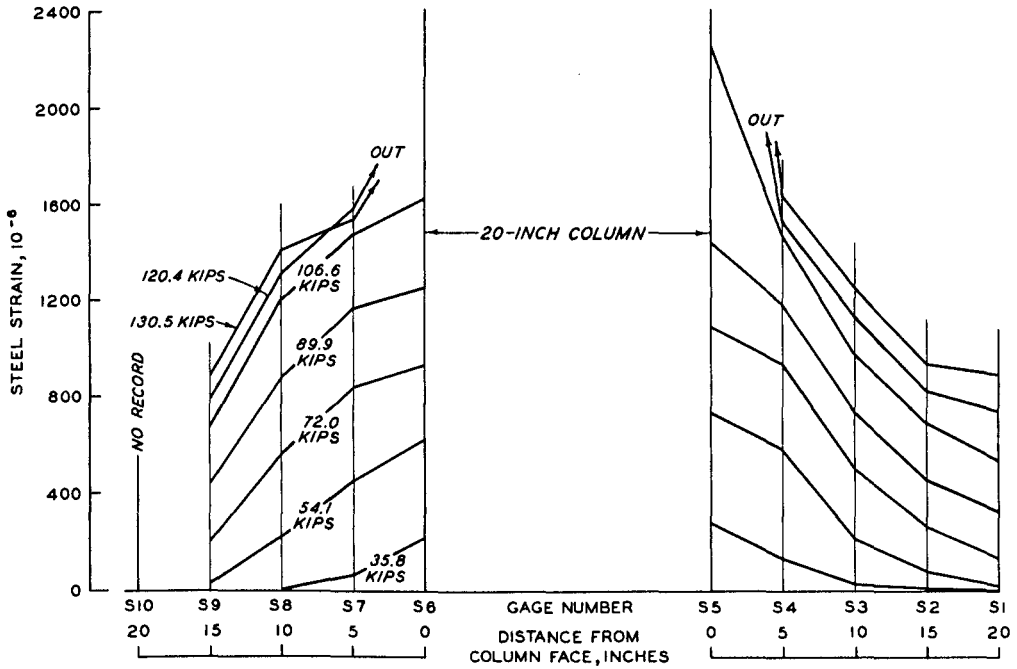


Figure 6.12 Concrete strains at column face, S4075 Specimens.



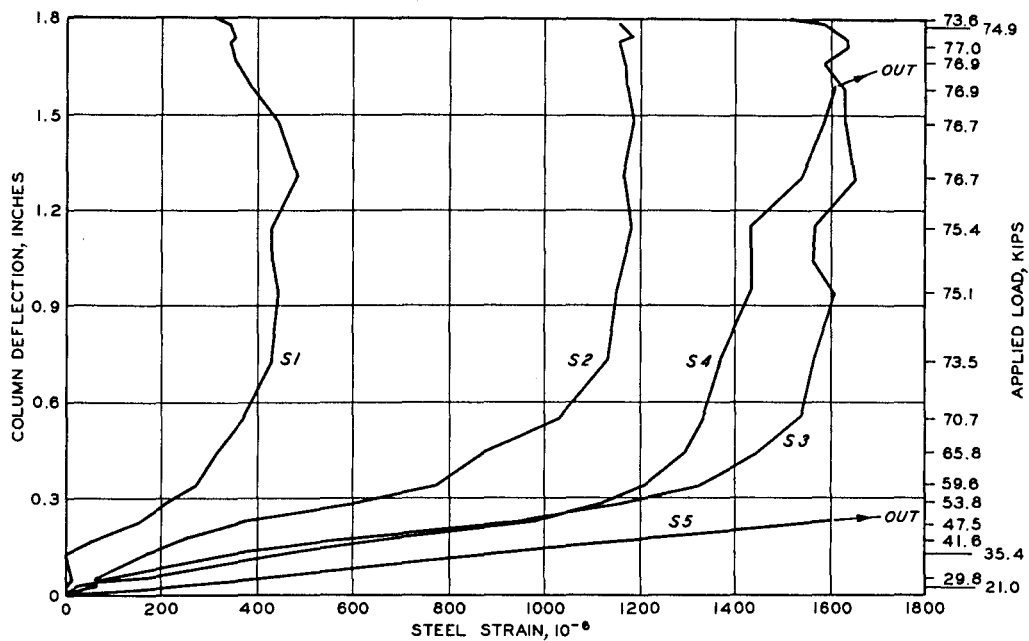


a. SPECIMEN S4075-1

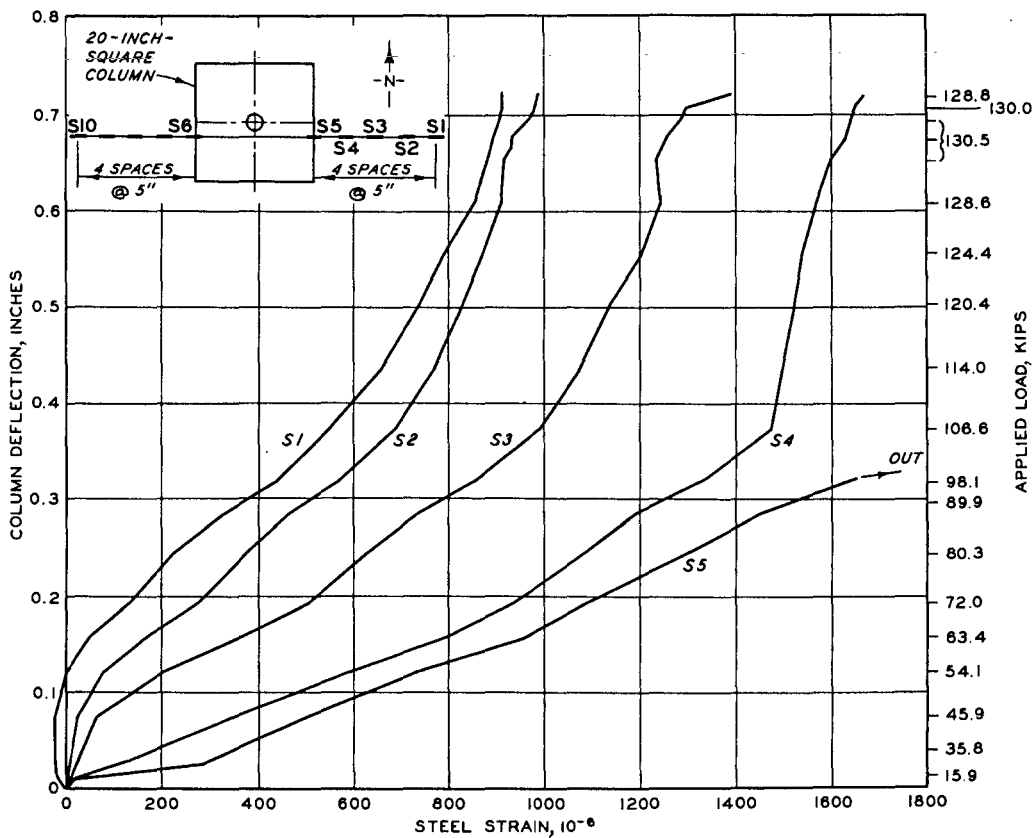


b. SPECIMEN S4150-2

Figure 6.13 Distribution of steel strains along slab centerline. S4000 Series.



a. SPECIMEN S4075-1



b. SPECIMEN S4150-1

Figure 6.14 Variation of steel strain with column deflection, S4000 Series.

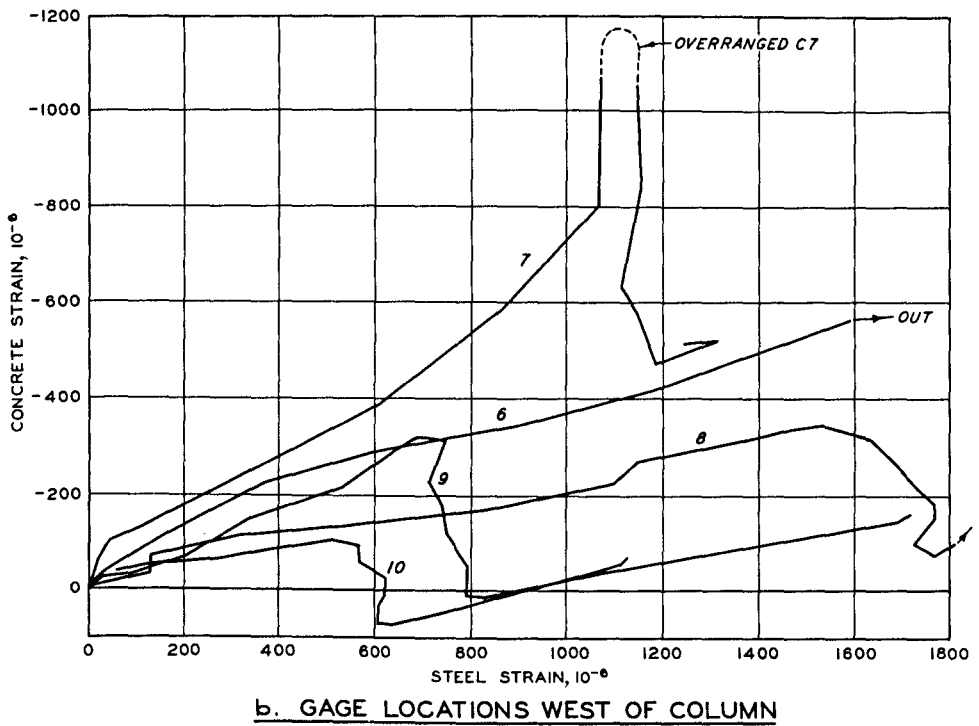
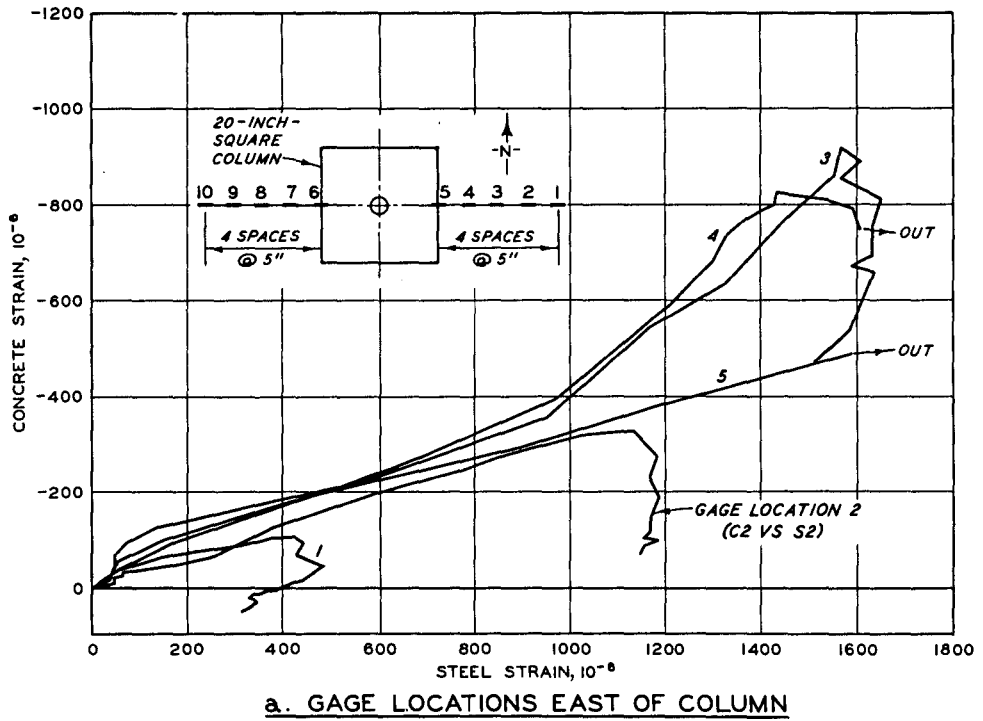
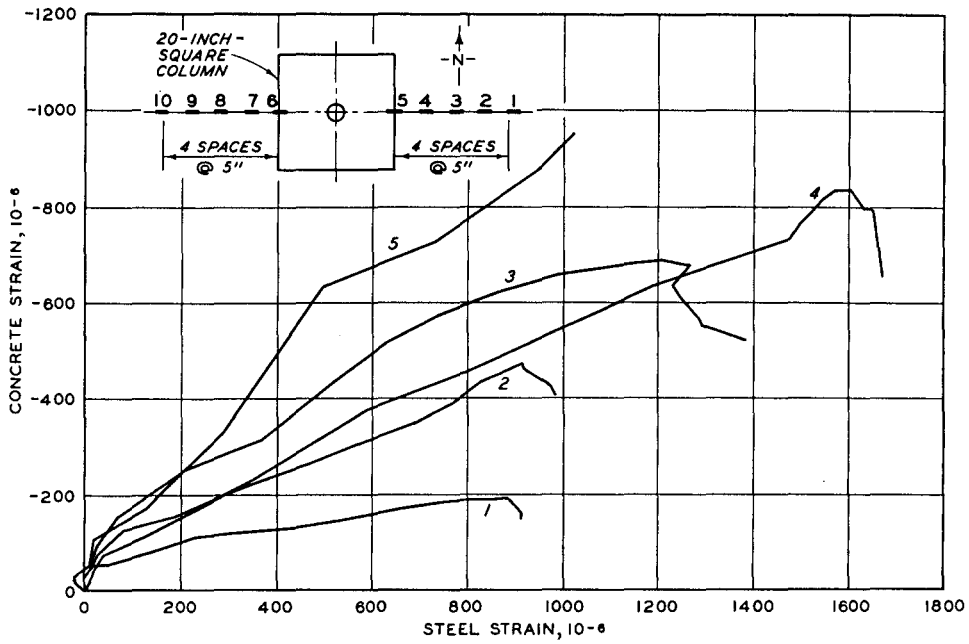
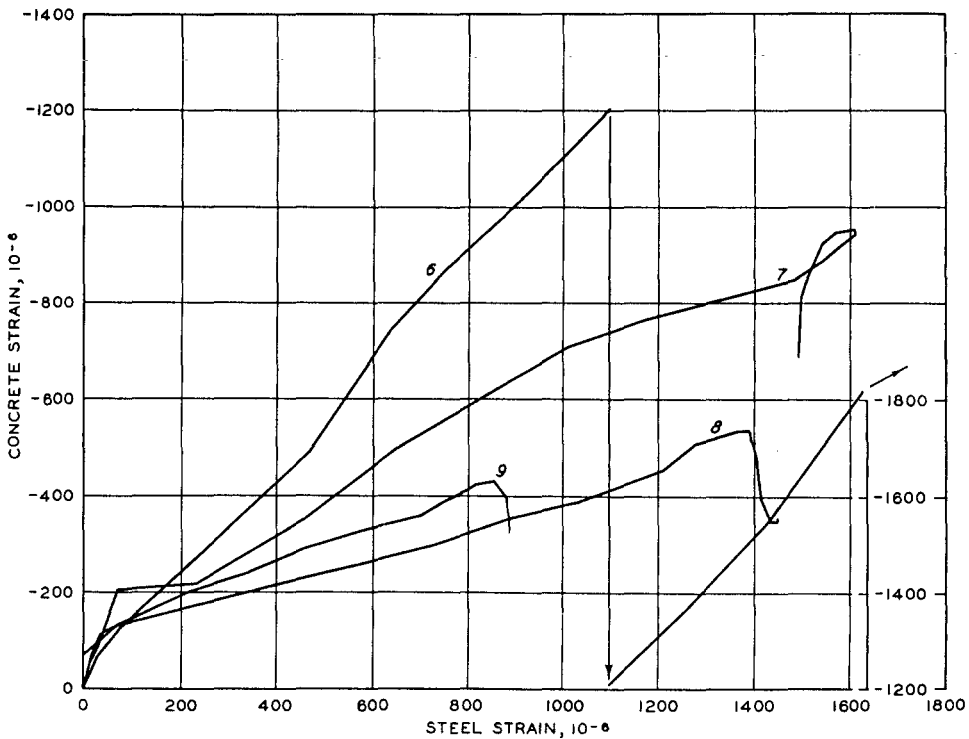


Figure 6.15 Concrete strains versus steel strains, Specimen S4075-1.



a. GAGE LOCATIONS EAST OF COLUMN



b. GAGE LOCATIONS WEST OF COLUMN

Figure 6.16 Concrete strain versus steel strain, Specimen S4150-2.

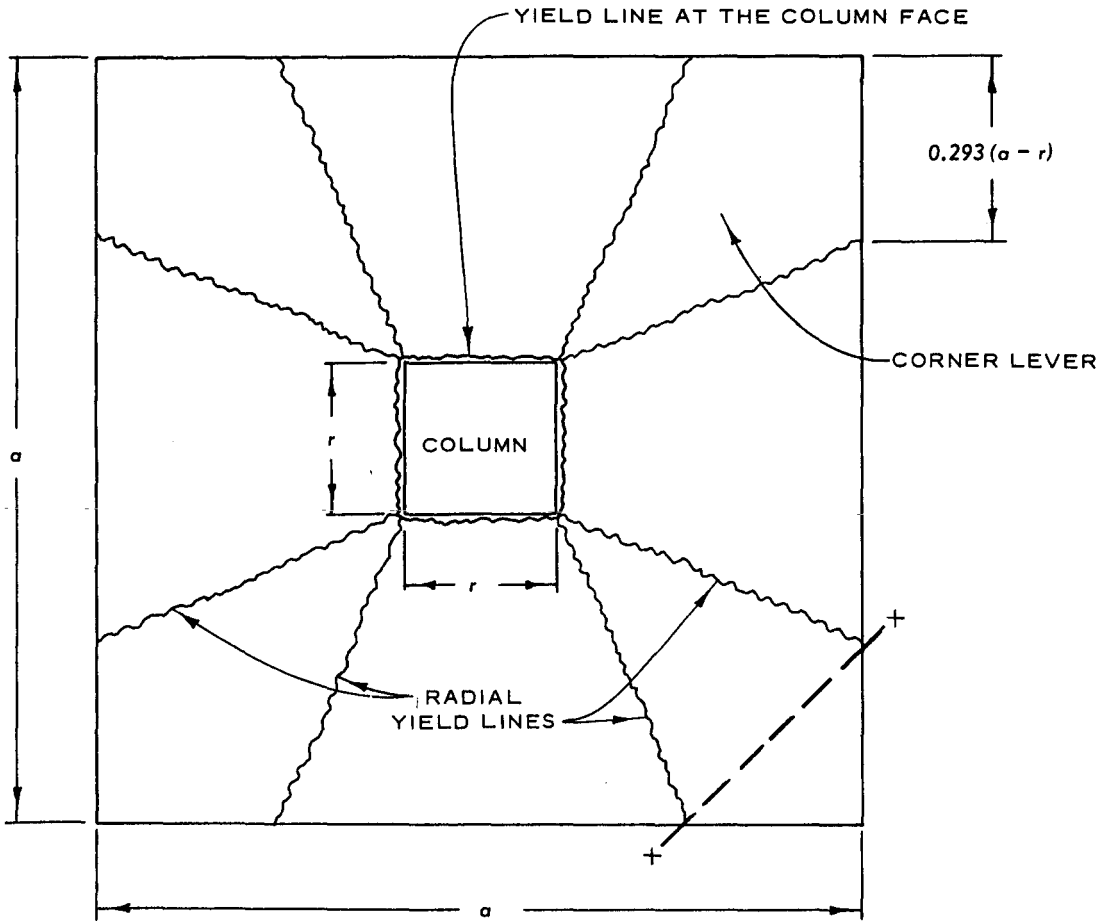
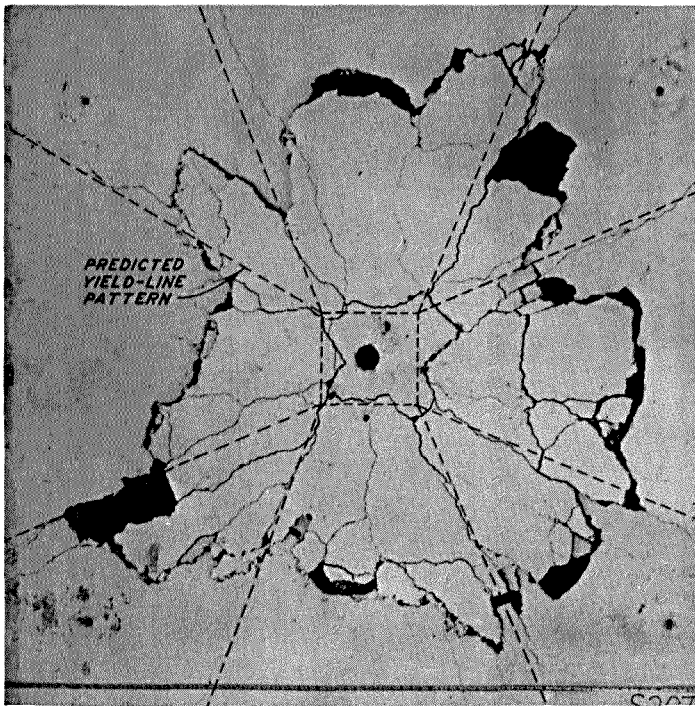
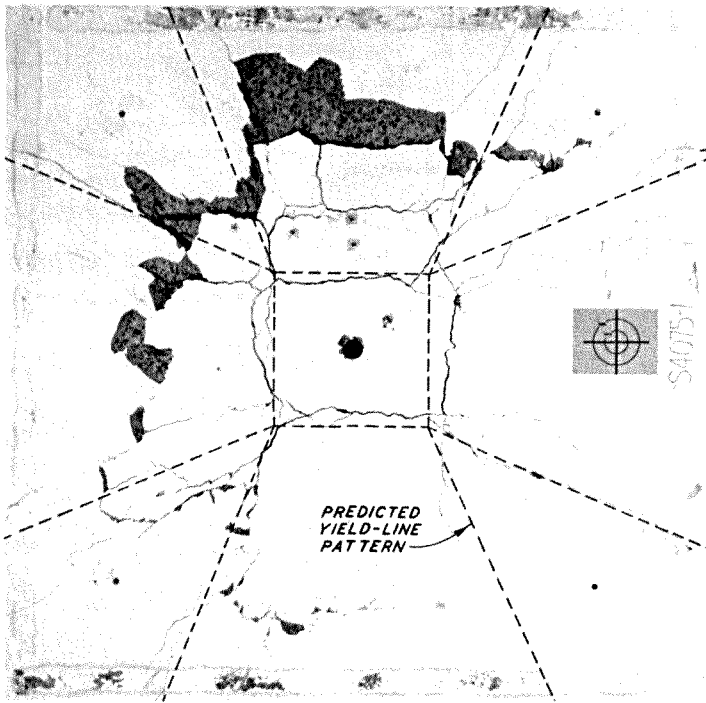


Figure 6.17 Predicted yield-line pattern.



a. SPECIMEN S2075-2



b. SPECIMEN S4075-2

Figure 6.18 Comparison of actual and predicted yield-line patterns.

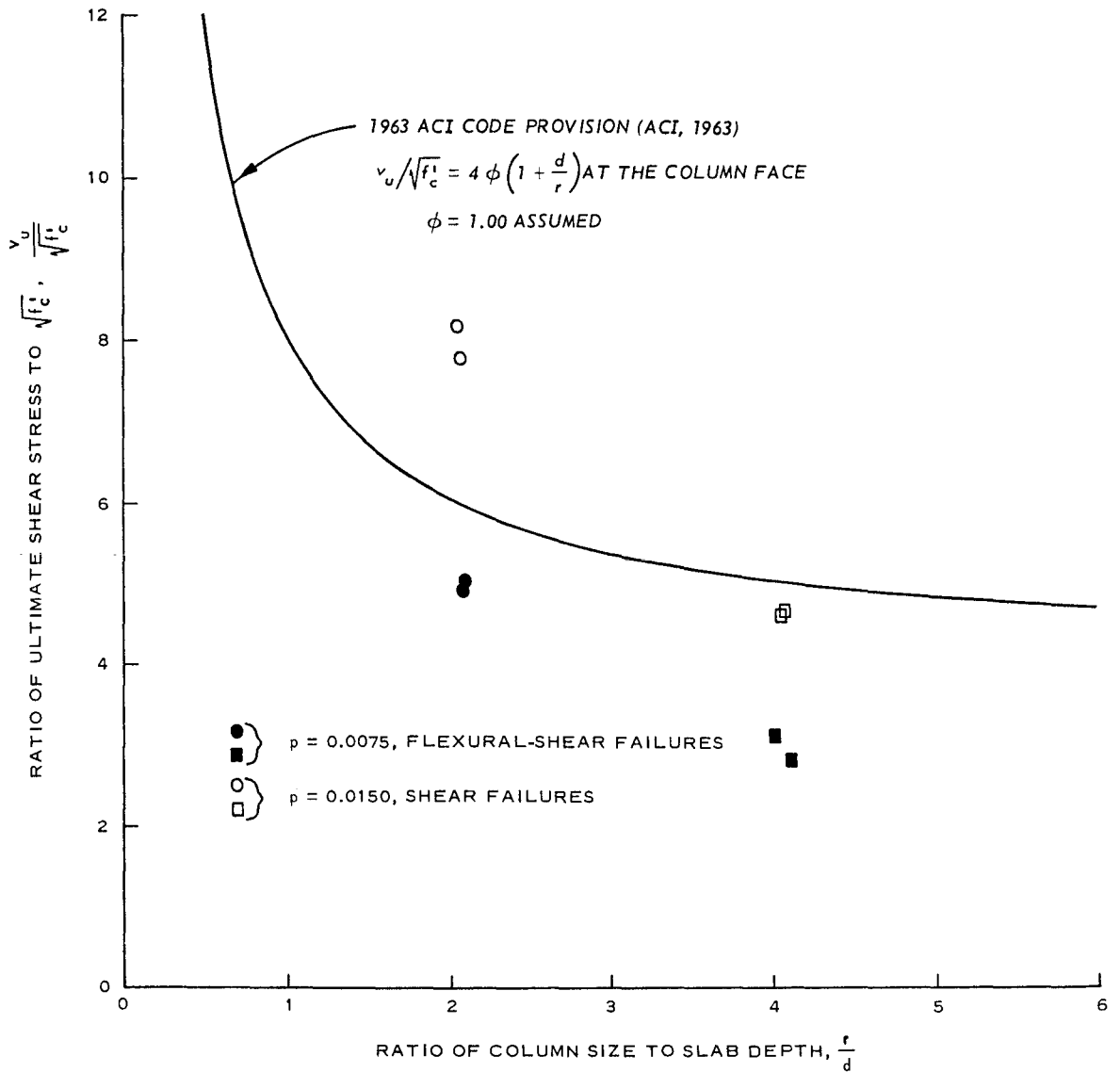


Figure 6.19 Comparison of ACI Code equation with static test results.

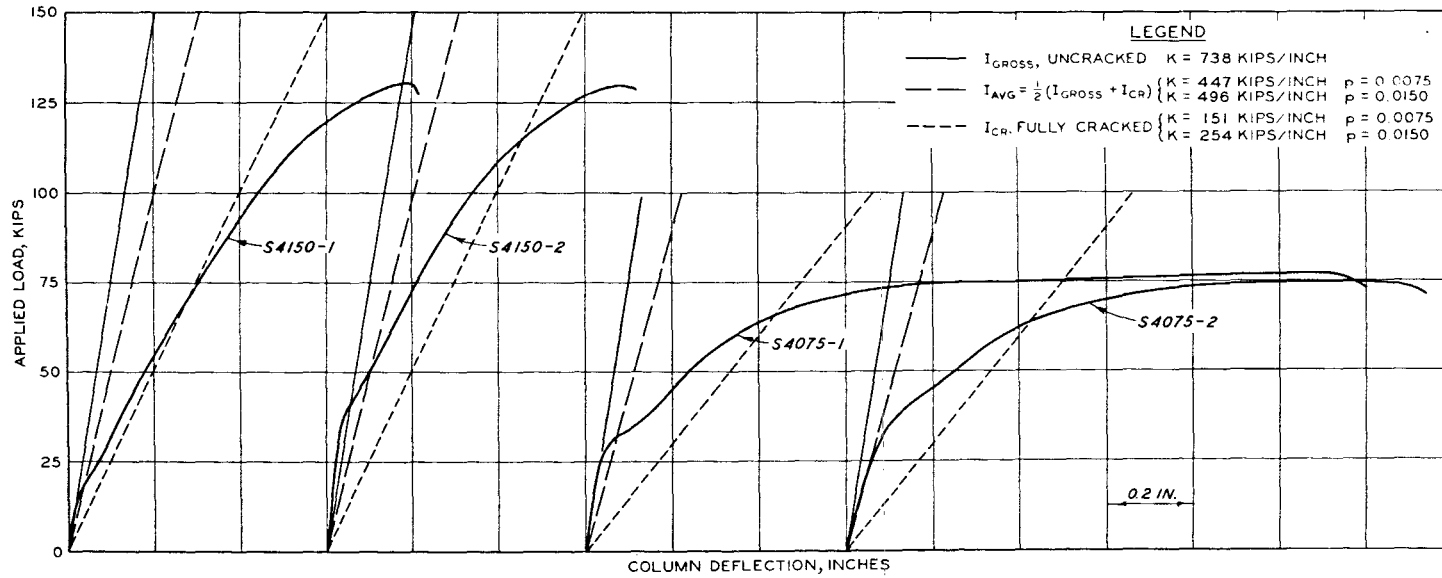
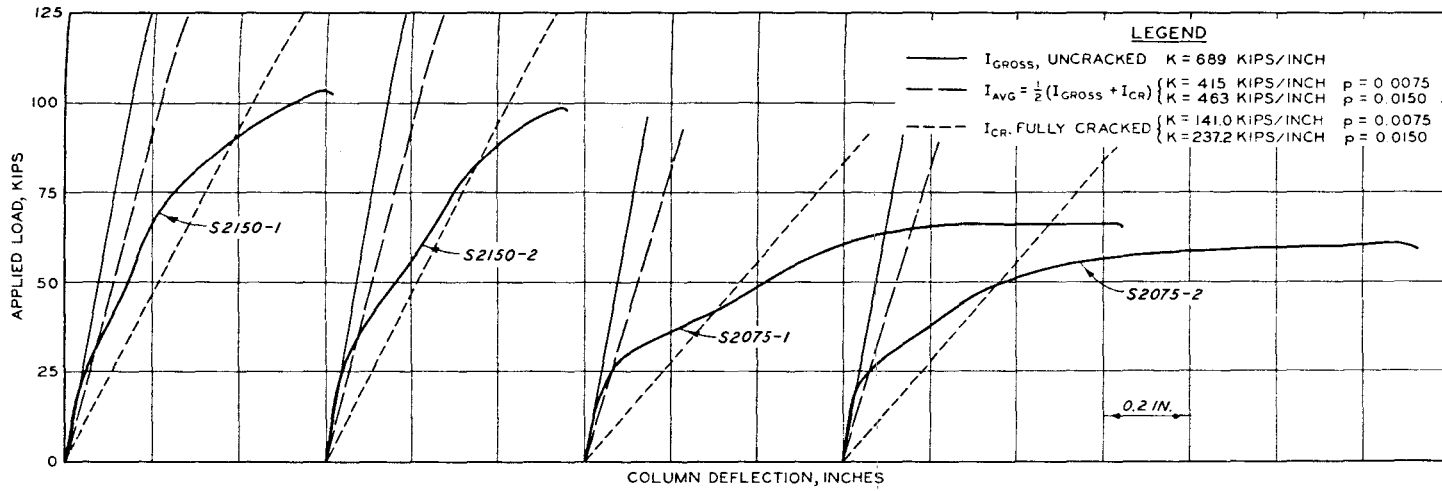
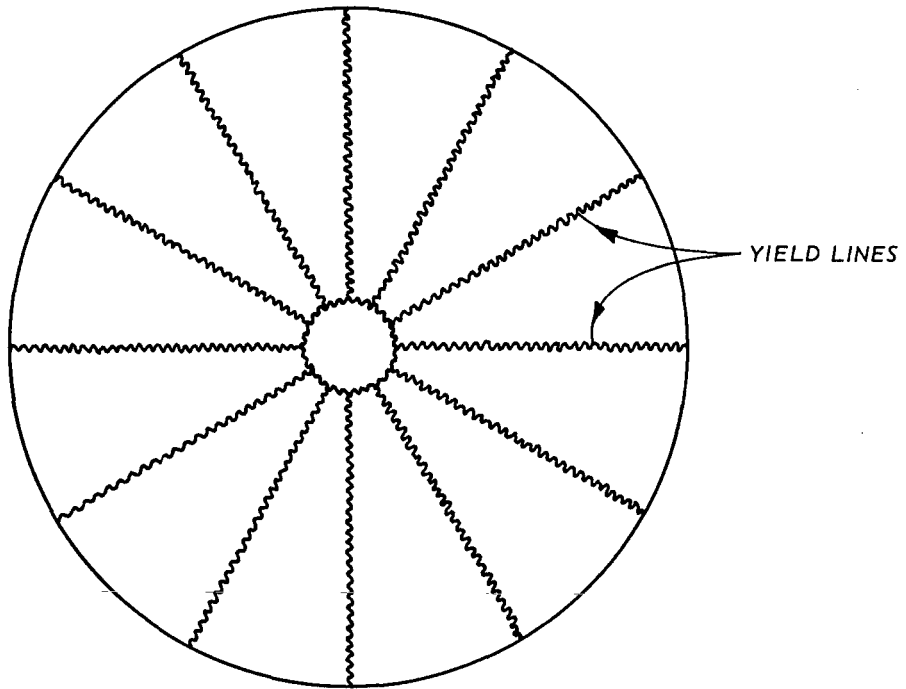
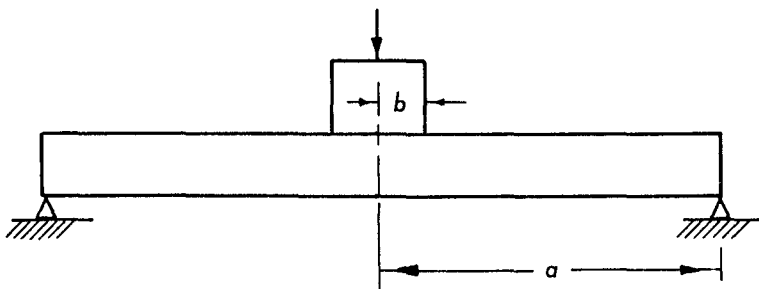


Figure 6.20 Comparison of calculated connection stiffnesses with the test results.



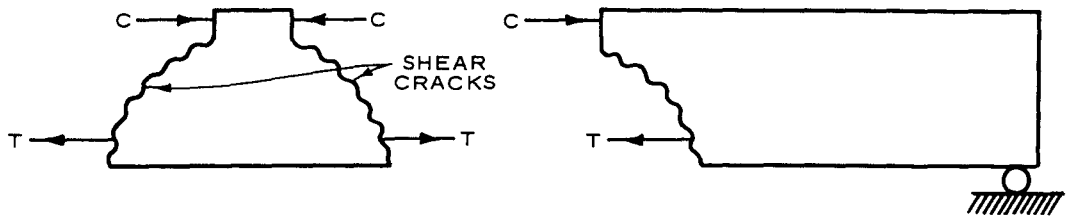


a. BOTTOM VIEW

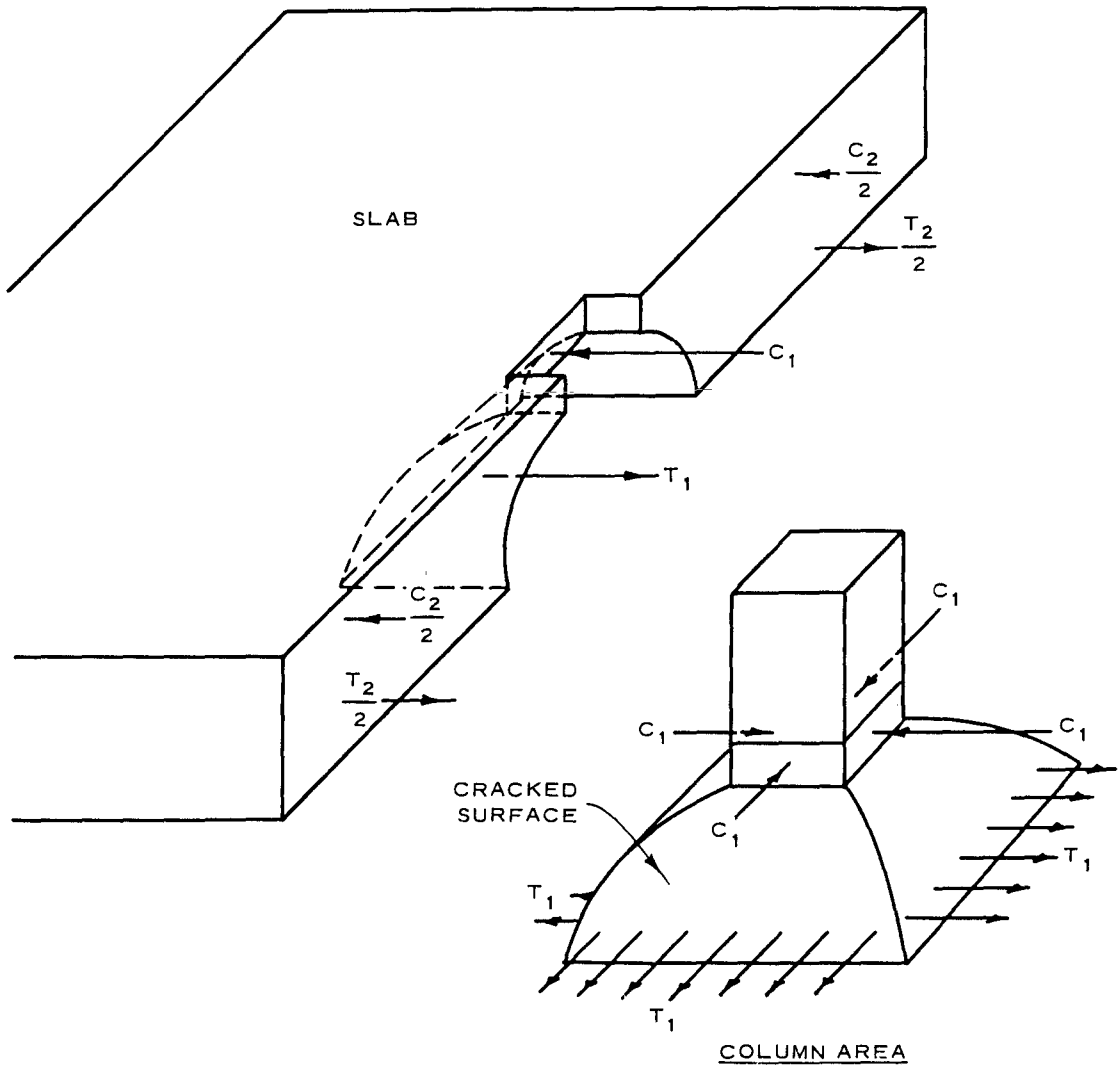


b. SIDE VIEW

Figure 6.21 Yield-line pattern for a circular slab loaded on a circular column.



a. HORIZONTAL FORCES ON A BEAM WITH AN INCLINED CRACK



b. HORIZONTAL FORCES ON A SLAB-COLUMN CONNECTION WITH AN INCLINED CRACK

Figure 6.22 Free-body diagrams.

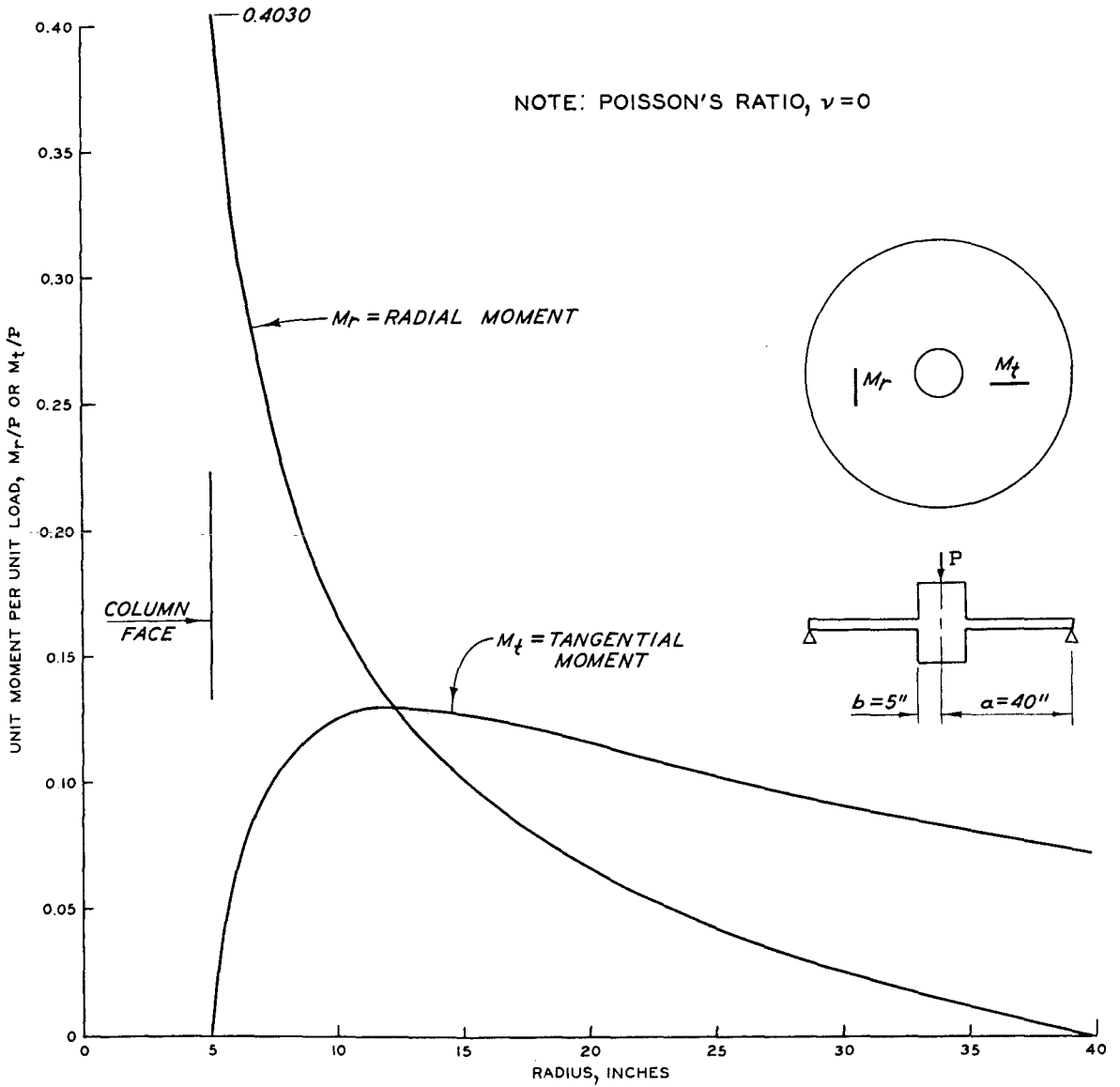


Figure 6.23 Elastic moments in a circular slab with a fixed center column.

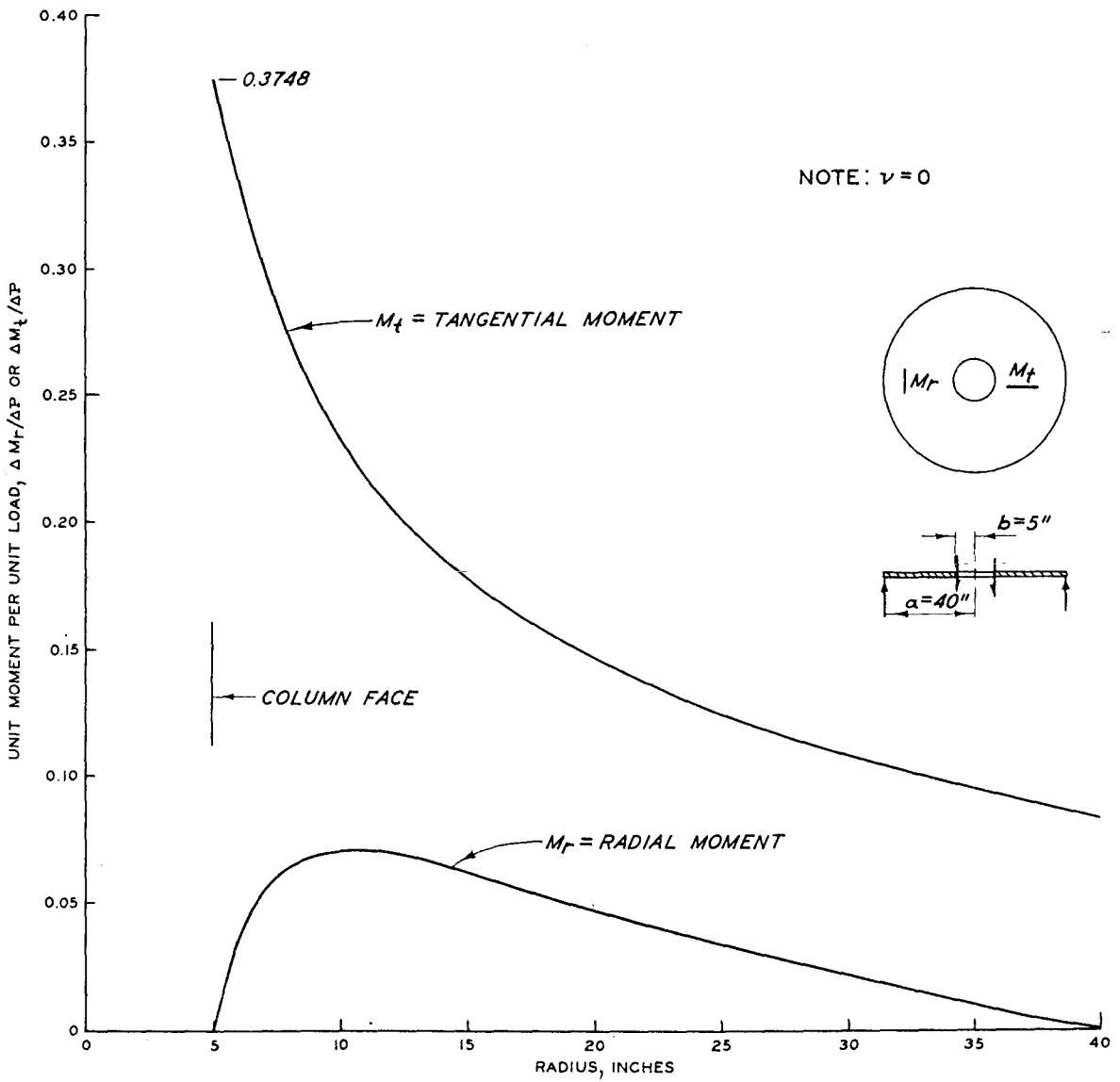


Figure 6.24 Elastic moments for a circular slab loaded along a centrally located hole.

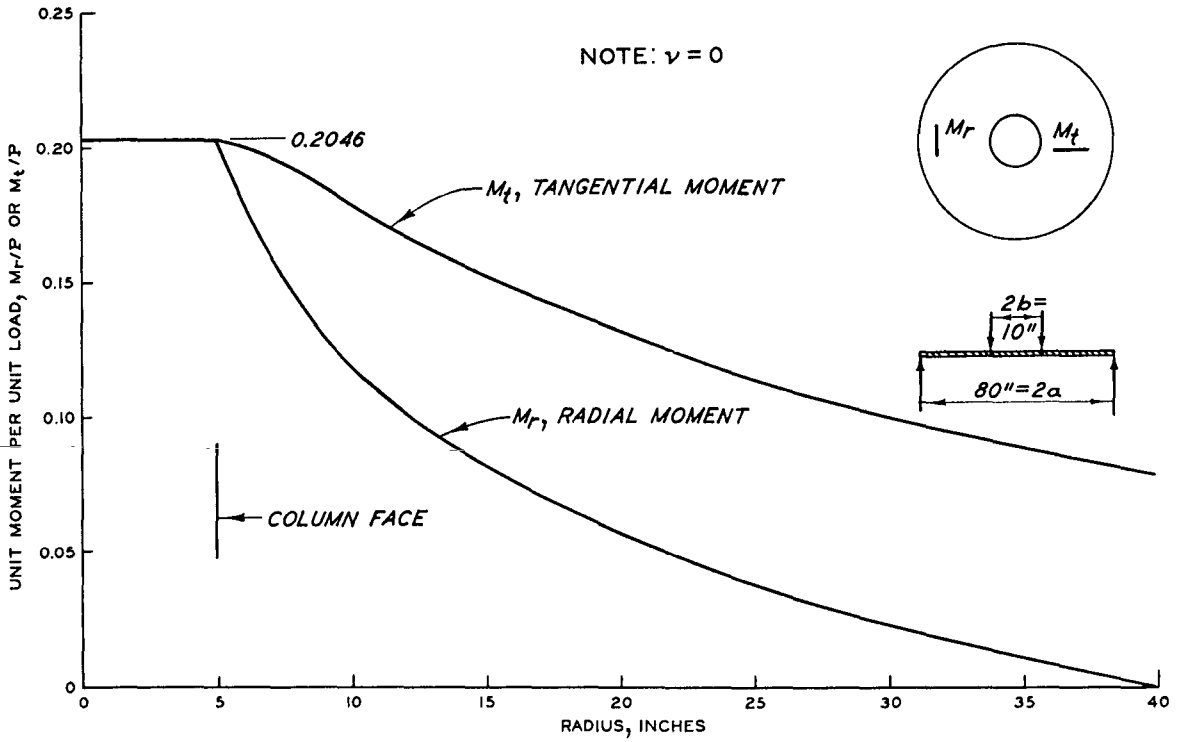
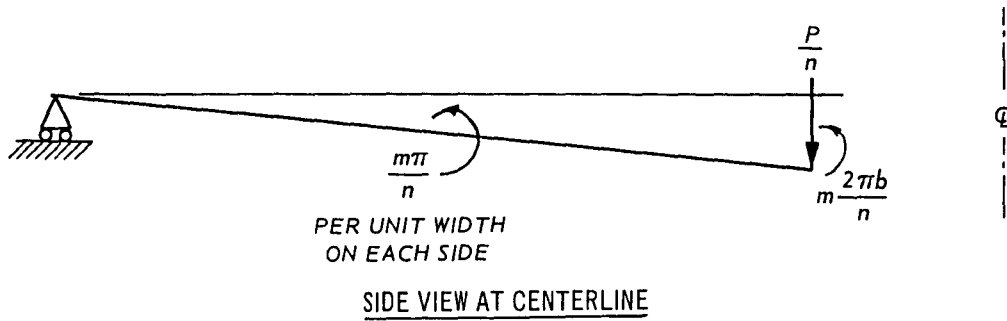
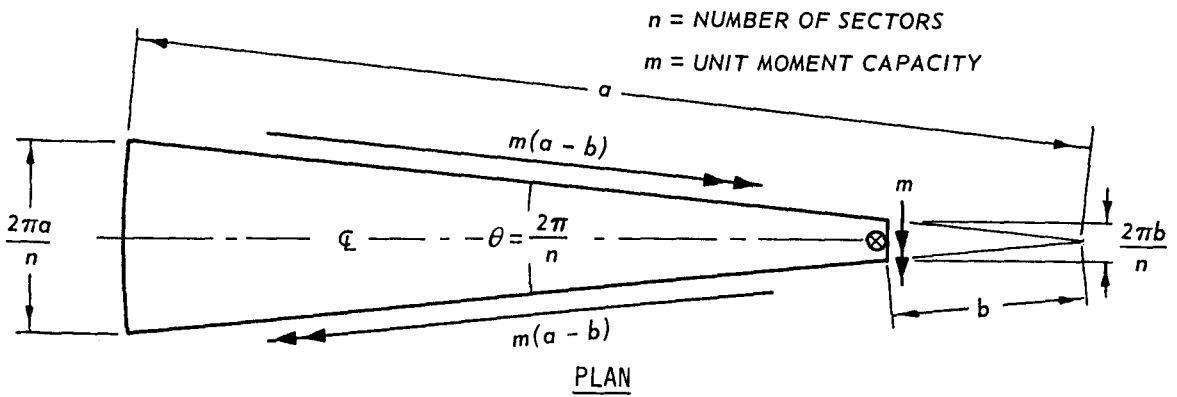
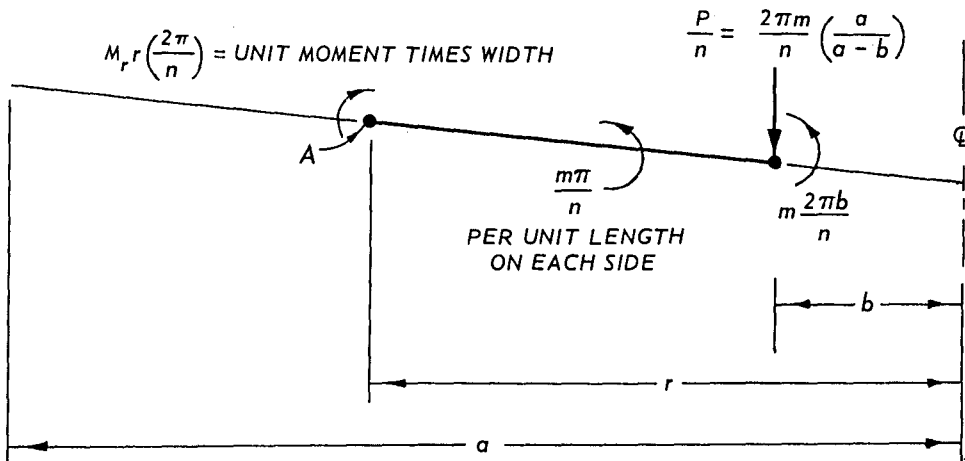


Figure 6.25 Elastic moments in a circular slab loaded along a circular ring.



a. FREE BODY DIAGRAMS USED TO DETERMINE P



b. FREE BODY DIAGRAM USED TO DETERMINE  $M_r$

Figure 6.26 Determination of load and radial moments for a circular slab at yield-line completion.

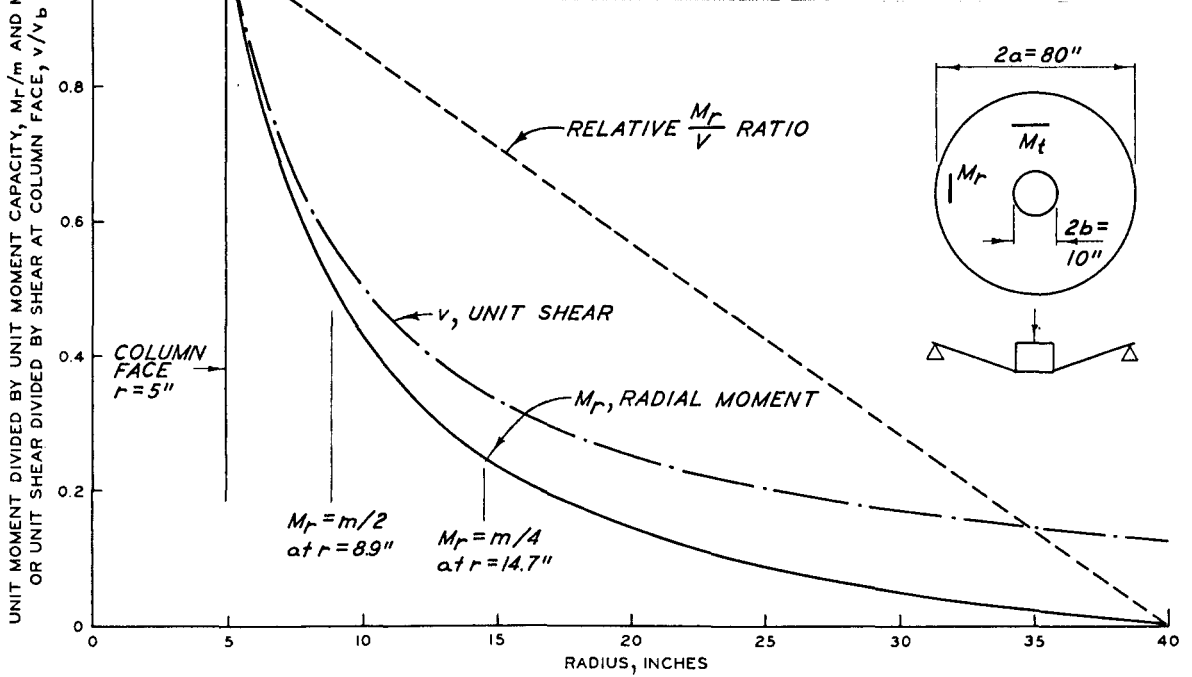


Figure 6.27 Moments in a circular slab at yield-line completion.

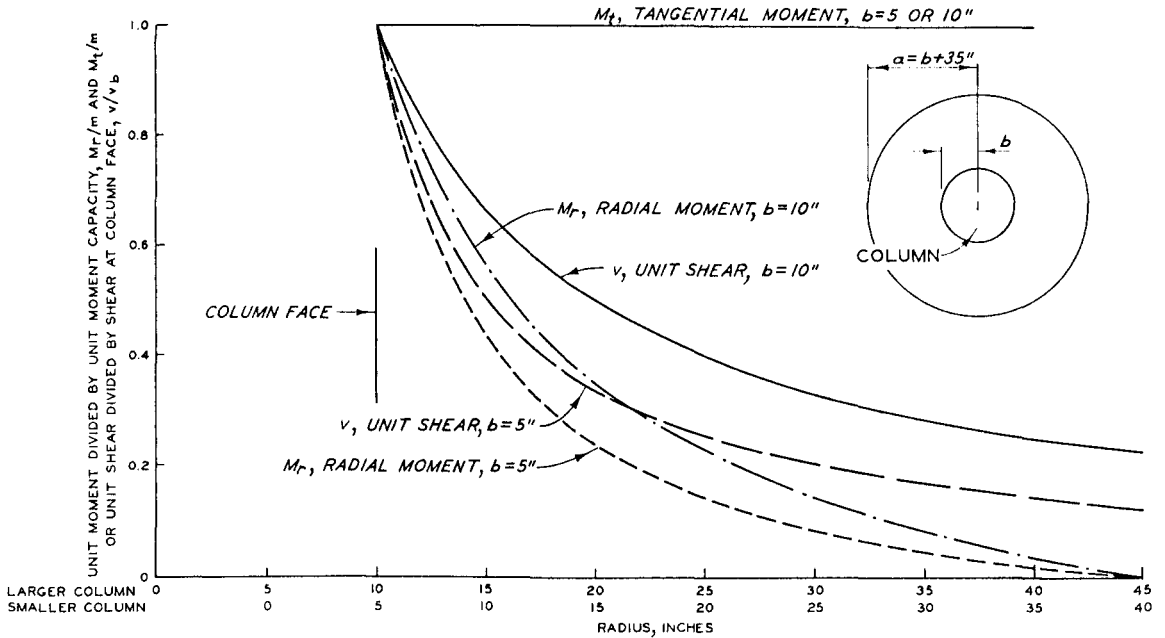


Figure 6.28 Moments and shears at yield-line completion for two column sizes.

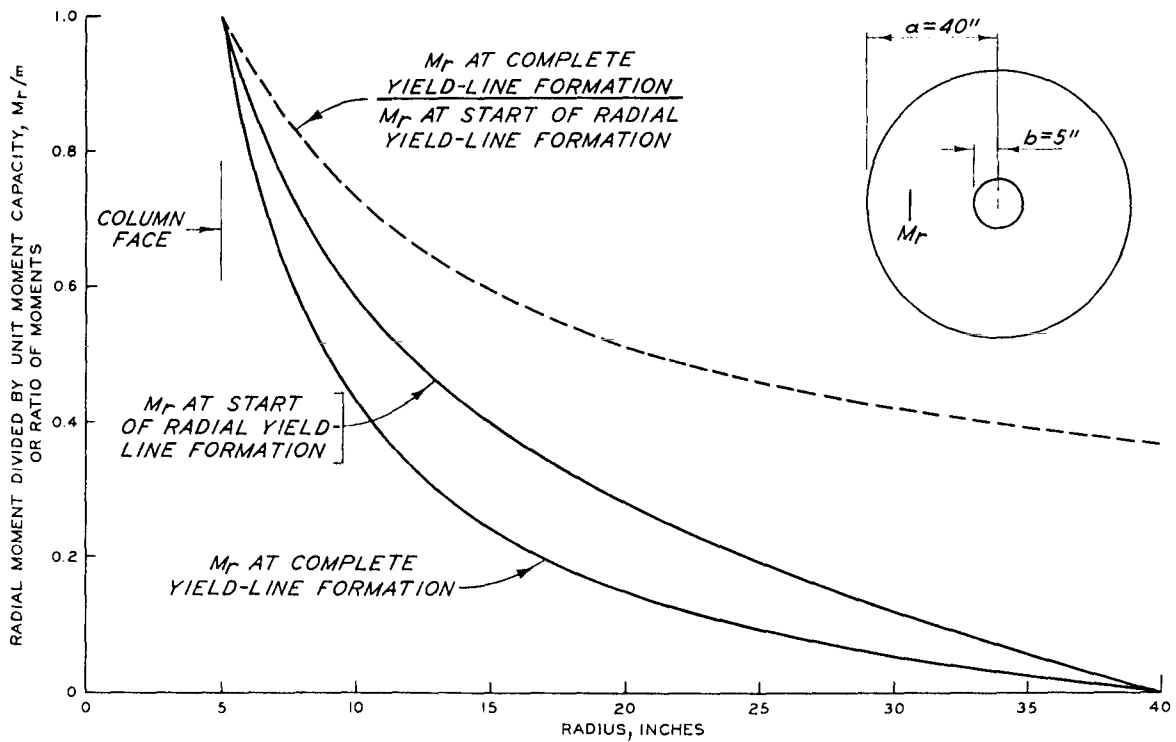


Figure 6.29 Decrease in radial moments with yield-line formation.



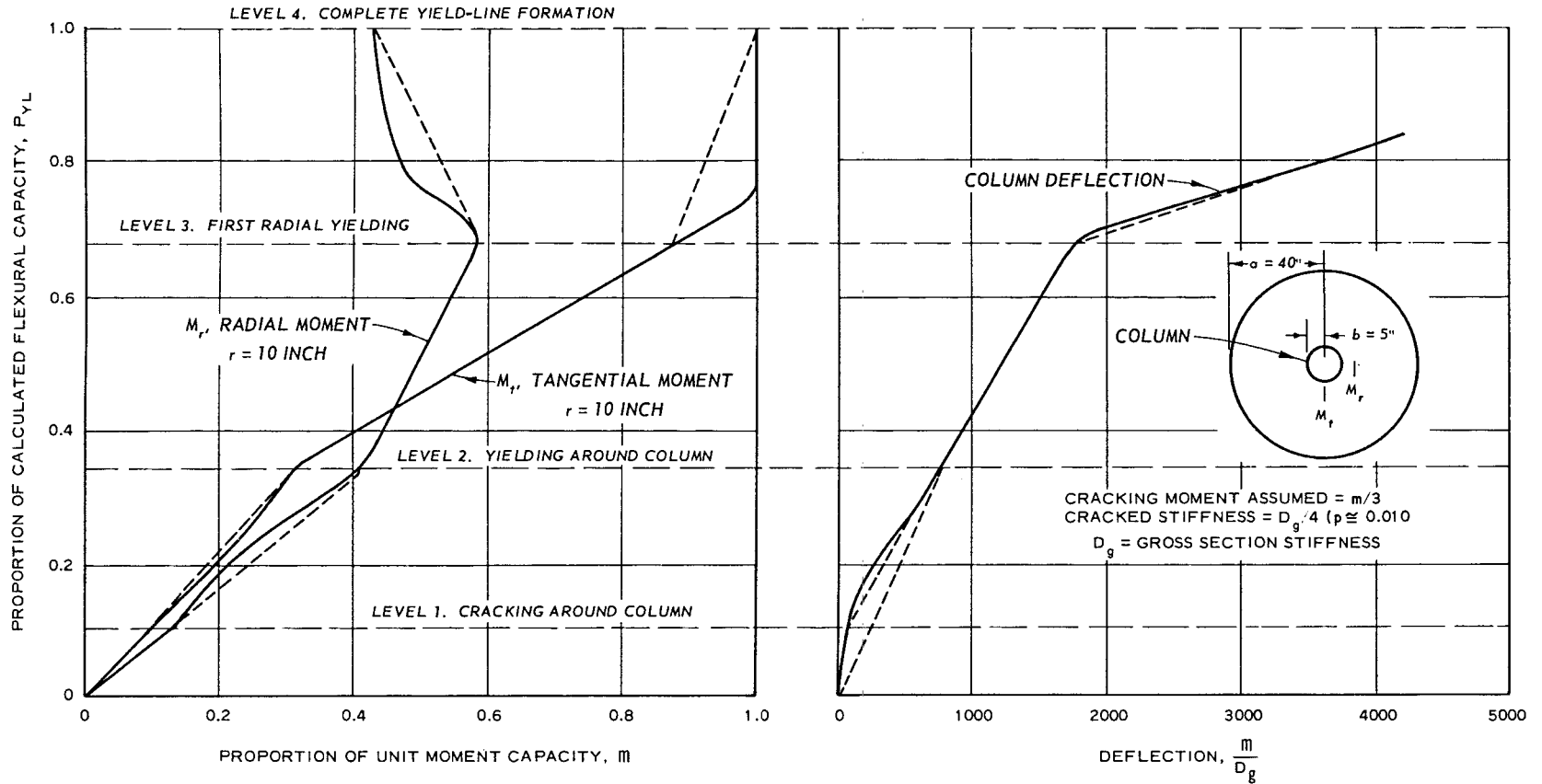


Figure 6.30 Column deflection and moments 5 inches from the column face.

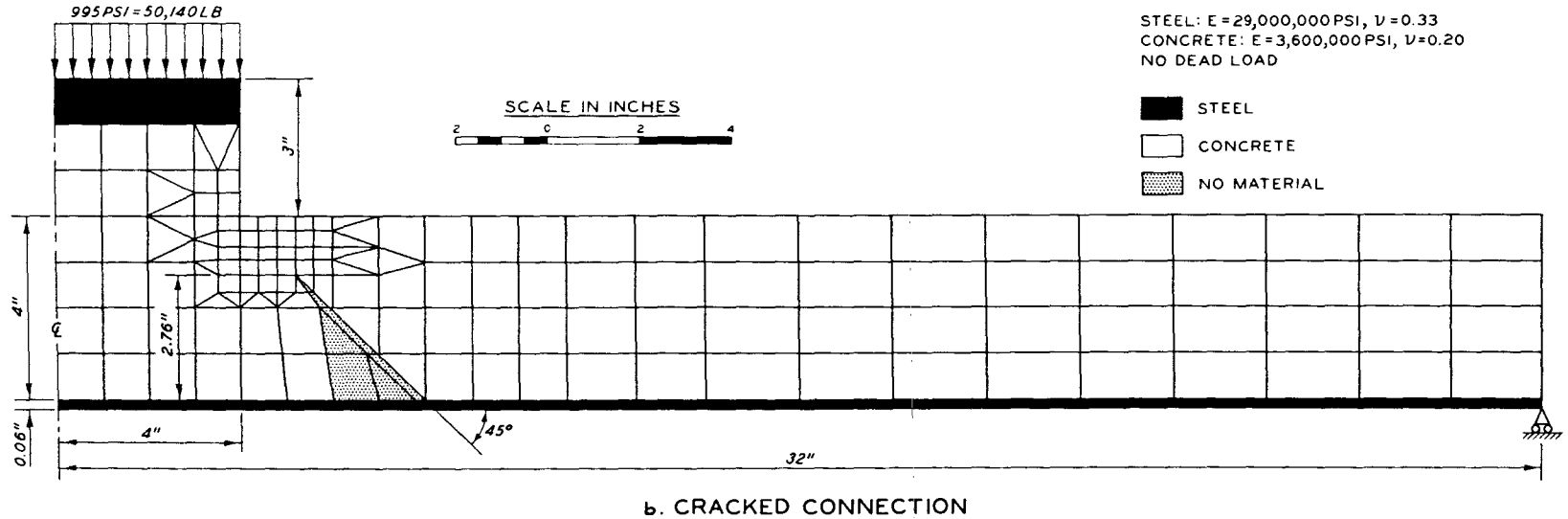
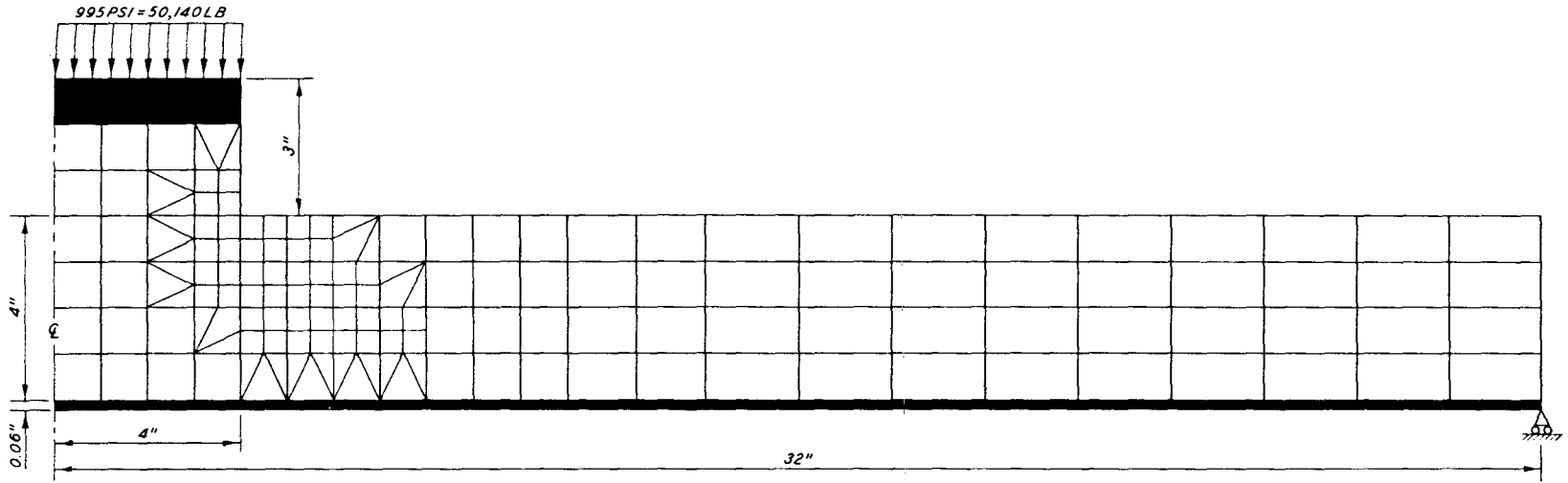
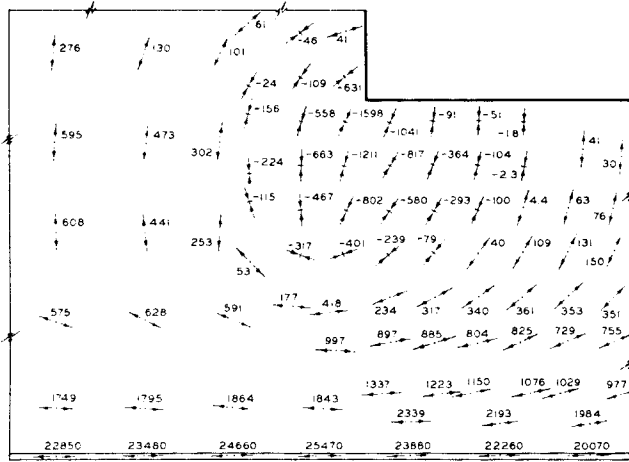
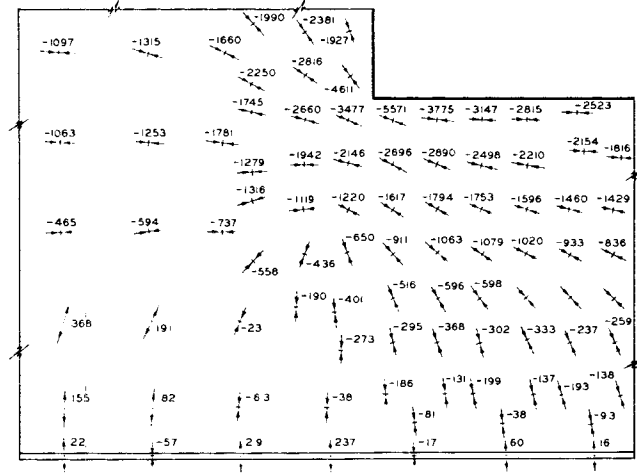


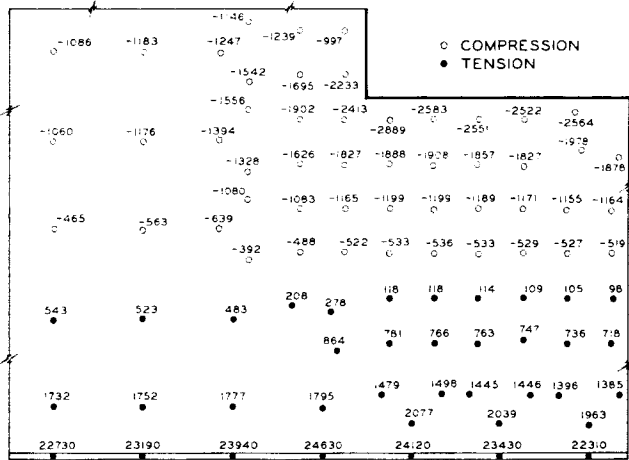
Figure 6.31 Finite-element representation of axially symmetric connection.



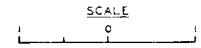
MAXIMUM PRINCIPAL STRESS



MINIMUM PRINCIPAL STRESS



RADIAL STRESS



TENSION POSITIVE  
 $\mu = 0.0150$

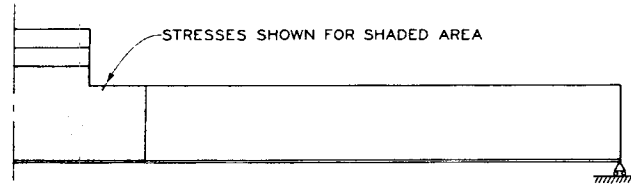
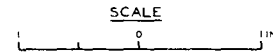
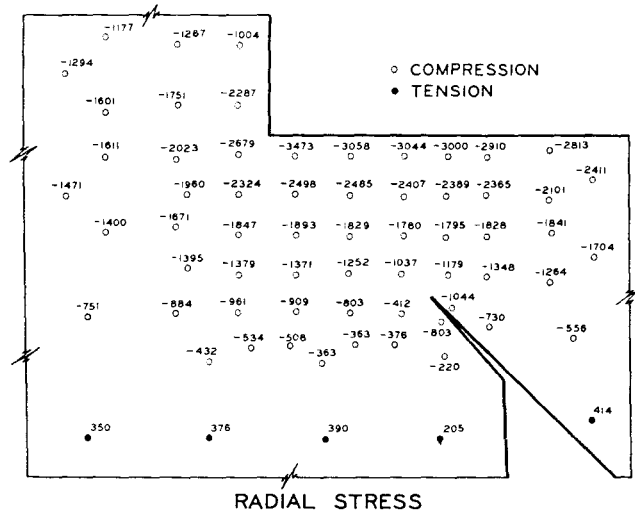
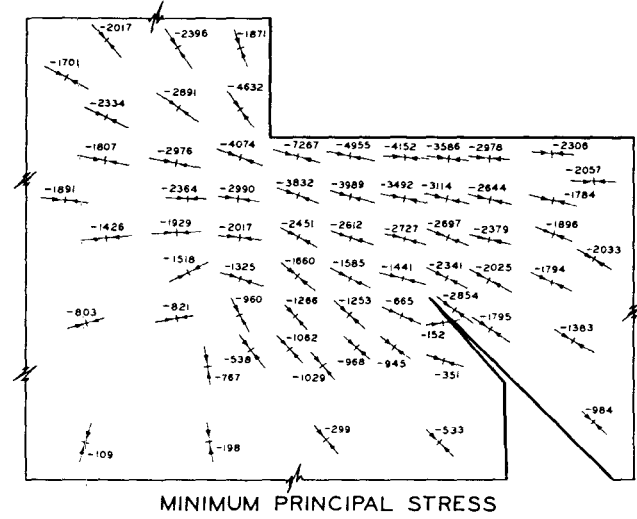
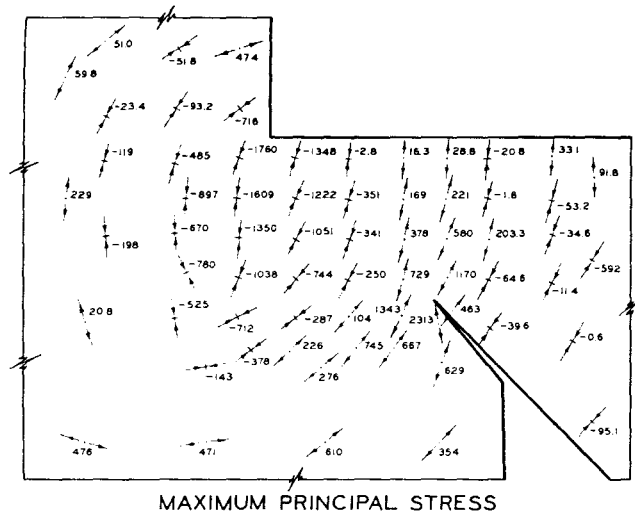


Figure 6.32 Stresses in an uncracked slab-column connection.



TENSION POSITIVE  
 $P = 0.0150$

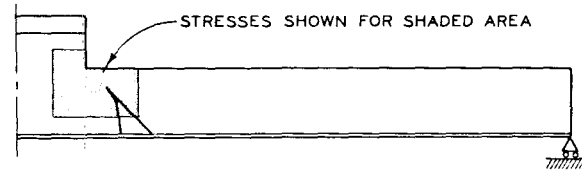
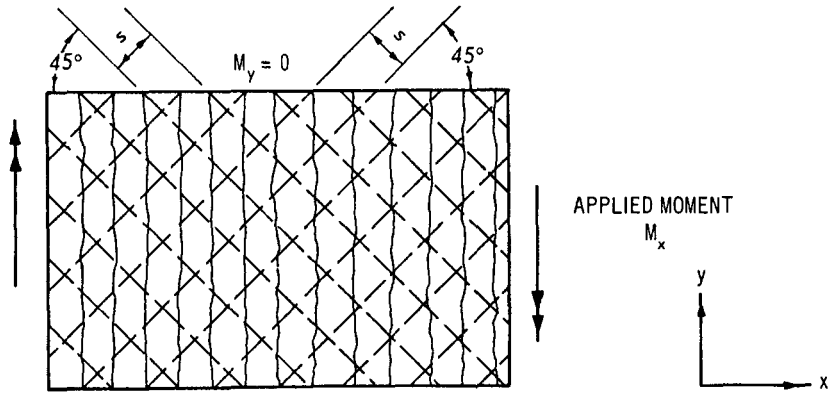
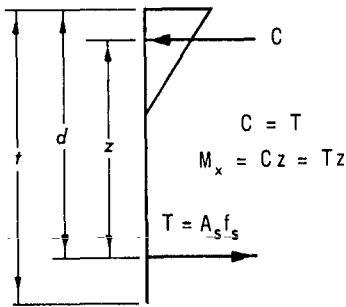


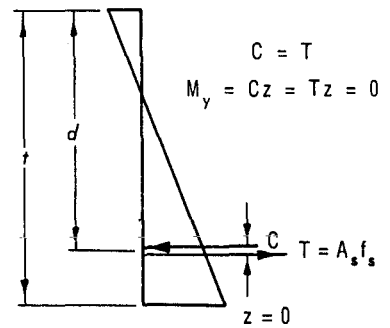
Figure 6.33 Stresses in a slab-column connection with an inclined crack.



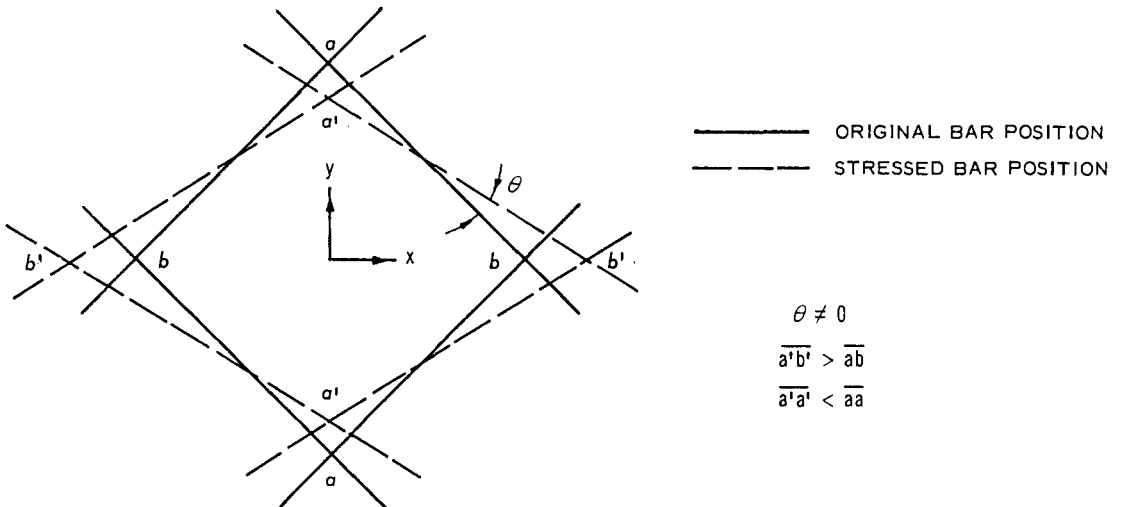
a. SLAB WITH REINFORCEMENT AND CRACK PATTERN SHOWN



b. STRESSES AT A SECTION PERPENDICULAR TO THE X-AXIS



c. STRESSES ON A SECTION PERPENDICULAR TO THE Y-AXIS



d. CHANGE IN REINFORCEMENT ORIENTATION

Figure 6.34 Uniaxially loaded slab with reinforcement 45 degrees from applied moment.

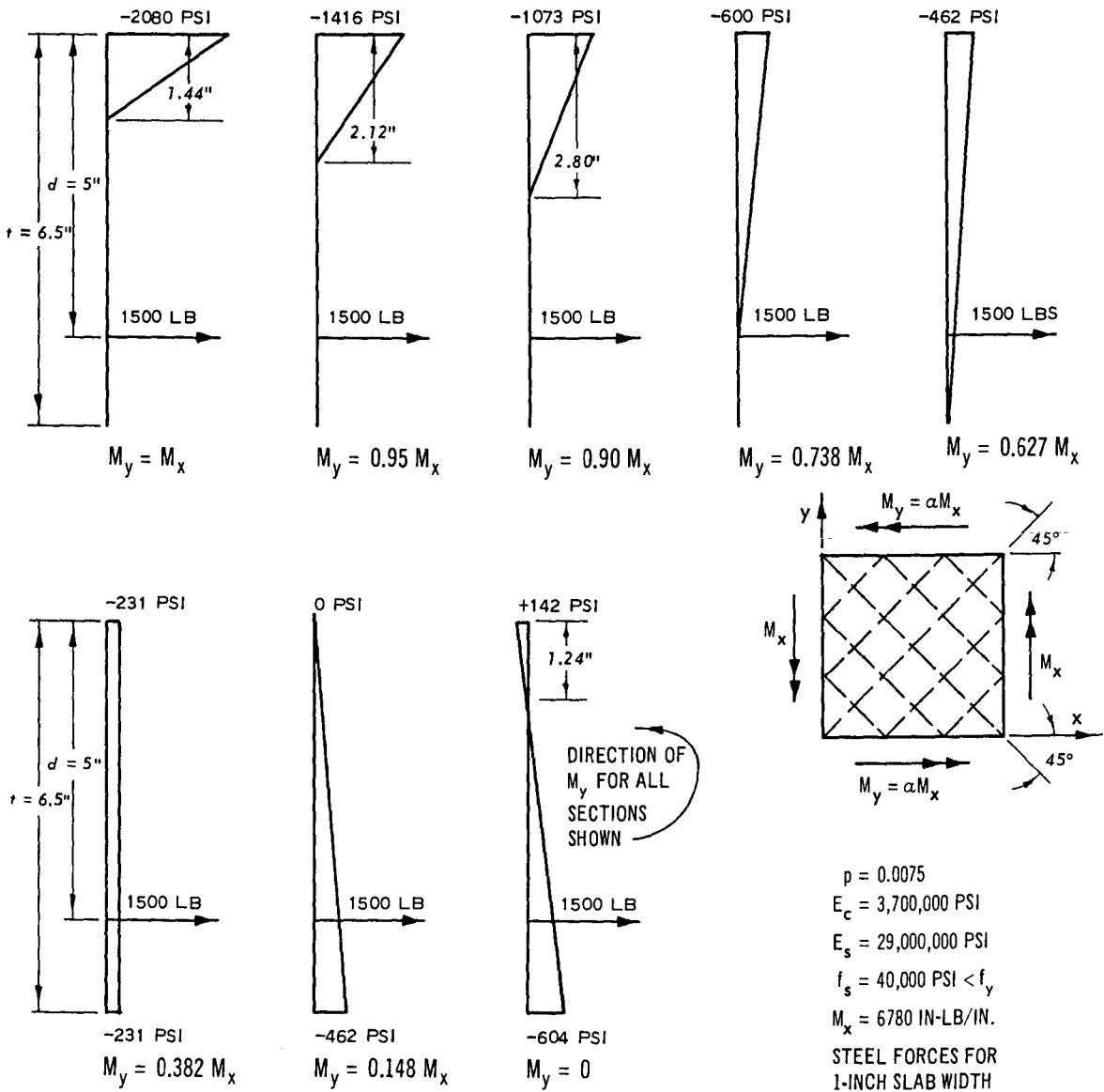
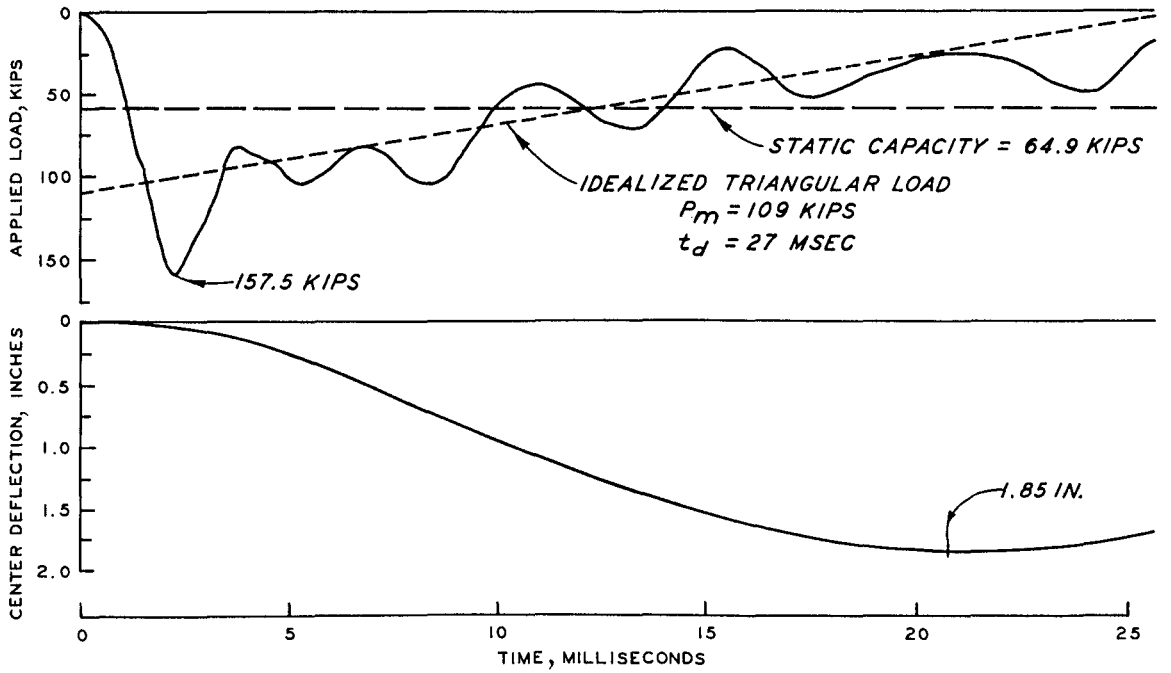
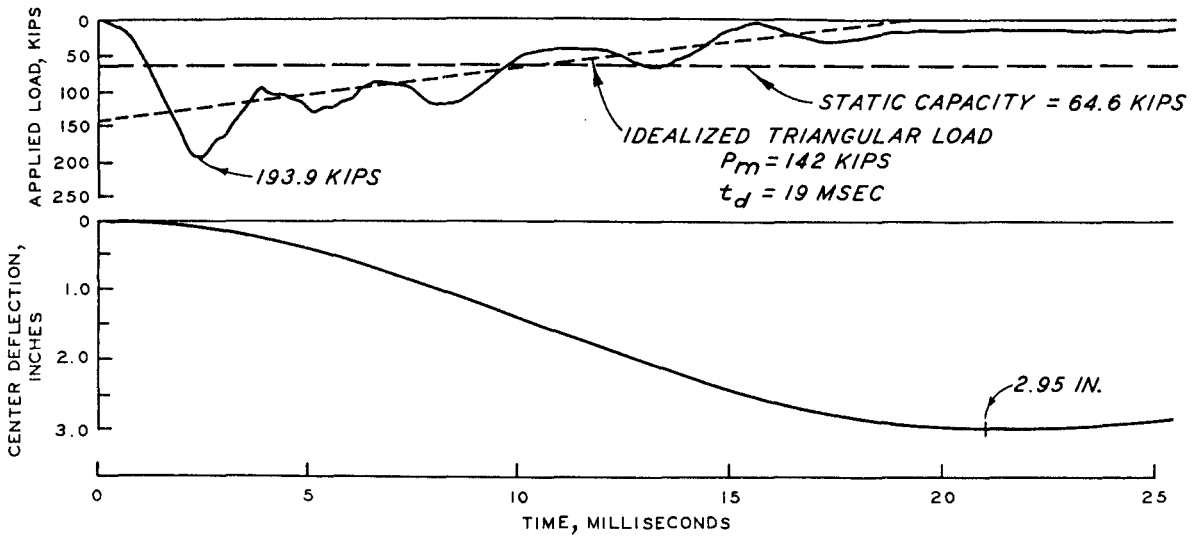


Figure 6.35 Effect of moment ratio on stresses in the direction of smaller principal moment, reinforcement 45 degrees from principal moment.



**a. SPECIMEN D2075-1**



**b. SPECIMEN D2075-2**

Figure 7.1 Load and deflection traces, Specimens D2075-1 and D2075-2.

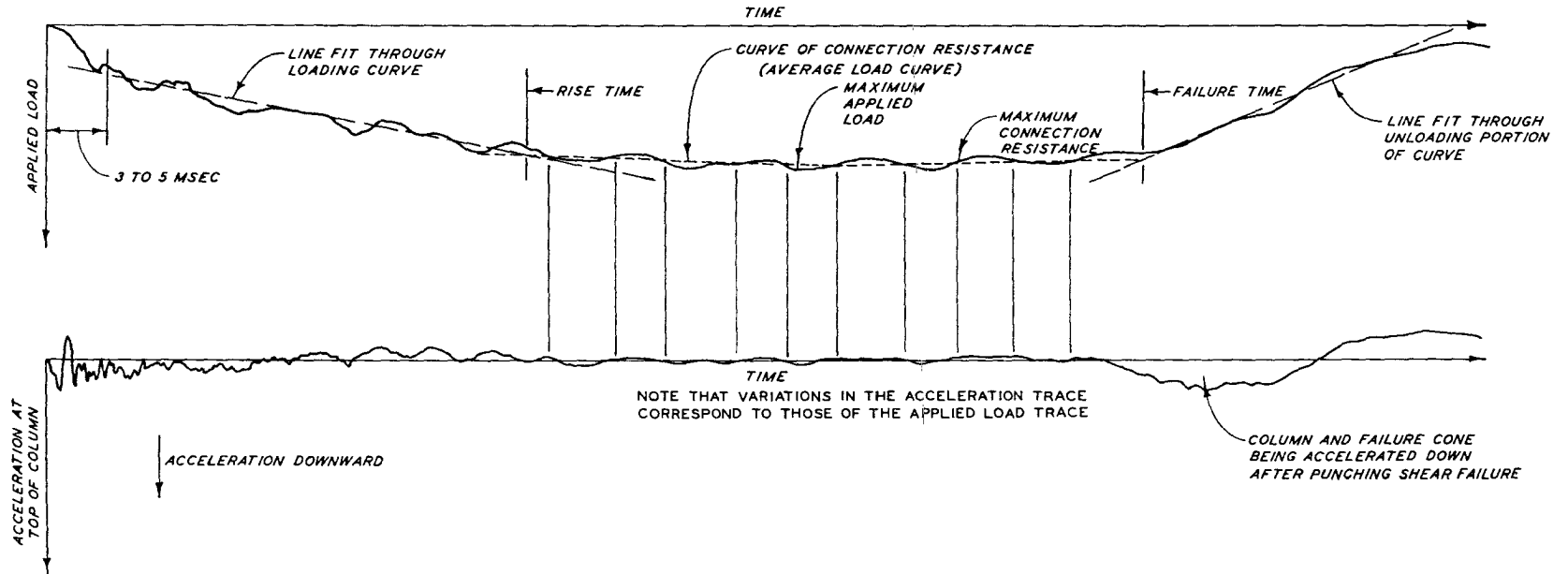
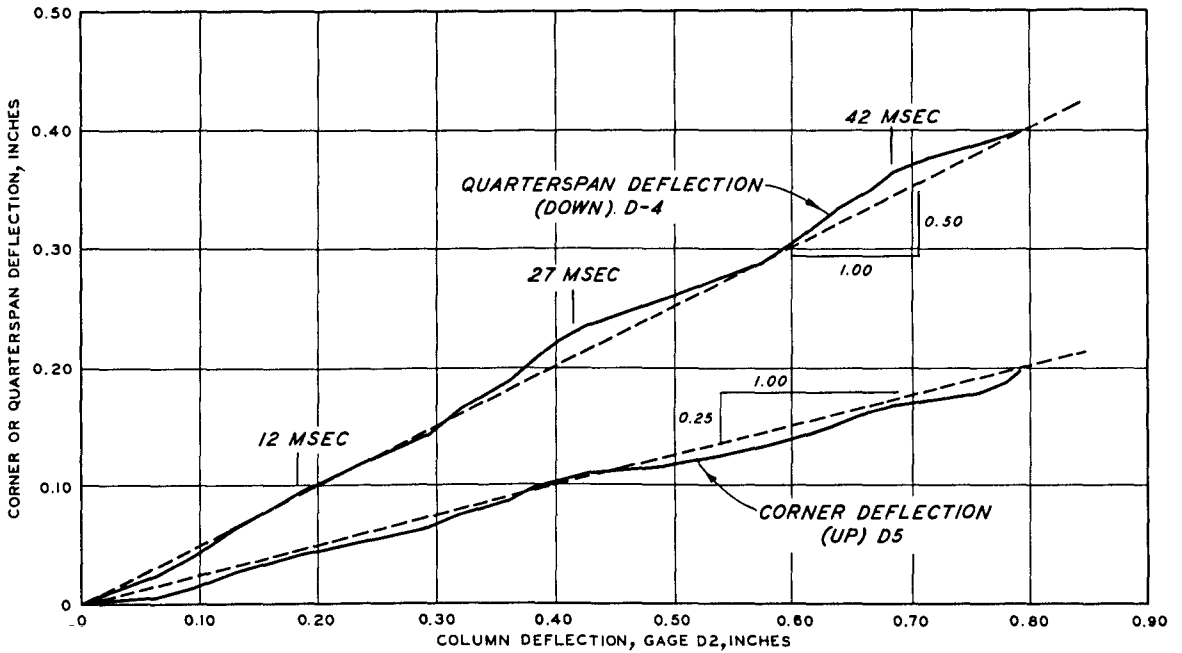
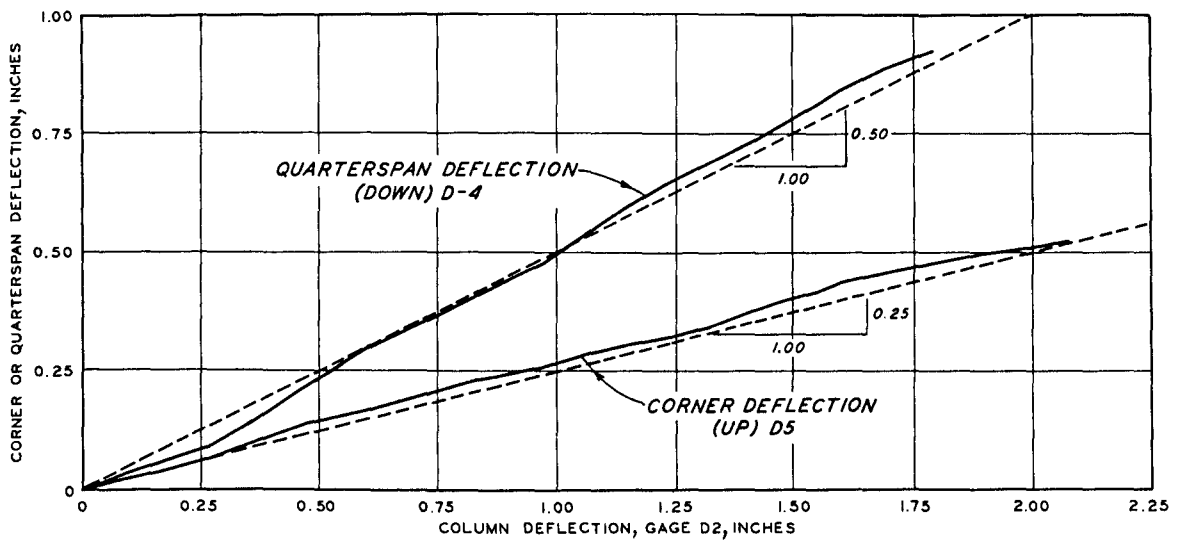


Figure 7.2 Determination of dynamic load characteristics.





a. SPECIMEN D2150-1



b. SPECIMEN D4075-2

Figure 7.3 Comparison of quarterspan and corner deflections with column deflections.

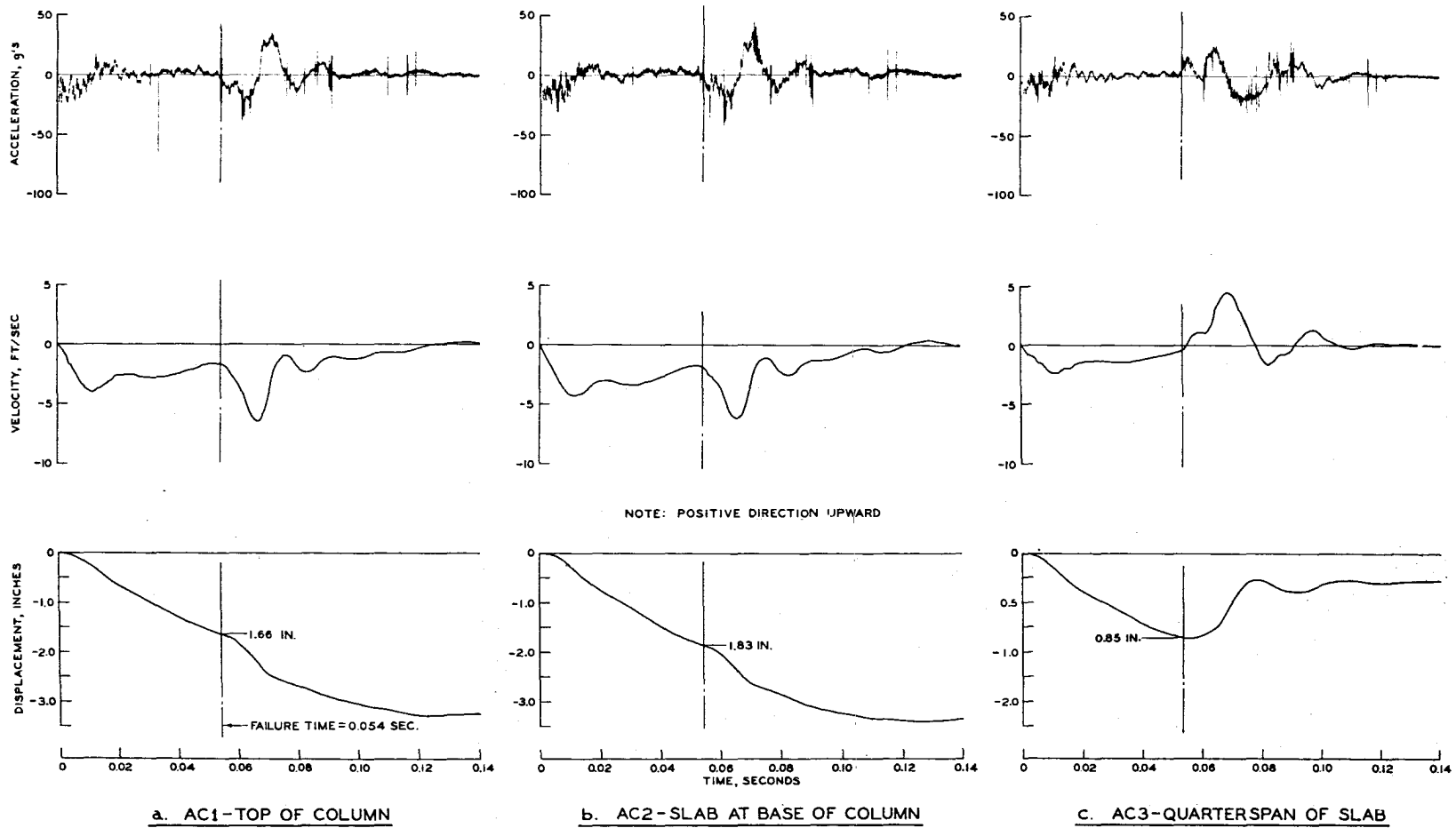


Figure 7.4 Acceleration-, velocity-, and displacement-time curves, Specimen D2075-3.

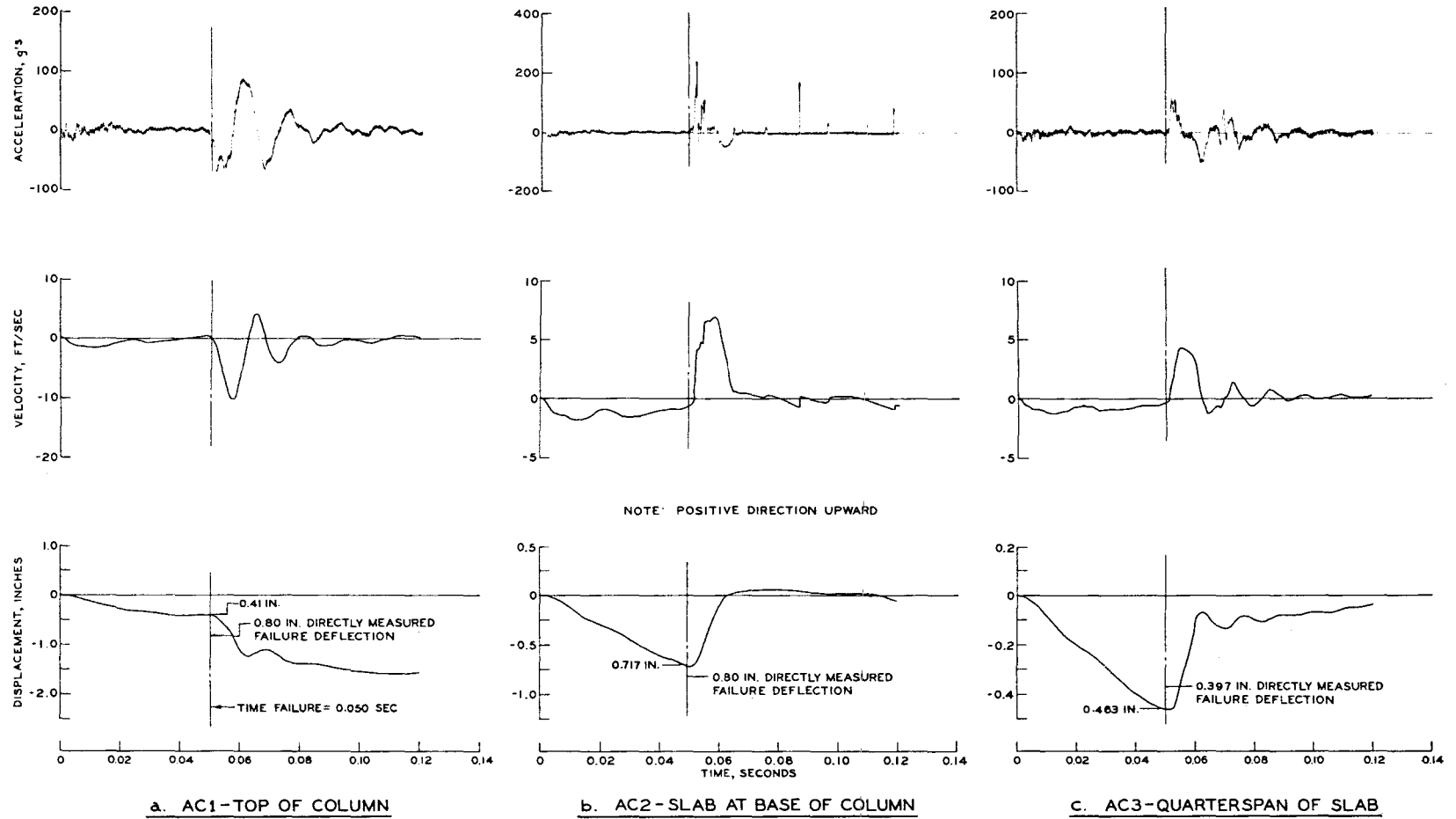


Figure 7.5 Acceleration-, velocity-, and displacement-time curves, Specimen D2150-1.

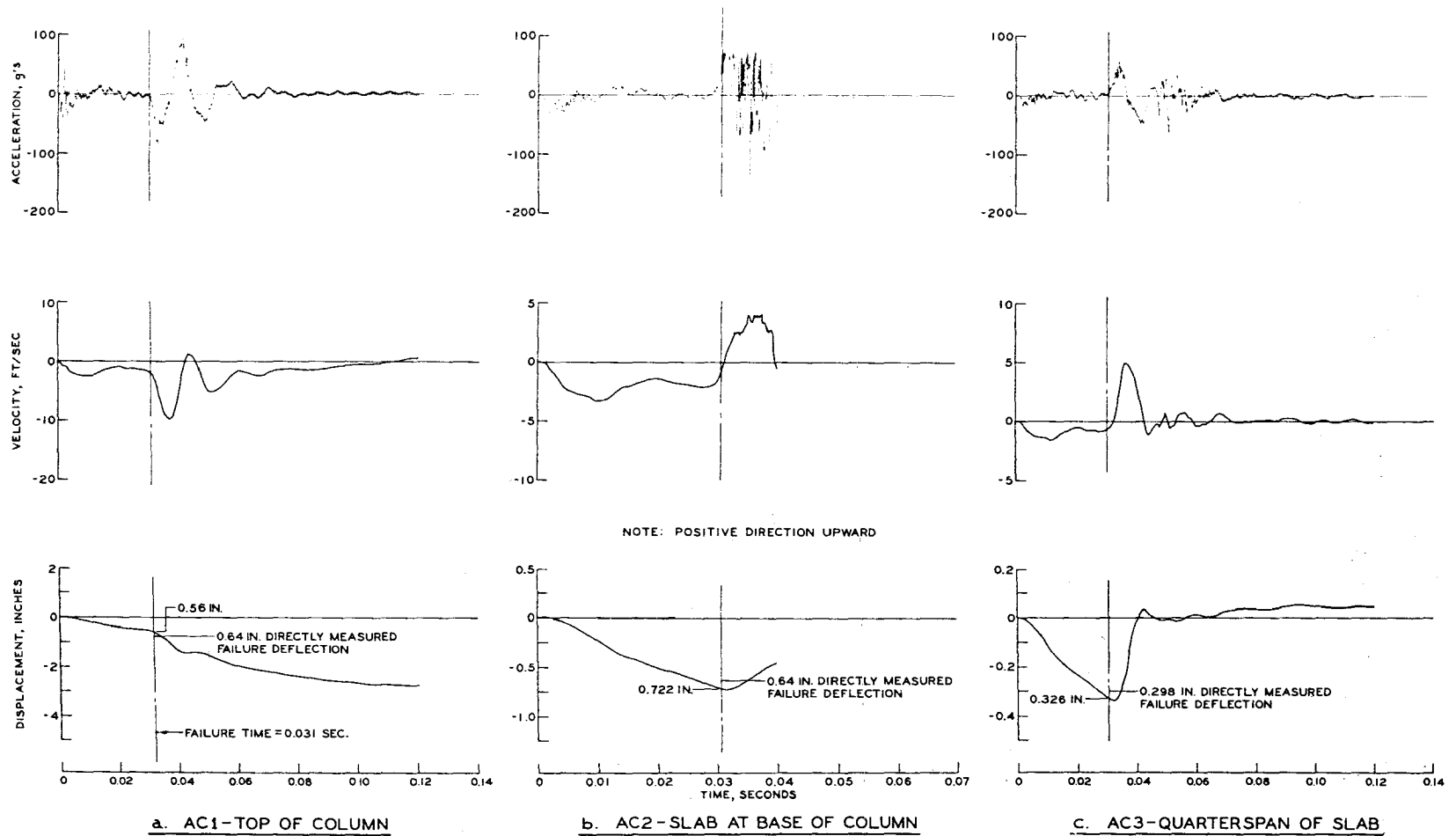


Figure 7.6 Acceleration-, velocity-, and displacement-time curves, Specimen D2150-2.

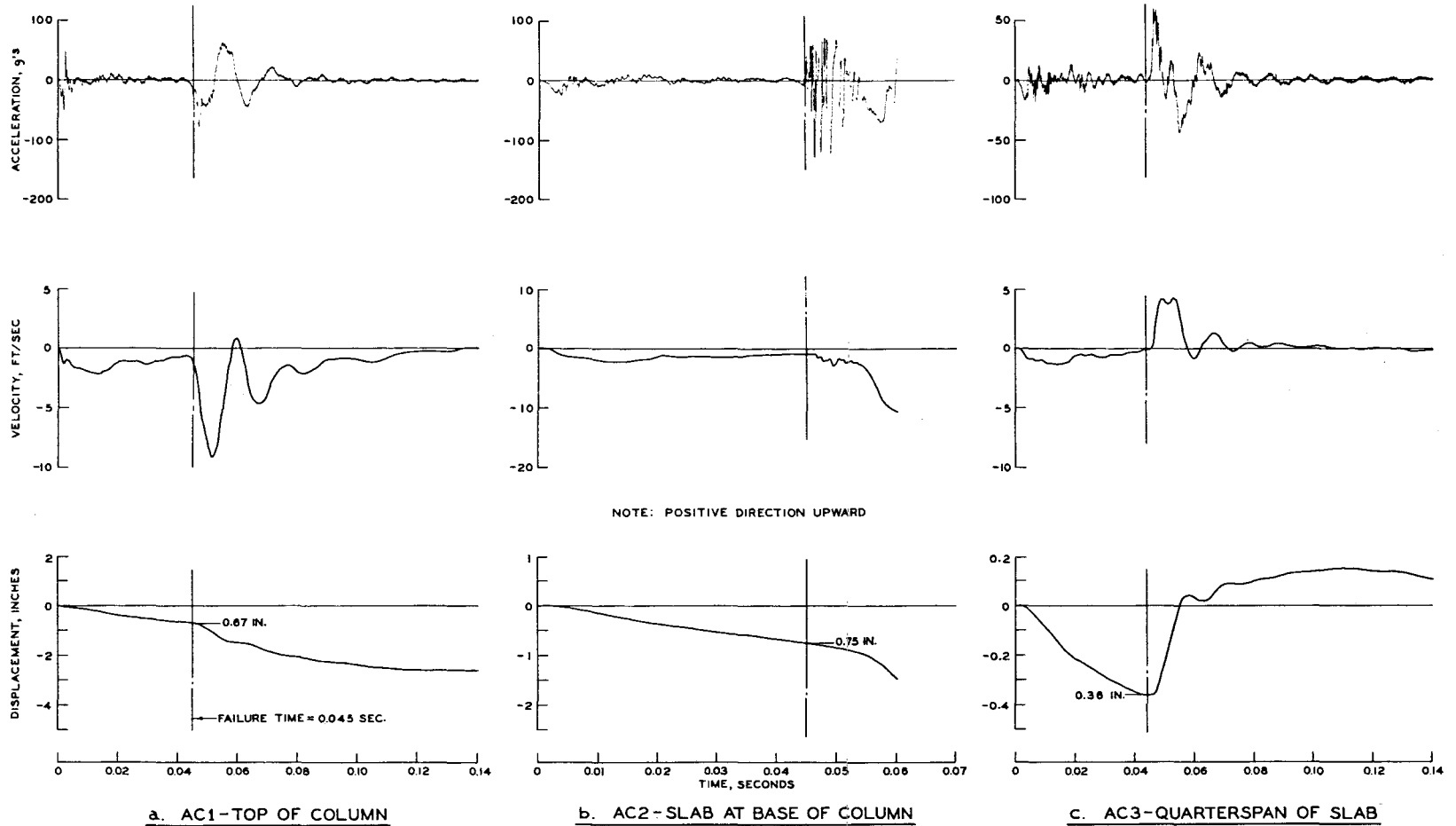


Figure 7.7 Acceleration-, velocity-, and displacement-time curves, Specimen D2150-3.

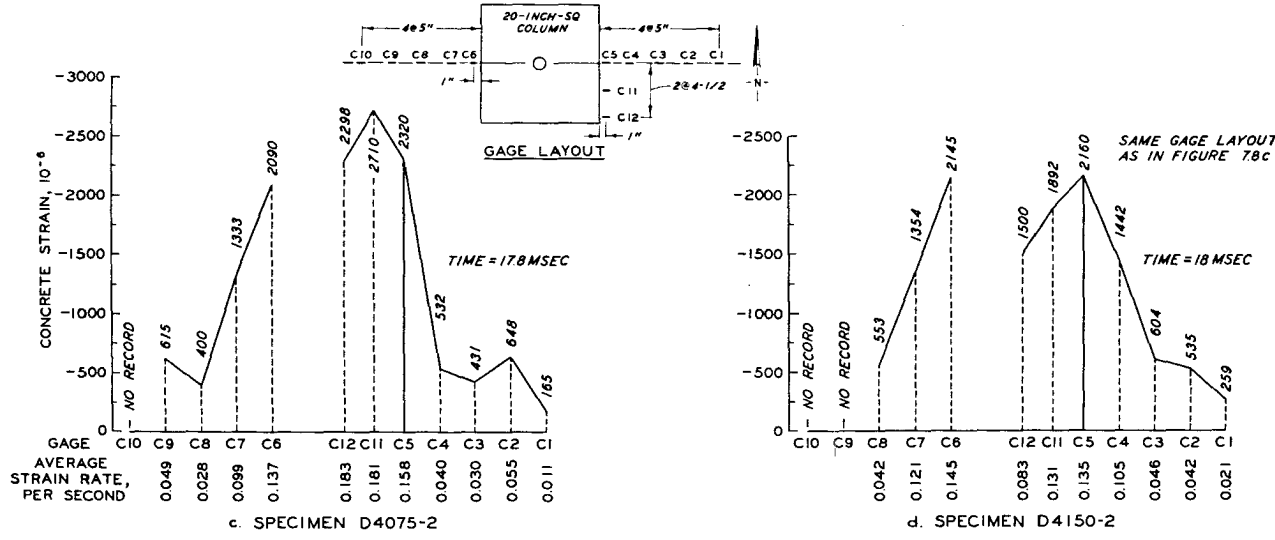
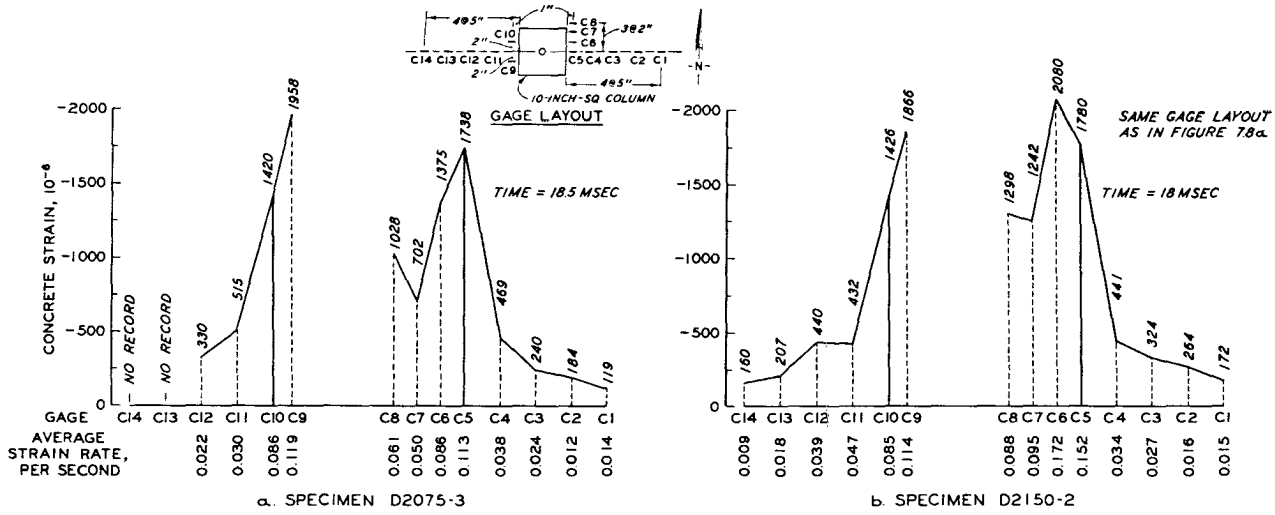
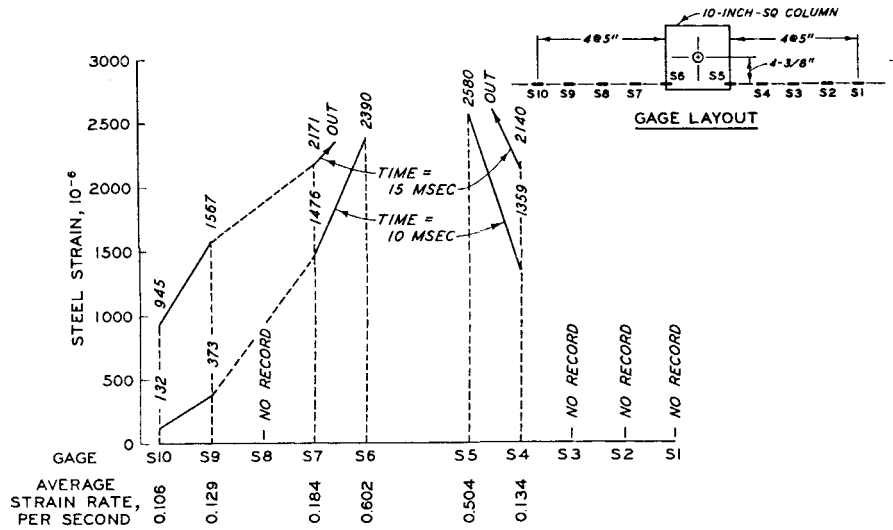
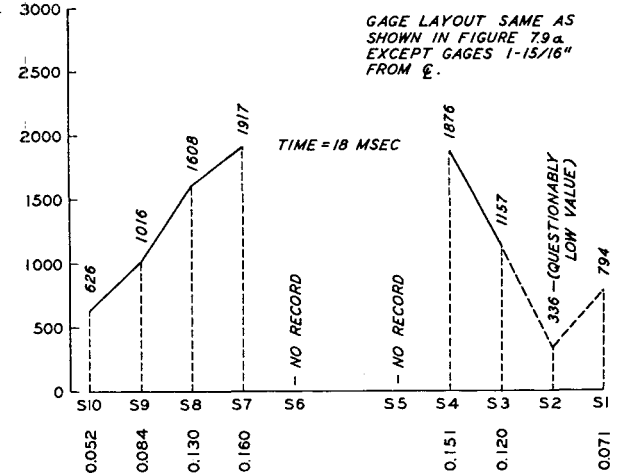


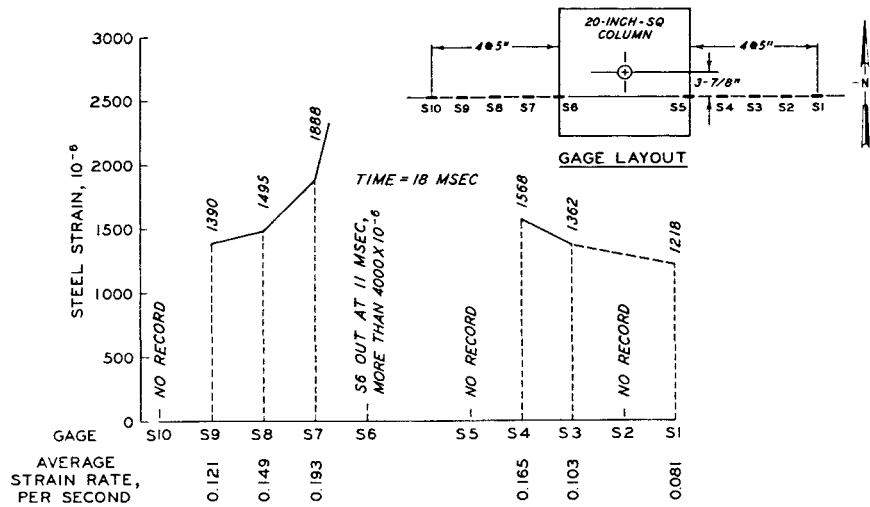
Figure 7.8 Concrete strain distribution and strain rates.



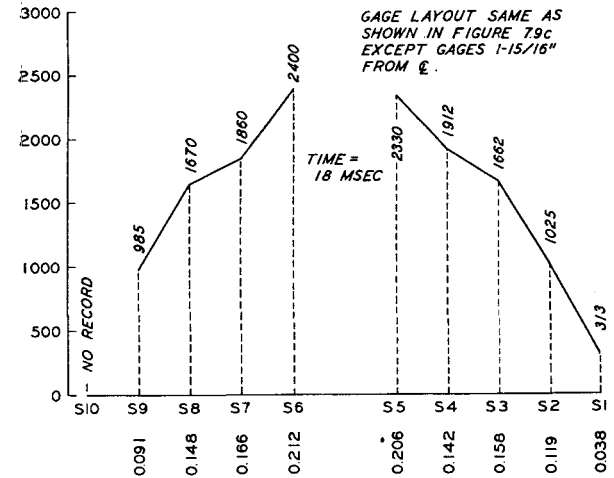
a. SPECIMEN D2075-3



b. SPECIMEN D2150-2



c. SPECIMEN D4075-1



d. SPECIMEN D4150-2

Figure 7.9 Steel strain distribution and strain rates.

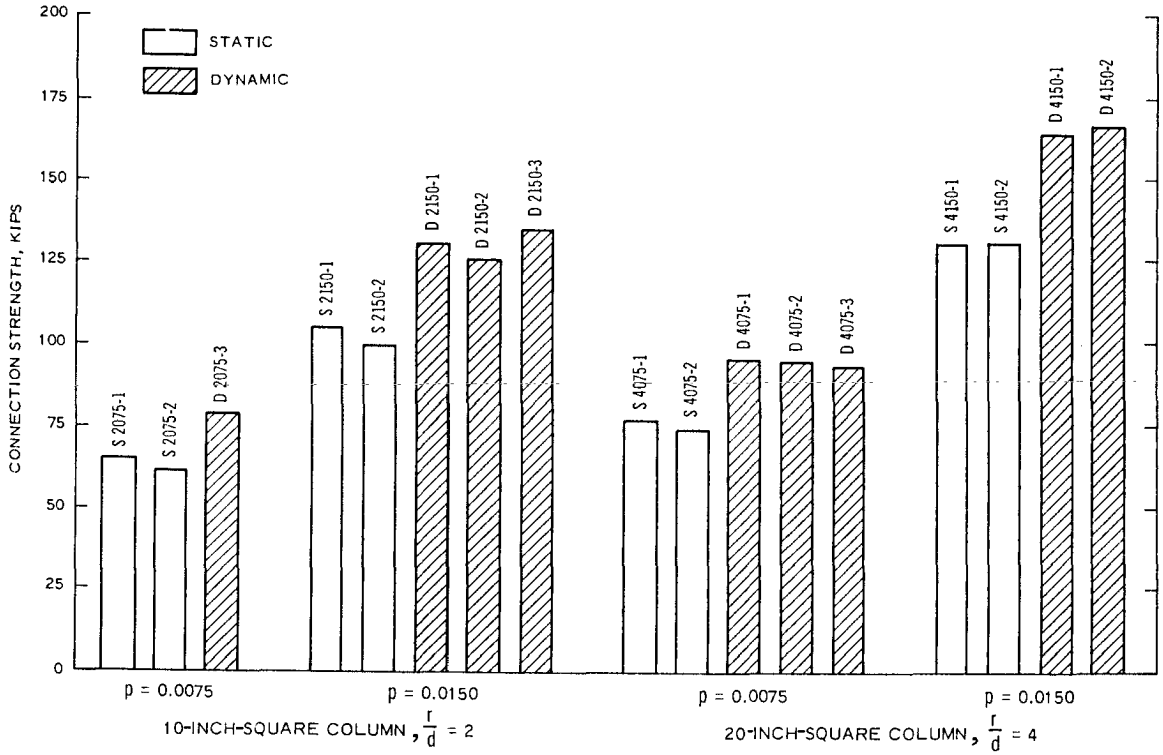
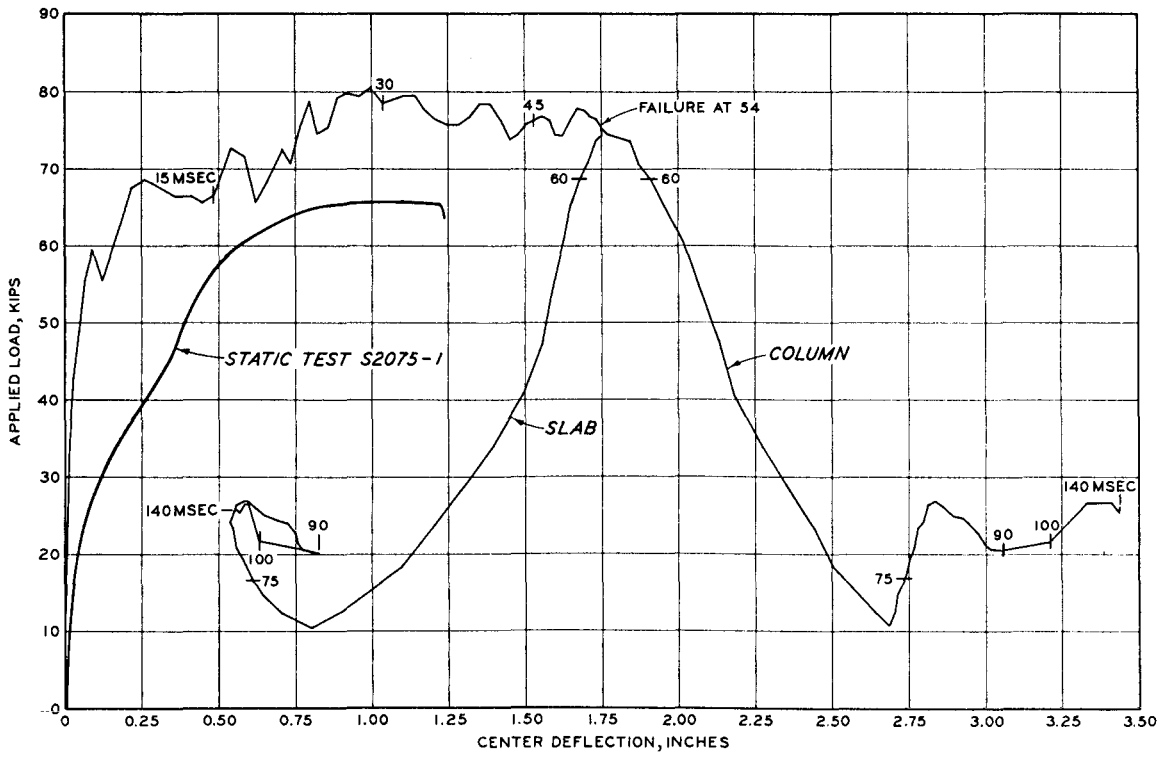
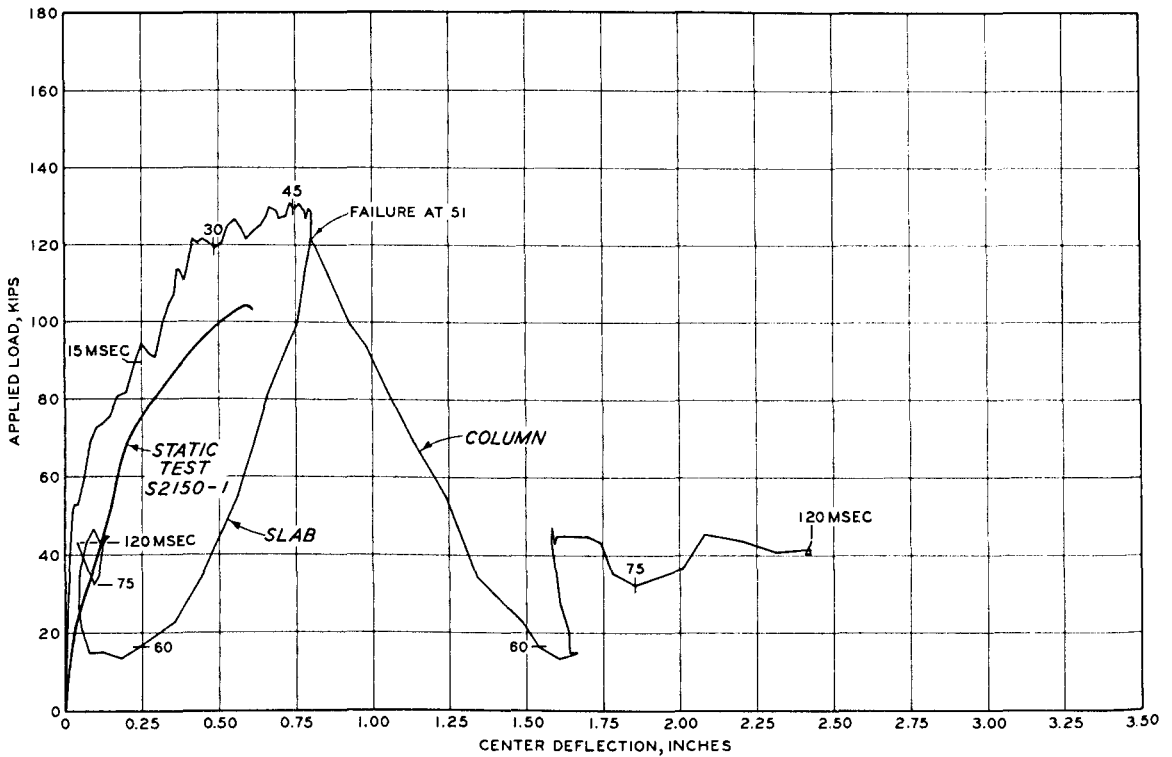


Figure 7.10 Comparison of static and dynamic connection strengths.



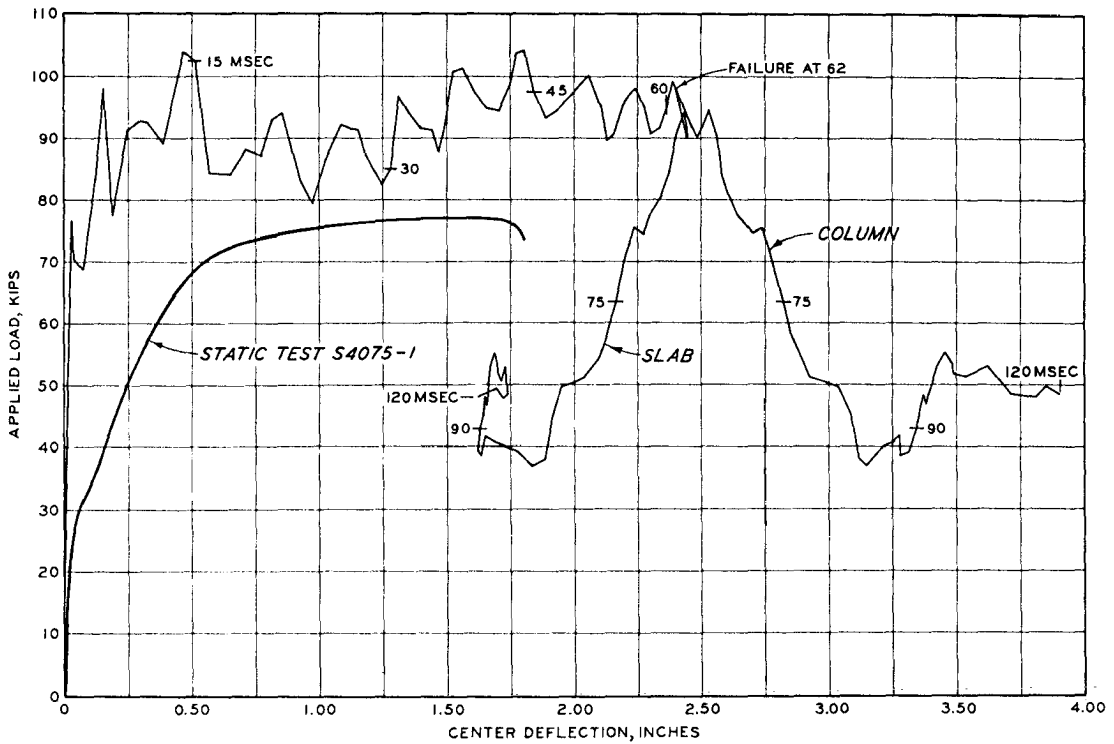


a. SPECIMEN D2075-3

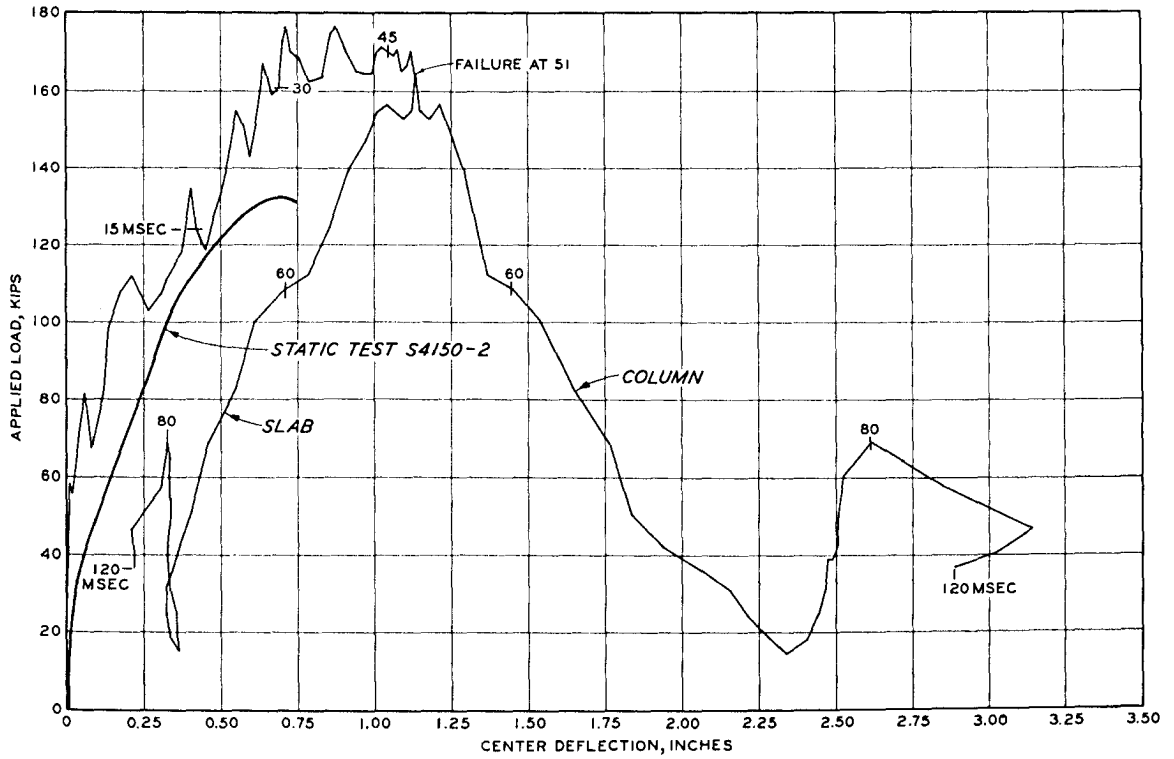


b. SPECIMEN D2150-1

Figure 7.11 Typical applied load-deflection curves, D2000 Series.



a. SPECIMEN S4075-1



b. SPECIMEN D4150-2

Figure 7.12 Typical applied load-deflection curves, D4000 Series.

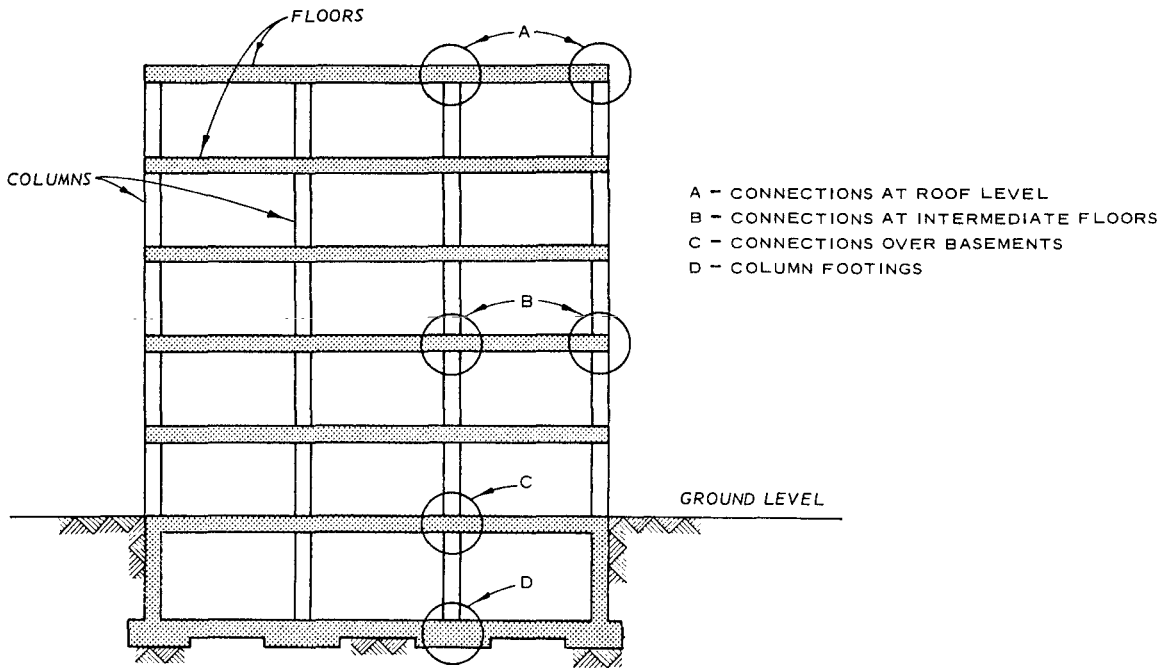
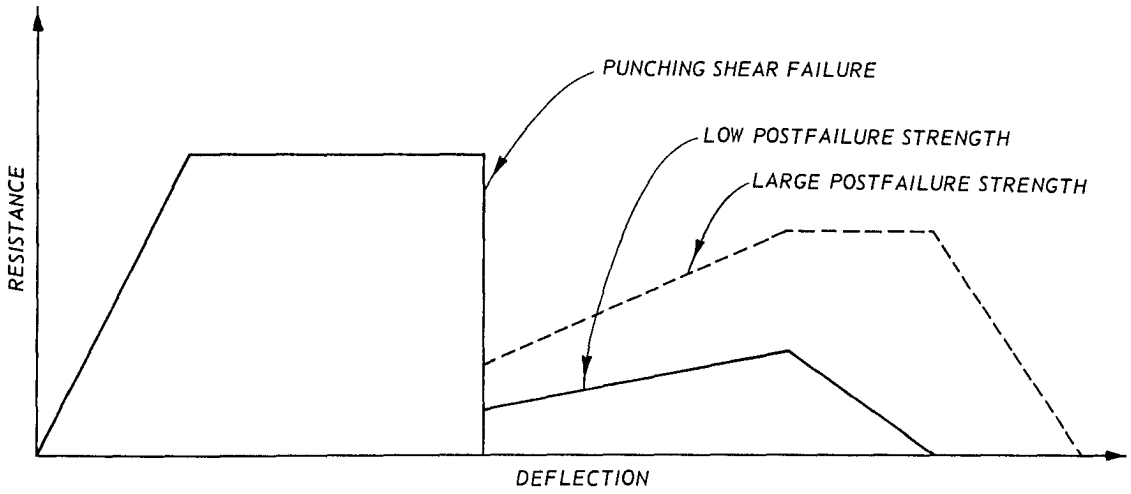
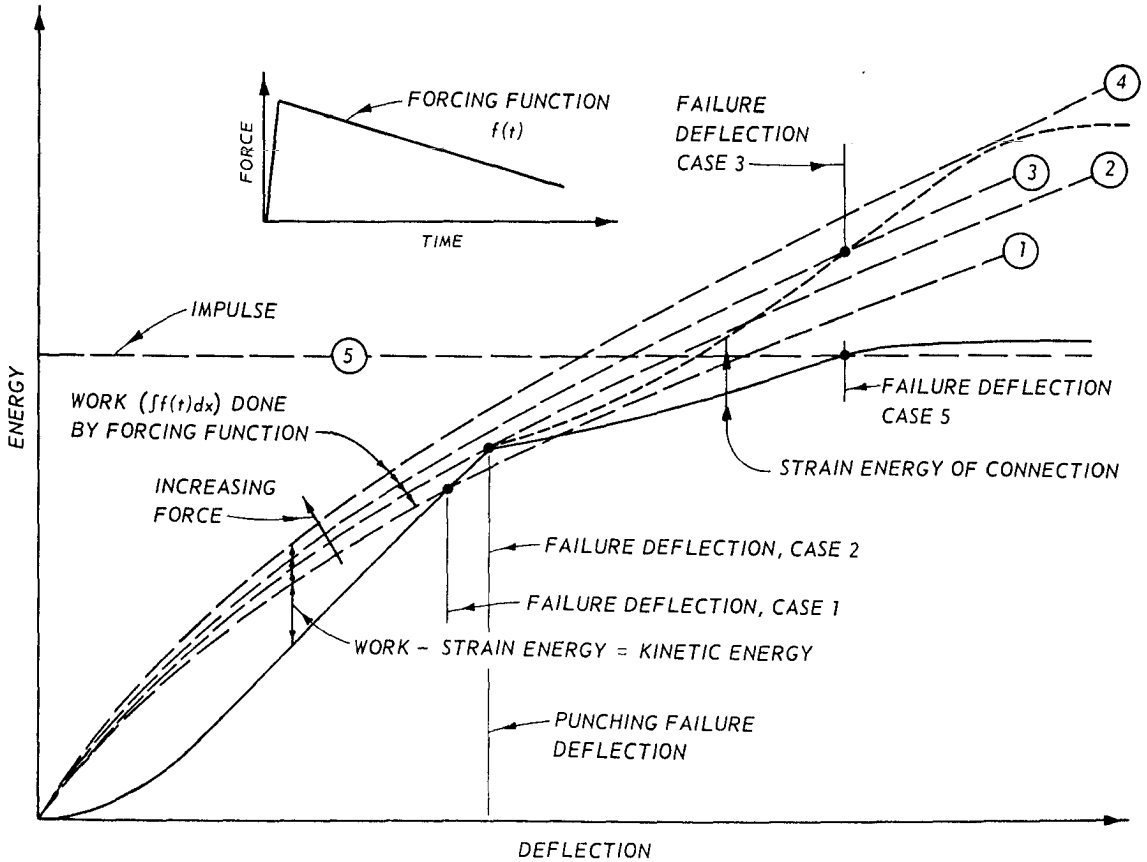


Figure 7.13 Connections in a building.

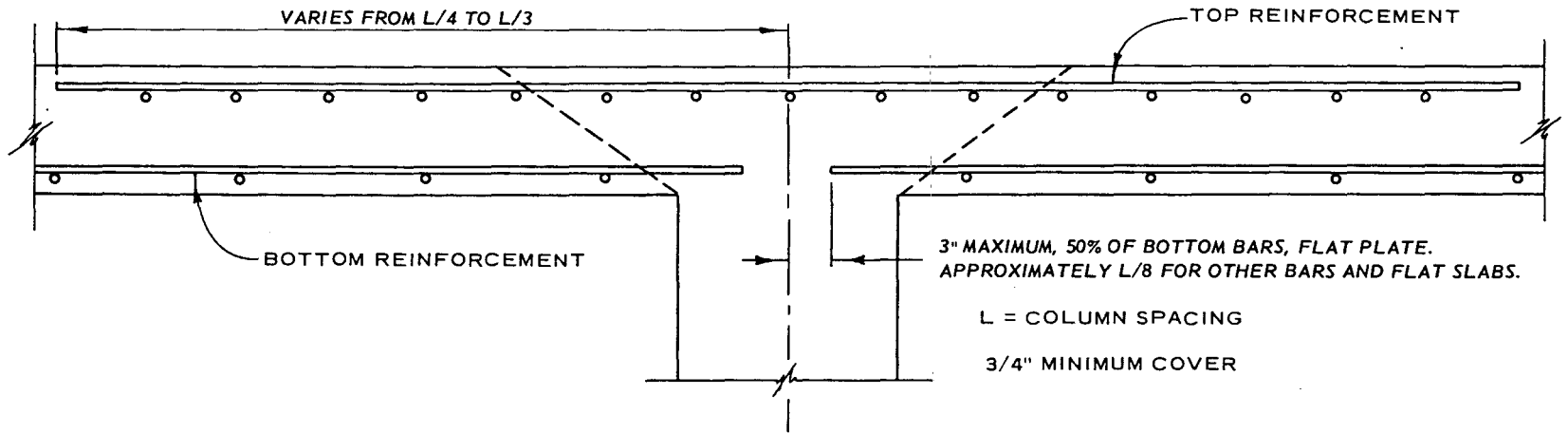


a. CONNECTION RESISTANCE (STRESS-STRAIN) CURVE

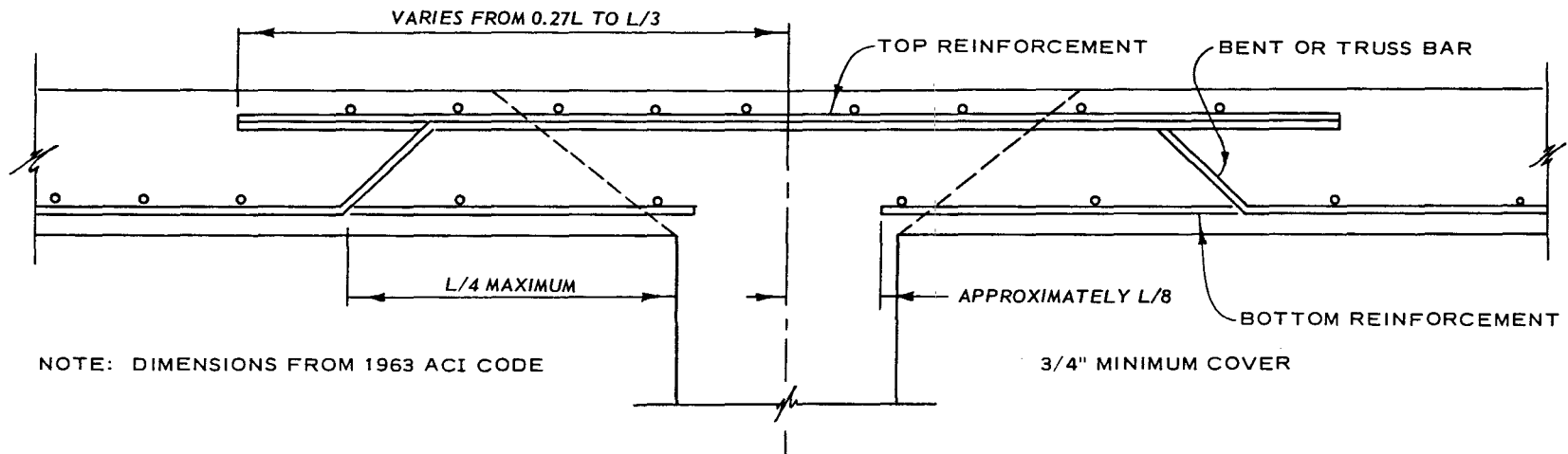


b. ENERGY DIAGRAM

Figure 7.14 Usefulness of postfailure resistance.



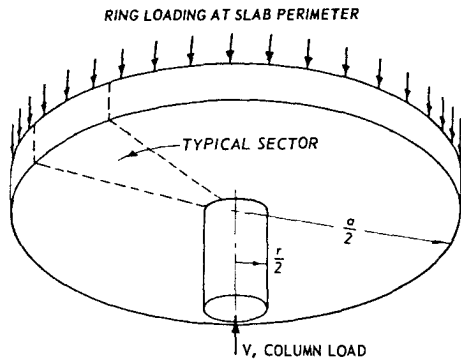
a. STRAIGHT BARS ONLY



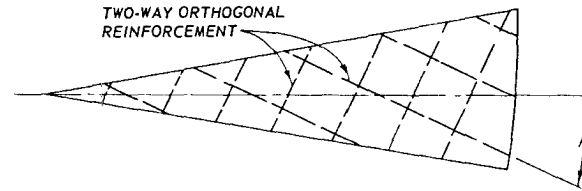
NOTE: DIMENSIONS FROM 1963 ACI CODE

b. STRAIGHT AND BENT BARS

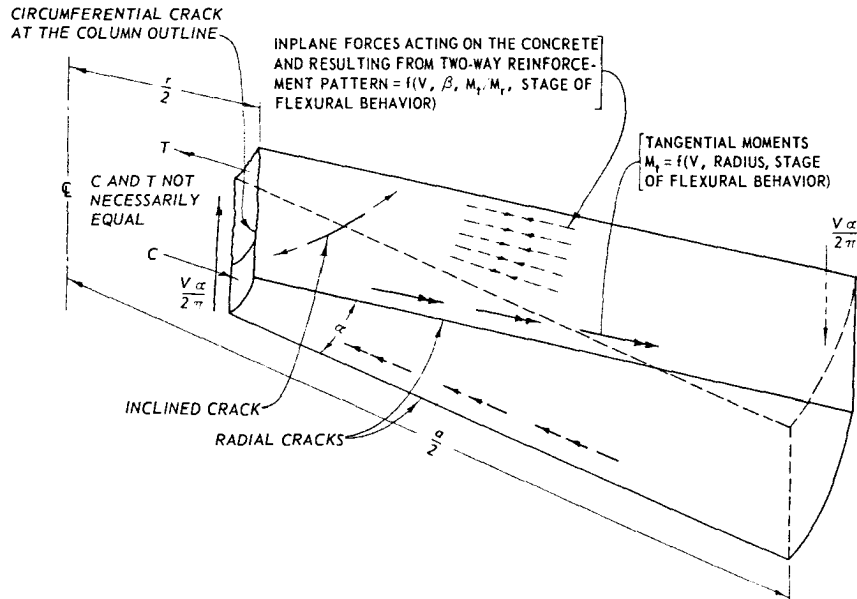
Figure 7.15 Reinforcement in flat plates and flat slabs near columns.



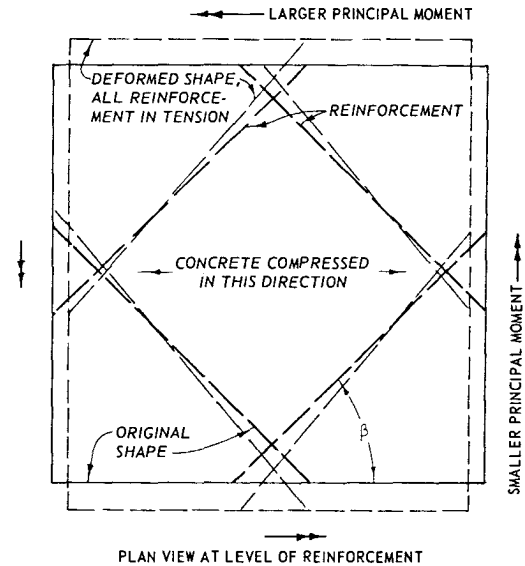
a. CONNECTION MODEL



b. REINFORCEMENT PLAN FOR A SLAB SECTOR



c. CRACKING AND FORCES FOR A SECTOR OF THE MODEL



d. MECHANISM CREATING INPLANE CONCRETE COMPRESSION

Figure 8.1 Idealized connection model.

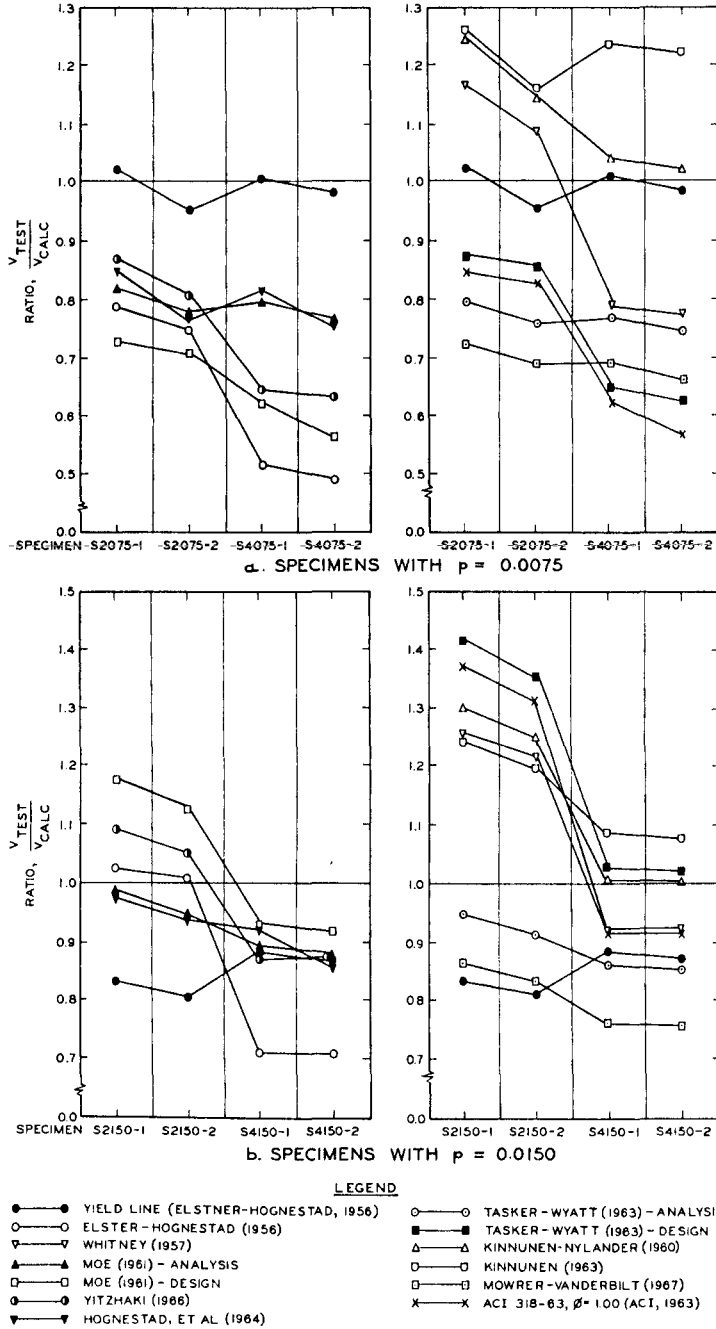


Figure 8.2 Comparison of observed and calculated strengths, static tests.

APPENDIX A  
THE 200-KIP LOADER



## A.1 DESCRIPTION

The 200-Kip Loader is an open-loop hydraulic loading device custom-built for the U. S. Army Engineer Waterways Experiment Station. The loader is capable of producing a load in excess of 200,000 pounds with a rise time as low as 1.5 msec. The maximum stroke is 6 inches. Figure A.1 shows a cutaway view of the loader and the girders that support it over a 4-foot-wide pit.

Specimens to be loaded in compression or flexure are placed below the loader. A tensile tower can be mounted over the loader for conducting tension tests, and reaction structures may be fitted around the loader.

The loader is basically a hydraulic cylinder containing a piston with a loading ram extending in either direction. Fluid chambers above and below the piston, a double rupture disk valve with orifice plate, and an expansion tank complete the system. Control of the system is entirely hydraulic and mechanical.

## A.2 OPERATION

The entire system, except for the expansion tank located below the piston, is filled with a silicone oil having an observed bulk modulus of approximately 140,000 psi. A low-volume high-pressure multiplier is used to pressurize the fluid in the loader system, which is filled with the silicon oil.

A.2.1 Static Loading. Static loads are normally produced by slowly pressurizing the upper chamber and maintaining little or no pressure in the lower chamber.

A.2.2 Dynamic Loadings. Dynamic loadings result from a suddenly created pressure difference across the piston of the loading device.

The following procedure is used:

1. Two rupture disks are installed along with an orifice plate between the air-filled expansion tank and the lower chamber of the loader. These disks are sheet-metal circles with an X scored on the expansion-tank side and with a known range of bursting strength. Disks with a nominal bursting strength of from 65 to 80 percent of the desired lower chamber pressure are selected.

2. Both the lower and upper chambers and the pressure tanks open to the upper chamber are pressurized to a predetermined level. A small pre-load on the specimen is maintained by properly adjusting the upper and lower chamber pressures. This keeps the piston in the proper position and the ram in contact with the specimen. The fluid pressure in the small space between the rupture disks is maintained at about one-half of the lower chamber pressure.

3. The rupture disks are broken, allowing the fluid in the lower chamber to escape into the expansion tank, thus lowering the pressure below the cylinder and creating the dynamic load. The disks are broken by either lowering the pressure between the disks until the upstream disk (nearest the lower chamber) ruptures or by pressurizing the fluid in this space until the downstream disk is broken. In either case, the remaining disk also ruptures as it cannot support the entire lower chamber pressure.

### A.3 CHARACTERISTICS OF THE LOADER

Although the concept and operation of the loader are relatively simple, the response of the system is quite complex.

The loads, strokes, and rise times are controlled primarily by the

volume and pressure of the fluid above the piston, the size of the orifice plate opening, and the properties of the resisting member being loaded.

The concept of potential load will be helpful in describing the loader characteristics. The potential load is the load at a given deflection with no pressure in the lower chamber and the piston at rest. This and other points on the load-stroke curve are shown in Figure A.2.

The maximum potential load is proportional to the pressure level above the piston. The potential load decays linearly with piston movement and at a rate dependent upon the volume of fluid above the piston. More fluid corresponds to a longer and therefore more flexible spring. The maximum stroke of the loader is influenced by both the system fluid volume and the fluid pressure level. The pressure controls the potential load at zero deflection; the fluid volume controls the slope of the decaying potential load-stroke curve.

The stiffness of the system could be varied from 42,000 to 265,000 lb/in with the tanks available during this investigation.

The size of the orifice opening and the stiffness of the loaded specimen act interdependently to control the rise time of the load. The shape of the loading curve cannot be directly controlled.

A larger orifice opening will allow fluid from the lower chamber to enter the empty expansion chamber more rapidly, resulting in a quicker relief of the lower chamber pressure and smaller rise times.

The constriction offered by the orifice plate and the ruptured disks prevent the lower chamber pressure from instantaneously dropping to zero. Thus the load may be considerably less than the potential load at that deflection.

A more flexible specimen will require more piston movement to obtain a

given load, thus requiring more fluid to pass through the orifice and thereby increasing the load rise time. This effect decreases as the loading rate increases.

If the rise time is small relative to the natural period of the specimen being loaded, the specimen appears to be very stiff and little piston movement and fluid flow from the lower chamber is needed to relieve most of the pressure in the lower chamber. With a rigid specimen, only enough fluid need escape to allow the pressurized fluid below the piston to expand to its nonpressurized volume. The rapid pressure drop in the lower chamber allows the applied load to quickly approach the potential load. The loader may be described as operating in the load-controlled mode; the applied load is very dependent upon the initial upper chamber pressure level.

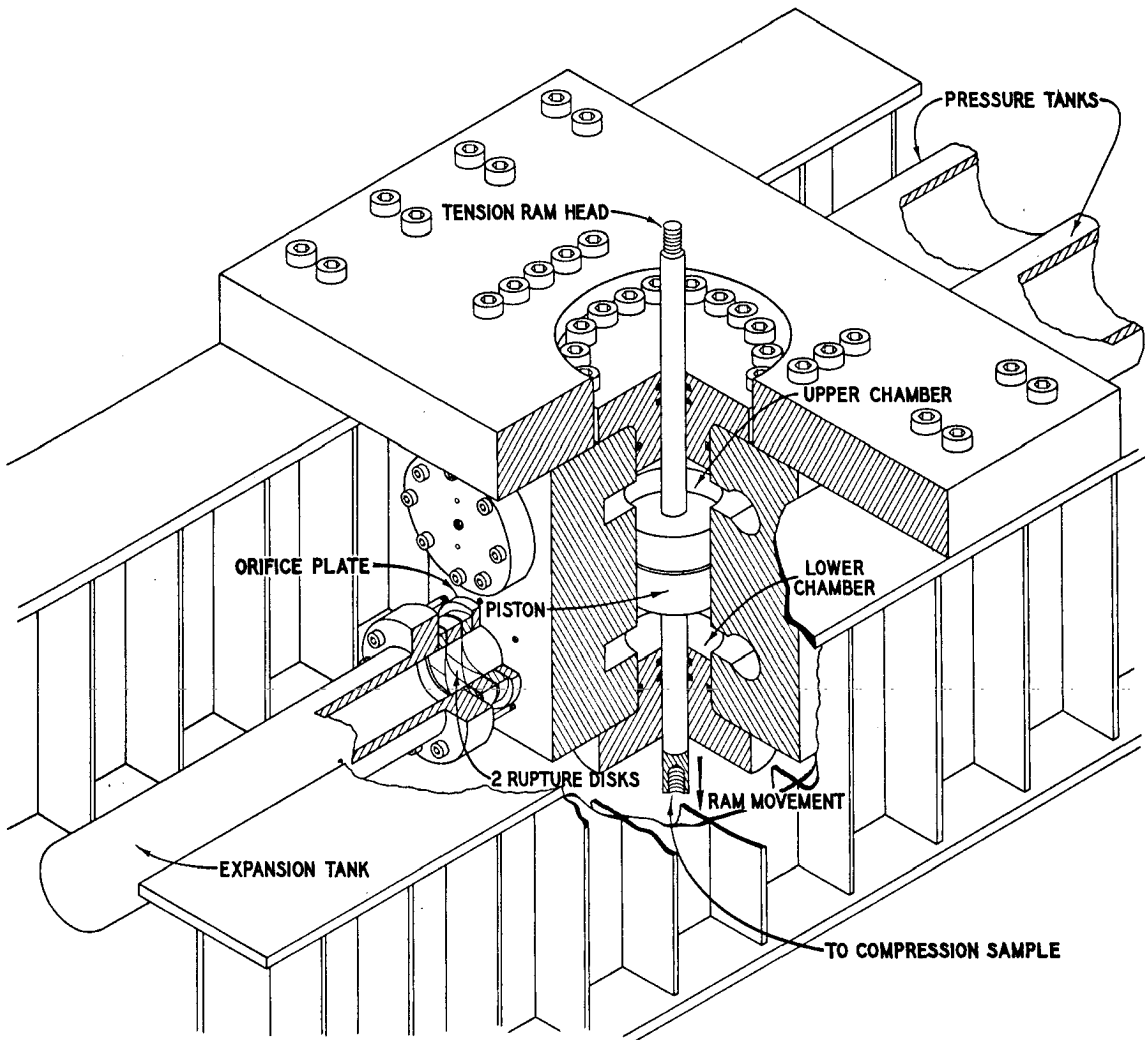
When the rise time of the load is long relative to the natural period of the specimen, the inertial resistance of the specimen is small and deflection (stroke) is needed for the specimen being tested to develop resistance to the ram movement. The stroke rate is controlled primarily by the rate at which fluid can escape from the lower pressure chamber. The lower chamber pressure is not quickly relieved. An obvious extreme of this deflection-controlled mode would be obtained by using a tiny orifice opening which would result in the piston moving very slowly (a static test). Large variations in the original fluid pressure level of the loader will have little to no effect on the magnitude of the load applied onto the specimen.

Most tests will be in a region intermediate to the load- and deflection-controlled mode.

The ram will stop at an equilibrium position only. After a specimen

failure, the piston and ram stops at a deflection where the potential load equals the residual resistance of the specimen, if any. This stroke can be several inches beyond the failure deflection. The load remains on a non-failing specimen until the fluid pressure is relieved.

The mass and dynamic properties of the loader will influence the loads and behavior obtained. The natural period of the system is controlled primarily by the fluid volume in the system. With the two large pressure tanks, the observed fundamental period is near 6 msec.



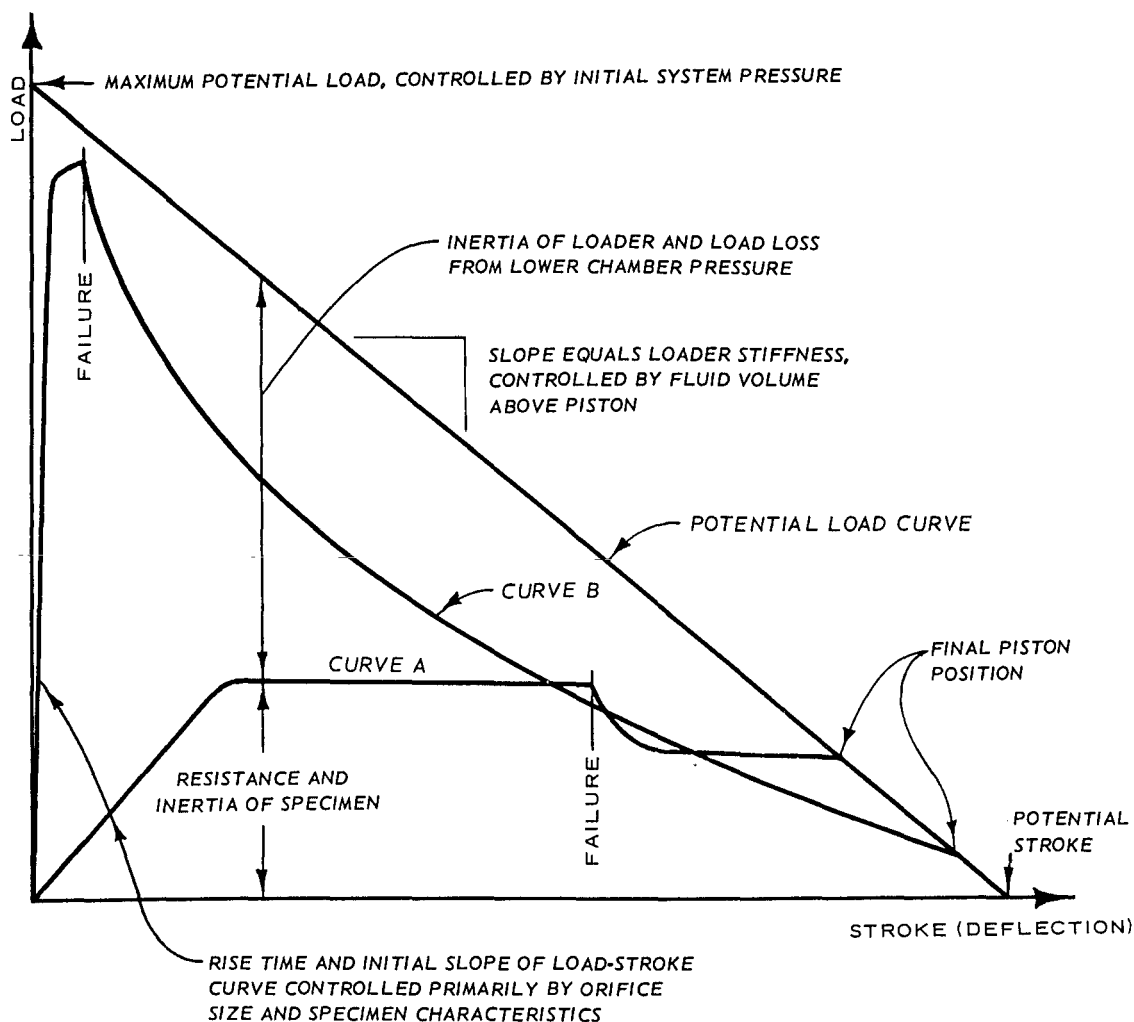
### CHARACTERISTICS

1. PEAK DYNAMIC LOAD: 200,000 LB IN LESS THAN 2 MSEC.
2. RISE TIME: 1 TO 200 MSEC.
3. HOLD TIME: 0 TO 200 MSEC.
4. DELAY TIME: 15 TO 500 MSEC.

### APPLICATIONS

1. DETERMINATION OF DYNAMIC STRESS-STRAIN PROPERTIES OF CONSTRUCTION MATERIALS.
2. DYNAMIC TEST OF STRUCTURAL ELEMENTS:
  - a. BEAMS UP TO 18 FEET IN LENGTH.
  - b. COLUMNS UP TO 8 FEET IN LENGTH.
  - c. TENSILE SPECIMENS UP TO 3 FEET IN LENGTH.
  - d. STRUCTURAL CONNECTIONS AND FRAMES.

Figure A.1 Cutaway view of the 200-Kip Loader.



CURVE A: LOAD APPLIED ON A DUCTILE SPECIMEN WITH CONSIDERABLE POST-FAILURE STRENGTH AND A NATURAL PERIOD SMALLER THAN THE RISE TIME (DEFLECTION-CONTROLLED MODE).

CURVE B: LOAD APPLIED ON A BRITTLE SPECIMEN WITH A NATURAL PERIOD MUCH LONGER THAN THE RISE TIME (LOAD-CONTROLLED MODE).

Figure A.2 Potential and actual applied load-stroke curves.

APPENDIX B  
DATA FROM THE STATIC TESTS



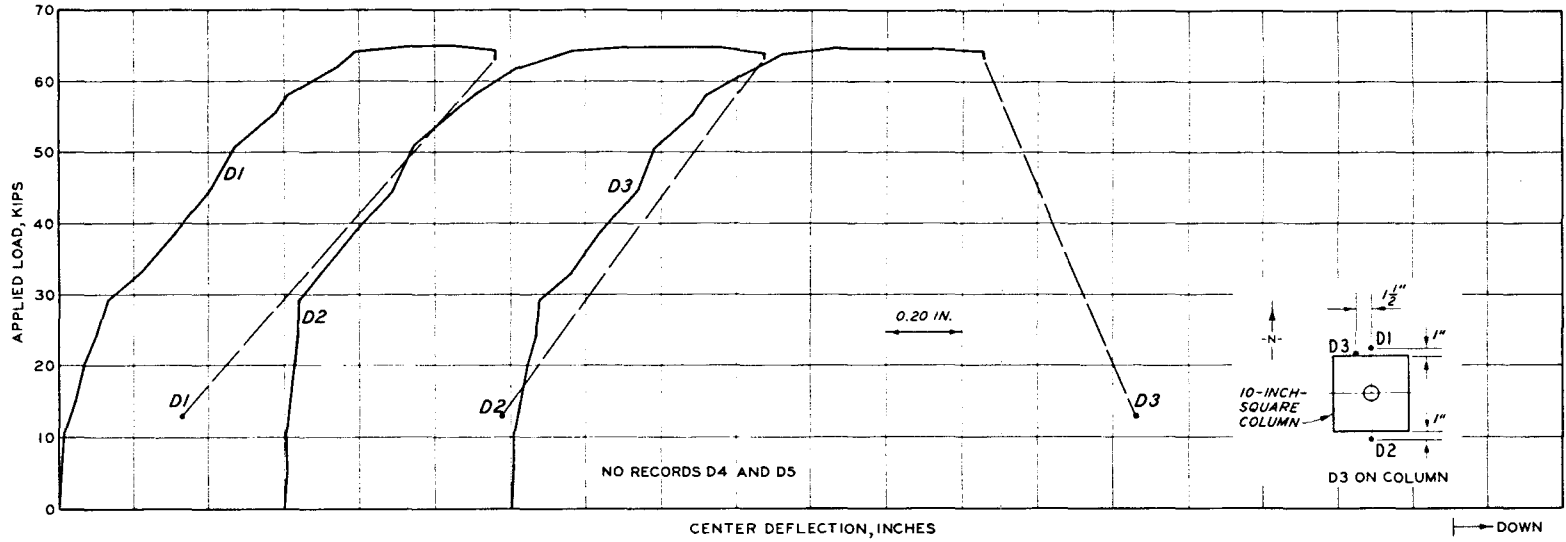
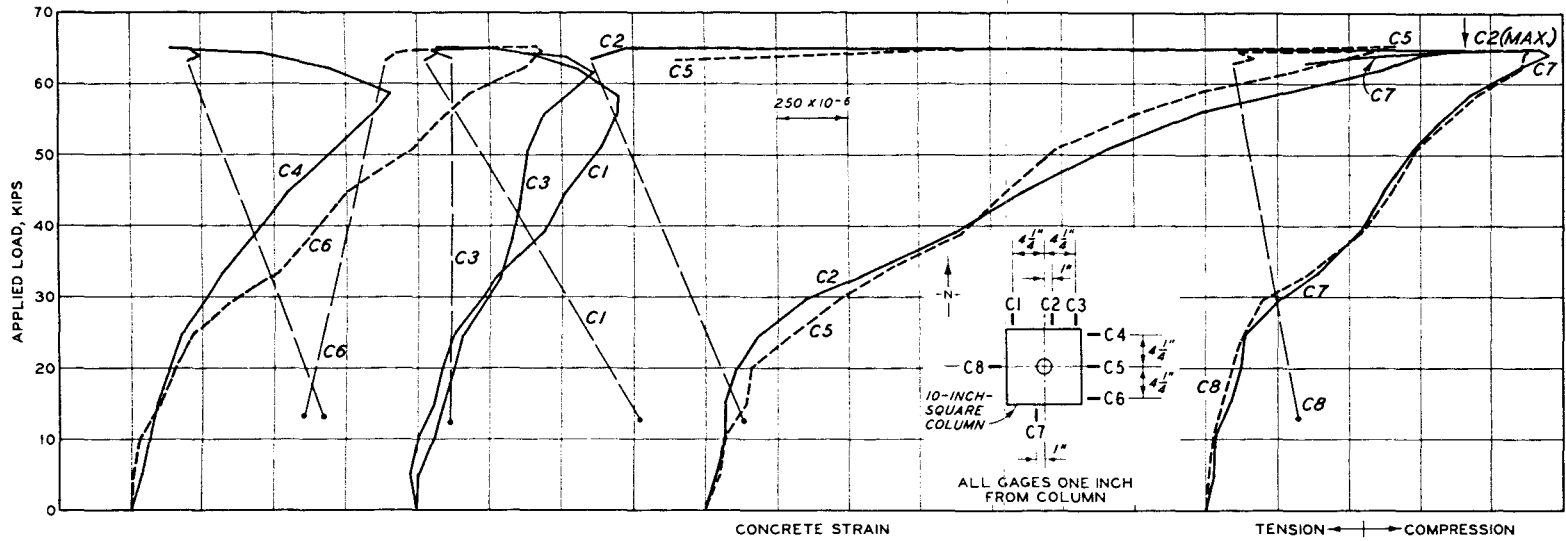


Figure B.1 Deflections and concrete strains, Specimen S2075-1.

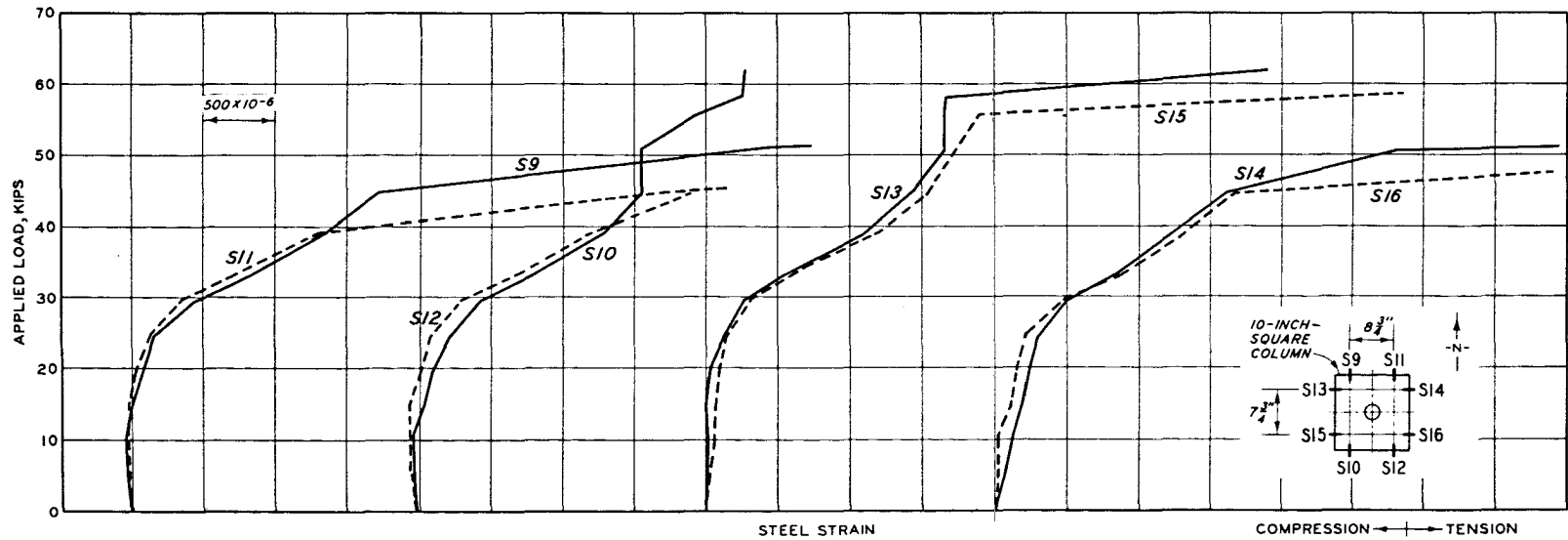
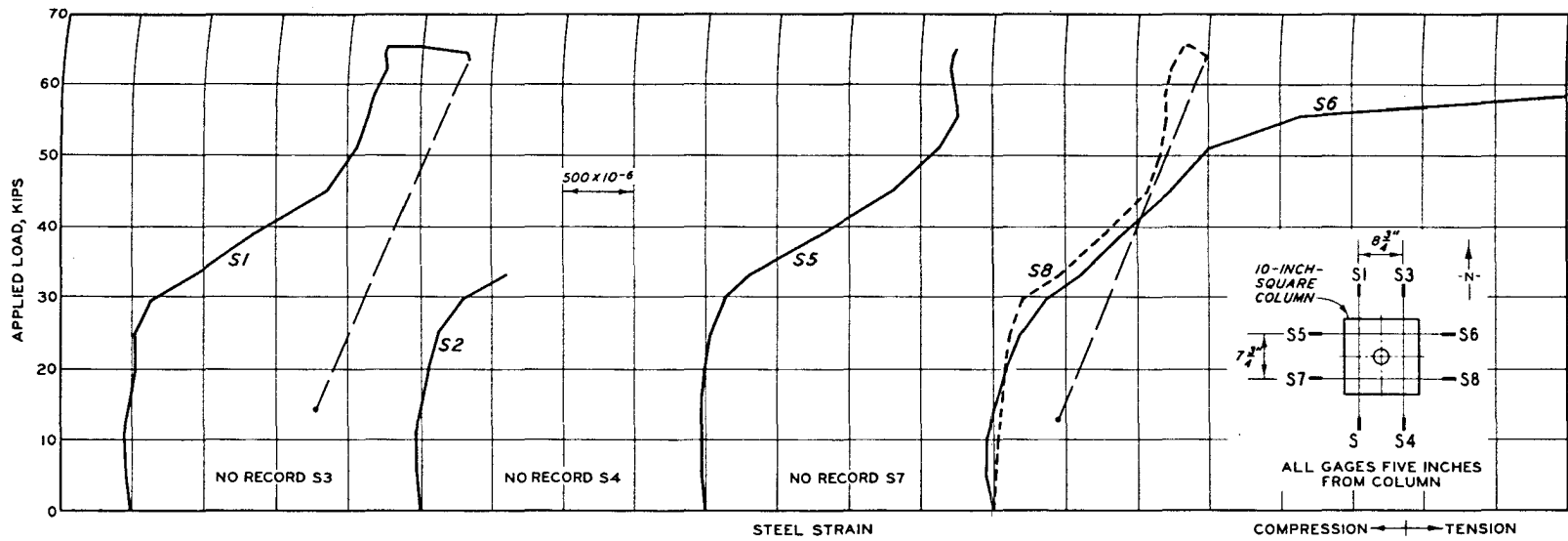


Figure B.2 Steel strains, Specimen S2075-1.

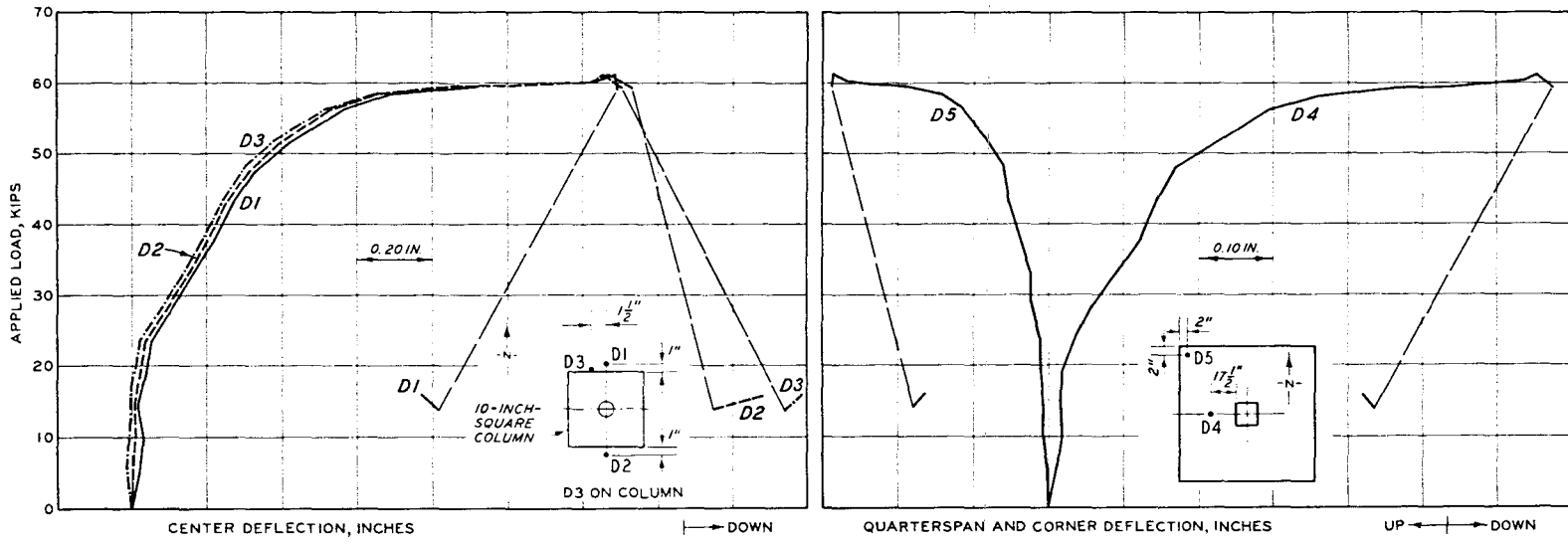
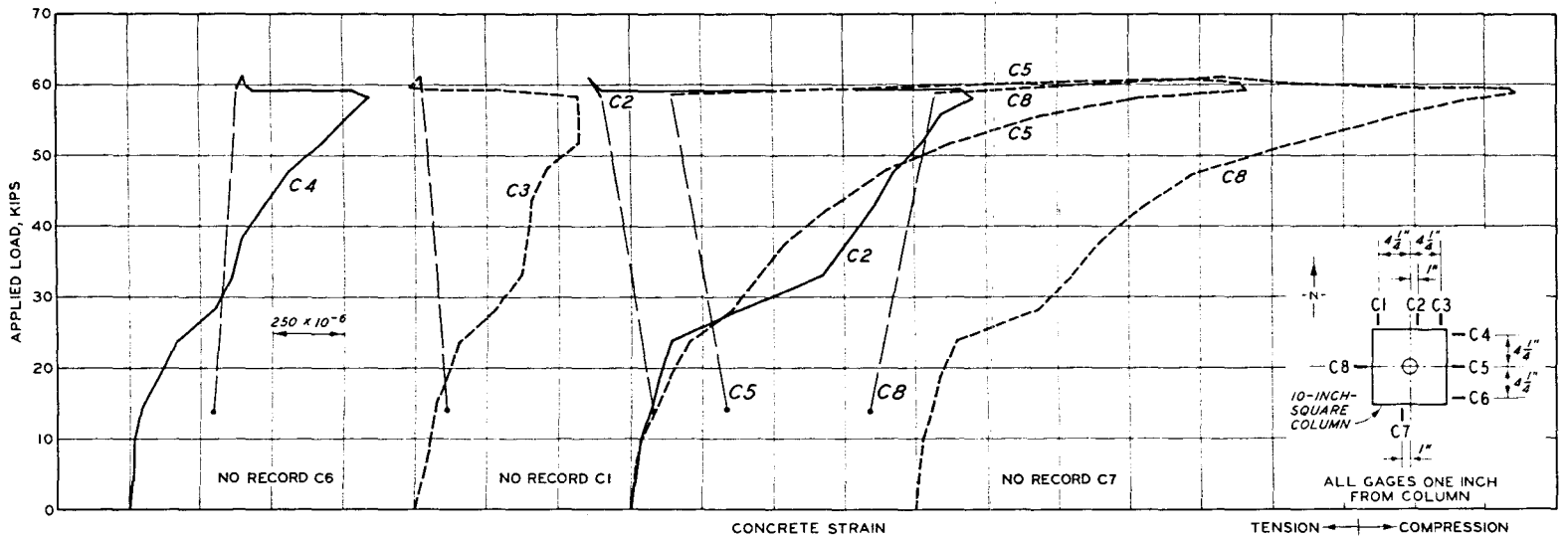


Figure B.3 Deflections and concrete strains, Specimen S2075-2.

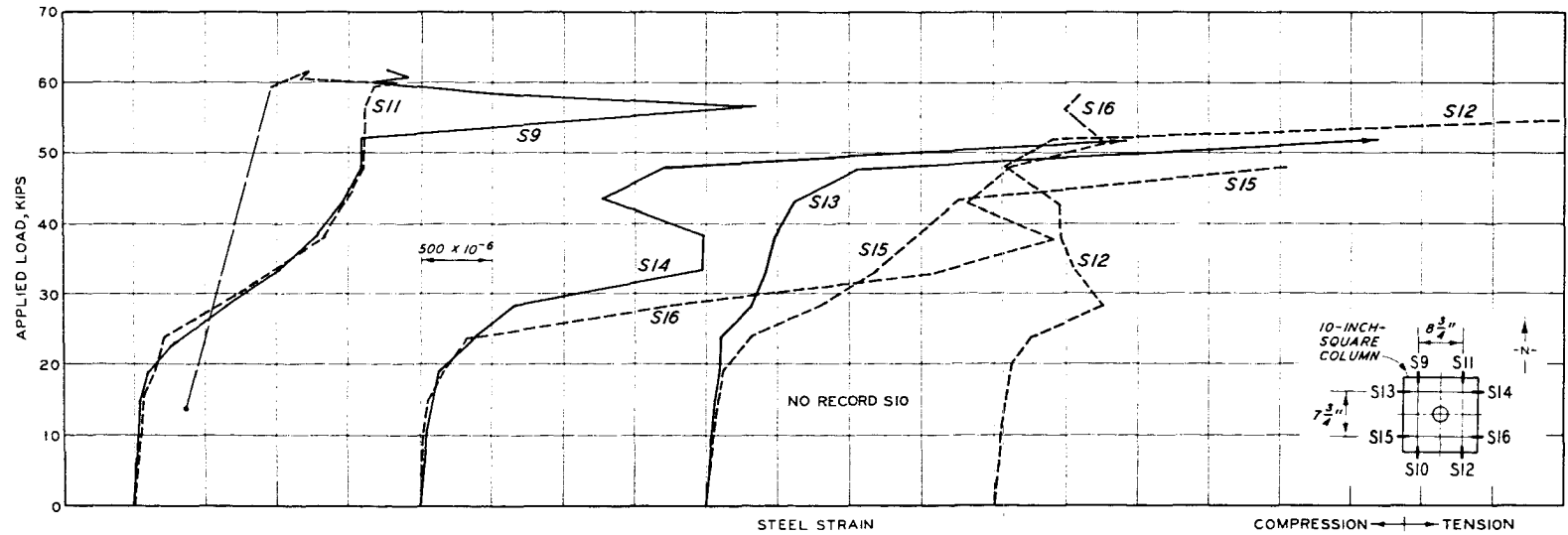
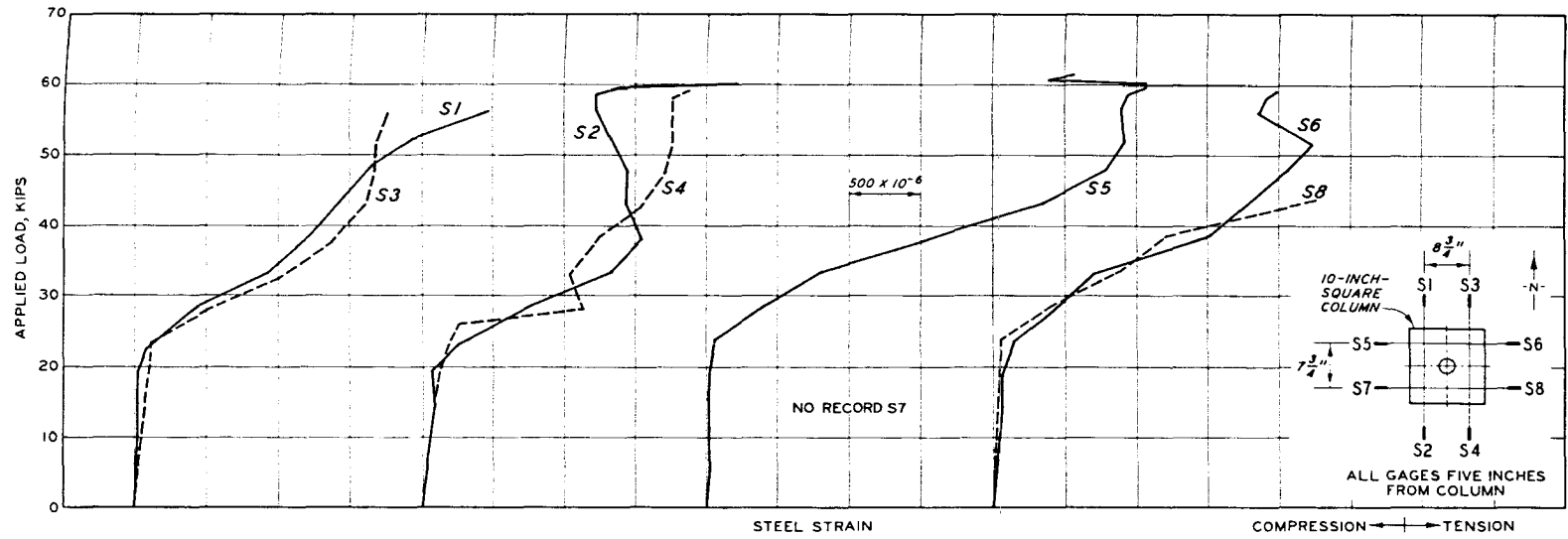


Figure B.4 Steel strains, Specimen S2075-2.

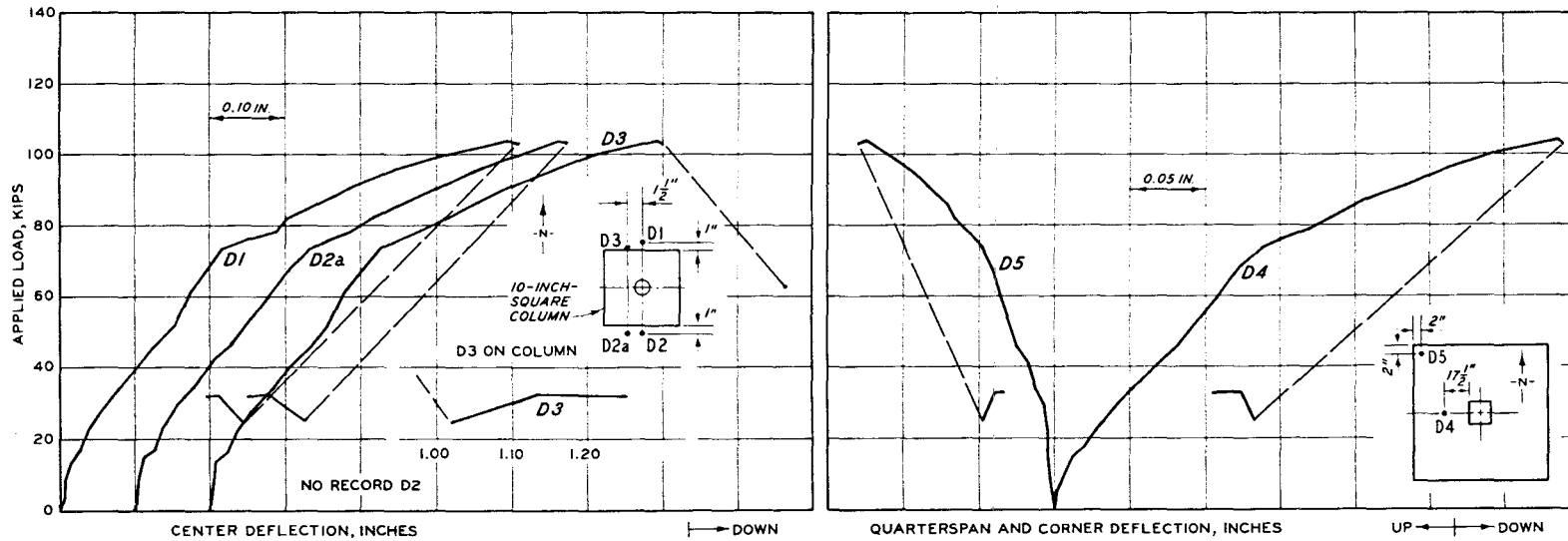
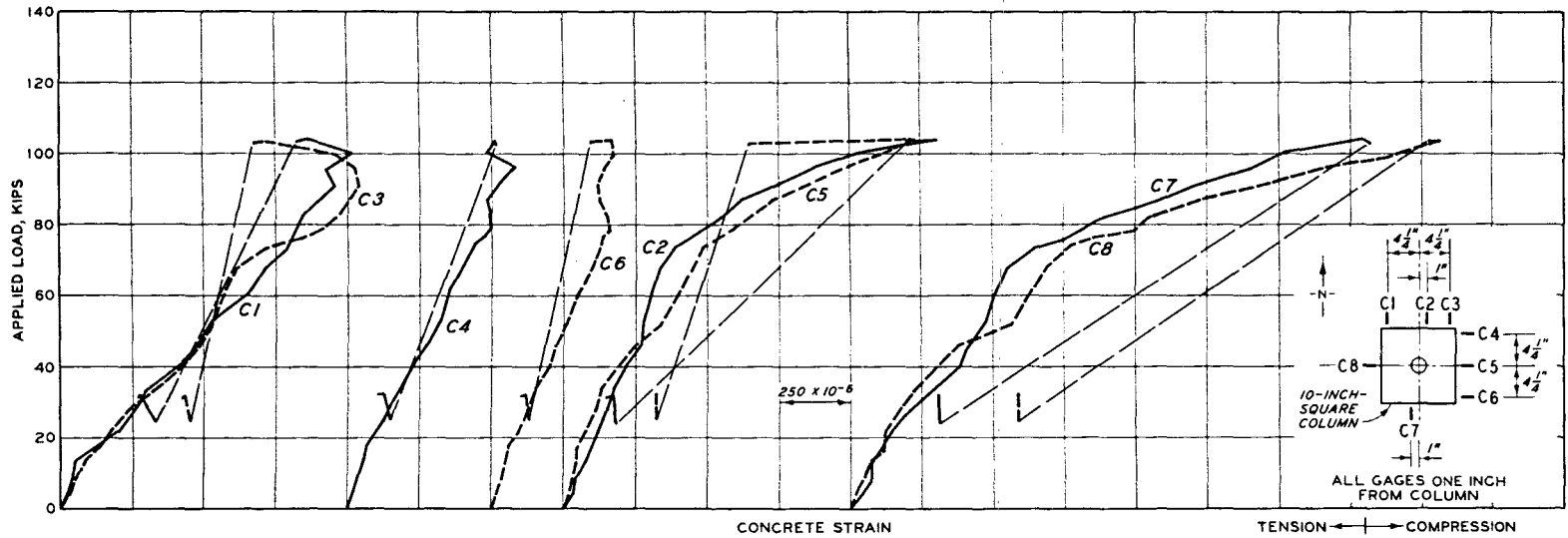


Figure B.5 Deflections and concrete strains, Specimen S2150-1.

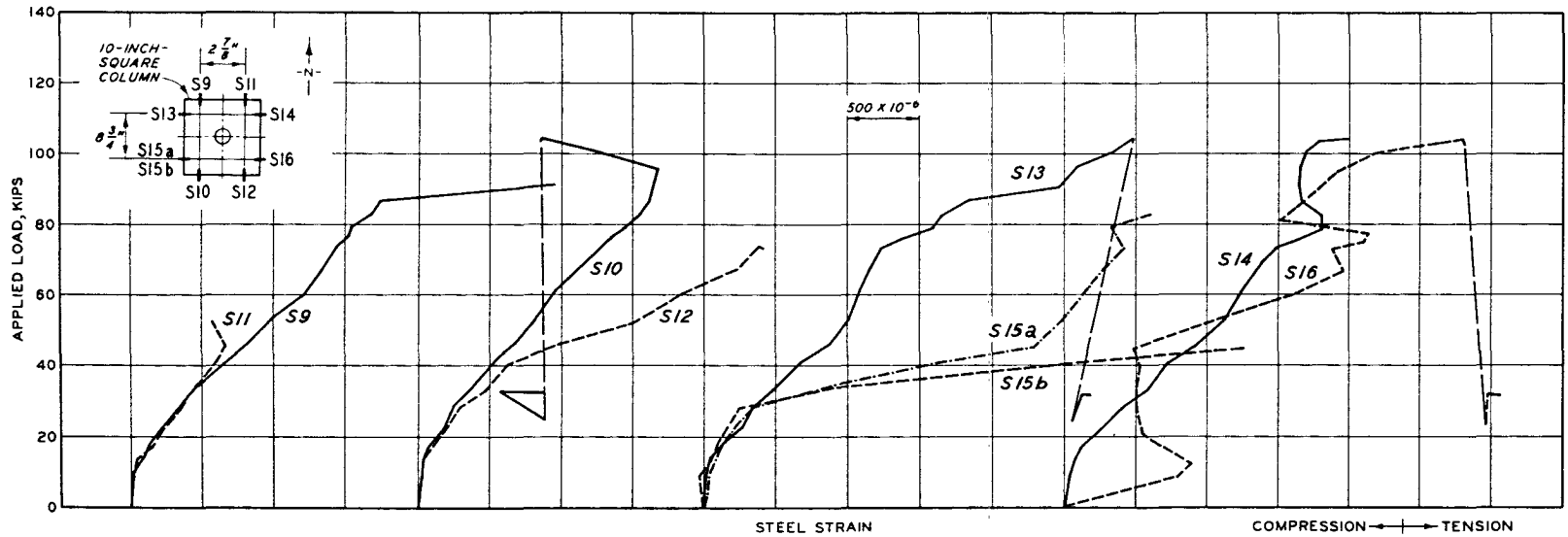
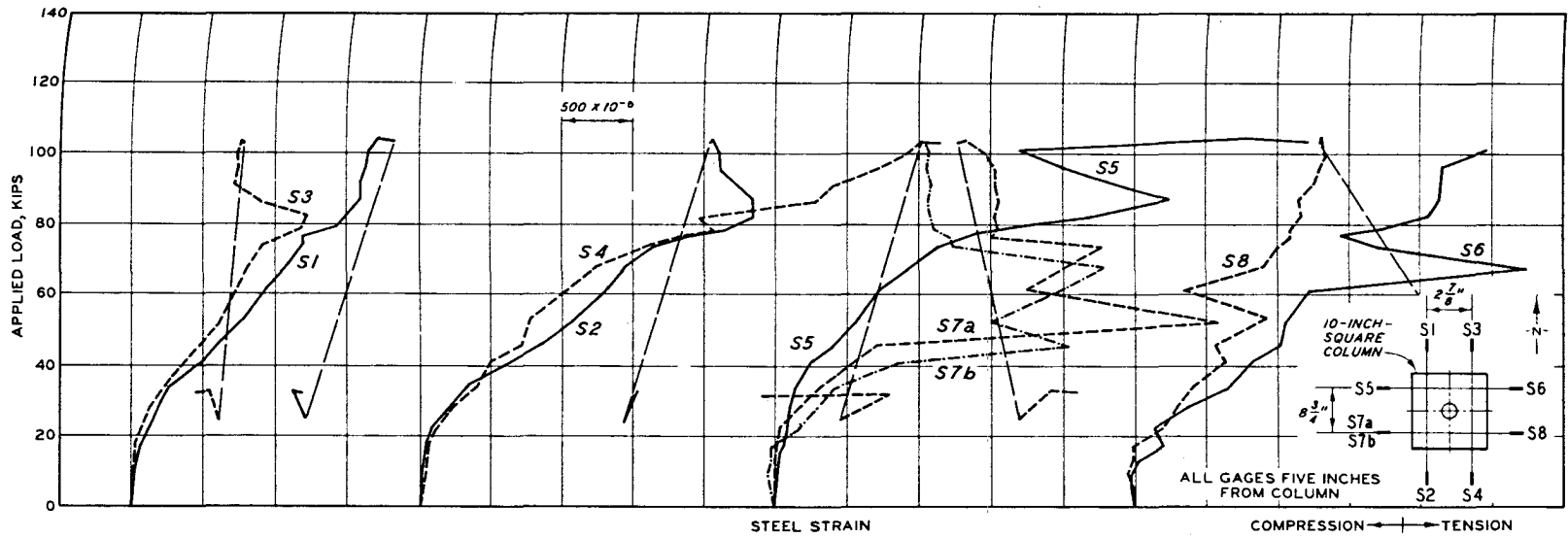


Figure B.6 Steel strains, Specimen S2150-1.

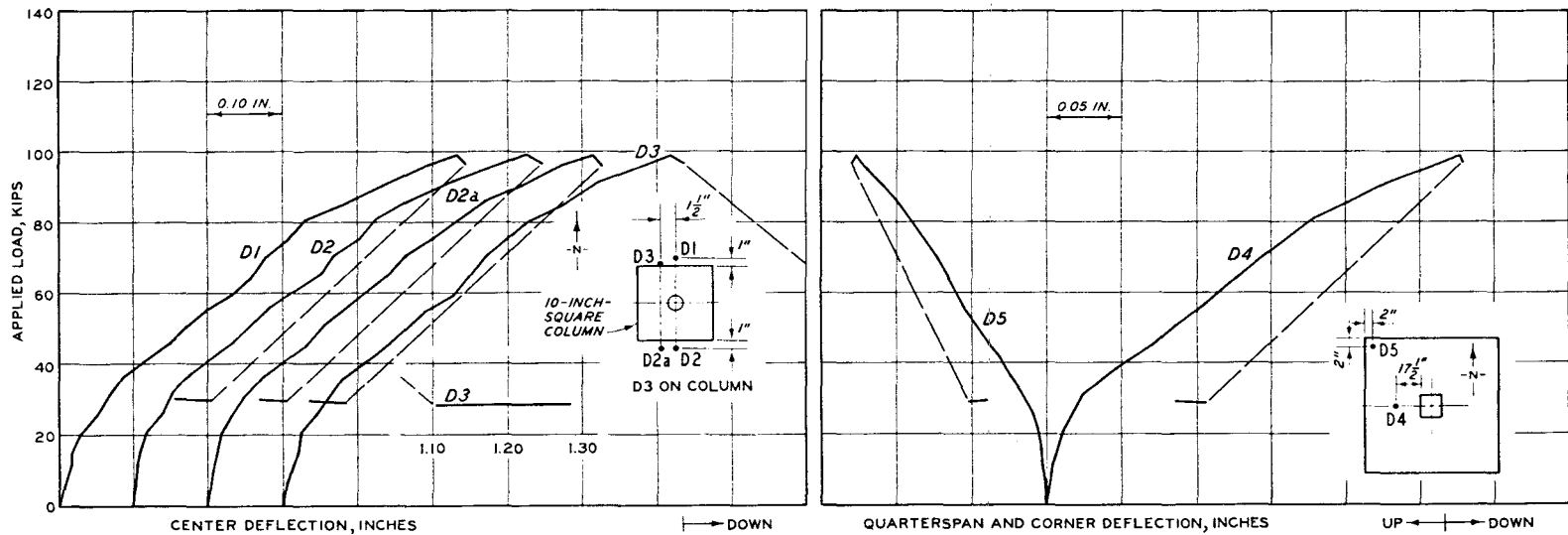
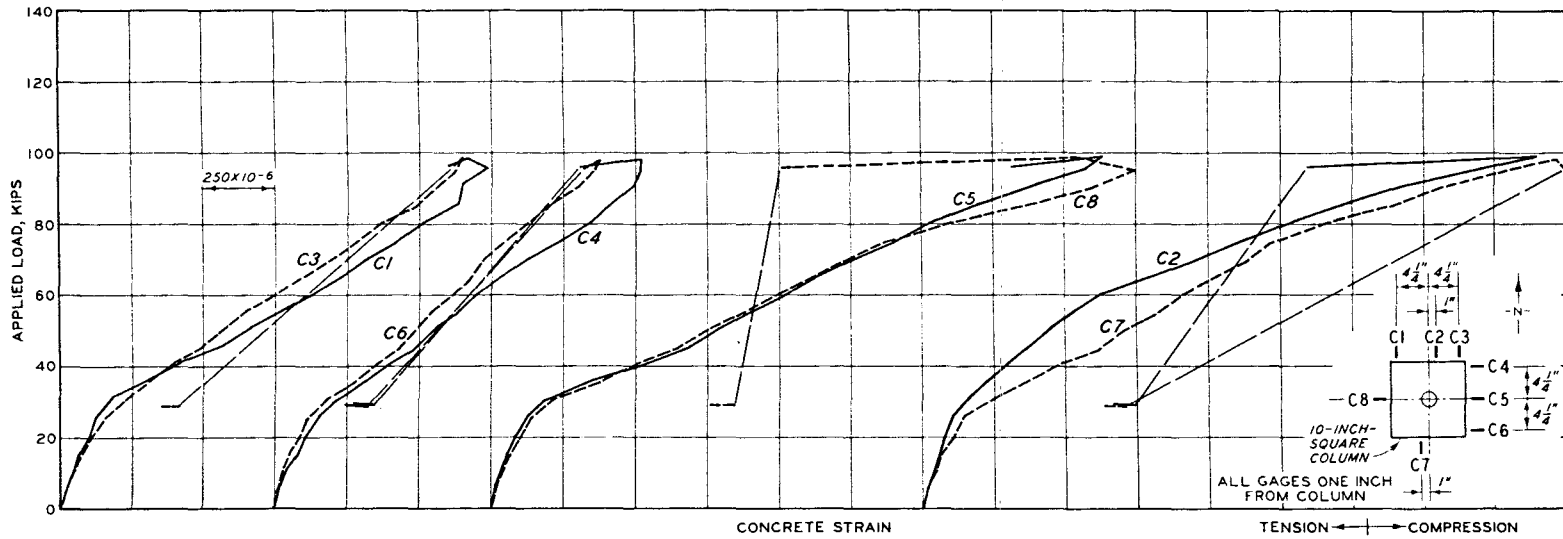


Figure B.7 Deflections and concrete strains, Specimen S2150-2.

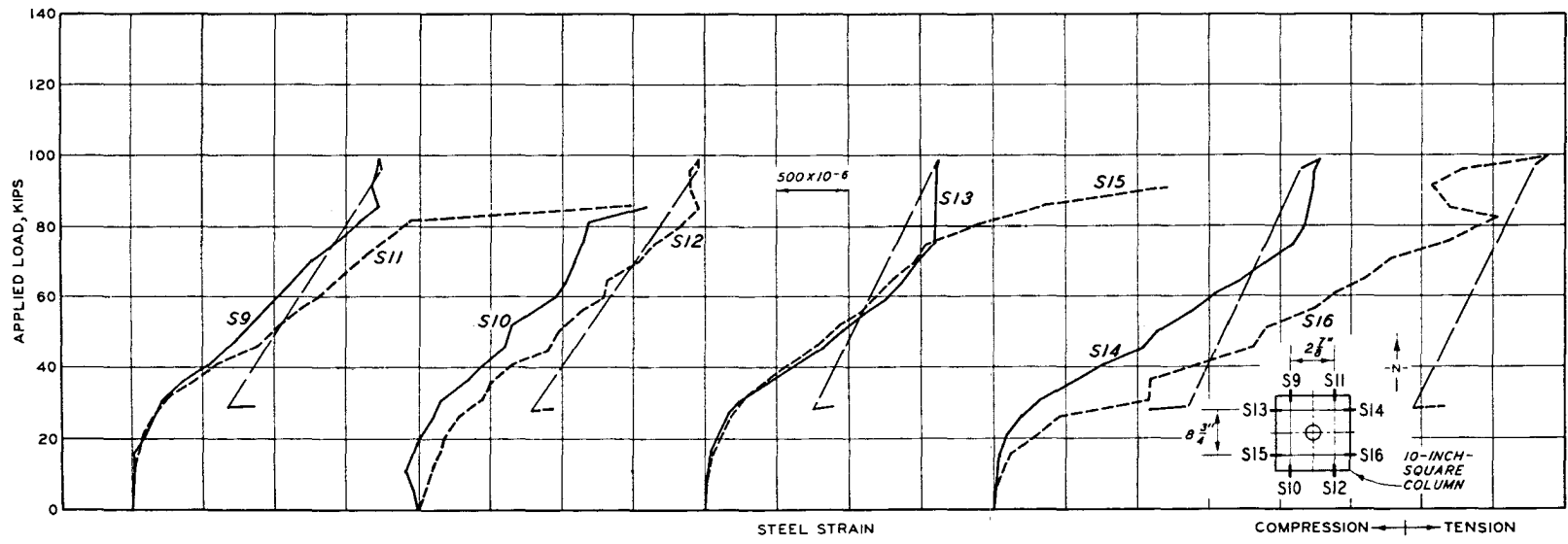
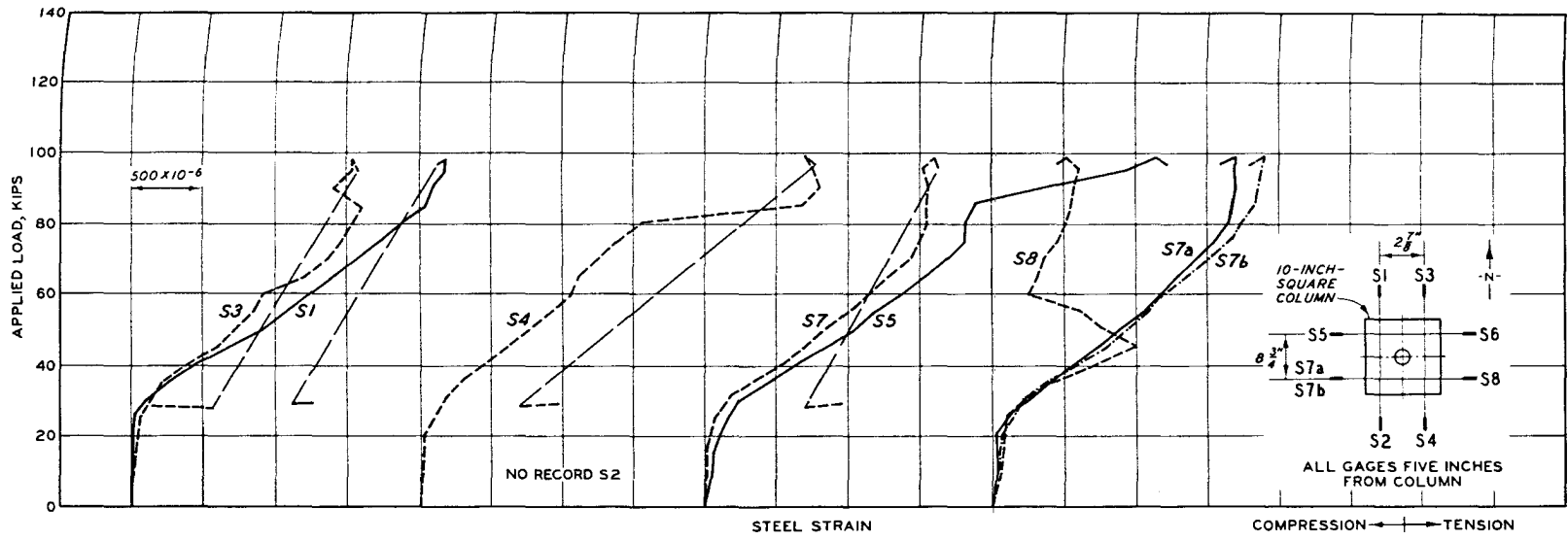


Figure B.8 Steel strains, Specimen S2150-2.



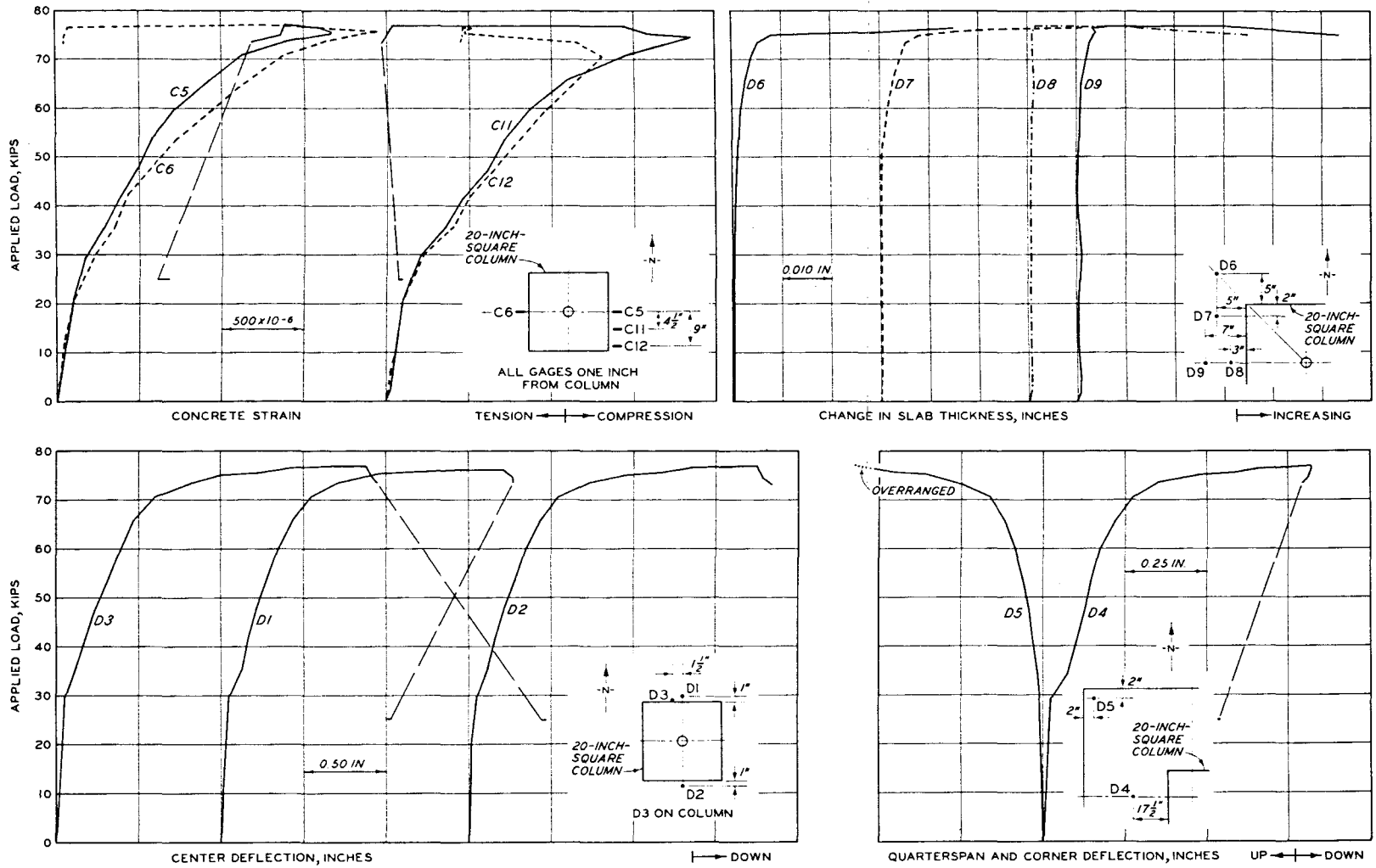


Figure B.9 Deflections and concrete strains, Specimen S4075-1.

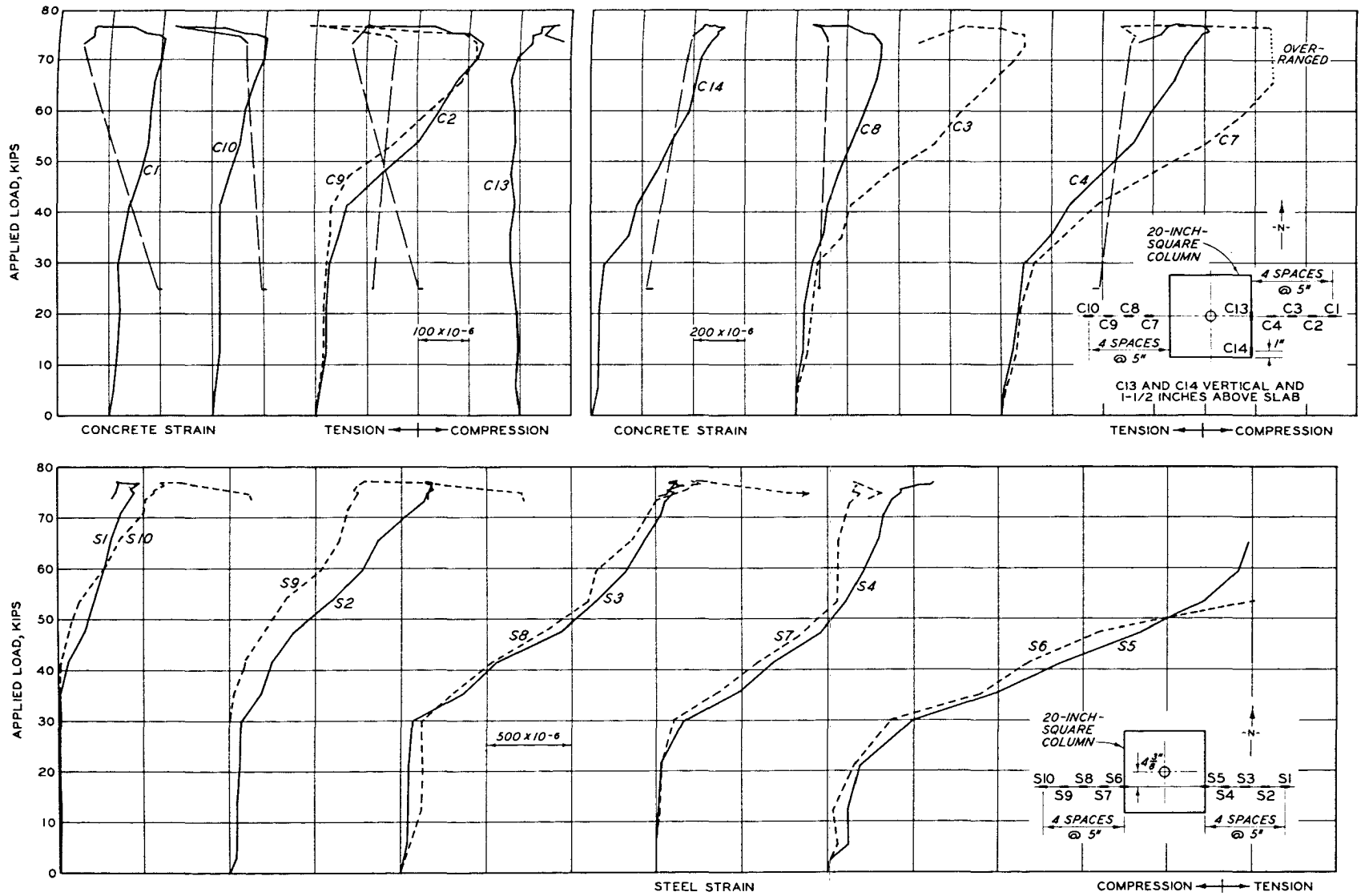


Figure B.10 Concrete and steel strains, Specimen S4075-1.

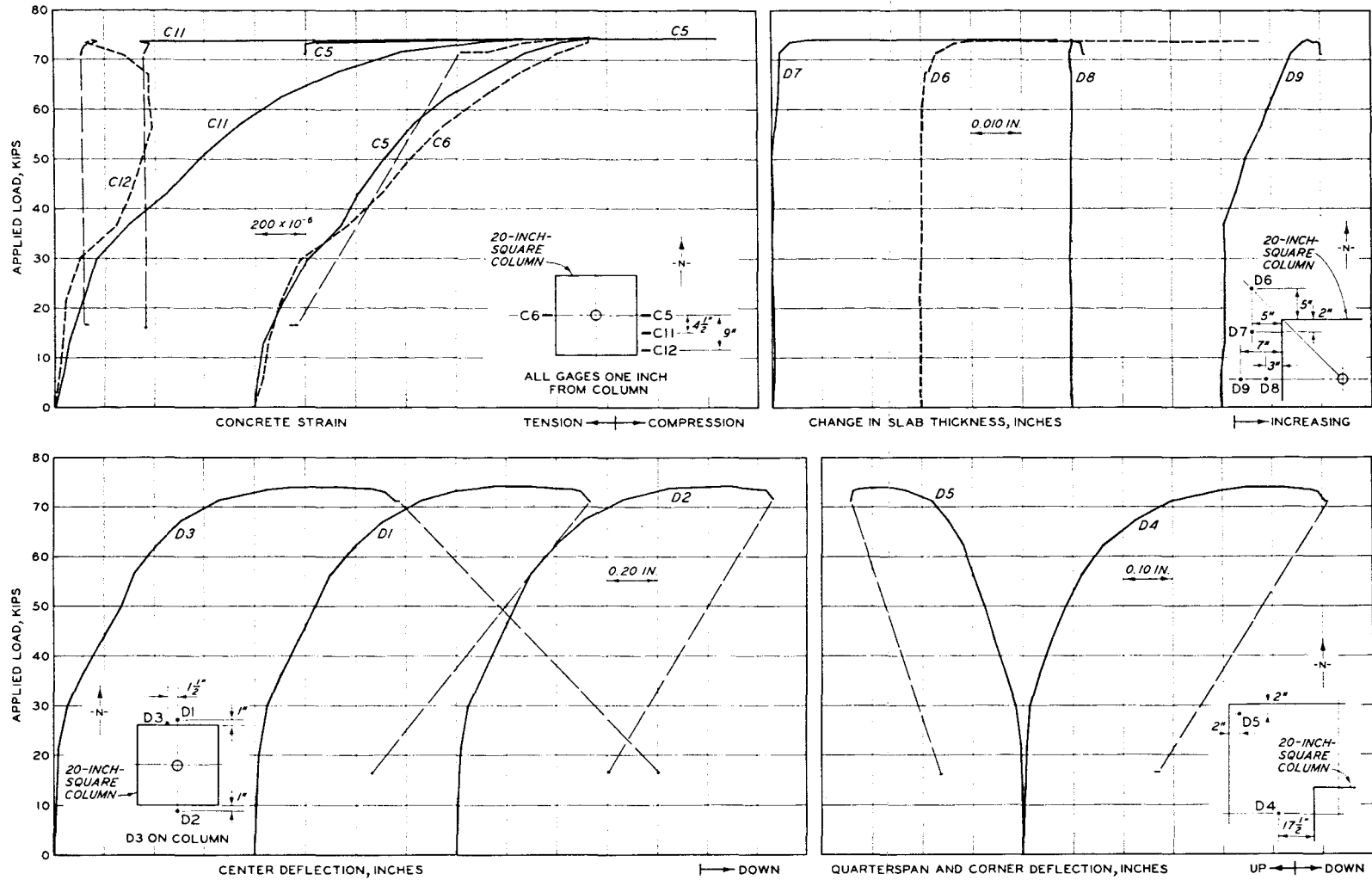


Figure B.11 Deflections and concrete strains, Specimen S4075-2.

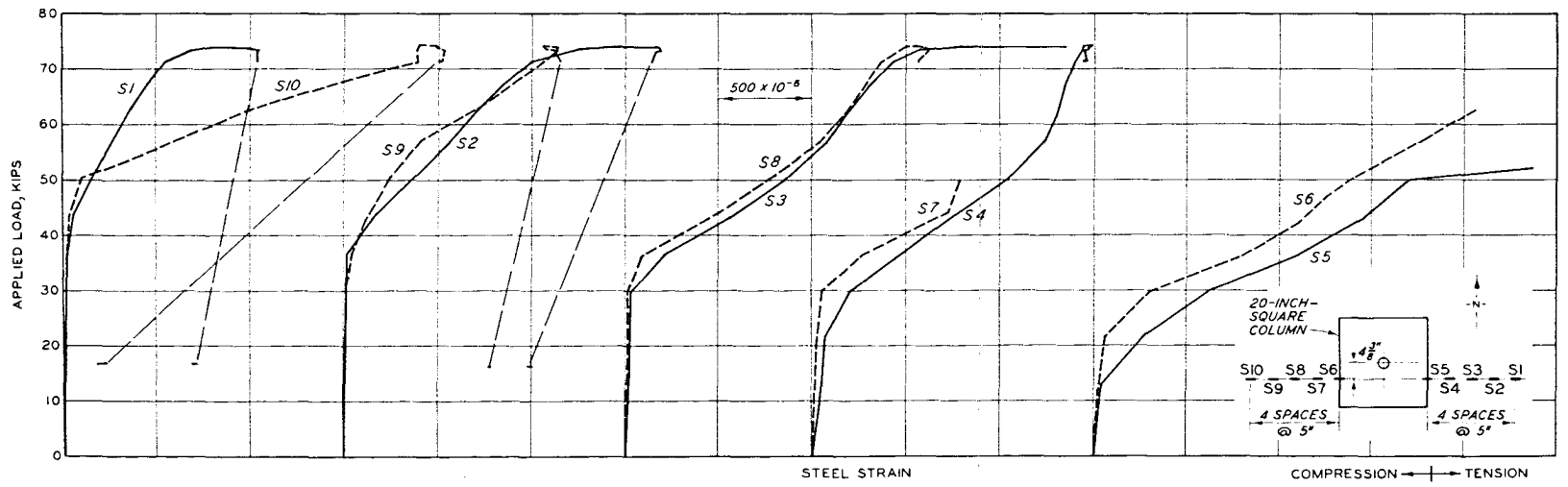
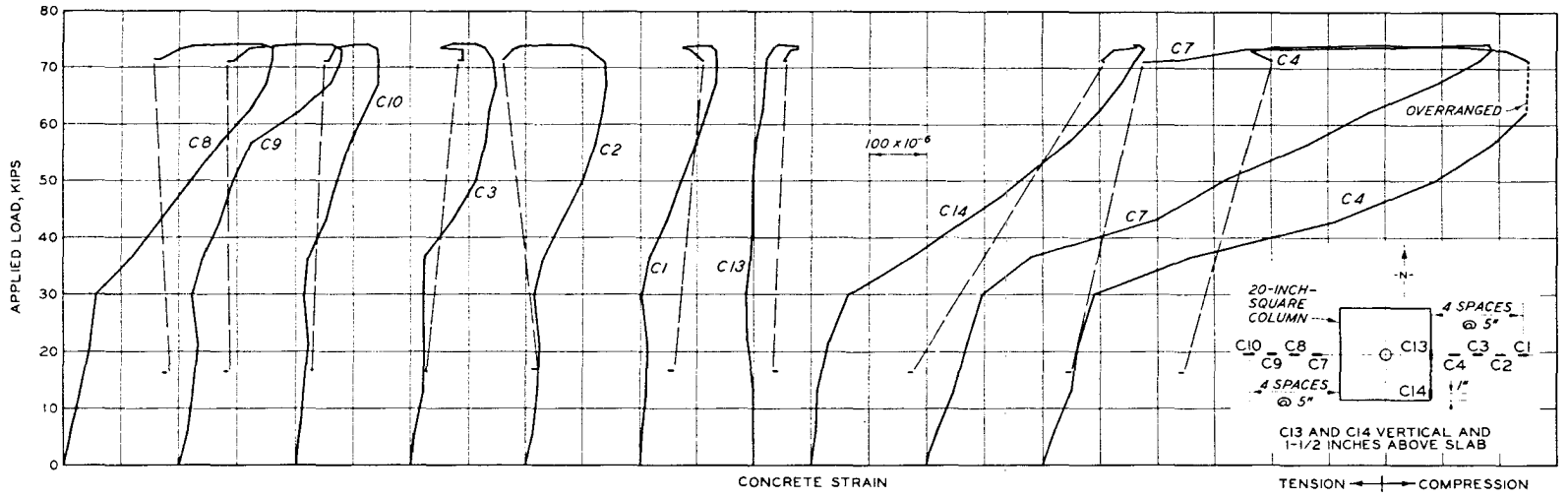


Figure B.12 Concrete and steel strains, Specimen S4075-2.

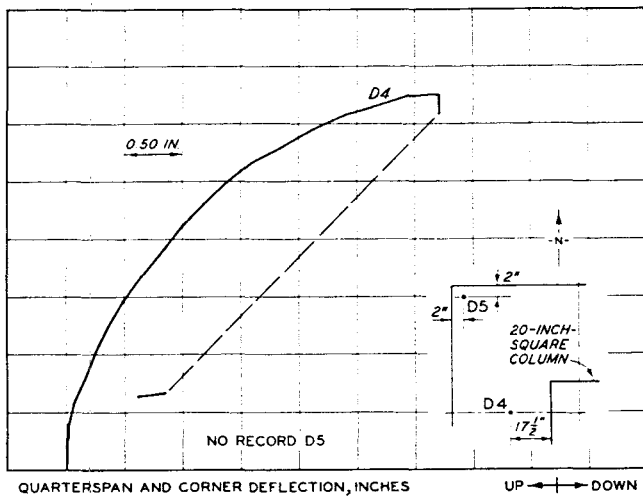
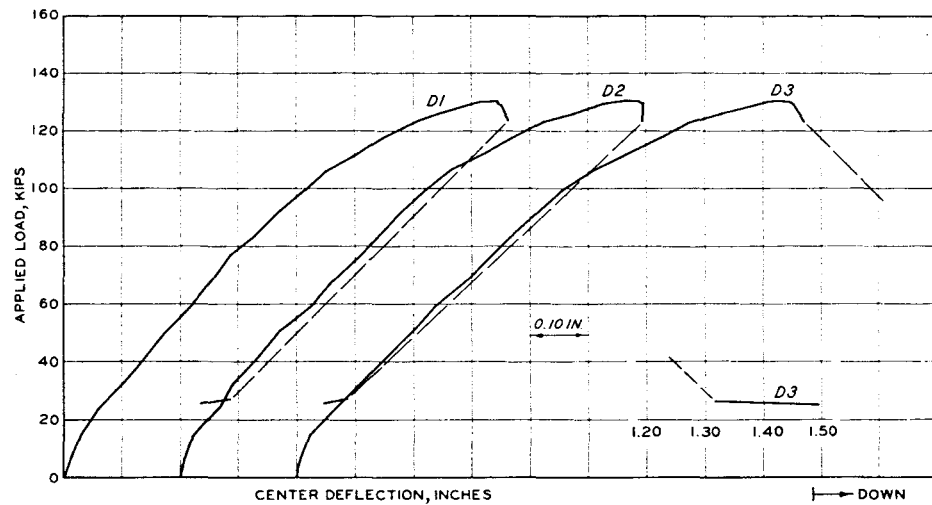
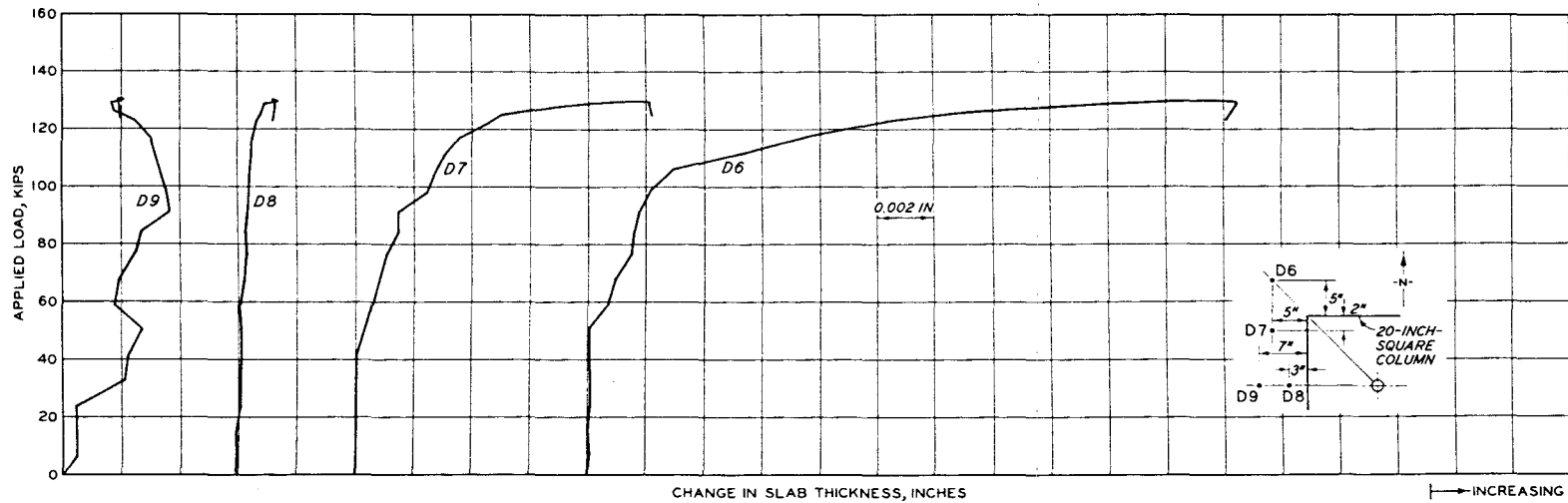
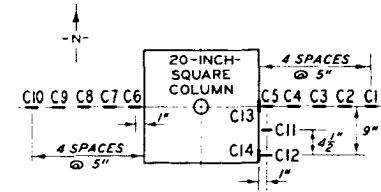
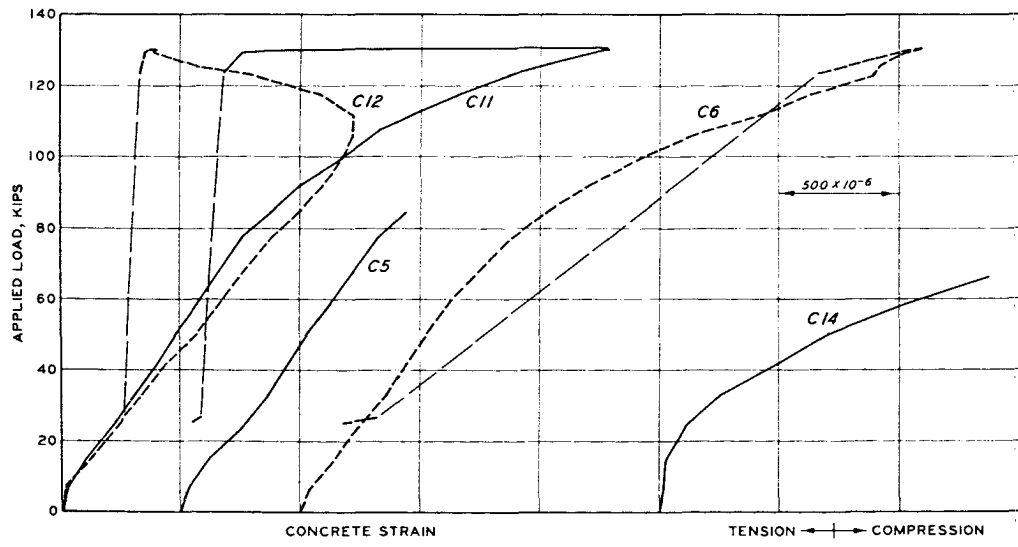
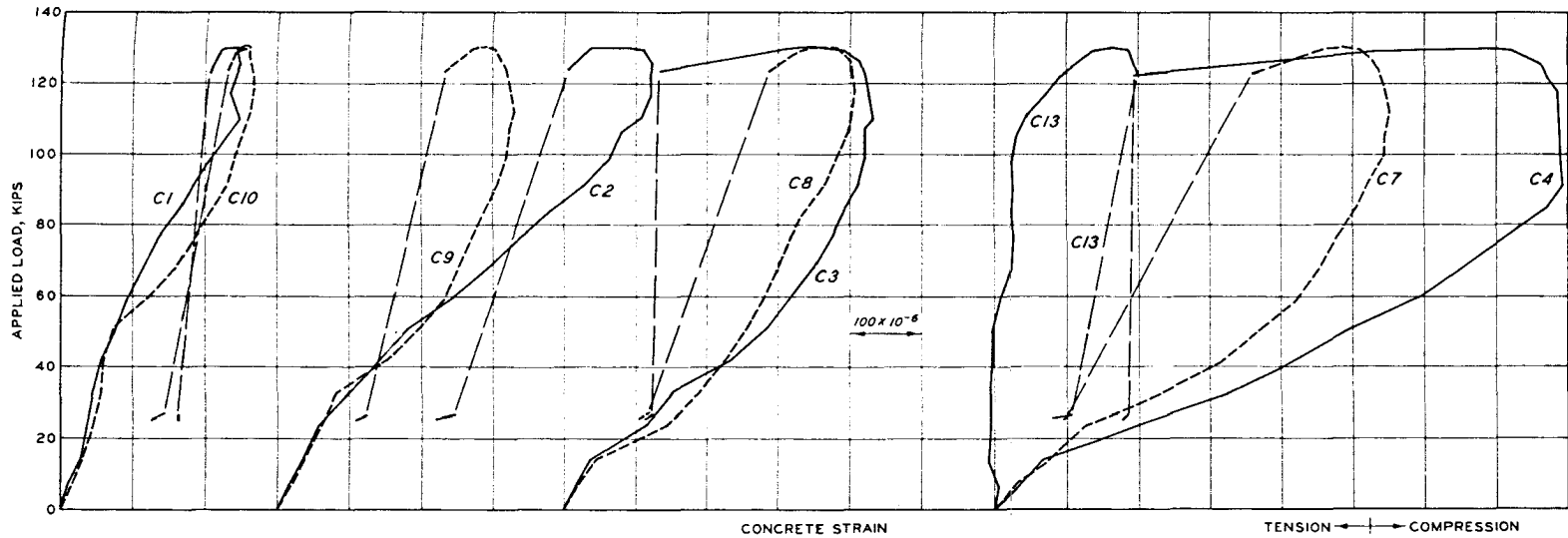


Figure B.13 Deflections, Specimen S4150-1.



NOTE: NO STEEL STRAIN RECORDS OBTAINED FOR THIS TEST; MALFUNCTION OF TAPE RECORDER UNIT.

Figure B.14 Concrete strains, Specimen S4150-1.

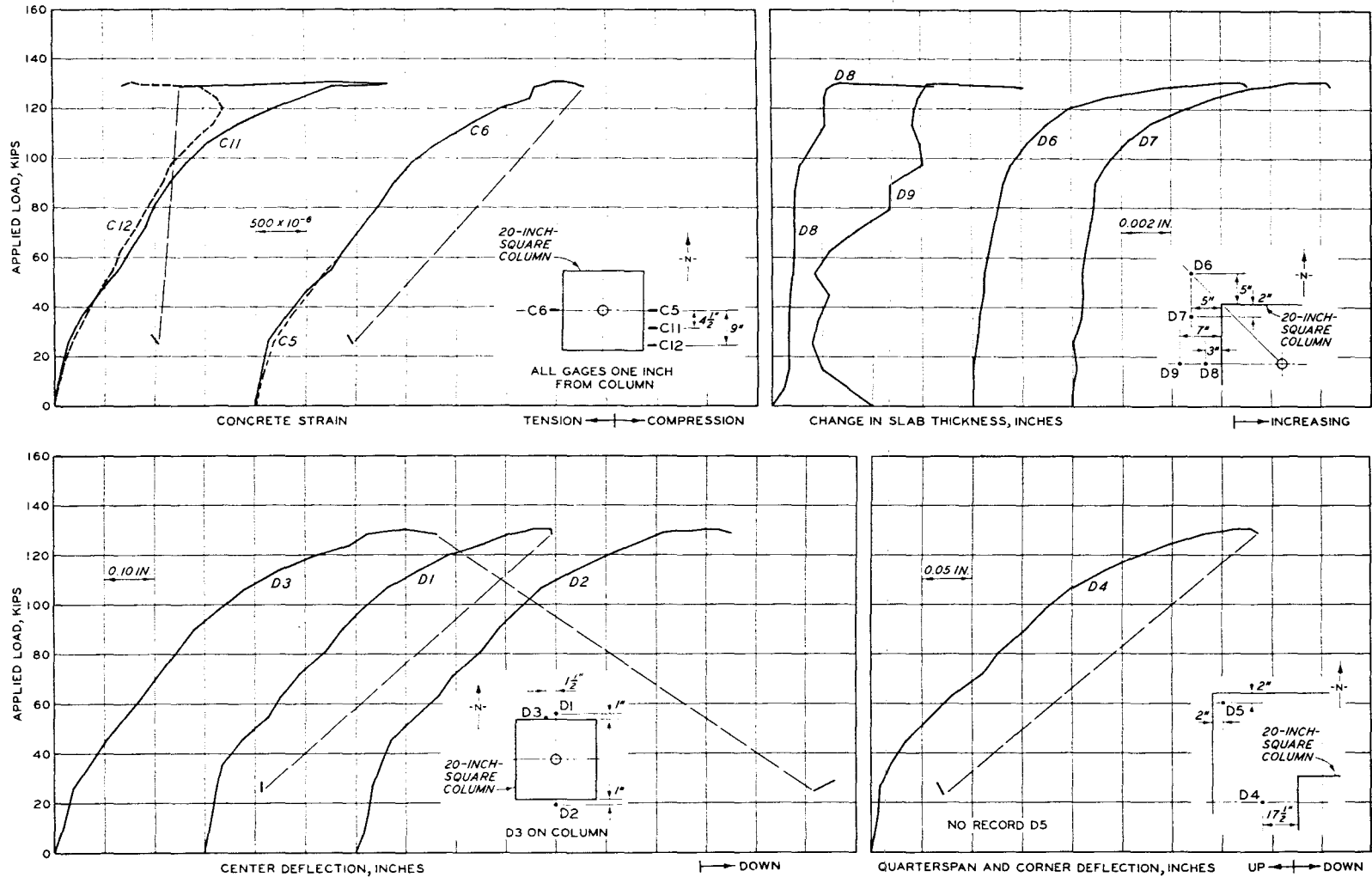


Figure B.15 Deflections and concrete strains, Specimen S4150-2.

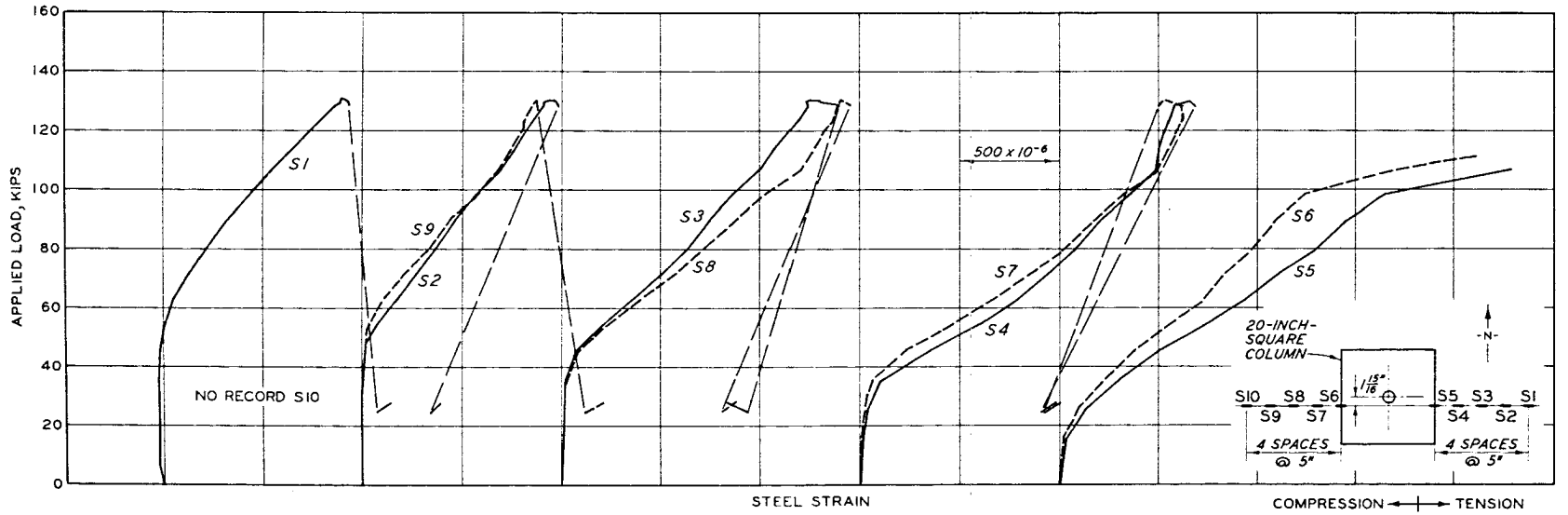
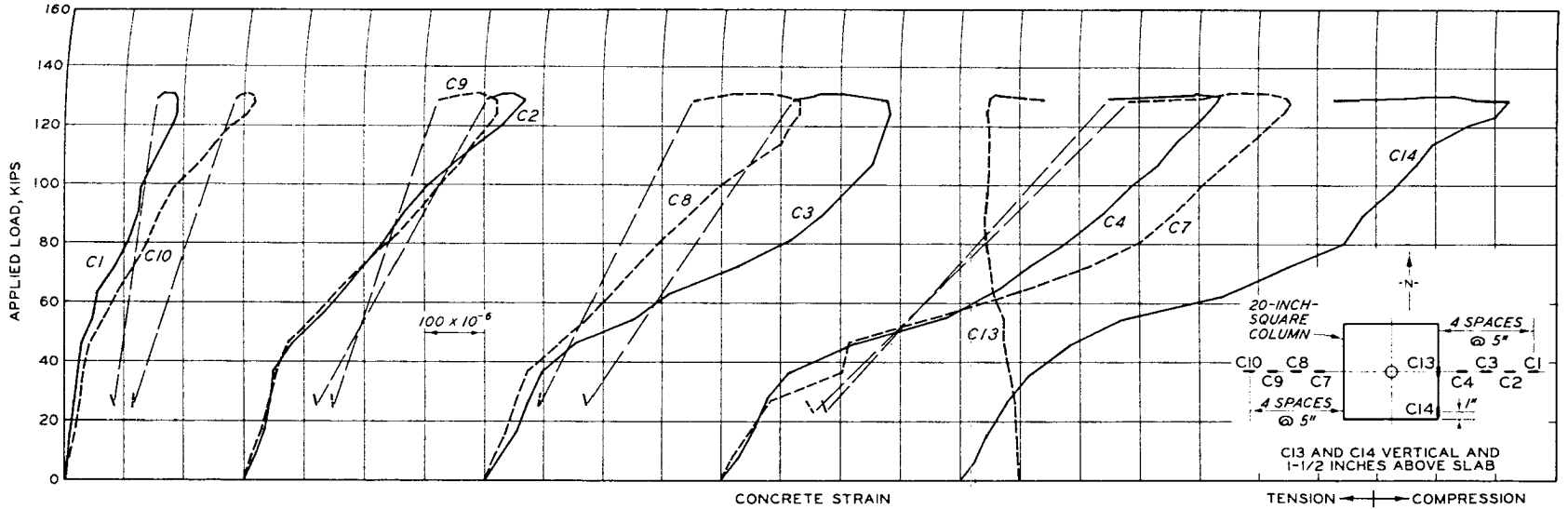


Figure B.16 Concrete and steel strains, Specimen S4150-2.



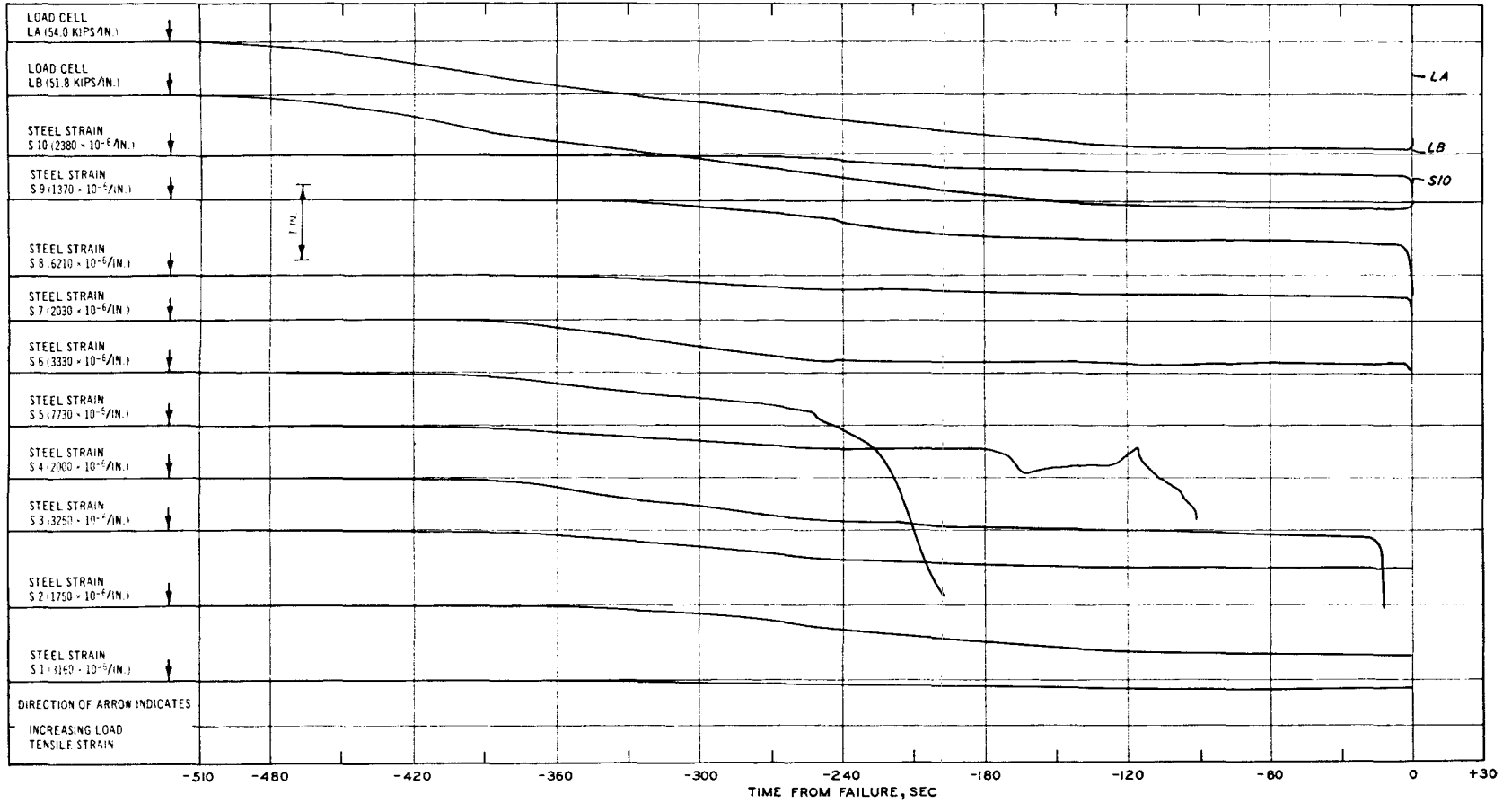


Figure B.17 Tracing from Recorder 1, Specimen S4075-1.

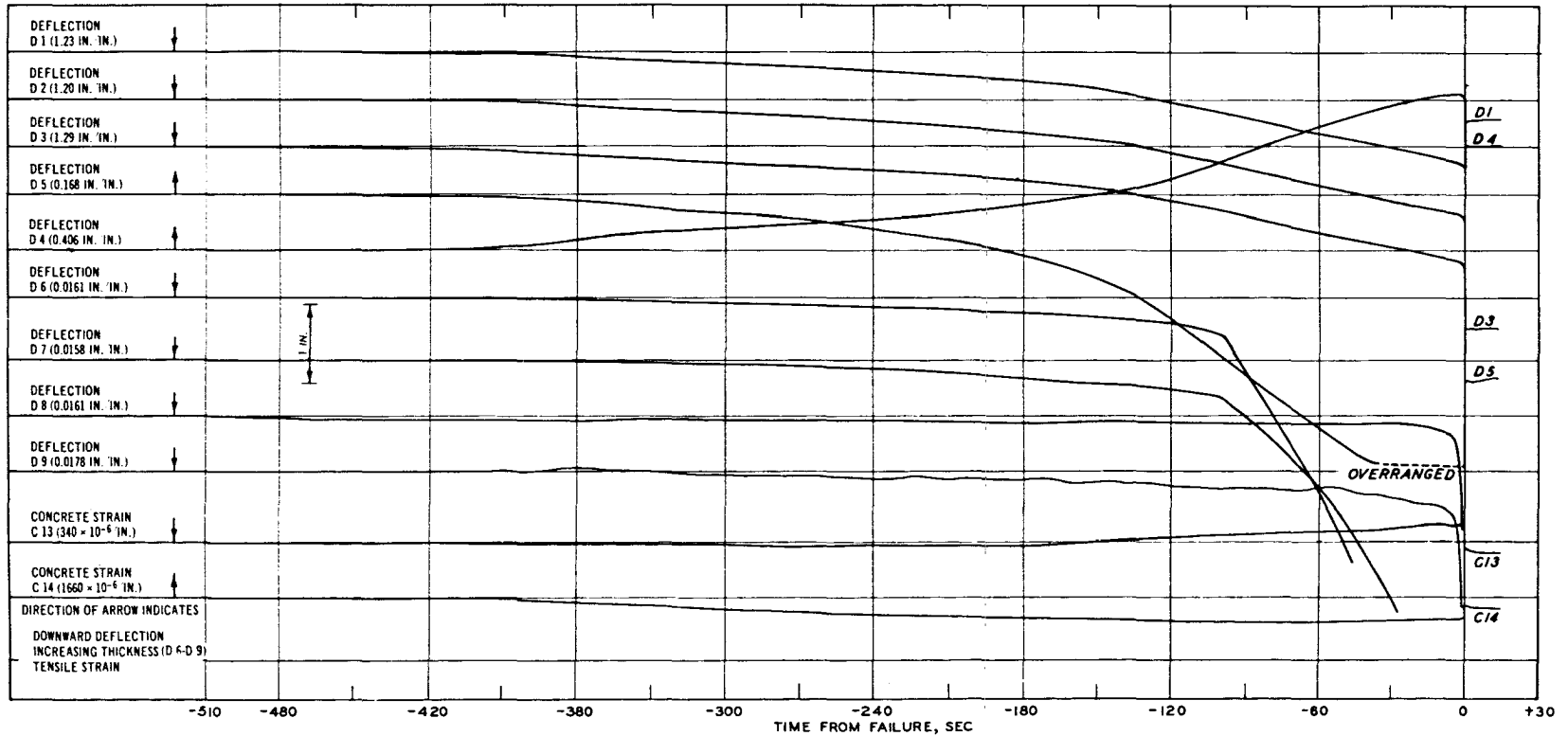


Figure B.18 Tracing from Recorder 2, Specimen S4075-1.

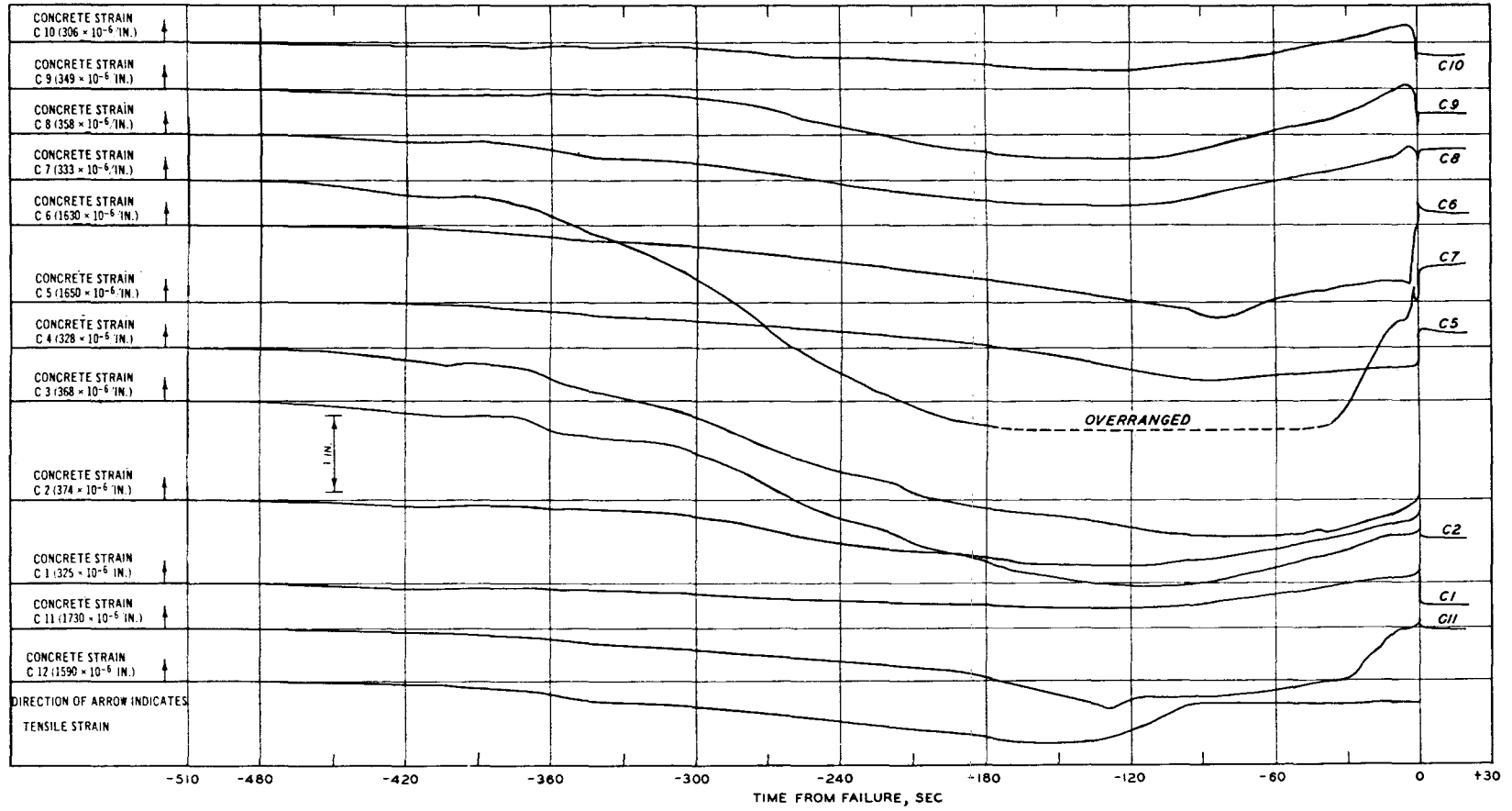


Figure B.19 Tracing from Recorder 3, Specimen S4075-1.

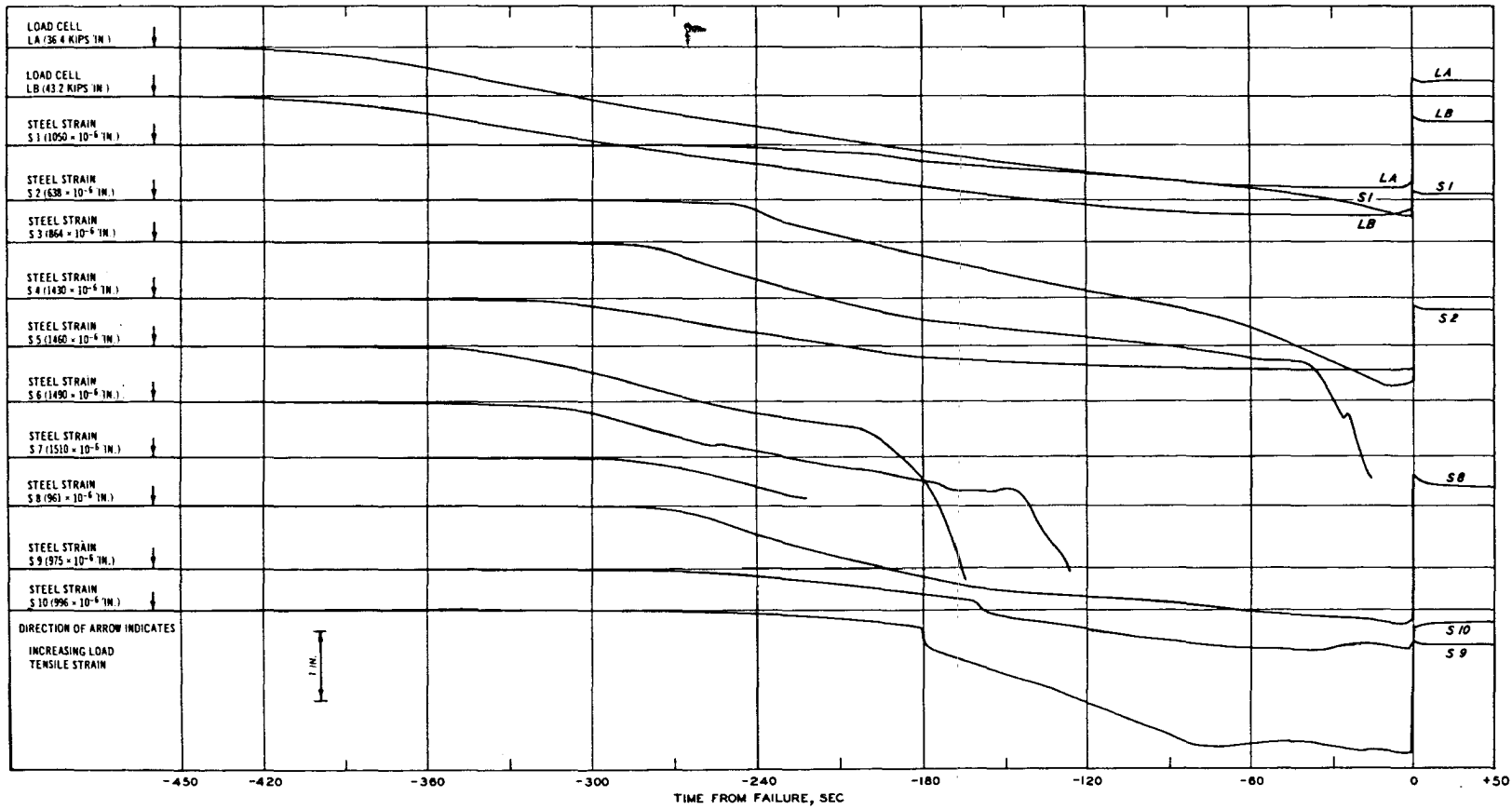


Figure B.20 Tracing from Recorder 1, Specimen S4075-2.

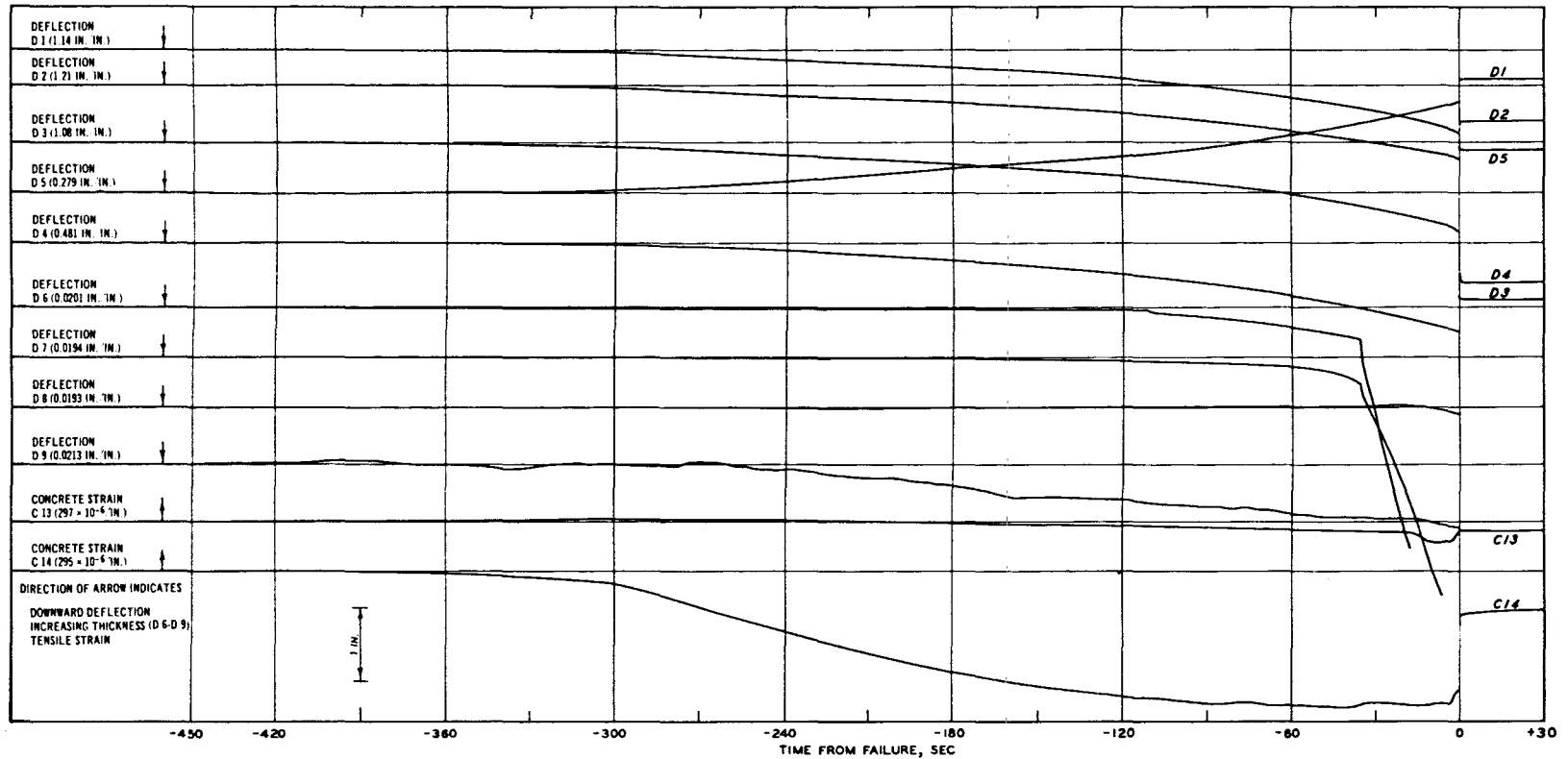


Figure B.21 Tracing from Recorder 2, Specimen S4075-2.

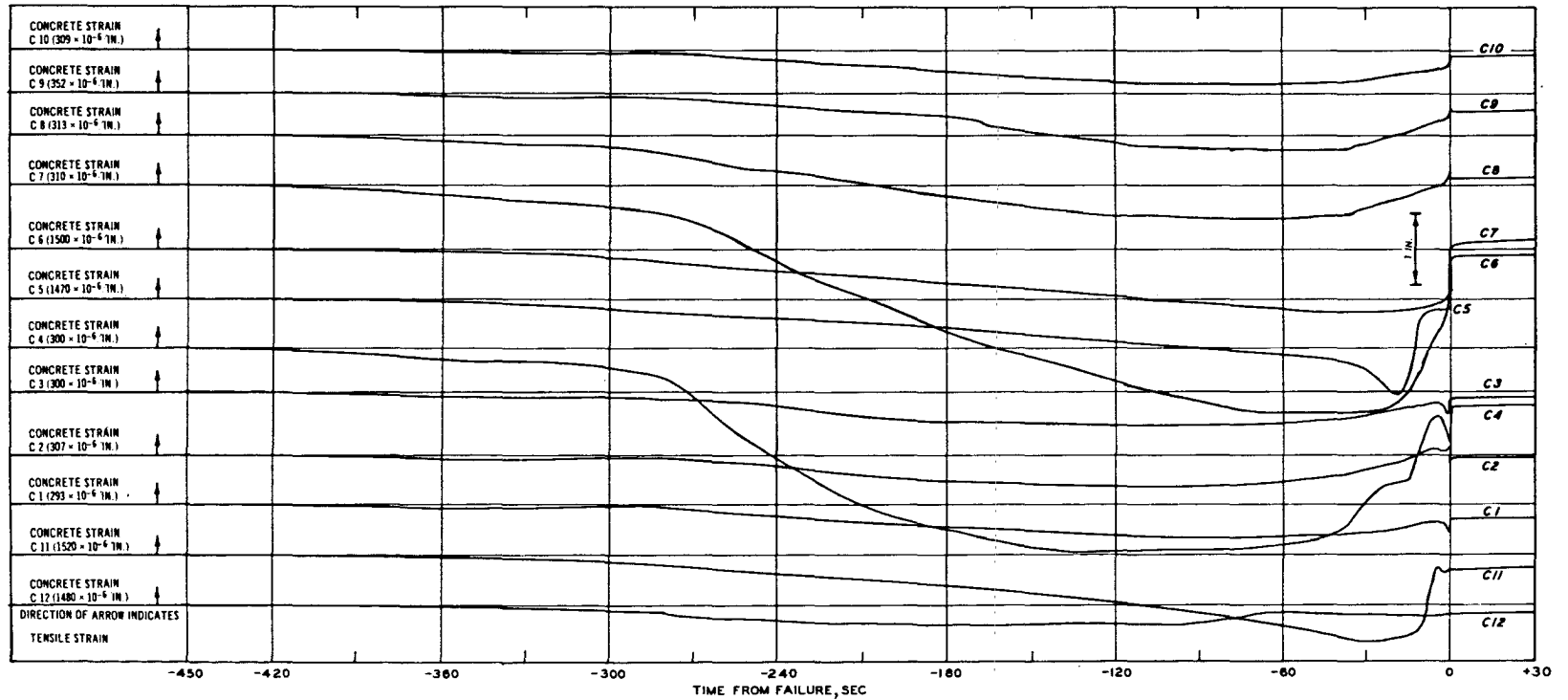


Figure B.22 Tracing from Recorder 3, Specimen S4075-2.

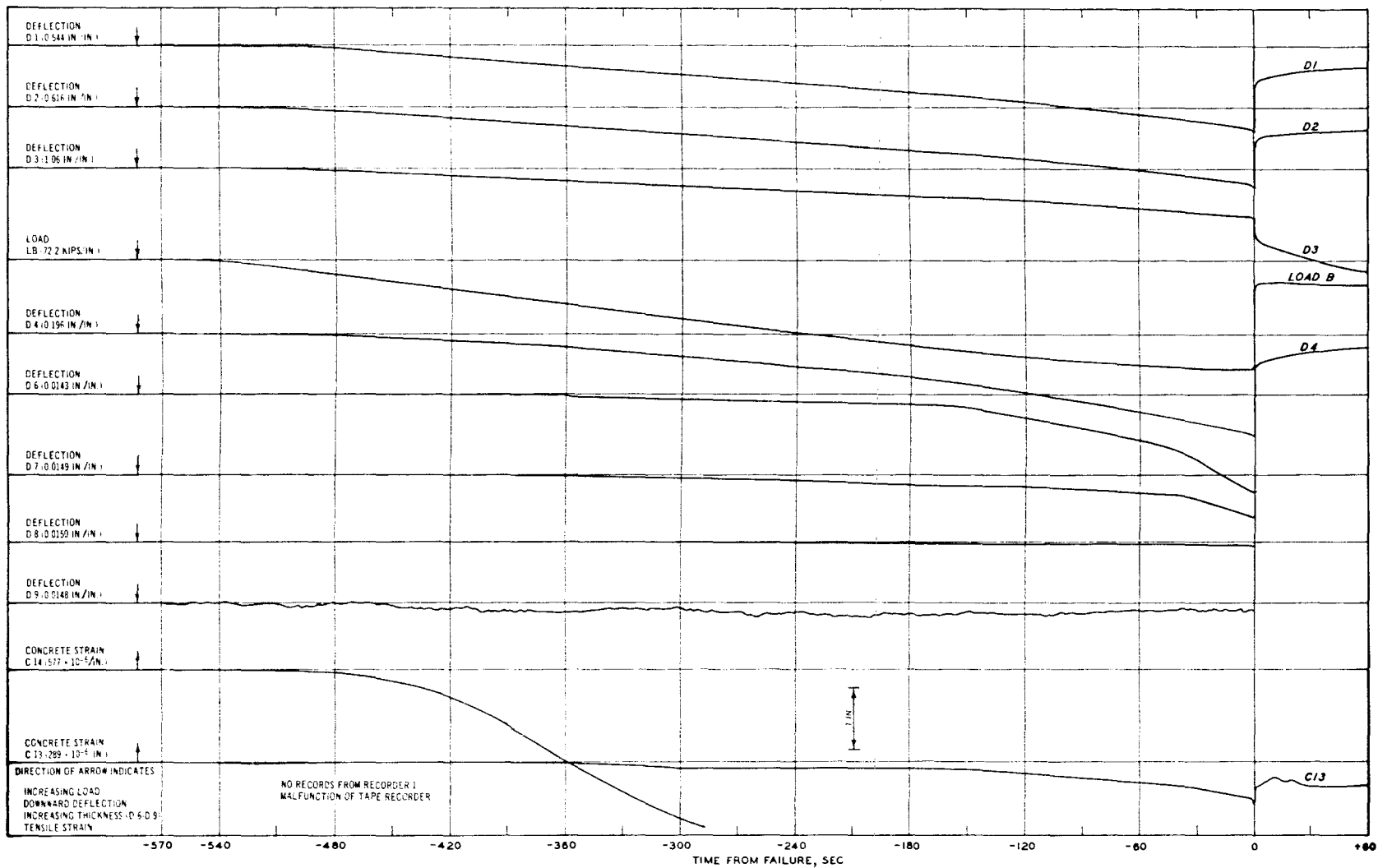


Figure B.23 Tracing from Recorder 2, Specimen S4150-1.

323

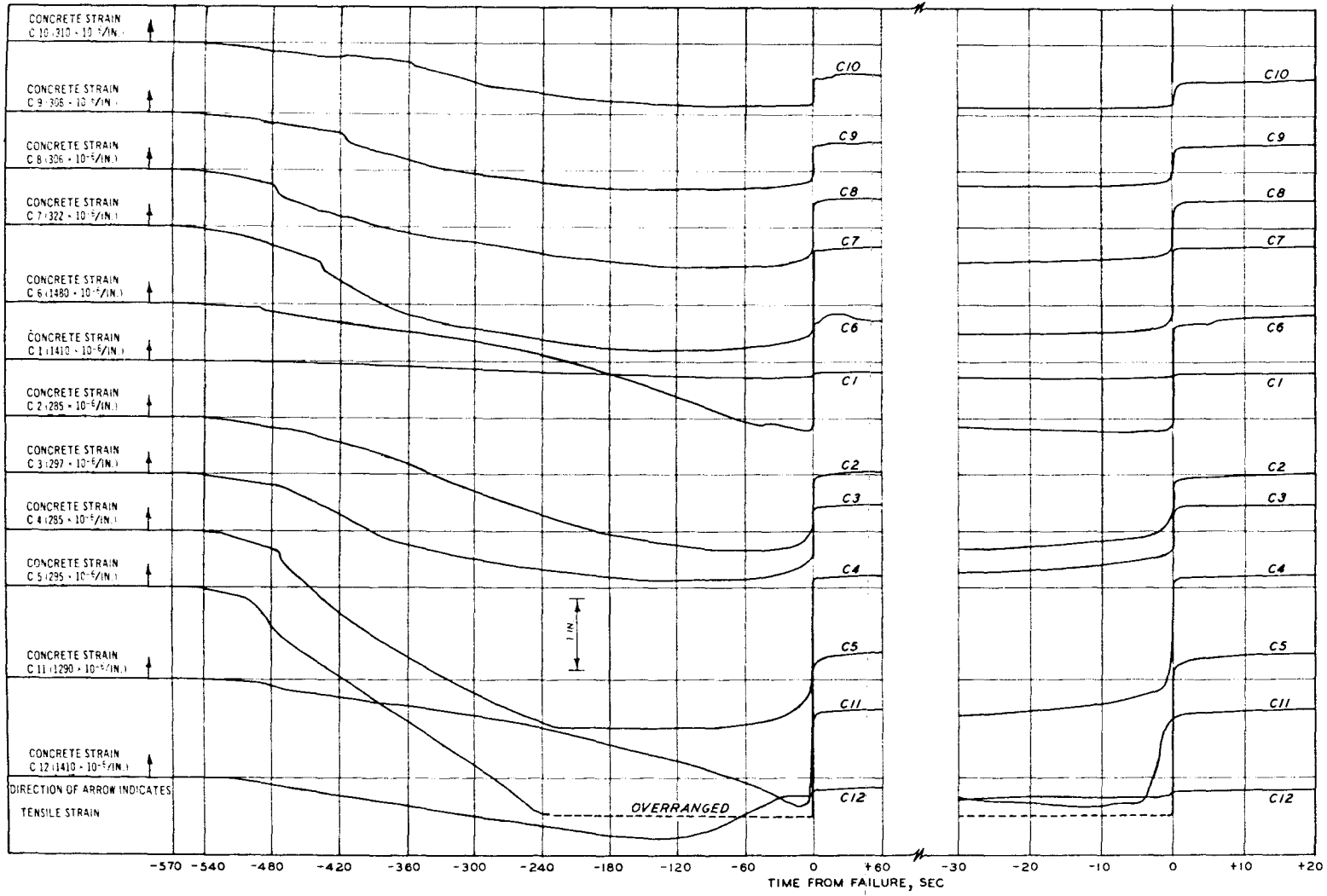


Figure B.24 Tracing from Recorder 3, Specimen S4150-1.



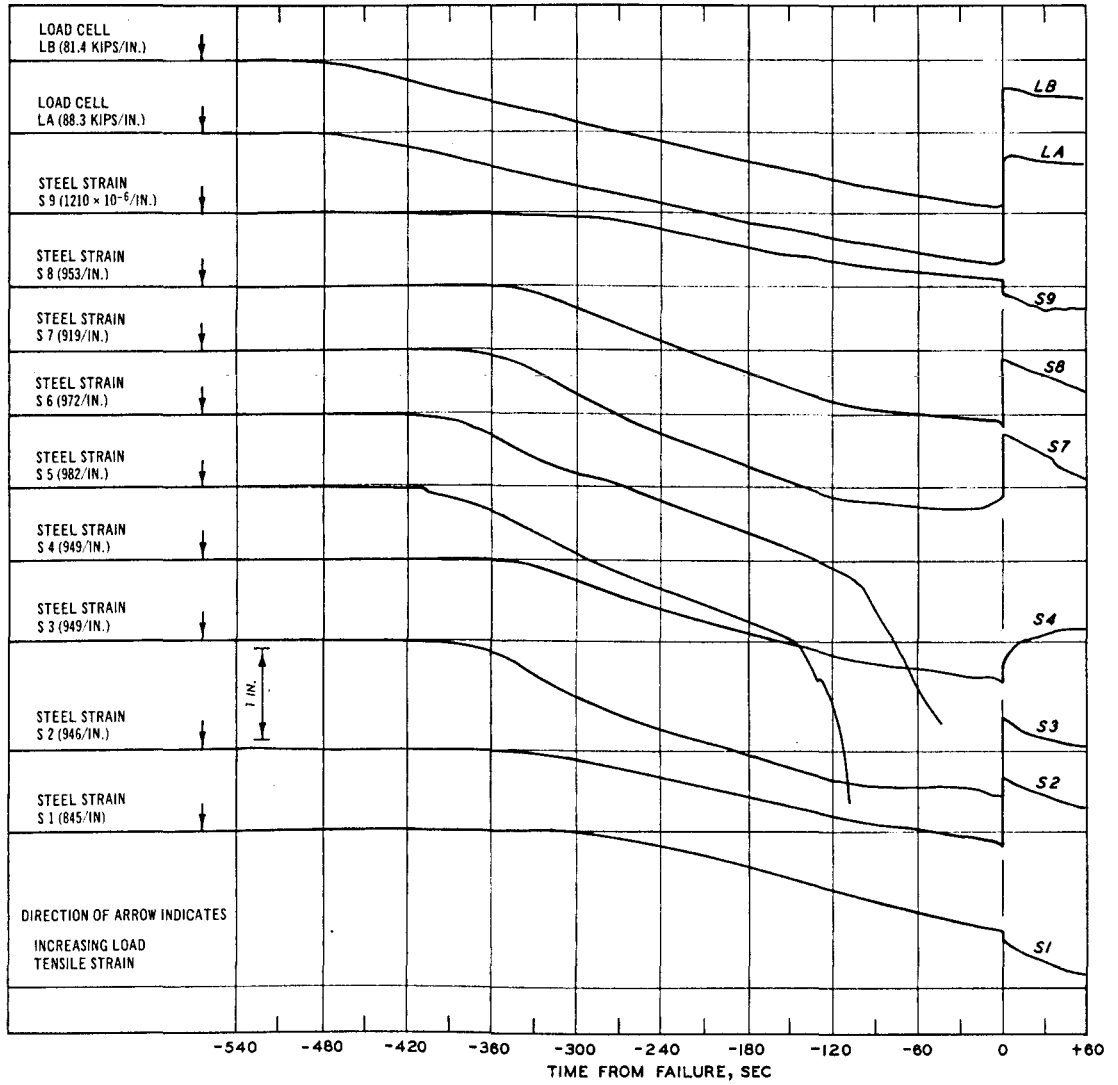


Figure B.25 Tracing from Recorder 1, Specimen S4150-2.

325

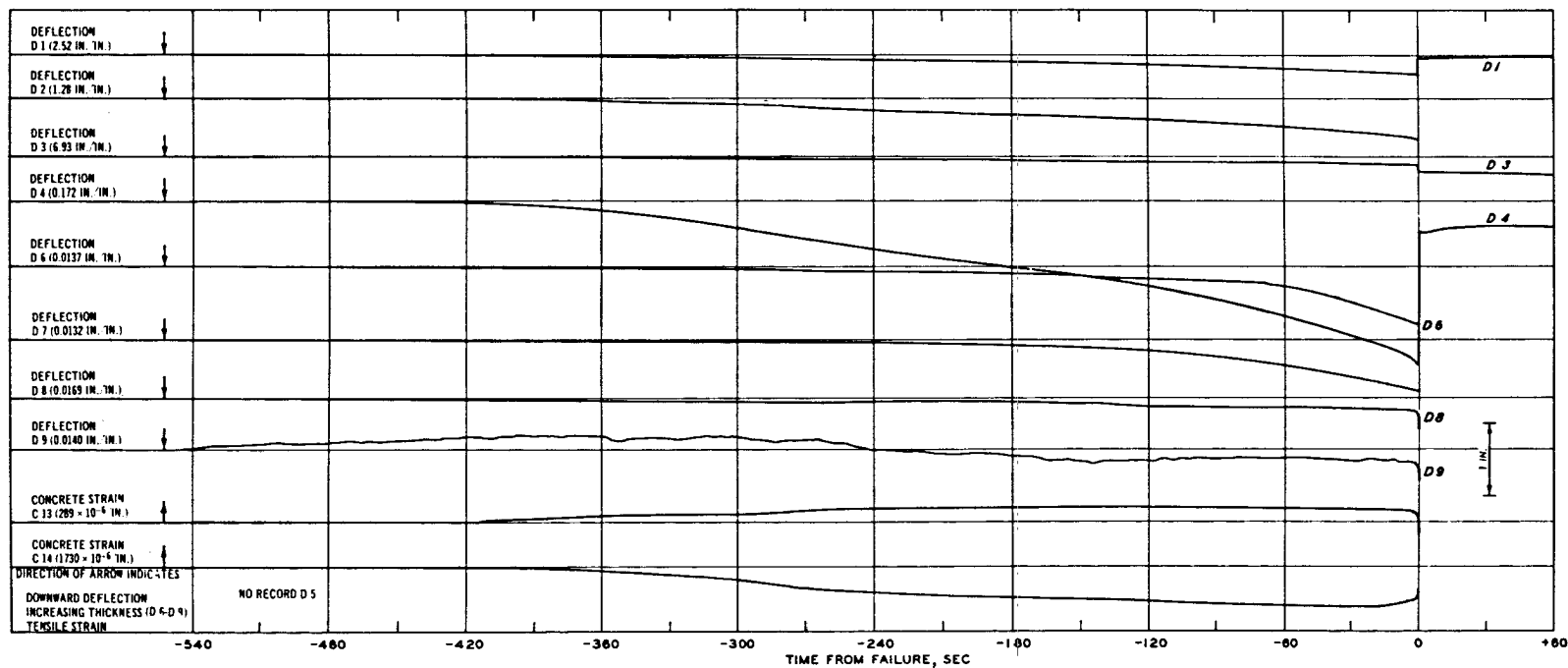


Figure B.26 Tracing from Recorder 2, Specimen S4150-2.

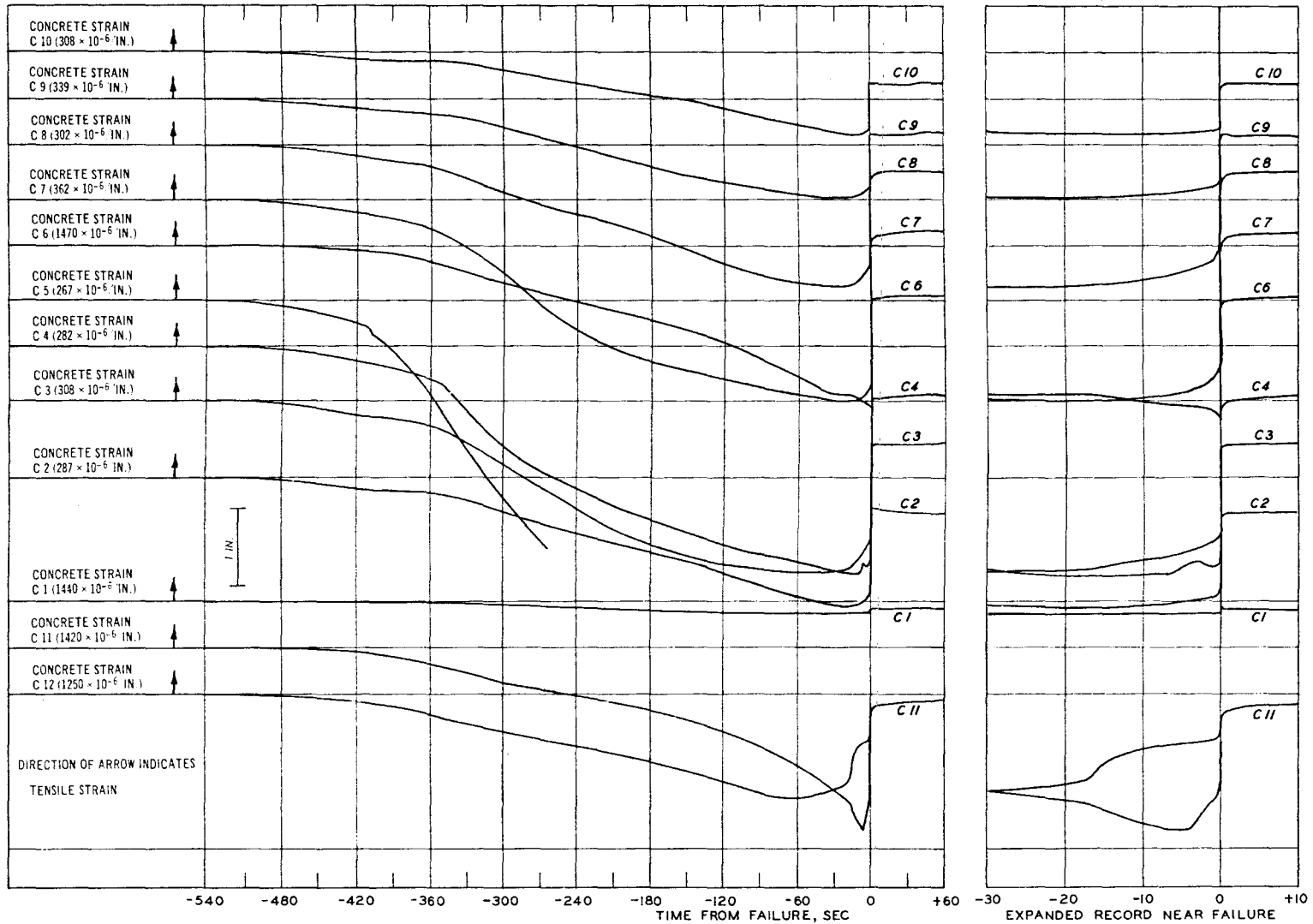


Figure B.27 Tracing from Recorder 3, Specimen S4150-2.

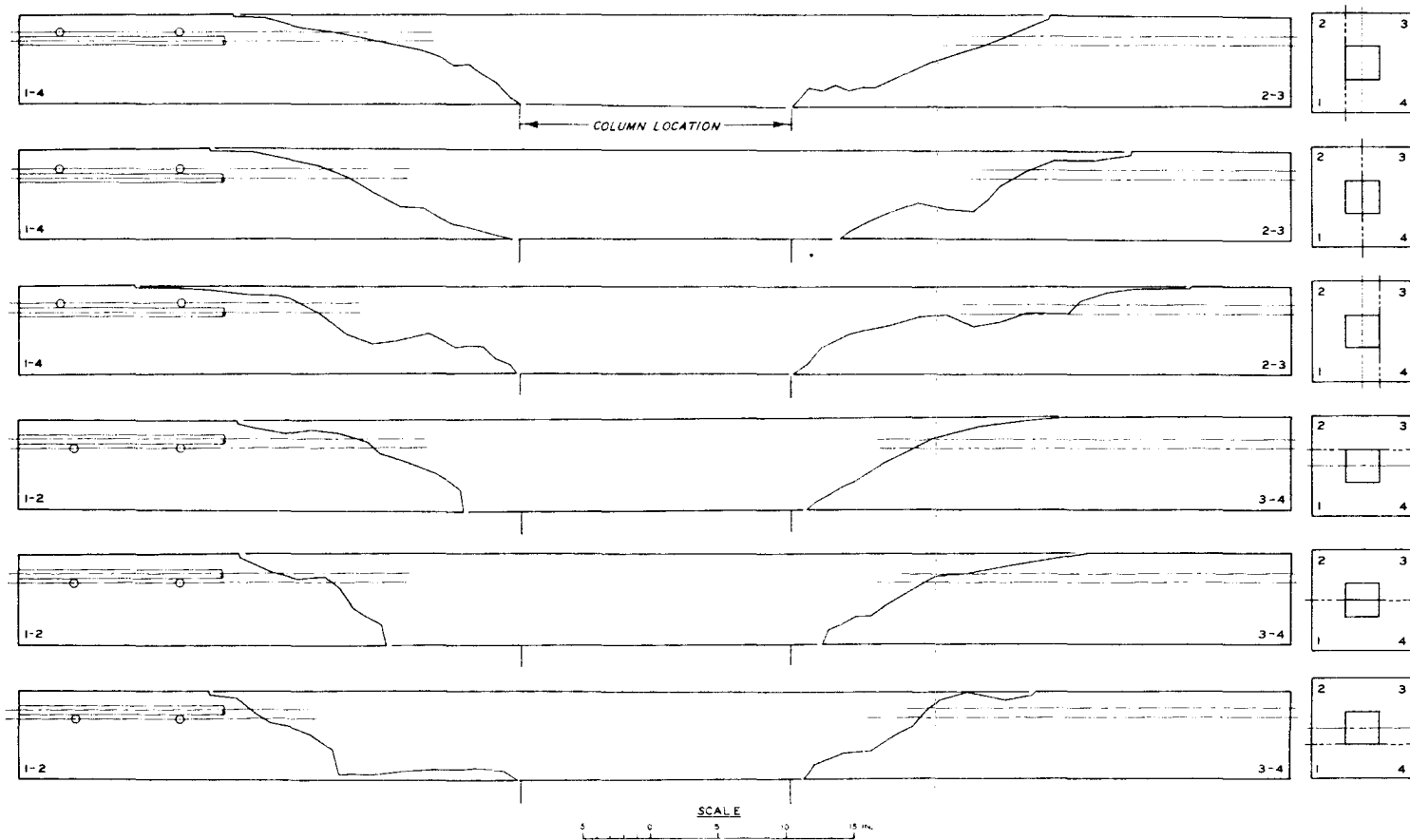
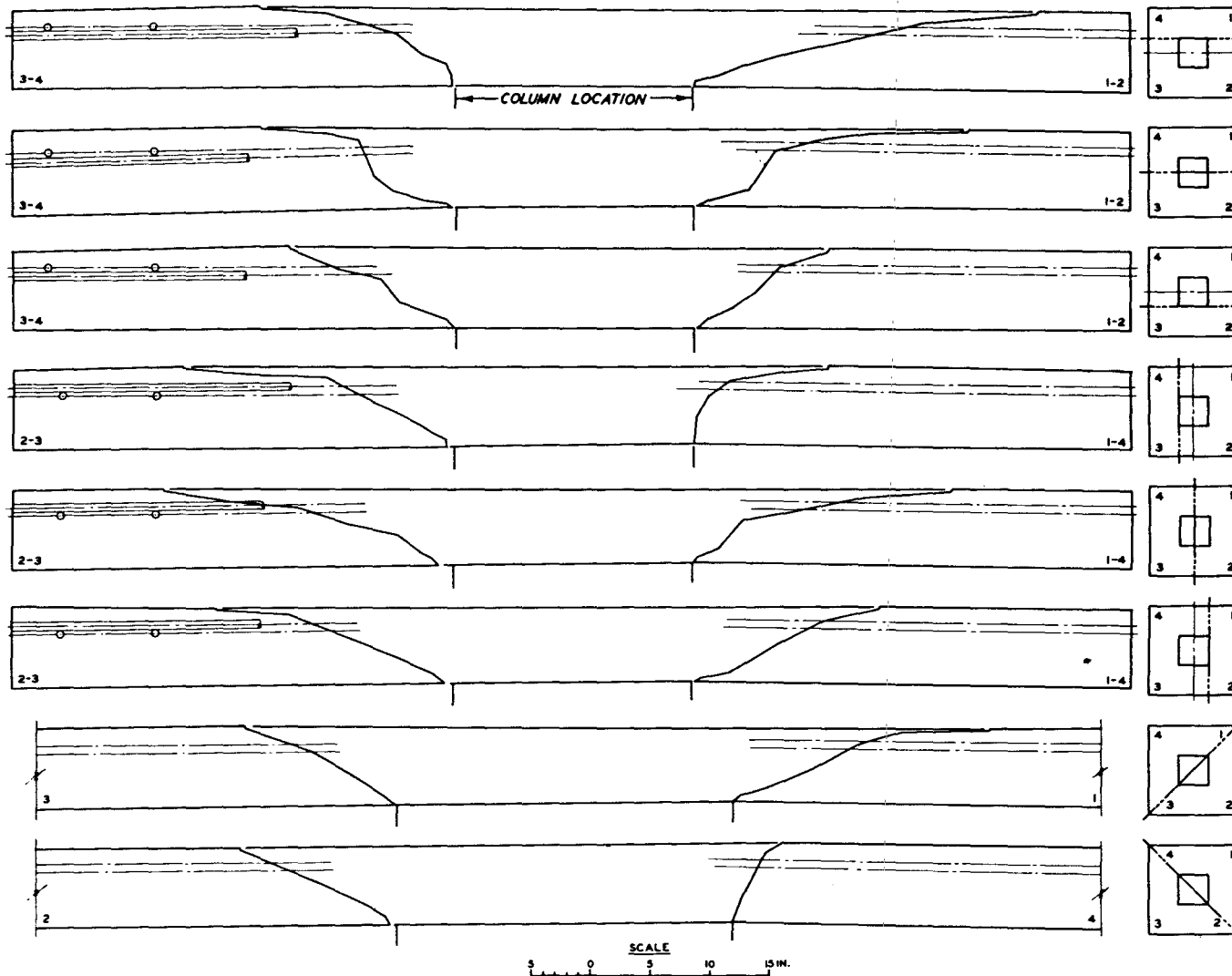


Figure B.28 Profiles of slab failure surface, Specimen S4075-1.



328

Figure B.29 Profiles of slab failure surface, Specimen S4075-2.

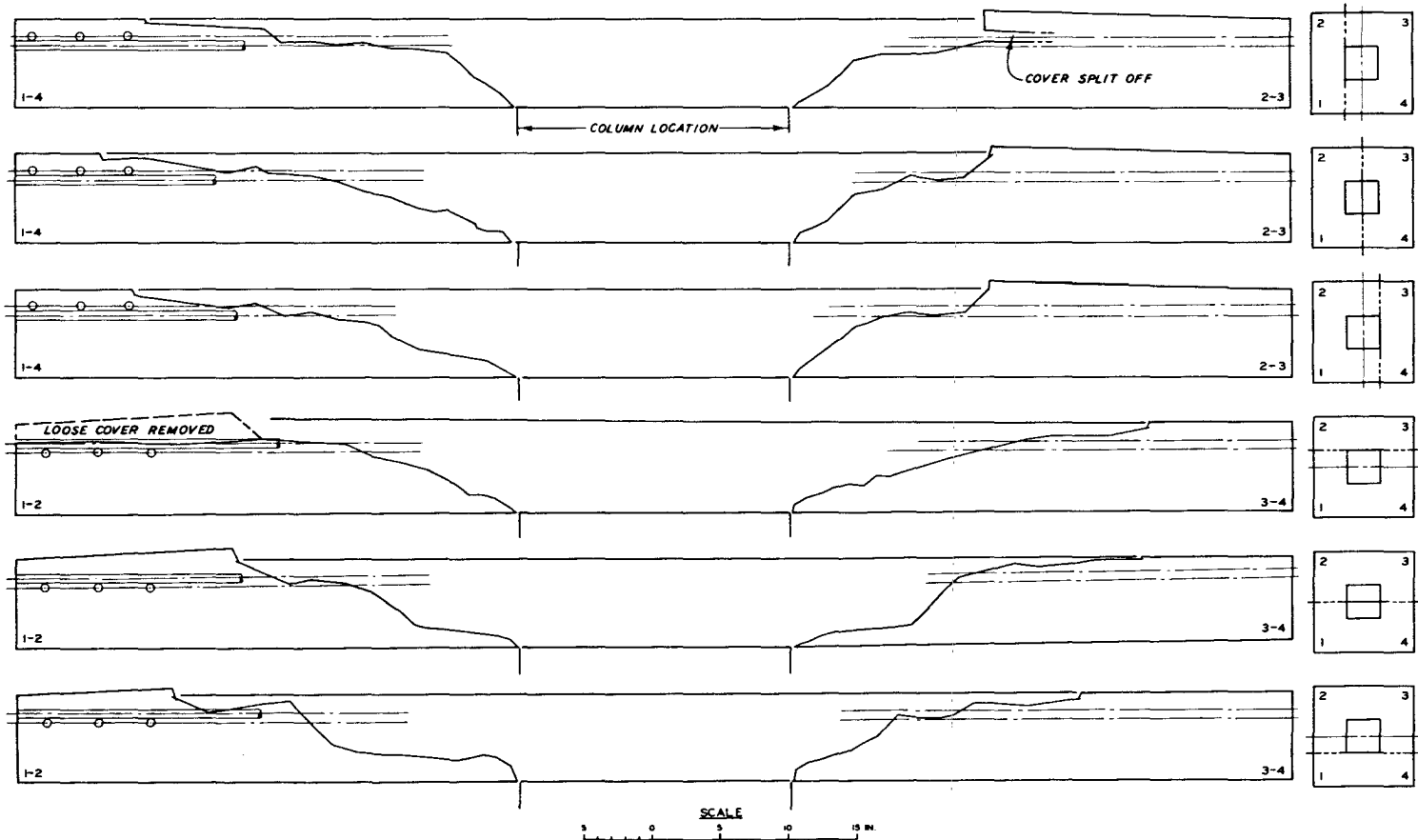


Figure B.30 Profiles of slab failure surface, Specimen S4150-1.

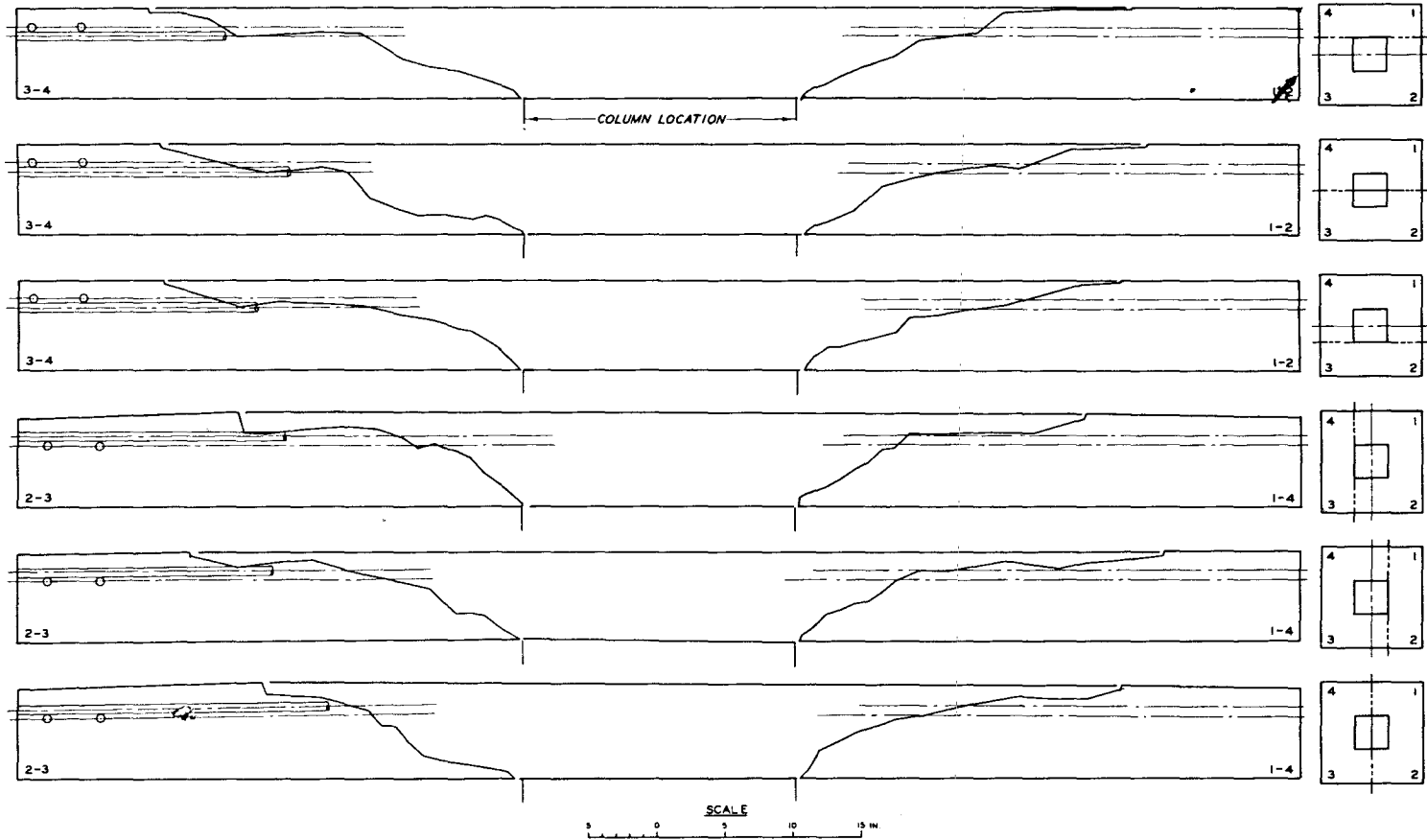


Figure B.31 Profiles of slab failure surface, Specimen S4150-2.

APPENDIX C  
DATA FROM THE DYNAMIC TESTS



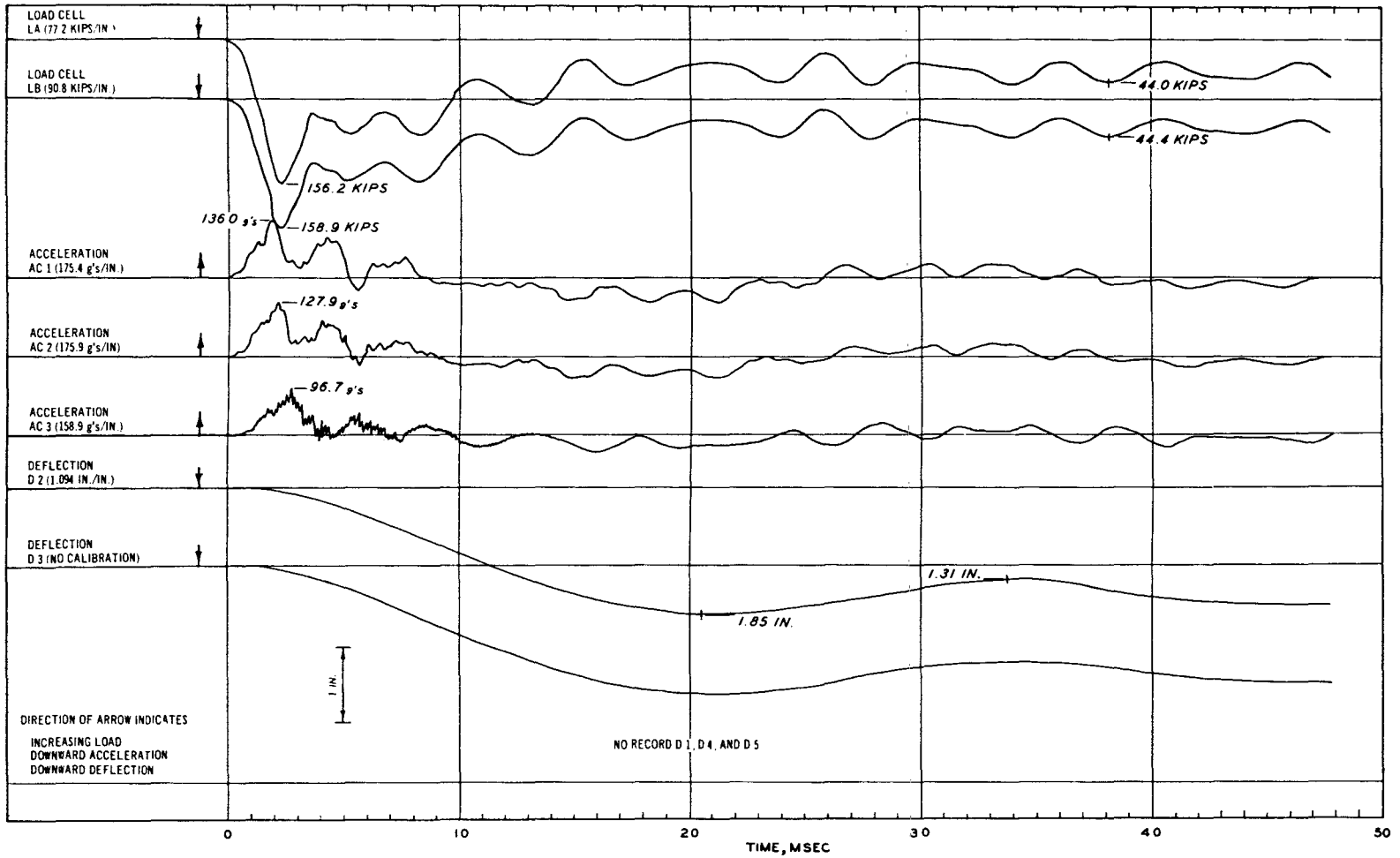


Figure C.1 Tracing from Recorder 1, Specimen D2075-1.

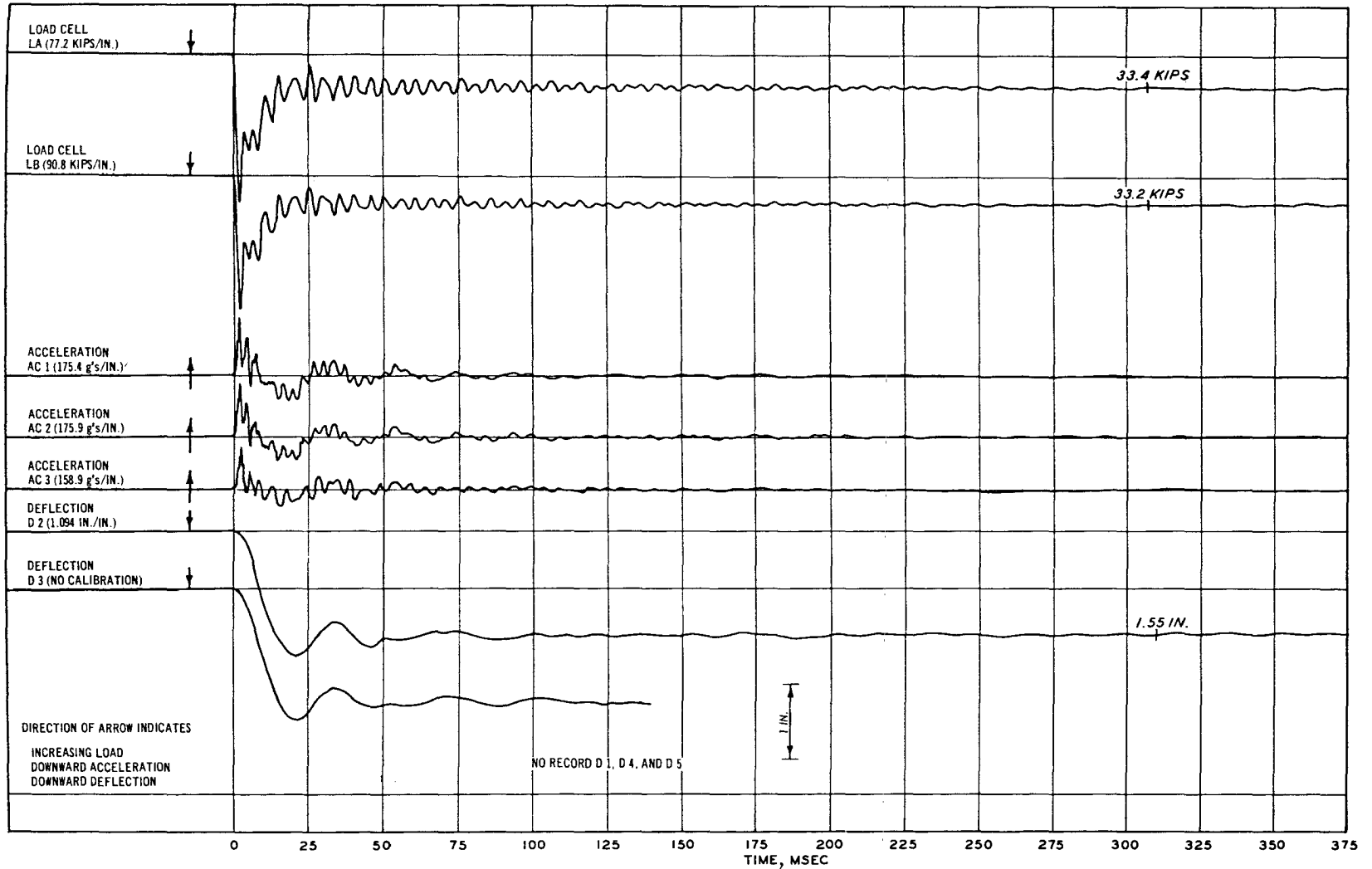


Figure C.2 Tracing from Recorder 1, condensed records, Specimen D2075-1.

334

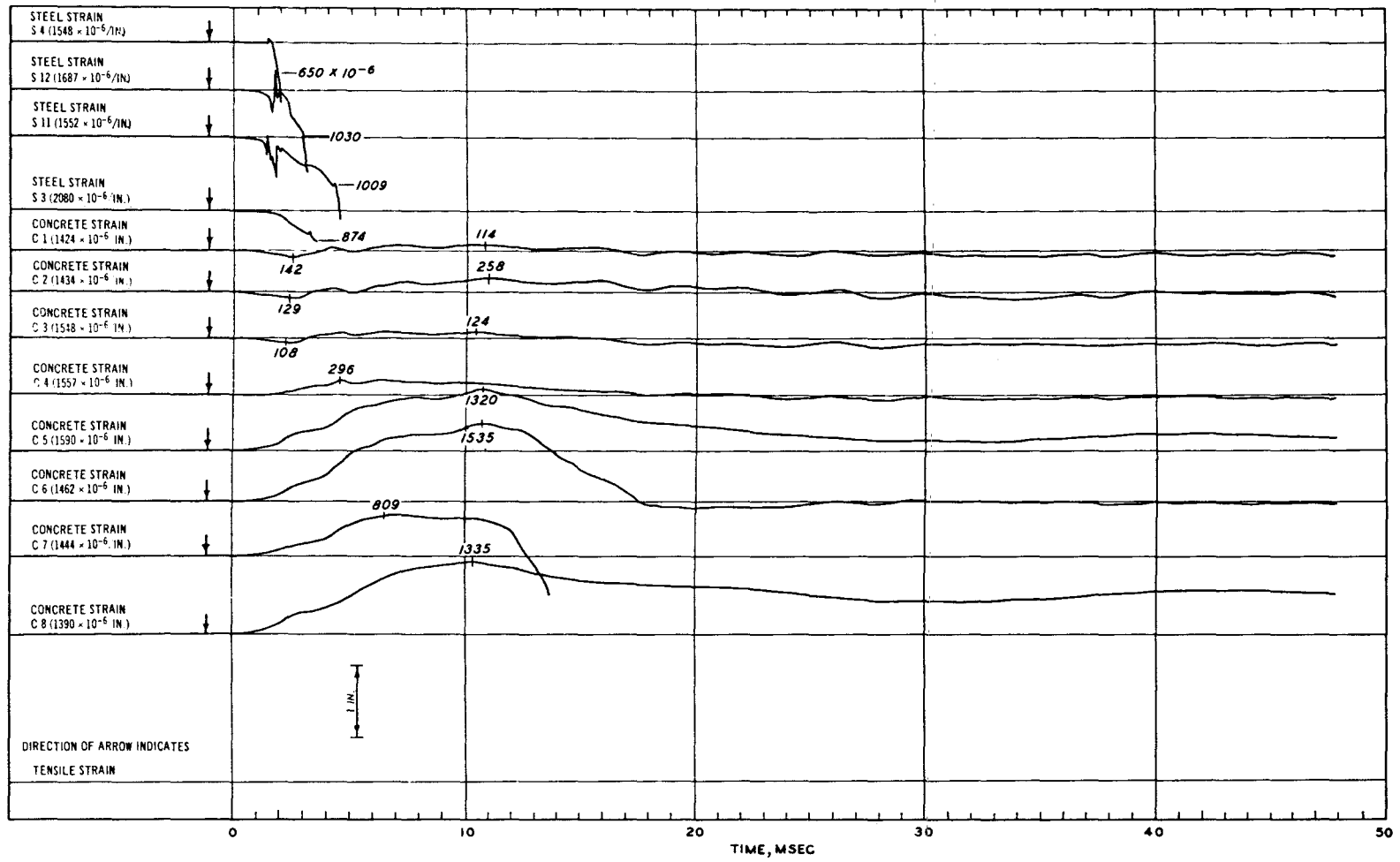


Figure C.3 Tracing from Recorder 2, Specimen D2075-1.

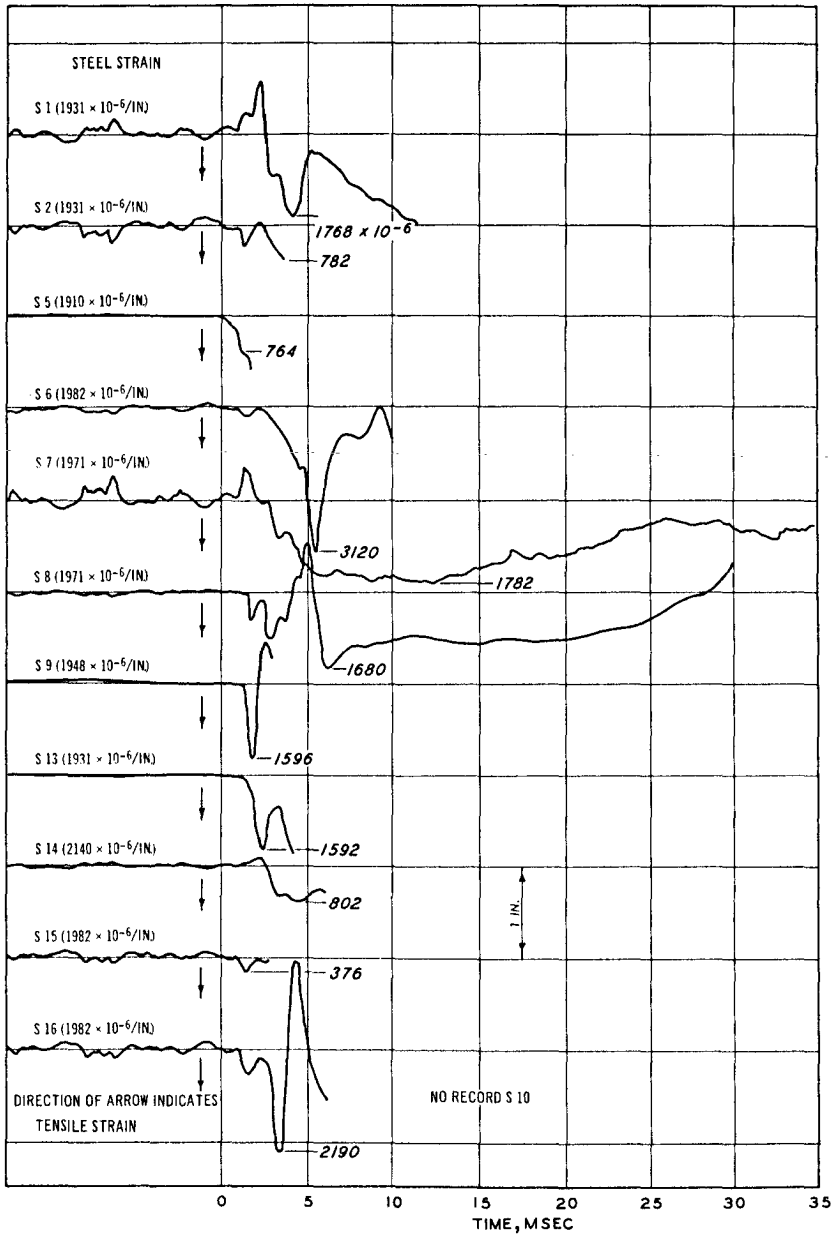


Figure C.4 Tracing from Oscillograph 1, Specimen D2075-1.

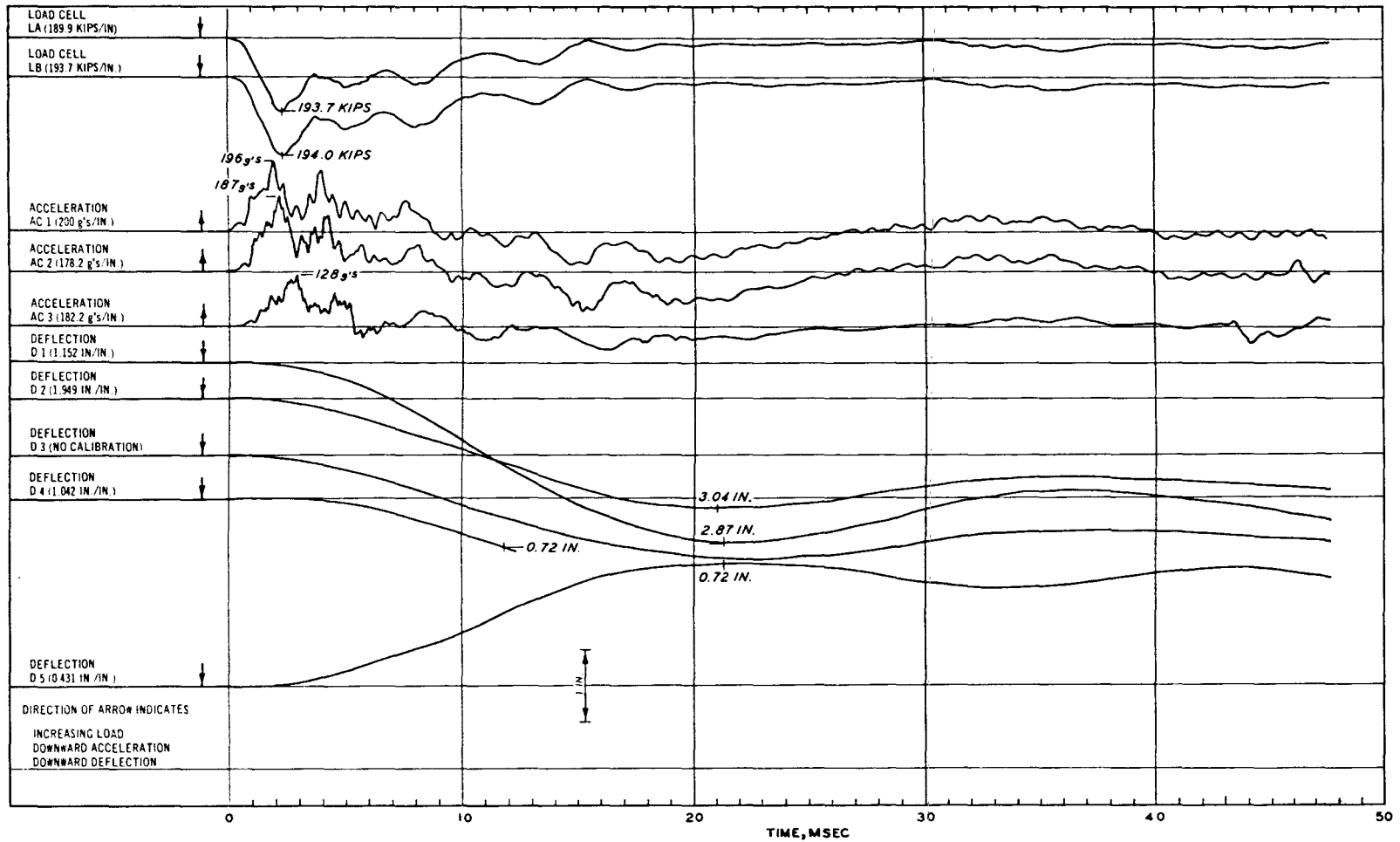


Figure C.5 Tracing from Recorder 1, Specimen D2075-2.

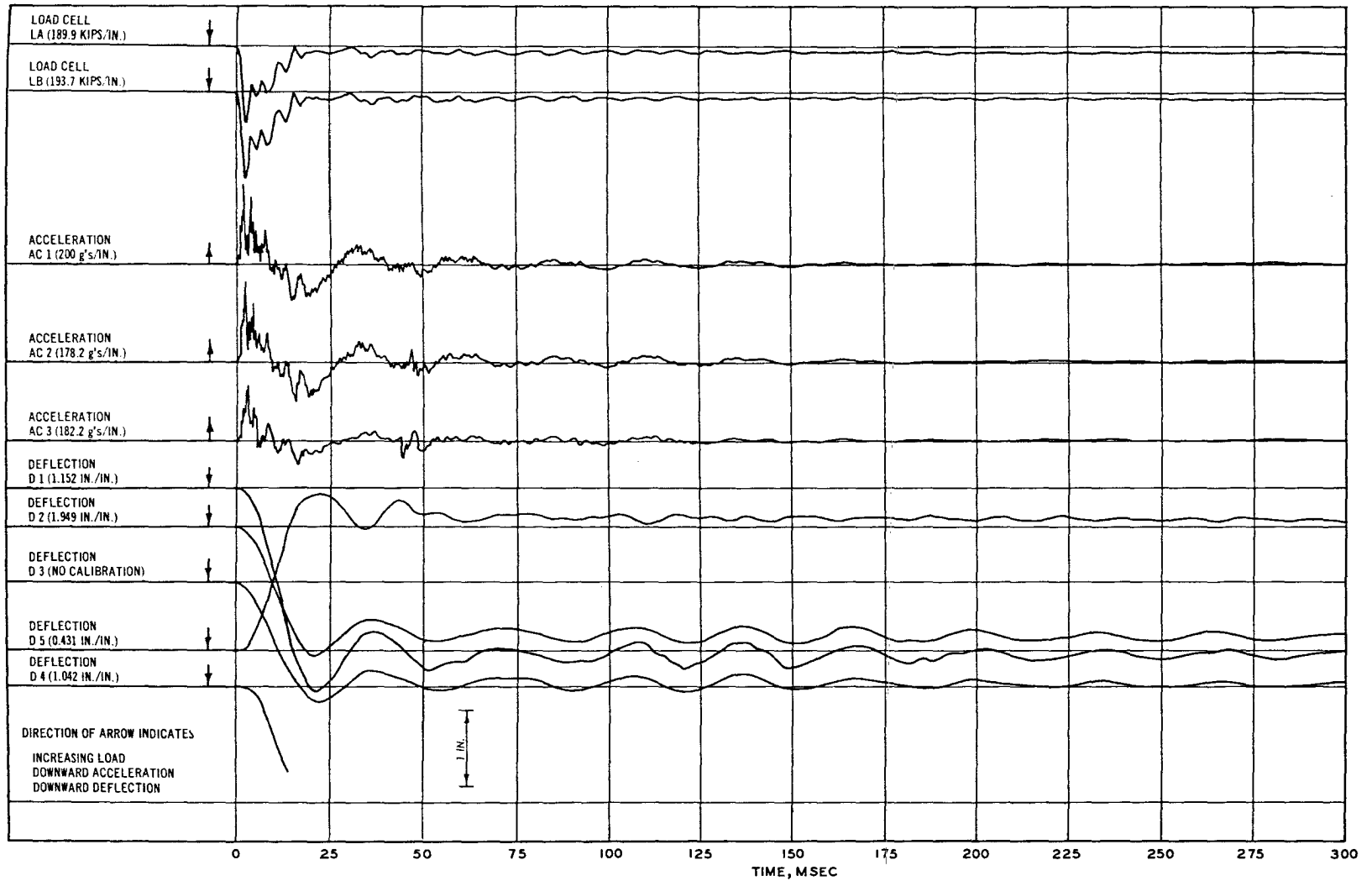


Figure C.6 Tracing from Recorder 1, condensed records, Specimen D2075-2.

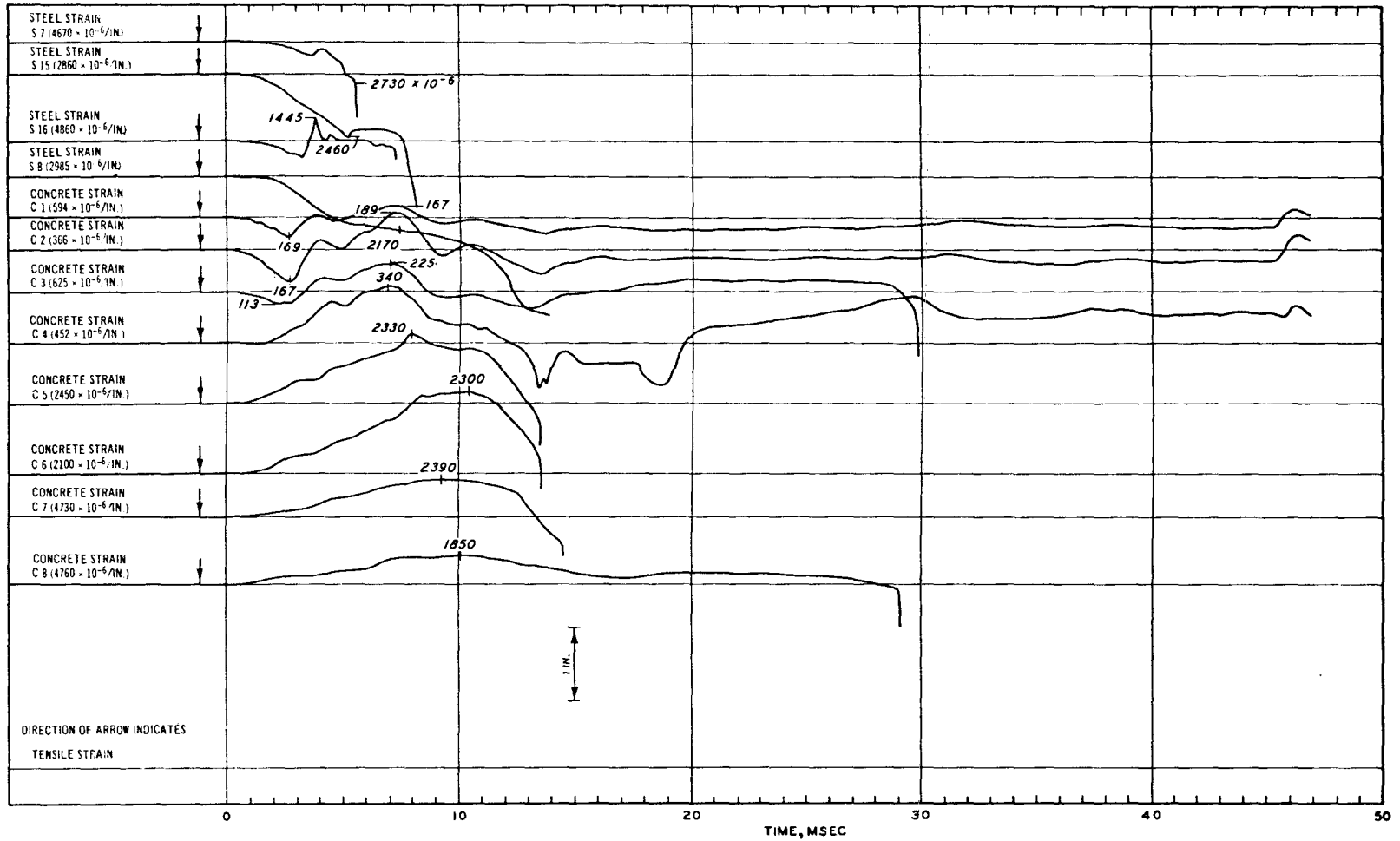


Figure C.7 Tracing from Recorder 2, Specimen D2075-2.

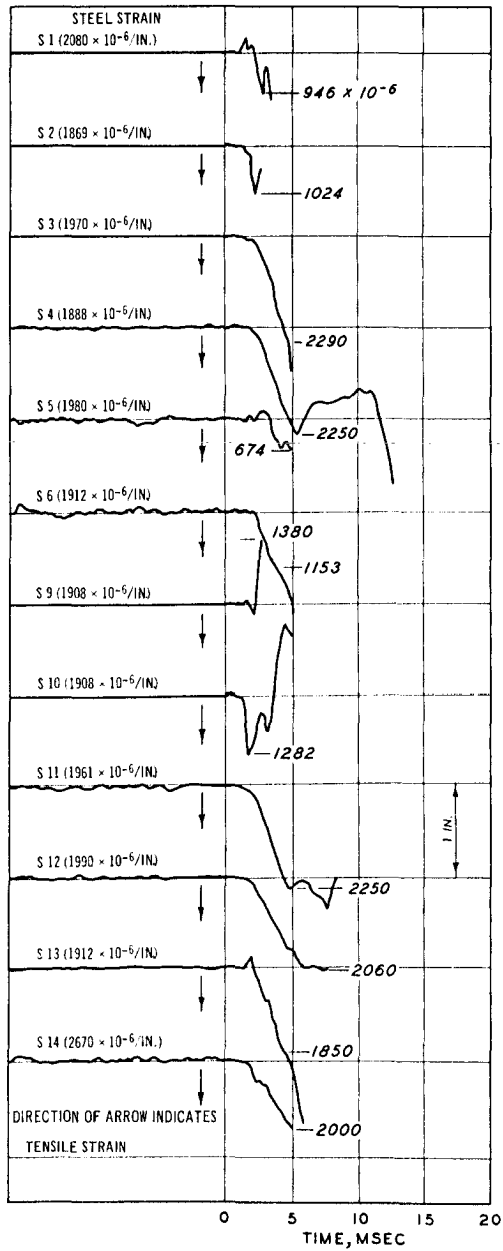


Figure C.8 Tracing from Oscillograph 1, Specimen D2075-2.



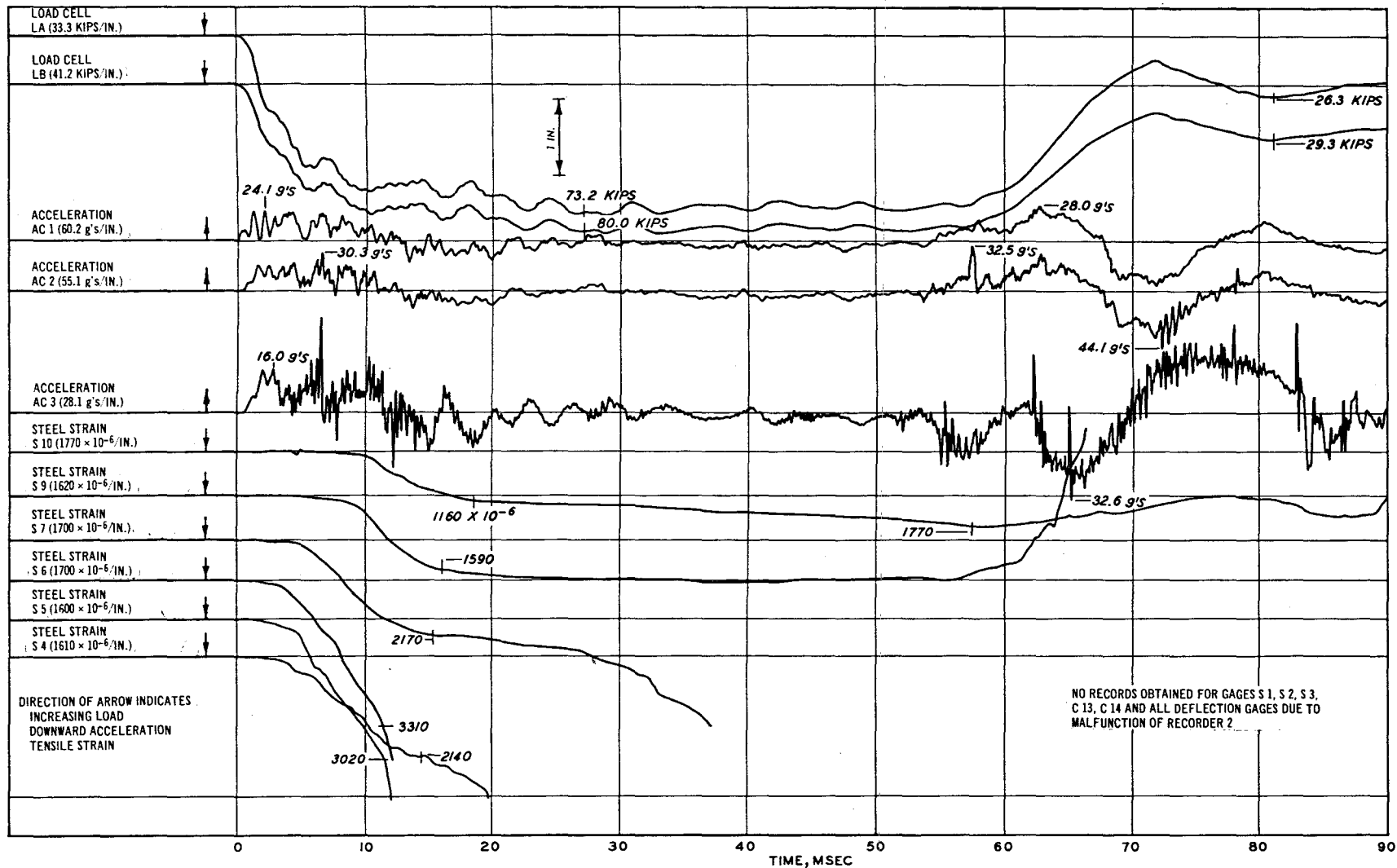


Figure C.9 Tracing from Recorder 1, Specimen D2075-3.

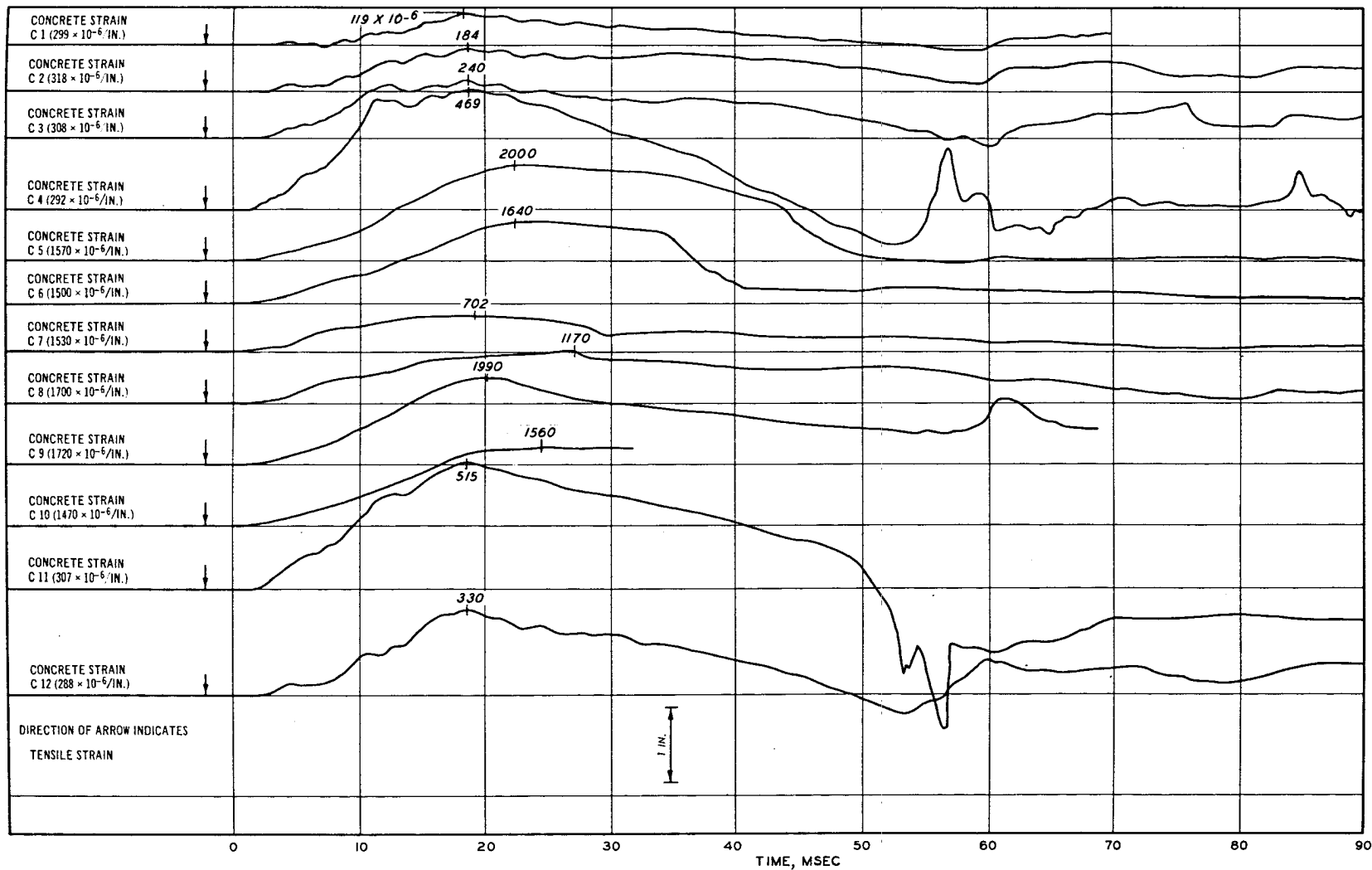


Figure C.10 Tracing from Recorder 3, Specimen D2075-3.

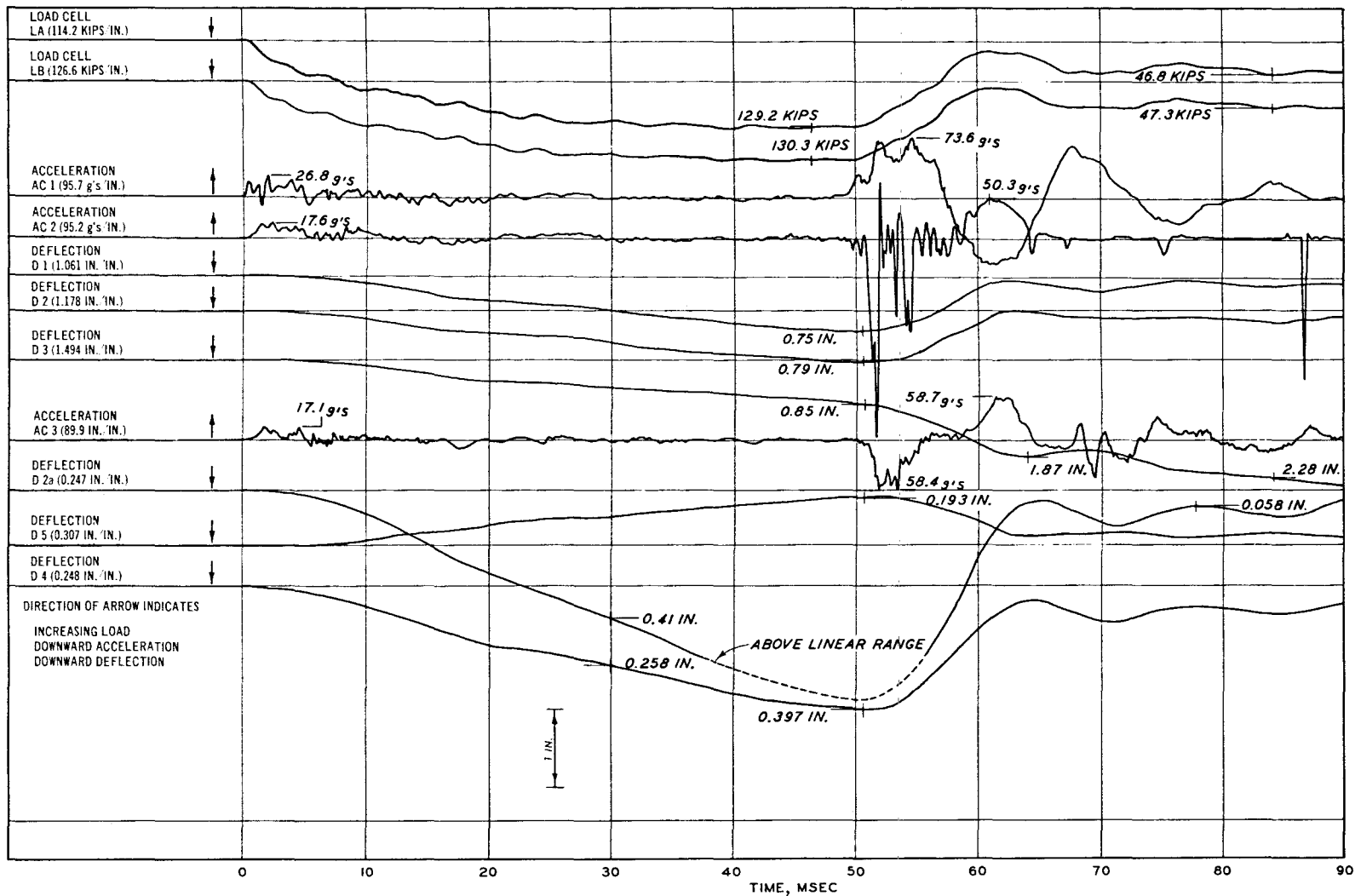


Figure C.11 Tracing of load, acceleration, and deflection records, Specimen D2150-1.

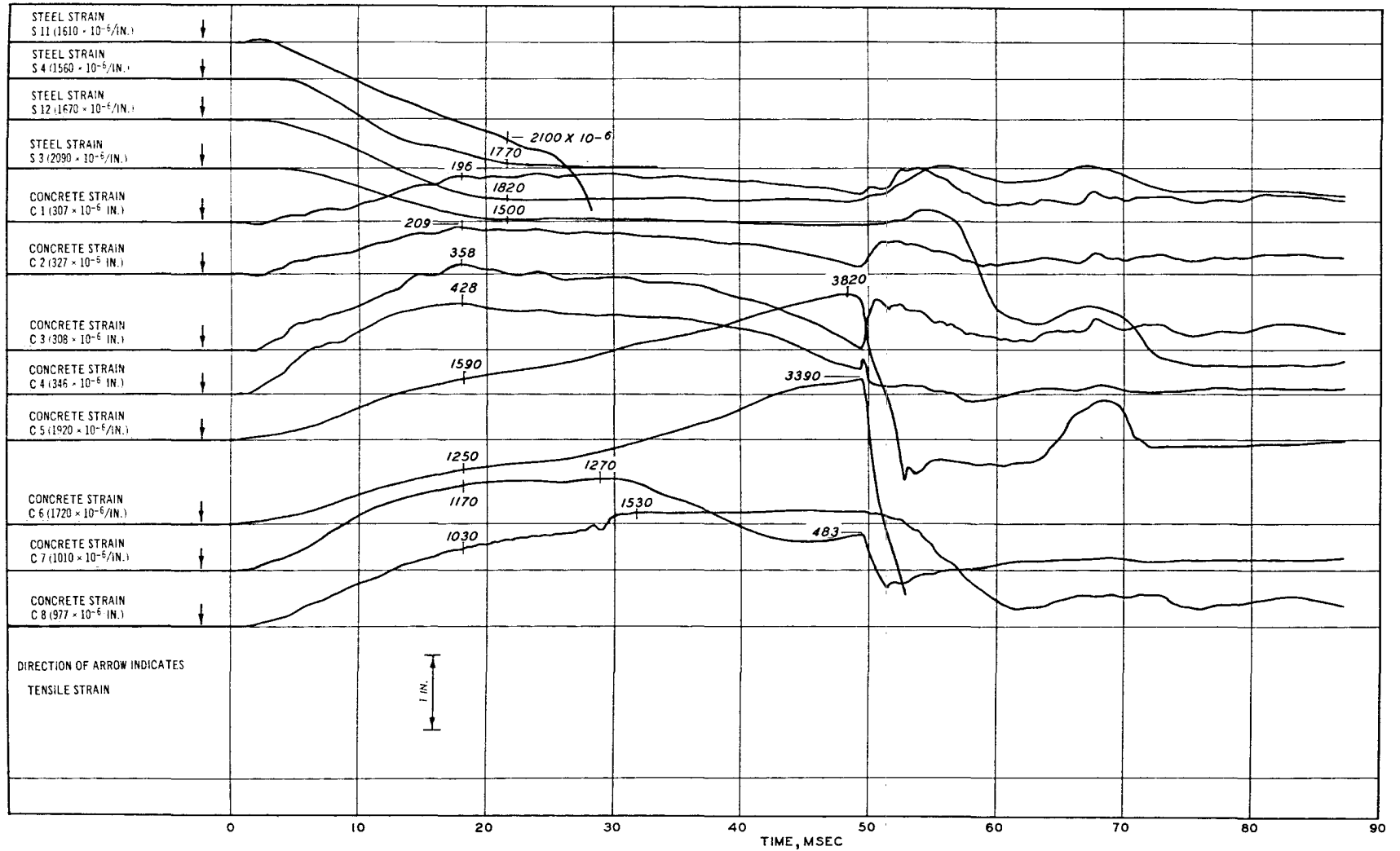


Figure C.12 Tracing of concrete and steel strain records, Specimen D2150-1.

344

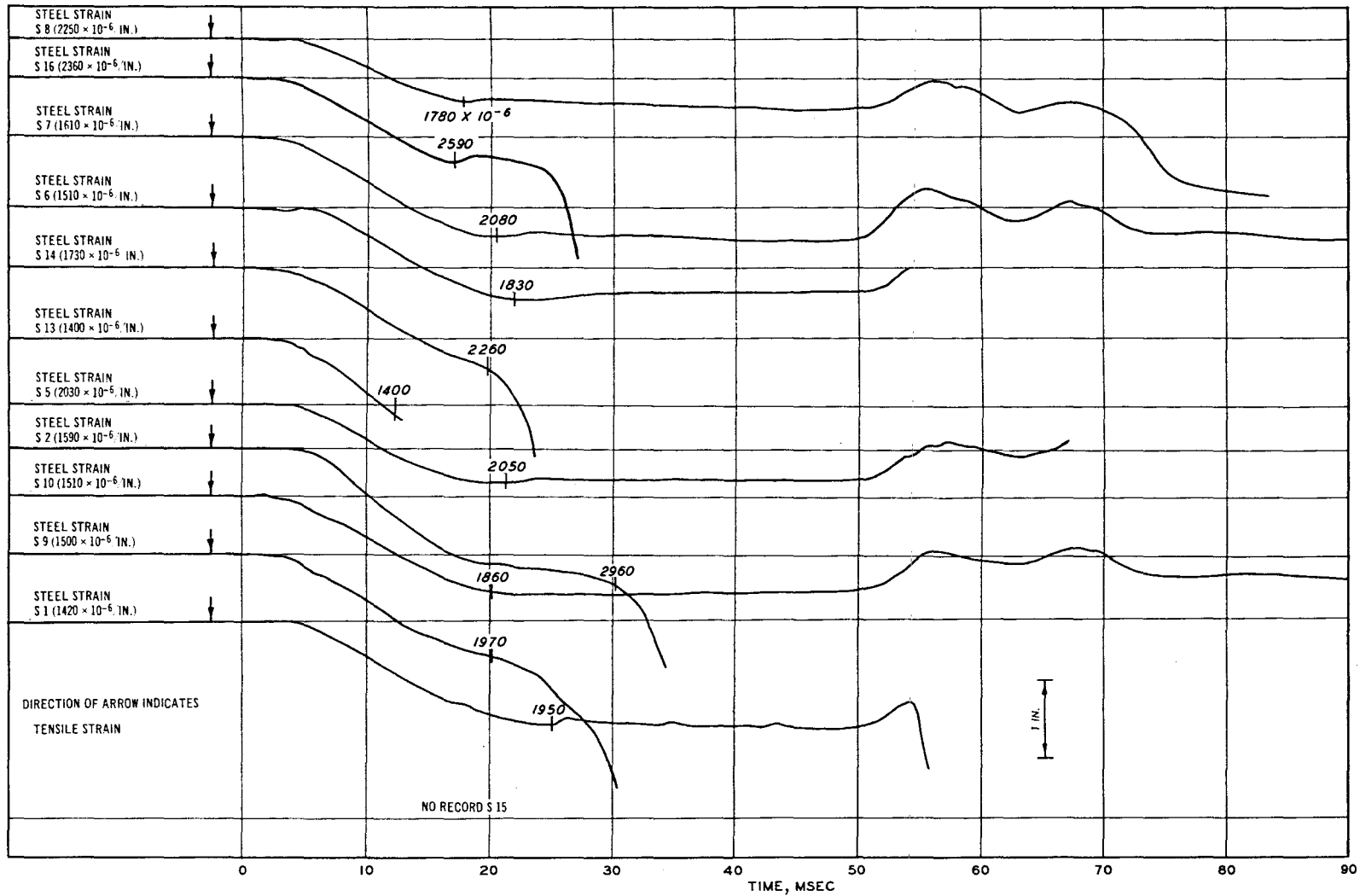


Figure C.13 Tracing of steel strain records, Specimen D2150-1.

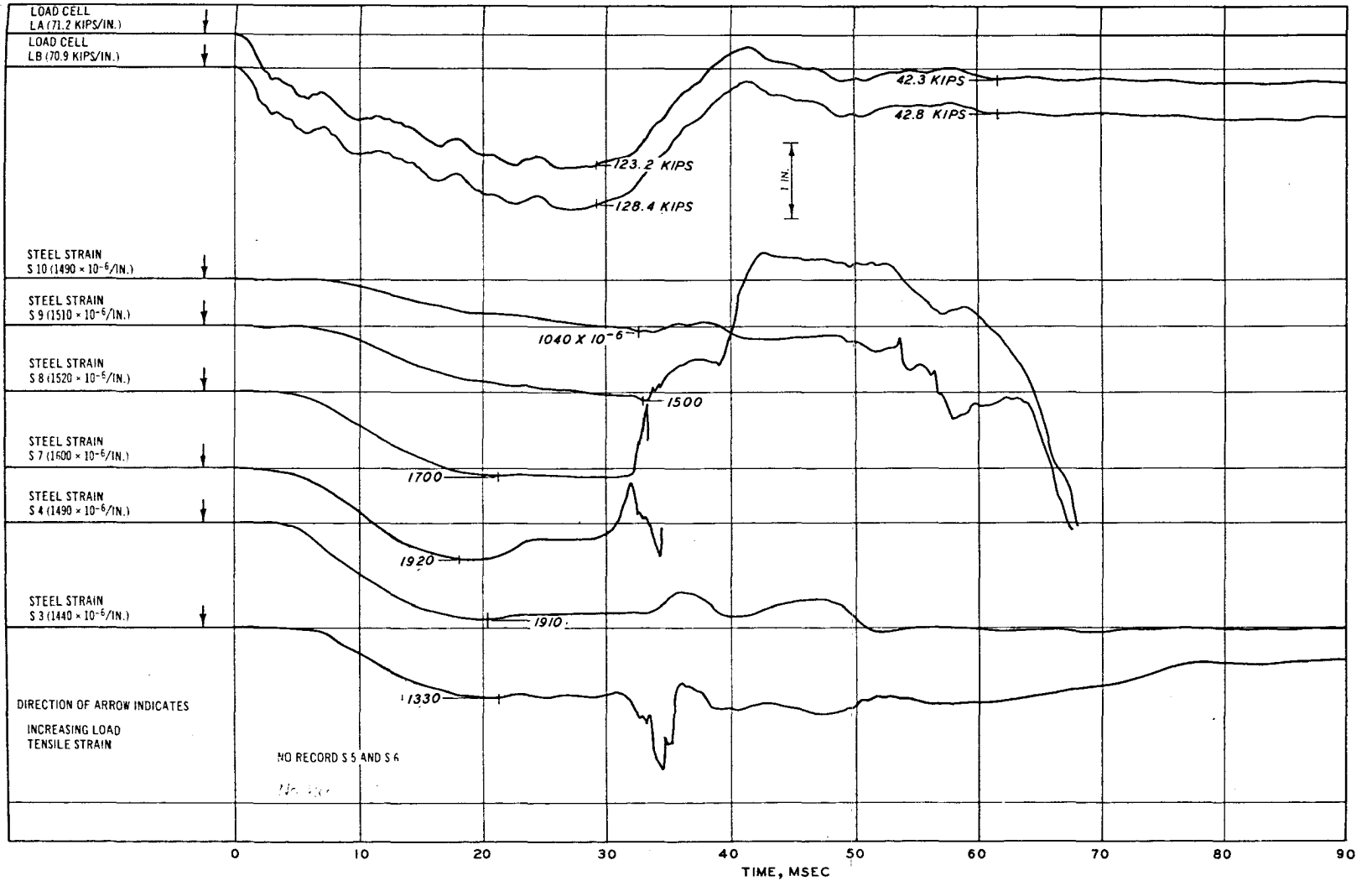


Figure C.14 Tracing of load and steel strain records, Specimen D2150-2.

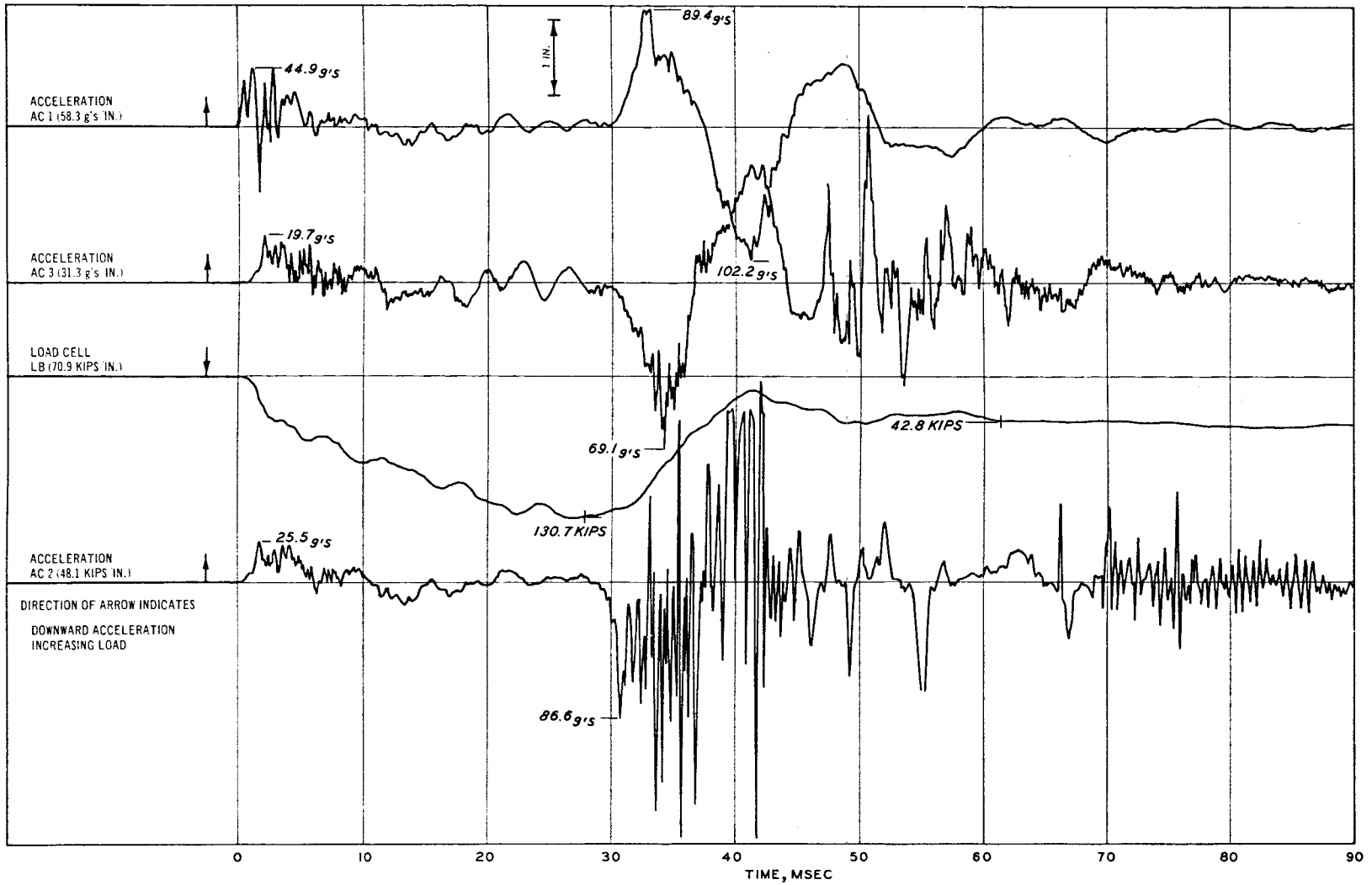


Figure C.15 Tracing of acceleration records, Specimen D2150-2.

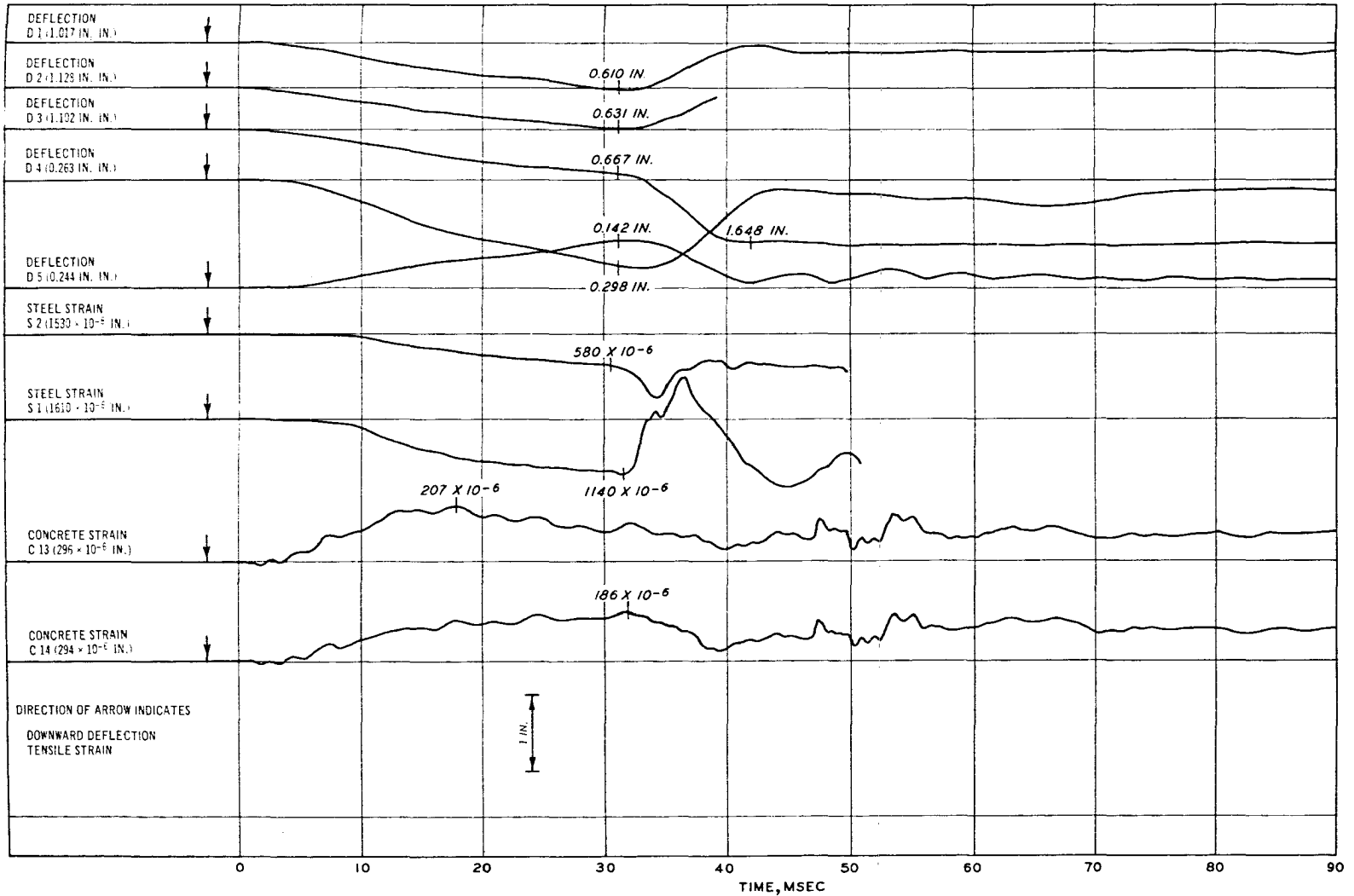


Figure C.16 Tracing of deflection, concrete strain, and steel strain records, Specimen D2150-2.



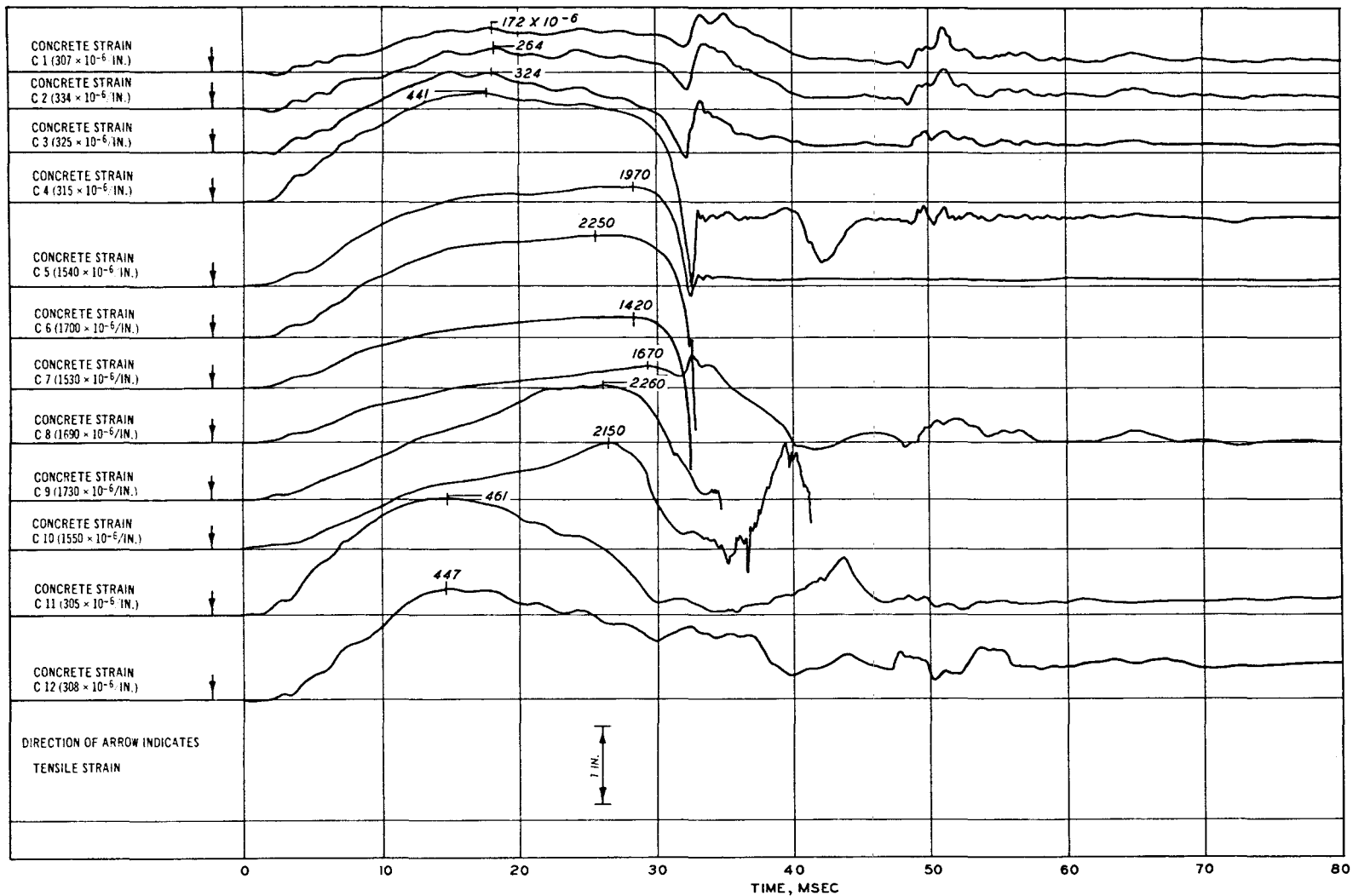


Figure C.17 Tracing of concrete strain records, Specimen D2150-2.

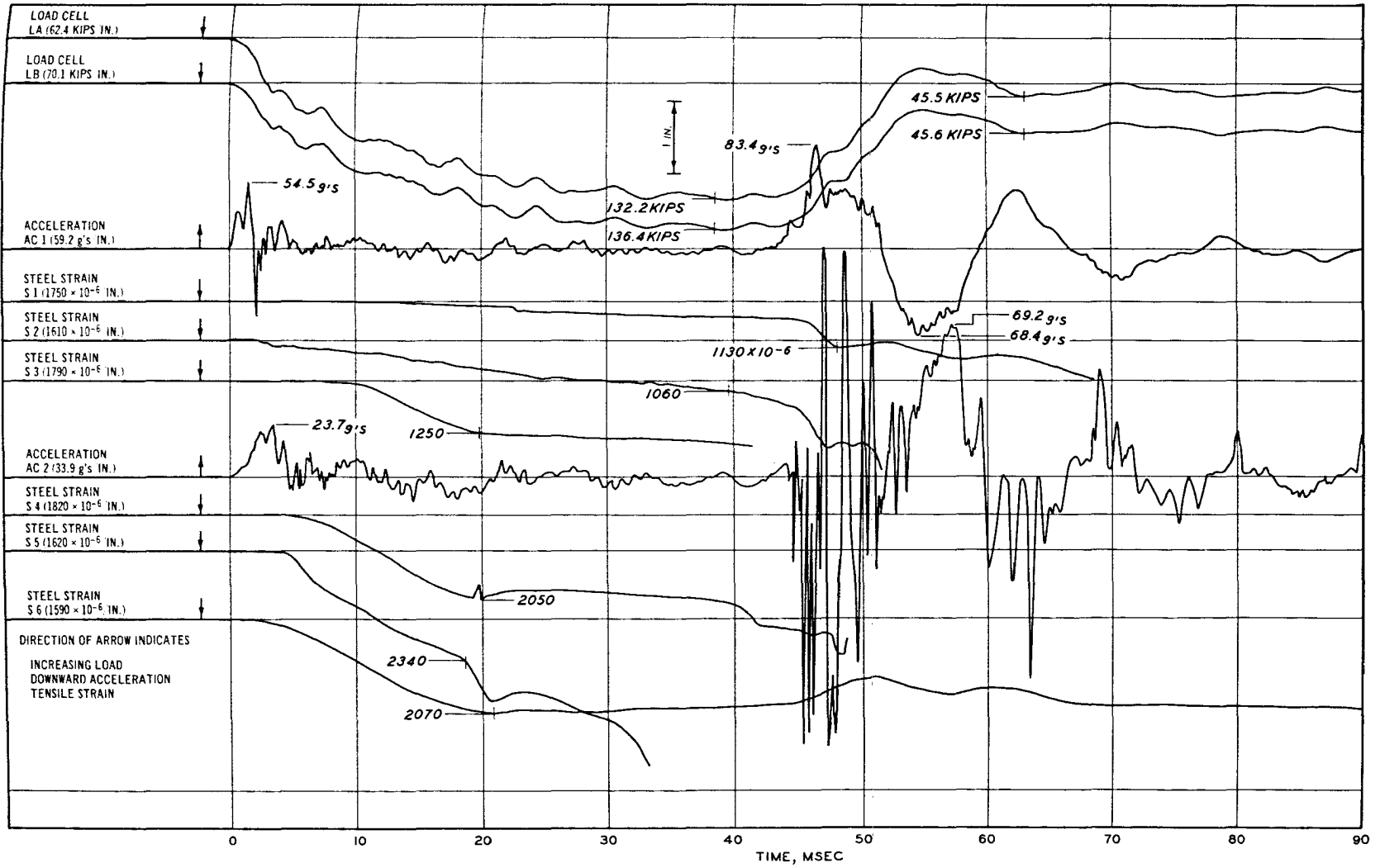


Figure C.18 Tracing of load, acceleration, and steel strain records, Specimen D2150-3.

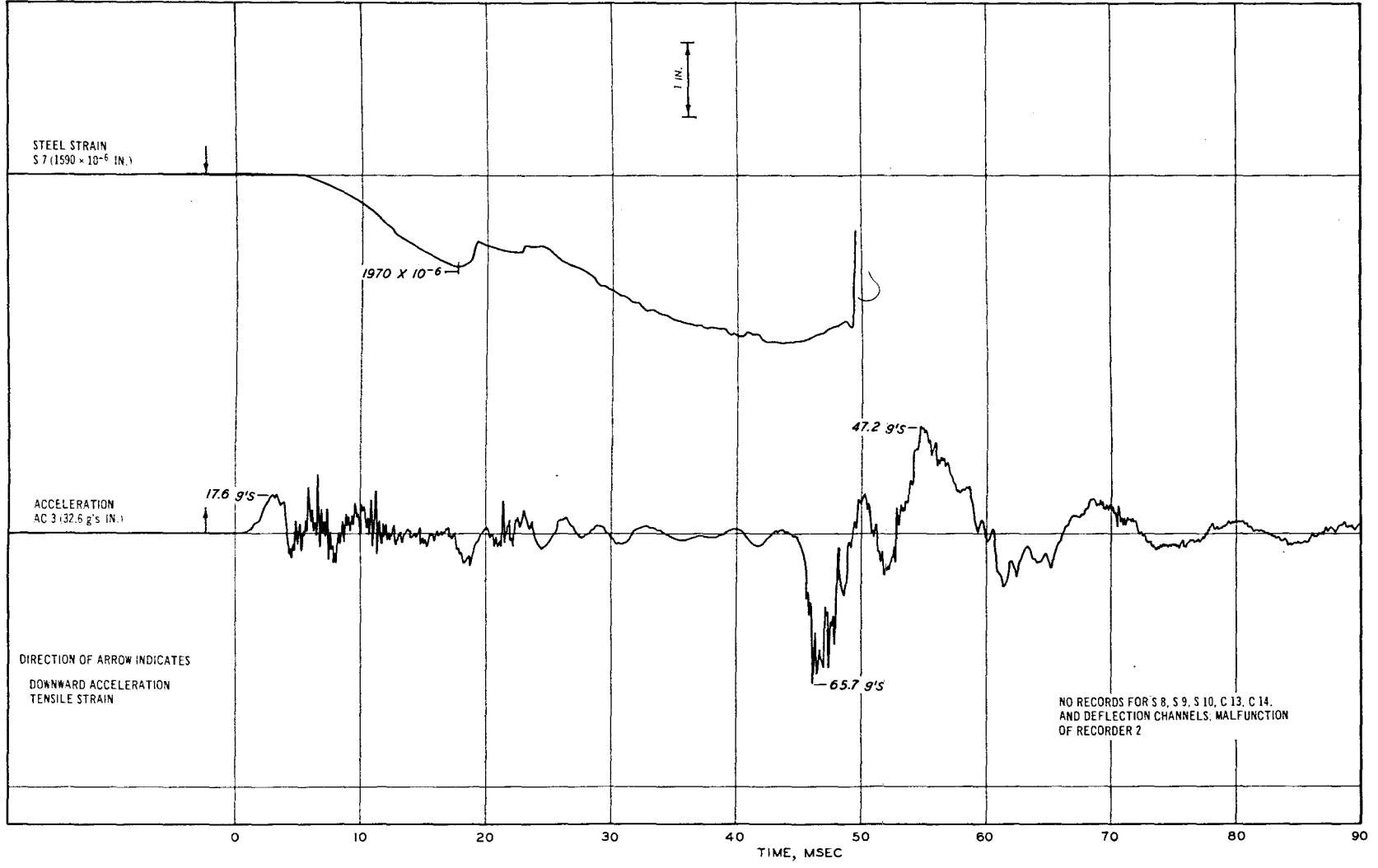


Figure C.19 Tracing of acceleration and steel strain records, Specimen D2150-3.

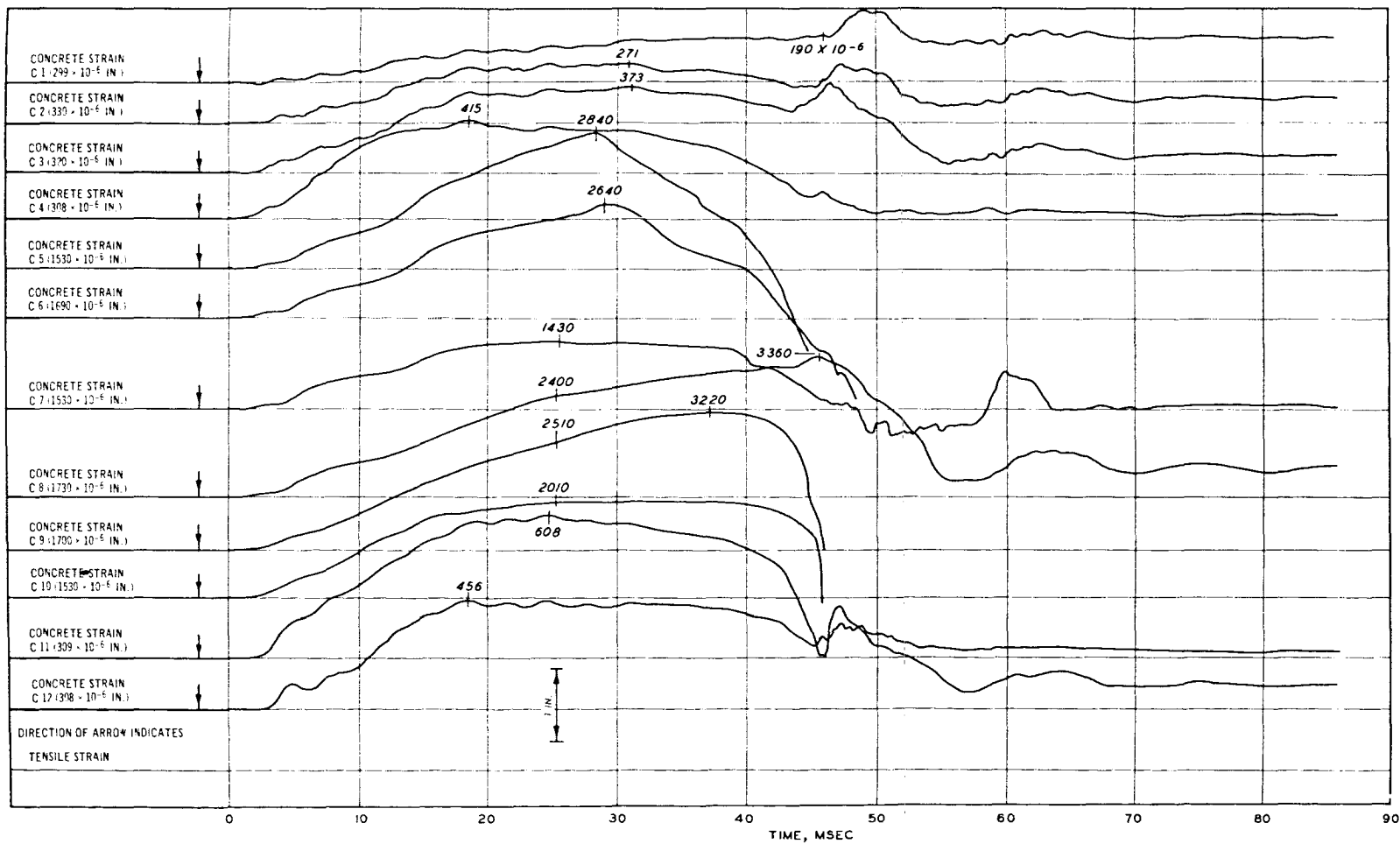


Figure C.20 Tracing of concrete strain records, Specimen D2150-3.

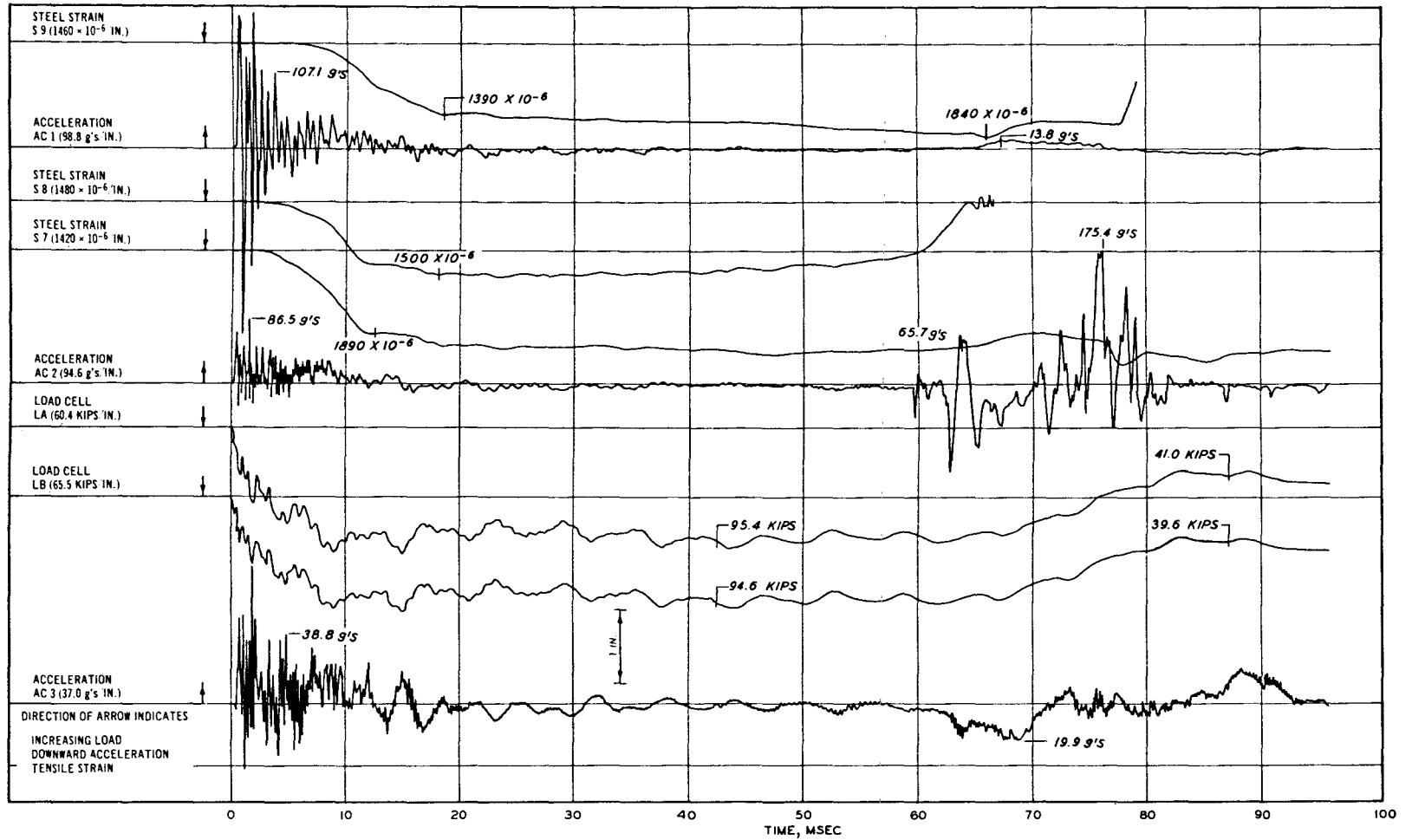


Figure C.21 Tracing of load, acceleration, and steel strain records, Specimen D4075-1.

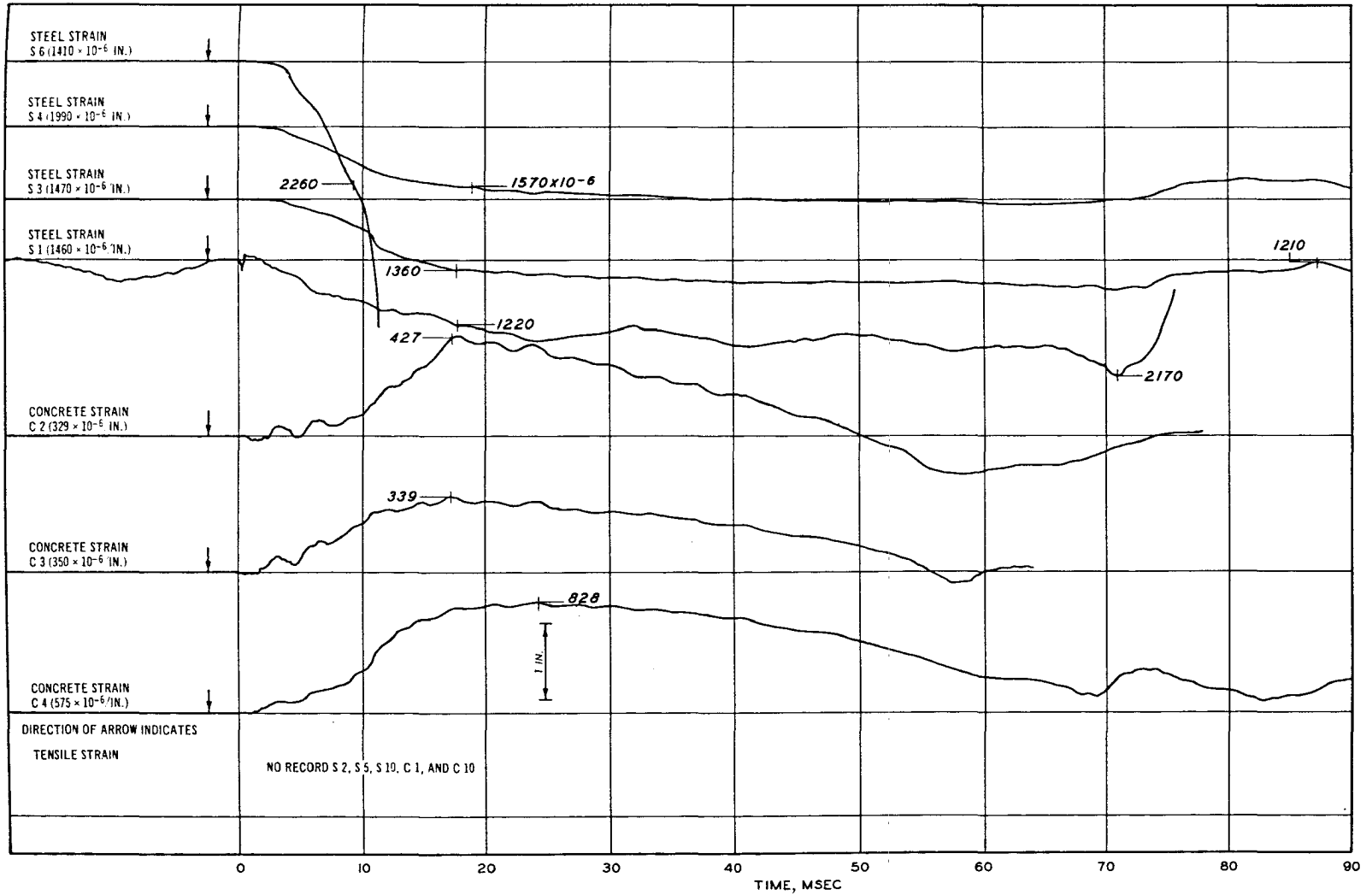


Figure C.22 Tracing of concrete and steel strain records, Specimen D4075-1.

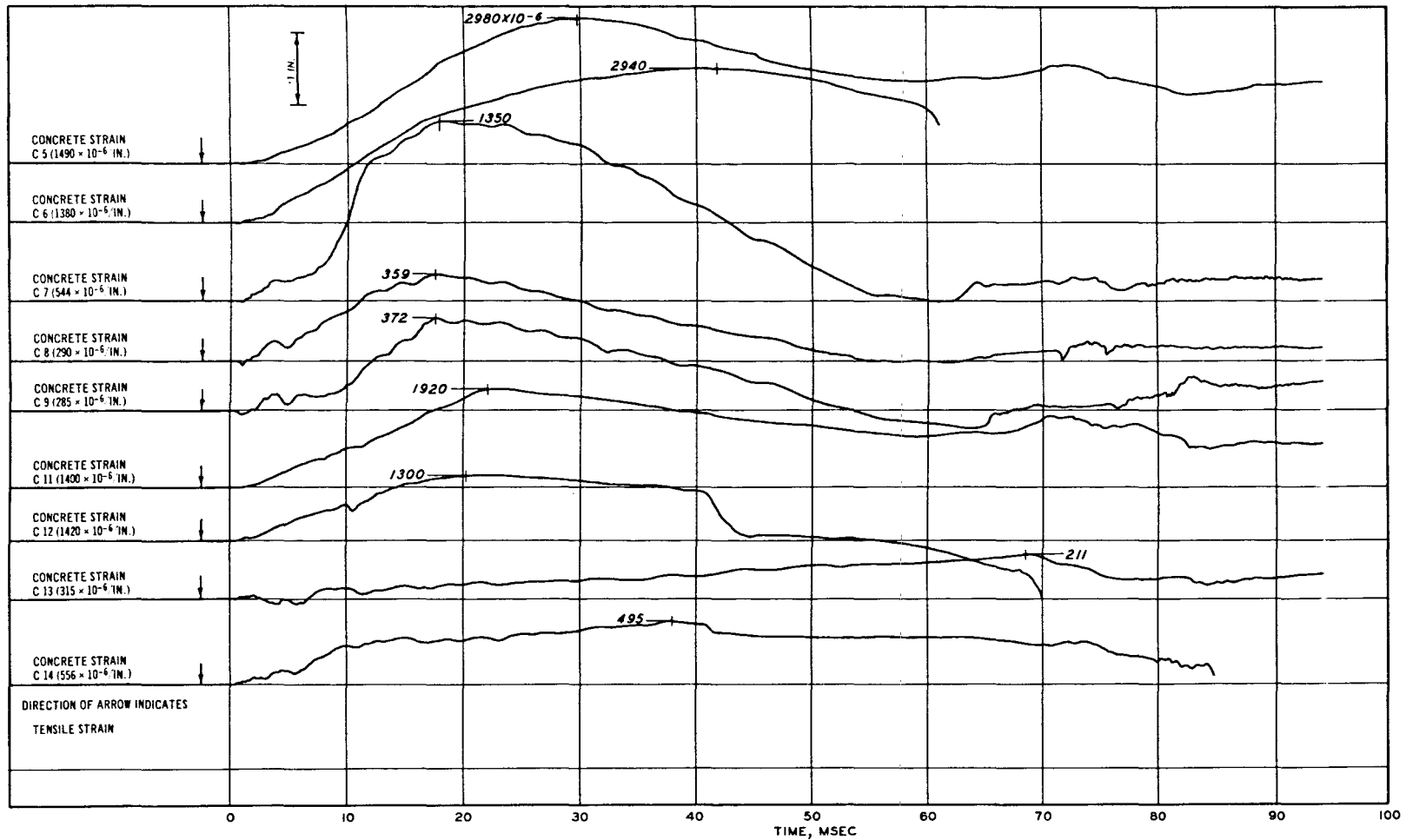


Figure C.23 Tracing of concrete strain records, Specimen D4075-1.

355

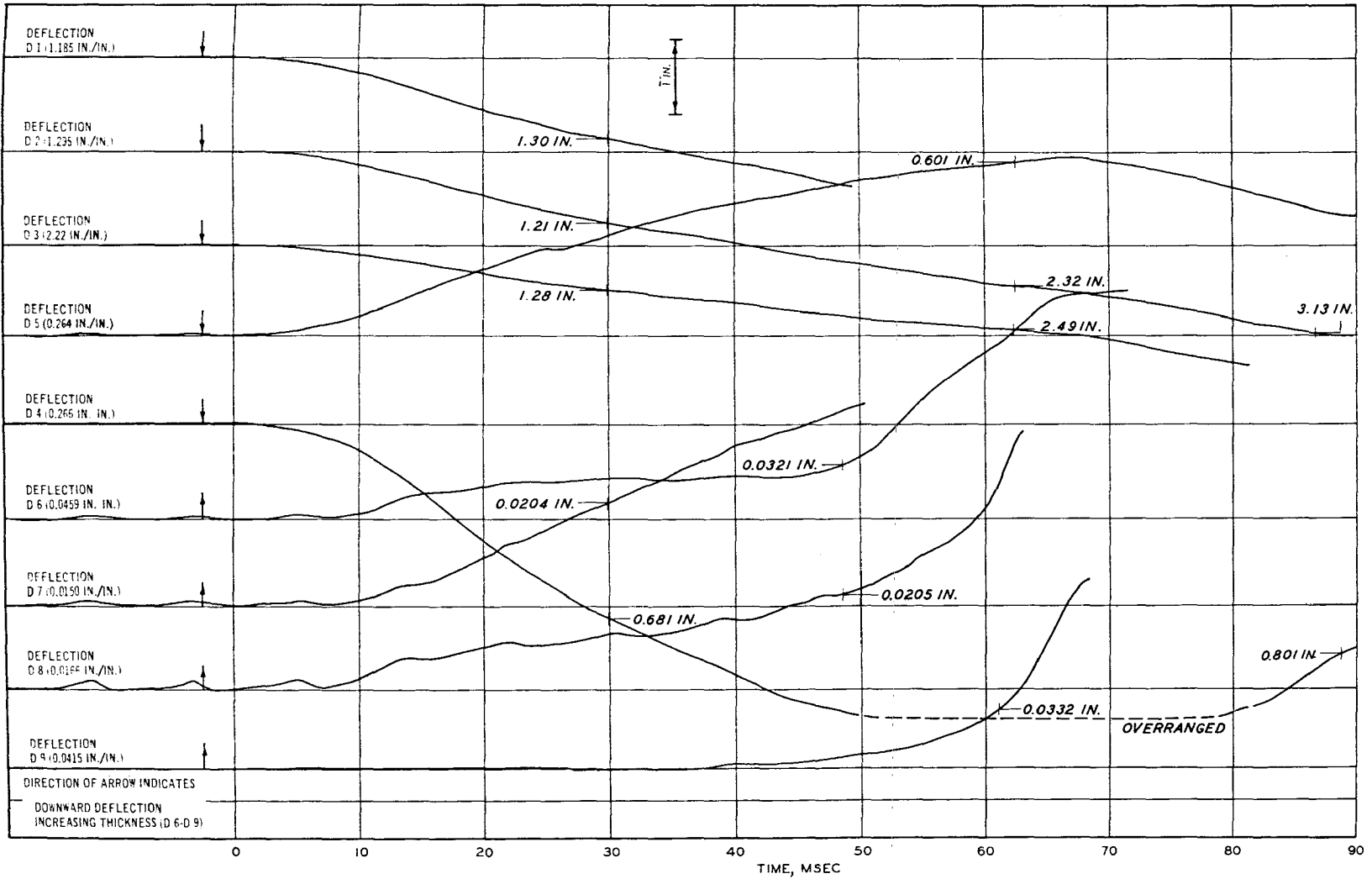


Figure C.24 Tracing of deflection records, Specimen D4075-1.



356

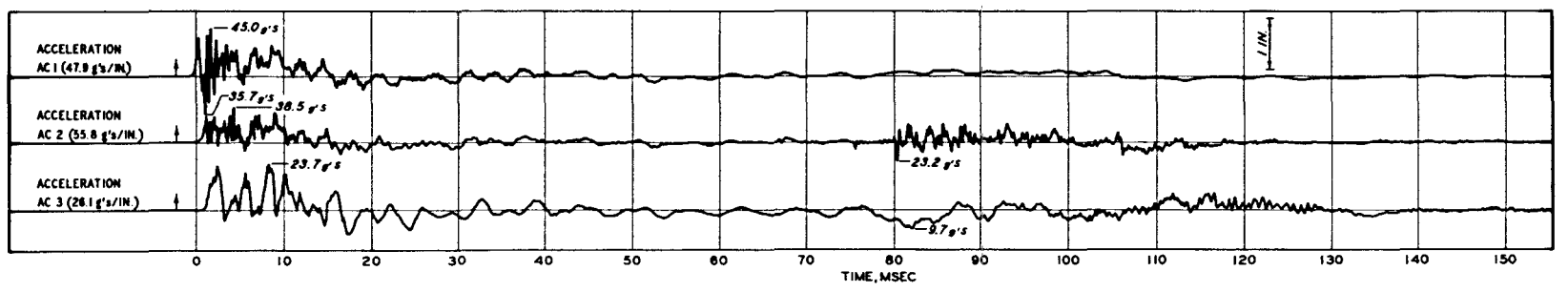
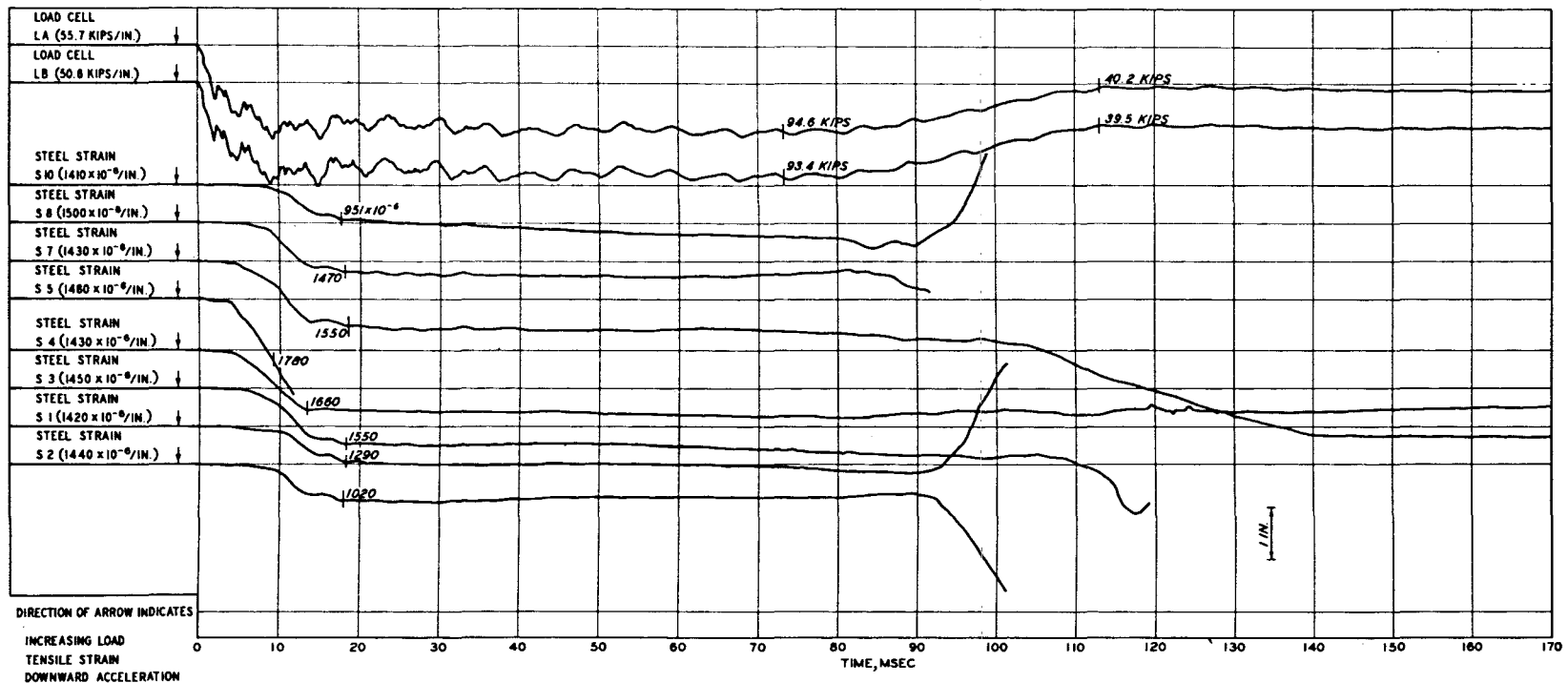


Figure C.25 Tracing of load, acceleration, and steel strain records, Specimen D4075-2.

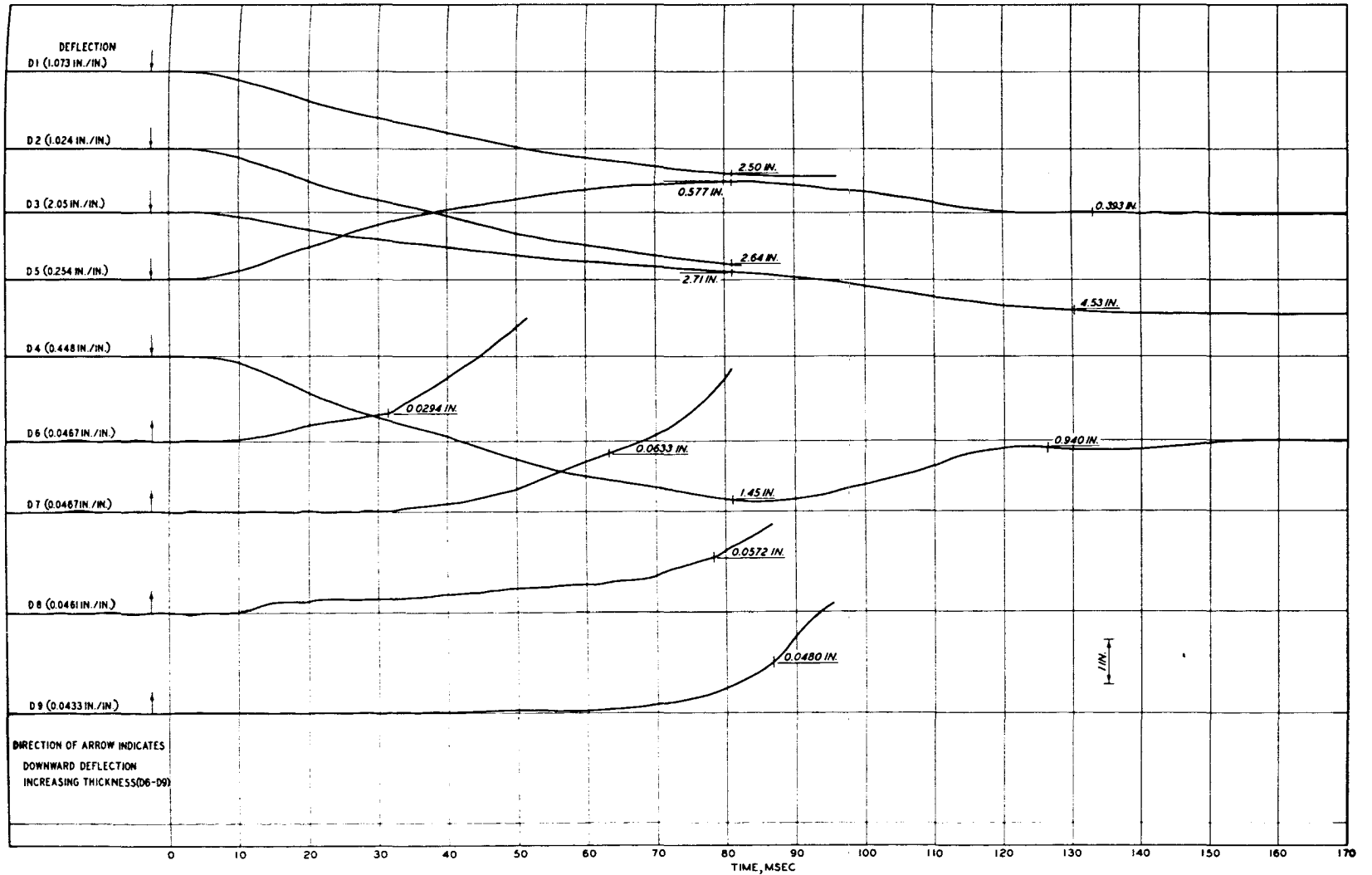


Figure C.26 Tracing of deflection records, Specimen D4075-2.

358

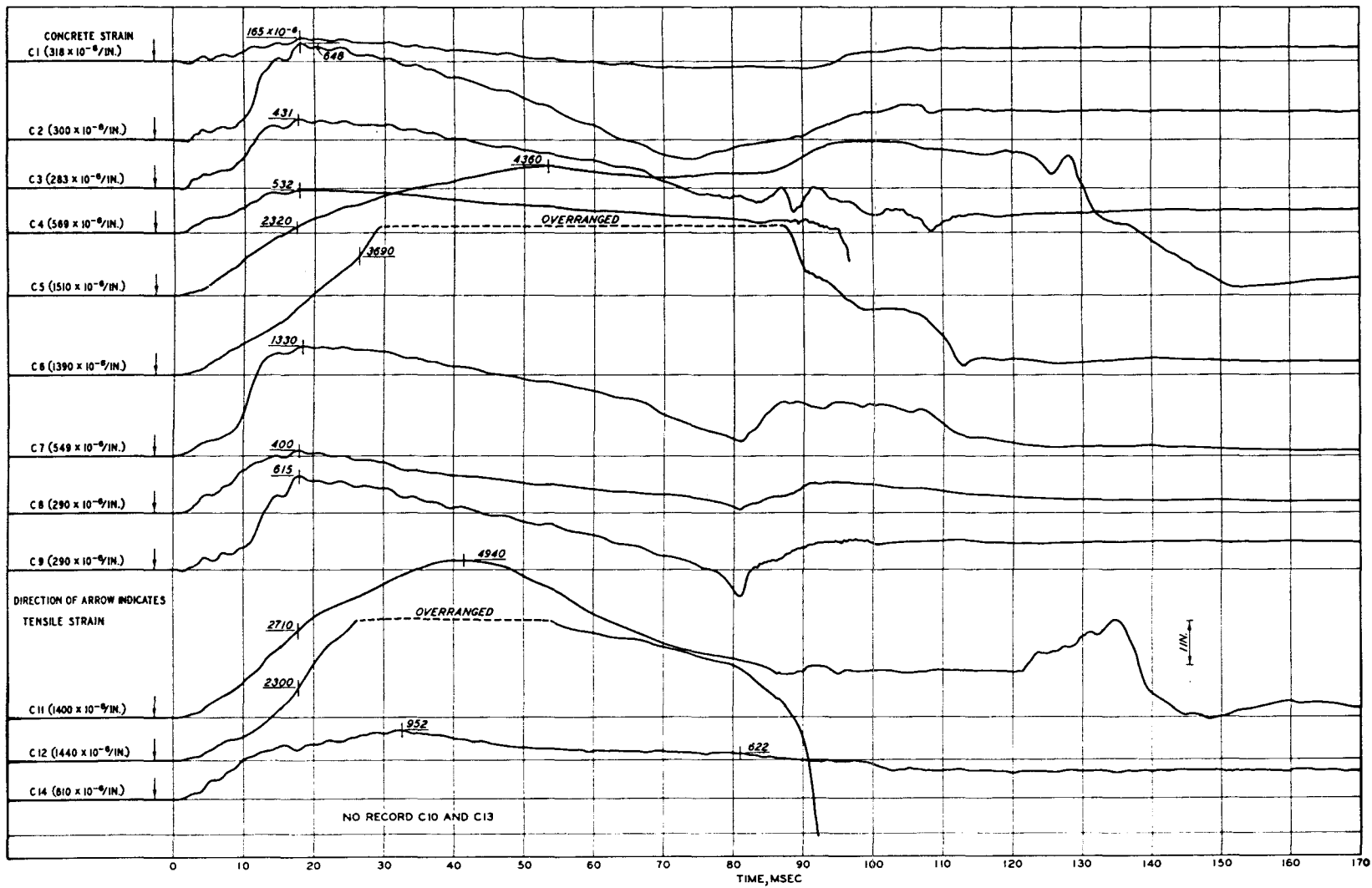


Figure C.27 Tracing of concrete strain records, Specimen D4075-2.

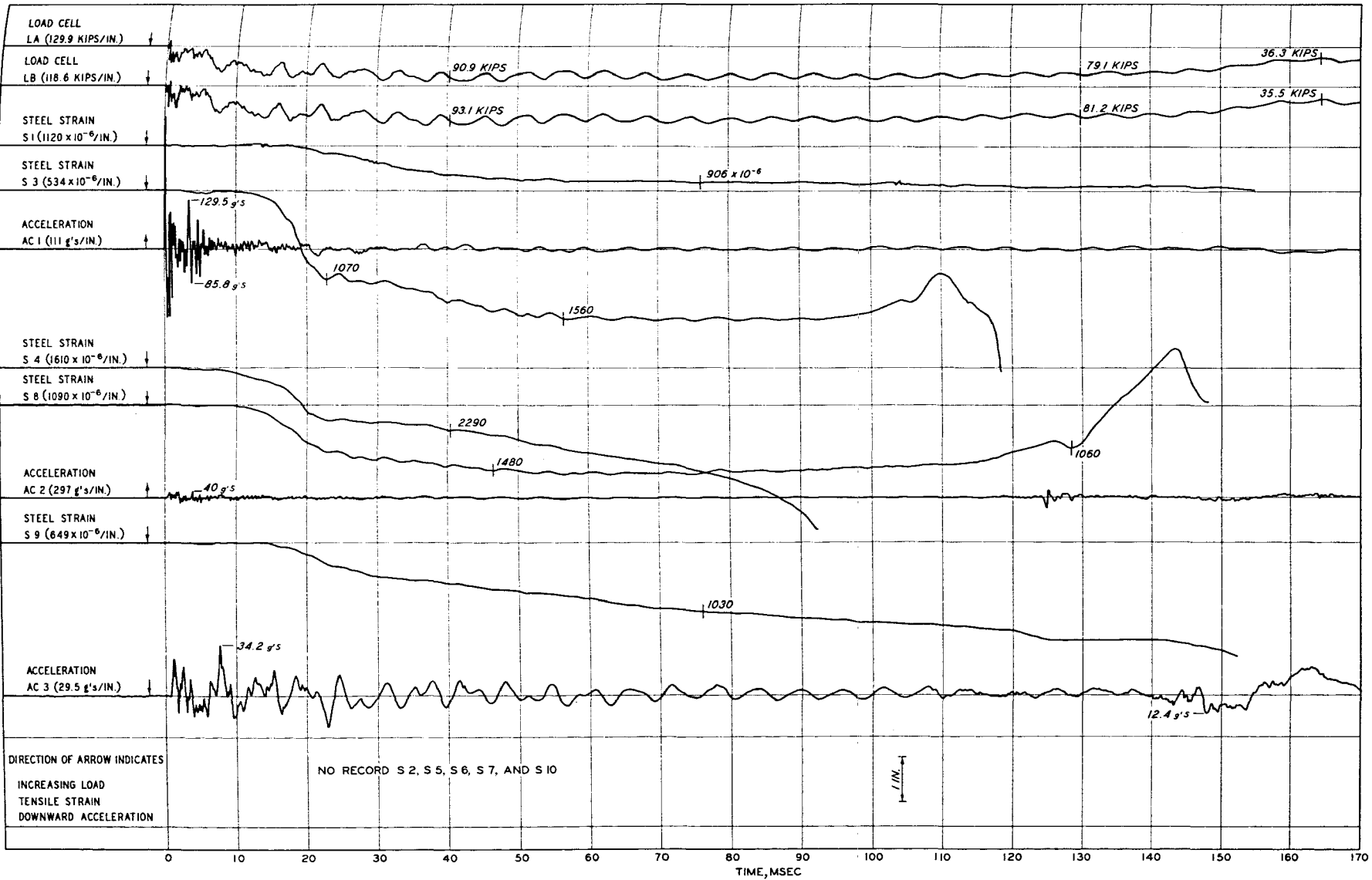


Figure C.28 Tracing of load, acceleration, and steel strain records, Specimen D4075-3.

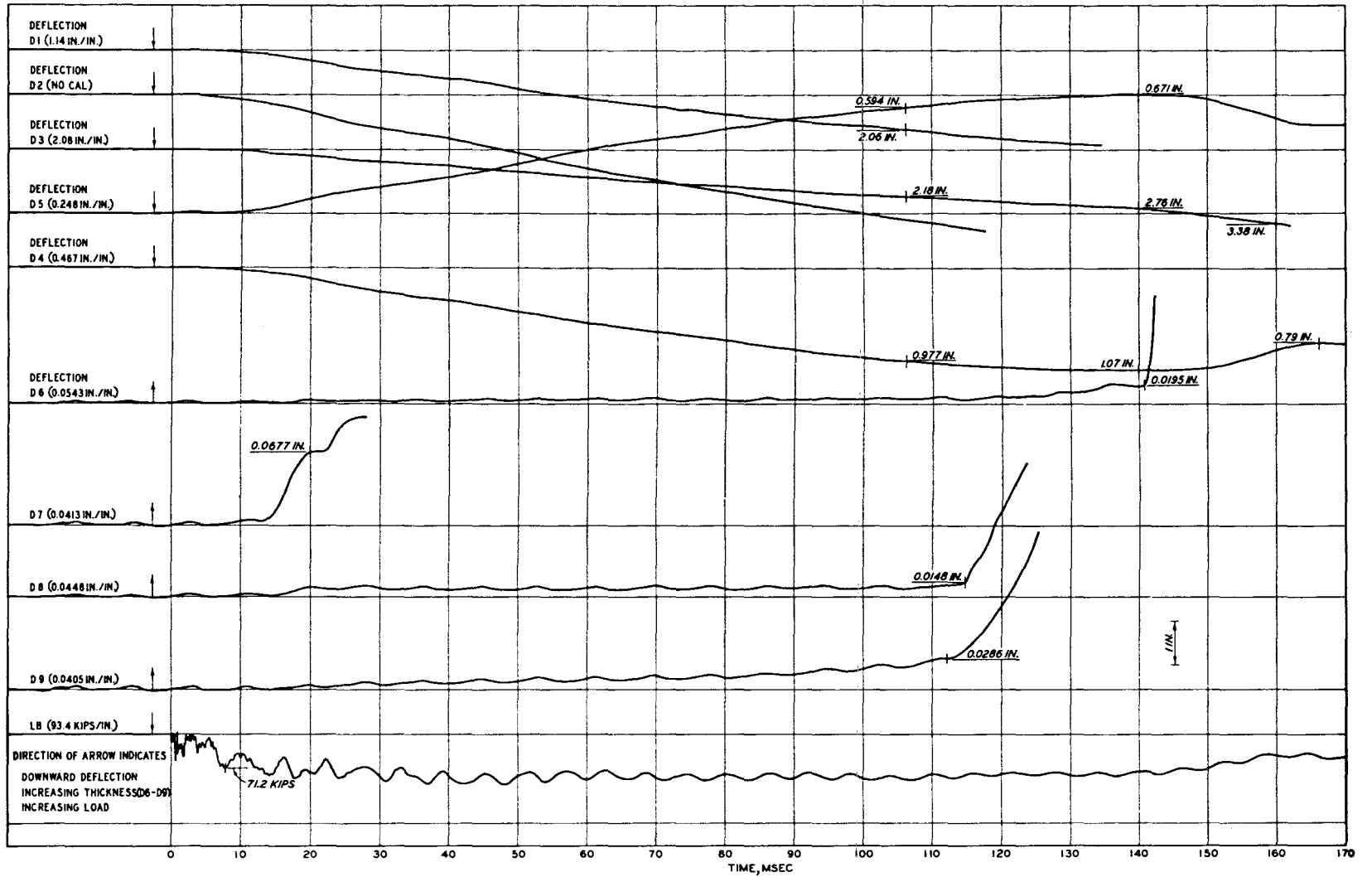


Figure C.29 Tracing of deflection records, Specimen D4075-3.

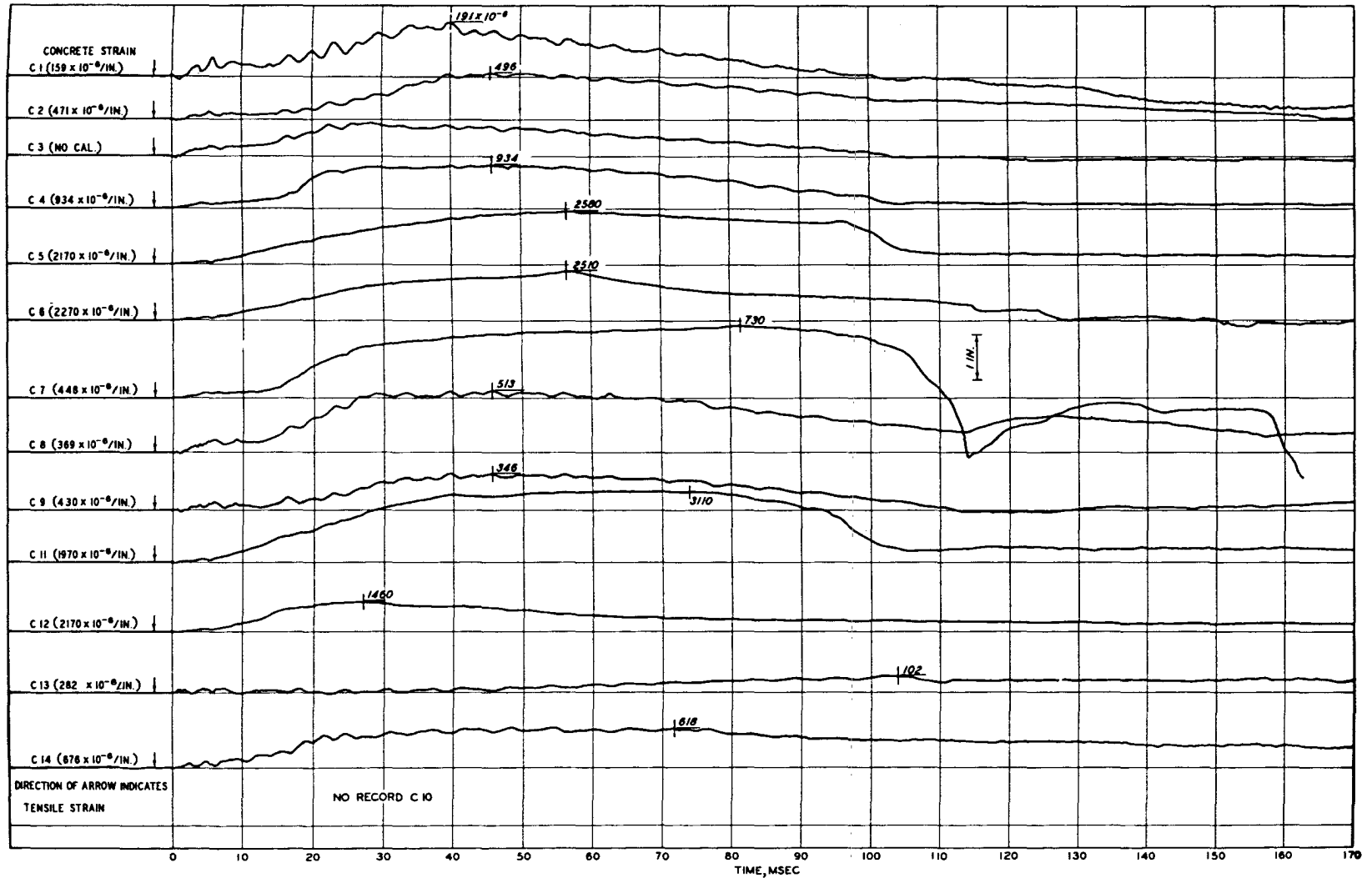


Figure C.30 Tracing of concrete strain records, Specimen D4075-3.

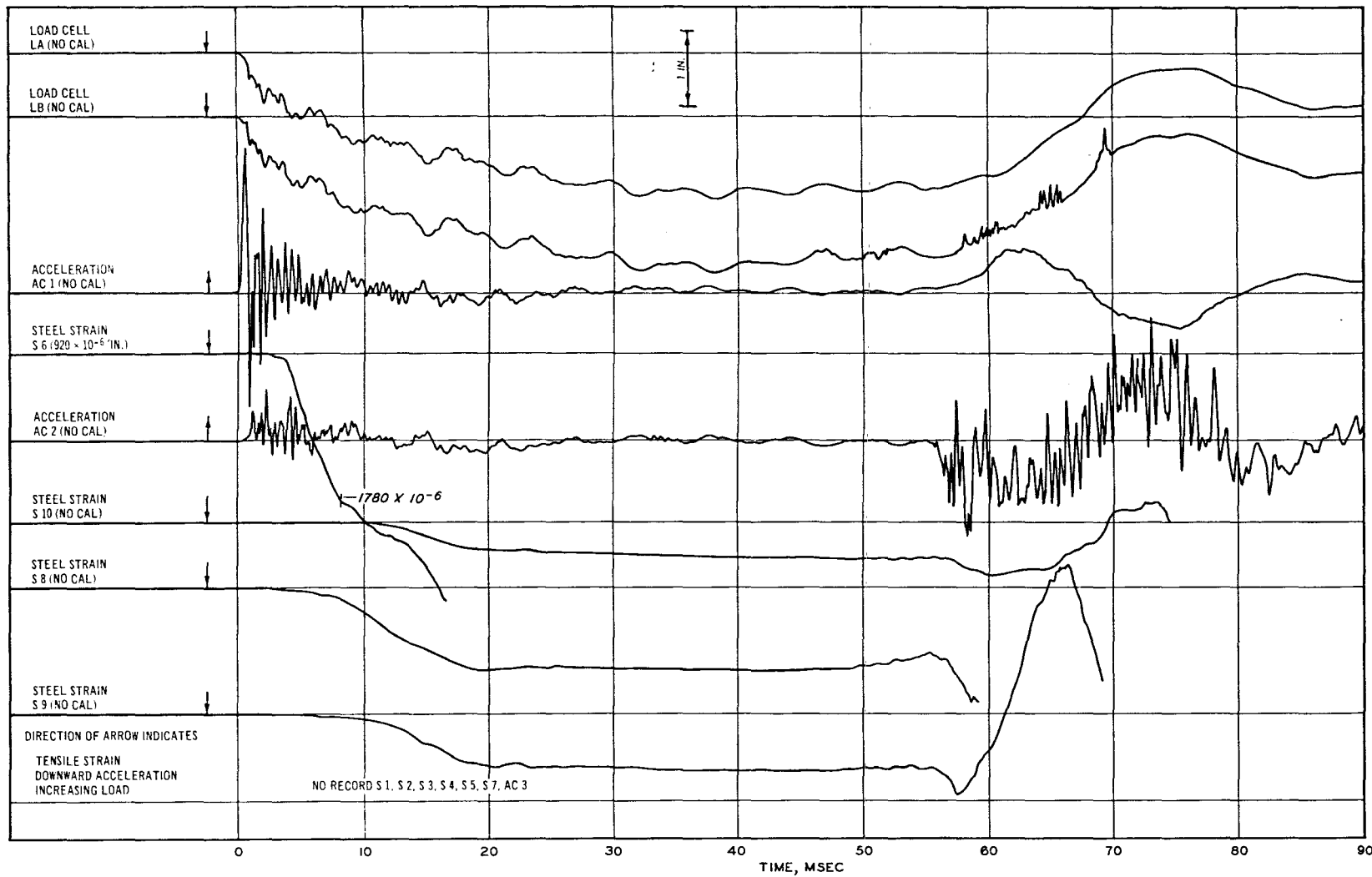


Figure C.31 Tracing of load, acceleration, and steel strain records, Specimen D4150-1.

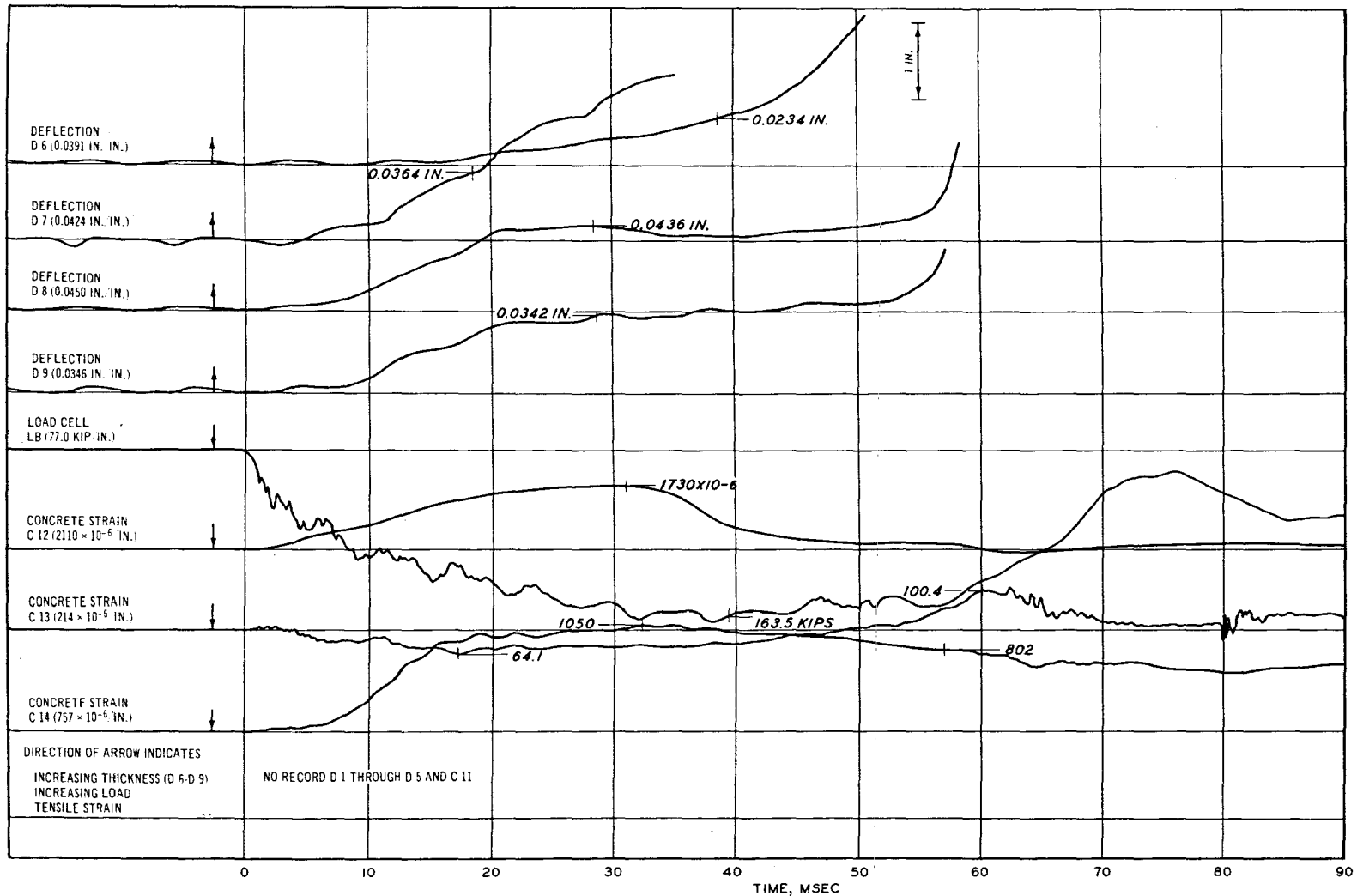


Figure C.32 Tracing of deflection, load, and concrete strain records, Specimen D4150-1.



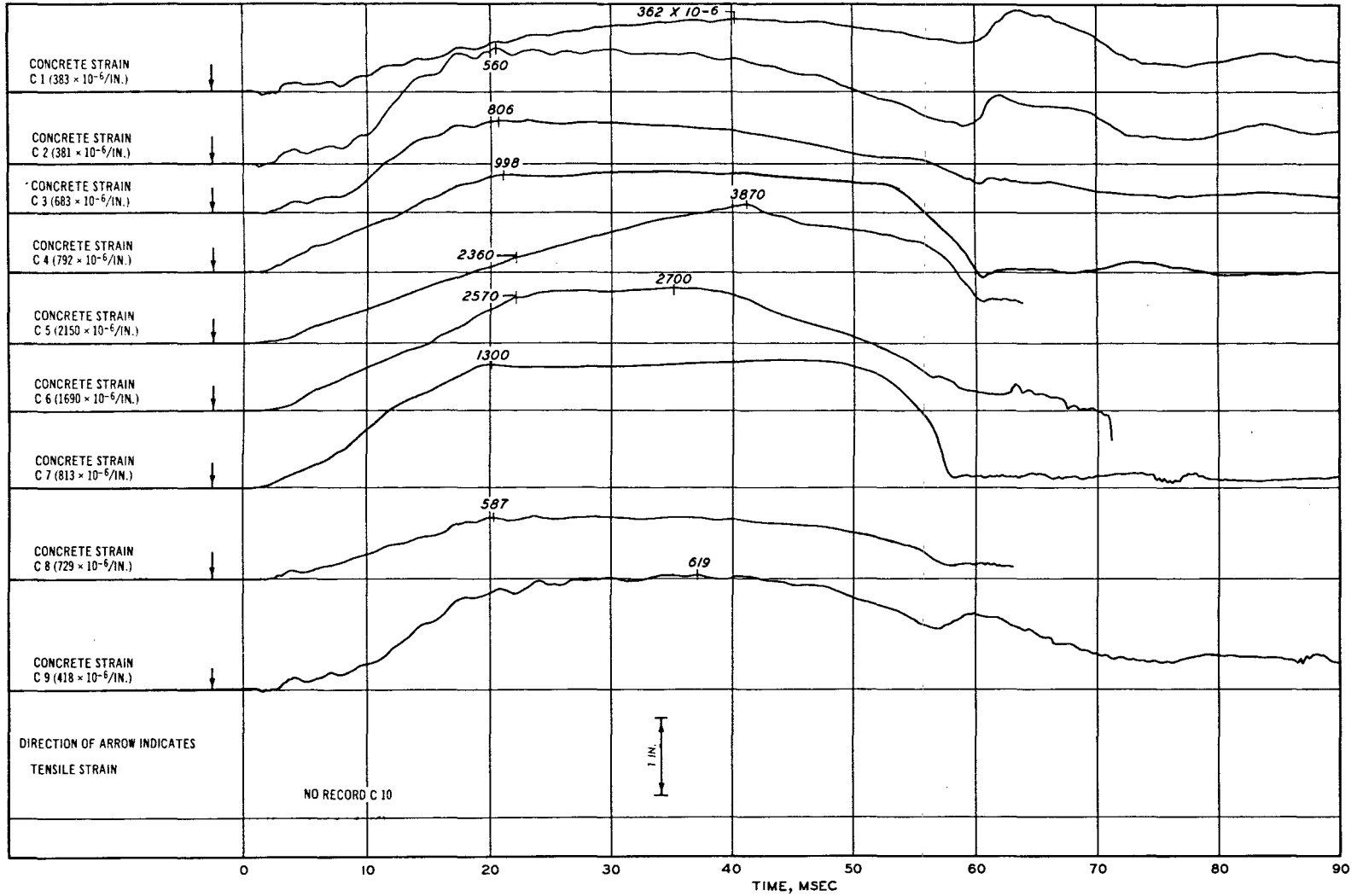


Figure C.33 Tracing of concrete strain records, Specimen D4150-1.

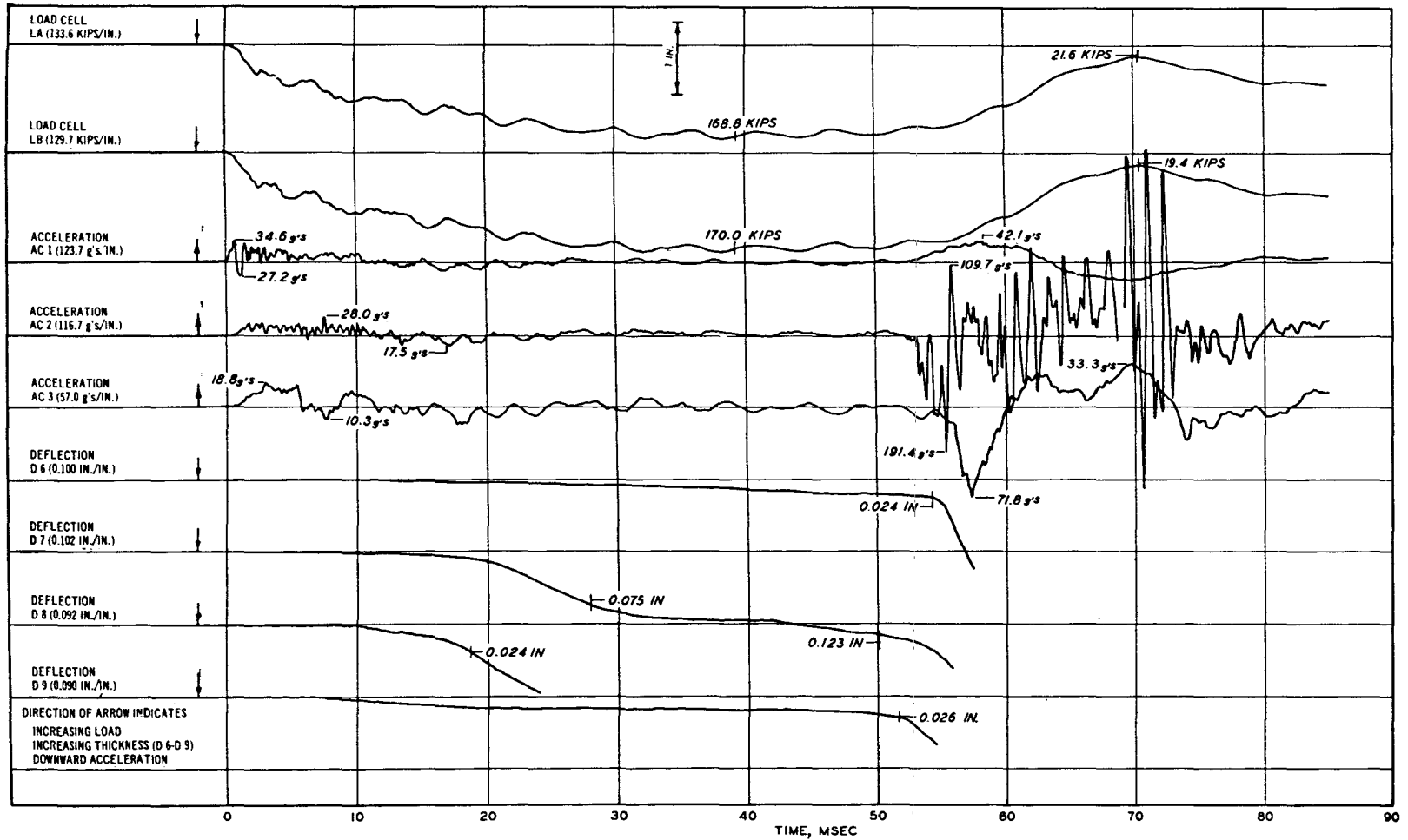


Figure C.34 Tracing of load, acceleration, and deflection records, Specimen D4150-2.

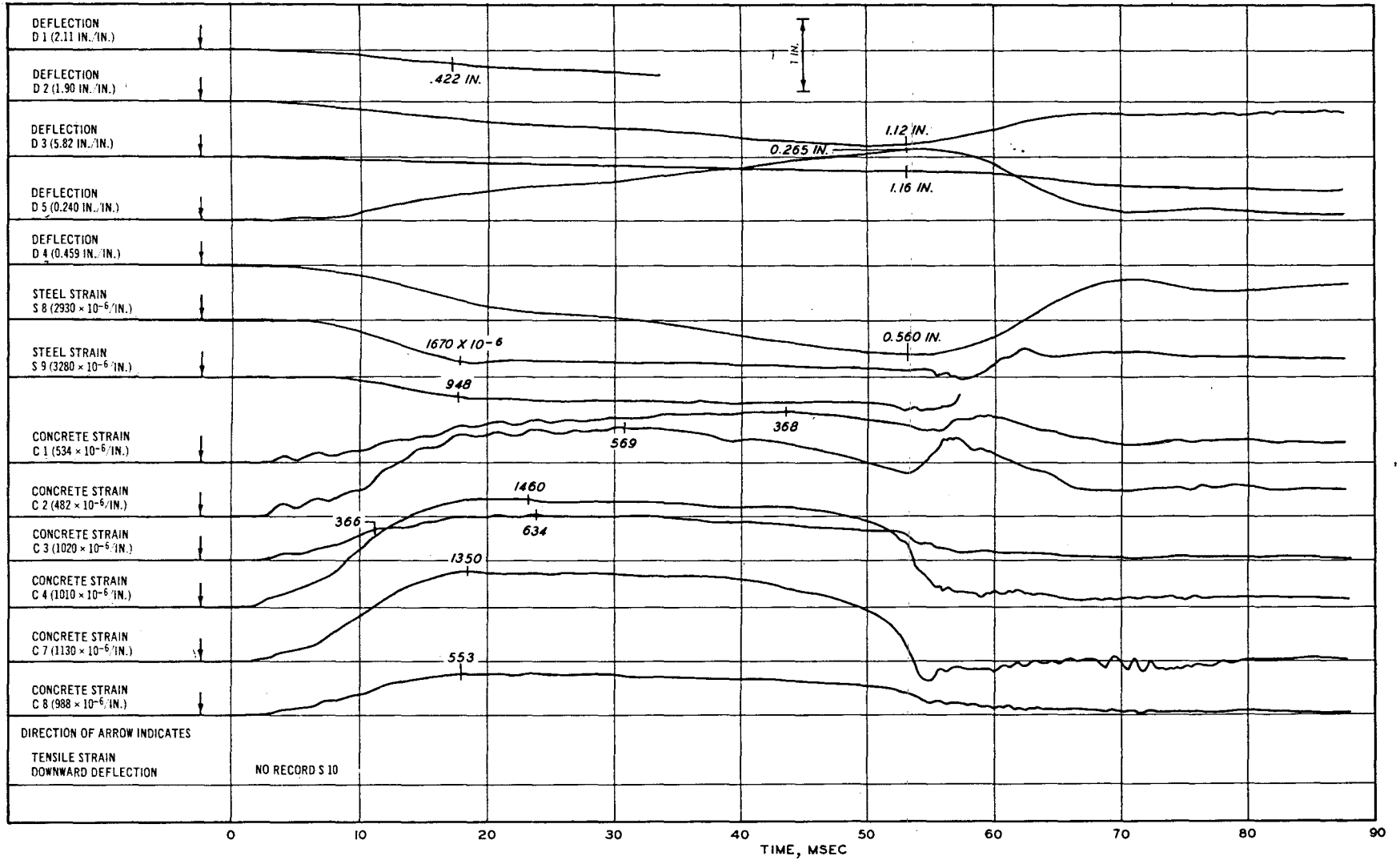


Figure C.35 Tracing of deflection, steel strain, and concrete strain records, Specimen D4150-2.

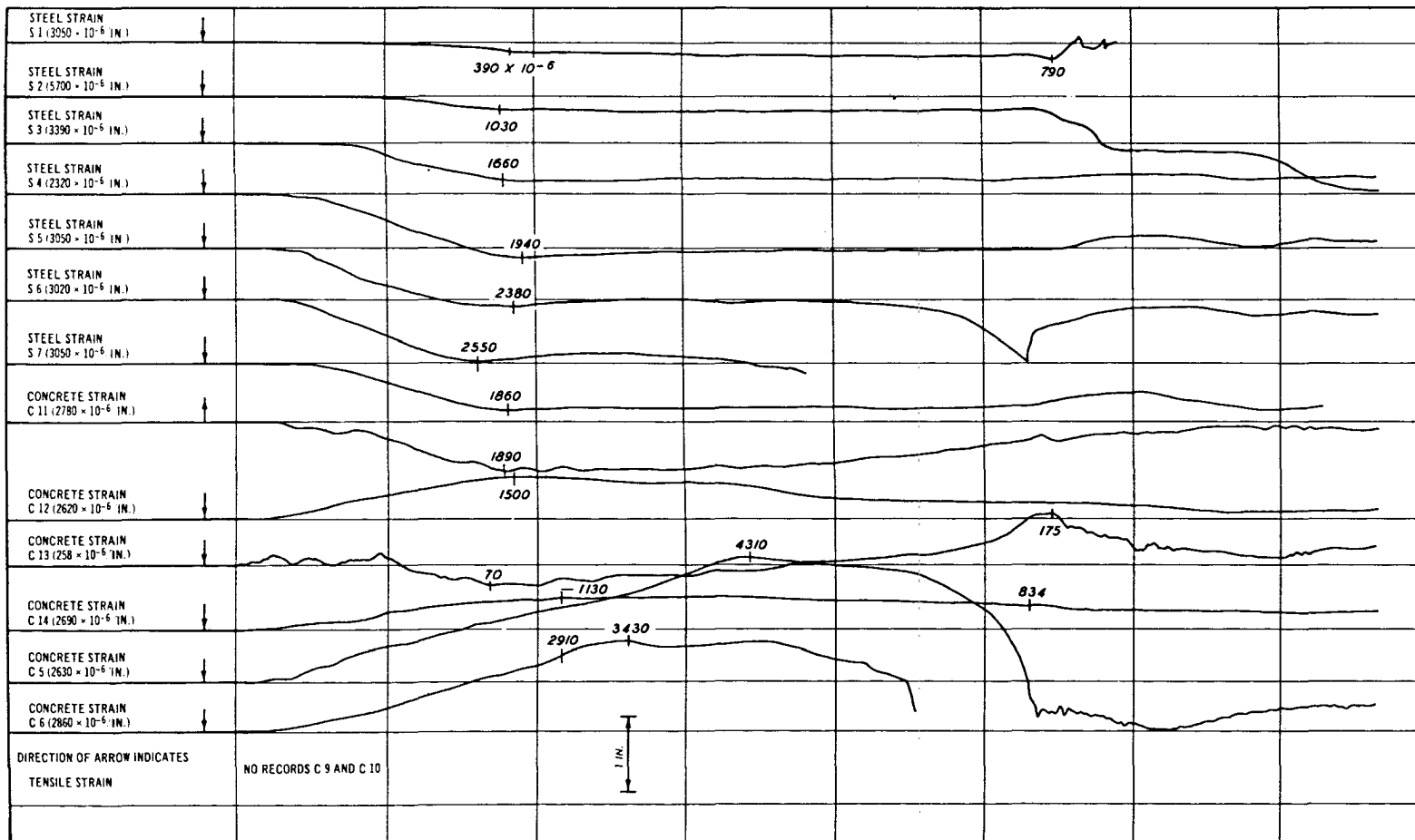


Figure C.36 Tracing of concrete strain and steel strain records, Specimen D4150-2.

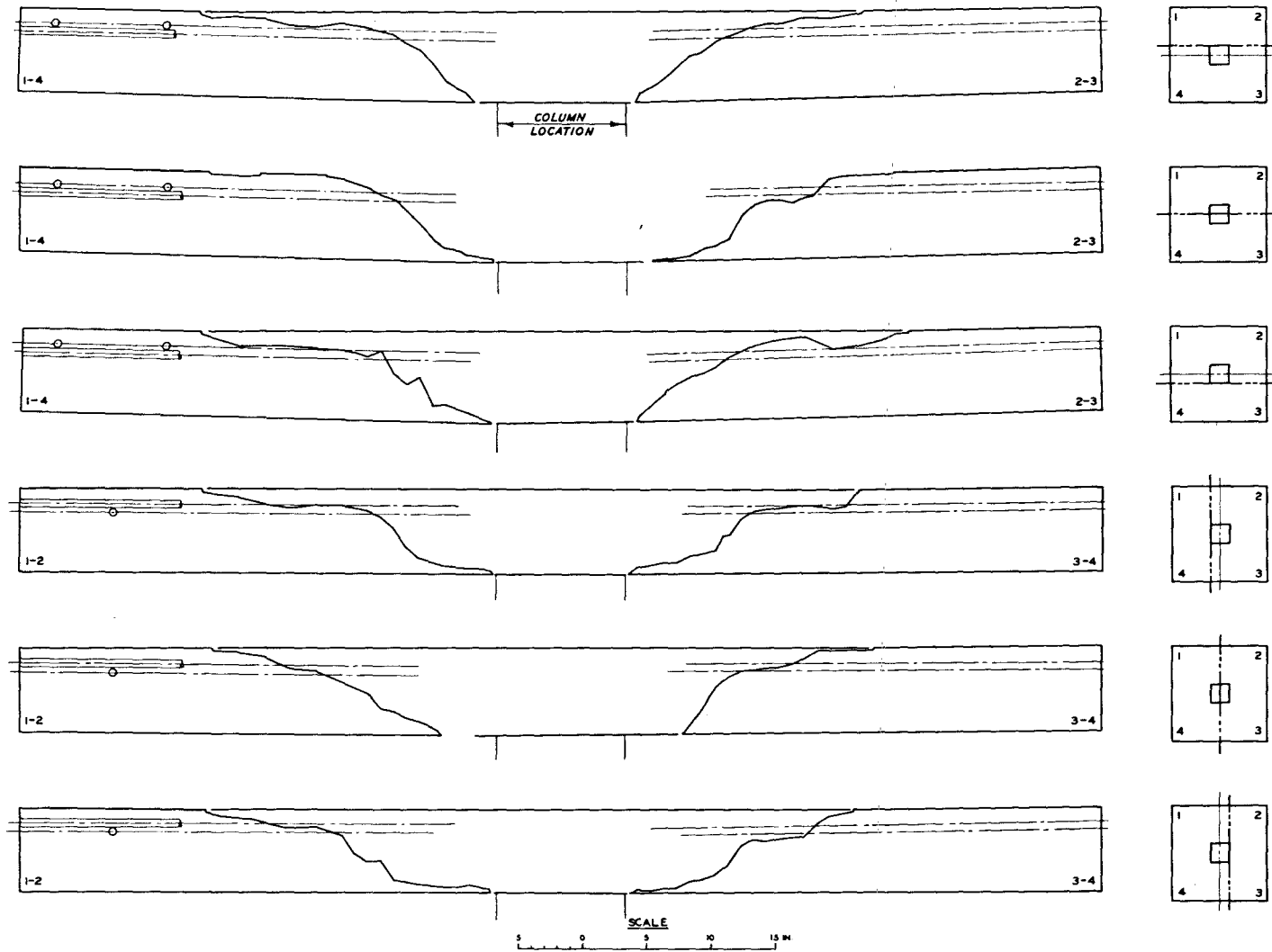


Figure C.37 Profiles of slab failure surface, Specimen D2075-3.

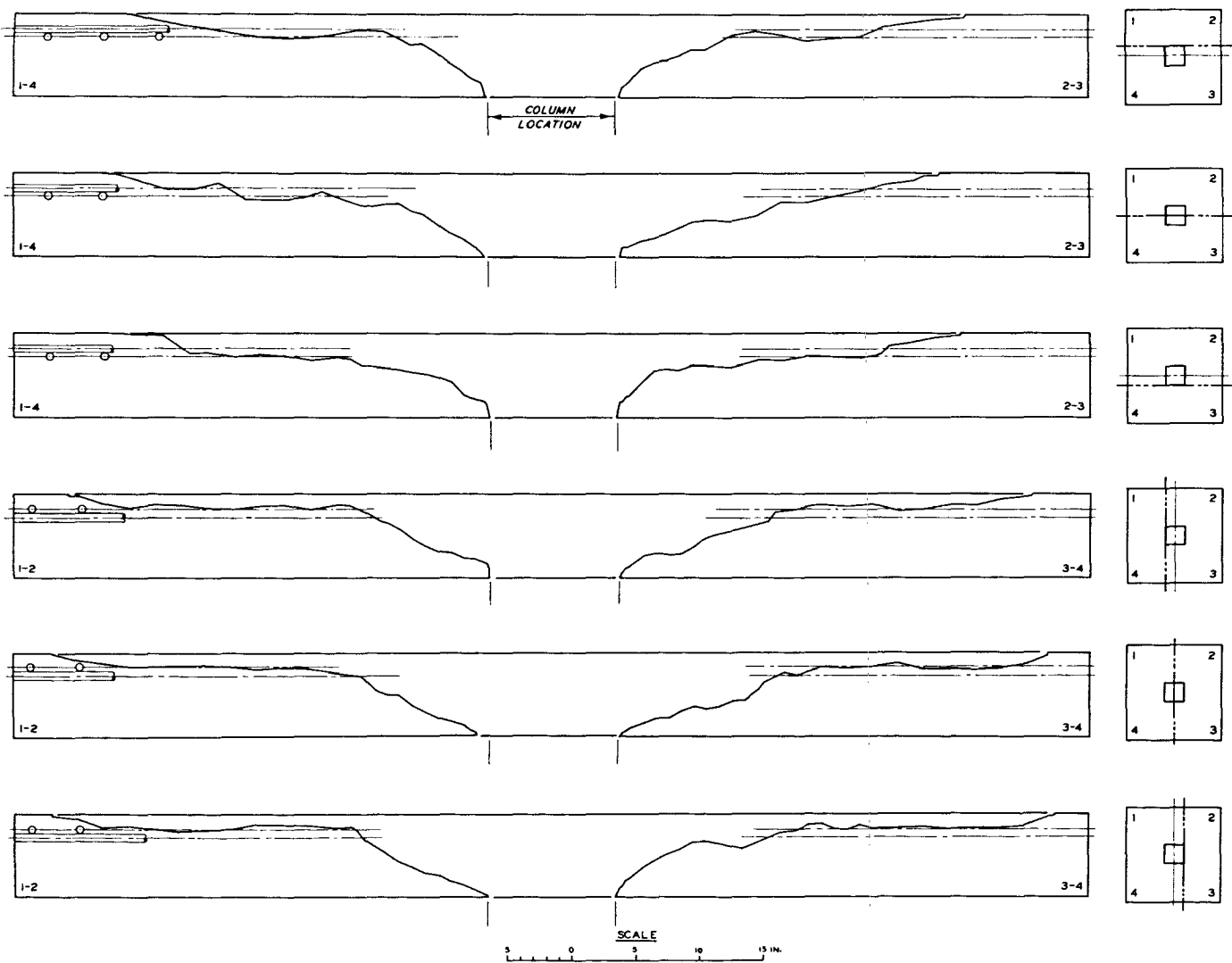


Figure C.38 Profiles of slab failure surface, Specimen D2150-1.

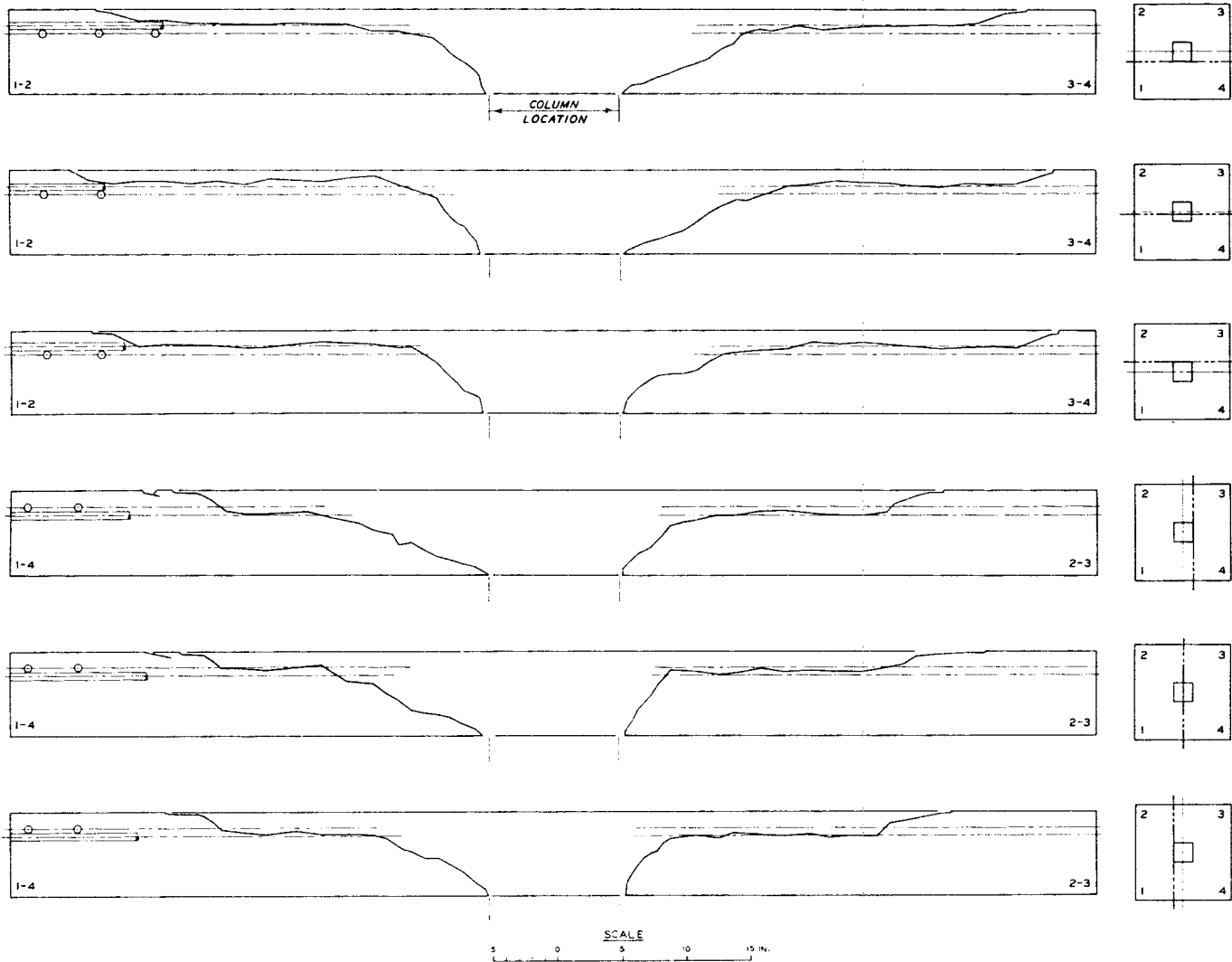


Figure C.39 Profiles of slab failure surface, Specimen D2150-2.

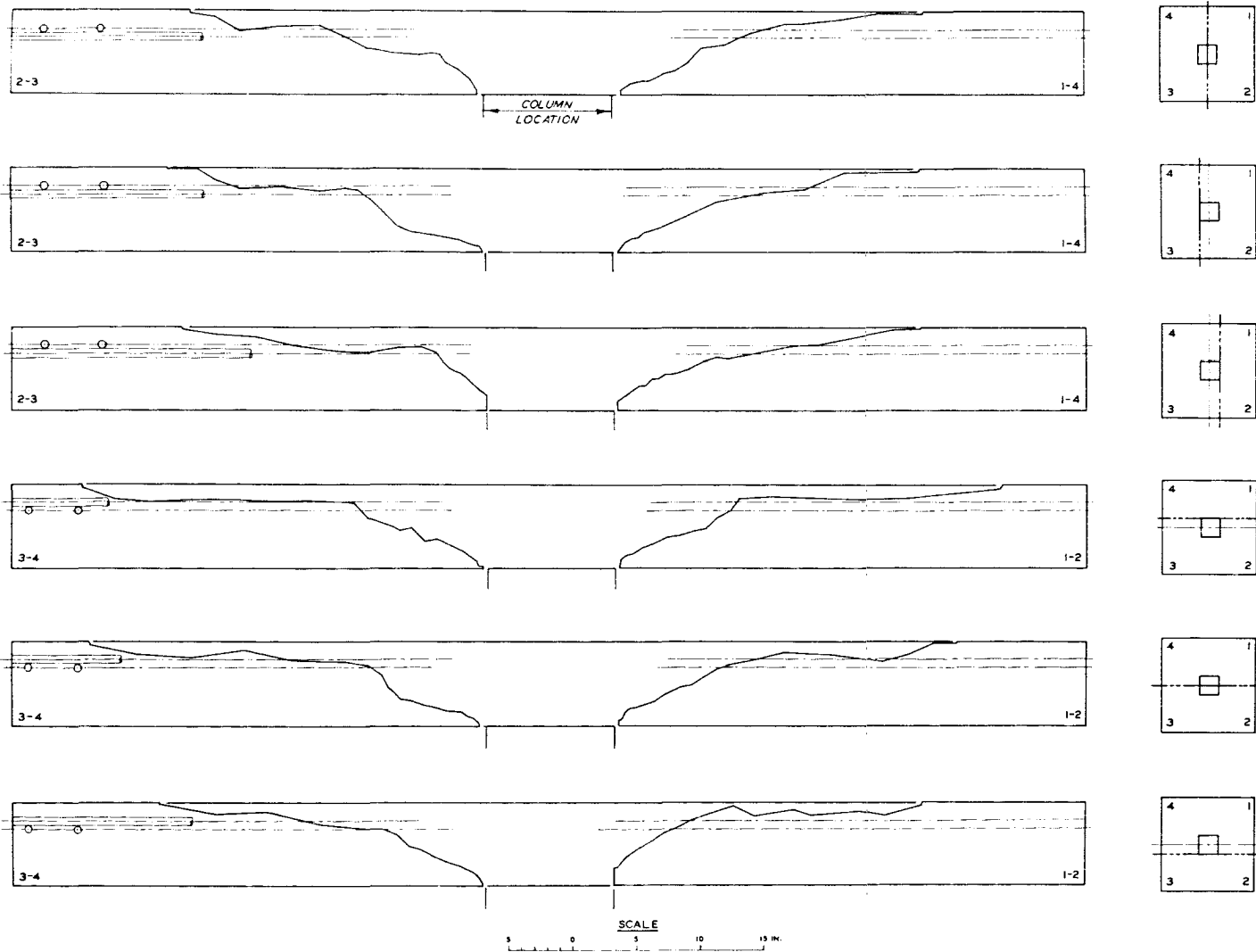


Figure C.40 Profiles of slab failure surface, Specimen D2150-3.



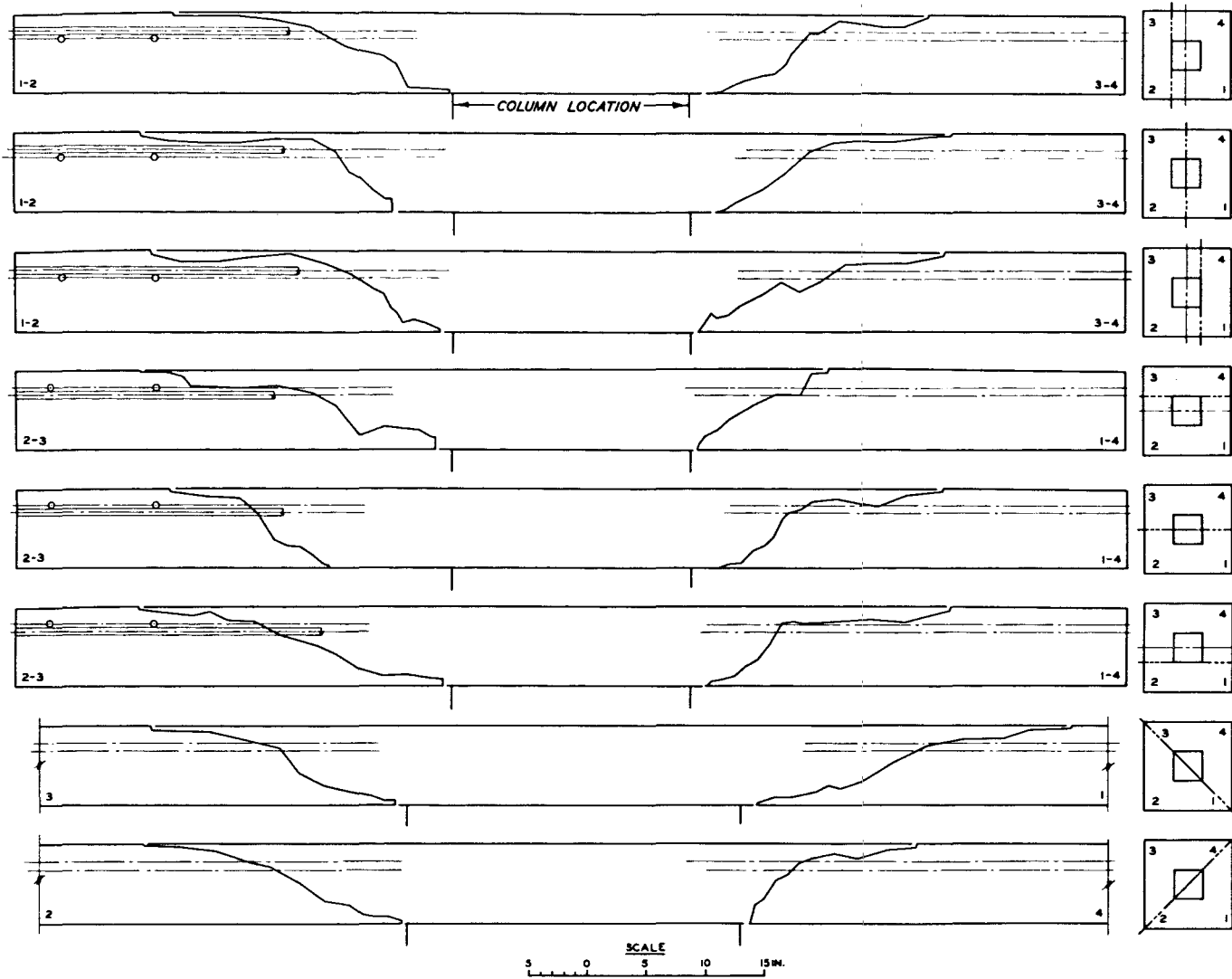


Figure C.41 Profiles of slab failure surface, Specimen D4075-1.

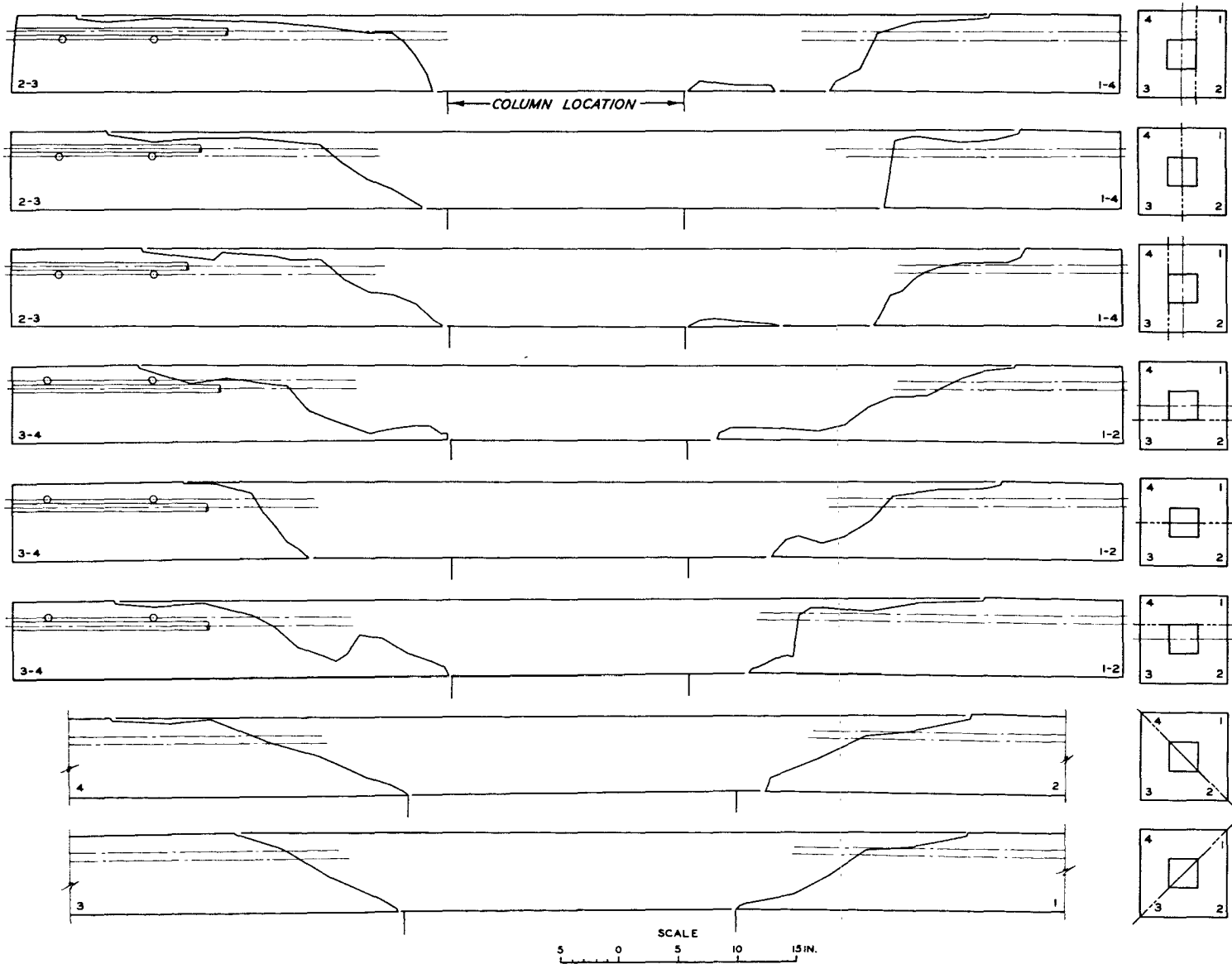


Figure C.42 Profiles of slab failure surface, Specimen D4075-2.

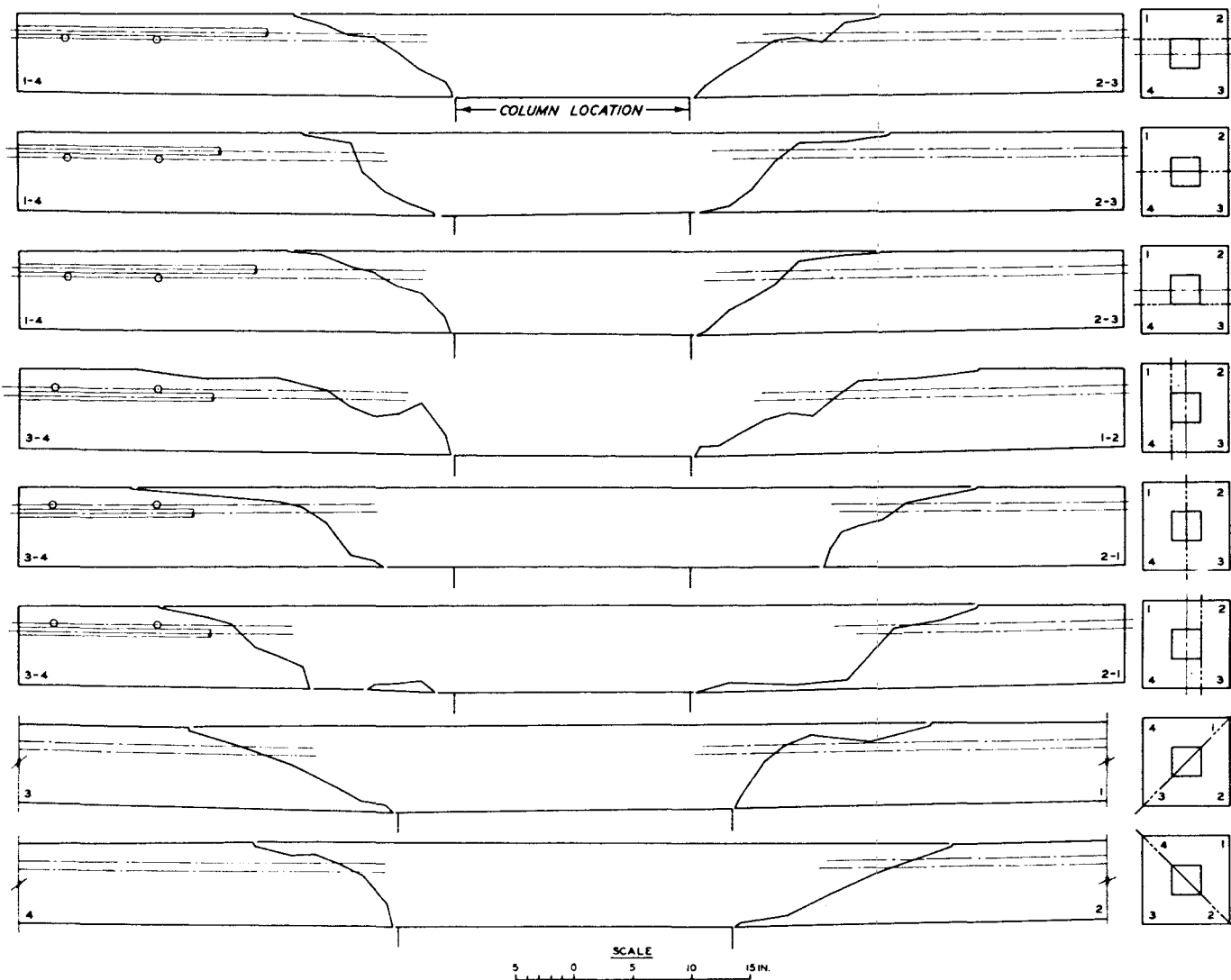


Figure C.43 Profiles of slab failure surface, Specimen D4075-3.

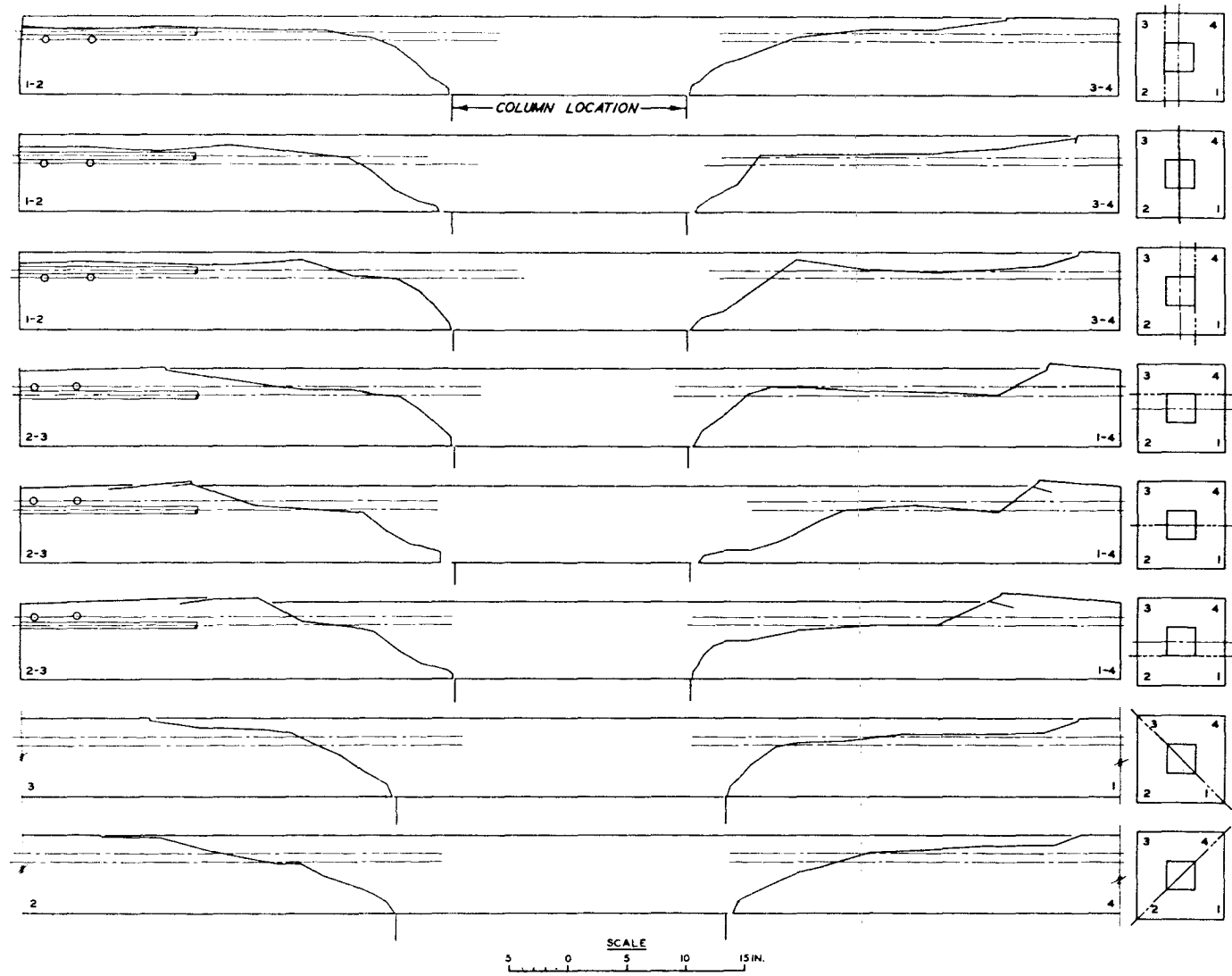


Figure C.44 Profiles of slab failure surface, Specimen D4150-1.

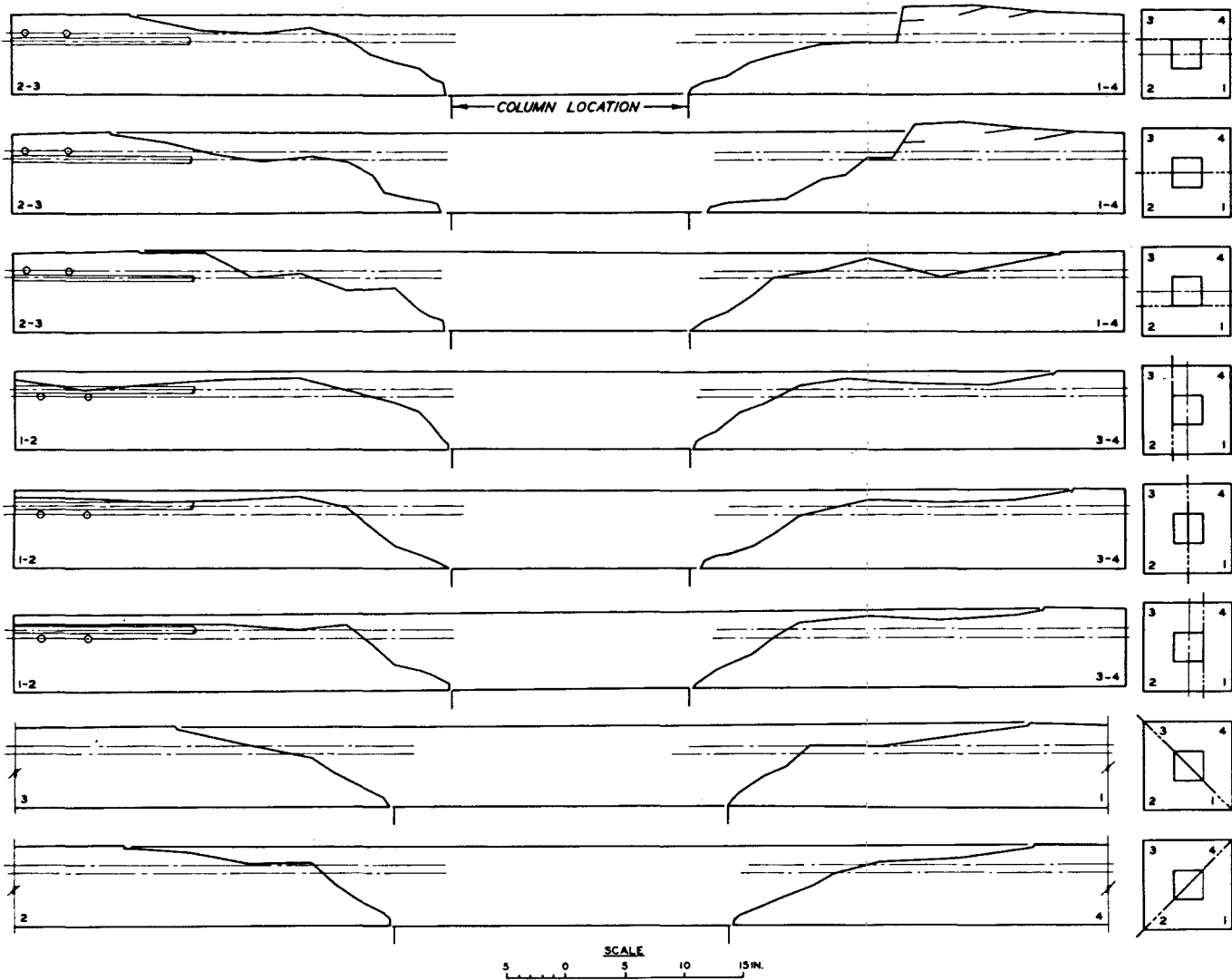


Figure C.45 Profiles of slab failure surface, Specimen D4150-2.

APPENDIX D

SHEAR STRENGTH ANALYSIS OF SLABS WITH TWO-WAY REINFORCEMENT  
BY THE METHODS OF KINNUNEN-NYLANDER AND KINNUNEN

The shear strength analyses presented by Kinnunen-Nylander (1960) and by Kinnunen (1963) involve the solution of numerous and sometimes lengthy equations. Iteration is necessary with either method to obtain a solution for a given design.

This appendix contains the equations and steps necessary to determine the predicted strength and rotation at failure by these two methods. Section 2.1.1 contains a short discussion of the method. The works of Kinnunen-Nylander and Kinnunen should be referred to for further details of the method and derivations of the equations.

#### D.1 METHOD OF KINNUNEN-NYLANDER

The physical model used by Kinnunen-Nylander is shown in Figure 2.2. The method includes constants fit to experimental data from circular connection specimens except where otherwise noted.

The column load is calculated separately from two equilibrium equations. The two values must be the same for a solution to be obtained.

Steps in the method are:

1. The following information is needed to start the analysis:

$f'_c$	concrete compressive strength, psi
$f_y$	yield stress of the reinforcement, psi
$d$	effective depth of the slab, inches
$p$	flexural reinforcement ratio in the slab
$B$	column diameter, inches
$c$	slab diameter, inches

2. If the column and slab are square, convert the column side dimension  $r$  and the slab side dimension  $a$  to an equivalent round shape:

$$B = 4r/\pi = \text{column diameter} \quad (\text{D.1})$$

$$c = 4a/\pi = \text{slab diameter} \quad (\text{D.2})$$

3. Calculate  $\sigma_t$ , the stress in the conical shell at failure. (From test results,  $\sigma_t = 2.35$  times the critical tangential stress on the slab surface at failure. Tangential strain values of failure are also from test results.)

If  $B/d \geq 2$

$$\sigma_t (\text{psi}) = 2290 + 1.09f'_c \quad (\text{D.3})$$

If  $B/d < 2$

$$\sigma_t (\text{psi}) = \left( 4110 + 1.95f'_c \right) \left( 1 - \frac{0.22B}{d} \right) \quad (\text{D.4})$$

4. Determine  $f(\alpha)$ , where  $\alpha =$  angle from the horizontal to the force  $T$  acting on the conical shell.  $f(\alpha) = \sin \alpha \cos \alpha (1 - \tan \alpha)$ .  $\alpha$  is solved from two equilibrium equations and is a function of  $c/d$ ,  $B/d$ , and  $y/d$ . The influence of  $y/d$ , where  $y$  is the depth of the compressive zone remaining above the inclined crack, is small.

Use Figure D.1, which gives  $f(\alpha)$  in terms of  $c/2d$  and  $B/d$ .

5. Assume a value for  $y/d$ . Usually,  $0.2 \leq y/d \leq 0.4$ . The value of  $y/d$  increases with  $p$ .

6. Determine  $P_1$ , the column load given by vertical equilibrium:

$$P_1 = \pi B y \sigma_t f(\alpha) \left[ \frac{1 + (2y/B)}{1 + (y/B)} \right] \quad (\text{D.5})$$

7. Calculate  $\psi$ , rotation of slab sectors at failure, in radians.



The formulas are fits to test results.

If  $B/d \geq 2$

$$\psi = 0.0019 \left( 1 + \frac{B}{2y} \right) \quad (D.6)$$

If  $B/d < 2$

$$\psi = 0.0035 \left( 1 - \frac{0.22B}{d} \right) \left( 1 + \frac{B}{2y} \right) \quad (D.7)$$

8. Compute  $r_y$ , the radius to which yielding in the slab extends, in inches:

$$r_y = \frac{29,000,000}{f_y} \psi (d - y) \quad (D.8)$$

9. Determine  $c_o$ , the radius to the shear crack at the level of the reinforcement. The following formula is a fit to data from two-way reinforced slabs only:

$$c_o = \frac{B}{2} + 1.8d \quad (D.9)$$

10. Compute  $R_1$ , the total tangential reinforcement force acting on the side of the slab sector:

If  $r_y \leq c_o$

$$R_1 = pf_y dr_y \ln \frac{c}{2c_o} \quad (D.10)$$

If  $c_o < r_y < c/2$

$$R_1 = pf_y d^2 \left[ \left( \frac{r_y - c_o}{d} \right) + \frac{r_y}{d} \ln \frac{c}{2r_y} \right] \quad (D.11)$$

If  $r_y \geq c/2$

$$R_1 = pf_y d \left( \frac{c}{2} - c_o \right) \quad (D.12)$$

11. Compute  $R_2$ , the total radial reinforcement force at the shear crack, divided by  $d\phi$ , the central angle of one slab sector.

If  $r_y \geq c_o$

$$R_2/d\phi = pf_y dc_o \quad (D.13)$$

If  $r_y < c_o$

$$R_2/d\phi = pf_y dr_y \quad (D.14)$$

12. Compute the column load  $P_2$  needed to satisfy moment equilibrium about the intersection of the radial resultant of the concrete compressive force in the slab and the force in the conical shell:

$$P_2 = \left( R_1 + \frac{R_2}{d\phi} \right) \frac{2\pi}{K_y} \quad (D.15)$$

where

$$K_y = \frac{(c - B)/2}{d - (y/3)} \quad (D.16)$$

13. If  $P_1$  does not equal  $P_2$ , select a new value for  $y/d$  and return to Step 6. Repeat until  $P_1 = P_2$ . If  $P_1 > P_2$ , decrease  $y/d$ .

14. Correct the column load  $P_1 = P_2$  for the effect of two-way reinforcement.

Kinnunen-Nylander observed that increasing the values of  $\psi$  and  $r_y$  by 60 percent and using a formula for  $c_o$  applicable for ring reinforcement (see Kinnunen-Nylander, 1960, p 79) resulted in the best fit for the data,

but recommended using the equations here designated as Equations D.1 through D.16 and using a calculated load  $P$  found by increasing  $P_1 = P_2$  by 10 percent:

$$P = 1.10P_1 = 1.10P_2 \quad (D.17)$$

## D.2 METHOD OF KINNUNEN

This method consists of the method of Kinnunen-Nylander modified to account for the dowel forces and the vertical force component present with a two-way reinforcement pattern and for the decrease in the tangential reinforcement force  $R_1$  resulting from the use of reinforcement not placed in an axisymmetric pattern.

1-3. Steps 1 through 3 are the same as for the method of Kinnunen-Nylander.

4. Determine  $\gamma$ , the proportion of the total load supported by reinforcement doweling and the vertical component of the steel force:

$$\gamma = 0.35 \text{ for two-way reinforcement}$$

$$\gamma = 0 \text{ for ring reinforcement}$$

Subsequent equations listed here are applicable for two-way reinforcement.

5. Determine  $f(\alpha)$  from Figure D.2 (for  $\gamma = 0.35$ )

$$f(\alpha) = f\left(\gamma, \frac{c}{d}, \frac{B}{d}\right)$$

6. Assume value of  $y/d$ .

7. Solve for  $P_1$ , the column load needed to satisfy vertical equilibrium:

$$P_1 = \frac{1}{1 - \gamma} f(\alpha) \sigma_t \pi B y \left[ \frac{1 + (2y/B)}{1 + (y/B)} \right] \quad (D.18)$$

8. Determine the rotation of the slab sectors at failure:

If  $B/d \geq 2$

$$\psi = 0.00195 (1 + \gamma) \left( 1 + \frac{B}{2y} \right) \quad (D.19)$$

If  $B/d < 2$

$$\psi = 0.0035 (1 + \gamma) \left( 1 - \frac{0.22B}{d} \right) \left( 1 + \frac{B}{2y} \right) \quad (D.20)$$

9. Calculate  $r_y$ , the maximum radius to which yielding extends:

$$r_y = \frac{29,000,000}{f_y} \psi (d - y) \quad (D.8)$$

10. Determine the radius to the shear crack at the level of the reinforcement,  $c_o$ :

$$c_o = \frac{B}{2} + 1.8d \quad (D.9)$$

11. Evaluate  $\eta$ , the coefficient of reduction of the reinforcement force tangential to the slab sector,  $R_1$ , because of the two-way reinforcement pattern. Use Figure D.3:  $\eta = f(c/2c_o, 2r_y/c)$ .

12. Modify  $\eta$  for design purposes:

$$\eta' = 0.5(1 + \eta) \quad (D.21)$$

13. Calculate  $R_1$ , the reinforcement force tangential to the slab sector for a ring reinforcement mat having the same spacing as the two-way reinforcement. Use Equations D.10 through D.12.

14. Calculate  $\theta$ , the slope of the inclined crack:

$$\cot \theta = \left[ \frac{1.8 - (y/d)}{1 - (y/d)} \right] \quad (D.22)$$

15. Compute  $R_2$ , the total radial reinforcement force at the shear crack, divided by  $d\phi$ , the central angle of one slab sector:

If  $r_y \leq c_o$

$$\frac{R_2}{d\phi} = p f_y' dr_y - \frac{\gamma P_1}{2\pi} \cot \theta \quad (D.23)$$

If  $r_y > c_o$

$$\frac{R_2}{d\phi} = p f_y' dc_o - \frac{\gamma P_1}{2\pi} \cot \theta \quad (D.24)$$

16. Determine  $\lambda$ , the distance from the slab compressive surface to the resultant concrete compressive force divided by the depth  $y$  of the compression zone above the inclined cracks. Use Figure D.4:

$$\lambda = f[c/(B+2y), \gamma] .$$

17. Evaluate  $P_2$ , the column load needed to satisfy moment equilibrium about the intersection of the reinforcement and the edge of the slab:

$$P_2 = 2\pi \left( \eta' R_1 + \frac{R_2}{d\phi} \right) \frac{1 - (\lambda y/d)}{\left( \frac{c - B}{2d} \right) - \gamma \left[ \frac{c_o - (B/2)}{d} \right]} \quad (D.25)$$

18. If  $P_2$  does not equal  $P_1$ , assume a new value of  $y$ . Repeat until  $P_1 = P_2$ .

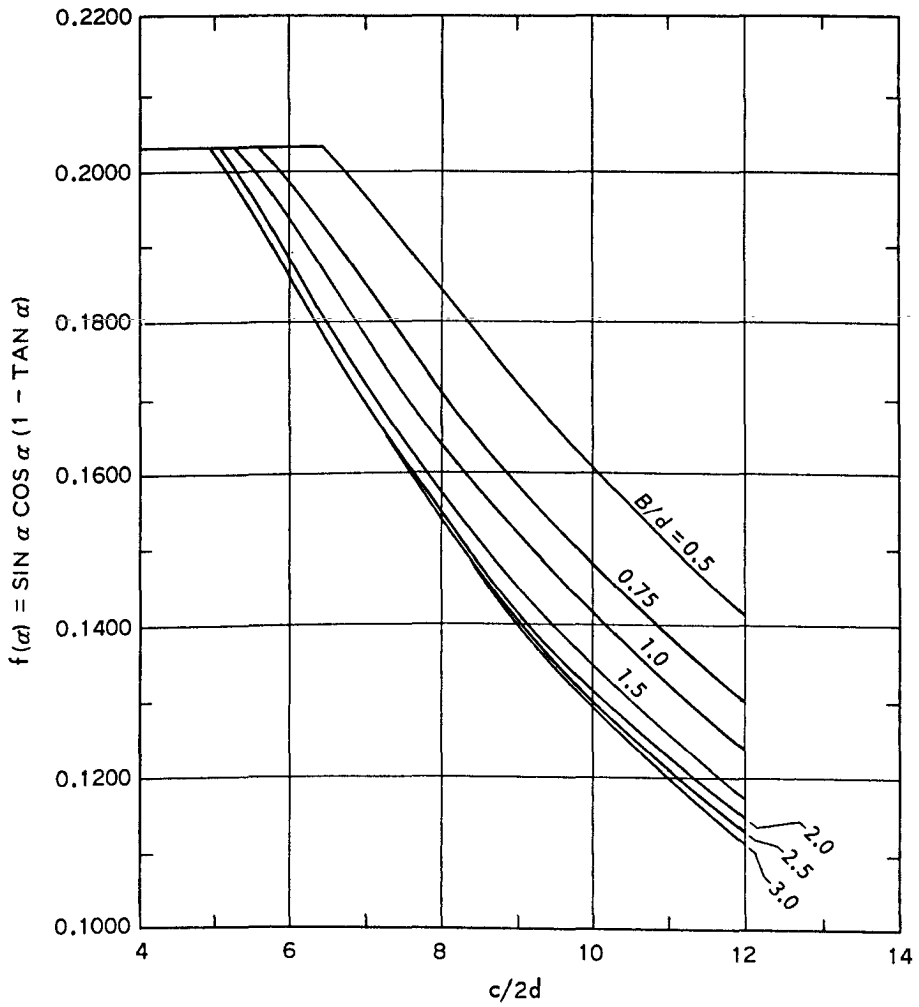


Figure D.1 Solution of  $f(\alpha)$ , from Kinnunen-Nylander (1960).

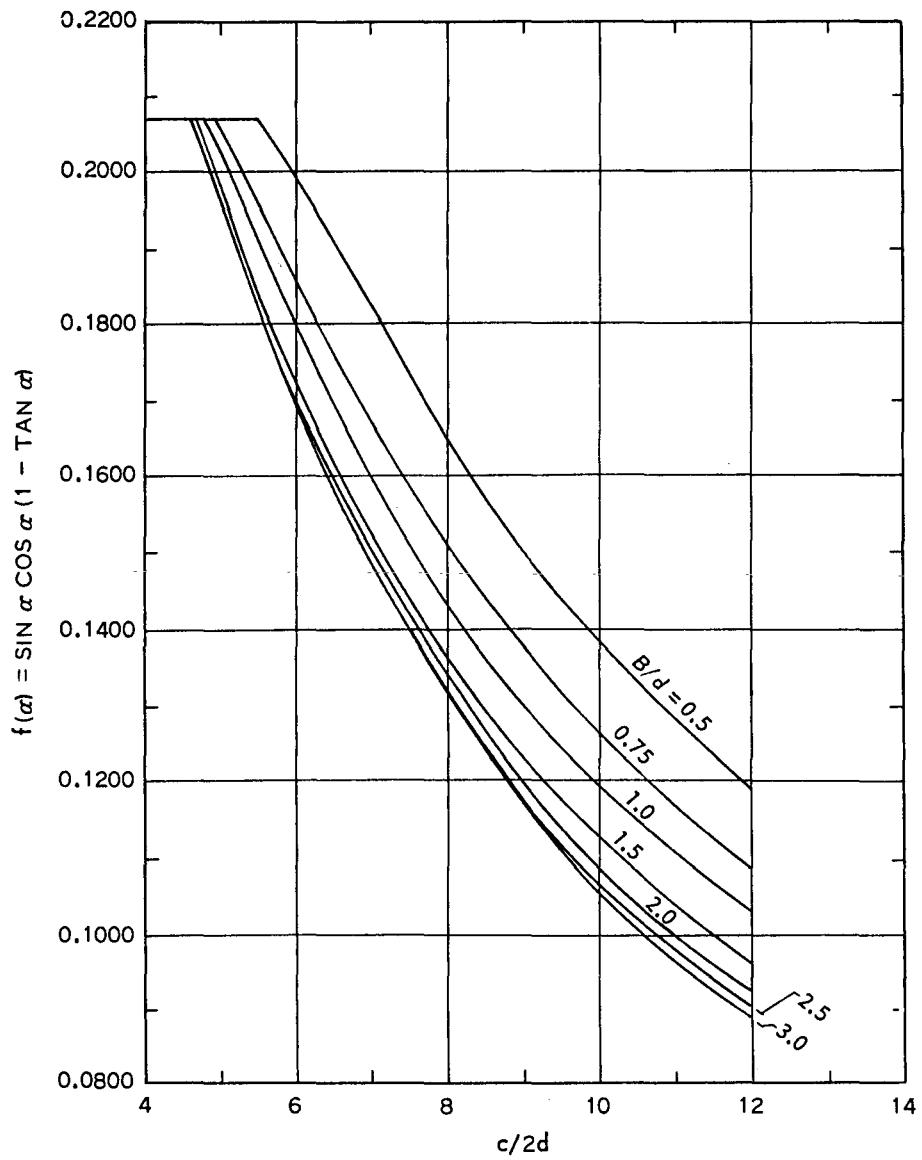


Figure D.2 Solution of  $f(\alpha)$ ,  $\gamma = 0.35$ , from Kinnunen (1963).

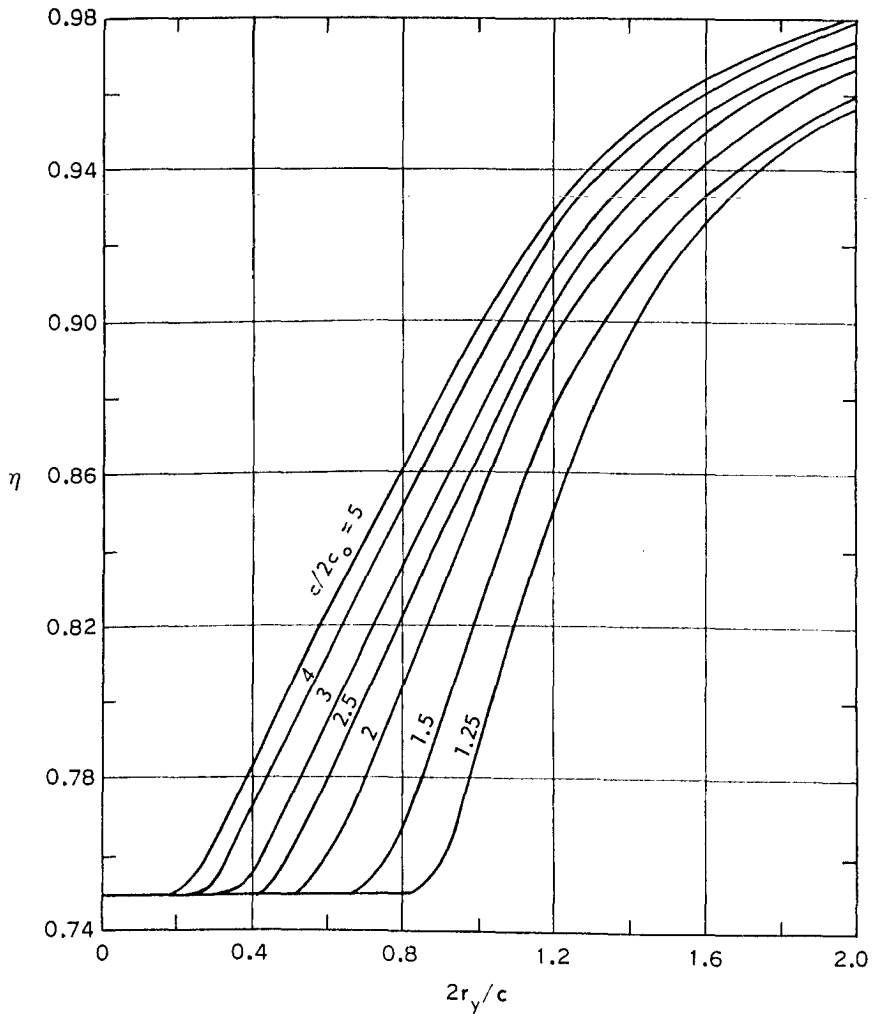
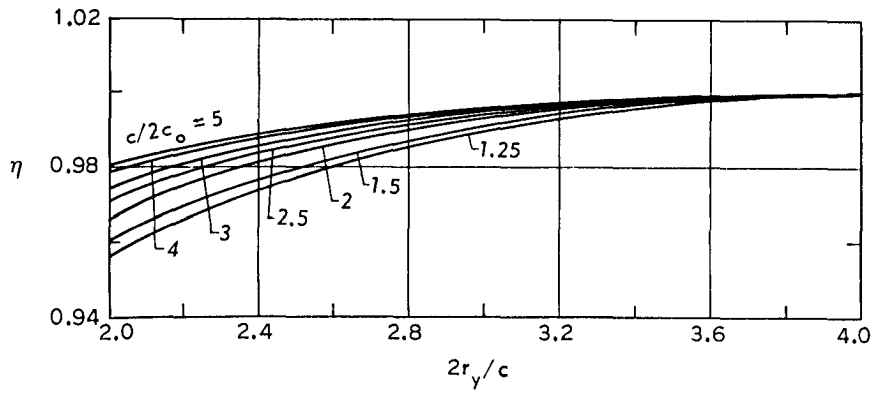


Figure D.3 Solution of  $\eta$ , from Kinnunen (1963).



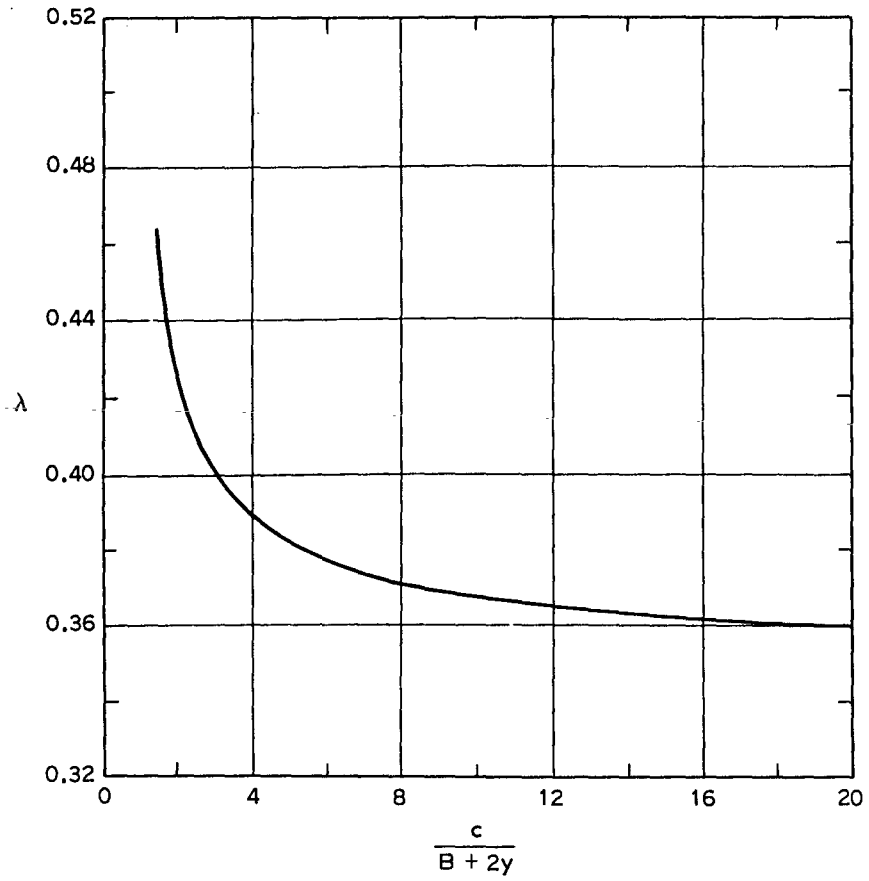


Figure D.4 Solution of  $\lambda$ ,  $\gamma = 0.35$ ,  
 from Kinnunen (1963).

DISTRIBUTION LIST FOR TECHNICAL REPORT N-70-1

Address	No. of Copies
Office of Civil Defense Office of the Secretary of the Army ATTN: Research Administration Office, Pentagon Washington, D. C. 20310	45
Army Library 1A 518, Pentagon Washington, D. C. 20310	1
Assistant Secretary of the Army (R&D) ATTN: Assistant for Research Washington, D. C. 20310	1
Chief of Naval Research Department of the Navy Washington, D. C. 20360	1
Commander, Naval Supply Systems Command (Code 0611C1) Department of the Navy Washington, D. C. 20360	1
Commander, Naval Facilities Engineering Command Research and Development (Code 0322C) Department of the Navy Washington, D. C. 20390	1
Mr. Richard Park Advisory Committee on Civil Defense National Academy of Sciences 2101 Constitution Avenue, N. W. Washington, D. C. 20418	1
Defense Documentation Center Cameron Station Alexandria, Va. 22314	20
Mrs. Joanne S. Gailar Civil Defense Research Project Oak Ridge National Laboratory P. O. Box X Oak Ridge, Tenn. 37830	1
Mr. Norward A. Meador Shelter Research Division, Office of Civil Defense Department of the Army - OSA, Washington, D. C. 20310	1

Address	No. of Copies
Chief of Naval Personnel (Code Pers M 12), Department of the Navy Washington, D. C. 20360	1
U. S. Naval Civil Engineering Laboratory Port Hueneme, Calif. 93041	1
Director, Disaster and Defense Services Staff Agricultural Stabilization and Conservation Service U. S. Department of Agriculture Washington, D. C. 20250	1
Mr. Bill Miller Department of Civil Engineering 307 More Hall, University of Washington Seattle, Wash. 98105	1
Professor Carl Koontz Department of Civil Engineering Worcester Polytechnic Institute Worcester, Mass. 01609	1
Mr. Franklin J. Agardy Department of Civil Engineering, San Jose State College San Jose, Calif. 95114	1
Professor Robert Bailey School of Civil Engineering, Civil Engineering Building Purdue University Lafayette, Ind. 47907	1
Mr. John A. Samuel Department of Mechanical Engineering, University of Florida Gainesville, Fla. 32601	1
Professor Gale K. Vetter School of Architecture, University of Colorado Boulder, Colo. 80302	1
Professor Richard E. Kummer 101 Eng. A, Pennsylvania State University University Park, Penn. 16802	1
Mr. George N. Sisson, Director Shelter Research Division, Office of Civil Defense Department of the Army - OSA Washington, D. C. 20310	1

Address	No. of Copies
Director, Defense Atomic Support Agency ATTN: Jack R. Kelso Washington, D. C. 20301	1
Mr. Edward R. Saunders, Jr. Deputy Director, National Resource Analysis Center Office of Emergency Preparedness, Executive Office of the President Washington, D. C. 20504	1
Director, Civil Effects Branch Division of Biology and Medicine, Atomic Energy Commission ATTN: Mr. L. J. Deal Washington, D. C. 20545	1
Los Alamos Scientific Laboratory ATTN: Document Library Los Alamos, N. Mex. 87544	1
Miss Nancy K. Barberii OCD Professional Advisory Service Center, University of Arizona Tucson, Ariz. 85721	1
Office, Chief of Engineers Department of the Army ATTN: ENGME-RD Washington, D. C. 20314	1
Chief, Joint Civil Defense Support Group Office, Chief of Engineers Department of the Army ATTN: ENGMC-D Washington, D. C. 20314	1
Director, Army Materials and Mechanics Research Center ATTN: Technical Library Watertown, Mass. 02172	1
Director, U. S. Army Ballistic Research Laboratory ATTN: Document Library Aberdeen Proving Ground, Md. 21005	1
Director, U. S. Army Ballistic Research Laboratory ATTN: Mr. William Taylor Aberdeen Proving Ground, Md. 21005	1

Address	No. of Copies
Director, Defense Atomic Support Agency ATTN: Technical Library Washington, D. C. 20301	1
District Engineer, U. S. Army Engineer District, Omaha ATTN: Chief, Engineering Division 6012 U. S. Post Office and Court House Omaha, Nebr. 68101	1
Mr. Carl K. Wiehle Civil Defense Technical Office, Stanford Research Institute Menlo Park, Calif. 94025	1
Mr. William L. White Civil Defense Technical Office, Stanford Research Institute Menlo Park, Calif. 94025	5
Mr. Werner Weber Director, New York State Civil Defense Commission Public Security Building, State Office Building Campus Albany, N. Y. 12226	1
Agbabian-Jacobsen Associates 8943 South Sepulveda Boulevard Los Angeles, Calif. 90045	1
Amman and Whitney 111 Eighth Avenue New York, N. Y. 10011	1
Mr. Arthur D. Caster Chairman, Coordinating Committee on Civil Defense American Society of Civil Engineers 2864 McFarlan Park Drive Cincinnati, Ohio 45211	1
The Dikewood Corporation 1009 Bardbury Drive, S. E., University Research Park Albuquerque, N. Mex. 87106	1
General American Transportation Corporation General American Research Division 7449 North Natchez Avenue Niles, Ill. 60648	1
Hudson Institute Quaker Ridge Road, Croton-on-Hudson, N. Y. 10520	1

Address	No. of Copies
Bell Telephone Laboratories, Inc. ATTN: Mr. R. W. Mayo Whippany Road Whippany, N. J. 07981	1
Dr. Harold Brode The RAND Corporation 1700 Main Street Santa Monica, Calif. 90401	1
Research Triangle Institute P. O. Box 12194 Research Triangle Park, N. C. 27709	1
Mr. Luke J. Vortman Division 5412, Sandia Corporation Box 5800, Sandia Base Albuquerque, N. Mex. 87115	1
URS Research Company 155 Bovet Road San Mateo, Calif. 94402	1
Massachusetts Institute of Technology Department of Civil and Sanitary Engineering Cambridge, Mass. 02138	1
University of Illinois, Civil Engineering Building ATTN: Dr. N. M. Newmark Dr. William Hall Dr. Mete Sozen Urbana, Ill. 61801	1 1 1
Dr. Merit P. White University of Massachusetts, School of Engineering Amherst, Mass. 01002	1
Dr. Abner Sachs Institute for Defense Analyses 400 Army-Navy Drive Arlington, Va. 22202	1
The Vertex Corporation 10400 Connecticut Avenue Kensington, Md. 20795	1

Address	No. of Copies
Office, Chief of Engineers Department of the Army ATTN: ENGMC-EM Washington, D. C. 20314	1
Dr. C. S. White President-Director, Lovelace Foundation 5200 Gibson Boulevard, S. E. Albuquerque, N. Mex. 87108	1
Dr. Charles Osterberg Acting Chief, Environmental Sciences Branch Division of Biology and Medicine U. S. Atomic Energy Commission Washington, D. C. 20545	1
Mr. J. J. Davis Effects Evaluation Division, Nevada Operations Office U. S. Atomic Energy Commission Las Vegas, Nev. 89101	1
Mr. Eugene F. Witt Bell Telephone Laboratories, Inc. Whippany Road Whippany, N. J. 07981	1
Mr. Paul Zigman Environmental Science Associates 770 Airport Boulevard Burlingame, Calif. 94010	1
Mr. J. W. Foss Supervisor, Buildings Studies Group Bell Telephone Laboratories Whippany Road Whippany, N. J. 07981	1
Commander, Air Force Weapons Laboratory ATTN: WLCO, MAJ Gerald Leigh WLIL (Tech. Library) Kirtland AFB, N. Mex. 87117	1 1
Division Engineer, U. S. Army Engineer Division, Huntsville ATTN: HNDSE-R (Mr. M. M. Dembo) HNDFE-S (Mr. H. O. Baker) P. O. Box 1600 West Station Huntsville, Ala. 35807	1 1

Unclassified

Security Classification

**DOCUMENT CONTROL DATA - R & D**

(Security classification of title, body of abstract and indexing annotation must be entered when the overall report is classified)

<b>1. ORIGINATING ACTIVITY (Corporate author)</b> U. S. Army Engineer Waterways Experiment Station Vicksburg, Miss.		<b>2a. REPORT SECURITY CLASSIFICATION</b> Unclassified	
		<b>2b. GROUP</b>	
<b>3. REPORT TITLE</b> STRENGTH AND BEHAVIOR OF REINFORCED CONCRETE SLAB-COLUMN CONNECTIONS SUBJECTED TO STATIC AND DYNAMIC LOADINGS			
<b>4. DESCRIPTIVE NOTES (Type of report and inclusive dates)</b> Final report			
<b>5. AUTHOR(S) (First name, middle initial, last name)</b> Marvin E. Criswell			
<b>6. REPORT DATE</b> December 1970		<b>7a. TOTAL NO. OF PAGES</b> 413	<b>7b. NO. OF REFS</b> 73
<b>8a. CONTRACT OR GRANT NO.</b>		<b>9a. ORIGINATOR'S REPORT NUMBER(S)</b>	
<b>b. PROJECT NO.</b>		Technical Report N-70-1	
<b>c. Work Order No. OCD-PS-66-67</b>		<b>9b. OTHER REPORT NO(S) (Any other numbers that may be assigned this report)</b>	
<b>d. Work Unit 1127B</b>			
<b>10. DISTRIBUTION STATEMENT</b> This document has been approved for public release and sale; its distribution is unlimited.			
<b>11. SUPPLEMENTARY NOTES</b> Report also submitted to University of Illinois, Urbana, Ill., as doctoral thesis, Department of Civil Engineering		<b>12. SPONSORING MILITARY ACTIVITY</b> Office of Civil Defense Office of the Secretary of the Army Washington, D. C.	
<b>13. ABSTRACT</b> The objectives of this investigation were to study the strength and behavior of slowly (statically) loaded reinforced concrete slab-column connections and to determine the effect of rapid (dynamic) loading on the strength and behavior by comparison with the static test results. Nineteen full-scale models of a connection and adjoining slab area, consisting of a simply supported slab 84 or 94 inches square and 6-1/2 inches thick loaded concentrically on a 10- or 20-inch-square stub column at the center of the slab, were tested. The main variables were the amounts of reinforcement in the slab (p = 0.75 and 1.50 percent), the column size, and the loading speed. Eight specimens were loaded to failure statically, two were subjected to a very rapidly applied load of short duration, and nine were loaded to failure by a rapidly applied load with a rise time chosen to represent the conditions in a blast-loaded structure. The behavior of the static and dynamic specimens was very similar. Failure deflections increased 25 to 50 percent at the rapid loading rate. The strength of specimens failing in shear after flexural yielding was reached (p = 0.0075) increased 18 percent with rapid loading; that of the more heavily reinforced specimens (p = 0.0150), 26 percent. These increases could be adequately explained by the effects of strain rate on material strength. The static test results are compared with 12 shear strength prediction methods. All methods became less conservative with the larger column size. The strengths of the specimens with p = 0.0075 were best predicted by a yield-line formula for flexural strength. Failure of connections with square columns was shown to start at the column corners and progress toward the column centerlines. Differences between the mechanism of shear failure in slabs and beams are examined. The shear-compression failure mechanism is shown to be not strictly applicable for slabs failing in shear.			

**DD FORM 1473**

FORM  
NOV 66

REPLACES DD FORM 1473, 1 JAN 64, WHICH IS OBSOLETE FOR ARMY USE.

Unclassified  
Security Classification



Unclassified

Security Classification

14.	KEY WORDS	LINK A		LINK B		LINK C	
		ROLE	WT	ROLE	WT	ROLE	WT
	Columns (Supports)						
	Concrete slabs						
	Connections						
	Dynamic loads						
	Reinforced concrete						
	Slab-column connections						
	Static loads						

Unclassified

Security Classification